FACULTY OF ENGINEERING
AND ARCHITECTURE

Unraveling the Pyrolysis and Oxidation Chemistry of Nitrogen, Oxygen and Sulfur Containing Hydrocarbon Mixtures

Cato Pappijn

Doctoral dissertation submitted to obtain the academic degree of
Doctor of Chemical Engineering

Supervisors

Prof. Kevin Van Geem, PhD - Prof. Marie-Françoise Reyniers, PhD

Department of Materials, Textiles and Chemical Engineering
Faculty of Engineering and Architecture, Ghent University

February 2022

GHENT
UNIVERSITY

FACULTY OF ENGINEERING
AND ARCHITECTURE

Unraveling the Pyrolysis and Oxidation Chemistry of Nitrogen, Oxygen and Sulfur Containing Hydrocarbon Mixtures

Cato Pappijn

Doctoral dissertation submitted to obtain the academic degree of
Doctor of Chemical Engineering

Supervisors
Prof. Kevin Van Geem, PhD - Prof. Marie-Françoise Reyniers, PhD

Department of Materials, Textiles and Chemical Engineering
Faculty of Engineering and Architecture, Ghent University

February 2022

GHENT
UNIVERSITY

ISBN 978-94-6355-573-9
NUR 952
Wettelijk depot: D/2022/10.500/14

Members of the Examination Board

Chair

Prof. Filip De Turck, PhD, Ghent University

Other members entitled to vote

Prof. Frédérique Battin-Leclerc, PhD, Institut National Polytechnique de Lorraine, France
Georgios Bellos, PhD, Dow Benelux, the Netherlands
Prof. Maarten Sabbe, PhD, Ghent University
Prof. Paul Van Steenberge, PhD, Ghent University

Supervisors

Prof. Kevin Van Geem, PhD, Ghent University
Prof. Marie-Françoise Reyniers, PhD, Ghent University

This work was supported by a doctoral fellowship fundamental research from the Fund for Scientific Research Flanders (FWO).

Acknowledgments

First of all I would like to thank Prof Guy B. Marin and my promotors Prof. Kevin M. Van Geem and Prof. Marie-Françoise Reyniers for giving me the opportunity to start my PhD research on this challenging topic at the Laboratory for Chemical Technology. I am very proud to have had these people as my guidance and I appreciate their continuous support and useful feedback on my research work over the last couple of years. I also would like to express my gratitude for the chances I have had to present my research at various conferences abroad and take part in different collaborations with academic groups and companies worldwide.

Second, I would like to thank Prof. Maarten Sabbe, Prof. Paul Van Steenberge and Prof. De Turck for their willingness to act as jury members for the defense of my thesis.

I would not have been able to connect the theoretical kinetic modeling work with experimental validation without the help of Aleksandar and Marko. Thank you for your support with the experimental datasets and for your general advice and assistance. Also many thanks to Florence and Ruben, who were always prepared to have valuable scientific discussions and provide guidance and support whenever needed throughout my PhD.

I have had the honor to work with different academic groups and companies and I would like to acknowledge them for their wonderful collaborations. I would like to thank Prof. Frédérique Battin-Leclerc and Olivier Herbinet for the opportunity to perform a research stay at their group at the Laboratoire Réactions et Génie des Procédés in Nancy, France. Thank you for sharing such a great deal of knowledge on all aspects of combustion chemistry and for making this stay such a good time. I also would like to express my gratitude to Georgios Bellos for giving me the opportunity to be a part of the academic project and for sharing all the expertise regarding heteroatomic compounds in hydrocarbon matrixes. Thank you for the

many scientific discussions and feedback opportunities that have provided me with valuable insights for my PhD research.

This PhD has been made possible via a fundamental PhD fellowship granted by the ‘Fonds voor Wetenschappelijk Onderzoek (FWO)’. I also would like to thank the COST Action CM1404 “Chemistry of smart energy carrier and technologies” for funding my research stay at Nancy in France.

There are many other people at the LCT who I would like to thank for the past four years. You have made my stay at the LCT, especially during the first two years, something to never forget. There are too many colleagues to list, but in particular a special thanks goes to Ismaël, Jia, Kevin, Lucas, Marvin, Pieter P., Pieter R. for spending many hours with me in the office.

Veel dank gaat ook uit naar vrienden en familie die me tijdens deze reis naar het behalen van een doctoraatsdiploma gesteund hebben. In het bijzonder zou ik mijn ouders en broer willen bedanken. Bedankt voor alle begrip en onvoorwaardelijke steun die jullie voor mij hadden en om mij van de nodige ontspanning te voorzien. Kortom bedankt om er altijd voor mij te zijn wanneer nodig gedurende deze interessante periode.

Cato Pappijn
Gent 2021

Contents

Contents i

Notation ix

Glossary xiii

Summary xvii

Samenvatting xxi

1 Introduction and outline 1

1.1. Heteroatomic compounds in the steam cracking process 1

1.2. Nitrogen-containing compounds 3

1.2.1. Feedstock impurities and additives 3

1.2.2. Thermal decomposition of nitrogen-containing compounds 5

1.2.2.1. Non-aromatic 5

1.2.2.2. Aromatic 8

1.2.3. Risks and safety hazards 10

1.3. Sulfur-containing compounds 12

1.3.1. Feedstock impurities and additives 12

1.3.2. Thermal decomposition of sulfur-containing compounds 14

1.3.2.1. Non-aromatic 14

1.3.2.2. Aromatic 16

1.3.3. Risks and safety hazards 18

1.4. Outline 19

1.5. References 21

2 Methodology 31
Abstract 31
2.1 Introduction 32
2.2 Quantum chemistry calculations 32
2.2.1 Stable species 32
2.2.2 Transition states 33
2.2.3 Thermodynamic parameters 34
2.2.4 Kinetic parameters 36
2.3 Group additivity method 38
2.3.1 Thermodynamic parameters 38
2.3.2 Kinetic parameters 40
2.4 Linear regression procedure 42
2.5 Kinetic modeling 45
2.6 Conclusions 49
2.7 References 50
3 Thermochemistry of nitrogen-containing compounds 55
Abstract 55
3.1. Introduction 57
3.2. Bond additivity corrections 60
3.2.1. Methodology 60
3.2.2. Results and discussion 63
3.2.2.1. Ab initio calculations 63
3.2.2.2. Comparison between ab initio calculated and experimental data 64
3.2.2.3. Regression 66
3.2.2.4. Application of the bond additivity corrections 73
3.3. Group additivity model for nitrogen-containing compounds 74
3.3.1. Methodology 74
3.3.2. Results and discussion 81
3.3.2.1. Ab initio calculations 81
3.3.2.2. Comparison between ab initio calculated and experimental data 81

3.3.2.3. Regression ... 82
3.3.2.4. Application of the group additivity scheme ... 93
3.4. Conclusions ... 95
3.5. References ... 96
4 Hydrogen abstraction reactions in nitrogen-containing compounds ... 101
Abstract ... 101
4.1. Introduction ... 102
4.2. Methodology ... 103
4.3. Results and discussion ... 107
4.3.1. Rate coefficients and Arrhenius parameters ... 107
4.3.2. Comparison between *ab initio* calculated and experimental data ... 109
4.3.3. Group additivity model ... 111
4.3.3.1. Initial model ... 111
4.3.3.2. Final model ... 112
4.3.3.3. Tunneling ... 118
4.3.3.4. Temperature dependence of group additive values ... 120
4.3.3.5. Thermodynamic consistency ... 121
4.3.3.6. Application ... 122
4.4. Conclusions ... 124
4.5. References ... 125
5 Pyrolysis and oxidation of aliphatic amines ... 129
Abstract ... 129
5.1. Introduction ... 131
5.2. Methodologies ... 133
5.2.1. Experimental data ... 133
5.2.2. Kinetic model development ... 136
5.2.3. Reactor simulations ... 137
5.3. Results and discussion ... 137
5.3.1. *Ab initio* calculations ... 137
5.3.2. Potential energy surfaces for low-temperature oxidation ... 140

5.3.3. Assessment of the kinetic model 143
5.3.3.1. Jet-stirred reactor experiments (DEA) 143
5.3.3.2. Shock tube ignition delay data (EA/DMA) 153
5.3.3.3. Laminar premixed flames (EA/DMA) 154
5.4. Conclusions 160
5.5. References 161
6 Steam cracking of sulfur-containing compounds 169
Abstract 169
6.1. Introduction 170
6.2. Methodologies 170
6.2.1. Kinetic model development 170
6.2.2. Experimental data 173
6.2.3. Reactor simulations 175
6.3. Results and discussion 176
6.3.1. *Ab initio* calculations 176
6.3.2. Potential energy surfaces 178
6.3.3. Assessment of the kinetic model 181
6.3.3.1. Dimethyl disulfide (DMDS) 181
6.3.3.2. Carbonyl sulfide (COS) 184
6.3.3.3. Heptane cracking with sulfur-containing compounds (CS_2, DMDS, DMS, DMSO) 186
6.4. Conclusions 190
6.5. References 191
7 Conclusions and future outlook 195
7.1. Conclusions 195
7.1.1 Quantum chemical calculations 195
7.1.2 Kinetic modeling with Genesys for H, C, N, O and S containing molecules 197
7.1.3 Experimental validation 198
7.2. Future outlook 198

Appendix A 203
A.1. Development of bond additivity corrections (BACs) 203
A.1.1. Database for regression of BACs and performance of CBS-QB3/BAC 203
A.1.2. CBS-QB3 methodology: Comparison with values of Montgomery et al. 213
A.2. Development of group additive values (GAVs) 215
A.2.1. CBS-QB3 methodology: Comparison with experimental entropies and heat capacities 215
A.2.2. Database for regression of GAVs 216
A.2.3. Differences between CBS-QB3 and GA approximated thermodynamic properties 226
A.2.4. Comparison with previously derived GAVs of Benson et al. 237
A.2.5. Comparison with previously derived GAVs of Holmes and Aubry 238
A.2.6. Comparison with previously derived GAVs of Ashcraft et al. 239
A.3. References 240
Appendix B 241
B.1. CBS-QB3 methodology: Experimental validation 241
B.2. H-H-N hydrogen abstractions 242
B.2.1. Single-event Arrhenius parameters for reference reaction 242
B.2.2. Rate coefficients in the temperature range 300-1800 K 243
B.2.3. Arrhenius parameters regressed at 1000 K 245
B.2.4. Reaction path degeneracy 246
B.2.5. Group additive values between 300 and 1800 K 247
B.2.6. Tunneling coefficients 251
B.3. N-H-N hydrogen abstractions 252
B.3.1. Single-event Arrhenius parameters for reference reaction 252
B.3.2. Rate coefficients in the temperature range 300-1800 K 253
B.3.3. Arrhenius parameters regressed at 1000 K 256
B.3.4. Reaction path degeneracy 258
B.3.5. Group additive values between 300 and 1800 K 260
B.3.6. Tunneling coefficients 264

B.4. C-H-N hydrogen abstractions 265
B.4.1. Single-event Arrhenius parameters for reference reaction 265
B.4.2. Rate coefficients in the temperature range 300-1800 K 266
B.4.3. Arrhenius parameters regressed at 1000 K 272
B.4.4. Reaction path degeneracy 275
B.4.5. Group additive values between 300 and 1800 K 279
B.4.6. Tunneling coefficients 283
B.5. References 285
Appendix C 287
C.1. Kinetic model development 287
C.2. Potential energy surfaces 289
C.2.1. Dimethylamine 289
C.2.2. Ethylamine 289
C.2.3. Diethylamine 290
C.3. Pyrolysis and oxidation of DEA 291
C.3.1. Tubular reactor 291
C.3.1.1. Discussion on plug flow reactor assumption 291
C.3.1.2. Temperatures profiles 292
C.3.2. Sensitivity analyses 292
C.3.2.3. Pyrolysis 292
C.3.2.4. Oxidation 293
C.4. Laminar premixed flames of DMA/EA 295
C.5. References 297
Appendix D 299
D.1. Pyrolysis of DMDS in N_2/C_2H_6 299
D.1.1. Experimental conditions 299
D.1.2. Temperature profiles 299
D.2. Pyrolysis of COS in N_2/C_2H_6 301
D.2.1. Experimental conditions 301
D.2.2. Temperature profiles 301

D.3. Steam cracking of C_7H_{16} with DMS/DMDS/DMSO/CS_2 302
D.4. References 303

Notation

Roman symbols

A	pre-exponential factor	s^{-1} or $m^3\ mol^{-1}\ s^{-1}$
$\tilde{A}$	single-event pre-exponential factor	s^{-1} or $m^3\ mol^{-1}\ s^{-1}$
C_p	heat capacity	$J\ mol^{-1}\ K^{-1}$
E_a	activation energy	$J\ mol^{-1}$
F	significance of regression	
G	Gibbs free energy	$J\ mol^{-1}$
$\Delta_r G$	reaction Gibbs free energy	$J\ mol^{-1}$
h	Planck's constant	$6.62\ 10^{-34}$ J s
H	enthalpy	$J\ mol^{-1}$
$\Delta_{atom} H$	enthalpy of atomization	$J\ mol^{-1}$
$\Delta_f H$	enthalpy of formation	$J\ mol^{-1}$
$\Delta_r H$	reaction enthalpy	$J\ mol^{-1}$
$\Delta^{\ddagger} H$	enthalpy of activation	$J\ mol^{-1}$
k	rate coefficient	s^{-1} or $m^3\ mol^{-1}\ s^{-1}$
$\tilde{k}$	single-event rate coefficient	s^{-1} or $m^3\ mol^{-1}\ s^{-1}$
k_B	Boltzmann constant	$1.38\ 10^{-23}\ J\ K^{-1}$
K_{eq}	equilibrium coefficient	units depend on reaction
n_e	number of single events	
n_{opt}	number of optical isomers	
p	pressure	Pa
q	molecular partition function	
R	universal gas constant	$8.314\ J\ mol^{-1}\ K^{-1}$
S	entropy	$J\ mol^{-1}\ K^{-1}$
$\tilde{S}$	symmetry-independent entropy	$J\ mol^{-1}\ K^{-1}$

$\Delta^{\ddagger}S$	entropy of activation	J mol^{-1} K^{-1}
T	temperature	K
$V(\varphi)$	potential energy	J
V_{ii}	Variance-covariance matrix	
X_{ij}	occurrence matrix	

Greek symbols

κ	tunneling coefficient	-
ν	frequency	cm^{-1} or s^{-1}
ρ	factor of deviation between rate coefficients	-
σ	rotational symmetry number	-
φ	equivalence ratio	-

Sub- and superscripts

‡	transition state
atom	atomization
elec	electronic
eq	equilibrium
exo	exothermic
exp	experimental
ext	external
for	forward
int	internal
opt	optical isomers
rot	rotational
tot	total
trans	translational
ref	reference
rev	reverse
vib	vibrational

Abbreviations

1D-HIR	one-dimensional hindered rotor
AI	ab initio
B3LYP	Becke-3-parameter-Lee-Yang-Parr hybrid functional
BAC	bond additive correction
BDE	bond dissociation energy
CBS-QB3	complete basis set quadratic Becke3
CDK	chemistry development kit
CIT	coil inlet temperature
CNRS	Centre National de la Recherche Scientifique
COP	coil outlet pressure
COT	coil outlet temperature
DFT	density functional theory
DEA	diethylamine
DMA	dimethylamine
DMDS	dimethyl disulfide
DMS	dimethyl sulfide
DMSO	dimethyl sulfoxide
EA	ethylamine
F	significance
FID	flame ionization detector
FTIR	Fourier transform infrared spectrometer
GA	group additivity
GAV	group additive value
GC	gas chromatography
InChI	international chemical identifier
IRC	intrinsic reaction coordinate
JSR	jet-stirred reactor
LCT	Laboratory for Chemical Technology
MAD	mean absolute deviation
MAX	maximum deviation

MD	mean deviation
NNI	non-nearest-neighbor interaction
PES	potential energy surface
RES	resonance correction
RMS	root-mean-square deviation
RRKM/ME	Rice-Ramsperger-Kassel-Marcus theory/Master Equation
RSC	ring strain correction
SMARTS	SMILES arbitrary target specification
SMILES	simplified molecular-input line-entry system
SOC	spin orbit correction
SSQ	sum of squares
TCD	thermal conductivity detector
TS	transition state
TST	transition state theory
VTST	variational transition state theory

Glossary

Ab initio	Calculations based on first principles for the determination of molecular properties using quantum chemical calculations.
Base mechanism	Used to describe the reaction network between the smallest species and reactions that occur between these species. Combined with thermodynamic and kinetic parameters it can be used to complement a kinetic model that is generated automatically.
Basis set	Set of functions used to describe the molecular orbitals in quantum chemical calculations.
Bond dissociation energy	Enthalpy change when breaking a bond by homolysis.
Chain branching	Reaction event in which one reactive free radical produces two other radical species.
Closed-shell compound	Compound with a completely filled valence shell or in other words with no unpaired electrons.
Coil outlet temperature	Highest temperature obtained at the outlet of the tubular reactor in a steam cracking plant.
Cold box	A separation unit in a steam cracking plant that separates methane and hydrogen from the ethylene-rich product of the cracking section.
Elementary reaction	A chemical reaction in which one or more species react(s) to form product(s) in a single step and with a single transition state.
Enantiomer	One of two stereoisomers that are mirror images of each other without being superimposable.

Equivalence ratio The ratio of the actual fuel to air ratio to the stoichiometric fuel to air ratio.

Fuel radical Radical that can be formed directly from the parent fuel molecule via an elementary initiation reaction.

Genesys In-house developed software tool used for the automatic generation of first-principles based kinetic models.

Group additivity method A set of techniques that allows the approximation of properties of molecules and reactions by summing different contributions for each group, which is a sub-molecular pattern existing of a small number of atoms.

High-pressure limit In the high-pressure limit collisions with the bath gas quickly establish a Boltzmann distribution of the population.

Internal standard A known concentration of a substance that is added to the analyzed sample to allow quantification.

Intrinsic reaction coordinate Calculations in which starting from a saddle point, the two wells on each side of the saddle point are searched for, corresponding to the reactants and products of a reaction.

Isodesmic reaction A reaction of which the bonds that are broken in the reactant are of the same type as the bonds that are formed in the product.

Jet-stirred reactor A reactor in which mixing is established using the kinetic energy of the process gas itself, which is injected at high velocity through a number of nozzles mounted centrally in the reactor. As it can be approximated by an ideal continuously stirred tank reactor, this reactor is typically used to obtain intrinsic kinetic information on gas phase reactions.

Level of theory Property of quantum chemical calculations that describes the treatment of the electron correlations and defines the basis set.

Microkinetic model A kinetic model that describes the behavior of a chemical system using only elementary reactions.

Potential energy surface	The electronic energy of chemical species and intermediates as a function of the geometrical arrangement of the atoms.
Pyrolysis	The uncatalyzed decomposition of compounds resulting from exposure to high temperature, in the absence of molecular oxygen or steam.
Radical pool	Combination of different small radical species that are in partial equilibrium.
Reaction family	A class of reactions that are characterized by the same pattern of electron rearrangement steps.
Reactive atom	An atom that changes in connectivity through an elementary reaction.
Reactive center	Collection of reactive atoms for one elementary reaction.
RRKM/ME calculations	Benchmark method to determine pressure dependent rate coefficients based on the ab initio calculated potential energy surface.
Shale gas	Natural gas trapped in shale formations.
Single events	A factor introduced in the rate coefficient to account for the equivalent ways for the reaction to occur. Also referred to as reaction path degeneracy.
Spin-orbit coupling	Interaction of the spin of a particle with the motion inside a potential.
Steam cracking	A petrochemical process in which saturated hydrocarbons are converted into small unsaturated hydrocarbons by exposure to high temperatures in the presence of steam.
Thermodynamic consistency	The forward and reverse rate coefficients are thermodynamically consistent if their ratio equals the equilibrium coefficient of the reaction.

Summary

Scope

The gradual shift from fossil to more sustainable and alternative feedstocks driven by the increasingly strict environmental regulations and process economics poses a challenge for the (petro)chemical industry. A common concern is the presence of heteroatomic compounds, i.e. containing oxygen, nitrogen, sulfur, which do not only have a higher concentration in these types of feedstocks, but also a different distribution of functional groups. Their decomposition can lead to the formation of hazardous species such HCN, NO_x, H_2S and SO_x, which can have a negative impact on the process, considering safety, operability and quality of the product streams. Because little is known about the pyrolysis or oxidation reactions of these heteroatomic compounds and how the occurring chemistry is affected by the presence of a hydrocarbon matrix, corresponding to steam cracking conditions, very global specifications are currently kept in place. The scope of this PhD thesis is to improve the understanding of the thermochemical reactions of heteroatomic compounds, present either as feedstock impurities or process additives, via a combination of quantum chemical calculations, first-principles based kinetic modeling and experimental work. While the majority of sulfur- and nitrogen-containing compounds is present in the form of aromatic structures, substantial amounts of non-cyclic compounds can be found in both fossil and renewable feedstocks, such as aliphatic amines, thiols and (di)-sulfides, which are also the classes of commonly used process additives. The gas phase chemistry of these classes is still poorly understood and hence the focus is on elucidation of their pyrolysis and oxidation chemistry, which can be regarded as a first step of the extension towards the more complex heteroatomic compounds.

Methodology

Microkinetic models are generated with the in-house developed software tool Genesys. The thermodynamic and kinetic parameters required for model simulation are determined with new *ab initio* calculations and group additivity schemes that enable a fast "on-the-fly" approximation procedure. The *ab initio* calculations are performed at the CBS-QB3 level of theory as implemented in the Gaussian 16 software. The performance of the kinetic models is evaluated with both available literature data as well as new datasets acquired with different experimental units, which can be approximated by ideal reactor models. These experimental units include a tubular reactor at the Laboratory of Chemical Technology in Ghent and a jet-stirred reactor at the Centre National de la Recherche Scientifique in Nancy.

Group additivity for nitrogen-containing compounds

Thermodynamic parameters

To address the scarcity of thermodynamic parameters for nitrogen-containing compounds, a consistent set of group additive values and non-nearest-neighbor interactions is determined from a large dataset of CBS-QB3 calculations for 300 species, including radicals. This dataset contains a wide range of nitrogen-containing functionalities, i.e. amine, imine, nitrile, nitro, nitroso, nitrite, nitrate and azo functional groups. The group additivity model enables the approximation of the standard enthalpy of formation and standard entropy at 298 K as well as the standard heat capacities over a large temperature range, i.e. 300-1500 K. Making use of a new set of bond additive corrections for the CBS-QB3 level of theory, both experimental results as well as the *ab initio* calculated values can be approximated with sufficient accuracy.

Kinetic parameters

One of the main reaction families important during pyrolysis and oxidation of nitrogen-containing compounds, including aliphatic amines, is the intermolecular hydrogen abstraction family. Reaction rate coefficients are calculated at the CBS-QB3 level of theory for a large set of 316 intermolecular hydrogen abstraction reactions from N-H and C-H bonds by a hydrogen atom, carbon-centered and nitrogen-centered radicals. The influence of substituents on both the attacking and attacked radical, being a hydrogen, carbon or nitrogen

atom, is investigated systematically. From this dataset, new group additive values are determined to approximate the kinetic parameters of hydrogen abstractions involving nitrogen-containing compounds, with sufficient accuracy. Complementary to the group additivity model, correlations for the tunneling coefficients, dependent on both the temperature and the activation energy of the reaction in the exothermic direction, are proposed.

Pyrolysis and oxidation of aliphatic amines

With the new group additive models for thermodynamic and kinetic parameters of nitrogen-containing compounds, a kinetic model for the pyrolysis and oxidation of three aliphatic amines, i.e. ethyl-, dimethyl- and diethylamine is generated with Genesys. This model is supported by new *ab initio* calculations for the low-temperature oxidation chemistry, while for the reactions between small nitrogen-containing compounds and C_1-C_2 hydrocarbons literature data is used. The kinetic model performance is evaluated with new experimental data gathered in a tubular reactor and a jet-stirred reactor for diethylamine pyrolysis and oxidation as well as available literature data from laminar premixed flames and shock tube experiments for ethyl- and dimethylamine. These datasets cover a wide range of experimental conditions with temperatures ranging from 500 to 2000 K and pressures from 4 to 170 kPa. A combination of rate of production and sensitivity analyses have been used to identify the dominant reaction pathways leading to the main products HCN, N_2, NH_3 and NO_x. Under the studied conditions, the amines are consumed via hydrogen abstraction from the N and C_α positions, and to a lesser extent homolytic C-C and C-N bond scission, followed by β-scission of the fuel radicals and no low-temperature reactivity has been observed in case of oxidation. This first-principles based kinetic model can be considered as an important step towards better understanding the pyrolysis and oxidation chemistry of larger more complex (cyclic) nitrogen-containing compounds present as feedstock impurities.

Steam cracking of sulfur-containing compounds

A new kinetic model has been constructed with Genesys to describe the thermal decomposition, both pure and in the presence of a hydrocarbon matrix, for a number of

sulfur-containing additives and feedstock impurities, i.e. dimethyl sulfide, dimethyl disulfide, dimethyl sulfoxide, carbonyl sulfide and carbon disulfide. Construction of the relevant potential energy surfaces is used for the identification of more complex reactions not belonging to the main reaction types, while thermodynamic and kinetic parameters important to accurately describe the initial decomposition pathways are obtained directly from *ab initio* calculations. The first-principles based kinetic model succeeds in predicting the main trends of three different datasets obtained from bench scale and pilot plant reactor experiments, without any fitting of the model thermodynamic or kinetic parameters. The weakening effect of the sulfur atoms on the bond strengths leads to a high reactivity under the studied steam cracking conditions, with H_2S the main sulfur-containing product and methane thiol, carbon disulfide and thiophene as minor products.

Samenvatting

Onderzoeksdoel

De graduele shift van fossiele naar hernieuwbare en alternatieve grondstoffen, gemotiveerd door de steeds strengere milieuvoorschriften en het nastreven van verhoogde winstgevendheid, vormt een uitdaging voor de (petro)chemische industrie. Deze grondstoffen bevatten namelijk heteroatomaire verbindingen, bestaande uit zuurstof, stikstof en zwavel, die niet enkel aanwezig zijn in een verhoogde concentratie in vergelijking met de traditionele feeds, maar ook met een verschillende distributie van de functionele groepen. Decompositie zorgt voor de vorming van gevaarlijke componenten zoals NO_x, H_2S en SO_x, die een negatieve invloed kunnen uitoefenen op de werking van het proces, op vlak van veiligheid, operabiliteit en kwaliteit van de productstromen. Aangezien er weinig kennis is m.b.t. tot de pyrolyse en oxidatie reacties van deze heteroatomaire verbindingen en hoe de chemie beïnvloed wordt door de aanwezigheid van een koolwaterstofmatrix, zoals het geval is in het stoomkraak proces, wordt vandaag de dag nog steeds gebruik gemaakt van algemene specificaties. Het doel van dit proefschrift is om de thermochemische reacties van heteroatomaire verbindingen, zowel onzuiverheden als typisch gebruikte proces additieven, te bestuderen d.m.v. een combinatie van kwantumchemische berekeningen, experimenteel werk en computergestuurde kinetische modellering. Zwavel en stikstof zijn voornamelijk in de vorm van aromatische verbindingen aanwezig, maar er zijn ook verschillende niet-cyclische klassen vertegenwoordigd in zowel fossiele als hernieuwbare grondstoffen, zoals amines, thiolen en (di-)sulfides, waartoe ook de meest gebruikte procesadditieven behoren. Omdat de gasfasechemie van deze componenten nog steeds onduidelijk is, ligt de focus in dit proefschrift op het verkrijgen van meer fundamenteel inzicht in hun pyrolyse en oxidatie reacties, wat kan beschouwd worden als een eerste stap van de uitbreiding naar de meer complexere cyclische heteroatomaire componenten.

Methodologie

De microkinetische modellen in dit proefschrift worden genereerd m.b.v. de software tool Genesys ontwikkeld binnen deze groep. De thermodynamische en kinetische parameters nodig voor het uitvoeren van reactor simulaties worden bepaald d.m.v. nieuwe kwantumchemische berekeningen en groep additieve modellen ontwikkeld voor een efficiënte parameterschatting tijdens de netwerk generatie procedure. De berekeningen worden uitgevoerd met de CBS-QB3 methode zoals geïmplementeerd in de Gaussian 09 of Gaussian 16 software. De werking van de microkinetische modellen wordt geëvalueerd door gebruik te maken van zowel beschikbare literatuur data als nieuwe datasets verworven met verschillende experimentele opstellingen, die omwille van hun specifiek design benaderd kunnen worden met ideale reactormodellen. Deze experimentele opstellingen zijn onder meer een tubulaire reactor in het Laboratorium voor Chemische Technologie en een continu geroerde reactor in het Centre National de la Recherche Scientifique in Nancy.

Groep additiviteit voor stikstofhoudende verbindingen

Thermodynamische parameters

Om het gebrek aan accurate thermodynamische parameters voor stikstofcomponenten aan te kaarten, is er een consistente set van nieuwe groep additieve waarden bepaald d.m.v. een dataset van kwantumchemische berekeningen uitgevoerd met de CBS-QB3 methode voor 300 moleculen, met inbegrip van radicalen. Deze dataset bevat een breed bereik van functionele groepen die een stikstof atoom bevatten, zoals amine, imine, nitrile, nitro, nitroso, nitriet, nitraat en azo groepen. Het groep additief model maakt het mogelijk om de standaard vormingsenthalpie en standard entropie bij een temperatuur van 298 K alsook de standaard warmtecapaciteiten over een groot temperatuur bereik van 300 tot 1500 K te benaderen. Door een nieuwe set van bondadditieve correcties in te voeren voor de CBS-QB3 methode, kunnen zowel de experimentele waarden als de waarden verkregen d.m.v. de kwantumchemische berekeningen met voldoende accuraatheid benaderd worden.

Kinetische parameters

Eén van de belangrijke reactiefamilies belangrijk voor de pyrolyse en oxidatie van stikstofhoudende verbindingen zijn de intermoleculaire waterstofabstracties. Via kwantumchemische berekeningen met de CBS-QB3 methode, zijn snelheidscoëfficiënten bepaald voor 316 intermoleculaire waterstofabstracties van N-H en C-H bindingen door een waterstofatoom, koolstof en stikstof gecentreerde radicalen. De invloed van substituenten op de atomen van het reactief centrum, die ofwel waterstof, koolstof en stikstof atomen zijn, wordt onderzocht op een systematische manier. Door gebruik te maken van deze data wordt een nieuwe set van groep additieve waarden bepaald om de kinetische parameters voor waterstofabstracties van stikstofhoudende verbindingen te benaderen. Complementair aan het groep additief model worden correlaties voorgesteld voor de tunneling coëfficiënten, die functie zijn van zowel de temperatuur als de activeringsenergie van de reactie in de exotherme richting.

Pyrolyse en oxidatie van amines

Gebruik makend van de nieuwe groep additieve modellen voor de thermodynamische en kinetische parameters van stikstofhoudende verbindingen, wordt een kinetische model ontwikkeld met Genesys voor de pyrolyse en oxidatie van drie niet-cyclische amines, i.e. ethyl-, dimethyl- en diethylamine. Dit model wordt ondersteund door nieuwe kwantumchemische berekeningen voor de chemie tijdens gasfase oxidatie op lage temperatuur. Voor reacties tussen stikstofcomponenten en C_1-C_2 koolwaterstoffen wordt literatuurdata gebruikt. De werking van het kinetisch model wordt geëvalueerd met nieuwe experimentele data verkregen in een tubulaire reactor en een continue geroerde reactor voor de pyrolyse en oxidatie van diethylamine, alsook literatuurdata uit laminaire voorgemengde vlammen en schokbuis experimenten voor ethyl- en dimethylamine. Deze datasets omvangen een groot bereik aan experimentele condities met temperaturen van 500 tot 2000 K en drukken van 4 kPa tot 170 kPa. Door gebruik te maken van een combinatie van reactiepad- en sensitiviteitanalyses worden de dominante reactiepaden geïdentificeerd die leiden tot de vorming van de belangrijkste stikstofhoudende producten, namelijk HCN, N_2, NH_3 en NO_x. Onder de bestudeerde condities worden de amines voornamelijk omgezet via

waterstofabstracties van de N en C_α posities, in mindere mate door homolytische scissie van de C-C en C-N bindingen, gevolgd door β-scissie van de gevormd radicalen en wordt er geen lage temperatuur reactiviteit geobserveerd in geval van oxidatie. Het microkinetisch model kan beschouwd worden als een belangrijke step om meer inzicht te krijgen in de pyrolyse en oxidatie chemie van complexere (eventueel cyclische) stikstofhoudende verbindingen.

Zwavelcomponenten in het stoomkraakproces

Een nieuw kinetisch model is ontwikkeld m.b.v. de Genesys softwaretool om de decompositie van zwavelhoudende proces additieven of onzuiverheden, waaronder dimethyl sulfide, dimethyl disulfide, dimethyl sulfoxide, carbonyl sulfide en carbon disulfide, zowel puur als in de aanwezigheid van een koolwaterstofmatrix te kunnen voorspellen. De constructie van de relevante potentieel energie oppervlakken zorgt ervoor dat complexere reacties die niet behoren tot de typische reactie families gebruikt voor de netwerk generatie, in rekening gebracht kunnen worden. De thermodynamische en kinetische paramaters van alle moleculen en reacties die deel uitmaken van de belangrijkste initiële decompositiepaden worden bepaald d.m.v. kwantumchemische berekeningen. Het microkinetisch model slaagt erin om de belangrijkste trends van drie verschillende experimentele studies uitgevoerd met twee tubulaire reactors op verschillende schaal te voorspellen, zonder thermodynamische of kinetisch model parameters te fitten. Het verzwakkend effect van het zwavelatoom op de sterkte van de naburige bindingen zorgt voor een hoge reactiviteit onder stoomkraakcondities, waarbij nagenoeg alle zwavel omgezet wordt naar H_2S met methaan thiol, carbon disulfide en thiofeen als belangrijkste bijproducten.

1

Introduction and outline

1.1. Heteroatomic compounds in the steam cracking process

The transition from fossil to more sustainable and alternative resources is driving today's research towards renewable feedstocks like bio-derived or waste-derived naphthas [1, 2]. As the composition of these alternative feedstocks differs substantially depending on the origin, this ongoing shift poses a challenge for the chemical industry. A common concern is the presence of substantial amounts of heteroatomic compounds (nitrogen, oxygen and sulfur) and their potential negative impact on the process. Current steam cracker units can handle various types of feedstocks from light gasses such as ethane, to liquids like naphthas and gas oils [3]. The economics of this process, which is the main production route for the platform chemical propene, 1,3-butadiene and benzene, are primarily determined by the feedstock cost, driving the interest to the alternative, cheaper feedstocks. At present primarily overall specifications on the presence of heteroatomic compounds in feedstocks are employed, e.g. total oxygen content below 100 ppmw [4], apart from some exceptions such as methanol, CO_2, COS and H_2S. An overview of the typical specifications for five different stream cracker feedstocks is given in Table 1-1 [4].

The total sulfur content is a key concern for all five different feedstocks, with maximum permissible concentrations ranging from 30 ppmw for ethane to 2300 ppmw for gas oil feedstocks [4]. Separate concentration limits are in place for two sulfur-containing compounds, carbonyl sulfide (COS) and H_2S. As the boiling point of COS is equal to 223 K, it mainly concentrates in the lower boiling point hydrocarbon fractions such as the C_3-C_4 fraction from refinery gases. COS is relatively stable towards acidic reagents and hence it is not effectively removed in the caustic wash tower (in contrast to H_2S and thiols). A maximum permissible concentration of 2000 ppmw is used for the total nitrogen content in gas oils, while 15 ppm mole of ammonia (NH_3) is a typical specification value applicable for ethane [4].

Table 1-1: The maximum permissible concentration of the most important heteroatomic impurities for typical steam cracker feedstocks. The average concentration from different questioned companies, i.e. number of responses, is presented [4].

Contaminant	Ethane or E/P mixtures	Propane or NGL	Raffinate from C_4, C_5 recovery	Naphthas and Condensates	Gas oils
Number of responses	29	27	12	22	10
Total S (ppmw)	30	50	500	200-500	2300
COS (ppm mole[a] or ppmw[b])	5[a]	1-2[a]	1[b]		
H_2S (ppm mole[a] or ppmw[b])	10[a]	10[a]	10[b]	10-15[b]	
Thiols (ppm mole)	1-20	50			
Sulfolane (ppmw)			150		
Total O (ppmw)		100	20-1000	100	
CO_2 (ppm mole)	1000-	1000			
CO (ppm mole)	1	1			
MeOH (ppm mole[a] or ppmw[b])	5-10[a]	20[a]	35[b]	100[b]	
O_2 (ppm mole)	5				
Total N (ppmw)					2000
NH_3 (ppm mole)	15				

[a] amounts are in ppm mole, [b] amounts are in ppmw

The primary concerns caused by the presence of heteroatomic compounds in steam cracker feedstocks are related to safety, operability and the quality of the product streams. Because there is little known about the pyrolysis reactions of these heteroatomic compounds and how their decomposition is affected by the changing hydrocarbon matrix under steam cracking conditions, these very global specifications are kept in place [5]. By making use of alternative feedstocks, which do not only have a higher heteroatomic concentration but also a different distribution of compounds, it can be questioned whether these specifications are still valid. Especially taking into account that the reactivity can differ substantially between different classes of heteroatomic compounds. This clear and important knowledge gap explains the recent large interest in gaining fundamental understanding of their pyrolysis behavior, ideally coming up with an individual specification for each compound or a predictive model that allows to estimate what is acceptable or not.

A major obstacle is quantification of these compounds and the resulting decomposition products on a molecular level. Fortunately, substantial progress has been made over the last few years by applying comprehensive characterization techniques with selective detectors such as sulfur

and nitrogen chemiluminescence detectors [6]. Moreover the use of mass spectrometry in selective ion mode permits identification of unknown contaminants in combination with reliable quantification at trace and ultratrace amounts [7], even online [8, 9]. This implies that experimental tools are now available to study the free radical reactions of heteroatomic compounds.

1.2. Nitrogen-containing compounds

1.2.1. Feedstock impurities and additives

Nitrogen-containing compounds are well known constituents of crude oil, with a typical range of 0.0 - 1.0 wt% and an average value of 0.25 wt% [10]. Most of the nitrogen in hydrocarbon mixtures is present in the form of aromatic compounds, but there is evidence that low concentrations of primary amines can be present [11, 12]. The aromatic nitrogen-containing compounds, mainly pyridine and pyrrole derivatives, can be classified according to basicity [13]. The six-ring structures, i.e. pyridines, anilines, quinolines, and acridines have been identified as the main classes of basic compounds, while the five-ring structures, i.e. pyrroles, indoles and carbazoles, are the main non-basic compounds, as depicted in Figure 1-1. According to Richter et al. [13], the ratio of basic to total nitrogen-containing compounds present in crude oil is approximately constant (25-30 wt%), regardless of the type of crude oil.

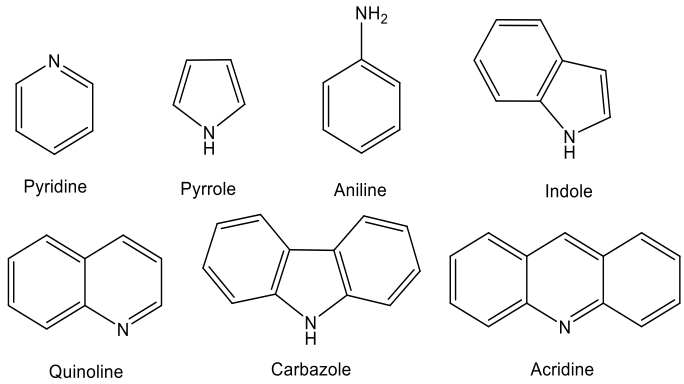

Figure 1-1: Different types of nitrogen-containing compounds found in hydrocarbon fractions.

Schmitter et al. [14] made an overview of the research concerning the presence of basic nitrogen-containing compounds in fuels. From the analysis of various crude oils, it was concluded that basic nitrogen in these feedstocks is solely present as substituted compounds, for example pyridines with a methyl substituent on the carbon atom adjacent to the heteroatom.

This is in contrast to shale oil, in which in addition to these substituted compounds also unsubstituted nitrogen-containing compounds such as pyridine and quinoline are present.

Ristic et al. [15] developed a novel method for quantitative analysis of nitrogen-containing compounds in complex hydrocarbon matrices. The following classes of compounds were identified in a shale oil: pyridines, anilines, quinolines, acridines, indoles and carbazoles. Overall, the analyzed sample contains 4.21 wt% of nitrogen-containing compounds, with the majority of them pyridines and indoles, 1.98 wt% and 1.10 wt% respectively. The remaining part of the nitrogen-containing compounds is present in the form of quinolines and anilines, 0.59 wt% and 0.46 wt% respectively, with only a very small fraction of acridines and carbazoles, both 0.04 wt%. Furthermore, from a detailed quantification of the individual compounds in each class, it could be concluded that the aromatic structures are mainly present as substituted homologs, which is in agreement with the study of Schmitter et al. [14]. As an example, the most abundant compound in the pyridine class has carbon number 9.

Untreated bio-oils produced by biomass fast pyrolysis can also contain substantial amounts of nitrogen-containing compounds, including amines, amino acids and heterocyclic structures, such as pyridine and pyrrole [16, 17]. Toraman et al. [16] investigated the composition of microalgae based bio-oils. As microalgae contain substantial amounts of oxygen- and nitrogen-containing compounds, the pyrolysis of the obtained bio-oils would be accompanied by considerable air pollution, due to the formation of both NO_x and sooth. Hence, a detailed compositional analysis is not only crucial for the development of efficient conversion processes, but also to optimize the required upgrading processes. The nitrogen content of the organic and aqueous fraction of the microalgae based bio-oil was determined to be equal to 3.68 wt% and 8.54 wt% respectively. Overall, thirteen different classes of nitrogen-containing compounds were identified: pyridines, indoles, quinolines, amines, imidazoles, amides, imides, nitriles, pyrazines, pyridines, pyrazoles, pyrimidines, pyrimidinediones and other compounds not assigned to a specific class. The additional classes of nitrogen-containing compounds, compared to crude and shale oil present in the analyzed sample are depicted in Figure 1-2.

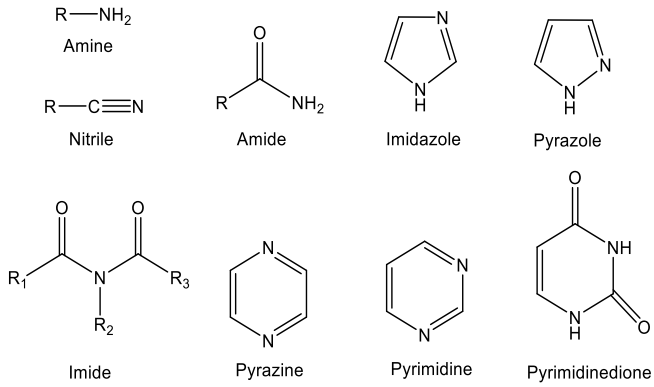

Figure 1-2: Nitrogen-containing compounds identified in a microalgae based bio-oil.

Aside from the compounds present as feedstock impurities, nitrogen-containing compounds can be used as process additives to reduce fouling, e.g. diethyl hydroxylamine (DEHA), or for pH control, e.g. mono ethanol amine (MEA). Nitrogen can also enter the process via recycle streams coming from process operations in which such compounds are used, for example extraction distillation solvents such as acetonitrile [18].

1.2.2. Thermal decomposition of nitrogen-containing compounds

The pyrolysis chemistry of the nitrogen-containing compounds encountered as feedstock impurities and process additives is poorly understood, and in some cases, even completely unknown. Aside from obtaining accurate data on the speciation of organic nitrogen-containing compounds of various streams, understanding its behavior during pyrolysis, combustion or any other thermal process is crucial considering the formation of hazardous species such as NO_x and NH_3. To this end, the pyrolysis of nitrogen-containing compounds has been investigated in different experimental, theoretical and kinetic modeling studies. Due to the numerous possible reactions and intermediates, studies have been restricted to the thermal decomposition of a set of model compounds, e.g. simple aliphatic amines and unsubstituted aromatic structures such as pyridine and pyrrole. Below the main findings are summarized for these compounds regarding the dominant decomposition pathways, product distributions and influence of a hydrocarbon matrix.

1.2.2.1. Non-aromatic

Amines are derivatives of ammonia in which one or more of the hydrogen atoms are replaced by an alkyl or aryl substituent. As depicted in Figure 1-3, amines can be subdivided into three different categories (primary, secondary and tertiary) depending on how many of the hydrogen

atoms have been replaced, corresponding to the substitution degree of the nitrogen atom. Furthermore, a distinction can be made between aliphatic and aromatic amines, depending on whether the nitrogen atom is connected to an aromatic ring or not.

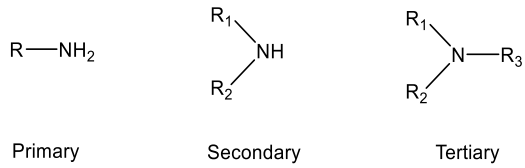

Figure 1-3: Classification of amines into primary, secondary and tertiary amines depending on the branching degree of the nitrogen atom.

While the pyrolysis of ammonia has been extensively investigated in the past [19-22], knowledge about the decomposition chemistry of its alkylated derivatives is much more scarce. Only a limited number of experimental and theoretical studies is available in literature focusing on the pyrolysis behavior of aliphatic amines. Higashihara et al. [23] studied the high temperature (1400-1820 K) thermal decomposition of methylamine (CH_3NH_2) by infrared laser kinetic absorption spectroscopy behind reflected shock waves. Hydrogen abstraction from methylamine by the radicals formed from initial C-N bond scission, followed by β-scission leads to formation of the relatively stable intermediate, i.e. methanimine (CH_2=NH), which is further converted to the main nitrogen-containing product HCN. For the pyrolysis of ethylamine ($CH_3CH_2NH_2$), Moldoveanu et al. [24] report the formation of the nitrogen-containing products HCN, acetonitrile, NH_3 and N_2 over the temperature range of 773-1273 K. The ratio of the different products depends on temperature with a decreasing yield of ethylene, the formation of which is initiated by C-N bond scission, with increasing temperature. In other words, the C-C bond scission gains importance as initiating reaction with temperature. The pyrolysis of propylamine ($CH_3CH_2CH_2NH_2$) occurs via similar reaction pathways as ethylamine. In addition to propylene formation, formation of ethylene indicates the importance of the decomposition pathway initiated by scission of the C-C bond. Higher molecular weight compounds can also be formed during the pyrolysis of these short chain amines as a result of termination reactions between the radicals [24].

A limited number of experimental studies have focused on more complex amines, such as 1,1-dimethyl propylamine [25], tert-butyl amine [26], aniline [27] and benzyl amine [28]. Similar to the simple aliphatic amines, the thermal decomposition is initiated by C-N and C-C bond scission, after which a sequence of hydrogen abstraction and β-scission reactions leads to formation of the main nitrogen-containing products NH_3, HCN and larger nitrile compounds

such as acetonitrile, acrylonitrile and benzonitrile. Although there is a general consensus on the dominant decomposition pathways, the kinetic modeling efforts have been limited to the most simple aliphatic amines, i.e. compounds with a maximum of three non-hydrogen atoms. By reviewing the nitrogen combustion chemistry research over the last decades, Glarborg et al. [29] have proposed a kinetic model to describe the formation of nitrogen-containing pollutants in non-catalytic gas phase processes. Based on available information from experiments and high-level theory, the mechanisms describing the nitrogen chemistry of light fuel-nitrogen species have been included in this recent model, with the amine species limited to methyl-, ethyl-, dimethyl- and hydroxylamine. Most of the kinetic parameters are based on an analogy with the corresponding reactions of hydrocarbons and oxygenates and experimental validation of the sub mechanisms for decomposition of these nitrogen-containing compounds is limited. A more thorough model validation with additional experimental datasets for over a wide range of conditions, also involving a hydrocarbon matrix to have more emphasis on the interactions with the hydrocarbon radical pool, is required.

Substituted hydroxyl amines, i.e. derivatives of hydroxylamine (NH_2OH) by replacing one of the hydrogen ligands by an alkyl substituent, are commonly used as process additives. The radicals formed after scission of the O-H bond are effective radical scavengers used to inhibit free-radical processes which can lead to for example fouling in a steam cracker plant. Very few studies focus on their decomposition chemistry, apart from the most simple compound hydroxylamine [30]. In general, the molecular structures of the nitroxides determine their reactivity. The vast majority of organic nitroxides is unstable, while some radicals such as di-tert-butyl nitroxide or TEMPO are stable, i.e. they can be isolated. This is due to the fact that with increasing steric hindrance, the reactivity of the corresponding radical decreases [31]. Examples of commonly used additives diethyl hydroxyl amine (DEHA) and 2,2,6,6-tetramethyl-1-piperidinol (TEMPOH) are shown in Figure 1-4.

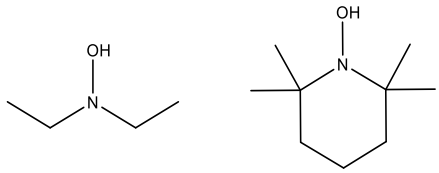

Figure 1-4: Molecular structures of DEHA (left) and TEMPOH (right).

A number of studies have focused on the use of DEHA as an atmospheric additive to inhibit smog formation [32-34]. Because the focus is on atmospheric chemistry, these experimental

and modelling studies of DEHA have been conducted at ambient temperatures. There are two possible reaction pathways for the decomposition of DEHA which each lead to the formation of different nitrogen-containing products, mainly HCN, NH_3 and NO_x. In the absence of abstracting radicals, the unimolecular decomposition is initiated by scission of the N-O bond. The formed nitrogen-centered radical, $(C_2H_5)_2N^{\cdot}$, can react further to form diethylamine, the decomposition of which leads mainly to HCN and NH_3. The other reaction pathway is initiated by hydrogen abstraction from the weak O-H bond, which is characterized by a bond dissociation energy (BDE) of approximately 290 kJ mol^{-1}, leading to the formation of the oxygen-centered nitroxide $(C_2H_5)_2NO^{\cdot}$ radical [32]. This radical further decomposes via β-scission of the C_α-N bond leading to nitroso ethane ($C_2H_5N{=}O$), which is converted to NO_x as main nitrogen-containing product [33].

The hydroxylamine TEMPOH or 2,2,6,6-tetramethylpiperidine 1-oxyl is another common process additive that can be used as a trapping agent for free radicals. Whereas the radical formed after hydrogen abstraction from DEHA is a reactive radical, oxygen-centered aminoxyl radicals derived from secondary amines with no hydrogens attached to the α- carbon atoms, i.e. the carbon atom next to the nitrogen atom, are stable or so-called persistent radicals (in view of their long lifetimes) [35]. The steric hindrance of the four methyl groups influences the reactivity, because formation of a double bond between the nitrogen atom and an adjacent carbon atom is prevented (in contrast to DEHA). According to the author's knowledge, no experimental studies have been reported focusing on the thermal decomposition of TEMPOH.

1.2.2.2. Aromatic

The decomposition of pyridine has been the focus of several experimental [36-43] and theoretical studies [44, 45]. Axworthy et al. [36] conducted pyrolysis experiments in a quartz capillary flow reactor at 213 kPa over the temperature range 1123-1373 K. Quinoline, benzonitrile, acrylonitrile, acetonitrile, hydrogen cyanide (HCN), and naphthalene were found as main nitrogen-containing products. The HCN yield was found to increase with temperature, with an almost complete conversion of pyridine to HCN at 1373 K. A reaction mechanism with a C-H bond scission as initiating reaction has been proposed, a route which is generally accepted as the major initiation reaction in many aromatic systems. Once a pool of radical species has been established, hydrogen abstraction becomes more important as initiating reaction. All three isomeric pyridyl radicals can undergo ring opening resulting in five different open-chain radicals, but only one out of the five possible β-scission reactions results in the formation of an open-chain cyano radical. This main decomposition pathway proceeding via C-N bond scission

of the ortho-pyridyl radical can lead to the formation of both HCN and cyanoacetylene (HC≡CC≡N), c.f. Figure 1-5. Similar to pyrolysis of aliphatic amines, formation of heavier products as a result of possible termination reactions between the pyridyl radicals has also been reported [41]. Analogous to the growth mechanism for polyaromatic hydrocarbons, acetylene can add to the pyridyl radical. However, the low reactivity of the meta position will inhibit the addition of the second acetylene molecule which is needed for the ring formation.

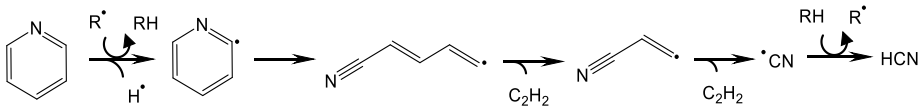

Figure 1-5: Radical decomposition pathway of pyridine leading to the formation of HCN.

Thermal decomposition of pyrrole has been evaluated under different experimental conditions [46-49]. For the pyrolysis experiments of Axworthy et al. [36] over the temperature range 1123-1373 K, acetonitrile, acrylonitrile and benzonitrile are the main nitrogen-containing compounds. A pyrrole conversion of 50% is reached at a temperature of 1173 K, while for pyridine this level of conversion is reached at a higher temperature of 1223 K. Pyrrole is mainly consumed by the 1,2-hydrogen shift to pyrrolenine, followed by a ring opening reaction resulting in the formation of allenic imine, c.f. Figure 1-6. This latter step occurs via a 1,4-hydrogen shift of the biradical intermediate, resulting from the ring opening reaction of pyrrolenine [50, 51]. According to Axworthy et al. [36], the decomposition of this allenic imine intermediate is the main source of HCN for pyrrole decomposition.

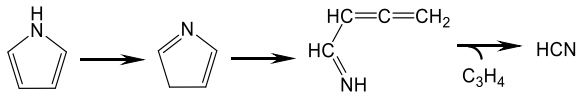

Figure 1-6: Ring opening reaction of pyrrole to allenic imine and subsequent unimolecular decomposition to HCN and propyne.

Formation of the intermediate pyrrolenine compound has been confirmed in the theoretical study of Zhai et al. [52]. The ring opening of the pyrrole radical, formed after C-H β-scission or hydrogen abstraction, followed by β-scission of the C-C bond results in the formation of the acetonitrile radical (Figure 1-7). In the presence of an initial pool of radical species, this decomposition pathway will gain importance [49].

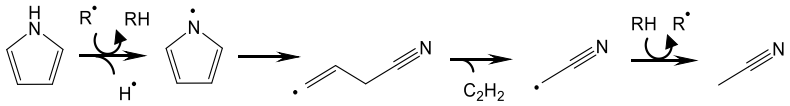

Figure 1-7: Radical decomposition pathway of pyrrole leading to the formation of acetonitrile.

A limited number of experimental and theoretical studies have focused on the pyrolysis of more complex nitrogen-containing aromatic structures, including (iso-)quinoline [47, 53-55], indole [47, 56] and carbazole [47, 57-59]. Note that there is an analogy between the decomposition of these larger ring systems and the decomposition of the constituting rings. For example, the decomposition of quinoline, which consists of a pyridine ring fused to a benzene ring, proceeds via the hydrogen abstraction reaction from the ortho site followed by a β-scission of the C-N bond, c.f. Figure 1-8. This radical decomposition pathway is similar to the main pathway of pyridine pyrolysis, c.f. Figure 1-5.

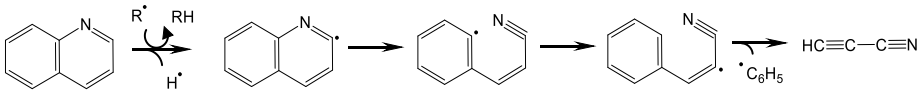

Figure 1-8: Radical decomposition pathway of quinoline leading to the formation of cyanoacetylene.

A subsequent scission of the C-C bond leads to formation of cyanoacetylene and a phenyl radical. A similar pathway for isoquinoline, in which the nitrogen atom can be found in the β-position instead of the α-position, leads to formation of benzonitrile, c.f. Figure 1-9.

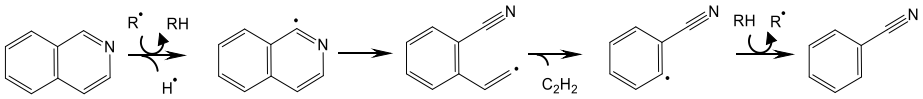

Figure 1-9: Radical decomposition pathway of isoquinoline leading to the formation of benzonitrile.

1.2.3. Risks and safety hazards

Catalytic hydrodenitrogenation is the most commonly applied method for removal of nitrogen in fossil-based feedstocks. Of the most abundant heteroatoms (S, N, and O), nitrogen is actually the most difficult to remove by hydroprocessing. Removal of pyridine derivatives is particularly challenging, because it requires one double bond and one single bond to be broken for denitrogenation to occur; in comparison with only two single bonds that need to be broken for desulfurization of thiophenic sulfur and deoxygenation of furanic oxygen [10]. Nitrogen removal is required to limit NO_x emissions and to guarantee process and product performance, but it can also affect the hydrodesulfurization process important to maintain the level of sulfur

below regulatory levels. Nitrogen-containing compounds can inhibit hydrodesulfurization and other reactions because of their preferential adsorption on catalytic sites [60].

While the main sources and decomposition chemistry of nitrogen-containing compounds are not yet completely understood, the risks and safety hazards of the presence of NH_3 and NO_x has been well documented. Ammonia can enter a steam cracking plant directly as feedstock impurity, for example in refinery gas feeds, but the primary source of ammonia is the decomposition of nitrogen-containing compounds in the cracking furnace. The decomposition of these species, either remaining feedstock impurities or process additives, is known to lead to the formation of small nitrogen-containing pollutants, such as NH_3 and HCN. The ethylene product quality is the main variable that can be negatively influenced by the ammonia content, followed by the contamination of the process water. Other possible concerns include the formation of ammonia nitrate in the chilling system and catalyst deactivation. It is known that nitrogen-containing compounds have a strong influence on the operation of catalytic processes. Basic nitrogen-containing compounds in particular, can poison acid catalysts and deactivate them through the formation of coke deposits [61]. This poisoning effect of basic nitrogen-containing compounds has been known for several decades. Another processing challenge that can be caused by the presence of ammonia is corrosion. Not all nitrogen-containing compounds are corrosive to metals and some are even considered to be corrosion inhibitors, for example pyridine. However, the main problem is that nitrogen-containing compounds can break down at high temperature resulting in the formation of ammonia, which can cause extensive corrosion by reaction with other nitrogen-containing compounds such as hydrogen cyanide [62]. Different strategies can be used to mitigate this ammonia contaminant with the most important ones: adjusting the feedstock specifications, removal of ammonia from the process water stream and making use of an amine removal step.

Possible sources of NO_x for the steam cracking process include refinery gas streams, dilution steam, i.e. make-up water contamination or boiler water feed additives and the thermal decomposition of nitrogen-containing compounds with the N-O functional group present. In theory, only NO enters the olefins processing train, as any NO_2 that was present will certainly be condensed before reaching the cold box. Due to its low boiling point, NO passes through the cold box without depositing. However, low levels of O_2 present in the cold box streams, i.e. generally less than 50 ppm (one or two orders of magnitude higher than the concentration of NO), can react with NO leading to the formation of NO_2. NO_2 then reacts with excess NO

forming nitrogen trioxide (N_2O_3). Being a solid at cold box conditions and insoluble in the hydrocarbon stream, N_2O_3 forms a solid deposit on the cold box equipment [63].

There are at least three possible ways in which NO_x compounds can present a safety hazard [63]. First of all, NO_x compounds can react with certain unsaturated hydrocarbons, mainly dienes such as butadiene or cyclopentadiene, leading to the formation of amorphous polymeric materials, or so-called nitrogenous gums. While in most cases their main concern is that they can lead to blockages of valves, NO_x gums formed at cryogenic conditions tend to be more unstable and are more likely to cause an explosion hazard. Second, some NO_x compounds are very reactive and can react violently with hydrocarbons under certain circumstances (although not with ethylene at cryogenic temperatures). After the NO_x condenses and accumulates in a small area, it can contact condensed hydrocarbons, which can result in an explosive reaction. In most hydrocarbon streams the NO_x concentration is extremely low, i.e. ppm level, and then the reactivity does not pose a problem. A third safety hazard related to the presence of NO_x compounds in the process, is their toxicity. NO_x compounds can accumulate in certain locations causing a potential health hazard in case of a sudden vapor release, leading to high local concentrations. Due to the low NO_x concentration in process streams combined with the fact that material from the cold box is normally not vented (apart from startups or shutdowns), toxicity is usually not a main concern.

1.3. Sulfur-containing compounds

1.3.1. Feedstock impurities and additives

Sulfur-containing compounds are found in almost every fossil-based feedstock for pyrolysis, with the sulfur content ranging from 0.1 wt% to 10.0 wt% [64]. The most common sulfur-containing compounds found in hydrocarbon fractions are thiols (mercaptans), sulfides, disulfides and aromatic sulfur-containing compounds, c.f. Figure 1-10 [65]. While a considerable amount of the sulfur impurities is present in the form of non-aromatic species, the majority are heterocyclic aromatic structures containing a thiophenic ring, such as alkyl homologs of thiophenes, (di-)benzothiophenes, and napthobenzothiophenes. The stability of thiols, sulfides and disulfides is comparable to that of alkanes, with disulfides being more reactive than sulfides. Thiophene and its homologs are more resistant to decomposition. In the order of decreasing reactivity, these sulfur-containing compounds can be ordered as: disulfides, sulfides, thiols, thiophenes and benzothiophenes [66].

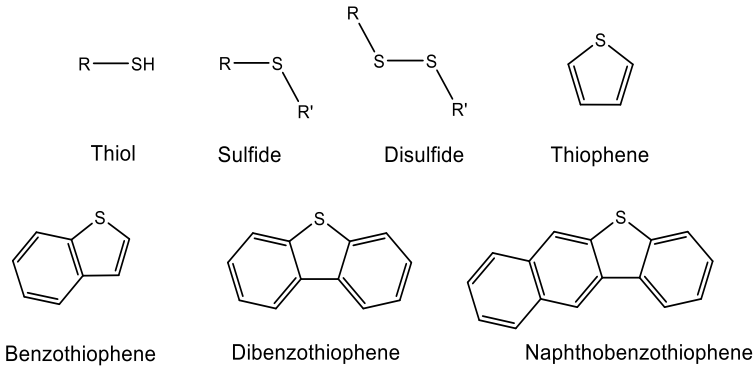

Figure 1-10: Different types of sulfur-containing compounds found in hydrocarbon fractions.

Dijkmans et al. [67] determined the detailed composition of a shale oil using a novel comprehensive 2D gas chromatographic (GC x GC) method, combining information of different detectors, including flame ionization detector (FID), sulfur chemiluminescence detector and a time of flight spectrometer. They succeeded in the quantification of the composition of the shale oil by carbon number and division into 20 different classes. A significant amount (2.2 wt%) of sulfur-containing groups was detected. The sulfur-containing compounds mainly consist of sulfides and thiols (0.93 wt%), benzothiophenes (1.11 wt%), naphthobenzothiophene (0.01 wt%) and dibenzothiophenes (0.16 wt%).

In addition to sulfur-containing compounds with single and aromatic bonds between the carbon and sulfur atoms, sulfur can also be present as compounds with a C=S bond. Although these are relatively uncommon, important compounds of this class include COS and carbon disulfide (CS_2). In addition to a feedstock impurity, COS can also be formed from decomposition of sulfur-containing compounds, for example in biomass pyrolysis [68]. As the boiling point of CS_2 is equal to 319 K, CS_2 has the tendency to concentrate in the C_5 stream. Some shale derived sources of light naphtha have high CS_2 content which may be explained by CS_2 being a constituent of the shale fracking solvent for enhanced oil recovery [69]. In most cases, the total sulfur content of the feedstock is measured rather than the CS_2 content. However, some ethylene producers have started to implement specific specifications of CS_2. For a naphtha feedstock, a typical number is 10 ppmw CS_2 [70].

Aside from the feedstock impurities, sulfur-containing compounds can also be added as process additives to influence CO and coke formation. One of the great advantages of the use of sulfur-containing compounds as additives is that they are added to the system only in low concentrations, compared to other additives for the same end [65].

1.3.2. Thermal decomposition of sulfur-containing compounds

Because thermal decomposition of sulfur-containing compounds can lead to formation of hazardous compounds such as H_2S and SO_x, which can exert a negative influence on both the product and process performance as well as on the environment, gaining insight into their governing chemistry of primary importance. Similar to nitrogen, research has been limited to a number of model compounds, with the focus on identification of the decomposition products and understanding of the main decomposition mechanism.

1.3.2.1. Non-aromatic

Thiols, which contain one or more -SH functional groups, can be considered as the sulfur analogs of alcohols or primary amines. The pyrolysis of several sulfides has been studied in continuous flow systems, i.e. for ethane thiol [71], butane thiol [72], pentane thiol [73], thiophenol [74]. The scission of the C-S bond, which has an experimental BDE of 312 kJ mol^{-1} compared to 345 kJ mol^{-1} for the C-C bond [75], is the main initiating reaction. As soon as a radical pool has been established, hydrogen abstractions from the S-H bond become more important. The predominant sulfur-containing product is H_2S representing more than 90% of the converted sulfur, while CS_2 is a common minor sulfur-containing product.

With two C-S bonds in their molecular structure, sulfides are characterized by a higher reactivity compared to thiols. Shum and Benson [76] investigated the thermal decomposition of dimethyl sulfide (DMS) in a batch reactor over the temperature range 681-723 K. The main product H_2S is formed via methyl radical addition to thioformaldehyde (CH_2=S) followed by isomerization and C-S β-scission. The formation of the minor product CS_2 is possible via reaction between the main intermediate thioformaldehyde with its corresponding radical, c.f. Figure 1-11.

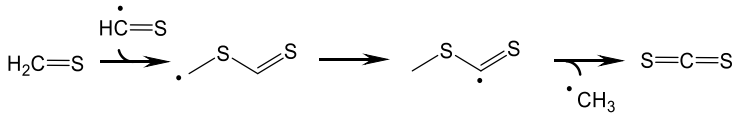

Figure 1-11: Radical reaction pathway leading to the formation of CS_2 starting from the intermediate thioformaldehyde according to Shum and Benson [76].

Zheng et al. [77] performed the pyrolysis in a tubular reactor over a temperature range of 903-1013 K of two sulfide compounds, i.e. diethyl sulfide and ethyl methyl sulfide, which results in the formation of the sulfur-containing products H_2S, methane thiol, thioformaldehyde and CS_2 [77]. Main initiating reactions for the decomposition are the homolytic scissions of the C-C and

C-S bonds, followed by hydrogen abstraction from C_α, i.e. the carbon next the sulfur atom [78]. The resulting radicals primary decompose via β-scission, resulting in the formation of unsaturated compounds such as thioformaldehyde, which is the main precursor for CS_2 formation, in agreement with Shum and Benson [76]. Zheng et al. [77] observed a yellowish deposit in the analysis section during the thermal decomposition of diethyl sulfide, which is most likely caused by the decomposition of elemental sulfur (which forms a polyatomic S_8 molecule). The sulfur dimer S_2 can be considered as an important precursor for S_8. During the decomposition of diethyl sulfide, small amounts of S_2 are formed via the bond scission of the methyl dithiyl radical ($CH_3SS^\bullet$), which originates from hydrogen abstraction from a disulfide. These disulfides are formed by recombination reactions or by homolytic substitution reactions involving thiyl radicals.

Disulfides are characterized by the presence of a S-S bond, which has a lower BDE compared to the C-S bond in sulfide species, i.e. an experimental BDE of 273 kJ mol^{-1}. Note that the BDE of the C-S bond in a disulfide decreases with approximately 60 kJ mol^{-1} compared to the analogous bond in a sulfide [79]. Several studies have focused on the thermal decomposition of dimethyl disulfide (DMDS), which is a common steam cracking process additive. Coope and Bryce [80] conducted an experimental study on the thermal composition of DMDS in a non-stirred batch reactor over the temperature range 589-646 K. The scission of the S-S bond was determined to be the dominant initiating reaction. The main decomposition products are methane thiol, H_2S, ethene and CS_2. Braye et al. [81] studied the thermal decomposition of DMDS and DMS in a toluene stream. They report that DMDS decomposition occurs at a significantly lower temperature (735-833 K) compared to DMS (931-982 K). Bock et al. [82] investigated the decomposition of different alkyl sulfides using photoelectron spectroscopy in the range of 300-1500 K. According to the authors, disulfides decompose at temperatures which are approximately 200 K lower than those for sulfides. Furthermore, the decomposition temperature decreases further with increasing alkyl substitution and chain branching, which is in agreement with the increasing importance of the C-S bond scission as initiating reaction, in addition to S-S bond scission, for larger disulfide species.

Thermal decomposition of COS and CS_2 has been studied in batch reactors [83], flow reactors [84-86] and shock tubes [87-90]. Woiki et al. [89] studied the reactions between hydrogen atoms and both COS and CS_2 behind reflected shock waves at over the temperature range 1170-1830 K. For both species, reaction with the hydrogen atom leads to the formation of a thiyl radical, with a reaction rate approximately one order of magnitude higher for the reactive COS

compound compared to CS_2. Glarborg and Marshall [91, 92] developed a kinetic model for the oxidation of COS and CS_2, which has not been validated under pyrolysis conditions.

Although the thermal decomposition of non-aromatic sulfur-containing compounds has gained a lot of attention over the past few years, elementary step kinetic model for model compounds are still limited. Some noteworthy examples include the work of Vandeputte et al. [93] and Van de Vijver et al. [78]. In the theoretical study of Vandeputte et al. [93], an elementary step kinetic model consisting of 36 reactions among 25 species was proposed to describe the formation of the main decomposition products in the thermal decomposition of DMDS, excluding thiophene. Because this model has been generated for the pure pyrolysis of DMDS, validation of important reactions with the hydrocarbon radical pool is limited. In addition, the formation of aromatic sulfur-containing compounds such as thiophene via interaction between unsaturated hydrocarbon species and thiyl radicals is not included in the model. Van de Vijver et al. [78] constructed a detailed kinetic microkinetic model for modeling of the thermal decomposition of diethyl sulfide and ethyl methyl sulfide. Experimental validation was performed with the tubular reactor pyrolysis data of Zheng et al. [77].

1.3.2.2. Aromatic

The most simple aromatic sulfur-containing compound is thiophene, which is the sulfur analogue of the five-membered planar ring structures furan and pyrrole. The resonance energy of thiophene (129.8 kJ mol^{-1}) is close to that of benzene (163.3 kJ mol^{-1}) [94]. However, thiophene has a more electron rich ring compared to benzene, because six lone electron pairs are distributed over five atoms compared to six atoms in benzene. This results in an increased reactivity and lower aromaticity of thiophene compared to benzene. Due to the lower electronegativity of the sulfur atom compared to oxygen and nitrogen, the free electron pair is delocalized more easily which results in a higher degree of aromatization. Both pyrrole and furan have a lower resonance energy (resulting in a lower aromaticity) compared to thiophene, i.e. 90.5 kJ mol^{-1} and 67.7 kJ mol^{-1} respectively [94].

A number of experimental and theoretical studies have focused on the thermal decomposition of thiophene [74, 95-97] and methyl thiophene [98]. In the tubular reactor experiments of Cullis and Norris [96], H_2S is found as the main sulfur-containing product at 1373 K. They state that ring opening by scission of the C-S bond dominates over scission of the C-C bond, in agreement with the decomposition of analogous heteroatomic compounds. Isomerization after C-S bond

scission leads to an unsaturated thiol which can either decompose or undergo a hydrogen substitution reaction to give H_2S, c.f. Figure 1-12.

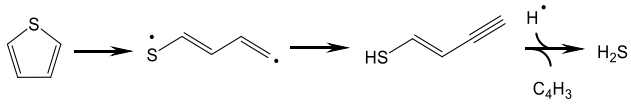

Figure 1-12: Decomposition pathway of thiophene initiated by C-S bond scission leading to formation of H_2S as proposed by Cullis et al. [96].

In the continuous flow pyrolysis experiments of Winkler et al. [99], thermal decomposition starts at approximately 873 K and complete conversion is obtained at 1273 K. The majority of the sulfur is converted to H_2S, while minor sulfur-containing products include CS_2, dithiophene and benzothiophenes. In contrast to the conclusion of Cullis and Noris [96], they report that the C-H scission is the main initiating reaction. At temperatures below 1073 K, the thiophene skeleton does not substantially fragment. Scission of the C-H bonds followed by recombination of the thiophene radicals leads to formation of larger condensation products. At a temperature of 1073 K, fragmentation of the thiophene structure starts.

Bajus et al. [65] studied the thermal decomposition of thiophene over the temperature range 300-700 K in the presence of hydrogen and identified only H_2S as sulfur-containing product. Hydrogen addition to C_α followed by β-scission leading to the formation of a sulfur-centered thiobutadienyl radical is proposed as the main decomposition pathway, c.f. Figure 1-13.

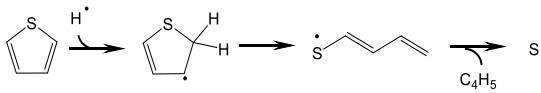

Figure 1-13: Decomposition pathway of thiophene initiated by hydrogen addition as proposed by Bajus et al. [65].

During the pyrolysis of thiophene in the temperature range 1073-1123 K, larger products such as benzothiophene can be formed via Diels-Alder addition of thiophene to another thiophene molecule, c.f. Figure 1-14.

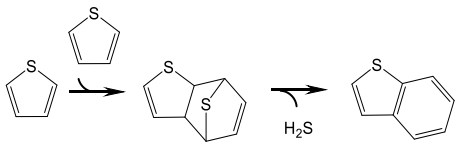

Figure 1-14: Formation of benzothiophene via Diels-alder reaction between two thiophene molecules.

Vasiliou et al. [71] studied thiophene pyrolysis in a microtubular reactor over the temperature range 300-1700 K. Thioketene ($H_2C{=}C{=}S$) is identified as the main intermediate sulfur-containing product and is formed via a 2,3-hydrogen shift followed by ring opening by C-S and C-C bond scission, c.f. Figure 1-15.

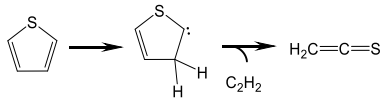

Figure 1-15: Decomposition pathway of thiophene initiated by hydrogen shift leading to formation of thioketene.

Hurd et al. [100] conducted pyrolysis experiments of thiophene and methyl thiophene at a temperature range of 1173-1198 K in a tubular reactor. Thiophene was found to be more thermally stable than 2-methylthiophene. According to Song et al. [97], methyl thiophenes have similar dominant decomposition pathways as unsubstituted thiophene. Because of the weakly electron-donating nature of the methyl group, the alkyl substituent does not have a significant effect on the main decomposition mechanism.

1.3.3. Risks and safety hazards

In general, sulfur-containing compounds are undesirable impurities that can lead to catalyst deactivation and corrosion problems [101]. Aside from H_2S, pyrolysis or combustion of sulfur-containing compounds can lead to the formation of other small sulfur-containing species, including sulfur oxides (SO_x), COS and CS_2. SO_x can be considered as a precursor to acid rain and contribute to air pollution by interaction with ozone, other gases and particulates to form airborne sulfonated smog particles [102]. For the steam cracking process, the presence of CS_2 has been linked to corrosion downstream of the furnace, problems related to the C_5 extraction from the pyrolysis gasoline stream and deterioration of hydrogenation catalysts [70]. In addition, almost all CS_2 entering the cracking furnace via the feedstock goes further downstream to the separation section [69, 70], as the decomposition of CS_2 in the furnace can be neglected. Note that similar to COS, CS_2 is relatively stable towards acidic reagents and hence it is not effectively removed in the caustic wash tower (in contrast to H_2S and thiols).

1.4. Outline

In this PhD thesis a microkinetic modeling approach is used to improve the fundamental understanding of the thermochemical reactions of nitrogen-, oxygen- and sulfur-containing model compounds present in renewable and alternative steam cracking feedstocks and energy carriers. Kinetic model construction, quantum chemistry calculations to determine thermodynamic and kinetic parameters and experiments to evaluate the model performance are combined in order to assess the effect of these different heteroatomic compounds in combination with the hydrocarbon feed.

In **Chapter 2**, the modeling strategy used in this PhD thesis is explained. The automatic kinetic model builder Genesys is used for kinetic model construction, with thermodynamic and kinetic parameters obtained from either quantum chemistry calculations or application of the group additivity method. The linear regression method is applied to determine new group additivity schemes for the heteroatomic compounds.

In **Chapter 3** a new **group additivity** scheme to approximate the **thermodynamic** parameters of nitrogen-containing compounds with a wide range of functionalities, including amine, imine, nitrile, nitro, nitroso, nitrite, nitrate and azo functional groups, is introduced. This consistent set of group additive values is obtained from a large dataset of CBS-QB3 calculations for 300 species with new **bond additive corrections** for the standard enthalpy of formation.

Chapter 4 reports new **group additivity** schemes for the intermolecular **hydrogen abstraction** reactions involving nitrogen-containing compounds, obtained from a dataset of 316 reaction rate coefficients calculated at the CBS-QB3 level of theory. The influence of substituents on both the attacking and attacked radical, being a carbon or nitrogen atom, is investigated systematically.

Chapter 5 deals with the pyrolysis and oxidation chemistry of the **nitrogen**-containing aliphatic **amines** ethylamine, dimethylamine and diethylamine. A new first-principles based kinetic model is developed making use of the group additivity schemes derived in Chapter 3 and Chapter 4. With three different experimental datasets covering a wide range of conditions for model validation, the effect of the branching degree as well as the length of the alkyl chain on the reactivity and the main product species is studied.

In **Chapter 6** the thermal decomposition of five **sulfur**-containing compounds under steam cracking conditions is studied. For dimethyl **sulfide**, dimethyl disulfide, dimethyl sulfoxide,

carbonyl sulfide and carbon disulfide, the influence of the molecular structure and the presence of a hydrocarbon matrix on the sulfur-containing product distribution and the main decomposition pathways is investigated.

In **Chapter 7** the main findings of this PhD thesis and outlook for further work on this research topic are summarized.

1.5. References

[1] R. De Bruycker, I. Amghizar, F.H. Vermeire, T. Nyman, M. Hakola, K.M. Van Geem, Steam cracking of bio-derived normal and branched alkanes: Influence of branching on product distribution and formation of aromatics, Journal of Analytical and Applied Pyrolysis 122 (2016) 468-478.

[2] B.O. de Beeck, M. Dusselier, J. Geboers, J. Holsbeek, E. Morré, S. Oswald, L. Giebeler, B.F. Sels, Direct catalytic conversion of cellulose to liquid straight-chain alkanes, Energy & Environmental Science, (2015).

[3] K. Weissermel, H.J. Arpe, Industrielle organische Chemie: bedeutende Vor- und Zwischenprodukte, Wiley-VCH1998.

[4] M. Brayden, A.J. Baumgartner, S.T. Coleman, D. Smith, L.A. Nairn, J. Lally, A. Bernard, Feedstock contaminants in ethylene plants - 2017 Update, Spring AIChE National Meeting, San Antonio, Texas, 2017.

[5] R. Van de Vijver, N.M. Vandewiele, P.L. Bhoorasingh, B.L. Slakman, F. Seyedzadeh Khanshan, H.-H. Carstensen, M.-F. Reyniers, G.B. Marin, R.H. West, K.M. Van Geem, Automatic Mechanism and Kinetic Model Generation for Gas- and Solution-Phase Processes: A Perspective on Best Practices, Recent Advances, and Future Challenges, International Journal of Chemical Kinetics 47 (2015) 199-231.

[6] H.E. Toraman, T. Dijkmans, M.R. Djokic, K.M. Van Geem, G.B. Marin, Detailed compositional characterization of plastic waste pyrolysis oil by comprehensive two-dimensional gas-chromatography coupled to multiple detectors, J Chromatogr A 1359 (2014) 237-246.

[7] K.M. Van Geem, J. Ongenae, J.L. Brix, J. Vercammen, G.B. Marin, Ultratrace Quantitative Analysis of Catalyst Poisoners Using a Dedicated GC-MS Analyzer, Lc Gc North America 30 (2012) 422-+.

[8] K.M. Van Geem, S.P. Pyl, M.F. Reyniers, J. Vercammen, J. Beens, G.B. Marin, On-line analysis of complex hydrocarbon mixtures using comprehensive two-dimensional gas chromatography, J Chromatogr A 1217 (2010) 6623-6633.

[9] N.D. Ristic, M.R. Djokic, K.M. Van Geem, G.B. Marin, On-line Analysis of Nitrogen Containing Compounds in Complex Hydrocarbon Matrixes, doi:doi:10.3791/54236(2016) e54236.

[10] G.H.C. Prado, Y. Rao, A. de Klerk, Nitrogen Removal from Oil: A Review, Energy & Fuels 31 (2017) 14-36.

[11] Y. Cho, A. Ahmed, S. Kim, Application of Atmospheric Pressure Photo Ionization Hydrogen/Deuterium Exchange High-Resolution Mass Spectrometry for the Molecular Level Speciation of Nitrogen Compounds in Heavy Crude Oils, Analytical Chemistry 85 (2013) 9758-9763.

[12] G.C. Laredo, S. Leyva, R. Alvarez, M.T. Mares, J. Castillo, J.L. Cano, Nitrogen compounds characterization in atmospheric gas oil and light cycle oil from a blend of Mexican crudes, Fuel 81 (2002) 1341-1350.

[13] F.P. Richter, P.D. Caesar, S.L. Meisel, R.D. Offenhauer, Distribution of Nitrogen in Petroleum According to Basicity, Industrial & Engineering Chemistry 44 (1952) 2601-2605.

[14] J.M. Schmitter, P.J. Arpino, Azaarenes in fuels, Mass Spectrometry Reviews 4 (1985) 87-121.

[15] N.D. Ristic, M.R. Djokic, K.M. Van Geem, G.B. Marin, On-line Analysis of Nitrogen Containing Compounds in Complex Hydrocarbon Matrixes, Jove - Journal of Visualized experiments, doi:doi:10.3791/54236(2016).

[16] H.E. Toraman, K. Franz, F. Ronsse, K.M. Van Geem, G.B. Marin, Quantitative analysis of nitrogen containing compounds in microalgae based bio-oils using comprehensive two-dimensional gas-chromatography coupled to nitrogen chemiluminescence detector and time of flight mass spectrometer, Journal of Chromatography A 1460 (2016) 135-146.

[17] A. Williams, J.M. Jones, L. Ma, M. Pourkashanian, Pollutants from the combustion of solid biomass fuels, Progress in Energy and Combustion Science 38 (2012) 113-137.

[18] A.J. Baumgartner, M.W. Blaschke, S.T. Coleman, R. Kohler, T.E. Paxson, Feedstock contaminants in ethylene plants - an Update, Spring AIChE National Meeting, New Orleans, LA, 2004.

[19] R.P. Lindstedt, F.C. Lockwood, M.A. Selim, Detailed Kinetic Modelling of Chemistry and Temperature Effects on Ammonia Oxidation, Combustion Science and Technology 99 (1994) 253-276.

[20] O. Mathieu, E.L. Petersen, Experimental and modeling study on the high-temperature oxidation of Ammonia and related NOx chemistry, Combustion and Flame 162 (2015) 554-570.

[21] C. Duynslaegher, F. Contino, J. Vandooren, H. Jeanmart, Modeling of ammonia combustion at low pressure, Combustion and Flame 159 (2012) 2799-2805.

[22] D.F. Davidson, K. Kohse-Höinghaus, A.Y. Chang, R.K. Hanson, A pyrolysis mechanism for ammonia, International Journal of Chemical Kinetics 22 (1990) 513-535.

[23] T. Higashihara, W.C. Gardiner, S.M. Hwang, Shock tube and modeling study of methylamine thermal decomposition, The Journal of Physical Chemistry 91 (1987) 1900-1905.

[24] S.C. Moldoveanu, Chapter 13 Pyrolysis of Amines and Imines, Techniques and Instrumentation in Analytical Chemistry, Elsevier2010, pp. 349-364.

[25] W. Tsang, Thermal stability of primary amines, International Journal of Chemical Kinetics 10 (1978) 41-66.

[26] H.O. Pritchard, R.G. Sowden, A.F. Trotman-Dickenson, The thermal decomposition of tert-butylamine, Journal of the Chemical Society (Resumed), doi:10.1039/JR9540000546(1954) 546-549.

[27] R. Cervellati, G. Corbelli, A.E. Esposti, D.G. Lister, P.E. Todesco, Identification of the pyrolysis products of some aromatic amines using microwave spectroscopy, Journal of the Chemical Society, Perkin Transactions 2, doi:10.1039/P29870000585(1987) 585-589.

[28] D.M. Golden, R.K. Solly, N.A. Gac, S.W. Benson, Very low pressure pyrolysis. V. Benzylamine, N-methylbenzylamine, and N,N-dimethylbenzylamine and the heat of formation of the amino, methylamino, and dimethylamino radicals, Journal of the American Chemical Society 94 (1972) 363-369.

[29] P. Glarborg, J.A. Miller, B. Ruscic, S.J. Klippenstein, Modeling nitrogen chemistry in combustion, Progress in Energy and Combustion Science 67 (2018) 31-68.

[30] Q. Wang, C. Wei, L.M. Pérez, W.J. Rogers, M.B. Hall, M.S. Mannan, Thermal Decomposition Pathways of Hydroxylamine: Theoretical Investigation on the Initial Steps, The Journal of Physical Chemistry A 114 (2010) 9262-9269.

[31] E.A. Lissi, M.A. Rubio, D. Araya, G. Zanocco, Reaction of di-tert-butylnitroxide radicals, International Journal of Chemical Kinetics 12 (1980) 871-881.

[32] T. Cáceres, E.A. Lissi, E. Sanhueza, Autooxidation of diethyl hydroxylamine, International Journal of Chemical Kinetics 10 (1978) 1167-1182.

[33] E. Abuin, M.V. Encina, S. Diaz, E.A. Lissi, On the reactivity of diethyl hydroxyl amine toward free radicals, International Journal of Chemical Kinetics 10 (1978) 677-686.

[34] J. Heicklen, The formation and inhibition of photochemical smog, Annals of the New York Academy of Sciences 502 (1987) 145-159.

[35] C. Galli, Nitroxyl Radicals, The Chemistry of Hydroxylamines, Oximes and Hydroxamic Acids, John Wiley & Sons, Ltd2008, pp. 705-750.

[36] A.E. Axworthy, V.H. Dayan, G.B. Martin, Reactions of fuel-nitrogen compounds under conditions of inert pyrolysis, Fuel 57 (1978) 29-35.

[37] T.J. Houser, M. Hull, R.M. Alway, T. Biftu, Kinetics of formation of HCN during pyridine pyrolysis, International Journal of Chemical Kinetics 12 (1980) 569-574.

[38] T.J. Houser, M.E. McCarville, T. Biftu, Kinetics of the thermal decomposition of pyridine in a flow system, International Journal of Chemical Kinetics 12 (1980) 555-568.

[39] R.D. Kern, J.N. Yong, J.H. Kiefer, J.N. Shah, Shock tube studies of pyridine pyrolysis and their relation to soot formation, Proceedings of the 16th International Symposium on Shock Tubes and Waves, (1987) 437-442.

[40] J.C. Mackie, M.B. Colket, P.F. Nelson, Shock tube pyrolysis of pyridine, The Journal of Physical Chemistry 94 (1990) 4099-4106.

[41] E. Ikeda, J.C. Mackie, Thermal decomposition of two coal model compounds - pyridine and 2-picoline - Kinetics and product distributions, Journal of Analytical and Applied Pyrolysis 34 (1995) 47-63.

[42] H.U.R. Memon, K.D. Bartle, J.M. Taylor, A. Williams, The shock tube pyrolysis of pyridine, International Journal of Energy Research 24 (2000) 1141-1159.

[43] X. Hong, T.-c. Zhang, L.-d. Zhang, F. Qi, Identification of Intermediates in Pyridine Pyrolysis with Molecular-beam Mass Spectrometry and Tunable Synchrotron VUV Photoionization, Chinese Journal of Chemical Physics 22 (2009) 204-209.

[44] N.R. Hore, D.K. Russell, Radical pathways in the thermal decomposition of pyridine and diazines: a laser pyrolysis and semi-empirical study, Journal of the Chemical Society, Perkin Transactions 2, (1998) 269-276.

[45] J. Liu, X. Fan, W. Zhao, S.-g. Yang, W. Xie, B. Hu, Q. Lu, A theoretical investigation on the thermal decomposition of pyridine and the effect of H2O on the formation of NOx precursors, Frontiers of Chemical Science and Engineering 15 (2021) 1217-1228.

[46] J.C. Mackie, M.B. Colket, P.F. Nelson, M. Esler, Shock tube pyrolysis of pyrrole and kinetic modeling, International Journal of Chemical Kinetics 23 (1991) 733-760.

[47] J.K. Winkler, W. Karow, P. Rademacher, Gas phase pyrolysis of heterocyclic compounds, part 3. Flow pyrolysis and annulation reactions of some nitrogen heterocycles: a product oriented study, ARKIVOC (Archive for Organic Chemistry) 1 (2000) 576-602.

[48] A. Lifshitz, C. Tamburu, A. Suslensky, Isomerization and decomposition of pyrrole at elevated temperatures: studies with a single-pulse shock tube, The Journal of Physical Chemistry 93 (1989) 5802-5808.

[49] M. Pelucchi, S. Arunthanayothin, Y. Song, O. Herbinet, A. Stagni, H.-H. Carstensen, T. Faravelli, F. Battin-Leclerc, Pyrolysis and Combustion Chemistry of Pyrrole, a Reference Component for Bio-oil Surrogates: Jet-Stirred Reactor Experiments and Kinetic Modeling, Energy & Fuels 35 (2021) 7265-7284.

[50] G.B. Bacskay, M. Martoprawiro, J.C. Mackie, An ab initio quantum chemical study of the electronic structure and stability of the pyrrolyl radical: Comparison with the isoelectronic cyclopentadienyl radical, Chemical Physics Letters 290 (1998) 391-398.

[51] G.B. Bacskay, M. Martoprawiro, J.C. Mackie, The thermal decomposition of pyrrole: an ab initio quantum chemical study of the potential energy surface associated with the hydrogen cyanide plus propyne channel, Chemical Physics Letters 300 (1999) 321-330.

[52] L. Zhai, X. Zhou, R. Liu, A Theoretical Study of Pyrolysis Mechanisms of Pyrrole, The Journal of Physical Chemistry A 103 (1999) 3917-3922.

[53] J.M. Patterson, C. Issidorides, E. Papadopoulos, W. Smith, The thermal interconversion of quinoline and isoquinoline, Tetrahedron Letters 11 (1970) 1247-1250.

[54] A. Laskin, A. Lifshitz, Thermal Decomposition of Quinoline and Isoquinoline. The Role of 1-Indene Imine Radical, The Journal of Physical Chemistry A 102 (1998) 928-946.

[55] L. Ling, R. Zhang, B. Wang, K. Xie, Pyrolysis Mechanisms of Quinoline and Isoquinoline with Density Functional Theory, Chinese Journal of Chemical Engineering 17 (2009) 805-813.

[56] A. Laskin, A. Lifshitz, Isomerization and Decomposition of Indole. Experimental Results and Kinetic Modeling, The Journal of Physical Chemistry A 101 (1997) 7787-7801.

[57] K. Ding, Y. Liu, Q. Xiao, Y. Luo, H. Yang, Pyrolysis of carbazole: Experimental results and kinetic study, Journal of Analytical and Applied Pyrolysis 113 (2015) 370-379.

[58] R. Guan, W. Li, H. Chen, B. Li, The release of nitrogen species during pyrolysis of model chars loaded with different additives, Fuel Processing Technology 85 (2004) 1025-1037.

[59] J.P. Hämäläinen, M.J. Aho, J.L. Tummavuori, Formation of nitrogen oxides from fuel-N through HCN and NH3: a model-compound study, Fuel 73 (1994) 1894-1898.

[60] E. Furimsky, F.E. Massoth, Hydrodenitrogenation of Petroleum, Catalysis Reviews 47 (2005) 297-489.

[61] G. Caeiro, A.F. Costa, H.S. Cerqueira, P. Magnoux, J.M. Lopes, P. Matias, F.R. Ribeiro, Nitrogen poisoning effect on the catalytic cracking of gasoil, Applied Catalysis A: General 320 (2007) 8-15.

[62] A. Groysman, Corrosion in Systems for Storage and Transportation of Petroleum Products and Biofuels: Identification, Monitoring and Solutions, Springer Netherlands2014.

[63] W.H. Henstock, NOx in the cryogenic hydrogen recovery section of an olefins production unit, Plant/Operations Progress 5 (1986) 232-237.

[64] M. R. Djokic, N. Ristic, N. Olahova, G. B. Marin, K. Van Geem, Quantitative On-line Analysis of Sulfur Compounds in Complex Hydrocarbon Matrices, 2017.

[65] M. Bajus, Sulfur compounds in hydrocarbon pyrolysis, Sulfur Reports 9 (1989) 25-66.

[66] M.K. Andari, H. Bchbehani, A. Stanislaus, Sulfur compound type distribution in naphtha and gas oil fractions of kuwaiti crude, Fuel Science and Technology International 14 (1996) 939-961.

[67] T. Dijkmans, M.R. Djokic, K.M. Van Geem, G.B. Marin, Comprehensive compositional analysis of sulfur and nitrogen containing compounds in shale oil using GC×GC – FID/SCD/NCD/TOF-MS, Fuel 140 (2015) 398-406.

[68] X. Wang, J. Si, H. Tan, L. Ma, M. Pourkashanian, T. Xu, Nitrogen, Sulfur, and Chlorine Transformations during the Pyrolysis of Straw, Energy & Fuels 24 (2010) 5215-5221.

[69] J. Gorawara, S. Caskey, J. Griffiths, Carbon disulfide removal to help meet new specifications for petrochemical grade naptha, Spring AIChE National Meeting, San Antonio, Texas, 2017.

[70] P. Coenen, E. Angueira, Carbon disulfide (CS2): A new challenge for steam cracker complexes?, Spring National AIChE Meeting, Houston, Texas, 2016.

[71] A.K. Vasiliou, D.E. Anderson, T.W. Cowell, J. Kong, W.F. Melhado, M.D. Phillips, J.C. Whitman, Thermal Decomposition Mechanism for Ethanethiol, The Journal of Physical Chemistry A 121 (2017) 4953-4960.

[72] T.O. Bamkole, The pyrolysis of alkanethiols. Part 1. Kinetics of the pyrolysis of butane-1-thiol, butane-2-thiol, and 2-methylpropane-2-thiol, Journal of the Chemical Society, Perkin Transactions 2, doi:10.1039/P29770000439(1977) 439-443.

[73] C. J. Thompson, R. A. Meyer, J. S. Ball, Thermal Decomposition of Sulfur Compounds. II. 1-Pentanethiol, 1952.

[74] O.S.L. Bruinsma, R.S. Geertsma, P. Bank, J.A. Moulijn, Gas phase pyrolysis of coal-related aromatic compounds in a coiled tube flow reactor: 1. Benzene and derivatives, Fuel 67 (1988) 327-333.

[75] J. Berkowitz, G.B. Ellison, D. Gutman, Three methods to measure RH bond energies, The Journal of Physical Chemistry 98 (1994) 2744-2765.

[76] L.G.S. Shum, S.W. Benson, The pyrolysis of dimethyl sulfide, kinetics and mechanism, International Journal of Chemical Kinetics 17 (1985) 749-761.

[77] X. Zheng, E.M. Fisher, F.C. Gouldin, L. Zhu, J.W. Bozzelli, Experimental and computational study of diethyl sulfide pyrolysis and mechanism, Proceedings of the Combustion Institute 32 (2009) 469-476.

[78] R. Van de Vijver, N.M. Vandewiele, A.G. Vandeputte, K.M. Van Geem, M.F. Reyniers, W.H. Green, G.B. Marin, Rule-based ab initio kinetic model for alkyl sulfide pyrolysis, Chemical Engineering Journal 278 (2015) 385-393.

[79] S. Nourbakhsh, C.L. Liao, C.Y. Ng, A 193 nm laser photofragmentation time-of-flight mass spectrometric study of CH3SSCH3, SSCH3, and SCH3, The Journal of Chemical Physics 92 (1990) 6587-6593.

[80] J.A.R. Coope, W.A. Bryce, THE THERMAL DECOMPOSITION OF DIMETHYL DISULPHIDE, Canadian Journal of Chemistry 32 (1954) 768-779.

[81] E.H. Braye, A.H. Sehon, B.d. Darwent, Thermal Decomposition of Sulfides, Journal of the American Chemical Society 77 (1955) 5282-5285.

[82] H. Bock, S. Mohmand, Unstable Intermediates in the Gaseous Phase: The Thermal Decomposition of Alkyl Sulfides RSnR, Angewandte Chemie International Edition in English 16 (1977) 104-105.

[83] J.R. Partington, H.H. Neville, 274. The thermal decomposition of carbonyl sulphide, Journal of the Chemical Society (Resumed), doi:10.1039/JR9510001230(1951) 1230-1237.

[84] K.H. Homann, G. Krome, H.G. Wagner, Schwefelkohlenstoffoxydation II. Zur Oxydation von Carbonylsulfid, Ber. Bunsen Phys. Chem. 73 (1969) 967-971.

[85] P.D. Clark, N.I. Dowling, M. Huang, W.Y. Svrcek, W.D. Monnery, Mechanisms of CO and COS Formation in the Claus Furnace, Industrial & Engineering Chemistry Research 40 (2001) 497-508.

[86] K. Karan, A.K. Mehrotra, L.A. Behie, Thermal Decomposition Of Carbonyl Sulfide At Temperatures Encountered In The Front End Of Modified Claus Plants, Chemical Engineering Communications 192 (2005) 370-385.

[87] A.J. Hay, R.L. Belford, High-Temperature Gas-Kinetic Study of Carbonyl Sulfide Pyrolysis Performed with a Shock Tube and Quadrupole Mass Filter, The Journal of Chemical Physics 47 (1967) 3944-3960.

[88] H.G. Schecker, H.G. Wagner, On the thermal decomposition of COS, International Journal of Chemical Kinetics 1 (1969) 541-549.

[89] D. Woiki, P. Roth, A shock tube study on the thermal decomposition of CS2 based on S(3P) and S(1D) concentration measurements, Shock Waves 4 (1994) 95-99.

[90] O. Masaaki, S. Hiroumi, T. Kentaro, M. Hiroyuki, Thermal Decomposition of COS, Bulletin of the Chemical Society of Japan 67 (1994) 2311-2313.

[91] P. Glarborg, B. Halaburt, P. Marshall, A. Guillory, J. Troe, M. Thellefsen, K. Christensen, Oxidation of reduced sulfur species: Carbon disulfide, The Journal of Physical Chemistry A 118 (2014) 6798-6809.

[92] P. Glarborg, P. Marshall, Oxidation of reduced sulfur species: Carbonyl sulfide, International Journal of Chemical Kinetics 45 (2013) 429-439.

[93] A.G. Vandeputte, M.-F. Reyniers, G.B. Marin, Theoretical study of the thermal decomposition of dimethyl disulfide, The Journal of Physical Chemistry A 114 (2010) 10531-10549.

[94] M. Bajus, V. Vesely, J. Baxa, P.A. Leclercq, J.A. Rijks, Steam cracking of hydrocarbons. 5. Effect of thiophene on reaction kinetics and coking, Industrial & Engineering Chemistry Product Research and Development 20 (1981) 741-745.

[95] P. Rademacher, Fragmentations of Five-Membered Rings, in: A.R. Katritzky (Ed.), Advances in Heterocyclic Chemistry, Academic Press1998, pp. 361-412.

[96] C.F. Cullis, A.C. Norris, The pyrolysis of organic compounds under conditions of carbon formation, Carbon 10 (1972) 525-537.

[97] X. Song, C.A. Parish, Pyrolysis Mechanisms of Thiophene and Methylthiophene in Asphaltenes, The Journal of Physical Chemistry A 115 (2011) 2882-2891.

[98] C.D. Hurd, J.I. Simon, Pyrolytic formation of arenes 3. Pyrolysis of pyridine, picolines and methylpyrazine, Journal of the American Chemical Society 84 (1962).

[99] J.K. Winkler, W. Karow, P. Rademacher, Gas-phase pyrolysis of heterocyclic compounds, part 1 and 2: flow pyrolysis and annulation reactions of some sulfur heterocycles: thiophene, benzo[b]thiophene, and dibenzothiophene. A product-oriented study11For part 3, see J.K. Winkler, W. Karow, P. Rademacher, ARKIVOC 1 (2000) 59. For part 4, see: J.K. Winkler, W. Karow, P. Rademacher, J. Anal. Appl. Pyrolys. 57 (2000) 133, Journal of Analytical and Applied Pyrolysis 62 (2002) 123-141.

[100] C.D. Hurd, R.V. Levetan, A.R. Macon, Pyrolytic Formation of Arenes. II. Benzene and Other Arenes from Thiophene, 2-Methylthiophene and 2-(Methyl-14 C)-thiophene, Journal of the American Chemical Society 84 (1962) 4515-4519.

[101] J. Dunleavy, Final Analysis: Sulfur as a Catalyst Poison, 2006.

[102] S. Albanese, D. Cicchella, Legacy Problems in Urban Geochemistry, 2012.

2

Methodology

Abstract

In this work, quantum chemistry calculations, kinetic modelling and experimental work are combined to improve the fundamental understanding of the pyrolysis or oxidation of nitrogen-, oxygen- and sulfur-containing model compounds present in renewable and alternative steam cracking feedstocks and energy carriers. With the microkinetic modelling approach, a kinetic model is generated that can describe the occurring chemistry as well as the effect of a hydrocarbon matrix over a wide range of conditions.

The automatic kinetic model generation software tool Genesys is used for construction of the kinetic models. To enable reactor simulations, thermodynamic and kinetic parameters need to be assigned to all species and reactions after the network generation step. If no accurate *ab initio* calculated values are available, the species properties and reaction kinetics are approximated with fast estimation methods such as the group additivity method. For heteroatom-containing compounds, the databases for these methods are scarce, which is one of the main challenges within this microkinetic modeling approach for the compounds of interest. Thermodynamic and kinetic group additive parameters are obtained with the unweighted least-squares linear regression analysis method making use of a reference dataset of *ab initio* data. A statistical analysis is performed to assess the reliability of the linear regression procedure, while the transferability of the regressed parameters using the so-called training set is validated using a second dataset, which has not yet seen that data, i.e. the test set.

The present Chapter introduces the methodology applied in this work to obtain the thermodynamic and kinetic parameters from *ab initio* calculations, the regression of new group additive parameters and the generation of an elementary step kinetic model with Genesys.

2.1 Introduction

First-principles based kinetic modeling not only provides understanding of the occurring chemistry, but also enables the development of predictive fundamental models that can be used to assess the influence of heteroatomic compounds present as impurities or process additives. For the majority of the technologically important processes, e.g. pyrolysis, oxidation and combustion, the kinetic models can become very large, i.e. they can contain hundreds of species and thousands of reactions, as discussed by Van de Vijver et al. [1]. In order to enable reactor simulations, thermodynamic and kinetic parameters need to be assigned to all species and reactions in the generated kinetic model. Due to the large number of radicals, many of which are radicals, obtaining experimental values for all these parameters is nearly impossible. When experimental data is lacking, quantum chemical calculations can be used as a complementary source for the assignment of thermodynamic and kinetic parameters to all species and reactions in a kinetic model. These methods can vary from *ab initio* calculations, i.e. based on first principles, to empirical methodologies [2]. The ever-growing computational power and the availability of high performance computing solutions have led to the increasing importance of *ab initio* calculations in the field of kinetic model generation.

In this Chapter, the approximations and methodology used to perform quantum chemistry calculations and the use of the group additivity methods to approximate the thermodynamic and kinetic parameters are discussed. The linear regression procedure required for the regression of new group additivity parameters as well as new bond additivity corrections is explained. The different steps in the microkinetic modeling approach are discussed.

2.2 Quantum chemistry calculations

2.2.1 Stable species

For stable species, *ab initio* calculations are carried out with the high-performance supercomputer available at Ghent University at the CBS-QB3 level of theory [3] as implemented in Gaussian 9 [4] and Gaussian 16 [5]. In-house developed algorithms are used to perform an automatic search of the lowest energy conformer with the Becke-3-parameter-Lee-Yang-Parr hybrid functional (B3LYP), i.e. at the B3LYP/6-31G(d) level of theory [6]. The conformers corresponding to the lowest 5 kJ mol^{-1} are further calculated at the complete basis set-quadratic Becke3 (CBS-QB3) level of theory. From these calculations, the lowest energy conformer is used as final geometry.

Harmonic frequency analysis is performed on the B3LYP/6-311G(2d,d,p) level of theory, which is also the level for geometry optimization within the CBS-QB3 method. Internal modes are treated as harmonic oscillators, except for modes which resemble rotations around single bonds. These internal modes are treated as one-dimensional (1D) hindered rotors, as long as the barrier does not exceed 50 kJ mol^{-1}. Assuming decoupled internal rotations, the 1D hindered rotor approach of Vansteenkiste et al. [7] is applied for the hindered rotor corrections. The hindrance potentials are determined at the B3LYP/6-31G(d) level of theory with relaxed surface scans in which all coordinates, except for the dihedral angle of interest, are re-optimized at each scan angle with a step size of 10°. In some cases, a relaxed surface scan does not result in a smooth energy surface and additional, carefully selected, bonds, angles or dihedrals are frozen during the scans. The potential energy of the hindered rotor scan is approximated by a function as shown in Eq. 2-1.

$$V(\varphi) = \sum_{k=1}^{n} \frac{1}{2} A_k (1 - \cos(k\varphi)) + \sum_{k=1}^{n} B_k (\sin(k\varphi)) \qquad \text{(Eq. 2-1)}$$

With the torsional angle φ, the coefficients A_k and B_k calculated using a linear least-squares regression method and a value of 10 for n. In Eq. 2-1, the potential energy is zero when φ is zero, i.e. the rotational scan starts at the lowest energy configuration of the species at the B3LYP/6-31G(d) level of theory. This function together with the reduced moment of inertia calculated at the I(2,3) level, as defined by East and Radom [8], is used to construct the Schrödinger equation for one-dimensional internal rotation. Numerical solution of this 1D Schrödinger equation yields the energy eigenvalues of the specific rotation. Note that for sulfur-containing compounds the B3LYP/6-311(2d,d,p) level of theory is used.

2.2.2 Transition states

The above methodology for *ab initio* calculations of stable species can also be applied for transition states. The transition state structure is generated using of in-house developed algorithms implemented in the Genesys software or, in case of more complex structures, the structure is obtained via manual *ab initio* calculations. Similar to stable species, internal modes with barriers lower than 50 kJ mol^{-1} are treated as 1D hindered rotors, including the rotation around the transition state bond. Forward and reverse intrinsic reaction coordinate (IRC) calculations are performed to confirm that the correct transition state structure has been found for the single-step reaction or to identify pre-reaction complexes.

2.2.3 Thermodynamic parameters

To obtain thermodynamic values from *ab initio* calculations for three thermodynamic properties, i.e. the enthalpy, entropy and heat capacity in a wide range of temperatures (300-1800 K), ideal gas statistical thermodynamics is used. The approach used in Genesys is similar to the work of Van Speybroeck [9] and Sabbe and coworkers [10, 11].

The molecular partition function can be considered as the link between the microscopic thermodynamic properties, such as the electronic energy and the vibrational frequencies, and the macroscopic thermodynamic properties of a species, i.e. the enthalpy, entropy and heat capacity. The energy of a molecule is quantized and can be written as a sum of various contributions: electronic, translational, rotational and vibrational energy. The coupling between these different contributions is often neglected. Input from the geometry optimization and energy calculation performed with Gaussian is required to construct the molecular partition function, c.f. Equation (Eq. 2-2).

$$q = q_{trans} \cdot q_{rot} \cdot q_{vib} \cdot q_{elec} \qquad \text{(Eq. 2-2)}$$

More information on the construction of this partition function can be found in Van de Vijver et al. [6]. Once the molecular partition function $q(T)$ is known, the macroscopic thermodynamic values can be calculated according to Eq. 2-3, Eq. 2-4 and Eq. 2-5.

$$H(T) = RT\left(1 + T\left(\frac{\partial ln(q(T))}{\partial T}\right)\right) \qquad \text{(Eq. 2-3)}$$

$$S(T) = R\left(1 + ln\left(\frac{q(T)}{N_A}\right) + T\frac{\partial ln(q(T))}{\partial T}\right) \qquad \text{(Eq. 2-4)}$$

$$C_P(T) = R\left(1 + 2T\frac{\partial ln(q(T))}{\partial T} + T\frac{\partial^2 ln(q(T))}{\partial T^2}\right) \qquad \text{(Eq. 2-5)}$$

The atomization method, as reported by Curtis et al. [12], is applied to calculate the standard enthalpy of formation ($\Delta_f H^{\circ}_{atom}$) at 298.15 K for a species with structural formula $H_{n_H}C_{n_C}O_{n_O}N_{n_N}S_{n_S}$, according to Eq. 2-6.

$$\Delta_f H^{\circ}_{atom}\left(H_{n_H}C_{n_C}O_{n_O}N_{n_N}S_{n_S}\right) = \sum_{X=H,C,O,N,S} \{n_X\, \Delta_{atom}H^{\circ}_{\mathrm{EXP}}(X)\} - \left[\sum_{X=H,C,O,N,S} \{n_X H^{\circ}_{AI}(X)\} - H^{\circ}_{AI}\left(H_{n_H}C_{n_C}O_{n_O}N_{n_N}S_{n_S}\right)\right] \quad \text{(Eq. 2-6)}$$

In Eq. 2-6, H°_{AI} is the *ab initio* calculated enthalpy, while $\Delta_{atom}H^{\circ}_{\mathrm{EXP}}$ is the atomization enthalpy, which is based on experimental data. All the values of $\Delta_f H^{\circ}_{atom}$, $\Delta_{atom}H^{\circ}_{\mathrm{EXP}}$ and H°_{AI} are evaluated at 298.15 K. The *ab initio* calculated enthalpies (H°_{AI}) and the experimentally determined atomization enthalpies of the elements constituting the species from their standard state ($\Delta_{atom}H^{\circ}_{EXP}$), taken from the NIST Chemistry WebBook [13] are given in Table 2-1.

Table 2-1: CBS-QB3 calculated atom enthalpies [Hartree] and experimental atomization enthalpies [kJ mol^{-1}] at 298 K taken from the NIST Chemistry WebBook [13] used as input in the atomization method.

Element	H°_{AI} [Hartree]	$\Delta_{atom}H^{\circ}_{\mathrm{EXP}}$ [kJ mol^{-1}]
H	-0.497	217.998
C	-37.783	716.68
O	-74.985	249.18
N	-54.518	472.68
S	-397.655	276.98

Two types of corrections are used to improve the accuracy of the standard enthalpy of formation calculated at the CBS-QB3 level of theory. First, Spin-Orbit Corrections (SOC) [12] are applied to account for the spin-orbit coupling of the atoms. These element-specific corrections to the *ab initio* calculated atom enthalpy (H°_{AI}), are taken from the work of Petersson et al. [14] and amount to -0.354 kJ mol^{-1} for a carbon atom, -0.933 kJ mol^{-1} for an oxygen atom and -2.345 kJ mol^{-1} for a sulfur atom. For the nitrogen atom, no SOC is taken into account. Considering Eq. 2-6, these negative values for the SOCs, lead to positive corrections for the standard enthalpy of formation ($\Delta_f H^{\circ}$). The second type of corrections are the bond-specific bond additive corrections (BAC), for which new values are determined in this work. Note that in the regression procedure for determination of the new set of BACs, the CBS-QB3 values including SOCs are used. Hence, these SOCs are used as input in the linear regression analysis and not optimized themselves. The standard enthalpy of formation at 298 K including SOCs and BACs is calculated according to Eq. 2-7, with i and j running over the different elements.

$$\Delta_f H^{\circ}_{atom+SOC+BAC} = \Delta_f H^{\circ}_{atom} + \sum_i n_i \cdot SOC_i + \sum_{ijk} N_{ij} \cdot BAC_{ij,k} \quad \text{(Eq. 2-7)}$$

$\Delta_f H^{\circ}_{atom}$ is the standard enthalpy of formation obtained with the atomization method, SOC_i are the element-specific spin orbit corrections, n_i is the number of occurrences of each element i, and $BAC_{ij,k}$ is the correction term for a given bond with bond order k between the elements i and j, which appears N_{ij} times in the molecule. While the SOCs are considered to be fixed for each atom type within the CBS-QB3 method, the BAC values depend on all details of the calculation methodology, such as the hindered rotor approximation, but the computational method as well as the basis set have the largest influence on the obtained value.

2.2.4 Kinetic parameters

The thermodynamic properties of the transition state species can be calculated with the same methodology as for the stable species. From the obtained thermodynamic properties, the rate coefficients can be calculated using the transition state theory (TST). The fundamental assumption of transition state theory is the existence of a hypersurface, i.e. a first order saddle-point on the potential energy surface (PES), which divides the phase space in a reactant and a product region [15]. In order to go to the products region, the reactants have to follow a trajectory which passes through this transition state. The transition state corresponds to the point with the highest energy on the minimum-energy path and has a vibrational spectrum which is characterized by one imaginary frequency. In conventional TST, the no-recrossing assumption is made, i.e. once the reactants have passed this so-called "dividing surface", no re-crossing to the well of the reactants can take place. With this method, the rate coefficient can be calculated with information about only two configurations, i.e. that of the reactants and that of the transition state. Hence, two points need to be localized on the potential energy surface, i.e. the stable reactant species and the first-order saddle-point corresponding to the transition state.

From the combined thermodynamic properties of reactants and transition state, the rate coefficients are calculated for using the transition state theory (TST) in the high-pressure limit according to Eq. 2-8.

$$k(T) = \kappa(T)\frac{k_B T}{h}\left(\frac{RT}{p}\right)^{-\Delta^{\ddagger}n} exp\left(-\frac{\Delta^{\ddagger}H - T\Delta^{\ddagger}S}{RT}\right) \qquad \text{(Eq. 2-8)}$$

In Eq. 2-8, $\Delta^{\ddagger}n$ is the change in number of moles upon formation of the transition state (i.e. 0 for unimolecular reactions such as β-scission, -1 for bimolecular reactions such as intermolecular hydrogen abstractions). The enthalpy difference $\Delta^{\ddagger}H$ and the entropy difference $\Delta^{\ddagger}S$ are calculated from the standard enthalpy of formation and entropy of the reactant(s) and

the transition state of the reaction. The contribution to the rate coefficient of quantum mechanical tunneling through the reaction barrier can be incorporated with a tunneling coefficient κ. The activation entropy can be written as a sum of two terms: a symmetry-independent entropy contribution and a term which contains all symmetry and optical contributions, c.f. Eq. 2-9.

$$\Delta^{\ddagger}S = \Delta^{\ddagger}\tilde{S} + R\,ln\frac{n_{opt,\ddagger}}{\prod_j n_{\mathrm{opt,j}}}\cdot\frac{\prod_j \sigma_{\mathrm{j}}}{\sigma_{\ddagger}} = \Delta^{\ddagger}\tilde{S} + R\,ln(n_e) \qquad \text{(Eq. 2-9)}$$

$$n_e = \frac{n_{opt,\ddagger}}{\prod_j n_{\mathrm{opt,j}}}\cdot\frac{\prod_j \sigma_{\mathrm{j}}}{\sigma_{\ddagger}} \qquad \text{(Eq. 2-10)}$$

In Eq. 2-10, n_{opt} is the number of optical isomers, with the index *j* running over the reactant(s), σ is the global symmetry number and finally n_e is the number of single events. In this work, the number of single events n_e corresponds to the reaction path degeneracy as defined by Pollak and Pechukas [16]. Substitution of the activation entropy in Eq. 2-8 and dividing both sides by the number of single events yields the single-event rate coefficient:

$$\frac{k(T)}{n_e} = \tilde{k}(T) = \kappa(T)\frac{k_B T}{h}\left(\frac{RT}{p}\right)^{-\Delta^{\ddagger}n} exp\left(-\frac{\Delta^{\ddagger}H - T\Delta^{\ddagger}\tilde{S}}{RT}\right) \qquad \text{(Eq. 2-11)}$$

The Gibbs free energy of a species can be calculated from the enthalpy and entropy according to Eq. 2-12.

$$G = H - TS \qquad \text{(Eq. 2-12)}$$

Once the Gibbs free energy of the reactant(s) and product(s) of a reaction is known, the equilibrium coefficient, corresponding to the ratio of the forward and reverse rate coefficient, can be calculated with Eq. 2-13 in which Δn is the change in number of moles between the products and reactants.

$$K_{eq} = \left(\frac{RT}{p}\right)^{-\Delta n} exp\left(-\frac{\Delta_r G^{\circ}}{RT}\right) \qquad \text{(Eq. 2-13)}$$

The Arrhenius parameters are obtained based on the linear least-squares regression of the *ab initio* rate coefficients to the Arrhenius equation (Eq. 2-14). For the fitting procedure, a set of five consecutive rate coefficients is used at temperature intervals of 100 K, i.e. from T – 200 to T + 200 with T the temperature of interest.

$$\ln\big(k(T)\big) = \ln(A) - \frac{E_a}{RT} \qquad \text{(Eq. 2-14)}$$

2.3 Group additivity method

2.3.1 Thermodynamic parameters

The basic assumption of the group additivity method is that the thermodynamic properties of an entire molecule can be determined from contributions of all the groups within the species. According to the method developed by Benson [17], a group is defined as a polyvalent atom together with all of its ligands. The central atom is defined as an atom that has at least two ligands and in special cases this central atom can also be a polyatomic group, such as the imine C=N group. The corresponding notation is X-$(A)_i(B)_j(C)_k(D)_l$, in which X represents the central atom surrounded by *i* ligands of atom A, *j* ligands of atom B and so on. Different types of carbon atoms can be distinguished with a distinct notation: C represents a single-bonded carbon atom with sp^3 hybrid orbitals, C_d a double-bonded carbon atom with sp^2 hybridization, C_t a triple-bonded carbon atom with sp hybridization and C_b a carbon atom which is part of an aromatic ring.

These group additive values or so-called GAVs need to be determined from a training set of species, for which accurate thermodynamic values are available. The accuracy of the GAVs does not only depend on how accurate the assumption of additivity is fulfilled, but also on the reliability of the database. In theory, both experimental data and data obtained from *ab initio* calculations can be used for the determination of these GAVs. Aside from group additive values that take into account the nature of the nearest-neighbor ligands, there are three other Benson group contributions: ring strain corrections (RSC), which account for the presence of rings compared to their acyclic counterparts, non-nearest-neighbor interactions (NNI), which model interactions between non-bonded sub-molecular fragments and finally resonance corrections (RES) which account for the stabilization effect of electron interactions in a molecule [17].

Symmetry is an important molecular property, which should be handled with care when calculating the thermodynamic properties of a species. Due to the non-local character of this property, symmetry cannot be accounted for within the group additivity scheme. A reliable group additivity scheme for estimation of the entropy requires that symmetry contributions are omitted from the calculated entropies, resulting in a symmetry-independent "intrinsic" entropy S_{int}. This can be done making use of Eq. 2-15, in which S represents the entropy obtained from the *ab initio* calculations, σ the global symmetry number and n_{opt} the number of optical isomers.

$$S_{int}^{\circ} = S^{\circ} + R \cdot \ln(\frac{\sigma}{n_{opt}}) \qquad \text{(Eq. 2-15)}$$

The rotational symmetry number of a molecule refers to the number of indistinguishable orientations of molecule [18]. The global symmetry number σ is the product of the external symmetry number σ_{ext} and the intrinsic symmetry numbers $\sigma_{int,k}$ (Eq. 2-16).

$$\sigma = \sigma_{ext} \prod_{k} \sigma_{int,k} \qquad \text{(Eq. 2-16)}$$

The external symmetry number can be obtained by rotating a molecule as a rigid body around its center of mass, assuming the internal coordinates of the atoms in the molecule do not vary. The internal symmetry number originates from rotation of sub-molecular fragments of the molecule around single bonds. Such rotations around internal bonds should only be taken into account when the energy barrier is sufficiently low, such that the time scale for rotation is much lower than the time scale of reaction.

Taking into account the contribution of each group, the standard enthalpy of formation ($\Delta_f H^{\circ}$), the intrinsic standard entropy (S_{int}°) and the standard heat capacity (C_p°) of the species can be estimated using Eq. 2-17.

$$\begin{cases} \Delta_f H^{\circ} \\ S_{int}^{\circ} \\ C_p^{\circ} \end{cases} = \sum_{j=1}^{n} GAV(X_j) + \sum_{j=1}^{m} NNI_j + \sum_{j=1}^{q} RSC_j + \sum_{j=1}^{p} RES_j \qquad \text{(Eq. 2-17)}$$

An example of the application of the group additivity method for approximation of the thermodynamic properties of the nitrogen-containing species ethyl isopropyl amine is given in Figure 2-1.

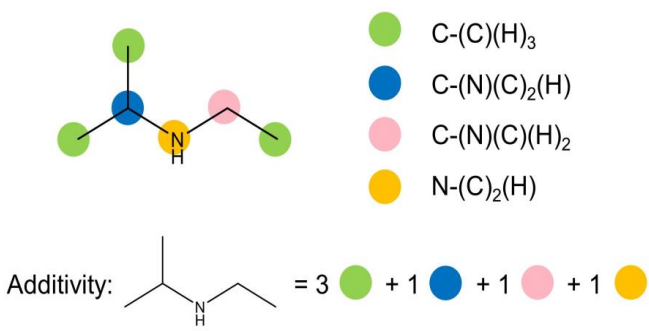

Figure 2-1: Identification of Benson groups in ethyl isopropyl amine for application of the group additivity method.

With the identification of four different Benson groups in this molecule, the standard enthalpy of formation can be approximated as:

$$\Delta_f H^\circ = 3 \cdot GAV[C-(C)(H)_3] + GAV[C-(N)(C)_2(H)] + GAV[C-(N)(C)(H)_2] + GAV[N-(C)_2(H)] \quad \text{(Eq. 2-18)}$$

2.3.2 Kinetic parameters

Group additivity was first developed to estimate the thermodynamic parameters of molecules and the corresponding radicals by summing over the contributions for each constituting group of the species. Marin and coworkers [19-27] extended this group additivity concept for kinetic data by defining the groups as the reactive atoms in the reactants. In this way, the group additivity method can also be used to estimate the pre-exponential factors and activation energies of reactions belonging to a reaction family.

By introducing the Arrhenius activation energy, as calculated from the rate coefficient via Eq. 2-19, the single-event rate coefficient can be rewritten as the product of the single-event pre-exponential factor $\tilde{A}$ and the exponential of this Arrhenius activation energy, c.f. Eq. 2-20.

$$E_a = RT^2 \frac{\partial}{\partial T} \ln k = \Delta^\ddagger H + (1-\Delta^\ddagger n)RT \quad \text{(Eq. 2-19)}$$

$$\tilde{k} = \underbrace{\frac{k_B T}{h}\left(\frac{RT}{p}\right)^{-\Delta^\ddagger n} exp\left(\frac{\Delta^\ddagger \tilde{S}}{R}\right) exp(1-\Delta^\ddagger n)}_{\tilde{A}} exp\left(-\frac{\Delta^\ddagger H + (1-\Delta^\ddagger n)RT}{RT}\right) \quad \text{(Eq. 2-20)}$$

From Eq. 2-20, it can be seen that in order to calculate the rate coefficient, estimates of the thermodynamic properties of both the transition state and the reactants are required. The applicability of the group additivity method is based on the assumption that the thermodynamic properties of the transition state can be estimated with the same accuracy as that of the species at the same level of theory. Instead of directly calculating group additive approximations for the transition state structures, the differences in the enthalpies and entropies of transition state and reactant(s) can be considered. Taking into account Eq. 2-20, it is clear that this corresponds to the approximation of the Arrhenius parameters, i.e. the Arrhenius activation energy and the pre-exponential factor.

Considering the differences between the group additive value of the transition state and the group additive value in the reactant, corresponding to the same polyvalent atom, ΔGAV° parameters are introduced. The "Δ" symbol corresponds to the difference between transition

state and reactant(s), while "°" refers to the definition of these group additivity values with respect to the Arrhenius parameters of a reference reaction. Because only the differences between the reactants and transition state are needed, systematic errors partially cancel out and the introduction of a reference reaction reduces the temperature dependency of the ΔGAV° values. For groups in which neither the central polyvalent atom nor the ligands change in connectivity during the reaction ΔGAV° is zero.

The activation energy can be calculated using Eq. 2-21 in which $\Delta GAV_{E_a}^{o} = \Delta GAV_{E_a} - \Delta GAV_{E_a,ref}$. The index i iterates over the groups that are transition state specific, which are referred to as the primary contributions. The term $\Delta E_{E_{a,res}}^{o}$ represents the additional stabilization of the transition state due to resonance effects that cannot be included in the $\Delta GAV_{E_a}^{o}$.

$$E_a(T) = E_{a,ref}(T) + \sum_i \Delta GAV_{E_a}^{o}(C_i) + \Delta E_{E_{a,res}}^{o} \qquad \text{(Eq. 2-21)}$$

As an example, for intermolecular hydrogen abstractions the attacking radical and the atom bonded to the abstracted hydrogen atom are considered as the primary contributions, as these are the main groups which will influence the kinetics. In case the reaction rate coefficients are dependent on groups which are not part of the reactive center, secondary contributions can be introduced. For example, non-nearest-neighbor interactions can account for interactions between secondary groups on both sides of the transition state. Similarly, the single-event pre-exponential factor is obtained according to:

$$\log \tilde{A}\,(T) = \log \tilde{A}\,(T)_{ref} + \sum_i \Delta GAV_{\log \tilde{A}}^{o}(C_i) + \Delta \log \tilde{A}_{\,res} \qquad \text{(Eq. 2-22)}$$

The group additive values for the pre-exponential factor and the pre-exponential factor of the reference reaction are evaluated without taking the number of single events into account. Hence, in order to obtain the correct rate coefficient, the pre-exponential as determined by group additivity still needs to be multiplied by the number of single events n_e, c.f. Eq. 2-23.

$$\log A\,(T) = \log \tilde{A}\,(T)_{ref} + \sum_i \Delta GAV_{\log \tilde{A}}^{o}(C_i) + \Delta \log \tilde{A}_{\,res} + \log n_e \qquad \text{(Eq. 2-23)}$$

The total reaction rate coefficient can be obtained with Eq. 2-24, with κ the tunneling contribution. As tunneling is a non-classical (quantum) effect, tunneling coefficients cannot be directly calculated from group additivity. The contribution of tunneling through the reaction barrier requires the imaginary frequency of the transition state as well as the energy profile along the reaction coordinate.

$$k(T) = \kappa n_e \tilde{A} \exp\left(-\frac{E_a}{RT}\right) \quad \text{(Eq. 2-24)}$$

In Figure 2-2, the application of the group additivity method is illustrated for determination of the Arrhenius parameters for the hydrogen abstraction reaction from the α carbon atom in ethylamine by a tert-butyl radical.

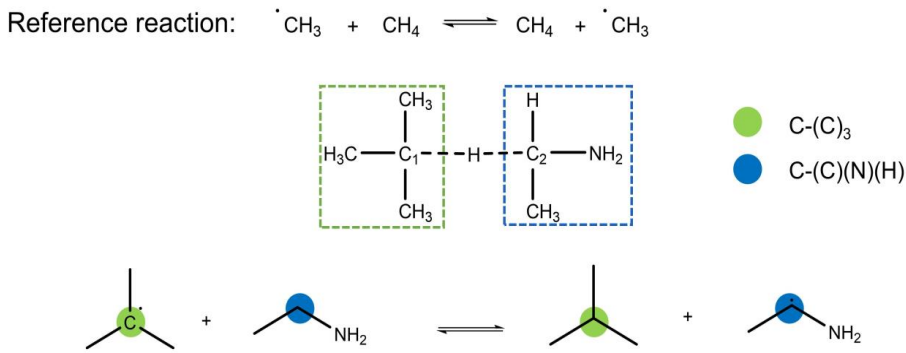

Figure 2-2: Application of the group additivity method for calculation of the kinetic parameters for the hydrogen abstraction from C_α in ethylamine by the tert-butyl radical.

In the transition state, the carbon atom labeled 1 corresponds to the abstracting atom, while the carbon atom labeled 2 refers to the carbon atom bound to the hydrogen atom which is abstracted. Considering abstraction from methane by a methyl radical as reference reaction, two different groups can be identified for this reaction, i.e. C-(C)$_3$ and C-(C)(N)(H). Not taking into account secondary contributions or non-nearest-neighbor interactions, the group additive approximated Arrhenius parameters can be calculated as follows:

$$\log \tilde{A} = \log\left(\tilde{A}_{ref}\right) + \Delta GAV^{o}_{\log \tilde{A}}(C_1 - (C)_3) + \Delta GAV^{o}_{\log \tilde{A}}(C_2 - (C)(N)(H))$$

$$E_a = E_{a,ref} + \Delta GAV^{o}_{E_a}(C_1 - (C)_3) + \Delta GAV^{o}_{E_a}(C_2 - (C)(N)(H))$$

2.4 Linear regression procedure

In Chapters 3 and 4 of this PhD thesis, parameter optimization is based on the unweighted least-squares linear regression analysis method. The optimal values for the BAC, thermodynamic and kinetic group additivity parameters are obtained by optimizing the agreement between two reference datasets, which can be experimental, *ab initio* or group additivity based. With this method, the property $\hat{y}_i$ of the ith species/reaction is approximated according to Eq. 2-25, with *m* the number of parameters and n the number of species or reactions.

$$\hat{y}_i = \sum_{j=1}^{m} X_{ij}\beta_j \quad i = 1, 2, \dots, n \qquad \text{(Eq. 2-25)}$$

In Eq. 2-25, $\hat{y}_i$ is equal to the difference between the experimental and *ab initio* calculated thermodynamic value for regression of BAC parameters or to the group additive approximated thermodynamic/kinetic value. This results in an overdetermined system of linear equations with X defined as the occurrence matrix in which the elements X_{ij} specify the number of occurrences of parameter β_j. For the ith species or reaction, the residual r_i can be defined according to Eq. 2-26 with y_i the observed value and $\hat{y}_i$ the predicted value.

$$r_i = y_i - \hat{y}_i = y_i - \sum_{j=1}^{m} X_{ij}\beta_j \quad i = 1, 2, \dots, n \qquad \text{(Eq. 2-26)}$$

The unweighted least-squares method consists of minimizing the target function, defined as the sum of squares of the unobservable errors, with respect to the unknown model parameters.

$$SSQ = \sum_{i}^{n} (y_i - \hat{y}_i)^2 \qquad \text{(Eq. 2-27)}$$

This minimization results in the following Eq. 2-28 for the optimized set of parameters.

$$\frac{\partial SSQ}{\delta \beta} = 0 \qquad \text{(Eq. 2-28)}$$

On the condition that the matrix $(X^T X)$ is not singular, which implies that no linear dependencies exist between the p columns of matrix, the following expression can be obtained for the parameter estimates b:

$$b = (X^T X)^{-1} X^T y \qquad \text{(Eq. 2-29)}$$

To assess the reliability of the linear regression procedure, a statistical analysis is performed. The quality of the regression procedure is expressed in terms of the mean deviation (MD), mean absolute deviation (MAD), maximum absolute deviation (MAX) and root-mean-square deviation (RMS). The significance of the regression F is calculated with Eq. 2-30, with n the number of species or reactions and p the number of model parameters in the linear regression.

$$F = \frac{\frac{\sum_{i=1}^{n} \hat{y}_i^2}{p}}{\frac{\sum_{i=1}^{n} (y_i - \hat{y}_i)^2}{n-p}} \qquad \text{(Eq. 2-30)}$$

For a probability level equal of 0.05, the null hypothesis, i.e. all parameters are equal to zero, can be rejected if Eq. 2-31 is satisfied, with values for $F_{0.05}(p, n-p)$ available in databases.

$$F > F_{0.05}(p-1, n-p) \quad \text{(Eq. 2-31)}$$

The variance-covariance matrix of the parameters is calculated according to:

$$V(b) = \sigma^2 (X^T X)^{-1} \quad \text{(Eq. 2-32)}$$

The diagonal elements of the variance-covariance matrix contain the variances of the parameters, while the off-diagonals contain the covariances between all possible pairs of variables. It follows from Eq. 2-32 that σ^2 needs to be known in order to be able to calculate the variance-covariance matrix. On the condition that the model is adequate, which means that no systematic deviation exists between the observed values and the model calculated values of the dependent variables, an unbiased estimator for the error variance σ^2 can be obtained as follows:

$$s^2 = \frac{SSQ}{n-p} \quad \text{(Eq. 2-33)}$$

The individual confidence intervals (CI_i) for the ith model parameter at 97.5% confidence level ($t_{97.5}$) can be calculated using Eq. 2-34, with the standard deviation on the estimate or the square root of the diagonal element of the variance-covariance matrix.

$$CI_i = t_{0.975}\sqrt{\hat{V}_{ii}} \quad \text{(Eq. 2-34)}$$

The general methodology followed in this work for parameter optimization with the unweighted least-squares linear regression analysis method based on the use of a training and test set, can be summarized as follows:

1) A training set is constructed containing a limited number of species/reactions for which the thermodynamic or kinetic parameters are obtained from high-level *ab initio* calculations (or from experimental databases in case of BAC parameters).
2) The unknown parameters are identified based on the molecular structures of the stable species or reactant(s)/products(s) of each reaction included in the training set. Initial values for these parameters are determined via linear regression of the training set, i.e. BAC parameters, GAV and NNI parameters for thermodynamics and ΔGAV° and ΔRES° for kinetics.
3) The performance of the regressed parameters is validated making use of a test set, which contains a limited number of species/reactions not included in the training set.

4) If a good performance is obtained, the final set of optimized parameters is obtained via regression of the combined training and test set. If this not the case, the parameter identification (corresponding to step 2) needs to be reassessed.

2.5 Kinetic modeling

Accurate chemical kinetic models are extremely powerful and valuable. They provide a starting point for gaining fundamental understanding of the underlying, controlling chemistry of several important industrial processes. In the chemical industry, detailed kinetic models have become an important asset to chemical engineers. The combination of a detailed kinetic model and simulation software results in an accurate prediction of the species concentrations, reaction rates, rates of production, but also other parameters such as heat transfer, pressure drop, etc. Hence, kinetic models cannot only be used for the design of an industrial plant, but also for the optimization of the day-to-day production by a facile exploration of diverse processing scenarios, such as a change in feedstock.

For the majority of the technologically important processes, e.g. pyrolysis, oxidation and combustion, these kinetic models can become very large, i.e. they can contain hundreds of species and thousands of reactions [1]. When considering such large models, it becomes obvious that the manual construction of such detailed kinetic models poses an almost impossible, or in either case a very time-consuming and error-prone task. This high complexity has motivated the development of automatic kinetic model generators, which cannot only be used to create the network, but also to assign accurate parameters to all species and reactions. The automatic kinetic model generator Genesys is used for the model construction for most of the model components in this PhD thesis. The main features of Genesys are discussed below. The reader is referred to Vandewiele et al. [28] and Van de Vijver et al. [1] for a more detailed explanation.

An initial set of species is provided as input to Genesys making use of either SMILES [29] or InChI [30] line identifiers. For the representation of molecules in the software, the molecule identifiers are converted to weighted graph structures by making use of the chemo informatics toolkit CDK [31]. An example of SMILES and InChI line identifiers for diethylamine as well as the representation of the weighted graph structure can be found in Figure 2-3.

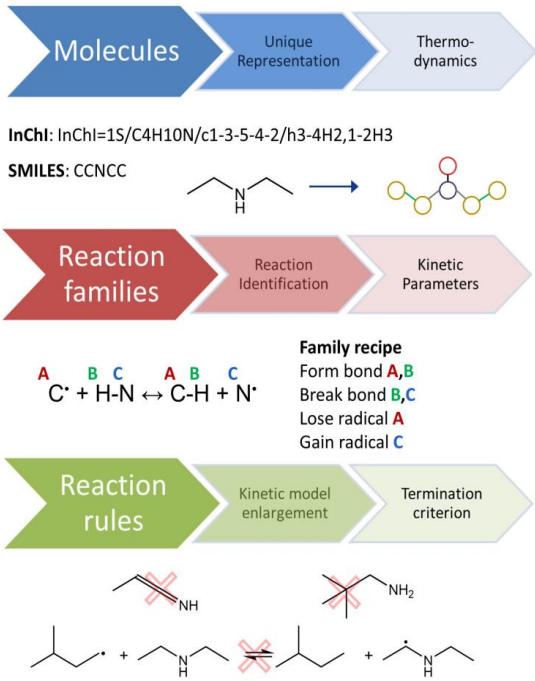

Figure 2-3: Schematic overview of the essential elements of the automatic kinetic model generator Genesys.

Genesys creates kinetic models based on the widely adopted strategy of condensing the relevant chemistry that molecules can undergo in reaction families [32]. The reaction family concept is the direct extension of the idea that sub-molecular patterns and more specifically functional groups inside a chemical species govern the reactivity of a molecule rather than the molecule in its entirety. Each reaction family specifies the rearrangement of bonds and atoms to go from the reactant(s) to the product(s) through the course of an elementary reaction. An example is the hydrogen abstraction by a carbon-centered radical from a N-H bond, c.f. Figure 2-3. The labels A,B and C are used to denote the reactive centers as defined in the family recipe. In addition to the list of reactants, the user must provide all possible reaction families that need to be considered in the network generation process as input to Genesys. The reactive moieties are defined by the user using the substructure SMARTS chemical language.

The algorithm that generates and systematically enlarges the reaction network starts from the set of input species and user-defined reaction families The input species are added to the pool of unreacted species or so-called source species. After selecting a species from the pool and adding it to the list of already reacted species (core species), it is checked whether it is eligible to undergo a specified reaction family. The possible molecular constraints are verified and the

subgraph isomorphism algorithm scans the species for the required reactive moiety. If the constraints are met and the particular reactive moiety is present, the product species emerge after the execution of the reaction family. In case of a bimolecular reaction, all core species are tested as second reactant. The product species can be added to the pool of unreacted species, only if they are not included yet in this list or in the list of reacted species. The reaction network enlargement phase finalizes with an empty pool of unreacted species.

To limit the kinetic model enlargement, a rule-based or rate-based termination criterion can be applied. In case of a rule-based termination criterion, rules or constraints are specified for the reaction families and the product species to prevent the formation of insignificant species and reactions. For example, user-defined rules can be adopted to limit the number of heavy atoms (or even atom types) or to avoid the formation of molecules with two consecutive double bonds. The chemical knowledge of the user can also be incorporated in a rule to evaluate whether or not a certain reactant species is eligible to undergo the structural rearrangements as defined by the reaction family. This can be translated in a number of constraints for a certain reaction family, for example hydrogen abstraction by carbon-centered radicals containing a maximum of five heavy (non-hydrogen) atoms. As an alternative, the rate-based criterion can be applied, which has a higher computational cost, but does not rely on prior knowledge of the chemistry. All of the possible product species are generated starting from an initial set of input species by performing on-the-fly reactor simulations with the CHEMKIN software [33]. Whether or not they are added to the reaction mechanism, depends on their calculated rate of formation. Only the product species with the highest rate are deemed significant and hence are added to the reaction network. All the reactions generated by the reaction families are implemented in the kinetic model as reversible reactions to preserve thermodynamic consistency.

After the generation of the network, thermodynamic and kinetic parameters are assigned to all species and reactions. Genesys is connected with user-defined databases containing species and reactions data from quantum chemical calculations at the CBS-QB3 level of theory, with the methodology as reported by Van de Vijver et al. [6]. If available, entries from these database are used. In case no unique data is available for the species and reactions, the group additivity method is applied to approximate the thermodynamic and kinetic parameters. The group additivity parameters used in this approximation procedure have been derived from a database of quantum chemical data. The use of the group additivity method to approximate the thermodynamic and kinetic parameters for the N-H hydrogen abstraction in diethylamine by a hydrogen atom is shown in Figure 2-4.

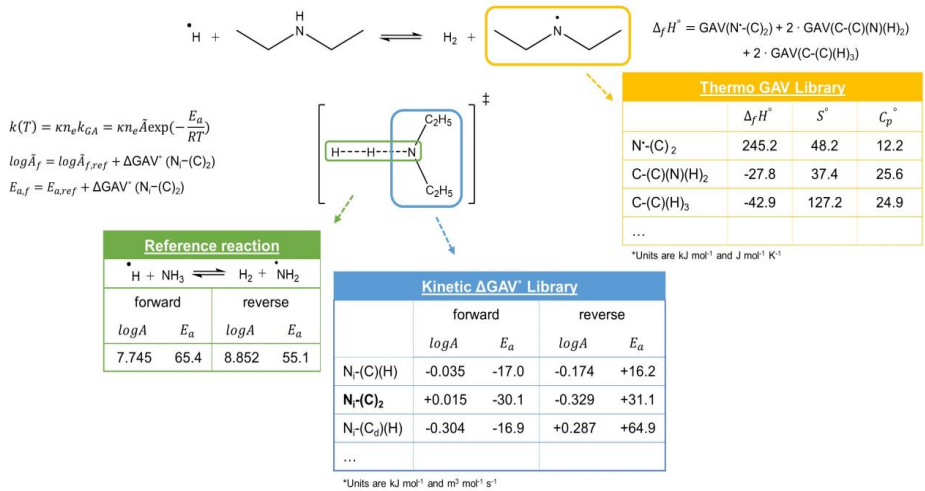

Figure 2-4: Use of the group additivity method to approximate the thermodynamic and kinetic parameters for the N-H hydrogen abstraction from diethylamine by a hydrogen atom.

In the post-processing step, human readable output formation is generated. The assigned thermodynamic properties for all species are provided as NASA polynomials in the output, c.f. Equations Eq. 2-35 - Eq. 2-37.

$$\frac{C_p(T)}{R} = a_1 + a_2 \cdot T + a_3 \cdot T^2 + a_4 \cdot T^4 + a_5 \cdot T^5 \qquad \text{(Eq. 2-35)}$$

$$\frac{\Delta_f H(T)}{R} = a_1 \cdot T + \frac{a_2 \cdot T^2}{2} + \frac{a_3 \cdot T^3}{3} + \frac{a_4 \cdot T^4}{4} + \frac{a_5 \cdot T^5}{5} + a_6 \qquad \text{(Eq. 2-36)}$$

$$\frac{S(T)}{R} = a_1 \cdot \ln(T) + a_2 \cdot T + \frac{a_3 \cdot T^2}{2} + \frac{a_4 \cdot T^3}{3} + \frac{a_5 \cdot T^4}{4} + a_7 \qquad \text{(Eq. 2-37)}$$

The output format of the kinetic model is dependent on the chemical reactor software package used for model simulations. By default, the input format is generated for integration with CHEMKIN.

2.6 Conclusions

In this PhD thesis a microkinetic modeling approach is used to acquire insight in the chemistry during the pyrolysis or oxidation of nitrogen-, oxygen- and sulfur-containing model compounds. This entails kinetic model construction, quantum chemistry calculations to determine thermodynamic and kinetic parameters and experiments to evaluate the model performance.

The kinetic models are generated using the in-house developed kinetic model generator software Genesys. A list of species represented by a SMILES of InChI identifier and all possible reaction families is required as input for the kinetic model generator. For the assignment of thermodynamic and kinetic parameters, Genesys is connected to user-defined databases with data obtained from quantum chemical calculations at the CBS-QB3 level of theory. If no such accurate data is available, Genesys makes use of the group additivity method for an efficient on-the-fly estimation of thermodynamic and kinetic parameters. For key species and reactions, parameters obtained from quantum chemical calculations at the CBS-QB3 level of theory are provided.

To address the scarcity of accurate thermodynamic and kinetic parameters for the compounds of interest, new group additivity schemes are determined via the unweighted least-squares linear regression analysis method. An assessment of the reliability of this linear regression procedure is performed via the use of several statistical parameters, while the transferability of the regressed parameters using the so-called training set is validated using a second dataset, which has not yet seen that data, i.e. the test set.

2.7 References

[1] R. Van de Vijver, N.M. Vandewiele, P.L. Bhoorasingh, B.L. Slakman, F.S. Khanshan, H.H. Carstensen, M.F. Reyniers, G.B. Marin, R.H. West, K.M. Van Geem, Automatic Mechanism and Kinetic Model Generation for Gas- and Solution-Phase Processes: A Perspective on Best Practices, Recent Advances, and Future Challenges, International Journal of Chemical Kinetics 47 (2015) 199-231.

[2] G. Andrew, Introduction to Computational Quantum Chemistry: Theory.

[3] J.A.M. Jr., M.J. Frisch, J.W. Ochterski, G.A. Petersson, A complete basis set model chemistry. VI. Use of density functional geometries and frequencies, The Journal of Chemical Physics 110 (1999) 2822-2827.

[4] M.J. Frisch, G.W. Trucks, H.B. Schlegel, G.E. Scuseria, M.A. Robb, J.R. Cheeseman, G. Scalmani, V. Barone, B. Mennucci, G.A. Petersson, H. Nakatsuji, M. Caricato, X. Li, H.P. Hratchian, A.F. Izmaylov, J. Bloino, G. Zheng, J.L. Sonnenberg, M. Hada, M. Ehara, K. Toyota, R. Fukuda, J. Hasegawa, M. Ishida, T. Nakajima, Y. Honda, O. Kitao, H. Nakai, T. Vreven, J.A. Montgomery Jr., J.E. Peralta, F. Ogliaro, M.J. Bearpark, J. Heyd, E.N. Brothers, K.N. Kudin, V.N. Staroverov, R. Kobayashi, J. Normand, K. Raghavachari, A.P. Rendell, J.C. Burant, S.S. Iyengar, J. Tomasi, M. Cossi, N. Rega, N.J. Millam, M. Klene, J.E. Knox, J.B. Cross, V. Bakken, C. Adamo, J. Jaramillo, R. Gomperts, R.E. Stratmann, O. Yazyev, A.J. Austin, R. Cammi, C. Pomelli, J.W. Ochterski, R.L. Martin, K. Morokuma, V.G. Zakrzewski, G.A. Voth, P. Salvador, J.J. Dannenberg, S. Dapprich, A.D. Daniels, Ö. Farkas, J.B. Foresman, J.V. Ortiz, J. Cioslowski, D.J. Fox, Gaussian 09, Gaussian, Inc., Wallingford, CT, USA, 2009.

[5] M.J. Frisch, G.W. Trucks, H.B. Schlegel, G.E. Scuseria, M.A. Robb, J.R. Cheeseman, G. Scalmani, V. Barone, G.A. Petersson, H. Nakatsuji, X. Li, M. Caricato, A.V. Marenich, J. Bloino, B.G. Janesko, R. Gomperts, B. Mennucci, H.P. Hratchian, J.V. Ortiz, A.F. Izmaylov, J.L. Sonnenberg, Williams, F. Ding, F. Lipparini, F. Egidi, J. Goings, B. Peng, A. Petrone, T. Henderson, D. Ranasinghe, V.G. Zakrzewski, J. Gao, N. Rega, G. Zheng, W. Liang, M. Hada, M. Ehara, K. Toyota, R. Fukuda, J. Hasegawa, M. Ishida, T. Nakajima, Y. Honda, O. Kitao, H. Nakai, T. Vreven, K. Throssell, J.A. Montgomery Jr., J.E. Peralta, F. Ogliaro, M.J. Bearpark, J.J. Heyd, E.N. Brothers, K.N. Kudin, V.N. Staroverov, T.A. Keith, R. Kobayashi, J. Normand, K. Raghavachari, A.P. Rendell, J.C. Burant, S.S. Iyengar, J. Tomasi, M. Cossi, J.M. Millam,

M. Klene, C. Adamo, R. Cammi, J.W. Ochterski, R.L. Martin, K. Morokuma, O. Farkas, J.B. Foresman, D.J. Fox, Gaussian 16 Rev. B.01, Wallingford, CT, 2016.

[6] R. Van de Vijver, K.M. Van Geem, G.B. Marin, On-the-fly ab initio calculations toward accurate rate coefficients, Proceedings of the Combustion Institute 37 (2019) 283-290.

[7] P. Vansteenkiste, V. Van Speybroeck, G.B. Marin, M. Waroquier, Ab Initio Calculation of Entropy and Heat Capacity of Gas-Phase n-Alkanes Using Internal Rotations, The Journal of Physical Chemistry A 107 (2003) 3139-3145.

[8] A.L.L. East, L. Radom, Ab initio statistical thermodynamical models for the computation of third-law entropies, The Journal of Chemical Physics 106 (1997) 6655-6674.

[9] V. Van Speybroeck, Ab initio and dynamic methods : A useful tool in the study of chemical reactions, Center for Molecular Modeling, Ghent University, 2001.

[10] M.K. Sabbe, M. Saeys, M.F. Reyniers, G.B. Marin, V. Van Speybroeck, M. Waroquier, Group additive values for the gas phase standard enthalpy of formation of hydrocarbons and hydrocarbon radicals, Journal of Physical Chemistry A 109 (2005) 7466-7480.

[11] M.K. Sabbe, F. De Vleeschouwer, M.-F. Reyniers, M. Waroquier, G.B. Marin, First Principles Based Group Additive Values for the Gas Phase Standard Entropy and Heat Capacity of Hydrocarbons and Hydrocarbon Radicals, The Journal of Physical Chemistry A 112 (2008) 12235-12251.

[12] L.A. Curtiss, K. Raghavachari, P.C. Redfern, J.A. Pople, Assessment of Gaussian-2 and density functional theories for the computation of enthalpies of formation, The Journal of Chemical Physics 106 (1997) 1063-1079.

[13] P.J. Lindstrom, W.G. Mallard, NIST Chemistry WebBook, NIST Standard Reference Database Number 69, National Institute of Standards and Technology, Gaithersburg MD.

[14] G.A. Petersson, D.K. Malick, W.G. Wilson, J.W. Ochterski, J.A. Montgomery Jr., M.J. Frisch, Calibration and comparison of the Gaussian-2, complete basis set, and density functional methods for computational thermochemistry, Journal of Chemical Physics 109 (1998) 10570 - 10579.

[15] D.G. Truhlar, B.C. Garrett, S.J. Klippenstein, Current Status of Transition-State Theory, The Journal of Physical Chemistry 100 (1996) 12771-12800.

[16] E. Pollak, P. Pechukas, Symmetry Numbers, Not Statistical Factors, Should be Used in Absolute Rate Theory and in Bronsted Relations, Journal of the American Chemical Society 100 (1978) 2984-2991.

[17] S.W. Benson, J.H. Buss, Additivity Rules for the Estimation of Molecular Properties. Thermodynamic Properties, The Journal of Chemical Physics 29 (1958) 546-572.

[18] N.M. Vandewiele, R. Van de Vijver, K.M. Van Geem, M.F. Reyniers, G.B. Marin, Symmetry calculation for molecules and transition states, Journal of Computational Chemistry 36 (2015) 181-192.

[19] M. Saeys, M.-F. Reyniers, G.B. Marin, V. Van Speybroeck, M. Waroquier, Ab Initio Calculations for Hydrocarbons: Enthalpy of Formation, Transition State Geometry, and Activation Energy for Radical Reactions, The Journal of Physical Chemistry A 107 (2003) 9147-9159.

[20] M. Saeys, M.F. Reyniers, G.B. Marin, V. Van Speybroeck, M. Waroquier, Ab initio group contribution method for activation energies for radical additions, AIChE Journal 50 (2004) 426-444.

[21] M.K. Sabbe, M.F. Reyniers, V. Van Speybroeck, M. Waroquier, G.B. Marin, Carbon-centered radical addition and beta-scission reactions: Modeling of activation energies and pre-exponential factors, Chemphyschem 9 (2008) 124-140.

[22] M.K. Sabbe, A.G. Vandeputte, M.F. Reyniers, M. Waroquier, G.B. Marin, Modeling the influence of resonance stabilization on the kinetics of hydrogen abstractions, Physical Chemistry Chemical Physics 12 (2010) 1278-1298.

[23] A.G. Vandeputte, M.K. Sabbe, M.F. Reyniers, G.B. Marin, Kinetics of alpha hydrogen abstractions from thiols, sulfides and thiocarbonyl compounds, Physical Chemistry Chemical Physics 14 (2012) 12773-12793.

[24] A.G. Vandeputte, M.F. Reyniers, G.B. Marin, Kinetics of Homolytic Substitutions by Hydrogen Atoms at Thiols and Sulfides, Chemphyschem 14 (2013) 1703-1722.

[25] P.D. Paraskevas, M.K. Sabbe, M.F. Reyniers, N.G. Papayannakos, G.B. Marin, Kinetic Modeling of a-Hydrogen Abstractions from Unsaturated and Saturated Oxygenate Compounds by Hydrogen Atoms, Journal of Physical Chemistry A 118 (2014) 9296-9309.

[26] P.D. Paraskevas, M.K. Sabbe, M.F. Reyniers, N.G. Papayannakos, G.B. Marin, Group Additive Kinetics for Hydrogen Transfer Between Oxygenates, Journal of Physical Chemistry A 119 (2015) 6961-6980.

[27] P.D. Paraskevas, M.K. Sabbe, M.F. Reyniers, G.B. Marin, N.G. Papayannakos, Group additive kinetic modeling for carbon-centered radical addition to oxygenates and -scission of oxygenates, Aiche Journal 62 (2016) 802-814.

[28] N.M. Vandewiele, K.M. Van Geem, M.F. Reyniers, G.B. Marin, Genesys: Kinetic model construction using chemo-informatics, Chemical Engineering Journal 207 (2012) 526-538.

[29] D. Weininger, SMILES, a chemical language and information system. 1. Introduction to methodology and encoding rules, Journal of Chemical Information and Computer Sciences 28 (1988) 31-36.

[30] S.R. Heller, A. McNaught, I. Pletnev, S. Stein, D. Tchekhovskoi, InChI, the IUPAC International Chemical Identifier, Journal of Cheminformatics 7 (2015) 34.

[31] C. Steinbeck, C. Hoppe, S. Kuhn, M. Floris, R. Guha, E.L. Willighagen, Recent developments of the Chemistry Development Kit (CDK) - An open-source Java library for chemo- and bioinformatics, Current Pharmaceutical Design 12 (2006) 2111-2120.

[32] E. Blurock, F. Battin-Leclerc, T. Faravelli, W.H. Green, Automatic Generation of Detailed Mechanisms, in: F. Battin-Leclerc, J.M. Simmie, E. Blurock (Eds.), Cleaner Combustion: Developing Detailed Chemical Kinetic Models, Springer London, London, 2013, pp. 59-92.

[33] R.J. Kee, F.M. Rupley, J.A. Miller, M.E. Coltrin, J.F. Grcar, E. Meeks, H.K. Moffat, A.E. Lutz, G. Dixon-Lewis, M.D. Smooke, J. Warnatz, G.H. Evans, R.S. Larson, R.E. Mitchell, L.R. Petzold, W.C. Reynolds, M. Caracotsios, W.E. Stewart, P. Glarborg, C. Wang, O. Adigun, Chemkin-Pro 15112, Reaction Design: San Diego, CA, USA, (2011).

3

Thermochemistry of nitrogen-containing compounds

Abstract

A prerequisite for the generation of detailed fundamental kinetic models is the availability of accurate thermodynamic properties. To address the scarcity of accurate experimental data, theoretical calculations and approximation methods based on these calculations can be used. The accuracy of these quantum chemistry methods for determination of the standard enthalpy of formation can be improved by making use of empirical correction methods, such as the isodesmic Bond Additivity Correction (BAC) method. In this work, *ab initio* calculations have been performed for a set of 371 species to determine a new set of 26 BAC parameters for the CBS-QB3 level of theory via linear regression analysis. This broad dataset of hydrocarbons and heteroatomic compounds contains (non)-cyclic molecules with a wide range of functional groups consisting of hydrogen, carbon, oxygen, nitrogen and sulfur atoms. The CBS-QB3 method combined with BACs succeeds in approximating the experimental standard enthalpy of formation at 298 K with an accuracy of 4 kJ mol^{-1} for almost all species. The BACs reduce the mean absolute deviation (MAD) for the complete dataset from 5.6 to 2.4 kJ mol^{-1}.

To address the scarcity of thermodynamic parameters for nitrogen-containing compounds, a consistent set of a total of 91 group additive values and three non-nearest-neighbor interactions have been determined from a dataset of CBS-QB3 calculations for 300 species, including 104 radicals. This dataset contains a wide range of nitrogen-containing functionalities, i.e. imine, nitrile, nitro, nitroso, nitrite, nitrate and azo functional groups. The group additivity model enables the approximation of the standard enthalpy of formation and standard entropy at 298 K as well as the standard heat capacities over a large temperature range, i.e. 300-1500 K. For a test set of 27 nitrogen-containing compounds, the group additivity model succeeds in approximating the *ab initio* calculated values for the standard enthalpy of formation with a

MAD of 2.3 kJ mol^{-1}. The MAD for the standard entropy and heat capacity is lower than 4 and 2 J mol^{-1} K^{-1}, respectively. For a test set of 11 nitrogen-containing compounds, the MAD between experimental and group additivity approximated values for the standard enthalpy of formation amounts to 2.8 kJ mol^{-1}.

This Chapter is based on the following publication:

Bond additivity corrections for CBS-QB3 calculated standard enthalpies of formation of H, C, O, N and S containing species. Pappijn C.A.R.; Vermeire F.H.; Van de Vijver R.; Reyniers M.-F.; Marin G.B.; Van Geem K.M. **International Journal of Chemical Kinetics**, 53, 345-355, 2021

3.1. Introduction

To enable reactor simulations, thermodynamic parameters need to be assigned to all species in a kinetic model. These are important while solving the energy equations and for the determination of reaction rates for reverse reactions via thermodynamic consistency. Due to the large number of species, many of which are radicals, obtaining experimental values for all these parameters is nearly impossible. To address the scarcity of reliable experimental data, theoretical calculations and approximation methods based on these calculations or on experiments are typically used [1]. It is important that reliable thermodynamic data are at hand for each of the species involved, as an under- or overestimation of the stability of intermediate compounds can result in for example the overlooking of important reaction paths during the actual simulation of the kinetic model.

The accuracy of the calculated thermodynamic properties depends on the employed model chemistry, i.e. the combination of level of theory and basis set. Ideally, in a kinetic model all standard enthalpies of formation should be within "chemical accuracy", which is often used to indicate the level of accuracy that matches the experimental uncertainty. The most commonly used values in the literature are 4 kJ mol^{-1} or 1 kcal mol^{-1} (4.184 kJ mol^{-1}) [2, 3]. According to the definition of Ruscic et al. [4], an uncertainty of 1 kcal mol^{-1} means that the 95% confidence interval is lower than 1 kcal mol^{-1}. An error of 1 kcal mol^{-1} on the enthalpy or a similar error of 1 cal mol^{-1} K^{-1} on the entropy corresponds to an error of about a factor of two on the rate coefficient at 1000 K. With high-level electronic structure methods based on coupled cluster calculations, which are considered to be the current gold-standard in model chemistries, this accuracy is within reach [5]. However, in spite of recent advances in computational capabilities, these methods remain limited in their application to molecules containing a large number of heavy (non-hydrogen) atoms [6]. This means that the use of these high-accuracy methods for the large range of molecules encountered in detailed chemical kinetic models is computationally too expensive. Composite methods, such as the CBS-QB3 method [7], are in widespread use across a range of different fields, due to their lower computational cost [8]. To assess the accuracy of this cost-effective alternative, Simmie et al. [9] benchmarked the CBS-QB3 method against the Active Thermochemical Tables (ATcT) [10]. For a dataset of 45 non-radical species containing between one to eight heavy atoms, the CBS-QB3 method is able to predict the ATcT values with a mean absolute deviation (MAD) of 6.1 kJ mol^{-1}. For 38 radical H/C/O species, the MAD amounts to 3.4 kJ mol^{-1} [11]. For a set of 28 nitrogen-containing molecules with an average of only three heavy atoms, the ATcT values are predicted with a MAD of 2.9 kJ mol^{-1}

[12]. This accuracy of the CBS-QB3 method is in agreement with the MAD of 4.6 kJ mol^{-1} originally reported by Montgomery et al. [7] for a dataset of 148 experimental standard enthalpies of formation at 298 K.

Because of the systematic nature of the deviations between experimental and theoretical values, correction methods can be used to improve the accuracy of the CBS-QB3 method [13]. The Bond Additive Correction (BAC) method developed by Petersson et al. [13] takes into account a contribution per bond type to correct the calculated standard enthalpy of formation. In case a large database of experimental data is lacking to determine separate contributions for each bond type, the Atom Additive Correction method can be used, which introduces more generic corrections per atom type [14]. Melius et al. [15] proposed a correction method with combined atom and bond corrections, which involves fitting of three parameters per atom type [16, 17]. Using these error-cancellation strategies, it has been shown that CBS-QB3 can predict the experimental values with chemical accuracy for hydrocarbons [18], oxygenates [19], organosulfur [8] and aromatic species [20]. In previous work [18-20], BACs have been determined for the CBS-QB3 method making use of datasets consisting of a limited number of small molecules and focusing on certain classes, such as hydrocarbons or oxygenates. Recently, Ince et al. [20] determined a new set of BAC values making use of a data set of 77 H/C/O molecules via the least-squares regression procedure. The MAD over the complete dataset is reduced from 8.2 to 1.4 kJ mol^{-1} when applying BACs.

Experimental thermochemical data available for molecules containing H/C/O/N/S is relatively limited and less accurate compared to H/C/O containing species. This lack of accurate experimental data is partly due to the high cost and time consuming nature of experiments, but also due to the aggregation state of the considered nitrogen compounds. For radicals, experimental data is even more scarce, mainly due to their instable nature and hence difficult determination. An alternative approach to obtain accurate thermodynamic values is to make use of computational methods. Computational chemical calculations are able to provide accurate thermochemistry values for all the gas phase species appearing in a reaction network [14]. Recent developments in processor technology, such as the use of multicore processers, have been beneficial for computational chemistry. However, in spite of this ever-growing computational power, performing on-the-fly *ab initio* calculations for each species during automated kinetic model generation remains computationally too expensive, especially for larger compounds. Therefore, as an alternative, high-level *ab initio* calculations are frequently performed for only a limited set of well-chosen smaller molecules. By making use of possible

approximation procedures based on parameters derived from this data set, the thermodynamic parameters of a broad range of molecules can then be calculated. The most widely used approximation method is the group additivity method as proposed by Benson [21], the theory of which has been introduced in Chapter 2. This method is based on an analogy between atoms in small molecules and atoms in large molecules but with similar surroundings. Using this method, it is possible to estimate the thermodynamic properties of species based on a limited number of parameters, the so-called group additive values (GAVs).

The main advantage of this approximation method is that it can easily be implemented in computer codes for a fast and accurate estimation of the thermodynamic parameters. Furthermore, if certain GAVs are not yet available, additional *ab initio* calculations can be performed to complement the GAV database. Also, in order to improve the accuracy of the estimated parameters for certain compounds, correction factors can be introduced, such as non-nearest-neighbor interactions or resonance interactions. Only a limited number of GAVs for non-radical nitrogen-containing compounds has been reported in literature. Based on experimental data, Benson et al. [22] derived 28 GAVs for nitrogen-centered groups and 26 carbon-centered groups with a nitrogen ligand. Their experimental dataset includes amine, imine, nitrile, amide, imide, nitro, nitroso, nitrite and azo functional groups. Due to the scarcity of experimental data, the accuracy of the reported Benson groups is lower and more variable as for the hydrocarbons. In addition, a significant number of Benson groups have been determined from only one molecular structure. Holmes and Aubry [23, 24] revised the GAV values for the standard enthalpy of formation using a combination of experimental and computational data. Ashcraft et al. [25] derived new GAV values from a database of CBS-QB3 calculations for 105 non-cyclic molecules. The molecules contain, amine, imine, nitrile, nitro, nitroso, nitrite, nitrate and azo functional groups. Because no GAVs are available for radical-centered nitrogen-containing groups as well as for a large number of other nitrogen functionalities, the set of GAVs available in literature is insufficient to study even small reaction schemes for nitrogen-containing compounds.

In the first part of this Chapter, a new set of BACs is derived to improve the accuracy of the standard enthalpy of formation at 298 K obtained from *ab initio* calculations at the CBS-QB3 level of theory. For a dataset of 371 molecules with a range from one to ten heavy (non-hydrogen) atoms, *ab initio* calculations are performed and experimental data is gathered from ATcT, Pedley et al. [26] and the NIST Chemistry Webbook [27]. This extensive dataset contains species consisting of the elements hydrogen, carbon, oxygen, nitrogen and sulfur

including cyclic, aromatic and radical species. The complete dataset is divided in two parts: a training set of 328 species to determine the initial set of BACs and a test set of 43 species to assess the performance of these BACs. To determine the final set of BACs, all species in both datasets are used. Three examples are discussed to demonstrate the use and the performance of these new BACs. In the second part of this Chapter, a dataset of CBS-QB3 calculations for 196 nitrogen-containing compounds and 104 nitrogen-containing radicals is used to determine 91 GAVs and three non-nearest-neighbor interactions. The GAVs enable the approximation of the standard enthalpy of formation and standard entropy at 298 K and the standard heat capacities over a temperature range 300-1500 K for a large set of nitrogen-containing compounds, including imine, nitrile, nitro, nitroso, nitrite, nitrate and azo functional groups. Similar to the BACs, the complete dataset is divided in two parts: a training set of 274 species to determine the initial set of GAVs and a test set of 26 species to assess the performance of these GAVs. An additional validation of the GAV scheme is performed with a second test set with 11 nitrogen-containing species, for which experimental values for the standard enthalpy of formation has been collected. The application of the group additivity method for nitrogen-containing species is demonstrated with two examples.

3.2. Bond additivity corrections

3.2.1. Methodology

Since its introduction in 1998, BACs have been widely used to improve the accuracy of theoretical calculations to approximate the standard enthalpy of formation. Similar to the well-known group additivity method developed by Benson et al. [22], this correction method is based on the idea that the property of a molecule can be obtained by summing up the separate contributions from its constituent parts. For the BAC method, the assumption is made that the error in the *ab initio* calculated standard enthalpy of formation of a molecule is equal to the sum of the errors of the different bonds. Determination of a new set of BACs requires a species database with experimental and *ab initio* calculated values for the standard enthalpy of formation. The BACs are obtained by unweighted least-squares analysis, for which the governing Equations can be found in Chapter 2. In Eq. 3-1, y_i is the experimental standard enthalpy of formation ($\Delta_f H^{\circ}_{EXP}$) of molecule i and $\hat{y}_i$ is the corrected CBS-QB3 calculated value, i.e. including SOCs and BACs ($\Delta_f H^{\circ}_{atom+SOC+BAC}$).

$$SSQ = \sum_{i}^{n} (y_i - \hat{y}_i)^2 \qquad \text{(Eq. 3-1)}$$

This leads to the following Eq. 3-2 for the optimized set of BAC parameters.

$$\overline{BAC} = (X^T X)^{-1} X^T y \qquad \text{(Eq. 3-2)}$$

$\overline{BAC}$ is the estimated vector of the BAC parameters, X is the matrix in which the elements X_{ij} specify the number of occurrences of BAC j in the molecule i and $\bar{y}$ is the vector containing the differences between the experimental and CBS-QB3 calculated values, including SOCs. The dimensions of the matrix X are M x N with N being the number of BACs and M the number of molecules in the reference dataset used to obtain the BACs. The methodology used to calculate a new set of BACs in this work is illustrated in Figure 3-1.

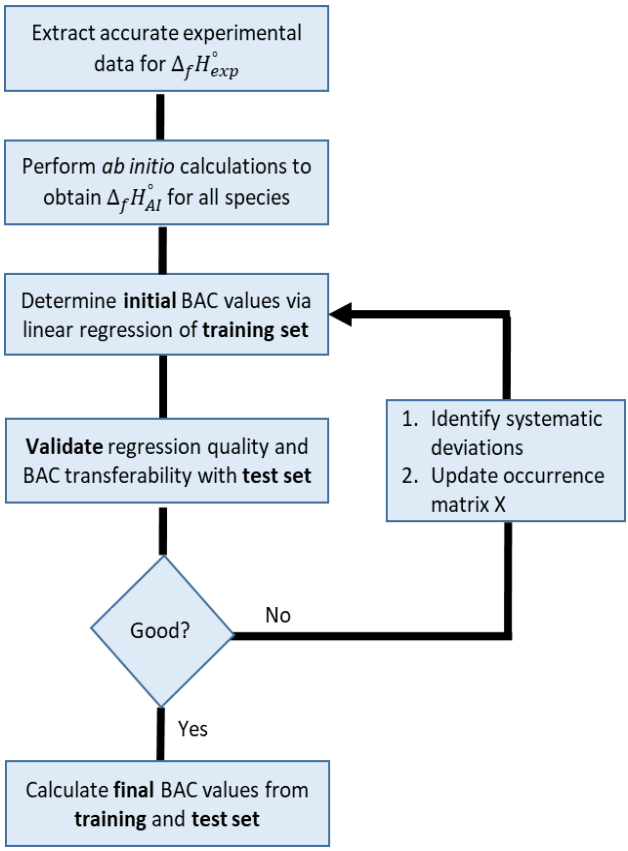

Figure 3-1: Methodology to determine a new set of bond additivity corrections (BAC) for hydrocarbons, oxygenates, nitrogen- and sulfur-containing species.

First, an experimental database is constructed by extracting data from different literature sources. Experimental standard enthalpies of formation are taken from ATcT [10, 28, 29], Pedley et al. [26] and the NIST Chemistry Webbook [27]. The ATcT values used in this work are based on TV ver. 122d [10]. Only experimental values with a reported uncertainty smaller than 3.0 kJ mol^{-1} are considered for all three sources, in agreement with Saeys et al. [14, 18]. Hydrocarbons, oxygenates, sulfur- and nitrogen-containing compounds are included with a range of one to ten heavy atoms, including radical species. For hydrocarbons, alkanes, alkenes, alkynes, cyclic non-aromatic and aromatic species are considered. The studied oxygen-containing compounds can be divided in alcohols, aldehydes, ethers, esters, ketones, and carboxylic esters. The nitrogen-containing species include amines, imines, nitriles, amides as well as a limited number of N/O-functionalities. The main sulfur-containing groups are thiols, (di-)sulfides and sulfoxides. By considering such a wide range of molecule classes, the most important functionalities are taken into account for the regression of new BACs. Note that species with more than one heteroatom are also included in the database. The complete database contains 371 molecules, including 41 radicals.

In a next step, *ab initio* calculations are performed to calculate the standard enthalpy of formation at 298 K of for each molecule. For radical species, no distinction is made between an atom with and without a radical center. For example, both ethane (C_2H_6) and the ethyl radical ($C_2H_5^{\cdot}$) are both assigned one C-C BAC and six and five C-H BACs respectively. Aromatic bonds, denoted as a bond between two atoms X_a, are distinguished from non-aromatic bonds. This leads to five types of aromatic BACs: C_a-C_a, C_a-O_a, C_a-N_a, C_a-S_a and N_a-N_a. For all bonds between an aromatic and non-aromatic atom, X_a is taken equal to X.

For the third step, the complete dataset is divided in a training and test set. The molecules in the test set represent a random selection of approximately 10% of all molecules included. The regression is first performed using the training set after which the obtained BACs are validated against the test set. Note that the set of BACs obtained from only the training set data are denoted as the preliminary BAC values. Except for the BACs of N_a-N_a and S=O, at least three different molecules are included in the complete dataset for the determination of each BAC. Note that SOCs are applied to the *ab initio* calculated values prior to the regression step. If a satisfactory agreement, i.e. a mean absolute deviation below 4 kJ mol^{-1}, is obtained between experimental and BAC corrected values, the final BACs are determined using both training and test set. These new BACs, can deviate slightly from the previously calculated values, but they improve the overall accuracy of the model. For the statistical analysis of the linear regression

step, the parameters as discussed in Chapter 2 are used, i.e. significance of the regression (*F*), mean deviation (MD), mean absolute deviation (MAD), root-mean-square deviation (RMS) and maximum deviation (MAX).

3.2.2. Results and discussion

3.2.2.1. Ab initio calculations

The *ab initio* calculated standard enthalpies of formation for all 371 molecules of the complete dataset are given in Table A-1 of Appendix A. Note that all molecules in the dataset have been calculated in their singlet or doublet state. For large deviations between calculated and experimental data, the triplet states have also been calculated, but in all cases the triplet state was significantly higher in energy. For the calculation of the standard enthalpy of formation, rotations around internal bonds are treated using the one-dimensional hindered rotor (1D-HIR) approximation. To investigate the influence of this approximation on the value of the standard enthalpy of formation, the 1D-HIR corrections have been calculated for an alkane, alcohol, amine and thiol with a chain length of four, c.f. Table 3-1. The difference between the standard enthalpies of formation with and without 1D-HIR corrections is similar for all four molecules, with the largest difference for the nitrogen-containing compound. The BACs obtained in this work are regressed on standard enthalpies of formation including 1D-HIR corrections. Using these BACs to correct values obtained with the harmonic oscillator approach, will result in additional errors.

Table 3-1: 1D-HIR corrections on the CBS-QB3 standard enthalpy of formation [kJ mol^{-1}].

Molecule	$\Delta_f H^{\circ}_{AI,HIR} - \Delta_f H^{\circ}_{AI,HO}$ [kJ mol^{-1}]
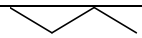	1.7
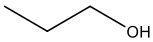	1.9
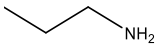	2.3
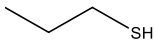	1.9

To investigate the influence of the employed basis set of the 1D-HIR corrections on the standard enthalpy of formation, the corrections have been calculated for five different molecules with the B3LYP functional using two different basis sets, i.e. 6-31G(d) and G-311G(2d,d,p), c.f. Table 3-2. Note that the considered molecules contain at least two different heteroatoms. The

difference between the corrections caused by a larger basis set size is more than one order of magnitude smaller than the desired accuracy of the *ab initio* calculated standard enthalpy of formation, i.e. 4 kJ mol^{-1}. For all molecules in the dataset, the hindrance potentials used for the 1D-HIR corrections have been determined at the B3LYP/6-31G(d) level of theory.

Table 3-2: 1D-HIR corrections on the CBS-QB3 standard enthalpy of formation [kJ mol^{-1}] calculated with the B3LYP functional using two different basis sets, i.e. 6-31G(d) and 6-311G(2d,d,p).

Molecule	$\Delta_f H^\circ_{AI,HIR} - \Delta_f H^\circ_{AI,HO}$ [kJ mol^{-1}]	
	6-31G(d)	6-311G(2d,d,p)
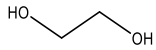	0.86	0.54
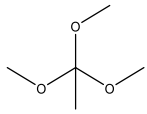	0.96	0.71
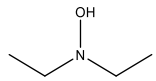	2.57	2.40
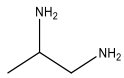	0.03	0.15
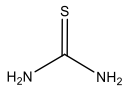	1.18	0.75

3.2.2.2. Comparison between ab initio calculated and experimental data

Figure 3-2 shows the differences between the uncorrected CBS-QB3 and experimental standard enthalpies of formation for a set of alkanes, alcohols, amines and sulfides with increasing alkyl chain length as a function of the number of heavy atoms. The vertical error bars correspond to the uncertainty on the experimental values. The molecule with one heavy atom is methane. The molecules with two heavy atoms correspond to respectively ethane, ethanol, ethylamine and ethane thiol, etc. The deviation between uncorrected CBS-QB3 and experimental values is proportional to the size of the molecules, which is an indication that the CBS-QB3 method can improve by using empirical corrections. All types of molecules give rise to approximately the same incremental difference when increasing the alkyl chain length with one heavy atom. This difference is indicative of the systematic errors on the C-C bond and C-H bond. For the alkanes and nitrogen-containing compounds, CBS-QB3 overestimates the standard enthalpy of formation for all molecules, while for oxygenates and sulfur-containing compounds the standard enthalpy of formation is underestimated for molecules with less than four heavy atoms.

Because of the higher absolute value of the standard enthalpy of formation for larger molecules, the increase in relative error as a function of the number of heavy atoms does not follow the linear trend that is obtained for the absolute error.

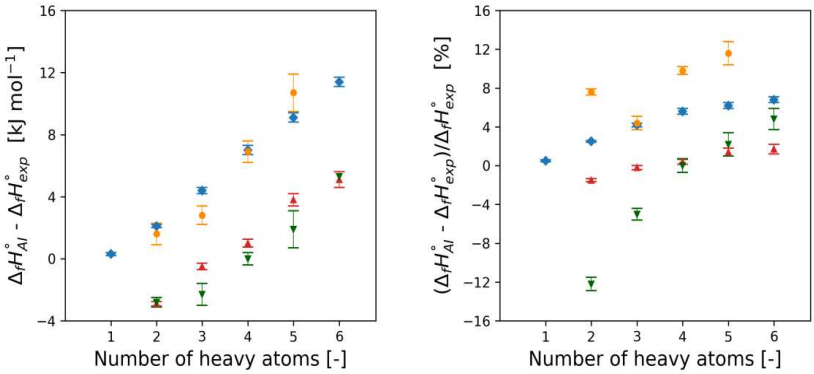

Figure 3-2: Absolute (left) and relative (right) differences between the uncorrected CBS-QB3 (AI) and experimental (exp) standard enthalpies of formation for a set of homologous alkanes (◆), alcohols (▲), amines (●) and thiols (▼) with increasing alkyl chain length as a function of the number of heavy atoms. For each molecule, the experimental uncertainty as reported in literature is indicated.

As discussed previously, higher-accuracy theoretical methods, such as coupled cluster calculations, are limited in their use for molecules with a high number of heavy atoms. For these molecules, CBS-QB3 is a cost-effective alternative, but will correspond to large deviations from the experimental values if no correction scheme is applied to reduce these systematic deviations. It can be noted that the average uncertainty on the experimental standard enthalpy of formation for the alkanes is significantly lower compared to the heteroatomic molecules.

In Figure 3-3, the deviations between uncorrected CBS-QB3 and experimental values are shown for the hydrocarbons, oxygen-, nitrogen- and sulfur-containing compounds. Note that also species which contain more than one type of heteroatom, are included in the dataset. For each class, a wide range of molecule sizes is taken into account, with a maximum of ten heavy atoms. In Figure 3-3, each species is included in only one dataset, i.e. the oxygen-containing compounds included in the set H/C/O/N also contain at least one nitrogen atom. The corresponding MADs are equal to 9.37, 3.62, 5.01 and 3.04 kJ mol^{-1} for respectively the hydrocarbons, oxygenates, nitrogen- and sulfur-containing compounds. The MAD for the complete dataset amounts to 5.62 kJ mol^{-1}. Although typically higher deviations are obtained for larger molecules, a wide spread of accuracies is observed. Apart from hydrocarbons, the trend as a function of the number of heavy atoms is less obvious for oxygen-, nitrogen- and sulfur-containing compounds. In addition, the standard enthalpy of formation of hydrocarbons

is always overpredicted, while for the heteroatomic compounds it can be both over- and under predicted, regardless of the number of heavy atoms. For sulfur-containing compounds, the average number of heavy atoms of all species included in the dataset is equal to six, while for the other classes it is equal to five.

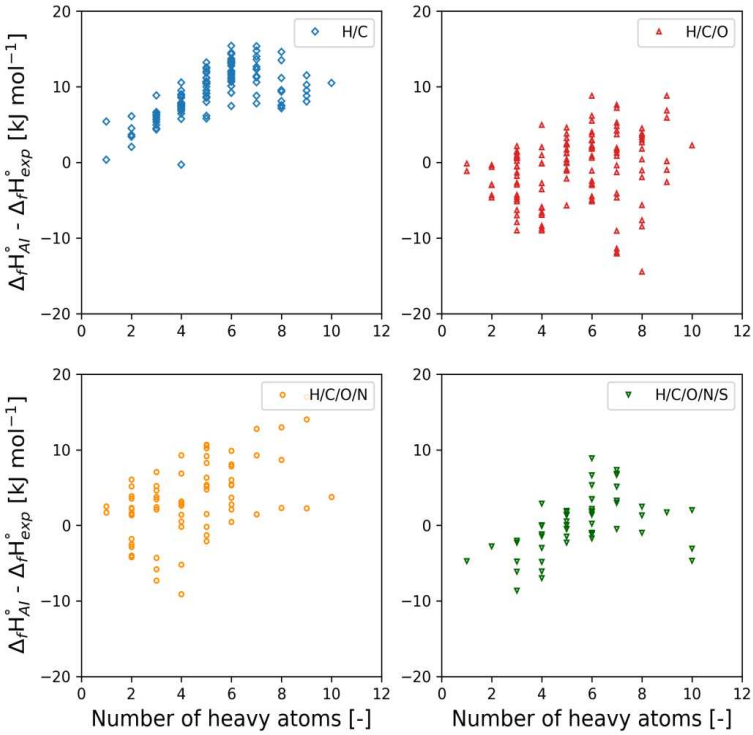

Figure 3-3: Absolute deviation between the uncorrected CBS-QB3 and experimental values of the standard enthalpy of formation [kJ mol^{-1}] as a function of the number of heavy atoms [-] for the hydrocarbons, oxygenates, nitrogen- and sulfur-containing species included in the complete dataset.

3.2.2.3. Regression

By least-squares regression, 26 BACs have been determined for the standard enthalpy of formation at the CBS-QB3 level of theory for hydrocarbons, oxygenates, nitrogen- and sulfur-containing molecules. Such a large set of consistent BAC values has not been reported before for the CBS-QB3 level of theory. The significance of the regression F has a value of 173.09, which is considerably higher value than the tabulated F value, i.e. $F_{0.05}$ (26, 345) = 1.53. With the preliminary set of BACs, determined with the training set data, the MAD between the calculated and the experimental values for the standard enthalpy of formation decreases from 5.64 to 1.67 kJ mol^{-1}. The maximum deviation without BACs, corresponding to 17.01 kJ mol^{-1}

for dibutylamine, is reduced to 4.12 kJ mol^{-1}. The maximum deviation with BACs is obtained for methylene cyclopropane, i.e. 8.55 kJ mol^{-1}.

To validate the transferability of the BACs, the thermodynamic properties have been determined for a test set using the preliminary BAC values obtained from regression of the training set data. This validation consisting of 43 molecules corresponds to a random selection of approximately 10% of all molecules of the complete dataset. The molecular structures included in this test set are shown in Figure 3-4.

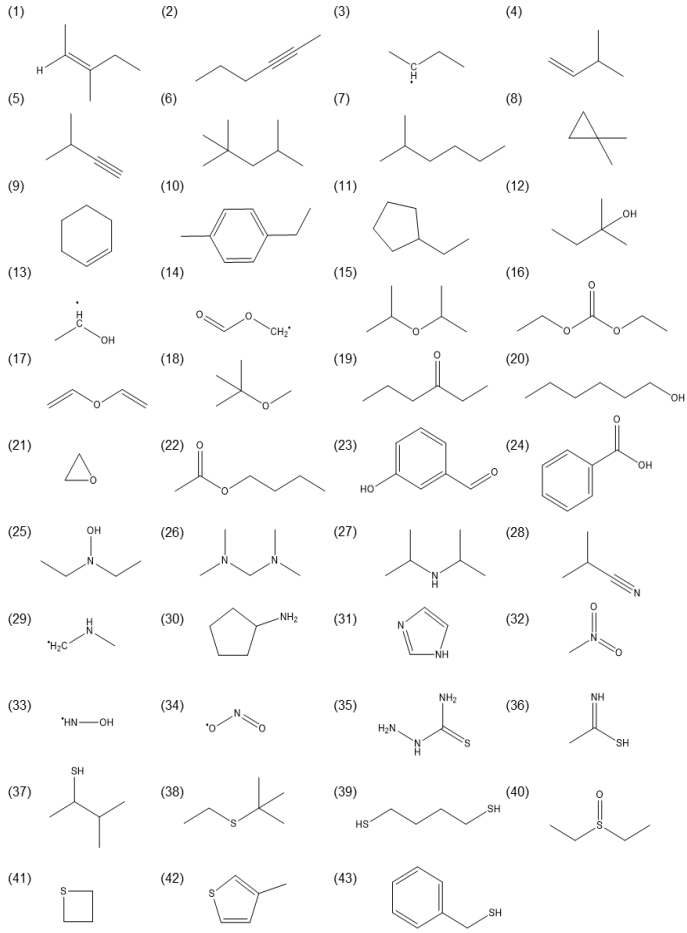

Figure 3-4: Test set of 43 hydrocarbons, oxygenates, nitrogen- and sulfur-containing molecules and radicals to validate the initial BAC estimates.

The results of this comparison between CBS-QB3 calculated values, with and without BACs, and experimental values for the standard enthalpy of formation at 298 K for the training set are shown in Table 3-3.

Table 3-3: Comparison between *ab initio* calculated (calc), with and without BACs, and experimental (exp) standard enthalpies of formation at 298 K [kJ mol^{-1}] for the test set. The experimental database entries are taken from ATcT [10], Pedley et al. [26] and the NIST database [27].

Molecule	$\Delta_f H^\circ_{exp}$ [kJ mol^{-1}]	$\Delta_f H^\circ_{calc} - \Delta_f H^\circ_{exp}$ [kJ mol^{-1}] CBS-QB3	CBS-QB3 + BAC
1	-62.3 ± 1.5	13.4	2.0
2	107.7 ± 2.4	9.2	-2.4
3	66.1 ± 2	8.6	2.7
4	-27.6 ± 1	9.2	-0.6
5	136.4 ± 2.1	13.2	3.2
6	-223.7 ± 1.5	9.3	-3.5
7	-194.6 ± 1	12.3	1.1
8	-8.2 ± 1.2	6.1	-2.0
9	-5.0 ± 0.7	11.7	0.1
10	-3.3 ± 1.5	10.3	-0.1
11	-127.1 ± 1.1	12.4	0.9
12	-330.8 ± 1.4	1.8	-2.7
13	-55.6 ± 0.7	0.9	1.7
14	-156.8 ± 1.7	-6.6	2.0
15	-319.2 ± 1.6	-0.4	-2.9
16	-640.0 ± 0.8	-8.4	1.9
17	-278.3 ± 0.9	3.7	-1.7
18	-13.6 ± 1.0	2.4	-0.5
19	-283.5 ± 1.1	-2.8	-3.6
20	-315.8 ± 0.6	7.2	1.0
21	-52.5 ± 0.4	-2.9	0.9
22	-485.6 ± 0.7	-1.0	0.6
23	-213.7 ± 1.0	0.2	0.6
24	-294.1 ± 2.2	-2.6	-2.2
25	-121.8 ± 0.7	0.5	-2.5
26	-17.7 ± 1.8	1.5	-2.2
27	-136.3 ± 0.5	9.3	0.1
28	24.3 ± 1.3	10.6	3.8
29	151.1 ± 1.0	5.2	3.0
30	-54.9 ± 0.9	9.9	0.4
31	132.9 ± 0.6	-0.2	-3.7
32	-74.8 ± 0.5	-9.1	-2.2
33	94.8 ± 0.9	-1.8	-0.8
34	33.1 ± 1.0	-7.3	-1.0
35	128.2 ± 1.6	-0.5	1.0
36	12.7 ± 1.2	-3.0	-1.5
37	-121.3 ± 0.8	1.7	-1.7
38	-148.0 ± 2.5	5.2	0.8
39	-50.4 ± 1.8	0.2	3.0
40	-205.0 ± 2.0	8.9	2.8
41	60.6 ± 1.4	2.9	3.2
42	83.6 ± 0.9	-1.1	-0.6
43	93.1 ± 1.1	2.5	-0.1

In Table 3-4, the mean (MD), mean absolute (MAD), root-mean-square (RMS) and maximum deviations (MAX) are given for both the training and test set. The statistical parameters are reported using both the initial and final set of BACs.

Table 3-4: Mean (MD), mean absolute (MAD), maximum (MAX) and root-mean-square deviations (RMS) between the calculated (calc) and experimental (exp) values for the standard enthalpy of formation (298 K) [kJ mol^{-1}] for the training and test set without BACs, with the initial set of BACs and with the final set of BACs.

	$\Delta_f H^\circ_{calc} - \Delta_f H^\circ_{exp}$ [kJ mol^{-1}]			
	MD	MAD	RMS	MAX
Without BACs				
Training set	3.45	5.64	6.94	17.01
Test set	3.31	5.53	6.95	13.36
Total	3.43	5.63	6.94	17.01
Initial set of BACs				
Training set	0.06	1.67	2.19	8.55
Test set	-0.14	2.06	2.50	4.90
Final set of BACs				
Training set	0.09	1.69	2.21	8.62
Test set	0.03	1.75	2.07	3.75
Total	0.07	1.70	2.20	8.62

The training and test set are characterized by very similar statistical values without and with BACs. This reflects not only the random selection of molecules for construction of the test set, but more importantly the good performance of the regressed BAC parameters. The MAD for the uncorrected CBS-QB3 values is equal to 5.63 kJ mol^{-1}. Note that this value is higher than the MAD of 4.6 kJ mol^{-1} reported by Montgomery et al. [7], which can be partly explained by the relatively larger molecules included in the current dataset. For 59 species, which are included both in the current dataset as well as in the dataset of Montgomery et al., the MAD between uncorrected CBS-QB3 and experimental values is equal to 3.95 kJ mol^{-1}. The MAD decreases to 1.69 kJ mol^{-1} when applying the new set of BACs to the *ab initio* calculated values reported in this work. The deviation using the (uncorrected) *ab initio* calculated values reported by Montgomery et al. is equal to 4.0 kJ mol^{-1}. The average number of heavy atoms for this set of species is equal to three heavy atoms. The deviations between experimental and *ab initio* calculated standard enthalpies of formation with and without BACs for the complete dataset as well as the comparison with the test set of Montgomery et al. can be found in Tables A-1 and A-2 of Appendix A, respectively.

Application of the new set of BACs leads to a decrease of the MAD for the training set from 5.64 to 1.67 kJ mol^{-1}, with a corresponding decrease in the RMS of 6.94 to 2.19 kJ mol^{-1}. The MAD for the test set after including the BACs is equal to 2.06 kJ mol^{-1} with an RMS of 2.50 kJ mol^{-1}. Using the final set of BACs, obtained by taking account both training and test set in the regression step, leads to a further reduction of this MAD, i.e. 1.75 kJ mol^{-1}, with an RMS of 2.07 kJ mol^{-1}. This improved accuracy of the final set of BACs can be expected, as a larger number of data points is used in the regression step. The maximum absolute deviation is equal to 8.62 kJ mol^{-1} including BACs compared to a deviation of 17.01 kJ mol^{-1} without BACs. The final set of BACs is shown in Table 3-5. Note that the reported BACs are not applicable to molecules with a triplet ground state, as all molecules in the dataset are in their singlet or doublet state and that the SOCs are not included in these BAC values.

Table 3-5: Final set of BACs [kJ mol^{-1}] obtained from regression of both training and test set.

Bond	BAC [kJ mol^{-1}]	Bond	BAC [kJ mol^{-1}]	Bond	BAC [kJ mol^{-1}]
C-H	-0.44	C_a-O_a	0.04	C_a-N_a	-0.35
C-C	-1.10	N-H	-0.97	N_a-N_a	3.14
C=C	-3.80	C-N	0.13	S-H	0.88
C≡C	-4.95	C=N	0.05	C-S	0.90
C_a-C_a	-0.82	C≡N	-1.87	C=S	1.20
O-H	-0.49	N-O	1.55	S=O	-5.91
C-O	2.52	N=O	2.91	S-S	4.12
C=O	2.30	N-N	2.46	C_a-S_a	1.30
O-O	1.77	N=N	3.34		

The highest BAC value is obtained for the S=O bond, i.e -5.91 kJ mol^{-1}. For the determination of this BAC, only two species containing the sulfoxide functional group have been included in the dataset, i.e. dimethyl and diethyl sulfoxide. The BACs for the non-aromatic hydrocarbon species correspond to negative values, while the BACs for the bonds between a carbon atom and a heteroatom are mainly positive. This is in agreement with the less systematic over prediction of the standard enthalpy of formation of heteroatomic compounds, in contrast to the hydrocarbons. For hydrocarbons, the outliers include cycloalkanes, alkadienes, alkynes and aromatic species. For oxygenates the largest deviations are obtained for species with at least two oxygen atoms, such as peroxides. This is also the case for the sulfur-containing species. For nitrogen-containing species, thermochemical accuracy is not reached for several aromatic species with C-N and N-N bonds, diazines (species with a single N-N bond) and species with a nitrile group including the cyanide radical.

Figure 3-5 depicts the differences between the *ab initio* calculated and experimental standard enthalpies of formation without and with BACs for all species in the complete dataset. Again, it can be seen that the largest systematic deviations are obtained for the hydrocarbon species. The largest difference for the BAC corrected values, i.e. 8.62 kJ mol^{-1}, corresponds to methylene cyclopropane.

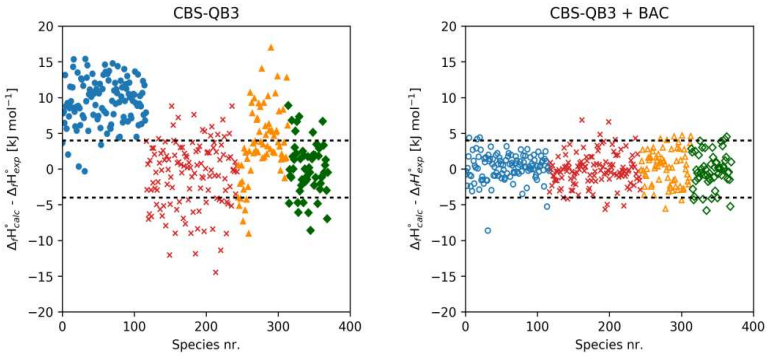

Figure 3-5: Differences between *ab initio* calculated (calc) and experimental (exp) standard enthalpies of formation [kJ mol^{-1}] without BACs (left) and with BACs (right) for hydrocarbons (●), oxygenates (×), nitrogen-containing (▲) and sulfur-containing (◆) compounds.

The corresponding decrease of the MAD for the hydrocarbons, oxygen-, nitrogen- and sulfur-containing compounds is given in Table 3-6. The scarcity of reliable experimental data for nitrogen and sulfur-containing compounds explains the smaller sizes of these classes.

Table 3-6: Mean absolute deviation (MAD) between the (un)corrected CBS-QB3 (calc) and experimental (exp) standard enthalpy of formation [kJ mol^{-1}] for the complete dataset and the different subsets of hydrocarbons, oxygenates, nitrogen-containing, sulfur-containing and aromatic compounds.

Elements	Size	MAD ($\Delta_f H^\circ_{calc} - \Delta_f H^\circ_{exp}$) [kJ mol^{-1}]	
		CBS-QB3	CBS-QB3 + BAC
H/C	117	9.47	1.43
H/C/O	127	3.61	1.67
H/C/O/N	71	5.06	2.05
H/C/O/N/S	56	2.89	1.85
Total	371	5.63	1.70

The distribution of the deviations between the *ab initio* calculated and experimental standard enthalpies of formation with and without BACs is shown in Figure 3-6. Without BACs, there is a very wide range of errors, especially for the hydrocarbons and nitrogen-containing compounds. For the majority of all species, the CBS-QB3 calculated values including BACs

deviate less than 4 kJ mol^{-1} from the experimental value.

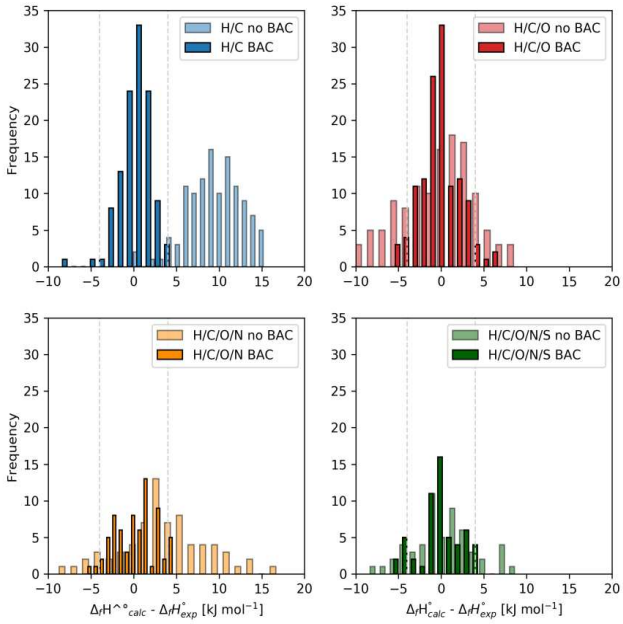

Figure 3-6: Distribution of the differences between the *ab initio* calculated (calc), with and without BACs, and experimental (exp) standard enthalpies of formation [kJ mol^{-1}] for all species included in the training and test set for hydrocarbons (top left), oxygenates (top right), nitrogen-containing (bottom left) and sulfur-containing compounds (bottom right). The gray lines correspond to a deviation of 4 kJ mol^{-1}.

In order to assess the influence of the experimental uncertainty of each species on the final BAC values and subsequently on the deviations between experimental and BAC including *ab initio* calculated data, the BACs have been determined making use of different 'perturbed' experimental datasets. The perturbations (deviations) of the experimental standard enthalpies of formation are determined assuming a normal distribution with the reported experimental uncertainty equal to twice the standard deviation [4]. The experimental uncertainties have the largest influence on the BACs of N_a-N_a and S=O. This is to be expected, as both BACs have been determined from only two species each. A change in these experimental values will thus have a significant influence on the values of the individual BACs. While the individual BACs are to some extent influenced by the exact experimental values, it is important to look at the overall performance of the BAC scheme to improve the accuracy of the standard enthalpies of formation. For 100 perturbed experimental datasets, the MAD is equal to 1.8 ± 0.1 kJ mol^{-1}. Note that not taking into account the uncertainty attributed to the experimental values resulted in a MAD of 1.7 kJ mol^{-1}. Hence, it can be concluded that the experimental uncertainties do not

have a significant influence on the performance of the BAC scheme, assuming that only experimental values with an uncertainty lower than 3.0 kJ mol^{-1} are considered.

3.2.2.4. Application of the bond additivity corrections

To demonstrate the use of the new set of BACs, three example calculations are done for the oxygen-containing methyl formate radical, the nitrogen-containing aromatic compound benzonitrile and the sulfur-containing compounds diethyl sulfoxide the structures of which are shown in Figure 3-7.

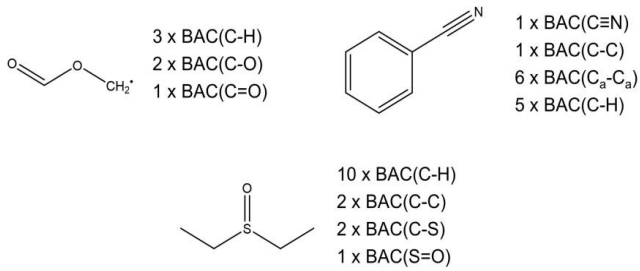

Figure 3-7: Application of the BAC procedure for calculation of the standard enthalpy of formation of the methyl formate radical, benzonitrile and diethyl sulfoxide.

The uncorrected CBS-QB3 standard enthalpy of formation of the methyl formate radical is equal to -163.4 kJ mol^{-1}. The experimental value is equal to -156.8 kJ mol^{-1}, which corresponds to an absolute deviation of 6.6 kJ mol^{-1}. The sum of the SOCs for the three hydrogen, two carbon and two oxygen atoms is equal to 2.6 kJ mol^{-1}. As can be seen from Figure 3-7, a total of six BACs can be identified, corresponding to three C-H bonds, two C-O bonds and one C=O bond, which equals a total correction of 6.0 kJ mol^{-1}. Hence, the corrected CBS-QB3 value including BACs and SOCs is equal to -154.8 kJ mol^{-1}, which only deviates 1.8 kJ mol^{-1} from the experimental value.

$$\Delta_f H^{\circ}_{calc} = 2 \cdot SOC(C) + 2 \cdot SOC(O) + 3 \cdot BAC(C-H) + 2 \cdot BAC(C-O) + BAC(C=O)$$
$$= -154.8\, kJ\, mol^{-1}$$

For benzonitrile, the CBS-QB3 value is equal to 224.4 kJ mol^{-1}, which is 8.7 kJ mol^{-1} higher than the experimental value. Summing up the SOCs for seven carbon, one nitrogen and five hydrogen atoms gives 2.5 kJ mol^{-1}. The total of the 13 BACs, i.e. one C≡N bond, one C-C bond, six aromatic C_a-C_a bonds and five C-H corresponds to a correction of -10.1 kJ mol^{-1}. The corrected CBS-QB3 value is thus equal to 216.8 kJ mol^{-1}, which is only 2.1 kJ mol^{-1} higher than the experimental value.

$$\Delta_f H^{\circ}_{calc} = 7 \cdot SOC(C) + SOC(N) + 5 \cdot BAC(C-H) + BAC(C-C) + 6 \cdot BAC(C_a - C_a) + BAC(C \equiv N) = 216.8\, kJ\, mol^{-1}$$

The uncorrected CBS-QB3 standard enthalpy of formation for diethyl sulfoxide is equal to -196.1 kJ mol^{-1}, which 8.9 kJ mol^{-1} higher than the experimental value. The sum of the SOCs for the ten hydrogen, four carbon, one oxygen and one sulfur atom is equal to 4.7 kJ mol^{-1}. The sum of the BACs, i.e. one S=O bond, two C-C bonds, two C-S bonds and ten C-H bonds is equal to -10.7 kJ mol^{-1}. The corrected CBS-QB3 value including SOC and BAC corrections is thus equal to -202.1 kJ mol^{-1}, which only deviates 2.9 kJ mol^{-1} from the experimental value.

$$\Delta_f H^{\circ}_{calc} = 4 \cdot SOC(C) + SOC(O) + SOC(S) + 10 \cdot BAC(C-H) + 2 \cdot BAC(C-C) + 2 \cdot BAC(C-S) + BAC(S=O) = -202.1\, kJ\, mol^{-1}$$

3.3. Group additivity model for nitrogen-containing compounds

3.3.1. Methodology

New group additive values for both carbon- and nitrogen-centered groups are determined. The different carbon, nitrogen and oxygen atom types as well as the polyatomic ligands considered are listed in Table 3-7.

Table 3-7: Different types of central atoms and polyatomic ligands.

Notation	Atom type
C	Single bonded carbon atom
C_d	Carbon atom double bonded to a carbon atom
C_I	Carbon atom double bonded to a nitrogen atom (imine)
C_t	Carbon atom triple bonded to a carbon atom
N	Single bonded nitrogen atom
N_I	Nitrogen atom double bonded to a carbon atom (imine)
N_A	Nitrogen atom double bonded to a nitrogen atom (azo)
CO	Carbonyl group
CN	Cyano group
NO	Nitroso group
ONO	Nitrite group
NO_2	Nitro group

The same notation as introduced by Benson et al. [22] for nitrogen-containing compounds is adopted in this work. C_I represents an sp^2 carbon atom bond double bonded to a nitrogen atom,

as is the case in imines. Similar to the carbon atom types, a distinction can be made between different types of nitrogen atoms. The symbols used for representation of a single bonded nitrogen atom, a nitrogen atom double bonded to a carbon atom and a nitrogen atom double bonded to another nitrogen atom are equal to N, N_I and N_A, respectively. In analogy to previous studies, when an sp^2 double bonded carbon atom (notation: C_I) is the central atom of a Benson group, it is implied that this atom is double bonded to another carbon atom and hence C_d is not mentioned as ligand in the definition of the GAV, for example C_d-$(H)_2$ and C_d-(N)(H). Five polyatomic groups are considered: carbonyl (notation: CO), cyano (notation: CN), nitroso (notation: NO), nitrite (notation: ONO) and the nitro group (NO_2). Aside from the carbonyl group (>C=O) which has two variable ligands, these groups are connected to only one ligand group. As their contributions are completely included in the GAV of the neighboring group, no separate GAV contributions are determined for Benson groups with these polyatomic groups as the center. In Figure 3-8, the use of these atom types is illustrated for eight different nitrogen-containing molecules.

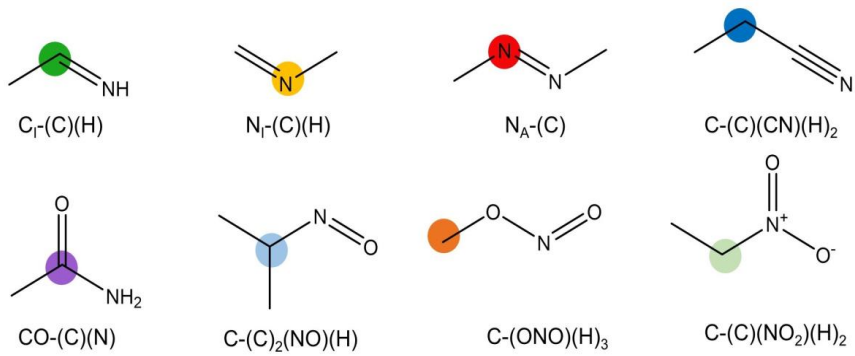

Figure 3-8: Identification of different Benson groups in nitrogen-containing species.

Note that for the imine group in ethanimine ($CH_3CH{=}NH$), N_I is also not mentioned as ligand in the definition of the GAV of C_I-(C)(H). Within the Benson group additivity method, a group is defined as a central atom together with all of its ligands. In radical-centered groups, the central atom is a radical, while in radical-adjacent groups one of the ligands has a radical character. For hydrocarbons [18], oxygenates [19] and sulfur-containing compounds [8], it has been shown that the GAVs for the radical-adjacent groups differ only slightly from the corresponding molecular groups, thereby allowing a significant reduction in the number of groups. In this work, it is assumed that the GAVs for radical-adjacent groups can be given the same values as the corresponding group for the closed-shell compounds. For example, the

corresponding non-radical group for C-(C)(N$^{\cdot}$)(H)$_2$ is obtained by replacing the radical nitrogen atom by its non-radical equivalent, e.g. C-(C)(N)(H)$_2$.

Group additivity approximations for resonance-stabilized radicals can be challenging. An unambiguous group additive prediction is only possible in case the ligands of the radical-centered group contain information about all the unsaturated bonds involved in electron delocalization. An example is the nitrogen-containing canonical structure C=C-N$^{\cdot}$-C=C, for which the N$^{\cdot}$-(C$_d$)$_2$ group includes both double bonds involved in the radical delocalization. Different equivalent canonical structures correspond to different group additive approximated enthalpies of formation, whereas the actual enthalpy of formation is equal. An example is the resonance stabilized radical $CH_3C(CH_3)$=CHNH$^{\cdot}$, for which the two different canonical structures are shown in Figure 3-9.

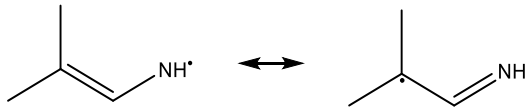

Figure 3-9: Resonance structures of the $CH_3C(CH_3)$=CHNH$^{\cdot}$ radical.

Because both resonance structures have different groups, application of group additivity will lead to different values for the enthalpy of formation. In accordance with the general rule for the application of Benson group additivity to radicals, the canonical structure yielding the lowest standard enthalpy of formation should selected. The best approximations for $S^{\circ}{}_{int}$ and C_p° are then obtained using the same groups that yield the lowest $\Delta_f H^{\circ}$. During the linear regression procedure, both resonance structures are initially included in the matrix of dependent variables in order to estimate all relevant GAVs. Next, only the resonance structure with the lowest group additivity approximated enthalpy of formation is kept and the GAVs are re-estimated. This procedure corresponds to what has been done in previous work by Sabbe et al. [18].

The GAVs for the non-nitrogen containing groups are taken from previous work of Sabbe and co-workers, who employed the same methodology for regression of GAVs and NNI corrections for hydrocarbon and oxygen-containing groups. These GAVs are summarized in Table 3-8.

Table 3-8: GAVs and NNIs for the standard enthalpy of formation [kJ mol^{-1}] and intrinsic standard entropy [J mol^{-1} K^{-1}] at 298 K and heat capacity [J mol^{-1} K^{-1}] at various temperatures for hydrocarbon and oxygen-containing groups taken from earlier studies by Sabbe et al. [18, 30].

	$\Delta_f H^\circ$	S°_{int}	C_p°						
Group			300 K	400 K	500 K	600 K	800 K	1000 K	1500 K
C-(C)(H)$_3$	-42.90	127.20	24.95	31.78	38.21	43.88	53.23	60.51	72.28
C-(C$_d$)(H)$_3$	-42.90	127.20	24.95	31.78	38.21	43.88	53.23	60.51	72.28
C-(C$_t$)(H)$_3$	-42.90	127.20	24.95	31.78	38.21	43.88	53.23	60.51	72.28
C-(C)$_2$(H)$_2$	-20.50	39.89	25.19	30.21	35.11	39.44	46.42	51.63	59.71
C-(C)(C$_d$)(H)$_2$	-18.90	41.91	21.93	28.33	33.87	38.47	45.63	50.93	59.18
C-(C)(C$_t$)(H)$_2$	-17.70	42.72	20.94	27.92	33.77	38.53	45.76	51.05	59.24
C-(C)$_3$(H)	-6.90	-48.30	23.31	29.20	33.51	36.70	41.01	43.82	47.82
C-(C)$_4$	3.90	-147.80	21.68	28.40	32.40	34.67	36.34	36.51	35.72
C$_d$-(H)$_2$	25.10	115.76	20.59	25.93	30.75	34.87	41.44	46.45	54.57
C$_d$-(C)(H)	37.10	32.91	18.44	21.74	25.02	27.96	32.65	36.06	41.17
C$_d$-(C$_d$)(H)	30.40	25.73	18.10	24.14	29.11	32.72	37.14	39.66	43.06
C$_d$-(C)$_2$	45.30	-55.90	19.58	21.71	23.12	24.25	25.94	27.02	28.35
C$_t$-(H)	113.80	102.94	21.61	24.75	26.96	28.65	31.28	33.41	37.21
C$_t$-(C)	115.60	26.45	13.78	15.34	16.73	17.93	19.82	21.15	22.98
C-(CO)(H)$_3$	-42.90	127.20	24.95	31.78	38.21	43.88	53.23	60.51	-42.90
C-(C)(CO)(H)$_2$	-21.51	40.32	26.91	30.80	34.98	38.91	45.56	50.73	-21.51
C$^{\cdot}$-(C)(H)$_2$	168.00	139.01	22.79	27.81	32.10	35.67	41.33	45.76	53.10
C$^{\cdot}$-(C)$_2$(H)	177.30	56.57	18.53	21.25	24.24	26.99	31.44	34.71	39.63
C$_d^{\cdot}$-(H)	275.80	121.36	20.59	23.57	25.74	27.44	30.14	32.31	35.96
gauche	2.9	-0.70	-0.90	-1.08	-1.10	-1.01	-0.76	-0.56	-0.35
1,5-interaction	7.1	2.72	-1.42	-0.18	0.55	0.83	0.67	0.18	-0.99

As a result, the obtained GAVs and NNIs for nitrogen-containing compounds form a complete and consistent dataset with the values reported by these authors. Due to linear dependencies, 12 GAV contributions cannot be determined independently from the remaining GAVs and are taken equal to analogous non-nitrogen containing groups. For example, the GAVs of the C-(N)(H)$_3$, C-(C$_I$)(H)$_3$, C-(N$_I$)(H)$_3$ and C-(N$_A$)(H)$_3$ groups are set equal to the values for the C-(C)(H)$_3$ group. The predefined GAV values can be found in Table 3-9.

Table 3-9: Predefined GAVs for the standard enthalpy of formation [kJ mol^{-1}] and intrinsic standard entropy [J mol^{-1} K^{-1}] at 298 K and heat capacity [J mol^{-1} K^{-1}] at various temperatures for nitrogen-containing compounds based on similar groups from earlier studies by Sabbe et al. [18, 30].

	$\Delta_f H^\circ$	S°_{int}	C_p°						
Fixed GAV			300 K	400 K	500 K	600 K	800 K	1000 K	1500 K
C-(N)(H)$_3$	-42.90	127.20	24.95	31.78	38.21	43.88	53.23	60.51	72.28
C-(N$_I$)(H)$_3$	-42.90	127.20	24.95	31.78	38.21	43.88	53.23	60.51	72.28
C-(C$_I$)(H)$_3$	-42.90	127.20	24.95	31.78	38.21	43.88	53.23	60.51	72.28
C-(N$_A$)(H)$_3$	-42.90	127.20	24.95	31.78	38.21	43.88	53.23	60.51	72.28
C$_I$-(H)$_2$	25.10	115.76	20.59	25.93	30.75	34.87	41.44	46.45	54.57
C$_d$-(N)(H)	37.10	32.91	18.44	21.74	25.02	27.96	32.65	36.06	41.17
C$_d$-(N$_I$)(H)	30.40	25.73	18.10	24.14	29.11	32.72	37.14	39.66	41.17
C$_d$-(C$_I$)(H)	30.40	25.73	18.10	24.14	29.11	32.72	37.14	39.66	41.17
C$_I$-(C$_t$)(H)	30.40	25.73	18.10	24.14	29.11	32.72	37.14	39.66	43.06
C$_t$-(N)	117.10	23.79	14.32	16.62	18.08	19.15	20.68	21.73	23.21
CO-(N)(H)	-123.42	145.46	26.24	31.22	35.94	40.13	46.74	51.39	57.73
O-(N)(H)	-165.22	125.32	19.07	19.80	20.85	22.07	24.57	26.95	31.66

Three NNI corrections for nitrogen-containing compounds are taken into account, c.f. Figure 3-10. These include a 1,4 gauche interaction along a carbon-nitrogen bond and two types of cis interactions. The first cis interaction is between a methyl (or alkyl) group and an amino group, along a carbon-carbon double bond. The second cis interaction is between two methyl groups, an alkyl group and a methyl group or between two alkylic groups, along a carbon-nitrogen double bond, i.e. as is the case in imines. The assignment of the number of gauche interactions is performed according to the revised gauche counting scheme as introduced by Benson et al. [22]. Note that hydrogen bonds which can be present in nitrogen-containing compounds as a stabilizing interaction are not considered.

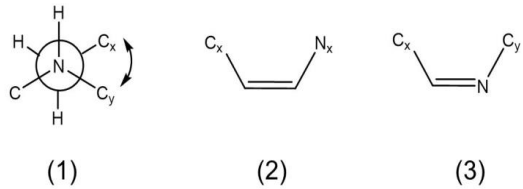

Figure 3-10: Definitions of non-nearest-neighbor interactions: (1) 1,4 gauche interaction along C-N bond, (2) single cis interaction between C_x and N_y substituents, and (3) single cis interaction between C_x and C_y substituents along C=N bond, with C_x, C_y methyl or alkyl substituents and N_x amino or amine substituent.

Symmetry cannot be accounted for within the group additivity scheme, due to the non-local character of this property. Aside from symmetry, it needs to be taken into account that different

stereoisomers can exist when calculating the thermodynamic properties of a molecule. Due to the presence of the lone electron pair on the nitrogen atom, ammonia has a trigonal pyramidal structure. The H-N-H bond angle is equal to 107°, which is slightly smaller than the corresponding H-C-H bond angle of 109.5° in methane.

In theory, a chiral centrum is defined by a tetrahedral central atom with four different substituents. When considering the lone electron pair on nitrogen as a fourth substituent, chirality can thus also occur in secondary and tertiary amines [31]. For example, considering the nitrogen atom in ethyl methyl amine as a chiral center, results in a pair of enantiomers as shown in Figure 3-11. This is also the approach that is followed in this work for determination of the number of optical isomers. A nitrogen atom with three different ligands is assigned a value of two for the number of optical isomers. Or as a corollary, the internal symmetry number of an amino group is assigned a value of one.

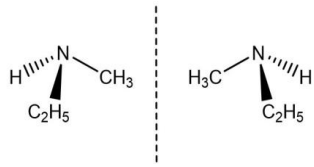

Figure 3-11: Pair of enantiomers of ethyl methyl amine

In reality, rapid inversion of the amine, passing through a planar transition state, will occur, even at 298 K. These nitrogen species should thus not be considered optically active in the traditional sense, because they have low barriers of conversion between the two mirror images. Nitrogen inversion allows its enantiomers to rapidly interconvert, making chiral resolution impossible unless the inversion process is prevented by steric or electronic effects [32]. The calculation of entropy via the group additivity method does not consider contributions from symmetry or chiral centers. A reliable group additivity scheme for estimation of the entropy requires that these contributions are omitted from the calculated entropies, resulting in a symmetry-independent entropy, S°_{int}, as introduced in Chapter 2.

Similar to the bond additive corrections, the GAVs for the standard enthalpy of formation, intrinsic entropy and heat capacity are obtained by unweighted least-squares regression analysis. This implies minimizing the sum of squares as defined in Eq. 3-1, with y_i the corrected CBS-QB3 calculated value, i.e. including SOCs and BACs ($\Delta_f H^{\circ}_{calc}$) of molecule i and $\hat{y}_i$ the

group additive estimate ($\Delta_f H^{\circ}_{GA}$). This results in the following Eq. 3-5 for the optimized set of GAV and NNI parameters:

$$\overline{GAV/NNI} = (X^T X)^{-1} X^T y \qquad \text{(Eq. 3-5)}$$

in which $\overline{GAV/NNI}$ is the estimated vector of the GAV and NNI parameters, X is the matrix in which the elements X_{ij} specify the number of occurrences of GAV or NNI j in the molecule i and $\bar{y}$ is the vector containing the differences between the corrected CBS-QB3 calculated and the group additivity approximated values. The dimensions of the matrix X are M x N with N being the number of GAVs and NNIs and M the number of molecules in the reference dataset used to obtain the group additive estimates. In general the order of matrix X is lower than the number of GAVs and NNIs that need to be determined, which indicates that linear dependencies between the different GAVs exist. The methodology used to calculate a new set of GAVs in this work is illustrated in Figure 3-12.

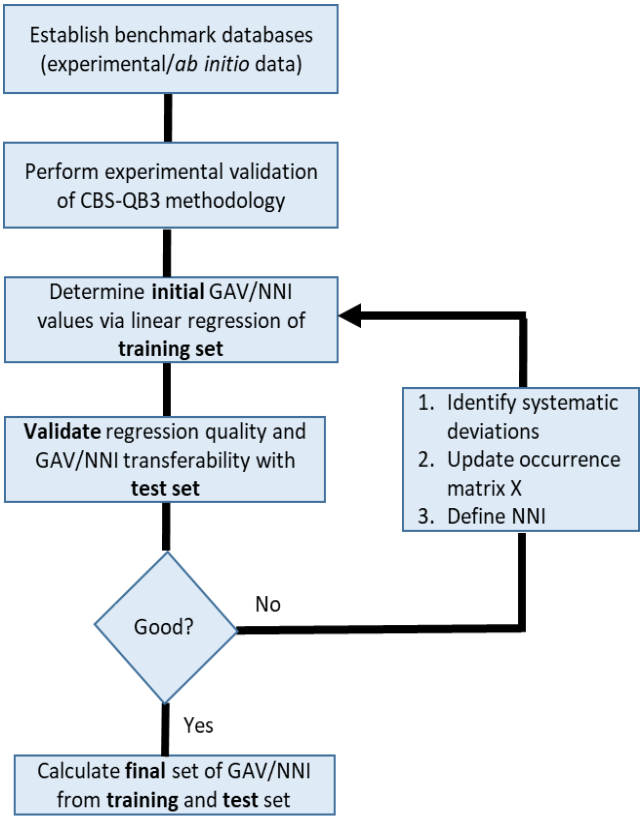

Figure 3-12: Methodology to determine a new set of group additive values (GAV) and non-nearest-neighbor interactions (NNI) for nitrogen-containing species.

Similar to the regression procedure for BACs, the complete dataset of nitrogen-containing compounds is divided in a training and test set. The test set represents a random selection of approximately 10% of all species included in the complete dataset. In a first step, a preliminary set of GAVs/NNIs is determined from the training data set only. These preliminary GAVs are subsequently used to approximate the thermodynamic properties of a large number of molecules not present in the training set, i.e. the test set. In case a satisfactory agreement is obtained between *ab initio* calculated and group additive approximated data for all species in the test set, the final set of GAVs/NNIs is determined from the complete dataset. If that is not the case, the NNIs need to be revised or changes to the group matrix X are required.

3.3.2. Results and discussion

3.3.2.1. Ab initio calculations

An overview of the *ab initio* calculated thermodynamic parameters for the complete dataset of 300 species, as well as the number of optical isomers and the total symmetry number, can be found in Table A-4 of Appendix A. All nitrogen-containing compounds have been calculated in their singlet or doublet states. In the case of large deviations between calculated and experimental data, the triplet states have also been calculated, but in all cases the triplet state is significantly higher in energy. Nitrogen-containing compounds containing a maximum of two nitrogen atoms and in total eight heavy atoms are considered. The average number of heavy atoms for the complete dataset is equal to six.

3.3.2.2. Comparison between ab initio calculated and experimental data

To further assess the performance of the CBS-QB3 level of theory for nitrogen-containing compounds, the *ab initio* calculated entropy and heat capacity at 298 K is compared with the available experimental values for the nitrogen-containing compounds included in the dataset for regression of BACs, c.f. Section 3.2. The experimental values for the standard entropy and heat capacity are taken from Dean and Lange [33]. From the total of 71 nitrogen-containing compounds, experimental values for the standard entropy are available for 22 species, while for the heat capacity there are only 16 experimental data points. The results of these comparisons are provided in Table A-3 of Appendix A for the entropies and heat capacities. For the standard enthalpy of formation, the deviations for these nitrogen-containing compounds are included in Table A-1 of Appendix A. The statistics of the comparison for all three thermodynamic parameters are given in Table 3-10.

Table 3-10: Statistics for the deviations between *ab initio* calculated (AI) and experimental values for the standard enthalpy of formation [kJ mol^{-1}], standard entropy [J mol^{-1} K^{-1}] and heat capacity [J mol^{-1} K^{-1}] at 298 K.

	$\Delta_f H^\circ$		S°	C_p°
	CBS-QB3	CBS-QB3 + BAC		
MD	5.2	0.3	1.3	0.8
MAD	5.1	2.0	2.2	2.1
MAX	17.0	4.7	8.9	7.8

As discussed in Section 3.2.2.3, the MAD between the experimental and *ab initio* calculated (CBS-QB3) standard enthalpy of formation for all 71 nitrogen-containing species is equal to 5.1 kJ mol^{-1}. With the introduction of BACs, this MAD is decreased to 2.0 kJ mol^{-1}. The standard entropy and heat capacity at 298 K are approximated with a MAD of 2.2 and 2.1 J mol^{-1} K^{-1} respectively.

3.3.2.3. Regression

By least-squares regression, GAVs for 40 carbon-centered and 22 nitrogen-centered groups have been determined for non-radical centered Benson groups. This includes 17 completely new groups and 15 groups for which only GAV values based on experimental datasets are available. For radical-centered groups, GAVs have been regressed for 17 carbon-centered groups, 11 nitrogen-centered groups and one oxygen-centered group. No radical-centered GAV contributions for nitrogen-containing compounds are available yet in literature. In addition, three NNI corrections have been obtained in this work, which have not been reported before. The statistics of the regression using the training set data are given in Table 3-11. All of the reported F values for the regression of the different thermodynamic properties are considerably higher than the tabulated F value, i.e. $F_{0.05}(93,207) = 1.326$. The new group additivity model is accurate for the molecules in the training set with a MAD of 1.5 kJ mol^{-1} for the standard enthalpy of formation and 2.5 J mol^{-1} K^{-1} for the standard entropy. The MAD for the heat capacities over the studied temperature range is equal to 1.0 J mol^{-1} K^{-1} on average. Maximum deviations amount to 6.6 kJ mol^{-1} for the standard enthalpy of formation, 8.2 J mol^{-1} K^{-1} for the standard entropy and 5.5 J mol^{-1} K^{-1} for the heat capacity.

Table 3-11: Statistics for the regression of the GAVs and NNI corrections for the standard enthalpy of formation [kJ mol^{-1}] and standard intrinsic entropy [J mol^{-1} K^{-1}] at 298 K and heat capacities [J mol^{-1} K^{-1}] at various temperatures for all 273 nitrogen-containing molecules in the training set.

	$\Delta_f H^\circ$	S°_{int}	C_p°						
			300 K	400 K	500 K	600 K	800 K	1000 K	1500 K
F	11236	2890	1256	2235	3232	4393	7648	12364	29372
MAD	1.5	2.5	1.4	1.3	1.1	1.1	0.9	0.8	0.5
RMS	1.9	3.2	1.8	1.6	1.6	1.5	1.3	1.1	0.8
MAX	6.6	8.2	5.5	5.0	5.8	6.1	5.0	4.0	3.9

In this work, the GAV and NNI corrections have been estimated simultaneously. In that case, it is crucial to monitor the correlation between the parameters. If one or more correlation coefficients are large, i.e. larger than 0.9, the values of the NNI corrections will influence the estimated GAVs. The largest correlation coefficient for this regression is 0.8 for the GAV for the N-(CO)(H)$_2$ and C-(CO)(N) groups.

To validate the transferability of the GAVs and NNIs, the thermodynamic properties are approximated for a test set using the preliminary values obtained from regression of the training set data. This test set consists of 16 molecules and 10 radicals, c.f. Figure 3-13, representing the different types of nitrogen-containing compounds included in the training set.

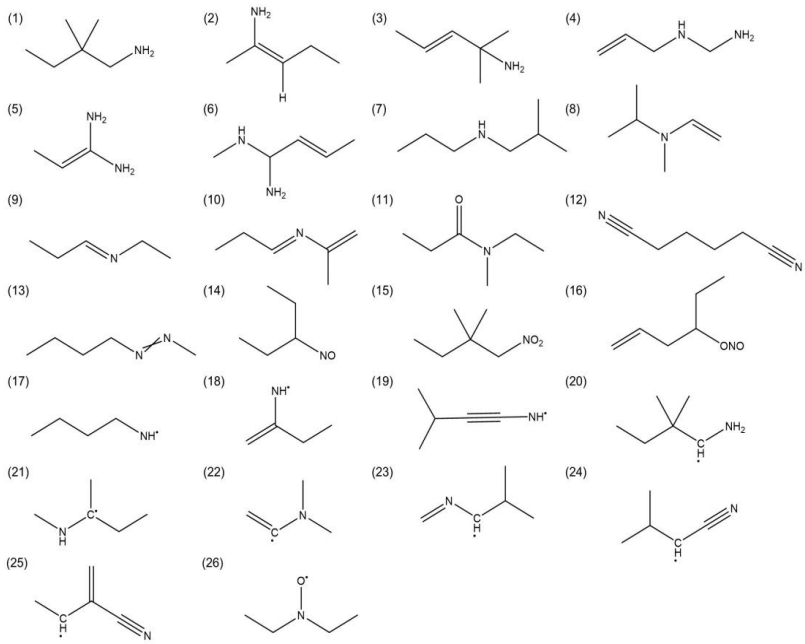

Figure 3-13: Test set of 26 nitrogen-containing molecules to validate the group value estimates.

The differences between the *ab initio* calculated and group additive approximated data are given in Table 3-12 for all test set species. The actual *ab initio* values of the standard enthalpy of formation, intrinsic entropy and standard heat capacities are given in Table A-4 of Appendix A. For the 26 molecules of the test set, the standard enthalpy of formation is predicted with a MAD of 2.3 kJ mol^{-1}. For the intrinsic entropy, the MAD amounts to 3.0 J mol^{-1} K^{-1} and for the heat capacities the MAD is less than 2.3 J mol^{-1} K^{-1} over the whole temperature range.

Table 3-12: Differences between the *ab initio* calculated (AI) and group additive approximated (GA) values for the standard enthalpy of formation [kJ mol^{-1}] and intrinsic standard entropy [J mol^{-1} K^{-1}] at 298 K and the heat capacities [J mol^{-1} K^{-1}] at different temperatures for all 26 molecules included in test set. The initial set of GAV and NNI values determined from the training set species only is used.

	$\Delta = AI - GA$			
	$\Delta_f H^\circ$	S°_{int}	C_p°	
Molecule			300 K	1000 K
1	2.2	3.1	1.9	0.0
2	0.9	-3.3	-4.2	0.2
3	-3.5	3.8	-1.6	-0.5
4	-0.1	-1.5	-0.5	0.3
5	-0.1	-1.6	5.4	-2.1
6	-2.9	-3.3	-0.6	4.4
7	1.2	4.6	-1.1	0.3
8	4.7	-8.5	0.0	-0.1
9	2.4	-2.4	-0.9	-0.2
10	-1.8	0.8	0.0	-0.5
11	-0.1	3.9	-3.1	0.8
12	3.2	-1.0	5.4	1.0
13	0.2	-3.2	-1.1	0.5
14	0.0	-4.6	6.8	1.6
15	3.4	-3.9	8.2	0.9
16	-2.6	-3.7	0.7	2.8
17	2.9	0.6	-2.3	-0.3
18	2.2	-3.6	-1.0	-0.5
19	-2.3	-5.4	1.4	1.8
20	-2.5	2.5	3.3	0.2
21	7.9	-2.4	-1.7	0.6
22	-1.4	3.2	0.1	3.0
23	2.4	3.5	0.3	-0.5
24	4.5	-1.5	1.1	0.7
25	1.4	-0.3	-0.2	-1.0
26	-2.1	2.6	-5.8	-1.5
Statistics				
MAD	2.3	3.0	2.3	1.0
RMS	2.8	3.5	3.2	1.4
MAX	7.9	8.5	8.2	4.4

As a final step, the GAV and NNI parameters have been optimized via a linear regression analysis based on both the training and test with a total of 300 molecules. The final values for the GAVs and NNI corrections are reported in Table 3-13 and Table 3-14 for non-radical and radical-centered Benson groups respectively. Note that each GAV and NNI correction is determined from at least three occurrences in three different molecules. The MAD for the combined data set is equal to 1.5 kJ mol^{-1} for the standard enthalpy of formation, 2.5 J mol^{-1} K^{-1} for the standard intrinsic entropy and 1.5 J mol^{-1} K^{-1} for the heat capacity over the complete temperature range. The maximum deviation with the final set of GAVs for the total dataset is obtained for 2,2-dimethyl-1-nitro-butane (Species 15 in Figure 3-13), i.e. 6.5 kJ mol^{-1}. The good agreement between the calculated and group additivity approximated values of $\Delta_f H^\circ$, $S^\circ{}_{int}$ and C_p° for all molecules included in the combined training and test set can also be seen from the corresponding histograms, available in Appendix A (Figure A-1).

Table 3-13: Group additive values for the standard enthalpy of formation [kJ mol^{-1}] and intrinsic standard entropy [J mol^{-1} K^{-1}] at 298 K and the heat capacities [J mol^{-1} K^{-1}] at different temperatures for nitrogen-containing molecules deduced by linear regression making use of both the training and test set. The subscripts d, t, I and A indicate that the corresponding atom is part of a carbon double bond, carbon triple bond, carbon nitrogen double bond and nitrogen double bond, respectively.

	$\Delta_f H^\circ$	$S^\circ{}_{int}$	C_p°						
Group			300 K	400 K	500 K	600 K	800 K	1000 K	1500 K
C-centered									
C-(C)(N)(H)$_2$	-27.83	37.39	25.65	31.37	36.33	40.58	47.18	52.19	60.00
C-(C)(C$_I$)(H)$_2$	-19.73	42.35	23.53	29.13	34.22	38.60	45.41	50.61	58.91
C-(C)(N$_I$)(H)$_2$	-27.57	35.96	22.81	30.33	36.25	40.88	47.58	52.46	60.03
C-(C)(CN)(H)$_2$	98.06	166.02	49.03	58.16	65.60	71.72	81.29	88.43	99.43
C-(C)(C$_A$)(H)$_2$	-26.93	42.35	22.37	28.80	34.26	38.82	45.79	51.01	59.16
C-(C$_d$)(N)(H)$_2$	-27.24	33.16	27.47	34.63	39.76	43.58	49.11	53.35	60.31
C-(C$_d$)(CN)(H)$_2$	101.10	170.17	45.45	55.12	63.18	69.79	79.97	87.44	98.80
C-(N)$_2$(H)$_2$	-46.75	37.90	28.44	33.85	38.53	42.53	48.58	53.21	60.54
C-(C)$_2$(N)(H)	-18.59	-51.76	24.91	30.57	34.62	37.60	41.46	44.00	47.55
C-(C)$_2$(C$_I$)(H)	-4.92	-46.70	21.52	27.36	31.62	34.78	38.99	41.88	46.24
C-(C)$_2$(CN)(H)	111.93	74.80	48.73	57.06	63.44	68.34	75.27	80.00	86.84
C-(C$_d$)$_2$(N)(H)	-14.88	-62.34	29.16	37.61	41.95	44.12	45.87	46.83	48.47
C-(C)(C$_d$)(N)(H)	-18.44	-55.79	25.25	33.12	37.90	40.76	43.71	45.45	47.98
C-(C)(N)$_2$(H)	-44.18	-54.25	25.82	32.68	37.46	40.74	44.27	46.28	48.90
C-(C$_d$)(N)$_2$(H)	-42.59	-65.05	30.71	42.07	48.49	51.48	52.46	51.92	51.10
C-(C)$_3$(N)	-11.98	-142.84	23.55	29.93	33.38	35.13	36.04	35.93	35.15
C-(C)$_3$(CN)	122.57	-18.51	50.50	59.37	64.67	67.92	71.41	73.18	75.14
C-(C)$_2$(C$_d$)(N)	-10.38	-144.93	27.45	33.37	36.25	37.40	37.38	36.68	35.27

C_d-(CN)(H)	149.27	157.83	41.03	48.19	54.34	59.44	67.17	72.67	80.75
C_d-(C)(N)	41.37	-51.33	16.77	19.25	21.23	22.88	25.11	26.40	27.82
C_d-(C)(N_I)	45.68	-44.46	13.17	12.90	13.96	15.81	19.53	22.31	25.94
C_d-(C)(CN)	165.45	71.80	41.58	47.26	51.56	54.97	59.98	63.32	67.83
C_d-$(N)_2$	35.86	-60.46	18.45	25.74	30.55	32.80	32.71	30.91	28.03
C_I-(C)(H)	23.93	32.35	16.78	20.77	24.60	27.78	32.76	36.34	41.29
C_I-(C_d)(H)	16.30	19.30	16.29	24.05	29.70	33.49	38.12	40.86	43.99
C_I-(C_t)(H)	32.56	43.59	15.31	20.41	25.07	28.77	34.15	37.94	43.28
C_I-$(C)_2$	25.49	-46.55	13.16	15.73	18.27	20.27	23.25	25.08	27.09
C_I=C_d	105.31	26.11	14.70	17.60	19.36	20.32	21.37	22.13	23.11
C_t-(CN)	245.60	145.15	42.05	46.46	49.63	52.21	56.24	59.19	63.45
CO-(C)(N)	-121.47	57.22	20.55	26.07	30.58	34.15	38.95	41.72	44.60
C-(C)(NO)$(H)_2$	88.68	184.00	48.33	55.97	63.22	69.48	79.17	86.11	96.40
C-$(C)_2$(NO)(H)	96.98	89.40	52.03	57.66	62.45	66.55	72.79	77.17	83.49
C-(C)(ONO)(H)	-54.80	205.23	61.65	72.44	82.18	90.27	102.26	110.49	122.10
C-$(C)_2$(ONO)(H)	-51.11	107.97	69.24	81.16	89.60	95.40	102.41	106.46	111.67
C-(C)(NO_2)(H)	-65.30	202.89	56.96	68.33	78.25	86.45	98.60	106.93	118.62
C-$(C)_2(NO_2)$(H)	-60.35	110.76	57.46	68.31	77.10	83.95	93.32	99.22	106.86
C-(NO)$(H)_3$[a]	71.64	269.42	52.05	60.41	68.54	75.78	87.50	96.30	109.97
C-$(NO_2)(H)_3$[a]	-61.70	295.65	64.26	74.86	84.90	93.69	107.61	117.80	133.18
C-(C)(ONO)$(H)_3$[a]	-76.97	290.17	57.24	69.70	81.10	90.81	105.77	116.46	132.41
C-(CN)$(H)_3$[a]	73.88	251.52	51.84	60.69	68.95	76.27	88.33	97.63	112.37
N-centered									
N-(CO)$(H)_2$	-72.38	122.89	28.25	30.91	33.47	36.04	40.99	45.39	53.59
N-(C)(CO)(H)	-28.14	29.78	17.26	20.51	23.85	26.74	31.33	34.65	40.22
N-$(C)_2$(CO)	18.04	-59.52	16.92	17.80	19.46	21.12	23.97	25.75	28.15
N-(C)$(H)_2$	20.99	124.63	21.33	25.86	30.06	33.63	39.44	43.92	51.57
N-$(C)_2$(H)	69.99	35.66	20.32	23.22	26.33	28.98	33.15	35.91	39.96
N-$(C)_3$	102.05	-54.69	15.22	19.68	23.47	26.04	28.94	29.78	29.55
N-$(C)_2(C_d)$	78.49	-56.59	16.50	19.57	22.28	24.37	27.40	28.92	30.03
N-$(C_d)(H)_2$	-6.78	116.11	24.87	31.18	35.93	39.50	44.77	48.64	54.9
N-(C)(C_d)(H)	37.62	28.60	20.78	25.52	29.45	32.50	36.94	39.71	43.20
N-$(C_d)_2$(H)	17.43	25.86	27.69	32.86	36.03	38.04	40.69	42.36	44.38
N-(C)(C_t)(H)	65.74	46.78	17.72	20.42	23.32	25.89	30.07	33.11	38.02
N-$(C_d)(C_t)$(H)	43.40	46.77	21.43	25.47	28.83	31.42	35.17	37.66	41.19
N-$(C_t)(H)_2$	18.83	126.30	27.69	31.23	34.68	37.77	42.90	47.05	54.43
N-(N)$(H)_2$	46.26	123.21	26.23	31.15	34.99	37.98	42.57	46.20	52.69
N-(C)(N)(H)	91.50	31.83	21.27	25.08	28.27	30.80	34.57	37.14	41.03
N-$(C)_2$(N)	123.34	-57.55	15.27	18.94	22.24	24.69	27.75	29.00	29.71
N_I-(H)	61.69	110.78	17.80	19.66	21.76	23.87	27.50	30.21	34.82

N_I-(C)	97.01	30.32	14.94	14.94	15.63	16.66	18.73	20.04	21.81
N_I-(C_d)	78.38	17.95	17.77	22.59	24.83	25.59	25.50	24.82	23.84
N_A-(C)	121.88	28.43	14.11	15.13	16.32	17.41	19.18	20.29	21.63
N-(C)(O)(H)	156.59	23.12	20.78	28.77	35.01	39.29	43.90	45.48	45.85
N-$(C)_2$(O)	181.97	-67.18	21.52	28.18	32.61	35.13	36.88	36.22	32.98
NNI									
cis-C-C=C-N	8.58	5.16	-4.50	-4.16	-3.34	-2.76	-2.36	-2.34	-2.22
cis-C-C=N-C	9.87	-1.50	-4.50	-3.49	-2.55	-1.82	-0.87	-0.38	0.02
gauche	5.14	0.40	0.96	-1.01	-1.80	-1.93	-1.51	-1.02	-0.33

[a]GAV derived from a single molecular structure

From Table 3-13, it can be seen that the GAV contributions for the $\Delta_f H^\circ$ of the carbon-centered groups increase with increasing number of non-hydrogen ligands. The addition of a carbon ligand results on average in an increase of the GAVs for $\Delta_f H^\circ$ with 21 kJ mol^{-1} for the first, 13 kJ mol^{-1} for the second and 9 kJ mol^{-1} for the third non-hydrogen ligand.

Also for the nitrogen-centered groups, a strong correlation is observed between the GAVs for $\Delta_f H^\circ$ and the number of carbon ligands. For example, the substitution of a hydrogen ligand of a primary amino group by a carbon ligand increases the GAV by approximately 46 kJ mol^{-1}. The GAVs for $\Delta_f H^\circ$ for the N-$(C)_2$(H), N-(C)(C_d)(H), N-(C)(C_t)(H), N-(C)(N)(H) and N-(C)(CO)(H) groups are 48.9, 44.7, 46.9, 45.2 and 44.3 kJ mol^{-1} higher than the values obtained for the N-$(C)(H)_2$, N-(C_d)$(H)_2$, N-(C_t)$(H)_2$, N-(N)$(H)_2$ and N-(CO)$(H)_2$ groups. In a similar way, going from a secondary to a tertiary amino group by addition of another carbon ligand increases the GAV for $\Delta_f H^\circ$ by approximately 35 kJ mol^{-1}. The GAVs for N-$(C)_3$, N-$(C)_2$(C_d)(H), N-$(C)_2$(N), N-$(C)_2$(CO) are 32.0, 40.7, 31.8 and 46.2 kJ mol^{-1} higher than the values obtained for N-$(C)_2$(H), N-(C)(C_d)(H), N-(C)(N)(H) and N-(C)(CO)(H).

For each subset with a fixed number of non-hydrogen ligands, there is also an effect of the number of nitrogen ligands. The replacement of a carbon by a nitrogen ligand for a nitrogen-centered group results in an increase of 23 kJ mol^{-1} on average. The differences between the GAV($\Delta_f H^\circ$) for the groups N-(C)$(H)_2$ and N-(N)$(H)_2$, N-$(C)_2$(H) and N-(C)(N)$(H)_2$, N-$(C)_3$ and N-$(C)_2$(N) are equal to 25.1, 21.5 and 21.3 kJ mol^{-1}, respectively. For carbon-centered groups, replacing a carbon by a nitrogen ligand corresponds to an average decrease of 12 kJ mol^{-1} for the first nitrogen ligand and 22 kJ mol^{-1} for the second ligand.

The correlation with the number of non-hydrogen ligands can also be seen for the GAV contributions for $S^\circ{}_{int}$ and C_p°. For carbon-centered groups, the GAV contributions for $S^\circ{}_{int}$

decrease approximately 90 J mol^{-1} K^{-1} with each successive substitution of a hydrogen ligand by a carbon or nitrogen ligand. This decrease in entropy contribution is due to the fact that the contribution of neighboring hydrogen atoms are accounted for within the considered group. On the contrary, the entropy contributions of neighboring carbon or nitrogen ligands are accounted for within the neighboring group. Similar to the carbon-centered groups, there is a decrease of approximately 90 J mol^{-1} K^{-1} in the GAV contributions for $S^{\circ}{}_{int}$ of nitrogen-centered groups with each successive substitution of a hydrogen ligand by a carbon or nitrogen ligand.

As the C_p° of the nitrogen-containing compounds increases with temperature, so does the GAV contributions for C_p°. From Figure 3-14, it can be seen that this temperature dependence of the GAVs is group-dependent. The strongest increase is obtained for the carbon-centered C-(N)(H)$_3$ and nitrogen centered N-(C)(H)$_2$ groups. With each additional non-hydrogen ligand, this increase is further moderated.

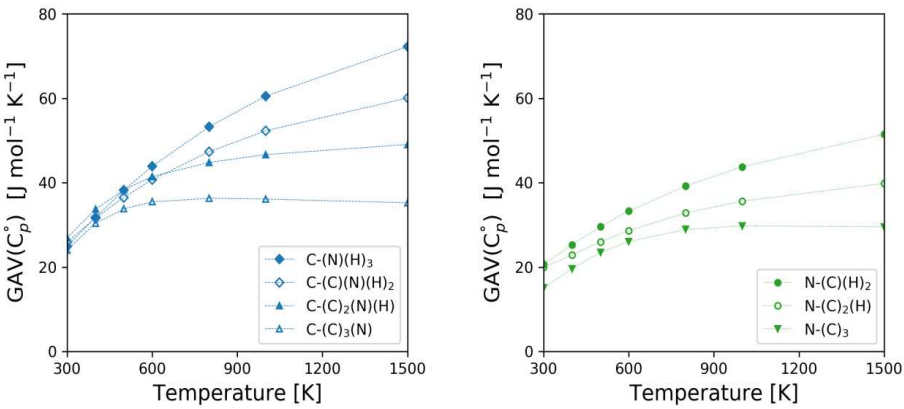

Figure 3-14: Temperature dependence of the GAVs for C_p° of various carbon-centered (left) and nitrogen-centered groups (right).

Similar to the carbon-centered GAVs determined by Sabbe et al., this trend is largely due to the C-H bonds, for which the contribution of their high-frequency stretch modes (3000 cm^{-1}) to the GAV for C_p° is only fully developed at about 3400 K. As a result, the GAV contributions of C_p° for carbon-centered groups will increase with temperature even for temperatures above 1000 K. For nitrogen-centered groups a similar trend can be seen, which is caused by the contributions of the high-frequency N-H stretch modes (3400 cm^{-1}) to the GAVs. The GAVs for the C_p° of carbon-centered groups decrease with increasing number of non-hydrogen ligands. This decrease can also be seen for the GAV contributions to C_p° of nitrogen-centered groups, e.g. approximately 6 J mol^{-1} K^{-1} at 300 K and 13 J mol^{-1} K^{-1} at 1500 K for the first substitution

of a hydrogen atom by a non-hydrogen ligand, 3 J mol^{-1} K^{-1} at 300 K and 9 J mol^{-1} K^{-1} at 1500 K for the second substitution.

In most cases, the carbon-centered groups with the same number of carbon and nitrogen ligands have similar GAV contributions. This is however not the case for the carbon-centered groups with cyano ligands. The GAVs for $\Delta_f H^\circ$ and $S^\circ{}_{int}$ are on average respectively 117 kJ mol^{-1} and 125 J mol^{-1} K^{-1} higher compared to those of similar carbon-centered groups with the same number of carbon ligands. This difference can be explained by the contribution of the –CN group, which is included in this group. Due to its definition as a supergroup, no separate contributions are introduced for groups with a cyanide carbon atom as central atom for approximation of the thermodynamic parameters of these molecules. It is assumed that the influence of the cyano group on the values of $\Delta_f H^\circ$, and C_p° is completely captured by the neighboring Benson group.

The destabilizing effect of the gauche interaction between alkyl substituents of a C-N bond corresponds to a positive contribution to the standard enthalpy of formation of 5.1 kJ mol^{-1}. For the analogous alkane gauche interaction along a C-C bond, which has an average bond length 1.54 Å compared to 1.47 Å for the C-N bond, the contribution equals 2.9 kJ mol^{-1}. The contributions for the intrinsic entropy and the heat capacities are less significant. The other two NNIs are cis-destabilizing interactions, with a positive contribution to the standard enthalpy of formation of 8.6 and 9.9 kJ mol^{-1} for cis-C-C=C-N and cis-C-C=N-C respectively. The single cis contributions to the intrinsic entropy are mainly caused by a change in the rotational barriers for the internal rotation around the bonds adjacent to the double bond. This leads to a contribution of 5.16 J mol^{-1} K^{-1} for cis-C-C=C-N and -1.50 J mol^{-1} K^{-1} for cis-C-C=N-C.

The final values for the GAVs of radical-centered Benson groups are included in Table 3-14. Due to the instability of the radicals, the GAVs for $\Delta_f H^\circ$ for radical-centered groups are in general much higher compared to the non-radical-centered groups. In most cases, the GAVs for $S^\circ{}_{int}$ and C_p° are slightly lower, which can be explained by the loss of a single bond and the corresponding loss of degrees of freedom.

Table 3-14: Group additive values for the standard enthalpy of formation [kJ mol^{-1}] and intrinsic standard entropy [J mol^{-1} K^{-1}] at 298 K and standard heat capacity [J mol^{-1} K^{-1}] at different temperatures for nitrogen-containing radicals deduced by linear regression making use of both the training and test set. The subscripts d, t, I and A indicate that the corresponding atom is part of a carbon carbon double bond, carbon carbon triple bond, carbon nitrogen double bond and nitrogen nitrogen double bond, respectively.

Group	$\Delta_f H^\circ$	S°_{int}	C_p°						
			300 K	400 K	500 K	600 K	800 K	1000 K	1500 K
C-centered									
$C^{\cdot}$-(N)(H)$_2$	127.49	132.66	27.23	31.77	35.30	38.27	43.10	47.17	54.25
$C^{\cdot}$-(N$_I$)(H)$_2$	110.64	116.33	23.57	31.09	36.64	40.80	46.65	50.92	57.80
$C^{\cdot}$-(CN)(H)$_2$	259.09	253.75	52.46	59.78	65.77	70.73	78.61	84.60	94.20
$C^{\cdot}$-(C)(N)(H)	140.33	44.73	25.18	28.80	31.37	33.37	36.21	38.34	41.65
$C^{\cdot}$-(C)(N$_I$)(H)	111.68	43.22	17.41	23.77	28.54	32.09	36.80	39.86	43.78
$C^{\cdot}$-(C)(CN)(H)	266.31	176.23	42.04	49.23	55.17	60.00	67.21	72.27	79.65
$C^{\cdot}$-(C$_d$)(N)(H)	79.35	31.95	19.59	25.96	30.53	33.90	38.38	41.41	45.79
$C^{\cdot}$-(C$_d$)(CN)(H)	217.69	160.00	41.40	50.38	57.45	62.90	70.65	75.90	83.47
$C^{\cdot}$-(C)$_2$(N)	141.47	-37.90	21.70	23.65	24.90	25.87	27.01	27.63	28.03
$C^{\cdot}$-(C)$_2$(N$_I$)	117.84	-40.93	15.65	20.35	24.25	27.19	30.42	31.61	31.55
$C^{\cdot}$-(C)$_2$(C$_I$)	127.73	-51.18	13.02	17.37	20.80	23.35	26.32	27.95	29.76
$C^{\cdot}$-(C)$_2$(CN)	269.58	93.76	39.60	44.39	48.71	52.39	57.85	61.43	66.01
$C^{\cdot}$-(C)(C$_d$)(N)	81.45	-53.68	19.28	23.67	26.46	28.38	30.52	31.59	32.34
C$_d^{\cdot}$-(N)	268.04	47.09	16.43	17.33	18.22	18.81	19.18	19.25	19.65
C$_d^{\cdot}$-(N$_I$)	238.59	47.71	14.19	13.95	14.81	16.31	19.21	21.18	23.20
C$_I^{\cdot}$-(H)	214.16	121.96	18.22	21.10	23.67	25.70	28.84	31.38	35.35
C$_I^{\cdot}$-(C)	206.49	40.24	13.01	15.44	17.29	18.49	20.05	20.99	21.88
N-centered									
$N^{\cdot}$-(C)(H)	224.64	130.79	16.64	18.68	21.08	23.19	26.62	29.13	33.19
$N^{\cdot}$-(C$_d$)(H)	142.89	115.04	15.77	20.77	24.56	27.28	30.99	33.55	37.46
$N^{\cdot}$-(C$_t$)(H)	160.22	131.02	24.17	25.64	27.36	28.96	31.56	33.55	36.87
$N^{\cdot}$-(C)$_2$	245.17	48.24	12.23	12.80	14.18	15.50	17.70	18.93	20.22
$N^{\cdot}$-(C)(C$_d$)	183.29	33.06	9.85	13.65	16.70	18.83	21.57	23.00	24.41
$N^{\cdot}$-(C$_d$)$_2$	133.79	8.85	16.85	25.75	31.88	35.81	39.10	38.51	32.77
$N^{\cdot}$-(C)(C$_t$)	198.61	53.51	11.35	12.08	13.53	14.92	17.09	18.31	19.67
$N^{\cdot}$-(C$_d$)(C$_t$)	157.45	36.11	21.09	25.32	27.64	28.90	30.11	30.39	29.55
$N^{\cdot}$-(C$_t$)$_2$	193.93	64.95	19.47	20.36	21.67	22.92	24.75	25.77	26.70
$N^{\cdot}$-(C)(O)	278.07	30.17	12.67	16.22	19.09	21.06	23.33	24.20	24.60
N$_I^{\cdot}$-	218.89	114.48	16.64	16.46	16.20	16.10	16.09	16.06	16.34
O-centered									
$O^{\cdot}$-(N)	-71.18	136.44	6.83	2.22	0.16	-0.28	1.29	3.99	9.91

Group additive values for nitrogen-containing compounds have been determined before by Benson et al. [22], Holmes and Aubry [23], and Ashcraft et al. [25]. The results of a direct comparison between the present GAVs and those previously derived values for all groups in common are provided in Table A-6, Table A-7 and Table A-8 in Appendix A. Large differences can be mainly explained by the different assumptions which have been made to address the linear dependencies. This illustrates that it is imperative to only use internally consistent GAV databases to approximate the thermodynamic properties. To enable a better comparison, the sum of the GAV values of pairs of linear dependent groups, for which there are large differences between their exact values, are also reported.

The majority of the GAV contributions determined in this work are similar to the experimental values reported by Benson et al. [22]. The largest difference is obtained for the group C_t-(CN), for which the GAV value for $\Delta_f H^\circ$ is 21 kJ mol^{-1} higher than the value calculated in this work. Benson et al. [22] determined this GAV from the experimental standard enthalpy of formation of a single molecule, i.e. 2-butyne dinitrile (N≡C-C≡C-C≡N). In the present work, this GAV has been determined from three different molecules containing one cyano group. Using the GAVs of Benson et al. [22] to calculate the standard enthalpy of formation for cyano acetylene (HC≡C-C≡N) a value of 378.7 kJ mol^{-1} is obtained, which is approximately 25 kJ mol^{-1} higher than the experimental value. With the GAVs calculated in this work, the approximated standard enthalpy of formation is equal to 359.4 kJ mol^{-1}. While there are minor differences for the values of the separate GAVs of amide compounds, i.e. CO-(N)(C), N-(CO)$(H)_2$ and N-(C)(CO)(H), the sum of GAV values for the pairs of the respective linear dependent groups agree well. The contribution of the azide Benson group N_A-(C) is 14 kJ mol^{-1} higher than the value reported here. In deriving the GAVs, Benson et al. [22] made the assumption that the incremental changes when replacing a hydrogen ligand by a methyl ligand of an azo nitrogen (N=N) is equal to those for the analogous olefins.

The largest differences with the GAVs of Holmes and Aubry [24] are obtained for the groups with cyano ligands. In their GAV scheme, separate contributions are introduced for cyano-centered groups. The reported GAV values for the $\Delta_f H^\circ$ of the groups CN-(C), CN-(C_d) and CN-(C_t) are all equal to 115.0 kJ mol^{-1}, with an uncertainty of 2.0 kJ mol^{-1}. The GAVs reported in this work for $\Delta_f H^\circ$ with a cyano group as ligand are on average 117 kJ mol^{-1} higher than those of similar carbon-centered groups with the same number of carbon ligands. The same approach regarding these cyano-centered ligands has been followed as in the work of Benson et al. [22] and Ashcraft et al. [25]. Holmes and Aubry [23] also made the assumption that the

sequence N-(CO)$(H)_2$, N-(C)(CO)(H), N-$(C)_2$(CO) is similar to that for N-(C)$(H)_2$, N-$(C)_2$(H), N-$(C)_3$.

When comparing with the GAVs reported by Ashcraft et al. [34], significant differences are observed for Benson groups with nitrogen and double bonded carbon ligands. This can be explained by the arbitrary fixing of GAV values to solve the linear dependencies. As an example, a difference of 27.0 kJ mol^{-1} is obtained for the single GAVs C_d-(C)(N), N-$(C_d)(H)_2$ and N-(C)(C_d)(H). Ashcraft et al. assigned the nitrogen-centered group N-$(C_d)(H)_2$ the same value as reported by Benson et al. for N-(C)$(H)_2$. While the differences can amount up to 27 kJ mol^{-1} for the single GAVs of $\Delta_f H^\circ$, the sum of the GAVs for the corresponding linear dependent groups agrees well, i.e. differences for N-$(C_d)(H)_2$+C_d-(C)(N) and N-(C_d)(C)(H)+C_d-(C)(N) are equal to only -0.3 and 0.5 kJ mol^{-1} respectively. In this work the value of C_d-(N)(H) was set equal to C_d-(C)(H), which is the similar to the assumption made for oxygenates and sulfur-containing compounds.

To further validate the GAV scheme, a test set is constructed containing experimental standard enthalpies of formation for 11 nitrogen-containing compounds, c.f. Figure 3-15.

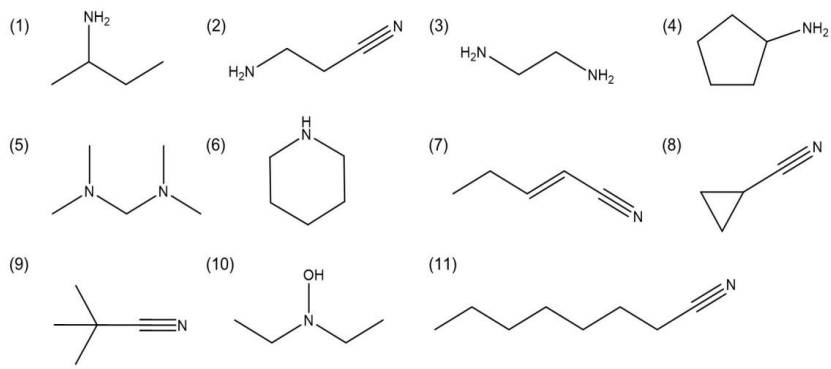

Figure 3-15: Test set of 11 nitrogen-containing molecules for experimental validation of the group value estimates.

The comparison between experimental and group additivity approximated $\Delta_f H^\circ$ for 11 nitrogen-containing compounds is given in Table 3-15 . The experimental values are taken from ATcT, Pedley et al. [26] and the NIST Chemistry Webbook [27].

Table 3-15: Comparison between group additivity approximated (GA) and experimental (exp) values for the standard enthalpy of formation [kJ mol^{-1}] for 11 nitrogen-containing compounds for the GAV scheme reported in this work, from Holmes and Aubry [24], and from Ashcraft et al. [34].

	$\Delta_f H^\circ_{exp}$	$\Delta_f H^\circ_{GA} - \Delta_f H^\circ_{exp}$		
Molecule		This work	Holmes et al.	Ashcraft et al.
1	-104.9 ± 1.0	1.0	-1.4	-1.4
2	89.8 ± 1.0	0.6	-0.8	-1.5
3	-17.6 ± 0.6	4.3	7.6	2.5
4	-54.9 ± 0.9	6.2	3.8	4.2
5	-17.7 ± 1.8	3.3	-	4.8
6	-47.2 ± 0.6	-0.3	4.7	6.3
7	119.8 ± 1.1	4.8	-	15.5
8	182.7 ± 0.7	6.8	-	2.8
9	-2.5 ± 0.8	-3.6	-	-4.1
10	-121.8 ± 0.7	-2.7	-	-
11	-50.6 ± 1.5	2.2	-0.8	1.0
Statistics				
	MAD	2.8	3.2	3.7
	RMS	3.9	4.0	6.0
	MAX	6.8	7.6	15.5

A good agreement is obtained between the experimental values and the group additivity approximations of the standard enthalpy of formation with a MAD of 2.8 kJ mol^{-1} and a MAX of 6.8 J mol^{-1} K^{-1}. By making use of the group additivity model of Holmes et al. , the standard enthalpy of formation for six species is approximated with a MAD of 3.2 kJ mol^{-1}, while for Ashcraft et al. a MAD of 3.7 kJ mol^{-1} is obtained for a set of 10 species.

3.3.2.4. Application of the group additivity scheme

To demonstrate the use of the group additivity model, two example calculations are done to obtain the standard enthalpy of formation for prop-1-ene-1,1-diamine (species 5 in Figure 3-13) and diethyl hydroxylamine (species 10 in Figure 3-15).

Four different groups can be identified in prop-1-ene-1,1-diamine, i.e. C-(C_d)$(H)_3$, C_d-(C)(H), C_d-$(N)_2$ and N-(C_d)$(H)_2$. The NNI correction of the destabilizing cis interaction between the methyl and amino group contributes 8.6 kJ mol^{-1}, which results in a final value of 23.6 kJ mol^{-1} for the standard enthalpy of formation of prop-1-ene-1,1-diamine. This group additive approximated value is 1.6 kJ mol^{-1} higher than the *ab initio* calculated value.

$$\Delta_f H^\circ = GAV(C-(C_d)(H)_3) + GAV\big(C_d-(C)(H)\big) + GAV(C_d-(N)_2) + GAV(N-(C_d)(H)_2) + NNI(cis) = (-42.9) + 37.1 + 34.6 + 2 \cdot (-6.9) + 8.6 = 15.0\ kJ\ mol^{-1}$$

Four different groups can be identified in diethyl hydroxylamine, i.e. two C-(C)(H)$_3$ groups, two C-(C)(N)(H)$_2$ groups, one N-(C)$_2$(O) group and one O-(N)(H) group. Using the group additivity approximation, the standard enthalpy of formation is equal to -124.6 kJ mol^{-1}. As can be seen from Table 3-15, this is an underestimation of the experimentally determined value with 2.7 kJ mol^{-1}.

$$\Delta_f H^\circ = 2 \cdot GAV(C-(C)(H)_3) + 2 \cdot GAV(C-(C)(N)(H)_2) + GAV\big(N-(C)_2(O)\big) + GAV(O-(N)(H)) = 2 \cdot (-42.9) + 2 \cdot (-27.8) + 182.0 + (-165.2) = -124.6\, kJ\, mol^{-1}$$

3.4. Conclusions

There is a systematic deviation between experimental and CBS-QB3 calculated standard enthalpies of formation at 298 K for hydrogen, carbon, oxygen, nitrogen and sulfur-containing species. In order to reach thermodynamic accuracy, i.e. predict the experimental values with a mean absolute deviation (MAD) of 4 kJ mol^{-1}, a correction method needs be applied, such as the Bond Additivity Correction (BAC) method. In this work, a new set of BACs has been derived to improve the accuracy of the standard enthalpy of formation obtained from *ab initio* calculations at the CBS-QB3 level of theory. The BAC parameters have been determined from a dataset of 371 hydrocarbons and heteroatom-containing molecules, for which accurate experimental data is available. The performance of the regressed BAC values has been validated with a test set of 41 species, for which the MAD decreases from 5.5 kJ mol^{-1} to 2.1 kJ mol^{-1} when applying BACs. For the complete dataset, the MAD between experimental and uncorrected CBS-QB3 calculated values is equal to 5.6 kJ mol^{-1}. Application of the optimized BAC parameters leads to a decrease of the MAD to 1.7 kJ mol^{-1}. The corresponding root-mean-square deviation decreases from 6.9 kJ mol^{-1} to 2.2 kJ mol^{-1}.

To address the scarcity of thermodynamic parameters for nitrogen-containing compounds, the available group additivity schemes have been extended for nitrogen-containing compounds. From a dataset of CBS-QB3 calculations for 300 species, 91 group additive values and three non-nearest-neighbor interactions have been determined via least-squares regression. This dataset contains a wide range of nitrogen-containing functionalities, i.e. imine, nitrile, nitro, nitroso, nitrite, nitrate and azo functional groups. The group additive model enables the approximation of the standard enthalpy of formation and standard entropy at 298 K and the heat capacity over the temperature range 300-1500 K for a large set of nitrogen-containing compounds. The general applicability of the new group additive model is validated with a test set of 27 nitrogen-containing compounds. The *ab initio* calculated values for the standard enthalpy of formation is approximated with a MAD of 2.3 kJ mol^{-1}. The MAD for the standard entropy and heat capacity is lower than 4 and 2 J mol^{-1} K^{-1}, respectively. A test set containing 11 nitrogen-containing compounds for which experimental values are available has been constructed to validate the new GAV values for standard enthalpies of formation. The MAD between experimental and group additive approximated values for the standard enthalpy of formation amounts to 2.8 kJ mol^{-1}.

3.5. References

[1] F. Battin-Leclerc, E. Blurock, R. Bounaceur, R. Fournet, P.-A. Glaude, O. Herbinet, B. Sirjean, V. Warth, Towards cleaner combustion engines through groundbreaking detailed chemical kinetic models, Chemical Society Reviews 40 (2011) 4762-4782.

[2] J.A. Pople, Nobel Lecture: Quantum chemical models, Reviews of Modern Physics 71 (1999) 1267-1274.

[3] C.W. Bauschlicher, S.R. Langhoff, Quantum Mechanical Calculations to Chemical Accuracy, Science 254 (1991) 394-398.

[4] B. Ruscic, Uncertainty quantification in thermochemistry, benchmarking electronic structure computations, and Active Thermochemical Tables, International Journal of Quantum Chemistry 114 (2014) 1097-1101.

[5] S.J. Klippenstein, C. Cavallotti, Chapter 2 - Ab initio kinetics for pyrolysis and combustion systems, in: T. Faravelli, F. Manenti, E. Ranzi (Eds.), Computer Aided Chemical Engineering, Elsevier2019, pp. 115-167.

[6] S.J. Klippenstein, V.S. Pande, D.G. Truhlar, Chemical Kinetics and Mechanisms of Complex Systems: A Perspective on Recent Theoretical Advances, Journal of the American Chemical Society 136 (2014) 528-546.

[7] J.A. Montgomery, M.J. Frisch, J.W. Ochterski, G.A. Petersson, A complete basis set model chemistry. VII. Use of the minimum population localization method, The Journal of Chemical Physics 112 (2000) 6532-6542.

[8] A.G. Vandeputte, M.K. Sabbe, M.F. Reyniers, G.B. Marin, Modeling the gas-phase thermochemistry of organosulfur compounds, Chemistry 17 (2011) 7656-7673.

[9] J.M. Simmie, K.P. Somers, Benchmarking Compound Methods (CBS-QB3, CBS-APNO, G3, G4, W1BD) against the Active Thermochemical Tables: A Litmus Test for Cost-Effective Molecular Formation Enthalpies, The Journal of Physical Chemistry A 119 (2015) 7235-7246.

[10] B. Ruscic, D.H. Bross, Active Thermochemical Tables (ATcT) values based on ver. 1.122d of the Thermochemical Network (2018); available at ATcT.anl.gov.

[11] K.P. Somers, J.M. Simmie, Benchmarking Compound Methods (CBS-QB3, CBS-APNO, G3, G4, W1BD) against the Active Thermochemical Tables: Formation Enthalpies of Radicals, The Journal of Physical Chemistry A 119 (2015) 8922-8933.

[12] J.M. Simmie, A database of formation enthalpies of nitrogen species by compound methods (CBS-QB3, CBS-APNO, G3, G4), The Journal of Physical Chemistry A 119 (2015) 10511-10526.

[13] G.A. Petersson, D.K. Malick, W.G. Wilson, J.W. Ochterski, J.A.M. Jr., M.J. Frisch, Calibration and comparison of the Gaussian-2, complete basis set, and density functional methods for computational thermochemistry, The Journal of Chemical Physics 109 (1998) 10570-10579.

[14] M. Saeys, M.F. Reyniers, G.B. Marin, V. Van Speybroeck, M. Waroquier, Ab initio calculations for hydrocarbons: Enthalpy of formation, transition state geometry, and activation energy for radical reactions, Journal of Physical Chemistry A 107 (2003) 9147-9159.

[15] B. Anantharaman, C.F. Melius, Bond Additivity Corrections for G3B3 and G3MP2B3 Quantum Chemistry Methods, The Journal of Physical Chemistry A 109 (2005) 1734-1747.

[16] C.A. Grambow, Y.-P. Li, W.H. Green, Accurate Thermochemistry with Small Data Sets: A Bond Additivity Correction and Transfer Learning Approach, The Journal of Physical Chemistry A 123 (2019) 5826-5835.

[17] M.R. Zachariah, P.R. Westmoreland, D.R. Burgess, W. Tsang, C.F. Melius, BAC-MP4 Predictions of Thermochemical Data for C1 and C2 Stable and Radical Hydrofluorocarbons and Oxidized Hydrofluorocarbons, The Journal of Physical Chemistry 100 (1996) 8737-8747.

[18] M.K. Sabbe, M. Saeys, M.F. Reyniers, G.B. Marin, V. Van Speybroeck, M. Waroquier, Group additive values for the gas phase standard enthalpy of formation of hydrocarbons and hydrocarbon radicals, Journal of Physical Chemistry A 109 (2005) 7466-7480.

[19] P.D. Paraskevas, M.K. Sabbe, M.F. Reyniers, N. Papayannakos, G.B. Marin, Group additive values for the gas-phase standard enthalpy of formation, entropy and heat capacity of oxygenates, Chemistry 19 (2013) 16431-16452.

[20] A. Ince, H.-H. Carstensen, M.-F. Reyniers, G.B. Marin, First-principles based group additivity values for thermochemical properties of substituted aromatic compounds, AIChE Journal 61 (2015) 3858-3870.

[21] S.W. Benson, J.H. Buss, Additivity Rules for the Estimation of Molecular Properties. Thermodynamic Properties, The Journal of Chemical Physics 29 (1958) 546-572.

[22] S.W. Benson, F.R. Cruickshank, D.M. Golden, G.R. Haugen, H.E. O'Neal, A.S. Rodgers, R. Shaw, R. Walsh, Additivity rules for the estimation of thermochemical properties, Chemical Reviews 69 (1969) 279-324.

[23] J.L. Holmes, C. Aubry, Group Additivity Values for Estimating the Enthalpy of Formation of Organic Compounds: An Update and Reappraisal. 2. C, H, N, O, S, and Halogens, The Journal of Physical Chemistry A 116 (2012) 7196-7209.

[24] J.L. Holmes, C. Aubry, Group Additivity Values for Estimating the Enthalpy of Formation of Organic Compounds: An Update and Reappraisal. 1. C, H, and O, The Journal of Physical Chemistry A 115 (2011) 10576-10586.

[25] R.W. Ashcraft, W.H. Green, Thermochemical Properties and Group Values for Nitrogen-Containing Molecules, The Journal of Physical Chemistry A 112 (2008) 9144-9152.

[26] J. Pedley, R.D. Naylor, S.P. Kirby, Thermochemical data of organic compounds, springer Netherlands, 1986.

[27] P.J. Lindstrom, W.G. Mallard, NIST Chemistry WebBook, NIST Standard Reference Database Number 69, National Institute of Standards and Technology, Gaithersburg MD.

[28] B. Ruscic, R.E. Pinzon, G.v. Laszewski, D. Kodeboyina, A. Burcat, D. Leahy, D. Montoy, A.F. Wagner, Active Thermochemical Tables: thermochemistry for the 21st century, Journal of Physics: Conference Series 16 (2005) 561-570.

[29] B. Ruscic, R.E. Pinzon, M.L. Morton, G. von Laszevski, S.J. Bittner, S.G. Nijsure, K.A. Amin, M. Minkoff, A.F. Wagner, Introduction to Active Thermochemical Tables: Several “Key” Enthalpies of Formation Revisited, The Journal of Physical Chemistry A 108 (2004) 9979-9997.

[30] M.K. Sabbe, F. De Vleeschouwer, M.-F. Reyniers, M. Waroquier, G.B. Marin, First Principles Based Group Additive Values for the Gas Phase Standard Entropy and Heat Capacity of Hydrocarbons and Hydrocarbon Radicals, The Journal of Physical Chemistry A 112 (2008) 12235-12251.

[31] A. Fernández-Ramos, B.A. Ellingson, R. Meana-Pañeda, J.M.C. Marques, D.G. Truhlar, Symmetry numbers and chemical reaction rates, Theoretical Chemistry Accounts 118 (2007) 813-826.

[32] M.B. Smith, J. March, March's Advanced Organic Chemistry, John Wiley & Sons, Inc.2006, pp. 136-233.

[33] J.A. Dean, N.A. Lange, Lange's Handbook of Chemistry, McGraw-Hill1999.

[34] R.W. Ashcraft, S. Raman, W.H. Green, Ab initio aqueous thermochemistry: application to the oxidation of hydroxylamine in nitric acid solution, J Phys Chem B 111 (2007) 11968-11983.

4

Hydrogen abstraction reactions in nitrogen-containing compounds

Abstract

New group additive values are presented to enable the modeling of a broad range of intermolecular hydrogen abstraction reactions involving nitrogen-containing compounds. From a dataset of 316 reaction rate coefficients calculated at the CBS-QB3 level of theory in the high-pressure limit, a total of 76 group additive values and 14 resonance corrections have been estimated. The influence of substituents on both the attacking and attacked radical, being a carbon or nitrogen atom, has been investigated systematically. The new group additivity models can be applied to approximate the Arrhenius parameters of hydrogen abstraction reactions of nitrogen-containing compounds by hydrogen atoms, carbon-centered and nitrogen-centered radicals in the temperature range 300-1800 K. Complementary to the group additivity model, correlations for the tunneling coefficients, which depend on both the temperature and the activation energy of the reaction in the exothermic direction, have been generated. The good overall accuracy of the new group additivity schemes has been demonstrated using a test set of reactions. At 1000 K, the rate coefficients for all test set reactions are approximated on average within a factor of a 1.45, 1.47 and 1.34, for the hydrogen abstractions with a reactive center of the type H-H-N, N-H-N and C-H-N respectively.

4.1. Introduction

In addition to thermodynamic parameters, assignment of kinetic parameters is necessary to enable model simulations. Due to the high complexity of kinetic models for industrially important processes such as pyrolysis and oxidation, one of the main challenges of kinetic model construction is the large amount of kinetic parameters required. The accuracy of the simulation is constrained primarily by the accuracy of the reaction rate coefficients which have been used and according to Green et al. [1], rate coefficients are likely to be the largest source of uncertainty in kinetic models for many years to come. Determining each elementary reaction rate from experimental measurements is not a feasible option. Especially, as it is required to characterize the reaction rate for different ranges of temperature and pressure. In spite of the increasing development of computational resources and methods, it is not yet possible to calculate all required kinetic parameters for each elementary reaction from first principles, as it requires even more time compared to the calculation of the thermochemistry.

Approximation methods have been developed to obtain accurate values for these parameters in a limited amount of time. Most of the reactions can be classified in a limited set of reaction families and the calculation of rate coefficients can be done per reaction family. Approximation methods are based on the idea that the reactive moiety within a certain reaction family is similar for all reactions in that family, such that for each reaction the rate coefficient can be estimated based on a contribution for the reactive moiety alongside reaction-specific contributions. These approximation methods are fast and scalable, and do not require any additional *ab initio* calculations during kinetic model generation. On the one hand, semi-empirical correlations exist, such as the Evans-Polanyi correlation [2] and the Blowers and Masel model [3]. On the other hand, there are methods which can be considered as an extension to Benson's group additivity method [4] and approximate the kinetic parameters based on the structure of the transition state. The *ab initio* derived group additivity method has been successfully applied to hydrogen abstraction reactions, radical addition reactions and homolytic substitution reactions in hydrocarbons [5-7], oxygenates [8, 9] and sulfur-containing compounds [10, 11].

One of the main reaction families important during steam cracking, pyrolysis and oxidation of nitrogen-containing compounds, including aliphatic amines, is the intermolecular hydrogen abstraction family. To the author's knowledge, there is only limited information available concerning the kinetic parameters of these reactions for these compounds. Lucassen et al. [12] combined literature data with *ab initio* calculations (B3LYP/6-311G(d,p)) to obtain reliable rate

coefficients for the oxidation of ethylamine. The kinetic parameters for the reactions of ethylamine with respectively hydrogen, methyl and amine radicals are assigned values based on analogous reactions involving propane and ethanol. Almatarnech et al. [13] studied the bimolecular and unimolecular reactions important for the decomposition of ethylamine making use of *ab initio* calculations.

Apart from a limited number of accurate data available for specific model compounds, a consistent database or a method to approximate the reaction rate coefficients for a wide range of hydrogen abstraction reactions involving nitrogen-containing compounds is still lacking. In this Chapter, the group additivity method is used to address this gap by introducing a new group additive model, consisting of a set of group additive values (ΔGAV°) as well as resonance corrections, for intermolecular hydrogen abstractions involving nitrogen-containing compounds. The influence of the ligands of the attacked nitrogen atom as well as the ligands of the attacking carbon and nitrogen atom are studied in detail. The application of the new group additivity model for approximation of the kinetic parameters of hydrogen abstractions of nitrogen-containing species is demonstrated with two examples.

4.2. Methodology

Three different reaction families are considered, that is 1) hydrogen abstraction from a nitrogen atom by a hydrogen atom and its reverse reaction, 2) hydrogen abstraction from a nitrogen atom by a nitrogen-centered radical and 3) hydrogen abstraction from a nitrogen atom by a carbon-centered radical and its reverse reaction. The first reaction family is characterized by a transition state of the H-H-N type and will therefore be referred to as H-H-N abstraction reactions. Hydrogen abstractions in which a hydrogen atom is exchanged between two nitrogen atoms are referred to as N-H-N abstractions. The third reaction family corresponds to C-H-N abstractions, in which a carbon and nitrogen atom are part of the reactive center. A schematic representation of these hydrogen abstractions is given in Figure 4-1.

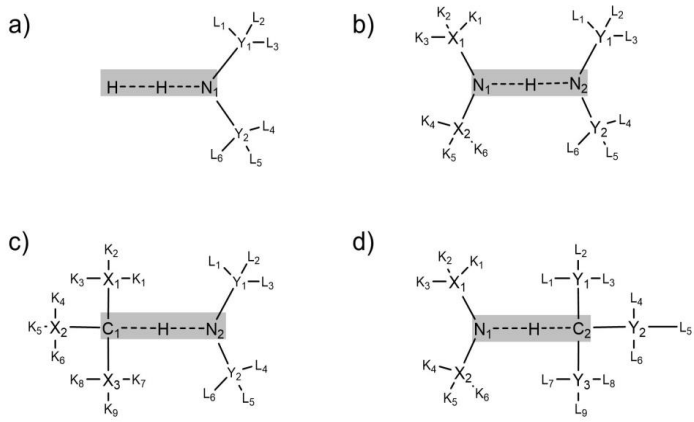

Figure 4-1: Schematic representation of the transition state for a) abstraction of a hydrogen atom bound to a nitrogen atom by a hydrogen atom, b) abstraction of a hydrogen atom bound to a nitrogen atom by a nitrogen atom, c) abstraction of a hydrogen atom bound to a nitrogen atom by a carbon-centered radical and d) its reverse reaction. The grey area indicates the central atoms of the primary contributions. The groups with X_i and Y_i as central atoms correspond to secondary contributions.

The groups with the carbon and nitrogen atoms labeled with subscripts 1 and 2 as central atoms, are referred to as the primary groups. Subscript 1 labels the hydrogen abstracting atom, while the atom from which the hydrogen atom is abstracted is labeled with subscript 2. The groups with X and Y as central atoms correspond to the secondary contributions. Non-nearest-neighbor interactions arise from interactions between the K and L-centered groups and the primary groups or between secondary groups located on both sides of the transition state. The reference reactions for these three reaction families are shown in Figure 4-2.

$$^{\bullet}H + NH_3 \rightleftharpoons H_2 + {}^{\bullet}NH_2$$

$$^{\bullet}NH_2 + NH_3 \rightleftharpoons NH_3 + {}^{\bullet}NH_2$$

$$^{\bullet}CH_3 + \text{—}NH_2 \rightleftharpoons CH_4 + \text{—}NH^{\bullet}$$

Figure 4-2: Reference reactions for the intermolecular hydrogen abstraction reactions of the type H-H-N, N-H-N and C-H-N.

For H-H-N and N-H-N abstraction reactions, the simplest reaction with that transition state is chosen as reference reaction, corresponding to abstraction from ammonia by a hydrogen atom and by the amino radical respectively. For C-H-N abstractions, the hydrogen abstraction by a methyl radical from ammonia is chosen as reference reaction. The single-event Arrhenius parameters for these reactions in the temperature range 300–1800 K can be found in Table B-2, Table B-8 and Table B-14 in Appendix B. Due to the introduction of a reference reaction,

the temperature dependence of the kinetic parameters is mainly accounted for by the Arrhenius parameters of the reference reaction, which decreases the temperature dependence of the ΔGAV° values to some extent. In addition, *ab initio* methods yield in general more accurate relative than absolute values. To determine new group additive values, an extensive dataset of 158 reactions is generated in which the hydrogen atoms attached to both the carbon and nitrogen atoms are substituted with different groups. The same notation as introduced in Chapter 3 is used to distinguish between the different carbon and nitrogen atom types. The different central atom types that are considered here include a single bonded carbon atom (C), a carbon atom double bonded to another carbon atom (C_d), a triple bonded carbon atom (C_t), a single bonded nitrogen atom (N), a carbon atom double bonded to a nitrogen atom (C_I), a nitrogen atom double bonded to a carbon atom (N_I). Note that the hydrogen atom exchanged during the abstraction reaction is not included in the group notation. For example, for hydrogen abstractions of the type C-H-N, the relevant groups identified in the reference reaction are equal to C-$(H)_3$ and N-(C)(H), which evidently have group additive values of zero.

To account for the (de)stabilizing effects of certain combination of ligands on the two nitrogen atoms for N-H-N hydrogen abstractions or on the carbon and nitrogen atom of asymmetric C-H-N abstractions, resonance corrections (RES) are regressed in addition to the group additive values. Because hydrogen abstraction from methylamine by a methyl radical is considered as reference reaction for C-H-N abstractions, cross-interactions with alkyl ligands on the nitrogen atom are already included in the ΔGAV°s. The interactions requiring additional attention are those obtained for combinations of an alkyl ligand, π-conjugating (C=C, C≡C, C=N, N=C, C≡C) ligand or nitrogen atom on the carbon atom, and a hydrogen ligand, vinyl ligand, ethynyl ligand on the primary nitrogen atom. These corrections are labeled $_{L1}N\text{-}N_{L2}$ or $_{L1}C\text{-}N_{L2}$, with L1 and L2 the possible ligands on the carbon and nitrogen reactive center atoms, i.e. L_i = H, $\beta_{C\text{-}H}$, πC=C, πC=N , πN=C , πC≡C, αN. Each resonance correction corresponds to a single cross interaction and the same counting scheme for the resonance interactions as defined in previous work is used [5].

Similar to the bond additive corrections and the thermodynamic group additive parameters, the kinetic group additive parameters are determined via unweighted least-squares regression analysis, for which the governing equations can be found in Chapter 2. This method implies the minimization of the sum as squares as defined in Eq. 4-1, with y_i the *ab initio* calculated value for the Arrhenius parameter and $\hat{y}_i$ the group additive approximated value for the Arrhenius parameter of reaction *i*.

$$SSQ = \sum_{i}^{n} (y_i - \hat{y}_i)^2 \qquad \text{(Eq. 4-1)}$$

This results in the following Eq. 4-2 for the optimized set of ΔGAV° and RES parameters.

$$\overline{\Delta GAV^{\circ}/RES} = (X^T X)^{-1} X^T y \qquad \text{(Eq. 4-2)}$$

The methodology used to calculate the new ΔGAV°s and RES in this work is illustrated in Figure 4-3. Similar to the regression procedure used for the thermodynamic parameters, c.f. Chapter 3, the complete dataset is divided into a training and test set for each reaction family. The preliminary set of ΔGAV°s and RES is determined in a straightforward manner from the limited training set data set, which contains one reaction for each value. In order to validate the group additivity approach, these preliminary ΔGAV°s and RES are subsequently used to approximate the kinetic properties of all reactions which have not been included in the training set, i.e. the test set. In case a satisfactory agreement is obtained between *ab initio* calculated and group additive approximated data for all reactions in the test set, the final set of ΔGAV°s and RES is determined from the complete dataset.

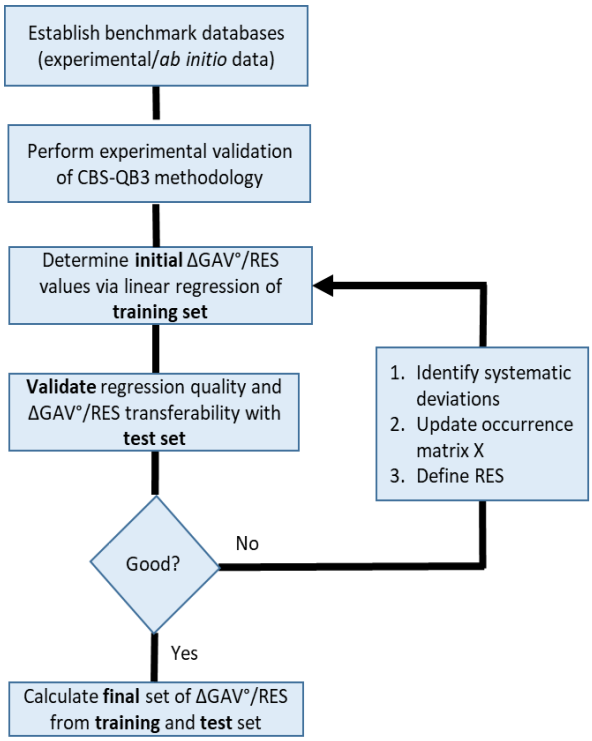

Figure 4-3: Methodology to determine a new set of group additive values (ΔGAV°) and resonance corrections (RES) for hydrogen abstractions of nitrogen-containing species.

The assessment of the accuracy of the group additivity method is performed by comparing the *ab initio* calculated (k_{AI}) rate coefficients with the group additive (k_{GA}) approximated rate coefficients. In analogy with previous studies [5, 7], the factor ρ, as defined in Eq. 4-3, is used to quantify the deviation between both values.

$$\rho = \frac{max(k_{AI}, k_{GA})}{min(k_{AI}, k_{GA})} \qquad \text{(Eq. 4-3)}$$

This factor ρ, which is a value larger than one, enables to determine a mean deviation $\langle\rho\rangle$ as well as a maximum deviation ρ_{max} for a set of reactions. This factor ρ is also used to assess the accuracy of the employed CBS-QB3 level of theory by comparing *ab initio* calculated rate coefficients with experimental rate coefficients in a similar fashion.

4.3. Results and discussion

4.3.1. Rate coefficients and Arrhenius parameters

Rate coefficients have been calculated from 300 up to 1800 K with intervals of 100 K for a total of 158 reactions, resulting in 316 distinct rate coefficients of single reactions at each temperature. For each reaction, the number of single events as well as the tunneling coefficients have been calculated separately, because for regression of the group additive values, the Arrhenius parameters excluding the number of single events and tunneling corrections are used. To regress the Arrhenius parameters at each temperature a set of five consecutive rate coefficients is used. Hydrogen abstraction reactions involving nitrogen-containing compounds containing a maximum of two nitrogen atoms and seven heavy (non-hydrogen) atoms are considered. The complete dataset contains 26 H-H-N abstraction reactions, 45 N-H-N reactions and 87 C-H-N reactions. A limited number of thermo-neutral reactions have identical reactants and products and thus the same rate coefficient in both the forward and reverse direction. The single-event rate coefficients, excluding the tunneling coefficient, can be found in Tables B-3, B-9 and B-15 of Appendix B for the H-H-N, N-H-N and C-H-N abstractions respectively.

To determine the primary contributions, the substituents of attacking and attacked atoms are varied between hydrogen atoms, alkyl groups, amine groups and π-conjugating groups (C=C, C≡C, C=N, N=C). The initial values for the ΔGAV°s are determined from a limited training set, in which one reaction is used to determine one group additive value. The influence of resonance effects due the simultaneous presence of groups on the carbon and nitrogen atoms on the activation energy and pre-exponential factors is also evaluated by including additional reactions for each possible cross-interaction in this training set. To validate the transferability

of the ΔGAV°s and RES, the kinetic properties are obtained for a test set using the preliminary values obtained from the training set data. The reactions in the test set for H-H-N abstractions are reactions in which the ligands of the non-hydrogen atom of the reactive center are substituted by larger groups, i.e. ethyl instead of methyl group. For N-H-N and C-H-N abstractions, the reactions included in the test set have different sets of ligands for both non-hydrogen atoms of the reactive center compared to the respective reference reactions. The Arrhenius parameters at 1000 K, regressed between 800 and 1200 K, for the reactions of both the training and test sets are given in Tables B-4, B-10 and B-16 of Appendix B for the H-H-N, N-H-N and C-H-N abstractions respectively

Considering all different types of hydrogen abstractions, the rate coefficients range between 10^{-1} and 10^{6} m^3 mol^{-1} s^{-1} at 1000 K. The lowest values are hydrogen abstractions by strongly resonance-stabilized radicals, such as the nitrogen-centered divinylamine radical $(CH_2{=}CH)_2N^{\cdot}$, while the highest values are evidently obtained for the corresponding reverse reactions. At 1000 K, the rate coefficients for H-H-N hydrogen abstractions reactions range from 4.8×10^{-1} m^3 mol^{-1} s^{-1} for hydrogen abstraction by the nitrogen-centered N-ethenylprop-1-en-2-amine radical from H_2 (Reaction 22) to 3.3×10^{6} m^3 mol^{-1} s^{-1} for hydrogen abstraction from methanimine ($CH_2{=}NH$) by a hydrogen atom (Reaction 2). For N-H-N and C-H-N abstractions, the lowest rate coefficients at 1000 K are obtained for hydrogen abstraction by the nitrogen-centered divinylamine radical from ammonia (Reaction 7) and methane (Reaction 8), i.e. 1.4 m^3 mol^{-1} s^{-1} and 1.2×10^{1} m^3 mol^{-1} s^{-1} respectively. The highest values correspond to formation of the resonance stabilized nitrogen-centered methyl ethynamine radical via hydrogen abstraction by $^{\cdot}NH_2$ (Reaction 8), i.e. 2.0×10^{5} m^3 mol^{-1} s^{-1}, and abstraction by the amino radical from the C_α-H bond in ethyl methylamine (Reaction 67), i.e. 8.7×10^{5} m^3 mol^{-1} s^{-1}. Hydrogen abstractions from the nitrogen atom in an imine are among the fastest N-H abstractions, while hydrogen abstraction from C_α-H bonds display the highest rate coefficients for abstraction from the carbon atom. The corresponding bond dissociation energies (BDE) obtained for these bonds are among the lowest in the studied nitrogen-containing molecule. The BDE of the N-H bond in methanimine is equal to 367 kJ mol^{-1}, while the BDE of the C_α-H bond in ethylamine amounts to 383 kJ mol^{-1}.

The activation energies, which are mainly dependent on the relative stabilities of the reactant and product radicals, also span a broad range, i.e. from 21 kJ mol^{-1} to 159 kJ mol^{-1} at 1000 K. Figure 4-4 depicts the *ab initio* calculated activation energies for all three types of hydrogen

abstractions as a function of the reaction enthalpy for all reactions included in both the training and test sets.

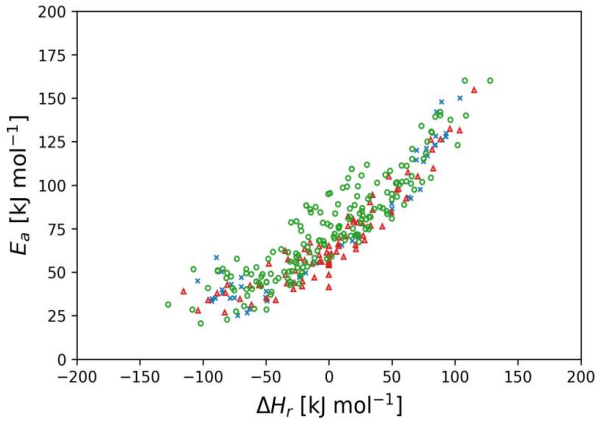

Figure 4-4: *Ab initio* calculated (CBS-QB3) activation energies as a function of the reaction enthalpy [kJ mol^{-1}] for all reactions in the complete dataset, calculated at 1000 K. The points correspond to the H-H-N (×), N-H-N (△) and C-H-N (○) hydrogen abstraction reactions.

The largest values for the activation energy and reaction enthalpy, i.e. 159 and 131 kJ mol^{-1}, are obtained for the hydrogen abstraction from the nitrogen atom in divinylamine by an ethyl radical. While a clear trend is visible in Figure 4-4, the use of a linear free-energy relationship such as Evans-Polanyi can be expected to lead to high deviations for the considered reaction families. Except for the reference reaction, all of the N-H hydrogen abstractions by a hydrogen atom are exothermic. This reflects that the formed H-H bond is stronger than the N-H bond. The direction of endo- and exothermicity for the N-H-N and C-H-N hydrogen abstractions depends on the type of C-H and N-H bonds in the reactive center. From the *ab initio* calculated reaction enthalpies of the studied reactions, the different N-H bonds can be ranked by increasing bond strength as follows: $(C_d)_2$N-H < (C_t)(C)N-H < (C_d)(C)N-H < (C_t)(H)N-H < N_I-H < (C_d)(H)N-H < $(C)_2$N-H < (C)(H)N-H < $(H)_2$N-H.

4.3.2. Comparison between *ab initio* calculated and experimental data

To assess the accuracy of the employed CBS-QB3 methodology for approximating the kinetic parameters of hydrogen abstractions involving nitrogen-containing compounds, the *ab initio* calculated rate coefficients are compared to available experimental values from literature studies for eight distinct reactions. The experimental rate coefficients have been obtained either directly from experimental measurements or from fitting to a complex reaction mechanism. The Arrhenius parameters and reported temperature ranges for these reactions can be found in Table

B-1 in Appendix B. The ρ parameter, obtained by dividing the highest by the lowest values for the rate coefficient at a specific temperature, is used to quantify the relative deviation between both rate coefficients. An overview of the comparison with literature data is given in Table 4-1. Overall, a good agreement is obtained between the *ab initio* calculated and experimental rate coefficients over a wide temperature range, i.e. 400-1600 K. The experimental values are approximated on average within a factor of 1.8, with a maximum deviation factor of 4.2 for the hydrogen abstraction from ethane by the amino radical at 1600 K. Note that this large deviation is obtained for the experimental rate coefficient reported by Hennig et al. [14] which corresponds to a pressure of 7.5 kPa.

Table 4-1: Comparison between experimental (k_{exp}) and *ab initio* (k_{AI}) calculated rate coefficients for eight hydrogen abstraction reactions involving nitrogen-containing compounds. The units of k are $m^3\ mol^{-1}\ s^{-1}$.

No	Reaction	Ref	T [K]	k_{exp}	k_{AI}	ρ^a
1	H + NH_3 ↔ H_2 + $^{\bullet}NH_2$	[15]	600	6.99×10^2	5.92×10^2	1.2
		[16]	600	9.14×10^2	5.92×10^2	1.5
		[17]	800	7.43×10^3	9.15×10^3	1.2
		[18]	1000	5.34×10^4	7.13×10^4	1.3
		[19]	1000	4.62×10^4	7.13×10^4	1.5
		[20]	1600	1.17×10^6	1.47×10^6	1.2
2	$^{\bullet}NH_2$ + CH_4 ↔ NH_3 + $^{\bullet}CH_3$	[21]	400	1.28×10^1	1.65×10^1	1.3
		[22]	1000	4.36×10^4	1.24×10^4	3.5
		[14]	1600	1.02×10^5	3.17×10^5	3.1
		[23]	1600	3.30×10^5	3.17×10^5	1.0
3	$^{\bullet}NH_2$ + ↔ NH_3 +	[21]	400	4.56×10^1	5.20×10^1	1.1
		[24]	800	1.22×10^4	1.68×10^4	1.4
		[14]	1600	2.63×10^5	1.01×10^6	4.2
4	$^{\bullet}CH_3$ + —NH_2 ↔ CH_4 + $^{\bullet}$—NH_2	[25]	400	1.71×10^0	1.58×10^0	1.1
5	$^{\bullet}CH_3$ + —NH_2 ↔ CH_4 + —$NH^{\bullet}$	[25]	400	2.72×10^0	1.73×10^0	1.6
6	$^{\bullet}CH_3$ + ↔ CH_4 +	[26]	400	2.02×10^1	5.59×10^1	2.8
7	$^{\bullet}CH_3$ + ↔ CH_4 +	[27]	400	5.58×10^0	3.42×10^0	1.6
8	$^{\bullet}CH_3$ + ↔ CH_4 +	[27]	400	2.28×10^0	3.28×10^0	1.4

[a] $\rho = max(k_{AI}, k_{exp})/min(k_{AI}, k_{exp})$

The hydrogen abstraction from ammonia by a hydrogen atom has been thoroughly investigated in several independent experimental studies. In Figure 4-5, the theoretical rate coefficient for this reaction is compared to six experimental studies in the temperature range 300-2000 K in the high-pressure limit. A good agreement is obtained between the *ab initio* calculated and

experimental rate coefficients over the complete temperature range. The temperature dependence at lower temperatures is well captured by the tunneling contribution. At 300 K, this corresponds to a tunneling coefficient of 4.3.

In Figure 4-5, the theoretical and experimental rate coefficients from four different studies are compared for the hydrogen abstraction from methane by an amino radical. The experimental values obtained by Hennig et al. [14] and Song et al. [23] at high temperatures (> 1500 K) and at a pressure of respectively 7.5 kPa and 110 kPa differ by a factor of three. The rate coefficients by Hack et al. [22] have been determined experimentally at a pressure of 0.4 kPa. For this reaction, there is a significant contribution of tunneling effects at lower temperatures, i.e. a tunneling coefficient of 36.8 at 300 K. Taking into account this tunneling contribution, the *ab initio* calculated rate coefficient succeeds in capturing the temperature dependence as seen from the experimental values of Demissy et al. [21].

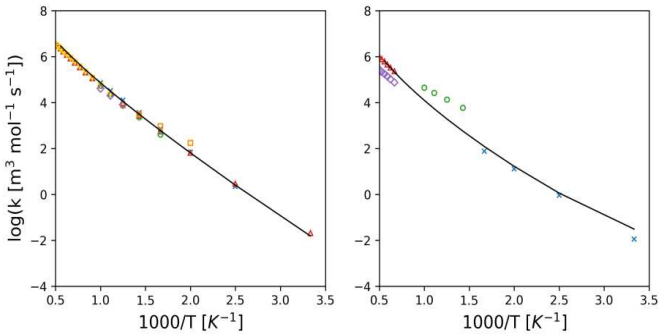

Figure 4-5: Arrhenius plot of the hydrogen abstraction from ammonia by a hydrogen atom, comparing the *ab initio* rate coefficients calculated in this work with experimental data from the literature of Marshal et al. [15] (×), Michael et al. [19] (△), Hack et al. [18] (○), Sutherland et al. [20] (▽), Willis et al. [16] (□), Aganesyan et al. [17] (◇) (right) and Arrhenius plot of the hydrogen abstraction from methane by the amino radical, comparing the *ab initio* rate coefficients calculated in this work with experimental data from the literature of Song et al. [23] (△), Hennig et al. [14] (◇), Hack et al. [22] (○) and Demissy et al. [21] (×) (left).

4.3.3. Group additivity model

4.3.3.1. Initial model

The initial set of ΔGAV°s and RES are deduced based on the reactions included in the training set. These reactions are characterized by a single change in group of one of the reactive atoms compared to the reference reaction and thus each value is determined from a single reaction. The training set for H-H-N hydrogen abstractions contains 9 reactions, including the reference reaction, from which initial values for the eight ΔGAV°s values are determined. For N-H-N and C-H-N hydrogen abstractions, respectively 14 and 29 reactions are included in the training set,

to obtain initial values for both the ΔGAV° values and RES corrections. Note that for H-H-N and N-H-N hydrogen abstractions, N-$(H)_2$ groups have group additive values equal to zero, as these correspond to the respective reference reactions. This also holds for the C-$(H)_3$ and N-(C)(H) groups for C-H-N hydrogen abstractions. The training set reactions for the H-H-N, N-H-N and C-H-N abstractions can be found in Tables B-4, B-10 and B-16 of Appendix B respectively.

The validity of this initial model is assessed by constructing a test set and comparing the group additive approximated and *ab initio* calculated rate coefficients for all reactions included in this test set. Apart from the H-H-N abstractions, the reactions in the test set deviate from the reference reaction by two different groups as reactive atoms. In Table 4-2 the mean and maximum values for the deviation factor ρ, which is obtained by dividing the highest by the lowest rate coefficient, are given. For all three types of hydrogen abstractions the deviation is each time smaller than a factor of two, which is a typical accuracy for group additivity [5]. This is also of the same order of magnitude as the uncertainty on the CBS-QB3 *ab initio* calculated rate coefficients. A few outliers are obtained for which the larger deviations can be attributed to either uncertainty of the *ab initio* calculations or the non-nearest-neighbor effects not taken into account.

Table 4-2: Deviations between the *ab initio* calculated (AI) and group additive approximated (GA) rate coefficients at 1000 K for the training and test set, with the initial set and final set of group additive values and resonance corrections. The deviations are expressed using the mean and maximum values for the ρ parameter, obtained by dividing the highest by the lowest rate coefficients.

	H-H-N		N-H-N		C-H-N	
	$\langle\rho\rangle$	ρ_{max}	$\langle\rho\rangle$	ρ_{max}	$\langle\rho\rangle$	ρ_{max}
Initial set of ΔGAV°/RES						
Test set	1.89	5.69	1.96	5.99	1.59	3.14
Final set of ΔGAV°/RES						
Training set	1.35	2.33	1.40	2.02	1.25	1.95
Test set	1.45	2.95	1.47	2.29	1.34	2.42
Total	1.42	2.95	1.44	2.29	1.31	2.42

4.3.3.2. Final model

To increase the accuracy of the group additivity scheme, the final values of the ΔGAV°s and RES parameters are determined via a linear regression analysis based on the reactions of both the training and test sets. Note that by using the combined datasets, the final ΔGAV° and RES values are regressed from at least three occurrences in three different molecules. This increase in accuracy can be seen from Table 4-2. The group additivity method succeeds in approximating

the *ab initio* calculated rate coefficients at 1000 K within a factor of 1.5 for all three reaction families, which is significant decrease compared to a factor of two when making use of the initial values. The maximum deviation values are also decreased, with the largest outlier having a deviation of approximately three.

The final values for the ΔGAV° at 300 and 1000 K are reported in Table 4-3, Table 4-4 and Table 4-6 for hydrogen abstraction by a hydrogen atom, a nitrogen-centered and carbon-centered radical respectively. The final values for the resonance corrections can be found in Table 4-5 for N-H-N and Table 4-7 for C-H-N abstractions. The corresponding parity plot of the *ab initio* calculated and group additive approximated rate coefficients for all three reaction families is given in Figure 4-6.

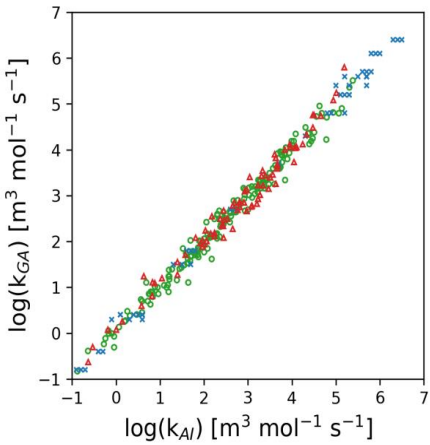

Figure 4-6: Parity plot of the *ab initio* calculated and the GA approximated single-event rate coefficients, for all reactions in the training and test set, calculated at 1000 K with the final set of group additive values and resonance corrections. The points correspond to the H-H-N (×), N-H-N (Δ) and C-H-N (○) hydrogen abstraction reactions.

For hydrogen abstractions of the type H-H-N, the ΔGAV°s for pre-exponential factors at 1000 K range from +0.278 for N_1-$(C_d)_2$ to -0.343 for N_1-$(C)_2$ for the abstracting radical and from +0.068 for $N_{2,1}$ to -0.268 for N_2-(C_d)(H) for the formed radical. In general, $\Delta GAV°_{logÃ}$ decreases with increasing number of methyl substituents on the abstracting radical. The ΔGAV°s for activation energies decrease with decreasing stability of the abstracting radical, i.e. from 89.2 for N_1-$(C_d)_2$ to 15.2 kJ mol^{-1} for N_1-(C)(H) at 1000 K. The *ab initio* calculated rate coefficients of the test set are approximated with a mean deviation of 1.42 and a maximum deviation of 2.95. The largest deviation is obtained for the hydrogen abstraction from CH_2=CH(C_2H_5)NHCH=CH_2, for which the group additive approximated rate coefficient

deviates from the *ab initio* calculated rate coefficient by a factor of approximately three at 1000 K.

Table 4-3: Primary group additive values ΔGAV°s at 300 and 1000 K for abstraction from a N-H bond by a hydrogen atom, deduced from the combined training and test set. For the reference reaction, the single-event pre-exponential factors are expressed in m^3 mol^{-1} s^{-1} and E_a is expressed in kJ mol^{-1}. The units for ΔGAV°$_{E_a}$ are kJ mol^{-1}.

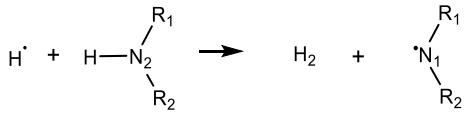

		300 K				1000 K			
		ΔGAV°(N_1)		ΔGAV°(N_2)		ΔGAV°(N_1)		ΔGAV°(N_2)	
No	Group	$log\tilde{A}$	E_a	$log\tilde{A}$	E_a	$log\tilde{A}$	E_a	$log\tilde{A}$	E_a
	Reference: H• + NH$_3$	7.124	57.7	6.048	48.2	7.746	65.4	6.545	55.1
1	**N_i-(C)(H)**	-0.374	13.1	-0.094	-17.9	-0.169	15.2	-0.024	-17.2
2	**$N_{i,I}$**	-0.250	37.6	-0.062	-39.7	-0.092	39.2	0.068	-38.5
3	**N_i-(C_d)(H)**	-0.476	61.3	-0.444	-26.8	-0.018	66.1	-0.268	-24.8
4	**N_i-(C_t)(H)**	-0.011	66.0	-0.150	-26.0	0.126	67.4	-0.120	-25.7
5	**N_i-(C)$_2$**	-0.745	27.3	0.007	-29.5	-0.343	31.4	0.037	-29.4
6	**N_i-(C_d)(C)**	-0.632	57.3	-0.361	-30.4	-0.060	63.6	-0.223	-28.7
7	**N_i-(C_d)$_2$**	0.303	90.3	-0.159	-16.8	0.278	89.2	-0.129	-16.6
8	**N_i-(C_t)(C)**	-0.597	68.7	-0.308	-31.8	-0.256	72.2	-0.201	-30.7

For hydrogen abstractions of the type N-H-N, the ΔGAV°s at 1000 K for pre-exponential factors range from +0.574 for N_1-(C_d)$_2$ to -0.273 for N_1-(C)$_2$ for the abstracting radical and from +0.074 for $N_{2,I}$ to -0.652 for N_2-(C_d)(H) for the formed radical. Note that these are the same groups as for the hydrogen abstraction by a hydrogen atom. The ΔGAV°s for activation energies decrease with decreasing stability of the abstracting radical, i.e. from 84.9 for N_1-(C_d)$_2$ to 18.0 kJ mol^{-1} for N_1-(C)(H) at 1000 K. The largest deviation, which is equal to 2.29, corresponds to the N-H-N type hydrogen abstraction with two non-hydrogen ligands on both nitrogen atoms, i.e. N_i-(C_t)(H) and N_i-(C_t)(C). Because these resonance corrections do not change significantly over the studied temperature range, the average values given in the last column of Table 4-5 can be used over the studied temperature range 300-1800 K. Overall, the influence of the cross interactions is more pronounced for the activation energies, which decrease in case of resonance stabilized transition states. The largest resonance corrections for activation energies are obtained for cross interactions between C=C and C≡C ligands of the reactive center atoms, which is in agreement with hydrogen abstractions of the type C-H-C [5]. Similar to hydrogen

abstractions of the type S-H-S [11], the resonance corrections are larger than the values obtained for C-H-C hydrogen abstractions which can be attributed to the increased electron delocalization in case of a heteroatom.

Table 4-4: Primary group additive values ΔGAV°s at 300 and 1000 K for abstraction from a N-H bond by a nitrogen-centered radical and its reverse reaction, deduced from the combined training and test set. For the reference reaction, the single-event pre-exponential factors are expressed in m^3 mol^{-1} s^{-1} and E_a is expressed in kJ mol^{-1}. The units for ΔGAV°$_{E_a}$ are kJ mol^{-1}.

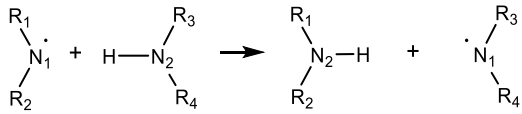

		300 K				1000 K			
		ΔGAV°(N_1)		ΔGAV°(N_2)		ΔGAV°(N_1)		ΔGAV°(N_2)	
No	Group	$log\tilde{A}$	E_a	$log\tilde{A}$	E_a	$log\tilde{A}$	E_a	$log\tilde{A}$	E_a
	Reference: $NH_2^{\bullet} + NH_3$	5.067	44.6	5.067	44.6	6.361	60.0	6.361	60.0
1	**N_i-(C)(H)**	-0.260	16.5	0.004	-15.4	-0.102	18.0	0.037	-15.2
2	**$N_{i,I}$**	-0.277	32.5	-0.072	-50.6	-0.164	33.5	0.074	-49.2
3	**N_i-(C_d)(H)**	-0.209	54.6	-0.553	-26.8	-0.105	55.2	-0.652	-28.2
4	**N_i-(C_t)(H)**	-0.387	55.5	-0.263	-32.2	-0.122	58.2	-0.070	-30.3
5	**N_i-(C)$_2$**	-0.703	22.9	0.054	-33.8	-0.273	27.1	0.064	-34.1
6	**N_i-(C)(C_d)**	-0.188	59.9	-0.332	-35.0	0.134	63.1	-0.353	-35.4
7	**N_i-(C_d)$_2$**	0.372	84.6	-0.636	-31.7	0.547	84.9	-0.530	-30.6
8	**N_i-(C)(C_t)**	-0.478	62.2	-0.151	-39.4	-0.123	65.7	-0.002	-38.0

Table 4-5: Corrections accounting for resonance stabilization of the transition state of N-H-N hydrogen abstraction reactions at 300 K, 1000 K and an average value over the complete temperature interval 300-1800 K. The single-event pre-exponential factors are expressed in m^3 mol^{-1} s^{-1} and E_a is expressed in kJ mol^{-1}.

No	Correction	Corresponding structure	300 K		1000 K		Average	
			$\Delta log\tilde{A}$	ΔE_a	$\Delta log\tilde{A}$	ΔE_a	$\Delta log\tilde{A}$	ΔE_a
1	**$\sigma_{\beta C\text{-}H}N{-}N_{\pi C=C}$**	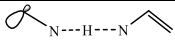	0.115	-2.1	0.057	-3.0	0.065	-2.7
2	**$\sigma_{\beta C\text{-}H}N{-}N_{\pi C\equiv C}$**	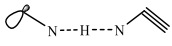	0.086	-4.9	-0.054	-6.7	-0.034	-6.3
3	**$_{\pi C=C}N{-}N_{\pi C=C}$**	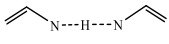	-0.124	-19.4	-0.107	-19.5	-0.112	-19.2
4	**$_{\pi C=C}N{-}N_{\pi C\equiv C}$**	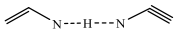	0.082	-17.8	-0.002	-19.1	0.010	-18.6
5	**$_{\pi C\equiv C}N{-}N_{\pi C\equiv C}$**	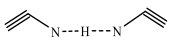	0.613	-15.4	0.368	-18.8	0.404	-17.8

For hydrogen abstractions of the type C-H-N, the $\Delta GAV°_{log\tilde{A}}$ values at 1000 K range from +0.708 for N_1-$(C_d)_2$ to -0.155 to N_1-$(C)_2$ and from +0.368 for C_1-$(C_I)(H)_2$ to -0.234 for C_1-$(C)(H)_2$ for the abstracting radical. In general, the group additive values for pre-exponential factors decrease with increasing number of alkyl ligands of both the carbon or nitrogen central atom. There is also a decrease when substituting a nitrogen-centered ligand by an alkyl ligand. For the formed radical, the largest influences are obtained for the groups $N_{2,I}$ and N_2-$(C_d)_2$, i.e. 0.171 and -0.516 respectively, and for $C_{2,d}$-(H) and C_2-$(N_I)(C)(H)_2$, i.e. 0.120 and -0.731 respectively. Similar to the hydrogen abstractions of the types H-H-N and N-H-N, the ΔGAV° for activation energies decrease with decreasing stability of the abstracting radical. The value of the ΔGAV° for the activation energy for the nitrogen-centered abstracting radical ranges from 71.9 kJ mol^{-1} for N_1-$(C_d)_2$ to -13.7 kJ mol^{-1} for N_1-$(H)_2$ and for the carbon-centered abstracting radical from 44.4 kJ mol^{-1} for C_1-$(C_d)(H)_2$ to -21.0 kJ mol^{-1} for C_{1d}-(H) at 1000 K. The value of the ΔGAV° for the activation energy for the formed radical ranges from 19.1 kJ mol^{-1} for N_2-$(H)_2$ to -25.7 kJ mol^{-1} for $N_{2,I}$ for nitrogen-centered radicals and from -0.7 kJ mol^{-1} for $C_{2,d}$-(H) to -38.6 kJ mol^{-1} for C_2-(N)(C)(H) for carbon-centered radicals.

Table 4-6: Primary group additive values ΔGAV°s at 300 and 1000 K for abstraction from a N-H bond by a carbon-centered radical and its reverse reaction, deduced from the combined training and test set. For the reference reaction, the single-event pre-exponential factors are expressed in m^3 mol^{-1} s^{-1} and E_a is expressed in kJ mol^{-1}. The units for $\Delta GAV°_{E_a}$ are kJ mol^{-1}.

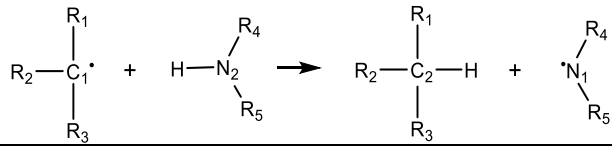

		300 K				1000 K			
		ΔGAV°(N_1)		ΔGAV°(N_2)		ΔGAV°(N_1)		ΔGAV°(N_2)	
No	Group	$log\tilde{A}$	E_a	$log\tilde{A}$	E_a	$log\tilde{A}$	E_a	$log\tilde{A}$	E_a
	Reference: $^{\bullet}CH_3 + CH_3NH_2$	5.751	48.1	6.013	70.7	6.192	60.8	6.501	86.9
1	**N_i-(H)$_2$**	0.461	-12.0	0.194	19.6	0.276	-13.7	0.131	19.1
2	**$N_{i,I}$**	0.122	24.7	0.077	-26.6	0.061	24.1	0.171	-25.7
3	**N_i-(C_d)(H)**	0.062	42.2	-0.532	-8.7	0.422	46.0	-0.293	-6.2
4	**N_i-(C_t)(H)**	0.259	41.6	0.127	-14.7	0.173	40.7	0.083	-15.1
5	**N_i-(C)$_2$**	-0.443	11.0	0.071	-14.1	-0.155	14.0	0.059	-14.4
6	**N_i-(C)(C_d)**	0.147	48.5	-0.265	-14.7	0.529	52.6	-0.072	-12.6
7	**N_i-(C_d)$_2$**	0.886	75.2	-0.426	-8.4	0.708	71.9	-0.516	-9.3
8	**N_i-(C)(C_t)**	-0.147	45.4	-0.074	-24.7	-0.023	46.6	-0.041	-24.4
		300 K				1000 K			
		ΔGAV°(C_1)		ΔGAV°(C_2)		ΔGAV°(C_1)		ΔGAV°(C_2)	
		$log\tilde{A}$	E_a	$log\tilde{A}$	E_a	$log\tilde{A}$	E_a	$log\tilde{A}$	E_a
	Reference: $CH_3NH^{\bullet} + CH_4$	6.013	70.7	5.751	48.1	6.501	86.9	6.192	60.8
1	**C_i-(C)(H)$_2$**	-0.482	2.0	-0.133	-14.7	-0.234	4.5	-0.166	-15.2
2	**C_i-(C)$_2$(H)**	-0.700	2.8	0.059	-26.6	-0.209	7.7	0.022	-27.4
3	**$C_{i,d}$-(H)**	0.041	-23.1	0.040	-1.3	0.265	-21.0	0.120	-0.7
4	**$C_{i,d}$-(C)**	-0.170	-20.0	0.054	-11.4	0.152	-16.8	0.090	-11.3
5	**C_i-(C_d)(H)$_2$**	-0.160	41.0	-0.920	-35.6	0.181	44.4	-0.666	-32.8
6	**C_i-(N)(H)$_2$**	-0.514	16.8	-0.611	-34.2	-0.156	20.5	-0.329	-31.2
7	**C_i-(C)(N)(H)**	-0.549	14.6	-0.428	-41.8	-0.073	19.9	-0.155	-38.6
8	**$C_{i,I}$-(H)**	0.008	5.6	-0.072	-33.4	0.366	9.2	0.105	-31.8
9	**$C_{i,I}$-(C)**	-0.093	7.5	0.008	-33.8	0.252	10.9	0.050	-33.6
10	**C_i-(C_I)(H)$_2$**	-0.018	27.2	-0.831	-31.0	0.368	30.9	-0.537	-27.9
11	**C_i-(N_I)(H)$_2$**	-0.127	41.0	-0.956	-29.6	0.174	43.8	-0.731	-27.3

Table 4-7: Corrections accounting for resonance stabilization of the transition state of C-H-N hydrogen abstraction reactions at 300 K, 1000 K and an average value over the complete temperature interval 300 – 1800 K. The single-event pre-exponential factors are expressed in m^3 mol^{-1} s^{-1} and E_a is expressed in kJ mol^{-1}.

No	Correction	Corresponding structure	300 K		1000 K		Average	
			$\Delta log\tilde{A}$	ΔE_a	$\Delta log\tilde{A}$	ΔE_a	$\Delta log\tilde{A}$	ΔE_a
1	$_{\pi C=C}C-N_H$	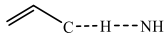	0.125	3.0	0.080	2.5	0.084	2.5
2	$_{\pi C=C}C-N_{\pi C=C}$	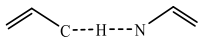	0.744	-3.0	0.428	-6.2	0.480	-5.7
3	$_{\pi C=C}C-N_{\pi C\equiv C}$	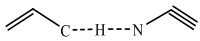	0.371	-5.8	0.296	-6.5	0.309	-6.4
4	$p_{\alpha N}C-N_{\pi C=C}$	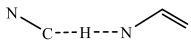	-0.267	-16.2	-0.184	-15.1	-0.188	-15.0
5	$p_{\alpha N}C-N_{\pi C\equiv C}$	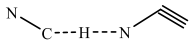	-0.556	-20.3	-0.447	-19.2	-0.453	-19.2
6	$_{\pi C=N}C-N_{\pi C=C}$	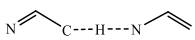	-0.068	1.8	-0.254	-0.1	-0.219	0.4
7	$_{\pi C=N}C-N_{\pi C\equiv C}$	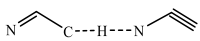	0.286	-1.6	0.229	-2.1	0.239	-1.9
8	$_{\pi N=C}C-N_{\pi C=C}$	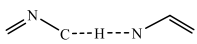	0.056	-0.9	-0.127	-2.7	-0.097	-2.3
9	$_{\pi N=C}C-N_{\pi C\equiv C}$	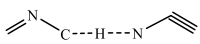	0.260	-0.7	0.224	-1.2	0.230	-1.1

4.3.3.3. Tunneling

Tunneling coefficients cannot be directly calculated from group additivity. Eckart tunneling coefficients are calculated using the electronic barrier and the imaginary frequency, which are only available when doing *ab initio* calculations. As an alternative, correlations can be constructed to model the tunneling coefficients from properties that can be obtained from group additivity. In this work the activation energy, which can be considered to be a good measure for the electronic tunneling barrier, is used to model the tunneling coefficients. For each reaction the activation energy of the reaction in the exothermic direction $E_{a,exo}$, i.e. the smallest activation energy when comparing the forward and reverse activation energy, is considered as tunneling can only proceed through the net electronic barrier, i.e. without endothermic contributions. These activation energies can be estimated with the group additivity method and no additional *ab initio* calculations are thus required.

For hydrogen abstractions of the C-H-C type involving hydrocarbons and organosulfur compounds, a fourth order polynomial with temperature-dependent coefficients has been proven to accurately approximate the tunneling coefficient over a large temperature range [5]. For hydrogen abstraction reactions involving nitrogen-containing compounds, new coefficients have been determined based on the tunneling coefficients between 300 and 1800 K of all

reactions in the complete dataset. These tunneling coefficients for all three types of hydrogen abstractions can be found in Tables B-7, B-13, B-19 of Appendix B. The tunneling coefficients for hydrogen abstractions of the H-H-N, N-H-N and C-H-N type can be modelled with Eq. 4-4, Eq. 4-5 and Eq. 4-6 for the temperature range 300-1800 K. Note that the second and third order terms of the fourth order polynomials were not significant. The obtained tunneling coefficients are always greater than one, decrease with increasing temperature and increase with increasing activation energy in the exothermic reaction. With the activation energy approaching zero, the tunneling coefficients will approach one at all temperatures.

$$\kappa_{H-H-N}(T) = 1 + \left(\frac{145}{T}\right)^3 E_{a,exo} + 2.48 \times 10^{-6} \exp(-(T-300)) {E_{a,exo}}^4 \qquad \text{(Eq. 4-4)}$$

$$\kappa_{N-H-N}(T) = 1 + \left(\frac{212}{T}\right)^3 E_{a,exo} + 6.31 \times 10^{-6} \exp(-(T-300)) {E_{a,exo}}^4 \qquad \text{(Eq. 4-5)}$$

$$\kappa_{N-H-C}(T) = 1 + \left(\frac{191}{T}\right)^3 E_{a,exo} + 6.53 \times 10^{-6} \exp(-(T-300)) {E_{a,exo}}^4 \qquad \text{(Eq. 4-6)}$$

For hydrogen abstractions of the type H-H-N, Eq. 4-4 can describe the tunneling coefficient with a mean factor of deviation $\langle\rho\rangle$ of only 1.08 over the complete temperature range 300-1800 K. At 300 K, a mean factor of deviation $\langle\rho\rangle$ of 1.39 is obtained. For hydrogen abstractions of the type N-H-N, $\langle\rho\rangle$ amounts to 1.08 using Eq. 4-5, while at 300 K $\langle\rho\rangle$ is equal to 1.38. For hydrogen abstractions of the type C-H-N, $\langle\rho\rangle$ amounts to 1.11 for the complete temperature range and 1.43 at 300 K. In Figure 4-7, the Eckart tunneling coefficients are presented for all reactions in the dataset as a function of the *ab initio* calculated activation energy $E_{a,exo}$ at 300 K, as well as the fit of the respective 4th order polynomials for hydrogen abstractions of the H-H-N, N-H-N and C-H-N type.

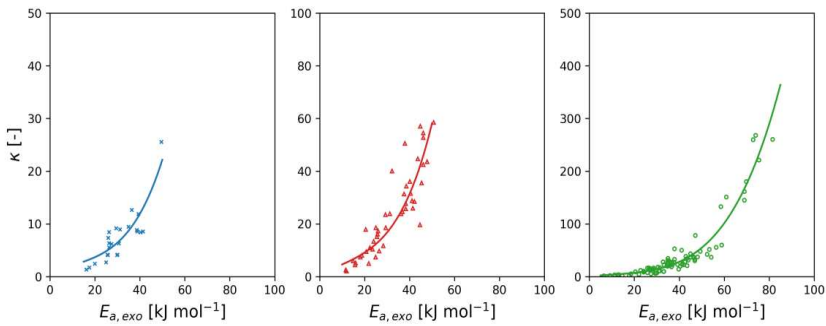

Figure 4-7: Tunneling coefficients [-] as function of the *ab initio* activation energy $E_{a,exo}$ [kJ mol^{-1}] at 300 K for hydrogen reactions of the type H-H-N (×), N-H-N (△) and C-H-N (○) and the corresponding fit from Eq. 4-4, Eq. 4-5 and Eq. 4-6.

4.3.3.4. Temperature dependence of group additive values

The limited temperature dependence of the ΔGAV°s due to the use of a reference reaction, enables the use of the group additive values over a large temperature range, without loss of accuracy. In Figure 4-8, the temperature dependence of the ΔGAV°s for both the pre-exponential factor as well as the activation energy with the highest temperature dependence per hydrogen abstraction reaction family is shown. The ΔGAV° value at 300 K is subtracted from the group additive values at higher temperature in order to obtain the depicted temperature dependency. For hydrogen abstractions of the type H-H-N, the group with the highest temperature dependence is N_1-(C)(C_d). The difference between 300 and 1800 K for $log\tilde{A}$ amounts to +0.703, while for E_a a difference of 9.6 kJ mol^{-1} is obtained. The group N_1-$(C)_2$ has the highest temperature dependency for N-H-N hydrogen abstractions, i.e. a change of +0.487 for $log\tilde{A}$ and 5.7 kJ mol^{-1} for E_a over the temperature range 300-1800 K. For C-H-N hydrogen abstractions, the group N_1-$(C_d)_2$ displays the largest temperature dependency for $log\tilde{A}$ (-0.647) and E_a (11.0 kJ mol^{-1}).

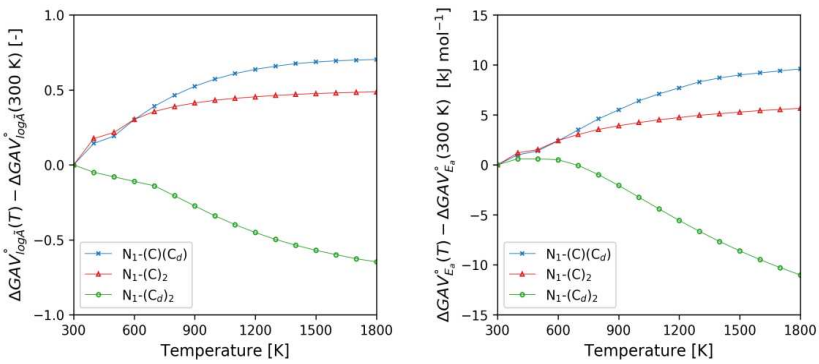

Figure 4-8: Temperature dependence of the group additive values: Difference between ΔGAV°(T) and ΔGAV°(300 K) for $log\tilde{A}$ (left) and E_a (right) for the groups with the highest temperature dependency for the H-H-N (×), N-H-N (△) and C-H-N (○) hydrogen abstractions.

Depending on the substituents of the reactive atoms, there can be a significant temperature dependence of the group additive values. Note that in Table 4-3, Table 4-4 and Table 4-6 the ΔGAV°s are given for 300 and 1000 K, while the ΔGAV°s determined at the other temperatures can be found in Table B-6, B-12 and B-18 in Appendix B. It is advised to use the ΔGAV°s in their relevant temperature range, i.e. the temperature range which has been used for regression of the Arrhenius parameters. For example, for the ΔGAV°s at 1000 K, this temperature range is equal to 800 to 1200 K.

4.3.3.5. Thermodynamic consistency

The forward and reverse rate coefficient are thermodynamically consistent if their ratio is equal to the equilibrium coefficient calculated from the *ab initio* thermodynamic parameters of the reactant(s) and product(s) of that reaction. When making use of a group additive model for approximation of the kinetic parameters, this is not necessarily the case. In Table 4-8, the ratio of the forward and reverse rate coefficients calculated from group additivity ($\frac{k_{for,GA}}{k_{rev,GA}}$) is compared to the *ab initio* equilibrium coefficient ($K_{eq,AI}$). The mean and maximum values of the ρ parameter, obtained by dividing the highest by the lowest values for the equilibrium coefficients, are reported for 1000 K. Note that for the hydrogen abstraction characterized by a N-H-N transition state, the deviations for the forward and reverse rate coefficients are of the same magnitude and thus cancel each other out when calculating the equilibrium coefficient. Overall, the ratios of the group additive approximated forward and reverse rate coefficients are in good agreement with the *ab initio* equilibrium coefficients. For both H-H-N and C-H-N, the highest deviation is obtained for reactions for which the forward rate coefficient deviates by more than a factor of two from the *ab initio* rate coefficient. For H-H-N, this reaction includes the group N_2-(C_d)(H), while for C-H-N the highest deviation is obtained for a reaction in which the groups C_1-(N)$(H)_2$ and N_2-$(C)_2$ are present.

Table 4-8: Comparison of the *ab initio* calculated equilibrium coefficient ($K_{eq,AI}$) with the ratio of the forward and reverse rate coefficients calculated from group additivity ($\frac{k_{for,GA}}{k_{rev,GA}}$) and the equilibrium coefficients calculated with group additive approximated thermodynamic data ($K_{eq,GA}$). The deviations are expressed as mean and maximum values for the ρ parameter, obtained by dividing the highest by the lowest values for the equilibrium coefficient at 1000 K for all reactions of the combined training and test set, with the final set of group additive values.

Reaction family	$\frac{k_{for,GA}}{k_{rev,GA}}$ versus $K_{eq,AI}$		$K_{eq,AI}$ versus $K_{eq,GA}$		$\frac{k_{for,GA}}{k_{rev,GA}}$ versus $K_{eq,GA}$	
	$\langle\rho_1\rangle$	$\rho_{1,max}$	$\langle\rho_2\rangle$	$\rho_{2,max}$	$\langle\rho_3\rangle$	$\rho_{3,max}$
H-H-N	1.41	3.08	1.72	3.68	1.65	3.04
N-H-N	1.00	1.00	1.63	3.81	1.62	3.83
C-H-N	1.26	2.87	1.63	4.26	1.72	5.20

[a] $\rho_1 = max(\frac{k_{for,GA}}{k_{rev,GA}}, K_{eq,AI}) / min(\frac{k_{for,GA}}{k_{rev,GA}}, K_{eq,AI})$, [b] $\rho_2 = max(K_{eq,AI}, K_{eq,GA}) / min(K_{eq,AI}, K_{eq,GA})$, [c] $\rho_3 = max(\frac{k_{for,GA}}{k_{rev,GA}}, K_{eq,GA}) / min(\frac{k_{for,GA}}{k_{rev,GA}}, K_{eq,GA})$

If thermodynamic data obtained directly from *ab initio* calculations is not available for a certain species during kinetic model generation, the group additivity method is used as approximation method. This approximation influences the value of the reverse rate coefficient, when it is implemented as a reverse reaction. From Table 4-8, it can be seen that the use of the equilibrium coefficient based on the group additive approximated thermodynamic parameters of reactant(s)

and product(s) ($K_{eq,GA}$), leads to a factor of uncertainty of around two for determination of the reverse rate coefficient based on thermodynamic consistency.

4.3.3.6. Application

In this section, the application of the new group additivity schemes for approximation of the kinetic parameters of hydrogen abstractions involving nitrogen-containing compounds, is illustrated for two reactions. The first example is the hydrogen abstraction by the nitrogen-centered methyl amino radical from n-methyl vinyl amine.

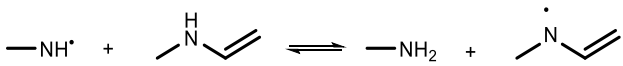

(R1)

During this reaction a hydrogen atom is exchanged between two nitrogen atoms. The values for $log\tilde{A}$ and E_a of the reference reaction amount to 6.361 and 60 kJ mol^{-1} respectively, c.f. Table 4-4. The contributions of the two primary groups N_1-(C)(H) and N_2-(C)(C_d) to the pre-exponential factor are equal to 18.0 and -35.4 kJ mol^{-1} and the activation energy -0.102 and -0.353. The resonance interaction between the methyl ligand on N_1 and the double bonded carbon atom on the N_2 atom corresponds to a correction of 0.057 for $log\tilde{A}$ and -3.0 for E_a. This results in a group additive approximated value of 5.963 for the single-event pre-exponential factor and 39.6 kJ mol^{-1} for the activation energy for the forward reaction.

$$\log\tilde{A}\,(1000\,K) = log\tilde{A}_{ref}(1000\,K) + GAV^{o}_{\log\tilde{A}}\big(N_1-(C)(H)\big) + GAV^{o}_{\log\tilde{A}}\big(N_2-(C)(C_d)\big) + \sigma_{\beta C-H}N - N_{\pi C=C} = 6.361 + (-0.102) + (-0.353) + 0.057 = 5.963$$

$$E_a(1000\,K) = E_{a,ref}(1000\,K) + \Delta GAV^{o}_{E_a}\big(N_1-(C)(H)\big) + \Delta GAV^{o}_{E_a}\big(N_2-(C)(C_d)\big) + \sigma_{\beta C-H}N - N_{\pi C=C} = 60.0 + 18.0 + (-35.4) + (-3.0) = 39.6\,kJ\,mol^{-1}$$

The activation energy for the reverse reaction is equal to 105.0 kJ mol^{-1}, which means that hydrogen abstraction from n-methyl vinyl amine by the methyl amino radical is the exothermic direction. Substitution of $E_{a,exo}$ in Eq. 4-5 yields a tunneling coefficient of 1.295 at 1000 K, which is in good agreement with the *ab initio* calculated Eckart tunneling coefficient of 1.274. To calculate the number of single events, the total symmetry numbers and the number of optical isomers of both reactants and the transition state are required. Both reactants have a methyl rotor and the number of optical isomers of methyl vinyl amine is equal to two, i.e. the nitrogen atom N_2 is a chiral center. The transition state has two methyl rotors and a number of optical isomers of four, as both nitrogen atoms N_1 and N_2 are chiral centers. The transition state thus exists as two pairs of diastereomers, for which the energy difference is neglected. This results

in a number of single events for the forward reaction of two. Considering all different contributions, the group additivity approach leads to a total rate coefficient of 2.0×10^4 m^3 mol^{-1} s^{-1} at 1000 K, which agrees with the *ab initio* calculated rate coefficient, i.e. 1.1×10^4 m^3 mol^{-1} s^{-1}, within a factor of two.

The second example is the hydrogen abstraction by the isopropyl radical from ethynamine.

(R2)

During this reaction, a hydrogen atom is abstracted from a nitrogen-centered group (N_2) by a carbon-centered radical (C_1). The values for $log\tilde{A}$ and E_a of the reference reaction, i.e. hydrogen abstraction from methylamine by methyl, are equal to 6.430 and 65.8 kJ mol^{-1}, c.f. Table 4-6. The contributions of the primary groups C_1-$(C)_2(H)$ and N_2-$(C_t)(H)$ amount to -0.213 and 0.086 for $log\tilde{A}$, while for E_a the values are equal to 7.6 and -15.0 kJ mol^{-1}. This results in a group additive approximated value of 6.303 for the single-event pre-exponential factor and 58.4 kJ mol^{-1} for the activation energy for the forward reaction. The activation energy for the reverse reaction is calculated as 105.4 kJ mol^{-1}, which means that hydrogen abstraction from ethynamine by the isopropyl radical is the exothermic direction. When substituting this value for $E_{a,exo}$ in Eq. 4-6, a tunneling coefficient of 1.341 is obtained at 1000 K, which is in good agreement with the *ab initio* calculated Eckart tunneling coefficient of 1.264. With two methyl rotors and an external symmetry of two, the total symmetry number of the isopropyl radical is 18. The transition state has two methyl rotors and one chiral center (N_2). The number of single events for the forward reaction is thus equal to four. This yields a total rate coefficient of 9.6×10^3 m^3 mol^{-1} s^{-1} which is in good agreement with the *ab initio* calculated rate coefficient of 1.2×10^4 m^3 mol^{-1} s^{-1}.

$$\log\tilde{A}\,(1000\,K) = log\tilde{A}_{ref}(1000\,K) + GAV^{o}_{\log\tilde{A}}\big(C_1 - (C)_2(H)\big) + GAV^{o}_{\log\tilde{A}}\big(N_2 - (C_t)(H)\big) = 6.430 + (-0.213) + 0.086 = 6.303$$

$$E_a(1000\,K) = E_{a,ref}(1000\,K) + \Delta GAV^{o}_{E_a}\big(C_1 - (C)_2(H)\big) + \Delta GAV^{o}_{E_a}\big(N_2 - (C_t)(H)\big) = 65.8 + 7.6 + (-15.0) = 58.4\,kJ\,mol^{-1}$$

4.4. Conclusions

The intermolecular hydrogen abstraction family is an important reaction family during pyrolysis and oxidation of nitrogen-containing compounds, including aliphatic amines. By making use of the group additivity method, the kinetics for a broad range of hydrogen abstraction reactions can be approximated based on a limited amount of parameters. In this work, new group additivity schemes have been determined to approximate the Arrhenius parameters of C-H and N-H hydrogen abstraction reactions involving nitrogen- and carbon-centered radicals. A dataset of 316 high-pressure limit rate coefficients calculated at the CBS-QB3 level of theory has been constructed, including 26 hydrogen abstractions by a hydrogen atom, 45 hydrogen abstractions by a nitrogen-centered radical and 87 hydrogen abstractions by a carbon-centered radical. A comparison with available experimental studies shows that the employed methodology using the CBS-QB3 composite method leads to accurate rate coefficients for the studied reaction families, i.e. the rate coefficients are approximated within a factor of two of the experimental values. From the Arrhenius parameters obtained for the training set reactions, 76 ΔGAV°s and 14 resonance corrections have been regressed. The resonance corrections are required to account for the cross-interactions between conjugated systems on the two primary atoms in the reactive center, being either a carbon or nitrogen atom.

A correlation has been proposed to account for the tunneling contributions with the temperature and activation energy of the exothermic reaction, which can be readily determined with group additivity, as input parameters. The performance of the group additive schemes is validated making use of a test set. At 1000 K, the *ab initio* calculated rate coefficient is approximated on average within a factor of 1.45 for H-H-N hydrogen abstractions, a factor of 1.47 for N-H-N hydrogen abstractions and a factor of 1.34 C-H-N hydrogen abstractions. The final ΔGAV°s and resonance corrections have been obtained making use of both the training and test sets in order to increase the accuracy of the group additivity scheme.

4.5. References

[1] W.H. Green, P.I. Barton, B. Bhattacharjee, D.M. Matheu, D.A. Schwer, J. Song, R. Sumathi, H.H. Carstensen, A.M. Dean, J.M. Grenda, Computer Construction of Detailed Chemical Kinetic Models for Gas-Phase Reactors, Industrial & Engineering Chemistry Research 40 (2001) 5362-5370.

[2] M.G. Evans, M. Polanyi, Inertia and driving force of chemical reactions, Transactions of the Faraday Society 34 (1938) 11-24.

[3] P. Blowers, R. Masel, Engineering approximations for activation energies in hydrogen transfer reactions, AIChE Journal 46 (2000) 2041-2052.

[4] S.W. Benson, J.H. Buss, Additivity rules for the estimation of molecular properties - Thermodynamic properties, Journal of Chemical Physics 29 (1958) 546-572.

[5] M.K. Sabbe, A.G. Vandeputte, M.-F. Reyniers, M. Waroquier, G.B. Marin, Modeling the influence of resonance stabilization on the kinetics of hydrogen abstractions, Physical Chemistry Chemical Physics 12 (2010) 1278-1298.

[6] M.K. Sabbe, M.-F. Reyniers, M. Waroquier, G.B. Marin, Hydrogen Radical Additions to Unsaturated Hydrocarbons and the Reverse β-Scission Reactions: Modeling of Activation Energies and Pre-Exponential Factors, Chemphyschem 11 (2010) 195-210.

[7] M.K. Sabbe, M.F. Reyniers, V. Van Speybroeck, M. Waroquier, G.B. Marin, Carbon-Centered Radical Addition and β-Scission Reactions: Modeling of Activation Energies and Pre-exponential Factors, Chemphyschem 9 (2008) 124-140.

[8] P.D. Paraskevas, M.K. Sabbe, M.-F. Reyniers, G.B. Marin, N.G. Papayannakos, Group additive kinetic modeling for carbon-centered radical addition to oxygenates and β-scission of oxygenates, AIChE Journal 62 (2016) 802-814.

[9] P.D. Paraskevas, M.K. Sabbe, M.-F. Reyniers, N. Papayannakos, G.B. Marin, Kinetic Modeling of α-Hydrogen Abstractions from Unsaturated and Saturated Oxygenate Compounds by Carbon-Centered Radicals, Chemphyschem 15 (2014) 1849-1866.

[10] A.G. Vandeputte, M.K. Sabbe, M.-F. Reyniers, G.B. Marin, Kinetics of α hydrogen abstractions from thiols, sulfides and thiocarbonyl compounds, Physical Chemistry Chemical Physics 14 (2012) 12773-12793.

[11] A.G. Vandeputte, M.-F. Reyniers, G.B. Marin, Kinetic modeling of hydrogen abstractions involving sulfur radicals, Chemphyschem 14 (2013) 3751-3771.

[12] A. Lucassen, K. Zhang, J. Warkentin, K. Moshammer, P. Glarborg, P. Marshall, K. Kohse-Höinghaus, Fuel-nitrogen conversion in the combustion of small amines using dimethylamine and ethylamine as biomass-related model fuels, Combustion and Flame 159 (2012) 2254-2279.

[13] M.H. Almatarneh, M. Altarawneh, R.A. Poirier, I.A. Saraireh, High level ab initio, DFT, and RRKM calculations for the unimolecular decomposition reaction of ethylamine, Journal of Computational Science 5 (2014) 568-575.

[14] G. Hennig, H.G.G. Wagner, A Kinetic Study About the Reactions of NH2(X2B1) Radicals with Saturated Hydrocarbons in the Gas Phase, Berichte der Bunsengesellschaft für physikalische Chemie 99 (1995) 863-869.

[15] T. Ko, P. Marshall, A. Fontijn, Rate coefficients for the H+NH3 reaction over a wide temperature range, The Journal of Physical Chemistry 94 (1990) 1401-1404.

[16] C. Willis, A.W. Boyd, O.A. Miller, Primary yields and mechanism in the radiolysis of gaseous ammonia, Canadian Journal of Chemistry 47 (1969) 3007-3016.

[17] K.T. Aganesyan, A.B. Nalbandyan, The determination of the rate constants for the reactions between hydrogen and oxygen atoms and ammonia molecules., Dokl. Phys. Chem. 160 (1965).

[18] W. Hack, P. Rouveirolles, H.G. Wagner, Direct measurements of the reactions NH2+H2→NH3 + H at temperatures from 670 to 1000 K, The Journal of Physical Chemistry 90 (1986) 2505-2511.

[19] J.V. Michael, J.W. Sutherland, R.B. Klemm, Rate constant for the reaction H + NH3 over the temperature range 750-1777 K, The Journal of Physical Chemistry 90 (1986) 497-500.

[20] J.W. Sutherland, R.B. Klemm, Kinetic studies of elementary reactions using the flash photolysis-shock tube technique, Symposium (International) on Combustion 16 (1987).

[21] M. Demissy, R. Lesclaux, Kinetics of hydrogen abstraction by amino radicals from alkanes in the gas phase. A flash photolysis-laser resonance absorption study, Journal of the American Chemical Society 102 (1980) 2897-2902.

[22] W. Hack, H. Kurzke, P. Rouveirolles, H.G. Wagner, Direct measurements of the reaction NH2+CH4→NH3+CH3 in temperature range 743≤T/K≤1023, Symposium (International) on Combustion 21 (1988) 905-911.

[23] S. Song, D.M. Golden, R.K. Hanson, C.T. Bowman, J.P. Senosiain, C.B. Musgrave, G. Friedrichs, A shock tube study of the reaction NH2 + CH4 → NH3 + CH3 and comparison with transition state theory, International Journal of Chemical Kinetics 35 (2003) 304-309.

[24] W. Hack, H. Kurzke, P. Rouveirolles, H.G. Wagner, Hydrogen Abstraction Reactions by NH2(X̃2B1)-Radicals from Hydrocarbons in the Gas Phase, Berichte der Bunsengesellschaft für physikalische Chemie 90 (1986) 1210-1219.

[25] P. Gray, J.C.J. Thynne, Arrhenius parameters for elementary combustion reactions: H-atom abstraction from N-H bonds, Symposium (International) on Combustion 10 (1965) 435.

[26] P. Gray, A. Jones, J.C.J. Thynne, Kinetics and sites of methyl radical attack on dimethylamine and deuterated dimethylamine, Transactions of the Faraday Society 61 (1965) 474-483.

[27] P. Gray, A. Jones, Methyl radical reactions with ethylamine and deuterated ethylamines, Transactions of the Faraday Society 62 (1966) 112-119.

5

Pyrolysis and oxidation of aliphatic amines

Abstract

Aliphatic amines are an important class of nitrogen-containing compounds present in renewable fuels such as bio-oils. Conversion of this fuel-bound nitrogen can lead to the formation of hydrogen cyanide (HCN) and NH_3, as well as NO_x emissions. The pyrolysis and oxidation chemistry of small aliphatic amines has been investigated via a combination of quantum chemical calculations, chemical kinetic modeling and experimental validation. A new kinetic model has been developed with the automatic kinetic model generator Genesys to describe the pyrolysis and oxidation of three model compounds, i.e. ethylamine ($CH_3CH_2NH_2$), dimethylamine ($(CH_3)_2NH$) and diethylamine ($(CH_3CH_2)_2NH$), over a wide range of conditions. This kinetic model makes use of the new group additivity databases for thermodynamic and kinetic parameters of nitrogen-containing compounds, as reported in Chapter 3 and Chapter 4. The thermodynamic and kinetic parameters for the main species and reactions are obtained directly from *ab initio* calculations. The kinetic model performance has been evaluated with new experimental data gathered in a tubular reactor and a jet-stirred reactor for diethylamine pyrolysis and oxidation and available literature data from laminar premixed flame and shock tube experiments for ethylamine and dimethylamine oxidation. The dominant decomposition pathway under all the studied conditions is a set of hydrogen abstractions from the C_α and N positions followed by β-scission of the fuel radicals. Among the unimolecular decomposition pathways, the homolytic C–C and C–N scissions and four-centered elimination play a minor role. HCN is the main intermediate nitrogen-containing species and at temperatures above 1100 K the amines are completely converted to N_2 and NO.

This Chapter is based on the following publications:

Experimental and kinetic modeling study of the pyrolysis and oxidation of diethylamine. Pappijn C.A.R.; Vin N.; Vermeire F.H.; Van de Vijver R.; Herbinet O.; Battin-Leclerc F.; Reyniers M.-F.; Marin G.B.; Van Geem K.M. **Fuel**, 275, 117744, 2020

Combustion of ethylamine, dimethylamine and diethylamine: Theoretical and kinetic modeling study. Pappijn C.A.R.; Vermeire F.H.; Van de Vijver R.; Reyniers M.-F.; Marin G.B.; Van Geem K.M. **Proceedings of the Combustion Institute**, 38, 585-592, 2021

5.1. Introduction

Untreated bio-oils produced by biomass fast pyrolysis contain substantial amounts of nitrogen containing compounds [1, 2]. The decomposition of these species is known to lead to the formation of small nitrogen-containing pollutants, such as hydrogen cyanide (HCN) and ammonia, as well as NO_x emissions, which has detrimental effects on the environment (e.g. acid rain, formation of ground-level ozone). In order to minimize the emission of these toxic compounds, it is essential to gain insight into the reactions governing the conversion of fuel-bound nitrogen so that compound specific maximum allowable quantities can be defined in fuel standards. For example, NO_x emissions from modern furnaces are limited to ppms, and to predict these quantities reliably, an in-depth investigation of the pyrolysis and oxidation chemistry of nitrogen-containing species is needed [3, 4]. To gain more insight into the nitrogen conversion, experimental and theoretical studies have focused on different classes of nitrogen-containing compounds, including amino acids [5, 6] and heterocyclic structures, such as pyridine [7-11] and pyrrole [12-16]. Another important class of nitrogen-containing species is amines, i.e. compounds which are derivatives of ammonia by replacing one or more hydrogen atoms by a substituent such as an alkyl group. The conversion of these amines can lead to the formation of NO_x, even more so compared to nitrogen-containing aromatic compounds [17-19]. Thus, even though they are present in bio-oils only in small quantities (a few percent), their conversion should be studied in depth.

The current understanding of the mechanisms responsible for the conversion of fuel-bound nitrogen has been reviewed in depth by Glarborg et al. [20] While both the pyrolysis and oxidation of ammonia have been extensively investigated in the past [21-24], knowledge about the chemical kinetics of its alkylated derivatives still has to be established. Some attention has been paid to the decomposition of the simplest primary amine, i.e. methylamine (CH_3NH_2). Kantak et al. [25] studied the oxidation of methylamine experimentally in a flow reactor over the temperature range 600-1400 K at pressures of 1 and 101 kPa. Votsmeier et al. [26] investigated the decomposition of methylamine with measurement of the NH_2 radical formation in a shock tube over the temperature range 1600-2100 K at a pressure of 162 kPa. They used the mechanism of Dean et al. [4] for the simulation of their experimental results. Lucassen et al. [27] investigated lean and rich flames of the two smallest isomeric amines ethylamine and dimethylamine. To develop a kinetic model, the thermodynamic parameters for several selected amine species were determined from quantum chemical calculations, while the kinetic parameters for the reactions of amines were approximated by analogy with the corresponding

reactions of hydrocarbons, methylamine and ethanol. They conclude that there is a significant difference between the decomposition chemistry of the better understood oxygenates ethanol and dimethyl ether and the analogous nitrogen-containing compounds ethylamine and dimethylamine. Li et al. [28, 29] studied the pyrolysis and oxidation of ethylamine in a shock tube over the temperature range 1200-1448 K at pressures of 86, 137 and 203 kPa. They made some changes to the model of Li et al. [30] to simulate the ignition delay times and NH_2 and OH time-history measurements.

A limited number of theoretical studies on the combustion chemistry of aliphatic amines is available in literature. Altarawneh et al. [31-33] studied the reaction pathways for the unimolecular and bimolecular decomposition of ethylamine using DFT calculations. Gong et al. [34] determined kinetic parameters for the reaction of DMA with a CH_3 radical using variational transition state theory. Galano et al. [35] and Onel et al. [36] studied the branching ratios in reactions of OH radicals with aliphatic amines. Recently, Shang et al. [37] investigated the kinetics of hydrogen abstractions from dimethylamine by a hydrogen atom and CH_3, HO and HO_2 radicals. They performed Rice-Ramsperger-Kassel-Marcus theory/Master Equation (RRKM/ME) calculations to determine pressure dependent rate coefficients and concluded that for these reactions, pronounced pressure dependency is observed under 400 K. Theoretical studies on the low-temperature oxidation of nitrogen-containing compounds, in which all the relevant potential energy surfaces are constructed for O_2 addition, are even more scarce. Rissannen et al. [38] combined experiments with theoretical calculations (CBS-QB3) to study the reactions of the two α-carbon-centered amino radicals of MEA and ethylamine with O_2. Alam et al. [39] investigated the reaction between O_2 and the nitrogen-centered aminyl radical of MEA. Overall, it can be concluded that the experimental database for the combustion chemistry of the aliphatic amines needs to be augmented and kinetic models need to be developed with a higher level of detail to further improve understanding of the underlying chemistry.

In this work the pyrolysis and oxidation of aliphatic amines is studied in detail by combining quantum chemical calculations, chemical kinetic modeling and experimental validation. The influence of the degree of substitution on the nitrogen atom and the alkyl chain length on the reactivity and product distribution is studied via three model compounds, i.e. ethylamine (EA, $CH_3CH_2NH_2$), dimethylamine (DMA, $(CH_3)_2NH$) and diethylamine (DEA, $(CH_3CH_2)_2NH$). The experimental data used for model validation includes shock tube ignition delay times reported by Li et al. [28, 29], species profiles measured in DMA and EA laminar premixed

flames by Lucassen et al. [27] and new datasets for the pyrolysis and oxidation of DEA in two different experimental units, i.e. a tubular reactor and a jet-stirred reactor [40]. These datasets cover a wide range of experimental conditions from very low residence times in the shock tube reactor of approximately 2 10^{-3} s to the much larger residence times in the jet-stirred reactor of 2 s. The studied temperatures range from 500 to 2000 K and pressures from 4 to 170 kPa. A new kinetic model containing accurate thermodynamic and kinetic parameters for the important species and crucial reactions determined with theoretical calculations at the CBS-QB3 level of theory, is proposed to describe the combustion of EA, DMA and DEA. The potential energy surfaces relevant for the low-temperature oxidation are investigated for all three amines. A large part of the kinetic model is constructed automatically with Genesys [41], applying the group additivity schemes for nitrogen-containing compounds as discussed in Chapter 3 and Chapter 4. The performance of the model is assessed for pyrolysis and oxidation at different equivalence ratios. Rate of production analyses reveal the important pathways for the pyrolysis and low- and intermediate temperature oxidation to HCN, acetonitrile, NO_x and others. Sensitivity analyses are used to identify the main reactions important to accurately describe the experimental results.

5.2. Methodologies

5.2.1. Experimental data

Three different types of experimental datasets are used to validate the developed kinetic model: species profiles measured in tubular and jet-stirred reactor experiments [40], shock tube ignition delay times [28, 29] and laminar premixed flames [27]. More specifically these datasets include: (1) tubular and jet-stirred reactor data of DEA pyrolysis and oxidation at three different equivalence ratios, a pressure of 107 kPa, temperatures between 500 and 1100 K, a residence time of 2 s and an inlet mole fraction of 0.01, (2) ignition delay times for stoichiometric mixtures of 2000 ppm of EA and DMA in argon with temperatures ranging from 1200 to 1450 K at a pressure of 137 kPa and (3) stoichiometric laminar premixed flames of EA and DMA with 25% argon dilution at 4 kPa. Detailed information is given below about the methodology used for the first set of experiments, i.e. DEA pyrolysis and oxidation. More information on the literature experimental data, i.e. the shock tube and laminar premixed flame experiments, can be found elsewhere [27-29].

The pyrolysis and oxidation of DEA has been studied experimentally using two different units: a jet-stirred reactor (JSR) and a tubular reactor (TR), both located in Centre National de la Recherche Scientifique (CNRS) in Nancy. The experimental results of diethylamine pyrolysis

have been reported before in the doctoral dissertation of Nicolas Vin, who has performed this set of experiments [42]. The pyrolysis and oxidation experiments in the jet-stirred reactor have been generated in the scope of this PhD thesis. The main features of both experimental units are discussed below, more details can be found elsewhere for the JSR [43] and the TR [44].

In the JSR, the diluent and the liquid fuel are mixed and passed through an evaporator. For the oxidation experiments, oxygen is added to the gaseous flow downstream. The gaseous mixture passes through an annular preheating zone, where it is heated to the reactor temperature, and enters the jet-stirred reactor through four nozzles. The gas residence time inside the annular preheater is very short compared to the residence time inside the reactor, i.e. approximately 1% of the residence time in the JSR. Therefore, the reactivity in this zone can be neglected. The nozzles and reactor are designed to limit temperature and concentration gradients inside the reactor. Thermocoax resistance wires provide heating for the annular preheating zone and the reactor. A type K thermocouple, for which the calibrated accuracy as reported by the manufacturer is ± 2.2 K or 0.75%, measures the temperature in the center of the reactor. Under unreactive conditions, the temperature gradients in the reactor are below 5 K. The temperature gradients have not been measured under reactive conditions. However, because of the perfect macro mixing obtained in the JSR and high dilution, i.e. 0.01 mole fraction of DEA, these temperature gradients are not expected to be significantly different from those under unreactive conditions. The pressure is set with a needle valve downstream of the reactor. The reactor has a fixed volume of 85 cm^3.

The TR consists of a horizontal 60 cm long alumina tube (volume of 294 cm^3) with an inner diameter of 2.0 cm and an outer diameter of 2.5 cm. The tubular reactor is heated by an electrical furnace from Vecstar equipped with an S-type thermocouple. For each reaction set point temperature, a temperature profile, i.e. temperature as a function of axial position in the TR, is measured in the absence of reaction using an R-type thermocouple, for which the calibrated accuracy as reported by the manufacturer is ± 1.5 K or 0.25%. These temperature profiles are available in Appendix C. Under unreactive conditions, the temperature gradients in the reactor are below 5 K. Because of the high dilution, i.e. 0.01 mole fraction of DEA, these temperature gradients are not expected to be significantly different under reactive conditions. For simulations, it can be assumed that the TR can be modeled as an ideal plug flow reactor [44]. The studied temperatures range from 500 to 1000 K for pyrolysis and to 1100 K for oxidation, with increments of 25 K, to cover the complete fuel conversion range. The pressure is kept constant at 107 kPa. The inlet mole fraction of DEA is set to 0.01 in the JSR and TR for all

experimental conditions. The volumetric flow rate in the JSR, calculated with the total molar inlet flow rate and the temperature and pressure in the reactor, is equal to 4.06 10^{-5} m^3 s^{-1}, corresponding to an average residence time (or space time) of 2 s. In the TR, the volumetric flow rate, calculated with the total inlet molar flow rate and the set point values of the temperature and pressure, is equal to 2.51 10^{-5} m^3 s^{-1}, corresponding to a space time of 2 s. Helium, argon, oxygen are provided by Messer (purity of 99.99%) and the nitrogen-containing compound DEA (purity ≥99.5%) is purchased from Sigma-Aldrich. The gaseous flow rates are controlled by mass flow controllers (Bronkhorst) and the liquid fuel mass flow rate is regulated by a liquid-Coriolis-flow controller (Bronkhorst).

In both experimental units, the products are analyzed using four different analytical techniques. The reactor outlet is connected to different gas chromatographs (GC), which enable online quantification of the product species. The connection with the GCs is done via heated transfer lines, kept at 433 K, to avoid product condensation. The first GC contains a Carbosphere packed column and a thermal conductivity detector (TCD). This GC is used to detect H_2, O_2, N_2, CO, CO_2, and CH_4. The carrier gas is He, except for the detection of H_2, for which Ar is used. The second GC is equipped with a PLOT-Q capillary column and a flame ionization detector (FID) preceded by a methanizer. The methanizer enables the detection and quantification of small oxygenates with the FID. The third gas chromatograph has a HP-5ms capillary column coupled to an FID. This GC is used to detect the main carbon- and nitrogen-containing products with more than 5 non-hydrogen atoms. The three preceding gas chromatographs are used for the analysis of species from the JSR. Two other gas chromatographs are used for the detection of species from the TR. The first is identical to the one used to detect the main carbon- and nitrogen-containing products with more than five non-hydrogen atoms from the JSR. The other one is equipped with a PLOT-Q capillary column, a TCD and FID (both detectors are installed in series). To enable on- or offline product identification, the reactor outlet is connected to a fourth gas chromatograph, which is equipped with either a PLOT-Q or HP-5ms capillary column, and has a quadrupole mass spectrometer as detector. The GC carrier gas is helium. A chemiluminescence NO_x analyzer (Thermo Scientific Model 42i) is adopted to measure the concentration of nitric oxide (NO) and nitric dioxide (NO_2). The quantitative range is 0 – 5000 ppm for NO and 0 – 500 ppm for NO_2 with a sensitivity of 0.01 ppm. A Fourier Transform InfraRed spectrometer (FTIR) from Thermo Scientific Antaris equipped with a Mercure Cadmium Telluride photoelectric detector is used to obtain a second quantification of NO, NO_2, DEA and HCN. The complete analysis section allows identification and quantification of all

oxidation and pyrolysis products ranging from the smallest hydrocarbons, oxygenates and nitrogen-containing compounds up to products with 9 non-hydrogen atoms.

The pyrolysis of DEA is studied both with the JSR and TR. For oxidation, three different equivalence ratios, i.e. φ = 1.0, 2.0 and 0.5, are studied with the JSR. Stoichiometry is based on complete conversion of nitrogen to N_2 rather than NO. In total, 32 species are identified and quantified for pyrolyis and oxidation using the described analytical techniques.The carbon and nitrogen balances are closed within 5% and all product yields can be found in in a summary of the experimental results on S:\vakgroep\ea12archief\SoftLib\c\cpappijn\1\. Because the configuration of the analysis section does not allow the quantification of water and hydrogen peroxide, the hydrogen and oxygen elemental balances are not available at oxidation conditions. The relative uncertainty on the experimental mole fraction is 5% for species calibrated using standards and 10% for species calibrated with the effective carbon number method, except for FTIR measurement for which the relative uncertainty can be estimated as 5%.

5.2.2. Kinetic model development

A kinetic model is constructed for the pyrolysis and oxidation of EA, DMA and DEA. This model consists of two parts, i.e. (1) a kinetic model to describe the oxidation chemistry of the small amines generated using the automatic kinetic model generation tool Genesys [41] and (2) a kinetic model to account for the reactions between the small hydrocarbon (C_1-C_2) and nitrogen-containing species, including the formation and destruction of NO_x, developed by Glarborg et al. [20].

Quantum chemical calculations are performed for all the main species and reactions important to accurately describe the EA, DMA and DEA chemistry, including the main low-temperature oxidation reaction pathways, for which the relevant potential energy surfaces are constructed. In case no *ab initio* thermodynamic data is available, Benson's group additivity method [45] is applied for hydrocarbons [46, 47] and oxygenates [48]. For nitrogen-containing species, the new group additivity scheme derived in Chapter 3 for approximation of the thermodynamic parameters is used. In case no *ab initio* kinetic data is available, the group additivity method developed by Saeys et al. [49] and extended by Sabbe et al. [50-52] for hydrocarbons and Paraskevas et al. [53] for oxygenates is used. For reactions with a nitrogen atom in the reactive center, either the developed group additivity schemes from Chapter 4 or rate rules are used [54].

This kinetic model describing the amine chemistry is merged with the mechanism of Glarborg et al. [20], which contains 150 species and 1397 reactions. It describes the chemistry of small

hydrocarbons (C_1-C_2) and nitrogen-containing species, including the formation and destruction of NO_x in a combustion process. In the case that the same species or reactions appear in both the automatically generated Genesys mechanism and the Glarborg et al. mechanism, it is opted to retain the kinetic parameters from the Genesys mechanism. Several reactions in the Glarborg et al. mechanism important to accurately describe the amine chemistry are approximated by analogy with hydrocarbon or oxygen-containing compounds. In the Genesys mechanism these reactions are obtained directly from quantum chemical calculations or at least based on similar reactions of nitrogen-containing compounds. In Appendix C, a comparison is done between a number of rate coefficients in the Glarborg et al. mechanism and calculated *ab initio* by Genesys. Not only do these rate coefficients differ several orders of magnitudes, also the relative importance of competing reactions is influenced. For the hydrogen abstraction by the hydroxyl radical from EA and DMA, the kinetic parameters computed with Variational Transition State Theory by Li et al. [55] are used. A number of reactions governing the low-temperature oxidation of DMA and EA have been refined with values based on nitrogen-containing compounds from the review of Dean et al. [4]. These reactions include reaction of the fuel radicals with other radical species, such as HO_2 and molecular oxygen. The complete kinetic model, which has 258 species and 2274 reactions, is available on S:\vakgroep\ea12archief\SoftLib\c\cpappijn\1\.

5.2.3. Reactor simulations

Reactor simulations are performed with the new kinetic model using CHEMKIN [56]. The JSR is modelled as a continuously stirred tank reactor (CSTR) and the TR as a plug flow reactor (PFR) using the temperature profiles measured under unreactive conditions as input. These profiles as well as a discussion on the PFR assumption are provided in Appendix C. The shock tube reactor is modelled as an adiabatic homogeneous batch reactor. The premixed laminar burner-stabilized flame is used for simulation of the flame experiments, with the reported experimental flame temperature profiles as input. Thermal diffusion is included in the simulations.

5.3. Results and discussion

5.3.1. *Ab initio* calculations

The pyrolysis and oxidation of aliphatic amines is driven by free radical reactions. During pyrolysis, the formation of radicals is initiated by a homolytic bond scission. In case of

oxidation, the initial radicals are formed via a hydrogen abstraction reaction by molecular oxygen (O_2) and to a lesser extent by a homolytic scission [40]. In Figure 5-1, the *ab initio* values calculated at the CBS-QB3 level of theory for the bond dissociation energies (BDE) of EA, DMA and DEA depicted. The BDEs of the analogous alkane bonds are included for comparison. The presence of the nitrogen atom influences the C-H and C-C BDEs at the α-carbon atom (C_α), i.e. the carbon atom next to nitrogen atom, significantly.

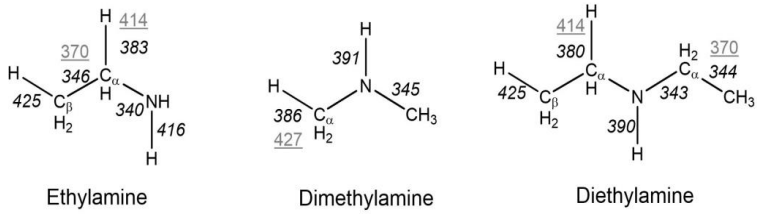

Figure 5-1: Bond dissociation energies (BDE) in kJ mol^{-1} for ethylamine, dimethylamine and diethylamine (*black*) and the analogous alkanes (grey) calculated at the CBS-QB3 level of theory.

The weakest bonds are the C_α-C_β and C_α-N bonds. The BDEs of the C_α-H bonds in EA, DMA and DEA are equal to 383, 386 and 380 kJ mol^{-1} respectively. This is approximately 30 kJ mol^{-1} lower than the BDE of a secondary alkane C-H bond, i.e. 414 kJ mol^{-1}. There is almost no effect of the alkylation of the carbon atom in the α-position on the BDE of the C_α-H bond. The hydrogen atom bonded to the α carbon atom is thus the preferred abstraction site. The calculated values agree well with the experimental BDE for the C_α–H bond in EA, i.e. 377 ± 8 kJ mol^{-1}, while for DMA an experimental BDE of 364 ± 8 kJ mol^{-1} has been reported [57]. Because the alkyl groups are able to stabilize the nitrogen-centered radical by hyperconjugation, the BDE of the N-H bond decreases when going from primary to secondary amines. The BDE of the N-H bond in EA is equal to 416 kJ mol^{-1}, which is approximately 25 kJ mol^{-1} higher than the BDE of the N-H bond in the secondary amines DMA and DEA. This calculated BDE of the N-H bond as well as the influence of the alkylation on the BDE is in agreement with experimental values gathered from Burkey et al. [58]. They report a value for the BDE of the N-H bond of 385 ± 8 kJ mol^{-1} for DMA, considering 33 kJ mol^{-1} for the stabilization by hyperconjugation due to adjacent alkyl groups. The lowest barrier for hydrogen abstraction from DEA by molecular oxygen is that for abstraction from C_α–H, i.e. 133 kJ mol^{-1}. The barriers for hydrogen abstraction from C_β–H and N-H are equal to respectively 197 and 143 kJ mol^{-1}. Taking into account the main initiating reactions, the oxidation of DEA will start at significantly lower temperatures compared to pyrolysis, due to the lower barrier of the main initiating reactions.

Besides typical pyrolysis and oxidation radical reactions, amines can undergo unimolecular 1,2-elimination reaction. In the case of EA this leads to the formation of ethene and NH_3, while elimination of DEA results in ethylene and EA. In Figure 5-2, both elimination reactions are depicted with the calculated concerted transition state structures. The energy barrier for the elimination reactions is equal to 290 and 283 kJ mol^{-1} for EA and DEA respectively. This is in agreement with the energy barrier of 285 kJ mol^{-1} for EA calculated by Almatarneh et al. [33] at the G3MP2B3 level of theory. For comparison, the energy barrier for the analogous elimination reaction of ethanol, leading to the formation of ethene and H_2O, amounts to 282 kJ mol^{-1} [59]. Both elimination reactions are endothermic, i.e. a reaction energy of 53 and 76 kJ mol^{-1} for EA and DEA respectively.

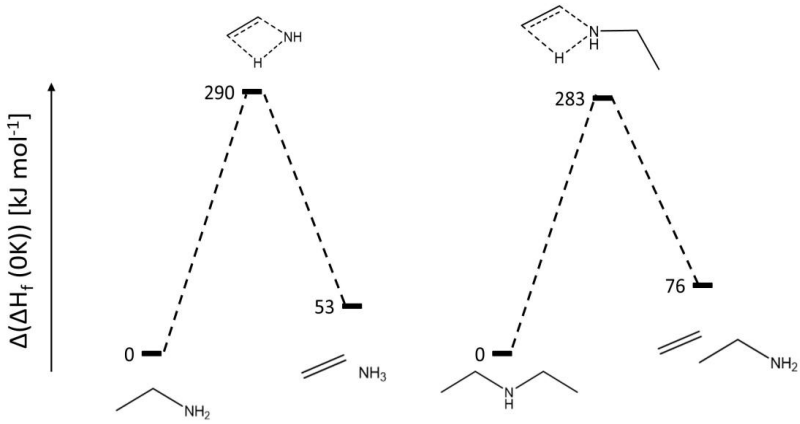

Figure 5-2: Potential energy surface for the unimolecular elimination of EA and DEA. The values are CBS-QB3 calculated enthalpies of formation at 0 K [kJ mol^{-1}] relative to EA and DEA.

Pressure dependent rate coefficients for the unimolecular elimination reactions of EA and DEA have been determined using the RRKM theory with the MESMER program [60]. Argon is used as bath gas and the energy transfer probability is modeled using a single exponential energy transfer model, with a ΔE_{down} of 130 cm^{-1}. The rate coefficients have been fitted to Chebyshev polynomials over the temperature range 300 to 2500 K and pressure range 1 to 10^4 kPa. The high-pressure limit rate coefficients expressed in Arrhenius form are given by:

$$k_{EA,uni} = 2.21 \cdot 10^{12}\, exp\left(-\frac{33.2 \cdot 10^3}{T}\right)\ s^{-1} \qquad \text{(Eq. 5-1)}$$

$$k_{DEA,uni} = 3.74 \cdot 10^{11}\, exp\left(-\frac{33.9 \cdot 10^3}{T}\right)\ s^{-1} \qquad \text{(Eq. 5-2)}$$

In Figure 5-3, an Arrhenius plot is shown for the calculated rate coefficients of EA and DEA at three different pressures, i.e. 1, 10^2 and 10^4 kPa. As expected for unimolecular reactions, the fall-off region shifts with increasing temperature towards increasing pressure [61].

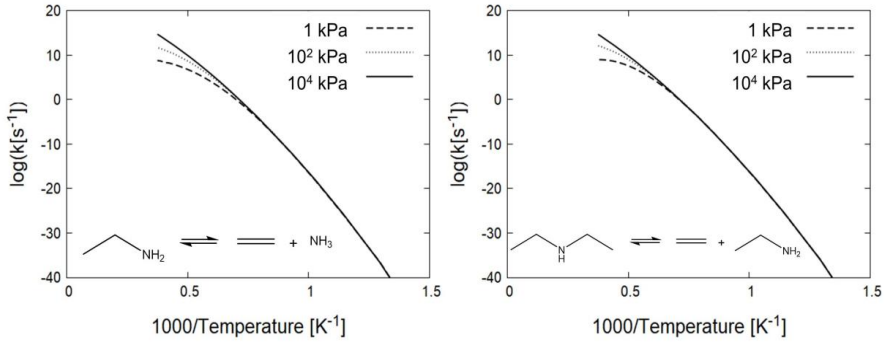

Figure 5-3: Arrhenius plot for unimolecular elimination reactions of EA (left) and DEA (right) comparing the rate coefficients obtained from RRKM calculations at three different pressures, i.e. 1, 10^2 and 10^4 kPa.

Note that for DEA, the reaction is still in the high-pressure limit at 10^3 kPa and 1100 K, which is the maximum temperature reached in the JSR experiments. In the low-pressure (4 kPa) laminar premixed flames of EA, the maximum temperature is approximately 2000 K. Under these conditions, the elimination reaction is in the fall-off regime. The contribution of the elimination reaction will thus increase with increasing pressure. In the present low-pressure flame of EA, the elimination reaction of EA plays only a minor role (< 1%) in the EA consumption.

5.3.2. Potential energy surfaces for low-temperature oxidation

To study the consecutive chemistry of the main amine radicals, i.e. the unimolecular reactions as well as their reactions with molecular oxygen, the relevant potential energy surfaces have been constructed. In the low-temperature oxidation (around 500-600 K) of hydrocarbons, a barrierless reaction between the alkyl radicals and O_2 can lead to the formation of the chemically activated $RO_2^{\cdot}$ adduct, which will either be stabilized or react via a concerted elimination of $HO_2^{\cdot}$ to give the conjugated alkene. Intramolecular hydrogen abstraction can lead to the formation of hydroperoxides, which can be considered as degenerate branching agents as the O-OH bond can easily be broken leading to the formation of two radicals. The reversibility of the addition of alkyl radicals to O_2 molecules benefits the direct formation of alkenes and hydroperoxy radicals with increasing temperature. Due to the higher activation energy barriers

(there is no energy barrier for the alkyl radical addition to O_2), unimolecular decomposition of the alkyl radicals will start to dominate at sufficiently high temperatures (≥ 800 K) [62].

Figure 5-4 depicts the potential energy surface (PES) for the addition of the carbon-centered DMA radical, i.e. $CH_2^{\cdot}NHCH_3$ labeled $R_1^{\cdot}$, to an O_2 molecule, leading to the formation of the peroxide $CH_2OO^{\cdot}NHCH_3$, labeled $R_1OO^{\cdot}$. The reaction enthalpy for the addition is equal to -138 kJ mol^{-1}. The direct HO_2 elimination has a barrier of only 82 kJ mol^{-1}. Of the three possible isomerization reactions for $R_1OO^{\cdot}$, the reaction in which a hydrogen atom migrates from C_α to the peroxy group via a six-membered cyclic transition state, has the lowest barrier, i.e. 71 kJ mol^{-1}. This reaction pathway leads to the formation of formaldehyde and methanimine after β-scission of the C-N bond. The second isomerization reaction proceeding via the three-membered cyclic transition state to form $CH_3NHCH{=}O$ and a hydroxyl radical, has a higher activation energy barrier compared to the reaction enthalpy of the addition reaction, i.e. 161 kJ mol^{-1}. The third possible isomerization reaction has a five-membered cyclic transition state with a barrier of 136 kJ mol^{-1}. After β-scission of the C-O bond of the resulting radical, $CH_2{=}NCH_3$ and a hydroxyl radical are formed, i.e. the same products as obtained from the HO_2 elimination reaction.

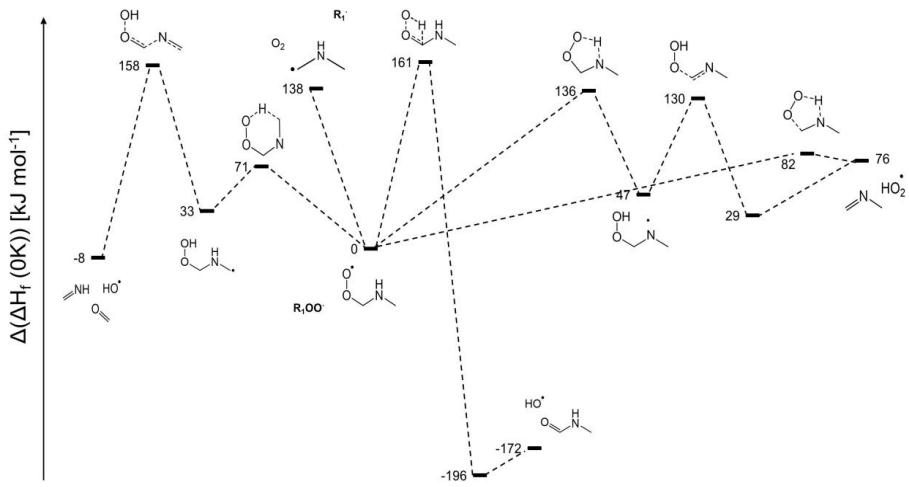

Figure 5-4: Selected part of the potential energy surface of the addition to O_2 of the $CH_2^{\cdot}NHCH_3$ radical, i.e. the radical formed after abstraction from the α carbon atom from DMA, labeled $R_1^{\cdot}$. The values are CBS-QB3 calculated enthalpies of formation at 0 K [kJ mol^{-1}] relative to enthalpy of formation of $R_1OO^{\cdot}$.

In Figure 5-5, the PES is shown for the addition of the radical formed after breaking of the weakest C-H bond in DEA, i.e. $CH_3CH^{\cdot}NHCH_2CH_3$ labeled $R_2^{\cdot}$, to an O_2 molecule, leading to the formation of the peroxide $CH_3CHOO^{\cdot}NHCH_2CH_3$ labeled $R_2OO^{\cdot}$. This PES is very similar

to the corresponding PES for the DMA radical. The reaction enthalpy of the addition reaction is equal to -149 kJ mol^{-1}, which is similar to the C-OO$^{\cdot}$ bond strength of propylperoxy radicals [63]. The peroxide $R_2OO^{\cdot}$ can react further via different reaction pathways, including cyclic ether formation and isomerization reactions. For the construction of the PES, only the isomerization reactions of $R_2OO^{\cdot}$ are considered, as these lead to the formation of product species which have been experimentally observed.

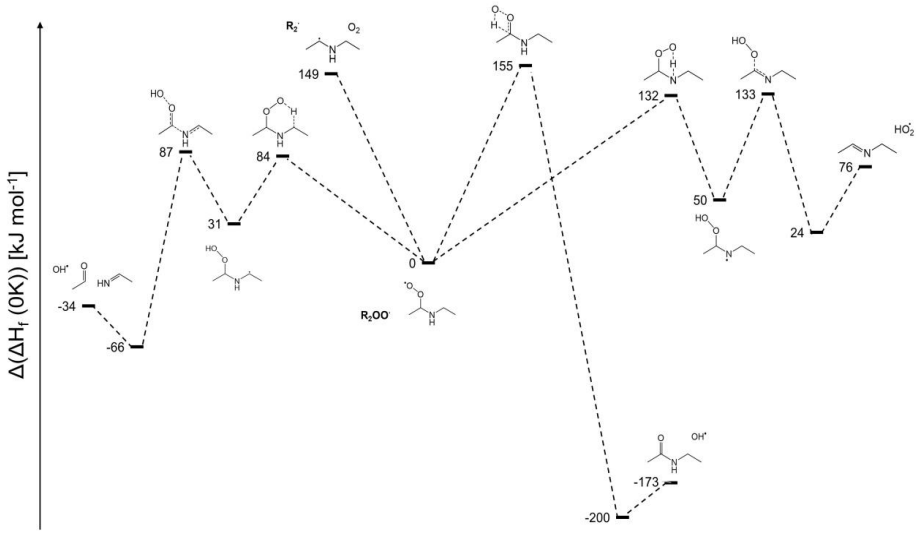

Figure 5-5: Selected part of the potential energy surface of the addition to O_2 of the $CH_3CH^{\cdot}NHCH_2CH_3$ radical, i.e. the radical formed after abstraction from the α carbon atom from DEA, labeled $R_2^{\cdot}$. The values are CBS-QB3 calculated enthalpies of formation [kJ mol^{-1}] at 0 K relative to enthalpy of formation of $R_2OO^{\cdot}$.

In the first pathway a hydrogen atom migrates from C_α to the peroxy group via a six-membered cyclic transition state, which is 84 kJ mol^{-1} higher in energy than $R_2OO^{\cdot}$. A subsequent β-scission leads to the formation of a hydroxyl radical, acetaldehyde and ethanimine ($CH_3CH{=}NH$). The second path starts with an isomerization reaction via a three-membered cyclic transition state, which is 155 kJ mol^{-1} higher in energy than $R_2OO^{\cdot}$. This path leads to the formation of ethyl ethanamide ($CH_3CH_2NHC(=O)CH_3$) and a hydroxyl radical. The third possible isomerization reaction proceeds via a five-membered cyclic transition state, and consists of a hydrogen abstraction from the nitrogen atom. The formed nitrogen-centered radical then undergoes a β-scission resulting in a methyl radical. As the transition states for these last two isomerization reactions have a higher energy compared to the addition of molecular oxygen to $R_2^{\cdot}$, these reactions will most likely be less important compared to the first isomerization. At the applied experimental conditions, no low temperature reactivity is observed. For this reason, the second addition of molecular oxygen to the hydroperoxy radical

leading to chain branching is omitted. According to Curran et al. [64], the contribution of the reaction leading to HO_2 radicals and alkenes decreases significantly with increasing number of carbon atoms in the alkyl radical, due to an increased possibility of stabilization of the adduct by vibrations. They neglect this reaction class for alkyl radicals containing more than four heavy atoms.

Abstraction from the N-H site leads to the formation of nitrogen-centered aminyl radicals, which are thought to react slowly with O_2 reflecting the thermodynamic instability of the O_2 adducts [65, 66]. In contrast to the barrierless formation of most alkyl peroxy radicals, addition to an O_2 molecule proceeds via a saddle point transition state. For example, O_2 addition of the $CH_3N^{\cdot}CH_3$ radicals proceeds via a barrier of 28 kJ mol^{-1}, with a corresponding reaction enthalpy of -29 kJ mol^{-1}. The consecutive isomerization reaction of the aminyl peroxy radical, in which a hydrogen atom migrates from C_α to the peroxy group via a five-membered cyclic transition state, has a barrier of 89 kJ mol^{-1}. This barrier is significantly higher compared to the barrier of the possible HO_2 elimination reaction of $CH_3NOO^{\cdot}CH_3$, i.e. 38 kJ mol^{-1}. This is in agreement with the findings reported by Alam et al. [39] for the reaction between O_2 and the nitrogen-centered $CH_3NH^{\cdot}$. The lowest energy pathway proceeds via the HO_2 elimination of $CH_3NHOO^{\cdot}$, with a barrier of 11 kJ mol^{-1}. Direct hydrogen abstraction and hydrogen transfer between the carbon and nitrogen atom have significantly higher barriers, i.e. 85 and 78 kJ mol^{-1}.

Also for DEA, the unstable aminyl peroxy radical causes the nitrogen-centered aminyl radicals to react slowly with O_2. The addition of molecular oxygen to the nitrogen-centered radical $CH_3CH_2N^{\cdot}CH_2CH_3$, i.e. the second most important radical, has an enthalpy of reaction of -33 kJ mol^{-1}. As both consecutive intramolecular hydrogen abstraction reactions have a higher reaction barrier compared to the O_2 addition, i.e. at least 181 kJ mol^{-1}, the formation of this peroxy radical can be neglected. The O_2 addition to the primary radical $CH_2^{\cdot}CH_2NHCH_2CH_3$ is not considered, due to the lower importance of this radical as a result of the higher BDE of the C_β-H bond. All of the relevant potential energy surfaces for the radicals formed from EA, DMA and DEA are provided in Appendix C.

5.3.3. Assessment of the kinetic model

5.3.3.1. Jet-stirred reactor experiments (DEA)

Figure 5-6 presents the experimental and simulated mole fractions of DEA and the main product species as a function of temperature for the pyrolysis of DEA in both the JSR and TR units. Under pyrolysis conditions, DEA starts to convert around 800 K in both reactor units. The type

of the reactor has an influence on the DEA conversion. A faster conversion is obtained in the TR than in the JSR. Full conversion is reached at 950 K in the TR reactor and at 1000 K in the JSR. This is in line with the theory of ideal reactors as it can be shown that for an elementary reaction A → products, the conversion in a PFR is larger than in a CSTR, under equal operating conditions [67].

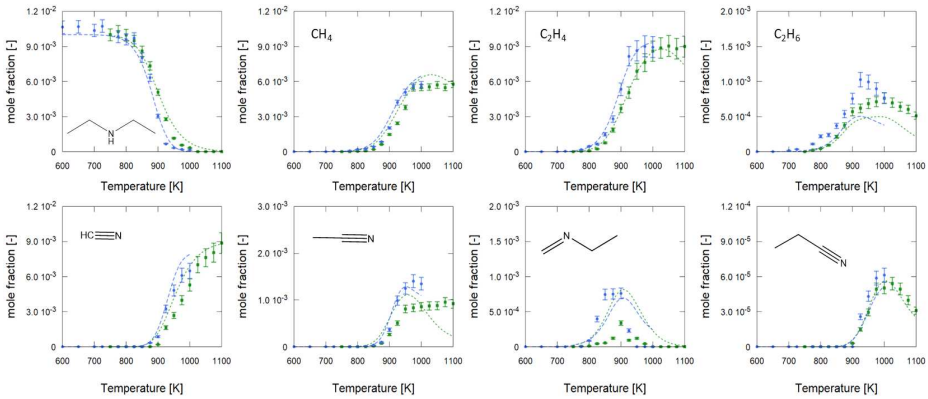

Figure 5-6: Species mole fractions as a function of temperature [K] for the pyrolysis of DEA in the JSR (green) and the TR (blue). Experiment (symbols) and simulation results (lines) are compared. Experimental conditions are 2 s residence time, a pressure of 107 kPa and an inlet DEA mole fraction of 0.01. For the TR, the depicted temperatures correspond to the set point temperatures.

The main hydrocarbon products observed are methane (CH_4), ethene (C_2H_4) and ethane (C_2H_6), while the main nitrogen-containing products are HCN, acetonitrile (CH_3CN), ethylmethanimine ($CH_2{=}NCH_2CH_3$) and propanenitrile (CH_3CH_2CN). Ethylmethanimine is one of the lowest temperature nitrogen-containing products that is formed. It is the smallest species containing an imine (C=N) group that is detected experimentally. The ethylmethanimine mole fraction increases with temperature and reaches a maximum at 900 K. The two main product species containing a nitrile group (C≡N) start to form at approximately 875 K. In contrast to acetonitrile, the HCN mole fraction does not reach a maximum and its mole fraction keeps increasing even when full fuel conversion is reached. The formation of propanenitrile starts at a temperature approximately 25 K higher, and reaches a maximum at 1000 K. HCN is by far the major nitrogen-containing product and ethene the main hydrocarbon product. Minor product species that are observed are propane, propene, 1-butene, 2-butene, butadiene, acrylonitrile and isobutyronitrile. There is almost no effect of the reactor type on the main product distribution and product selectivity. In the TR, the formation of the products starts at a slightly lower temperature. In the intermediate temperature range, large recombination products are formed, containing at least five carbon atoms and two nitrogen atoms, and also an imine (C=N) or nitrile

(C≡N) functional group. Figure 5-7 depicts the molecular structures of two experimentally detected nitrogen-containing recombination products. In the TR a lower number of recombination products are formed compared to the JSR.

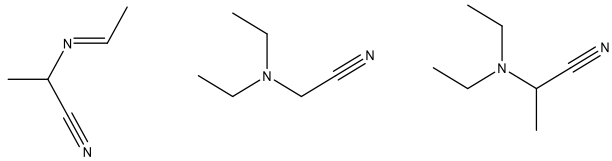

Figure 5-7: Large nitrogen-containing recombination products formed during the pyrolysis of DEA.

Oxidation experiments of DEA are performed at fuel-rich, stoichiometric and fuel-lean conditions, corresponding to the equivalence ratios, φ = 2.0, 1.0 and 0.5. The experimental results are depicted in Figure 5-8, Figure 5-9 and Figure 5-10 respectively. The conversion of DEA starts at 600 K, approximately 200 K lower compared to pyrolysis. The equivalence ratio does not have a significant influence on the conversion profile. The formation of acetaldehyde is observed at low temperatures, probably corresponding to the addition of molecular oxygen on the parent radical, as discussed previously. Similar recombination products are formed in the JSR as during the pyrolysis of DEA. Oxidation products that are not formed during the pyrolysis of DEA, include CO, CO_2, N_2, NO, NO_2 and nitromethane. For φ = 1.0 and φ = 0.5, the mole fraction of CO goes through a maximum indicating that CO is further oxidized to CO_2. At fuel-rich conditions, CO keeps increasing with temperature and the mole fraction of CO_2 is significantly less. The hydrocarbon mole fractions decrease when going from fuel-rich to fuel-lean conditions. Compared to pyrolysis, the maximum mole fractions of methane and ethene are much lower. The maximum ethene mole fractions are 3.8×10^{-3} at 875 K, 3.3×10^{-3} at 850 K and 2.8×10^{-3} at 825 K for φ = 2.0, φ = 1.0 and φ = 0.5 respectively. Similar to DEA pyrolysis, HCN and acetonitrile are the most important product species containing a nitrile group (C≡N). Formation of acetonitrile starts at a temperature lower with 100 K compared to HCN. With increasing O_2 concentration, the peak of HCN mole fraction decreases and shifts towards lower temperatures, i.e. 8.1×10^{-3} at 1025 K, 6.0×10^{-3} at 975 K and 5.2×10^{-3} at 925 K for φ = 0.5, φ = 1.0 and φ = 2.0 respectively. The consumption of HCN leads to the formation of N_2 as main nitrogen-containing product at high temperatures for the fuel-lean and stoichiometric conditions.

The simulation results obtained with CHEMKIN [56], are compared to the experimental data in Figure 5-6 for pyrolysis and Figure 5-8 to Figure 5-10 for oxidation. Overall, the new kinetic model succeeds in predicting the experimental trends. The difference in reactivity for DEA

pyrolysis in the JSR and TR is captured by the model. The absolute mole fractions of the major species are predicted well, with an average deviation of 10%. The largest discrepancies are found for the hydrocarbons species methane and ethane. While for acetaldehyde the trend is captured by the model, it is clearly overpredicted. The formation of minor nitrogen-containing products NO, NO_2 and nitromethane (CH_3NO_2) starts at approximately 700 K, with mole fractions an order of magnitude lower compared to the main nitrogen-containing products. In contrast to the complete conversion of carbon to CO_2, nitrogen is only partially oxidized to NO and NO_2 at the highest temperatures, even in excess of O_2.

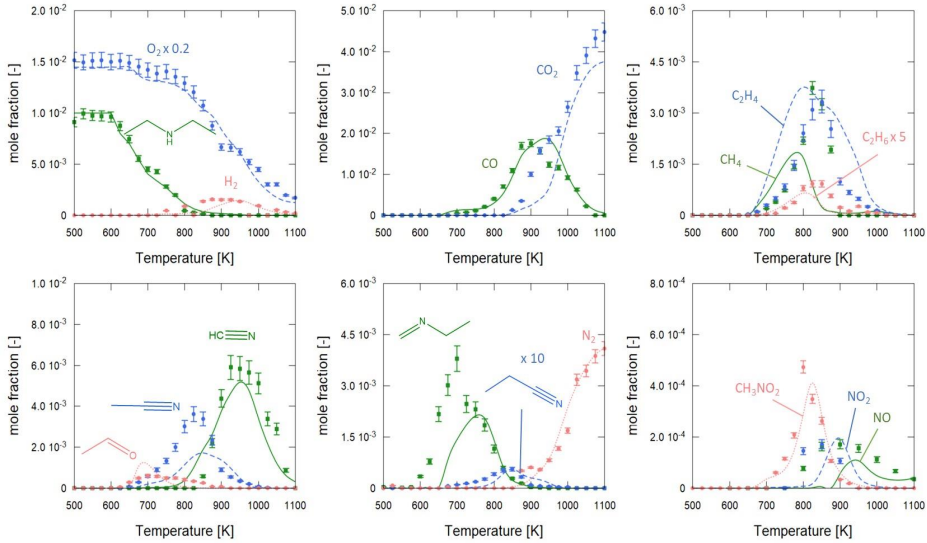

Figure 5-8: Species mole fractions as a function of temperature [K] for the oxidation of DEA for an equivalence ratio of 1.0. Experiment (symbols) and simulation results (lines) are compared. Experimental conditions are 2 s residence time, 107 kPa and an inlet mole fraction of DEA 0.01. The mole fractions of molecular oxygen for experimental points and simulations are divided by a factor 5. The mole fractions of ethane for experimental points and simulations are multiplied by a factor 5 and for propanenitrile by a factor 10.

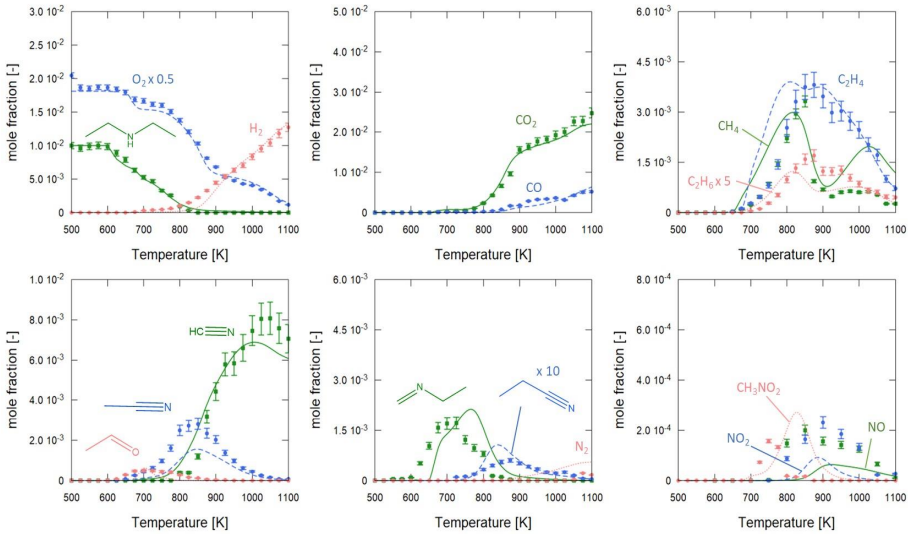

Figure 5-9: Species mole fractions as a function of temperature [K] for the oxidation of DEA for an equivalence ratio of 2.0. Experiment (symbols) and simulation results (lines) are compared. Experimental conditions are 2 s residence time, 107 kPa and an inlet mole fraction of DEA 0.01. The mole fractions of molecular oxygen for experimental points and simulations are divided by a factor 2. The mole fractions of ethane for experimental points and simulations are multiplied by a factor 5 and for propanenitrile by a factor 10.

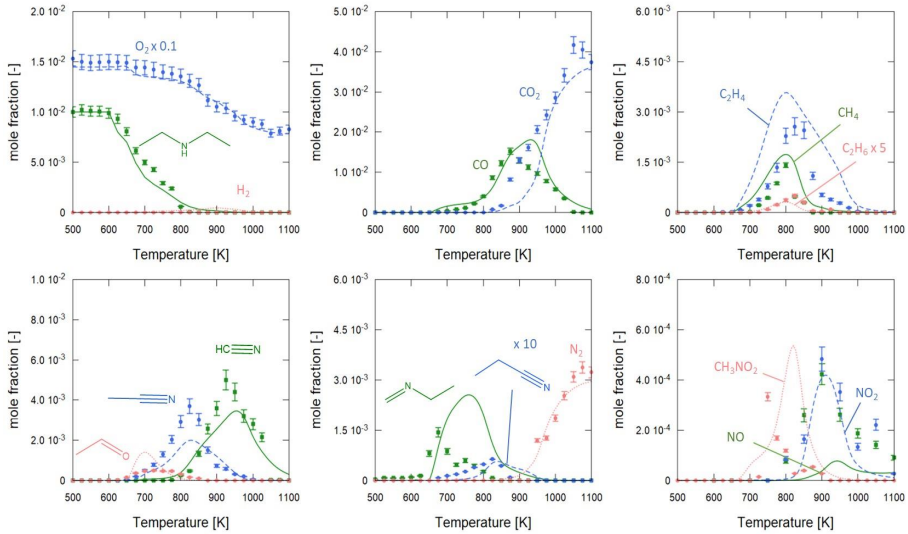

Figure 5-10: Species mole fractions as a function of temperature [K] for the oxidation of DEA for an equivalence ratio of 0.5. Experiment (symbols) and simulation results (lines) are compared. Experimental conditions are 2 s residence time, 107 kPa and an inlet mole fraction of DEA 0.01. The mole fractions of molecular oxygen for experimental points and simulations are divided by a factor 10. The mole fractions of ethane for experimental points and simulations are multiplied by a factor 5 and for propanenitrile by a factor 10.

A rate of production analysis for the pyrolysis of DEA at 900 K in the JSR is presented in Figure 5-11. At these experimental conditions, the DEA conversion is equal to 50%. At 900 K, DEA consumption is dominated by hydrogen abstractions. The contribution of both the homolytic scissions of the C-N and C-C bonds and the unimolecular elimination reaction of EA are small. The scissions, especially the C-N scission, become more important at higher temperature and under pyrolysis conditions. In pyrolysis, the main abstracting species are the hydrogen atoms and methyl radicals. Hydrogen abstraction from C_α is the main consumption channel. β-scission of the formed radical leads to the formation of ethanimine, which is mainly consumed via hydrogen abstraction. β-scission of the C-C bond of the nitrogen-centered radical ($CH_3CH{=}N^{\cdot}$) results in the formation of HCN, while β-scission of the C-H bond leads to acetonitrile. At 900 K, this β-scission is the dominant formation pathway of hydrogen cyanide. Another important pathway for the formation of HCN proceeds via C-H β-scission of the imine radical ($CH_2{=}N^{\cdot}$) formed from the ethylamine radical ($CH_3CH_2NH^{\cdot}$). This ethylamine radical is produced either via C-N scission of DEA or via hydrogen abstraction from the carbon atom in β position followed by β-scission. This HCN formation pathway becomes more important at higher temperatures.

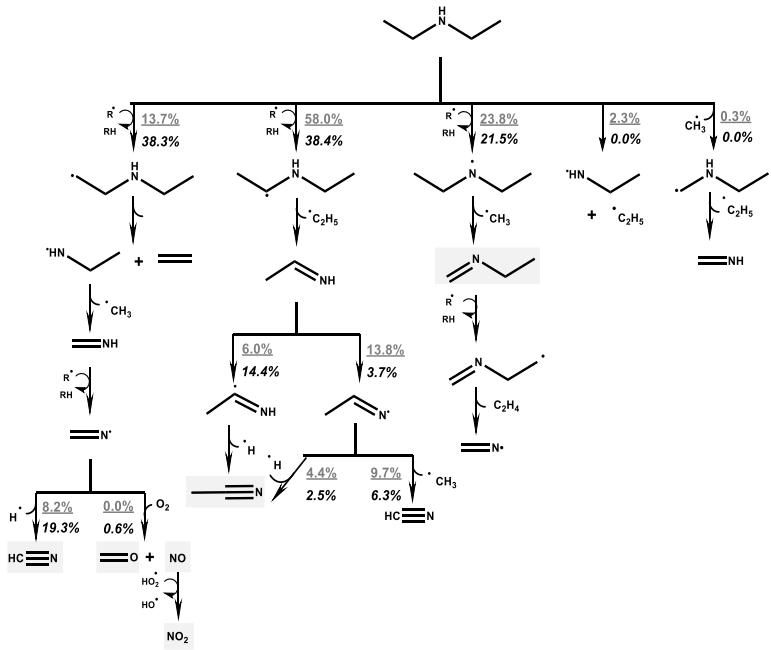

Figure 5-11: Rate of production analysis in the JSR for the pyrolysis and oxidation at intermediate temperatures. Percentages report the rate of productions relative to the total consumption of DEA at 900 K for pyrolysis (grey) and oxidation at φ = 2 (*black*). Species that are detected experimentally are marked.

The oxidation of DEA at 900 K is governed by the same reaction pathways as in pyrolysis, c.f. Figure 5-11. The main hydrogen abstraction species are the hydroperoxy radicals, followed by hydroxyl radicals. Both for pyrolysis and oxidation, hydrogen abstraction reactions by nitrogen-containing species, i.e. the amino radical (NH_2) are much less important. In pyrolysis, NH_2 is formed via a sequence of hydrogen addition and β-scission reaction steps, starting from the C_α-centered radical. In oxidation, NH_2 is formed via the reaction between the important intermediate HNCO and a hydrogen atom (R1). Subsequent reaction of NH_2 with HO_2 results in the formation of H_2NO, which is further oxidized to NO and finally to NO_2 (with a small fraction passing through HONO).

$$HNCO + H \rightleftarrows NH_2 + CO \qquad \text{(R1)}$$

HCN is mainly consumed by reaction with OH and O radicals (R2) - (R5), resulting in the formation of NCO, CN and NH. Because an increase in the availability of O_2 increases the formation of these radicals important for HCN conversion, there is a decrease of the peak HCN mole fraction with decreasing equivalence ratio.

$$HCN + O \rightleftarrows NCO + H \qquad \text{(R2)}$$

$$HCN + O \rightleftarrows NH + CO \qquad \text{(R3)}$$

$$HCN + OH \rightleftarrows CN + H_2O \qquad \text{(R4)}$$

$$HCN + OH \rightleftarrows HNCO + H \qquad \text{(R5)}$$

Reaction between the intermediates NH and CN with molecular oxygen O_2 leads to the formation of NO and NCO respectively. Methanimine (CH_2=NH), an important intermediate for HCN formation, is also consumed by reaction with O resulting in formaldehyde and NH (R6). However, due to the weak N-H bond, hydrogen abstraction dominates for methanimine and the increasing O/OH radical concentration does not have any significant influence on the mole fraction.

$$CH_2NH + O \rightleftarrows CH_2O + NH \qquad \text{(R6)}$$

At 900 K, the dominant formation pathway of acetonitrile proceeds via the β-scission of the weak N-H bond of the ethanimine radical $CH_3C^{\cdot}$=NH. Acetonitrile is further converted to HCN via hydrogen addition followed by β-scission of the C-N bond. Another consumption pathway for acetonitrile is the reaction with O, leading to the formation of a methyl radical and NCO (R7).

$$CH_3CN + O \rightleftarrows CH_3 + NCO \qquad \text{(R7)}$$

The reaction with O is only a minor consumption pathway of acetonitrile compared to hydrogen addition and hence the equivalence ratio has only a limited influence on its peak concentration compared to HCN. After hydrogen abstraction, HNCO reacts with a hydrogen atom forming the amino radical as well as CO (R1), which subsequently leads to CO_2. At higher temperatures, NCO leads directly to the formation of NO via reaction with O (R8).

$$NCO + O \rightleftarrows NO + CO \tag{R8}$$

Another decomposition pathway of HCN proceeds via the isomerization reaction resulting in the intermediate HNC, which reacts with OH producing HNCO.

$$HCN + H \rightleftarrows HNC + H \tag{R9}$$

$$HNC + OH \rightleftarrows HNCO + H \tag{R10}$$

Formation pathways of N_2 pass through NO interaction with NH_2 and NCO via reactions (R11) and (R12). For the reaction (R12), there is an important competing product channel (R13) leading to the formation of N_2O. Under stoichiometric and fuel-lean conditions, the dominant formation pathway of N_2 proceeds via this very reactive N_2O species, i.e. (R14).

$$NH_2 + NO \rightleftarrows N_2 + H_2O \tag{R11}$$

$$NCO + NO \rightleftarrows N_2 + CO_2 \tag{R12}$$

$$NCO + NO \rightleftarrows N_2O + CO \tag{R13}$$

$$N_2O + CO \rightleftarrows N_2 + CO_2 \tag{R14}$$

NCO can be considered as a key species for the formation of N_2. Due to the smaller O/OH radical pool, N_2 formation is negligible at fuel-rich conditions and the HCN mole fraction drops only slightly at higher temperatures. At stoichiometric and fuel-lean conditions, N_2 is the main nitrogen-containing product at the highest temperatures. The formation of NO starts at approximately 800 K via the reaction of the nitrogen-centered imine radical ($CH_2{=}N^{\cdot}$) with O producing formaldehyde and NO.

$$CH_2N + O \rightleftarrows NO + CH_2O \tag{R15}$$

At this temperature, NO is immediately converted to NO_2 via the reaction between NO and a hydroperoxy radical producing NO_2 and a hydroxyl radical, causing a maximum of the mole fraction of NO_2 at lower temperatures compared to NO. At 900 K, NO_2. By reaction with a hydrogen atom, NO_2 is converted back into NO. The balance between these two reactions is crucial for determination of the maximum of both the NO and NO_2 mole fractions.

$$NO + HO_2 \rightleftarrows NO_2 + OH \tag{R16}$$

$$NO_2 + H \rightleftarrows NO + OH \qquad \text{(R17)}$$

For all three equivalence ratios, the simulated maxima of the NO and NO_2 mole fractions are at 950 and 900 K, respectively. From 900 K, the formation of NO starts to be favored over NO_2. This is not the case for oxidation at fuel-lean conditions. The higher amount of hydroperoxy radicals in the system leads to higher NO_2 mole fractions. At 900 K, the main NO formation pathway proceeds via H_2NO starting from NCO, while at higher temperatures NCO leads directly to NO formation. Regarding NCO formation, the pathway via HCN (R2) increases in importance with increasing temperature compared to the pathway via acetonitrile (R7).

In Figure 5-12, the rate of production analysis is shown for the oxidation at stoichiometric conditions at a temperature of 700 K. Under these experimental conditions, the conversion of DEA is equal to 47%.

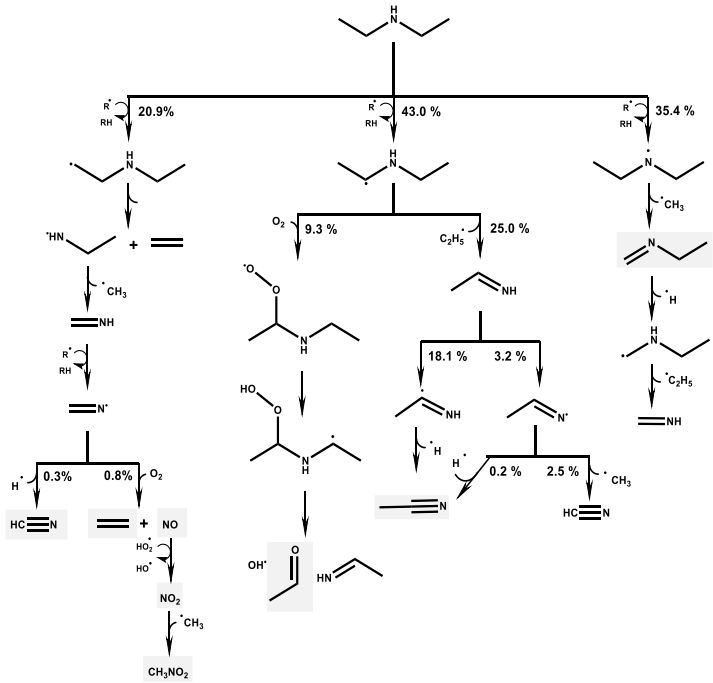

Figure 5-12: Rate of production analysis for the low-temperature oxidation at φ = 1. Percentages report the rate of production relative to the total consumption of DEA at 700 K. Species that are detected experimentally are marked.

The consumption of DEA proceeds completely via hydrogen abstraction. The main abstracting species are the hydroxyl radicals, followed by the hydroperoxy radicals. Hydrogen abstraction from C_α is favored. The formed radical can either undergo β-scission or addition to molecular oxygen. At 700 K, the β-scission is more important compared to the addition to molecular

oxygen. Addition to molecular oxygen leads to the formation of acetaldehyde after isomerization and β-scission, as discussed in Section 5.3.2. With increasing temperature, this β-scission becomes even more favored and the addition of molecular oxygen cannot compete anymore. NO_2 combines with a methyl radical leading to the formation of nitromethane.

Sensitivity analyses are performed to study both the decomposition of DEA during pyrolysis and oxidation (φ = 1.0) at different temperatures as well as the reactions driving the NO/N_2 selectivity. The most sensitive reactions for the decomposition of DEA in both pyrolysis and oxidation are those directly related to DEA decomposition by homolytic scissions and hydrogen abstraction reactions and those that increase the number of radicals and hence the reactivity, e.g. recombination of methyl radicals for pyrolysis and recombination of hydroperoxy radicals for oxidation. Note that the model is able to capture the fluctuations in the mole fractions of DEA and O_2, caused by the onset of different kinetic regimes. More detailed results are given in Appendix C. Figure 5-13 depicts the results of the sensitivity analysis with respect to the mole fractions of NO and N_2 for oxidation at φ = 1 and T = 1000 K, corresponding to complete conversion of DEA.

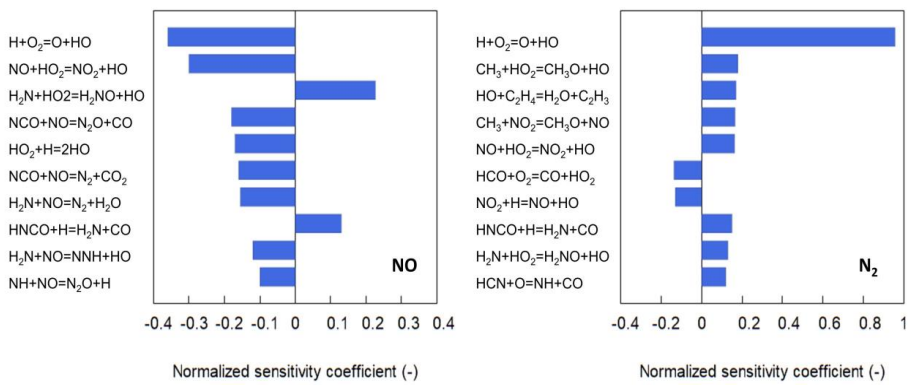

Figure 5-13: Normalized sensitivity coefficients for the mole fraction of NO (left) and N_2 (right) in DEA oxidation. Experimental conditions are φ = 1, p = 107 kPa, $x_{DEA,0}$ = 0.01 and T = 1000 K.

The chain branching reaction which is also the main controlling reaction in hydrocarbon combustion chemistry (R18) is also both for NO and N_2 the most sensitive reaction at these conditions.

$$H + O_2 \rightleftarrows O + OH \qquad \text{(R18)}$$

Apart from the reactions which directly convert NO by interactions with NCO and NH_2, the system is controlled by reactions influencing the O/OH radical pool and reactions important for the NO/NO_2 interconversion. The availability of O/OH radicals is crucial for the conversion of

HCN and acetonitrile to NCO and NH_2, which subsequently leads to N_2 formation. This is reflected in the large value of the sensitivity coefficient of the chain branching reaction (R18) in the case of N_2.

5.3.3.2. Shock tube ignition delay data (EA/DMA)

The influence of the substitution degree of the nitrogen atom and the alkyl chain length on the reactivity of the amine compound is studied making use of shock tube experimental data reported by Li et al. [28, 29]. Ignition delay times are determined by extrapolating the steep pressure increase concurrent with ignition back to the baseline pressure. Figure 5-14 depicts the experimentally measured ignition delay times of EA and DMA along with the simulated values for EA, DMA and DEA at stoichiometric conditions and at a pressure of 137 kPa. The ignition delay times of DMA measured at 148 kPa have been scaled to a pressure of 137 kPa using the derived correlation for ignition delay times. Li et al. report the uncertainty on the experimental ignition delay times to be ± 10%.

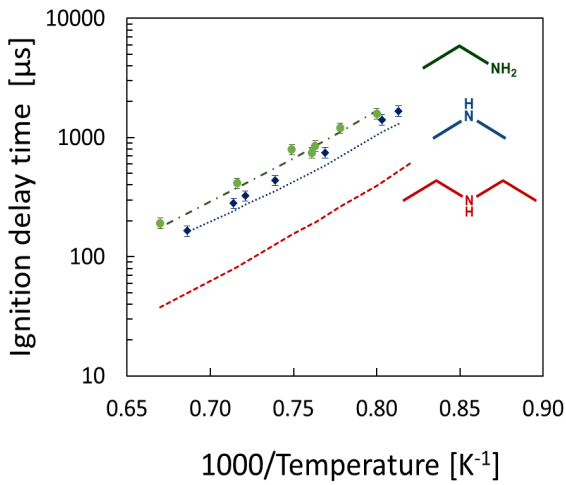

Figure 5-14: Experimental data for the ignition delay times of EA [28] and DMA [29] measured in a shock tube (symbols) and model predictions for the ignition delay times of EA, DMA and DEA in stoichiometric mixtures and at a pressure of 137 kPa.

For all three amine species, the ignition delay times show a strong Arrhenius dependence with temperature that is well captured by the model with an average deviation of 10% and a maximum deviation of 20%. Within the studied range of conditions, i.e. 1200-1500 K and 137 kPa, EA has the longest ignition delay times and DEA the shortest. The ignition delay time of DEA is approximately a factor of three lower than that of EA. This difference in reactivity can

be explained considering the degree of substitution on the nitrogen atom and the chain length of the alkyl substituents.

At the conditions considered in these shock tube experiments, the consumption of DMA and EA is dominated by hydrogen abstraction. The formed fuel radicals react further via C-C, C-N and C-H β-scissions producing mainly methyl radicals and hydrogen atoms. The main abstracting species are hydrogen atoms and hydroxyl radicals, which are formed from the reaction between a hydrogen atom and an oxygen molecule. The contribution of the homolytic scissions of C-C and C-N bonds is much less compared to the hydrogen abstraction reactions, but their importance increases with temperature. Under the studied conditions, these unimolecular reactions contribute very little, i.e. less than 5%, to the decomposition of the amines. From the BDE values, it can be seen that the hydrogen atom bonded to C_α is the preferred abstraction site. As DMA only contains C_α-H bonds, this increases the rate of abstraction compared to EA, which also contains C_β-H bonds. The second most preferred abstraction site is the hydrogen bonded to the nitrogen atom, especially in secondary amines, due to the weaker N-H bonds. With increasing alkyl chain length, more hydrogen abstraction sites become available as well as additional C-C and C-N bonds that can undergo homolytic scission. This explains the increased reactivity, or equivalently lower ignition delay times, of DEA compared to DMA.

5.3.3.3. Laminar premixed flames (EA/DMA)

The third validation set consists of species profiles from laminar premixed stoichiometric flames reported by Lucassen et al. [27]. The experimental conditions correspond to a pressure of 4 kPa, and inlet mole fraction of DEA of 0.16. The temperatures in these flames range from 500 to 2000 K. The products at a distance of 3.5 cm from the burner are assumed to consist of CO, CO_2, H_2, H_2O, N_2, and NO. The uncertainty on their mole fraction profiles is reported to be less than 30%. The estimated uncertainty on the species concentrations of stable intermediates, such as HCN, is reported to be within a factor of two. The experimental and simulated mole fractions as a function of the distance from the burner of the main hydrocarbon and nitrogen-containing oxidation products as well as a limited number of stable intermediate species are shown in Figure 5-15 and Figure 5-16 for flames of DMA and EA, respectively. A more detailed comparison for a larger range of products species can be found in Appendix C.

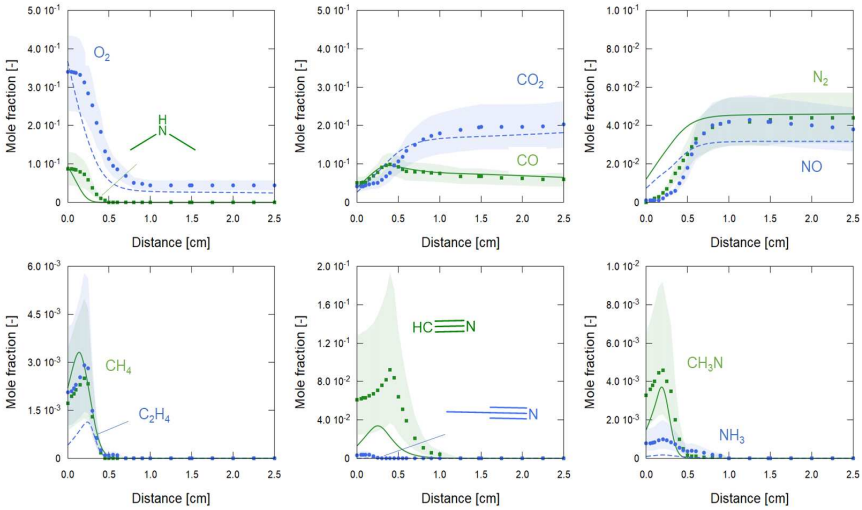

Figure 5-15: Comparison between experimental [6] and simulated mole fractions in stoichiometric premixed flames of DMA (experiment: points, simulation: lines). The shaded area corresponds to the experimental uncertainty. Experimental conditions are a pressure of 4 kPa, and inlet mole fraction of DMA equal to 0.16.

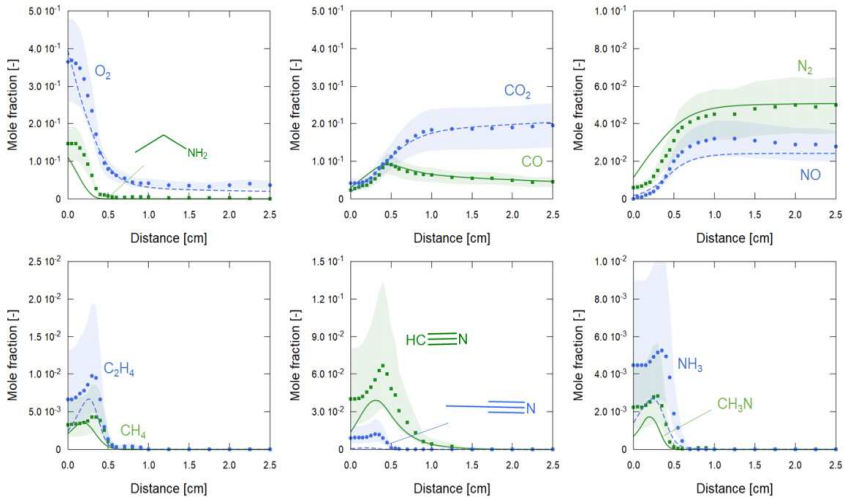

Figure 5-16: Comparison between experimental [6] and simulated mole fractions in stoichiometric premixed flames of EA (experiment: points, simulation: lines). The shaded area corresponds to the experimental uncertainty. Experimental conditions are a pressure of 4 kPa, and inlet mole fraction of EA equal to 0.16.

Both DMA and EA are completely consumed close to the burner, i.e. at a distance of 0.5 cm. Similar to the DEA oxidation, HCN is the main nitrogen-containing intermediate product. The

model underpredicts the maximum HCN yields, but it captures the correct trend with higher HCN yields in the DMA flames compared to the EA flames. Near the end of the flame, the fuel-nitrogen is completely converted to N_2 and NO, but the N_2/NO ratio is significantly smaller compared to the DEA oxidation in the JSR. In the stoichiometric flames, conversion of DMA leads to higher NO levels compared to EA. In Figure 5-17, the rate of production analysis is given at a distance of 0.1 cm from the burner, corresponding to a temperature of 750 K and EA and DMA conversion of 56 % and 85% respectively. A high enough conversion has been selected in order to be able to also study the consumption of the primary products.

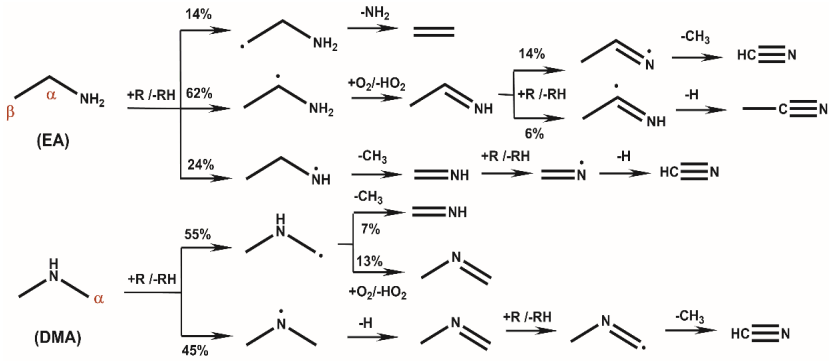

Figure 5-17: Rate of production analysis for the oxidation of EA and DMA. Percentages report the rate of products relative to the total consumption of DEA at 750 K corresponding to a distance of 0.1 cm from the burner and a EA and DMA conversion of 56% and 85% respectively.

In the region close to the flame, the consumption of both DMA and EA is dominated by hydrogen abstraction by fuel-propagating radicals, mainly hydroxyl radicals and hydrogen atoms. The contribution of the homolytic C-C and C-N scissions and the unimolecular elimination reaction of EA to the fuel consumption is negligible (< 1% of the total consumption rate of DMA and EA). Because of the lower BDE, hydrogen abstraction occurs mainly at the C_α. Hydrogen abstraction from the N-H bond in DMA is more important compared to EA as a result of the lower N-H BDE in secondary amines.

At low temperatures, i.e. between 500 and 700 K, the fuel radicals mainly react with molecular oxygen to form HO_2 and an imine. Above 700 K, the fuel radicals formed after hydrogen abstraction decompose primarily via β-scission to form imine species. The two EA radicals, i.e. $CH_3CH^{\cdot}NH_2$ and $CH_3CH_2NH^{\cdot}$, undergo N-H and C-N β-scission leading to the formation of $CH_3CH{=}NH$ and methanimine ($CH_2{=}NH$). The methyl radicals formed after β-scission from the fuel radicals, mainly lead to the formation of CH_2O, via reaction with oxygen atoms. Hydrogen abstraction form the carbon atom in β position followed by β-scission of the C-N bond leads to the formation of the amino radical. In the case of a secondary amine such as

DMA, there is no direct formation pathway for NH_2. The nitrogen-containing radicals formed after hydrogen abstraction from DMA, i.e. $^{\cdot}CH_2NH_2CH_3$ and $CH_3N^{\cdot}HCH_3$, undergo C-N and C-H β-scission leading to the formation of $CH_2{=}NH$ and $CH_2{=}NCH_3$. These imines are important intermediate products, which are further converted to HCN and CH_3CN. The selectivity towards these two species is influenced by the degree substitution of the nitrogen atom. EA has a more direct pathway towards CH_3CN and hence less HCN is formed compared to DMA.

N_2 and NO are mainly produced by reactions which are part of the base mechanism of Glarborg et al. [20]. For the conversion of the fuel nitrogen in the studied amines, HCN and NH_3 (or equivalently the amino radical NH_2) are important intermediate species and their concentration influences the dominant formation pathways for NO/N_2. The main routes for the formation of NO_x and N_2 from the simple amines EA and DMA are depicted in Figure 5-18.

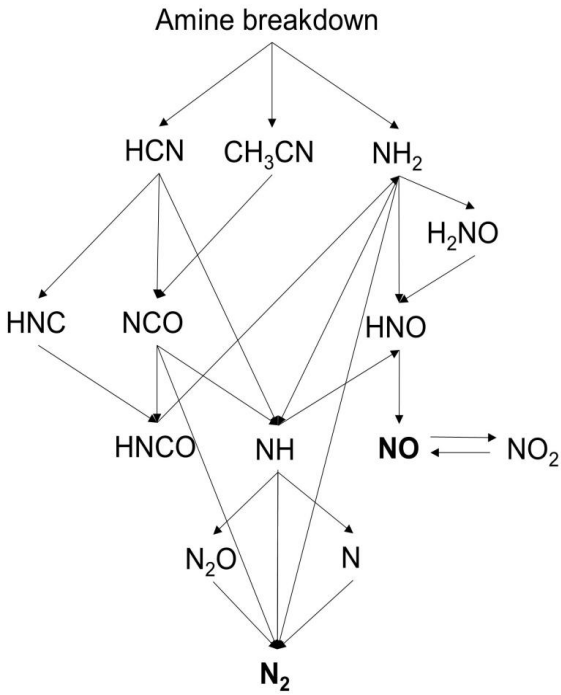

Figure 5-18: General reaction path diagram for formation of NO and N_2 from oxidation of the amines EA and DMA.

At lower temperatures, the NO formation is governed by the formation of H_2NO via the reaction between NH_2 and HO_2 radicals. In the EA flame, the amino radical is directly formed after β-scission of the fuel radical $^{\cdot}CH_2CH_2NH_2$. In the DMA flame, NH_2 is formed via the reaction

pathway HCN→HNC→HNCO→H_2N. Formation of NO via interaction of the methanimine radical with the O/OH radical pool is negligible under these conditions. Reaction between NO and NH_2 leads to N_2 formation. As HO_2 is readily available close to the flame front, from interaction between the fuel radicals and O_2, NO_2 is produced as soon as NO is formed early in the flame. At higher temperatures (> 1000 K), the increased availability of O/OH radicals in the amine flames opens up new pathways. The reaction between H_2N and O allows to bypass the H_2NO intermediate.

$$NH_2 + O \rightleftarrows HNO + H \qquad \text{(R19)}$$

Another pathway gaining importance at higher temperatures proceeds via NH. This intermediate radical is formed after hydrogen abstraction from NH_2, directly via reaction between O and HCN (R3) or via the reaction pathway HCN→NCO→NH. Subsequent reaction with O results in NO formation (R20), while reaction with NO further results in N_2, either directly (R21) or via N_2O as intermediate. The fraction of the fuel-nitrogen that decomposes via HCN influences the ratio NO/N_2. A higher HCN mole fraction in the DMA flame corresponds to a higher NO/N_2 ratio compared to the EA flame. Note that also for methanimine, which is the main intermediate imine species leading to the formation of HCN, a higher peak concentration is obtained in the DMA flame.

$$NH + O \rightleftarrows NO + H \qquad \text{(R20)}$$

$$NH + NO \rightleftarrows N_2 + OH \qquad \text{(R21)}$$

Due to the fast reaction between NO and a hydroperoxy radical, the ratio between NO and NO_2 ratio is influenced by the HO_2 radical concentration. When NO is formed at a distance > 1 cm, there is no further oxidation towards NO_2, which is in accordance with the thermochemistry at these temperatures that favors NO formation.

Figure 5-19 depicts the results of the sensitivity analysis with respect to the mole fractions of NO and N_2, at a burner distance of 0.5 cm, corresponding to complete conversion of both EA and DMA. For both amines the reactions with the largest sensitivity coefficients are part of the Glarborg et al. submechanism. The main reactions with negative sensitivity coefficients for NO selectivity are the reactions with NH and N, and also with NCO in the case of DMA. For N_2 the absolute values of the sensitivity coefficients are significantly lower compared to NO.

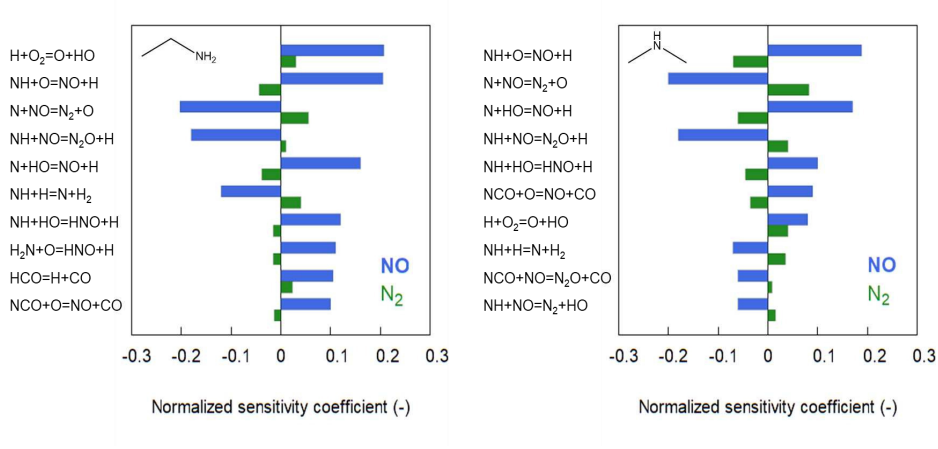

Figure 5-19: Normalized sensitivity coefficients for the mole fractions of NO and N_2 for the laminar premixed flames of EA (left) and DMA (right) for a burner distance of 0.5 cm, corresponding to complete conversion of both EA and DMA.

5.4. Conclusions

The pyrolysis and oxidation chemistry of aliphatic amines has been studied via a combination of theoretical calculations, kinetic modelling and experimental validation. The new group additive schemes for nitrogen-containing compounds combined with additional theoretical calculations at the CBS-QB3 level of theory for important species and reactions have been used to determine accurate thermodynamic species parameters and high-pressure limit reaction rate coefficients. The new model describing the combustion of ethylamine, dimethylamine and diethylamine, which contains 258 species and 2274 reactions, has been validated with shock tube, JSR and low-pressure flame experimental datasets.

The model succeeds in capturing the main trends in ignition delay times and species concentrations, without any fitting of the model thermodynamic and kinetic parameters over the wide range of conditions with temperatures ranging from 500 to 2000 K and pressures from 4 to 170 kPa. The ignition delay data are predicted with an average deviation of 10%. The difference between experimental and simulated species concentrations from laminar premixed flames is for the major species on average 50%. For the JSR, an even better agreement is obtained, with an average deviation of 10% for the major species. Hydrogen abstractions from the C_α and N positions followed by β-scission of the fuel radicals are the major decomposition pathways of the amine species. HCN is the main intermediate nitrogen-containing product, while at high temperatures the amines are completely converted to N_2 and NO. The fraction of the fuel-nitrogen that decomposes via HCN influences the NO/N_2 at high temperatures. Higher concentrations of HCN lead to higher ratios of NO/N_2.

5.5. References

[1] H.E. Toraman, K. Franz, F. Ronsse, K.M. Van Geem, G.B. Marin, Quantitative analysis of nitrogen containing compounds in microalgae based bio-oils using comprehensive two-dimensional gas-chromatography coupled to nitrogen chemiluminescence detector and time of flight mass spectrometer, Journal of Chromatography A 1460 (2016) 135-146.

[2] A. Williams, J.M. Jones, L. Ma, M. Pourkashanian, Pollutants from the combustion of solid biomass fuels, Progress in Energy and Combustion Science 38 (2012) 113-137.

[3] J.A. Miller, C.T. Bowman, Mechanism and modeling of nitrogen chemistry in combustion, Progress in Energy and Combustion Science 15 (1989) 287-338.

[4] A.M. Dean, J.W. Bozzelli, Combustion Chemistry of Nitrogen, in: W.C. Gardiner (Ed.), Gas-Phase Combustion Chemistry, Springer New York2000, pp. 125-341.

[5] G. Chiavari, G.C. Galletti, Pyrolysis—gas chromatography/mass spectrometry of amino acids, Journal of Analytical and Applied Pyrolysis 24 (1992) 123-137.

[6] R.K. Sharma, W.G. Chan, J. Wang, B.E. Waymack, J.B. Wooten, J.I. Seeman, M.R. Hajaligol, On the role of peptides in the pyrolysis of amino acids, Journal of Analytical and Applied Pyrolysis 72 (2004) 153-163.

[7] Z. Tian, Y. Li, T. Zhang, A. Zhu, F. Qi, Identification of Combustion Intermediates in Low-Pressure Premixed Pyridine/Oxygen/Argon Flames, The Journal of Physical Chemistry A 112 (2008) 13549-13555.

[8] N.R. Hore, D.K. Russell, Radical pathways in the thermal decomposition of pyridine and diazines: a laser pyrolysis and semi-empirical study, Journal of the Chemical Society, Perkin Transactions 2, (1998) 269-276.

[9] J.C. Mackie, M.B. Colket, P.F. Nelson, Shock tube pyrolysis of pyridine, The Journal of Physical Chemistry 94 (1990) 4099-4106.

[10] E. Ikeda, P. Nicholls, J.C. Mackie, A kinetic study of the oxidation of pyridine, Proceedings of the Combustion Institute 28 (2000) 1709-1716.

[11] T.J. Houser, M. Hull, R.M. Alway, T. Biftu, Kinetics of formation of HCN during pyridine pyrolysis, International Journal of Chemical Kinetics 12 (1980) 569-574.

[12] L. Zhai, X. Zhou, R. Liu, A Theoretical Study of Pyrolysis Mechanisms of Pyrrole, The Journal of Physical Chemistry A 103 (1999) 3917-3922.

[13] Z. Tian, Y. Li, T. Zhang, A. Zhu, Z. Cui, F. Qi, An experimental study of low-pressure premixed pyrrole/oxygen/argon flames with tunable synchrotron photoionization, Combustion and Flame 151 (2007) 347-365.

[14] J.C. Mackie, M.B. Colket, P.F. Nelson, M. Esler, Shock tube pyrolysis of pyrrole and kinetic modeling, International Journal of Chemical Kinetics 23 (1991) 733-760.

[15] X. Hong, L. Zhang, T. Zhang, F. Qi, An Experimental and Theoretical Study of Pyrrole Pyrolysis with Tunable Synchrotron VUV Photoionization and Molecular-Beam Mass Spectrometry, The Journal of Physical Chemistry A 113 (2009) 5397-5405.

[16] G.B. Bacskay, M. Martoprawiro, J.C. Mackie, The thermal decomposition of pyrrole: an ab initio quantum chemical study of the potential energy surface associated with the hydrogen cyanide plus propyne channel, Chemical Physics Letters 300 (1999) 321-330.

[17] M. Zheng, X. Li, L. Guo, Investigation of N behavior during coal pyrolysis and oxidation using ReaxFF molecular dynamics, Fuel 233 (2018) 867-876.

[18] L. Zhang, D. Su, M. Zhong, The effect of functional forms of nitrogen on fuel-NOx emissions, Environmental Monitoring and Assessment 187 (2014) 4195.

[19] X. Liu, Z. Luo, C. Yu, B. Jin, H. Tu, Release Mechanism of Fuel-N into NOx and N2O Precursors during Pyrolysis of Rice Straw, Energies 11 (2018) 520.

[20] P. Glarborg, J.A. Miller, B. Ruscic, S.J. Klippenstein, Modeling nitrogen chemistry in combustion, Progress in Energy and Combustion Science 67 (2018) 31-68.

[21] R.P. Lindstedt, F.C. Lockwood, M.A. Selim, Detailed Kinetic Modelling of Chemistry and Temperature Effects on Ammonia Oxidation, Combustion Science and Technology 99 (1994) 253-276.

[22] O. Mathieu, E.L. Petersen, Experimental and modeling study on the high-temperature oxidation of Ammonia and related NOx chemistry, Combustion and Flame 162 (2015) 554-570.

[23] C. Duynslaegher, F. Contino, J. Vandooren, H. Jeanmart, Modeling of ammonia combustion at low pressure, Combustion and Flame 159 (2012) 2799-2805.

[24] D.F. Davidson, K. Kohse-Höinghaus, A.Y. Chang, R.K. Hanson, A pyrolysis mechanism for ammonia, International Journal of Chemical Kinetics 22 (1990) 513-535.

[25] M.V. Kantak, K.S. De Manrique, R.H. Aglave, R.P. Hesketh, Methylamine oxidation in a flow reactor: Mechanism and modeling, Combustion and Flame 108 (1997) 235-265.

[26] M. Votsmeier, S. Song, D.F. Davidson, R.K. Hanson, Shock tube study of monomethylamine thermal decomposition and NH2 high temperature absorption coefficient, International Journal of Chemical Kinetics 31 (1999) 323-330.

[27] A. Lucassen, K. Zhang, J. Warkentin, K. Moshammer, P. Glarborg, P. Marshall, K. Kohse-Höinghaus, Fuel-nitrogen conversion in the combustion of small amines using dimethylamine and ethylamine as biomass-related model fuels, Combustion and Flame 159 (2012) 2254-2279.

[28] S. Li, D.F. Davidson, R.K. Hanson, Shock tube study of ethylamine pyrolysis and oxidation, Combustion and Flame 161 (2014) 2512-2518.

[29] S. Li, D.F. Davidson, R.K. Hanson, Shock tube study of dimethylamine oxidation, International Journal of Chemical Kinetics 47 (2015) 19-26.

[30] S. Li, D.F. Davidson, R.K. Hanson, N.J. Labbe, P.R. Westmoreland, P. Oßwald, K. Kohse-Höinghaus, Shock tube measurements and model development for morpholine pyrolysis and oxidation at high pressures, Combustion and Flame 160 (2013) 1559-1571.

[31] M. Altarawneh, M.H. Almatarneh, A. Marashdeh, B.Z. Dlugogorski, Decomposition of ethylamine through bimolecular reactions, Combustion and Flame 163 (2016) 532-539.

[32] M.H. Almatarneh, L. Barhoumi, B. Al-Tayyem, A.A.-A.A. Abu-Saleh, M.M. Al-A'qarbeh, F. Abuorabi, E. AlShamaileh, M. Altarawneh, A. Marashdeh, Computational study for the second-stage cracking of the pyrolysis of ethylamine: Decomposition of methanimine, ethenamine, and ethanimine, Computational and Theoretical Chemistry 1075 (2016) 9-17.

[33] M.H. Almatarneh, M. Altarawneh, R.A. Poirier, I.A. Saraireh, High level ab initio, DFT, and RRKM calculations for the unimolecular decomposition reaction of ethylamine, Journal of Computational Science 5 (2014) 568-575.

[34] S. Gong, Q. Luo, G.M. Wei, Theoretical Study of Mechanism and Dynamics on Reaction of (CH3)2NH with CH3, The Journal of Physical Chemistry A 119 (2015) 4746-4754.

[35] A. Galano, J.R. Alvarez-Idaboy, Branching Ratios of Aliphatic Amines + OH Gas-Phase Reactions: A Variational Transition-State Theory Study, Journal of Chemical Theory and Computation 4 (2008) 322-327.

[36] L. Onel, M. Blitz, M. Dryden, L. Thonger, P. Seakins, Branching Ratios in Reactions of OH Radicals with Methylamine, Dimethylamine, and Ethylamine, Environmental Science & Technology 48 (2014) 9935-9942.

[37] Y. Shang, H. Ning, J. Shi, H. Wang, S.-N. Luo, Chemical kinetics of H-abstractions from dimethyl amine by H, CH3, OH, and HO2 radicals with multi-structural torsional anharmonicity, Physical Chemistry Chemical Physics 21 (2019) 12685-12696.

[38] M.P. Rissanen, A.J. Eskola, T.L. Nguyen, J.R. Barker, J. Liu, J. Liu, E. Halme, R.S. Timonen, CH2NH2 + O2 and CH3CHNH2 + O2 Reaction Kinetics: Photoionization Mass Spectrometry Experiments and Master Equation Calculations, The Journal of Physical Chemistry A 118 (2014) 2176-2186.

[39] M.A. Alam, Z. Ren, G. da Silva, Nitramine and nitrosamine formation is a minor pathway in the atmospheric oxidation of methylamine: A theoretical kinetic study of the CH3NH + O2 reaction, International Journal of Chemical Kinetics 51 (2019) 723-728.

[40] C.A.R. Pappijn, N. Vin, F.H. Vermeire, R. Van de Vijver, O. Herbinet, F. Battin-Leclerc, M.-F. Reyniers, G.B. Marin, K.M. Van Geem, Experimental and kinetic modeling study of the pyrolysis and oxidation of diethylamine, Fuel 275 (2020) 117744.

[41] N.M. Vandewiele, K.M. Van Geem, M.F. Reyniers, G.B. Marin, Genesys: Kinetic model construction using chemo-informatics, Chemical Engineering Journal 207 (2012) 526-538.

[42] N. Vin, Étude cinétique de la pyrolyse en phase gazeuse de molécules organiques contenant des hétéroatomes représentatives de composés toxiques présents dans les sols pollués, 2019.

[43] O. Herbinet, F. Battin-Leclerc, Progress in Understanding Low-Temperature Organic Compound Oxidation Using a Jet-Stirred Reactor, International Journal of Chemical Kinetics 46 (2014) 619-639.

[44] N. Vin, F. Battin-Leclerc, O. Herbinet, A study of thermal decomposition of bromoethane, Journal of Analytical and Applied Pyrolysis 136 (2018) 199-207.

[45] S.W. Benson, F.R. Cruickshank, D.M. Golden, G.R. Haugen, H.E. O'Neal, A.S. Rodgers, R. Shaw, R. Walsh, Additivity rules for the estimation of thermochemical properties, Chemical Reviews 69 (1969) 279-324.

[46] M.K. Sabbe, M. Saeys, M.F. Reyniers, G.B. Marin, V. Van Speybroeck, M. Waroquier, Group additive values for the gas phase standard enthalpy of formation of hydrocarbons and hydrocarbon radicals, Journal of Physical Chemistry A 109 (2005) 7466-7480.

[47] M.K. Sabbe, F. De Vleeschouwer, M.-F. Reyniers, M. Waroquier, G.B. Marin, First Principles Based Group Additive Values for the Gas Phase Standard Entropy and Heat Capacity of Hydrocarbons and Hydrocarbon Radicals, The Journal of Physical Chemistry A 112 (2008) 12235-12251.

[48] P.D. Paraskevas, M.K. Sabbe, M.F. Reyniers, N. Papayannakos, G.B. Marin, Group additive values for the gas-phase standard enthalpy of formation, entropy and heat capacity of oxygenates, Chemistry 19 (2013) 16431-16452.

[49] M. Saeys, M.F. Reyniers, G.B. Marin, V. Van Speybroeck, M. Waroquier, Ab initio group contribution method for activation energies for radical additions, AIChE Journal 50 (2004) 426-444.

[50] M.K. Sabbe, A.G. Vandeputte, M.-F. Reyniers, M. Waroquier, G.B. Marin, Modeling the influence of resonance stabilization on the kinetics of hydrogen abstractions, Physical Chemistry Chemical Physics 12 (2010) 1278-1298.

[51] M.K. Sabbe, M.F. Reyniers, V. Van Speybroeck, M. Waroquier, G.B. Marin, Carbon-Centered Radical Addition and β-Scission Reactions: Modeling of Activation Energies and Pre-exponential Factors, Chemphyschem 9 (2008) 124-140.

[52] M.K. Sabbe, M.-F. Reyniers, M. Waroquier, G.B. Marin, Hydrogen Radical Additions to Unsaturated Hydrocarbons and the Reverse β-Scission Reactions: Modeling of Activation Energies and Pre-Exponential Factors, Chemphyschem 11 (2010) 195-210.

[53] P.D. Paraskevas, M.K. Sabbe, M.-F. Reyniers, G.B. Marin, N.G. Papayannakos, Group additive kinetic modeling for carbon-centered radical addition to oxygenates and β-scission of oxygenates, AIChE Journal 62 (2016) 802-814.

[54] L. Cai, H. Pitsch, S.Y. Mohamed, V. Raman, J. Bugler, H. Curran, S.M. Sarathy, Optimized reaction mechanism rate rules for ignition of normal alkanes, Combustion and Flame 173 (2016) 468-482.

[55] S. Li, E. Dames, D.F. Davidson, R.K. Hanson, High-Temperature Measurements of the Reactions of OH with Ethylamine and Dimethylamine, The Journal of Physical Chemistry A 118 (2014) 70-77.

[56] R.J. Kee, F.M. Rupley, J.A. Miller, M.E. Coltrin, J.F. Grcar, E. Meeks, H.K. Moffat, A.E. Lutz, G. Dixon-Lewis, M.D. Smooke, J. Warnatz, G.H. Evans, R.S. Larson, R.E. Mitchell, L.R. Petzold, W.C. Reynolds, M. Caracotsios, W.E. Stewart, P. Glarborg, C. Wang, O. Adigun, Chemkin-Pro 15112, Reaction Design: San Diego, CA, USA, (2011).

[57] P.J. Lindstrom, W.G. Mallard, NIST Chemistry WebBook, NIST Standard Reference Database Number 69, National Institute of Standards and Technology, Gaithersburg MD.

[58] T.J. Burkey, A.L. Castelhano, D. Griller, F.P. Lossing, Heats of formation and ionization potentials of some .alpha.-aminoalkyl radicals, Journal of the American Chemical Society 105 (1983) 4701-4703.

[59] M.R. Nimlos, S.J. Blanksby, G.B. Ellison, R.J. Evans, Enhancement of 1,2-dehydration of alcohols by alkali cations and protons: a model for dehydration of carbohydrates, Journal of Analytical and Applied Pyrolysis 66 (2003) 3-27.

[60] D.R. Glowacki, C.-H. Liang, C. Morley, M.J. Pilling, S.H. Robertson, MESMER: An Open-Source Master Equation Solver for Multi-Energy Well Reactions, The Journal of Physical Chemistry A 116 (2012) 9545-9560.

[61] H.-H. Carstensen, A. Dean, The Kinetics of Pressure-Dependent Reactions, 2007, pp. 105–187.

[62] F. Battin-Leclerc, Detailed chemical kinetic models for the low-temperature combustion of hydrocarbons with application to gasoline and diesel fuel surrogates, Progress in Energy and Combustion Science 34 (2008) 440-498.

[63] C.A. Taatjes, Uncovering the Fundamental Chemistry of Alkyl + O2 Reactions via Measurements of Product Formation, The Journal of Physical Chemistry A 110 (2006) 4299-4312.

[64] H.J. Curran, P. Gaffuri, W.J. Pitz, C.K. Westbrook, A Comprehensive Modeling Study of n-Heptane Oxidation, Combustion and Flame 114 (1998) 149-177.

[65] C.J. Nielsen, H. Herrmann, C. Weller, Atmospheric chemistry and environmental impact of the use of amines in carbon capture and storage (CCS), Chemical Society Reviews 41 (2012) 6684-6704.

[66] C. Lindley, J. Calvert, J. Shaw, Rate studies of the reactions of the (CH3)2N radical with O2, NO, and NO2, Chemical Physics Letters 67 (1979) 57-62.

[67] G.B. Marin, G.S. Yablonsky, D. Constales, Kinetics of Chemical Reactions: Decoding Complexity, Wiley2019.

6

Steam cracking of sulfur-containing compounds

Abstract

Sulfur-containing compounds play a key role in many industrial processes. Particularly for the steam cracking process they have been linked with increased olefin selectivity, decreased CO formation and coke inhibition. In this work, the pyrolysis chemistry of a number of sulfur-containing additives and feedstock impurities, including dimethyl sulfide, dimethyl disulfide, dimethyl sulfoxide, carbonyl sulfide and carbon disulfide, has been studied by combining quantum chemical calculations, chemical kinetic modeling and experimental validation. A new kinetic model has been developed with the automatic kinetic model generator Genesys to investigate both the pure pyrolysis as well as the pyrolysis in a hydrocarbon matrix. The thermodynamic and kinetic parameters important to accurately describe the main species and reactions of the initial decomposition pathways are obtained directly from *ab initio* calculations. Experimental data obtained on two different experimental units, i.e. a bench-scale and pilot plant reactor unit, are used for experimental validation of the new model over a wide range of conditions. The thermal decomposition of the (di-)sulfide compounds is initiated by homolytic scission of the C-S and S-S bonds. Due to the low bond dissociation energy of these sulfur bonds compared to the alkane bonds, these are also the dominant initiating reactions when a hydrocarbon matrix is present. Decomposition of the less reactive COS and CS_2 compounds proceeds via radical addition by a hydrogen atom or methyl radical. Similar formation pathways consisting of a sequence of hydrogen abstraction, substitution and β-scission reactions can be identified for the main sulfur-containing products H_2S, CS_2 and thiophene. The presence of a large hydrocarbon radical pool, corresponding to steam cracking conditions, decreases the occurrence of reactions between the sulfur-containing compounds, corresponding to an almost complete conversion to H_2S on a sulfur basis and a negligible formation of sulfur-containing products with two sulfur atoms (CS_2). Thiophene formation via interaction between a thiyl radical and an unsaturated species with at least four heavy atoms gains importance with increasing chain length of the hydrocarbon.

6.1. Introduction

For the steam cracking process, it is well known that sulfur-containing additives decrease CO production by passivating active nickel sites and thus forming nickel sulfides [1]. The influence of these additives on coke formation is much less understood and many contradictory findings have been reported in literature [2-5]. While the effect of sulfur-containing additives on CO and coke production has been well studied over the past few years, much less focus has been paid to the decomposition mechanism of these compounds. For the majority of these sulfur-containing additives, the main product is H_2S, but minor compounds can be also be formed, including carbon disulfide (CS_2), thiophene and SO_2. Both the molecular structure of the sulfur-containing additive, i.e. the functional group containing the sulfur atom, as well as the hydrocarbon matrix, influence the reactivity and product distribution.

In this Chapter the thermal decomposition of five different sulfur-containing compounds, that are typically used as additives or present as feedstock impurities, is discussed both experimentally and theoretically under typical pyrolysis and steam cracking conditions. The aim is to gain insight into the main decomposition pathways and investigate the formation of the most important sulfur-containing product species, including H_2S, CS_2 and SO_2. In a first part, the kinetic model development and experimental datasets used for validation are discussed. In the second part, the focus is on the performance of the newly developed microkinetic model for three different experimental datasets: (1) pyrolysis of dimethyl disulfide (CH_3SSCH_3, DMDS), (2) pyrolysis of carbonyl sulfide (O=C=S, COS) and (3) steam cracking of CS_2, DMDS, dimethyl sulfide (CH_3SCH_3, DMS) and dimethyl sulfoxide ($CH_3S{=}OCH_3$, DMSO). A rate of production analysis is performed to determine the most important decomposition pathways and to investigate the main differences between the sulfur-containing compounds.

6.2. Methodologies

6.2.1. Kinetic model development

A kinetic model is constructed for the thermal decomposition of DMDS, DMS, COS, CS_2 and DMSO in a hydrocarbon matrix. This model consists of two parts, i.e. (1) a kinetic model to describe the decomposition chemistry of the sulfides generated using the automatic kinetic model generation tool Genesys [6] and (2) a kinetic model to account for the reactions between the small hydrocarbons (C_1-C_2) and sulfur-containing species, including the formation and

destruction of SO_x, developed by Alzueta et al. [7]. More details regarding the automatic kinetic model generation software Genesys can be found in Chapter 2.

Genesys is connected to an extensive species and reaction database with data obtained from *ab initio* calculations at the CBS-QB3 level of theory. The thermodynamic properties for all species are obtained either from this database, if available, or from Benson's group additivity method [8] for hydrocarbons [9, 10], oxygenates [11] and sulfur-containing compounds [12]. For the β-scission reaction of ethyl and vinyl radicals to ethene and acetylene respectively, the pressure dependent rate coefficients proposed by Miller et al. [13] are used. In case no *ab initio* kinetic data is available, the group additivity method developed by Saeys et al. [14] and extended by Sabbe et al. [15-17] for hydrocarbons and by Paraskevas et al. [18] for oxygenates is used. New *ab initio* calculations at the CBS-QB3 level of theory have been performed for the main species and reactions important to accurately describe the thermal decomposition of the sulfur-containing compounds of interest. The accuracy of the CBS-QB3 method for approximation of the thermodynamic and kinetic parameters of organosulfur compounds has been validated by Vandeputte et al. [19]. Details of the methodology used for the *ab initio* calculations can be found in Chapter 2. In Table 6-1, an overview of all the reaction families used for kinetic model generation with Genesys for the sulfur-containing compounds is given, including an example of each reaction family and the source of the kinetic parameters. To address the lack of certain group additive values for sulfur-containing compounds, existing group additivity databases have been extended with new values obtained from *ab initio* calculations for specific reactions.

Homolytic bond scission reactions are implemented as the reverse reactions of the barrierless recombination reactions. The single-event pre-exponential factor is fixed to 2.50×10^6 m^3 mol^{-1} s^{-1}. Taking into account the number of single events, this results in a value of 10^7 m^3 mol^{-1} s^{-1} for most radical recombinations. For the homolytic scissions of DMDS, the kinetic parameters as obtained by Vandeputte et al. [20] with Variational transition state theory are used. The calculated activation energies are very close to the corresponding reaction enthalpy values, with a pre-exponential factor varying between 10^{16} – 10^{17} s^{-1}.

For intermolecular hydrogen abstractions involving sulfur-containing radicals, the group additive values reported by Vandeputte et al. [21] are used. New *ab initio* calculations have been performed for intramolecular hydrogen abstractions at the CBS-QB3 level of theory, because of the lack of a group additive scheme for these reactions. For the most important intramolecular abstractions of the studied sulfur-containing compounds, i.e. reactions involving

the parent radicals, accurate values are available. For all other intramolecular hydrogen abstractions involving sulfur-containing radicals, the kinetic parameters are based on a limited number of these *ab initio* calculated reference reactions.

For β-scission and the reverse radical addition reactions of sulfur-containing compounds, no group additive databases are available in literature. For intermolecular radical addition reactions, unpublished GAVs based on new *ab initio* data are used. Similar to the intramolecular hydrogen abstraction reactions, the kinetic parameters of the intramolecular radical addition reactions are based on a limited set of *ab initio* calculated reference reactions.

An important reaction family for sulfur-containing compounds are the substitution reactions. A bimolecular homolytic substitution corresponds to a concerted process in which a radical $R_1^{\cdot}$ binds to a molecule R_2X with the simultaneous scission of the R_2–X bond and the expulsion of the leaving radical $X^{\cdot}$. The kinetic parameters of intermolecular homolytic substition reactions of hydrogen atoms at thiols and sulfides are approximated with the group additive values of Vandeputte et al. [21].

This kinetic model describing the sulfur-containing chemistry is merged with the mechanism of Alzueta et al. [7], which contains 117 species and 775 reactions. It describes the chemistry of small hydrocarbons (C_1-C_2) and sulfur-containing species, including the formation and destruction of SO_x. For species or reactions appearing in both the automatically generated Genesys mechanism and the Alzueta et al. [7] mechanism, it is opted to retain the kinetic parameters from the Genesys mechanism.

Table 6-1: List of reaction families used for kinetic model generation for the thermal decomposition of the sulfur-containing compounds.

No.	Reaction family	Example reaction	Kinetic source
1	Radical recombination/ homolytic bond	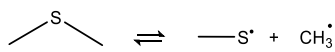	Vandeputte et al. [20] or single event fixed to 2.50 10^6 m^3 mol^{-1} s^{-1}
2	Intermolecular hydrogen abstraction by $H^{\cdot}$, $C^{\cdot}$ and $S^{\cdot}$	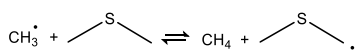	GAV scheme [22, 23]

3	Intramolecular hydrogen abstraction by $C^{\cdot}$ and $S^{\cdot}$	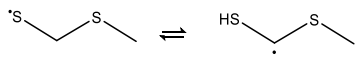	Analogy with new CBS-QB3 data
4	Intermolecular addition/ β-scission	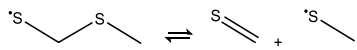	Unpublished GAVs based on new CBS-QB3 data
5	Intramolecular addition to C_5 rings/ β-scission	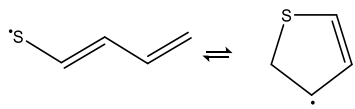	Analogy with new CBS-QB3 data
6	Intermolecular homolytic substitution	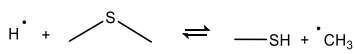	GAV scheme [21]
7	Intramolecular homolytic substitution	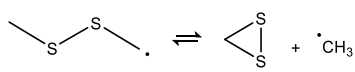	Analogy with new CBS-QB3 data

The kinetic model generation step is constrained using the rule-based termination criterion. Rules are applied to both product species and reaction families in order to limit the generation of redundant species and reactions. As an example, product species obtained by executing reaction families that can lead to larger chains of carbon or sulfur atoms are constrained to a maximum of five carbon atoms and two sulfur atoms. Moreover, the assumption is made that only species with three or less heavy atoms are important abstraction radicals or can participate in bimolecular addition and substitution reactions, as larger species mainly decompose via unimolecular reaction pathways. The complete kinetic model is available on S:\vakgroep\ea12archief\SoftLib\c\cpappijn\1\.

6.2.2. Experimental data

An overview of the experiments used for model validation is given in Table 6-2. These experimental datasets are the result of collaborations with other PhD students and have been obtained with two different experimental units, i.e. the bench-scale and pilot plant unit, both located at the Laboratory for Chemical Technology (LCT) at Ghent University. Detailed information about the employed experimental units can be found elsewhere for the bench-scale

unit [24-26] and the steam cracking pilot plant unit [27]. The main aspects with respect to these three experimental datasets are discussed below.

The first dataset corresponds to DMDS pyrolysis in nitrogen as well as in the presence of a C_2H_6 hydrocarbon matrix with steam used as diluent. Experiments are performed in an annular reactor of approximately 1 m long, with an inner tube with a 10 mm diameter and an annulus with an inner diameter of 15 mm and outer diameter of 21 mm. For simulations purposes, an equivalent diameter of 15 mm is considered. Experimental conditions correspond to a temperature range of 673 to 1073 K with 100 K temperature increments, a fixed pressure of 102 kPa, a residence time of 0.6-1.1 s and an inlet concentration of 1000 ppmwS/H_2O. The flow rate of steam is kept fixed at 80 g h^{-1}, while the C_2H_6 and nitrogen gas flow rate is equal to 200 g h^{-1}. Six different sulfur-containing compounds are detected, i.e. H_2S, methane thiol (CH_3SH), CS_2, DMS and DMDS, corresponding to a sulfur balance ± 5%. These experimental results as well as a preliminary model for the decomposition of DMDS has been reported in the doctoral thesis of Olahova et al. [28]. Note that the model presented in this work contains new *ab initio* calculated rate coefficients for the initiating reactions of DMDS and for the formation pathways of the main sulfur-containing products. In addition, new reaction pathways have been included in this model, for example for the formation of minor sulfur-containing products such as thiophene.

The second experimental dataset focuses on the pyrolysis of COS in nitrogen as well in the presence of hydrocarbons (C_2H_6). Experiments are performed in an annular reactor over a temperature range of 873 to 1173 K, at a fixed pressure of 150 kPa, a residence time of approximately 0.5 s and an inlet concentration of 417 ppmwS/total. The flow rate of nitrogen and C_2H_6 is equal to respectively 120 and 180 g h^{-1}. Four different sulfur-containing compounds are detected, i.e. H_2S, COS, CS_2 and thiophene, corresponding to a sulfur balance ± 5%. This dataset is a result of collaboration with other PhD students and has not yet been published.

The third set of experimental data corresponds steam cracking of C_7H_{16}, as a surrogate feedstock for light naphtha, in the presence of the sulfur-containing additives CS_2, DMDS, DMS and DMSO. These experimental results have already been reported in literature, but in contrast to the DMDS experiments, these experiments have not yet been used for validation of a kinetic model [29]. The reactor coil is made of Incoloy 800HT and has a length of 12.8 m with an internal diameter of 9 mm. Steam cracking of C_7H_{16} is performed with a coil outlet temperature (COT) of 1123 K, a coil outlet pressure (COP) of 170 kPa and with addition of 842 ppmwS/HC from CS_2, 841 ppmwS/HC from DMDS, 826 ppmwS/HC from DMS and 821

ppmwS/HC from DMSO. The C_7H_{16} flow rate is equal to respectively 4 x 10^3 g h^{-1} with a dilution of 0.5 kg_{steam} $kg_{heptane}^{-1}$. Nine different sulfur-containing compounds are detected, including H_2S, CS_2, SO_2, DMS, DMDS, thiophene together with its alkyl-substituted homologues and benzothiophene. For all four sulfur-containing additives the sulfur balance reaches approximately 90%.

Table 6-2: Overview of the experimental datasets used for model validation for the pyrolysis of DMDS, DMS, COS, CS_2 and DMSO.

No.	Sulfur compound	Experimental unit	Hydrocarbon matrix	Steam cracking?	Temperature [K]	Pressure [kPa]
1	DMDS	Bench-scale unit	/	No	673 - 1073	120
	DMDS		C_2H_6	Yes	673 - 1073	120
2	COS	Bench-scale unit	C_2H_6	No	873 - 1123	150
3	CS_2, DMDS, DMS, DMSO	Pilot plant unit	C_7H_{16}	Yes	1123	170

For both the bench-scale and the steam cracking pilot plant experiments, a dedicated analysis section is available that enables the online quantification of the wide boiling range mixture of components in the reactor effluent. The combination of two-dimensional gas chromatography with a sulfur chemiluminescence dual plasma detector online allows the accurate and complete determination of the decomposition products of the sulfur-containing compounds, since the detector is especially designed to detect and measure these compounds in complex hydrocarbon matrices up to ppm level. Note that it is possible that surface reactions contribute to the decomposition chemistry in addition to the expected gas phase reactions. For now, it is assumed that no surface reactions take place, even in the case of the stainless steel reactor. An overview of all experimental results and temperature profiles in the reactor measured during the experiments can be found on S:\vakgroep\ea12archief\SoftLib\c\cpappijn\1\.

6.2.3. Reactor simulations

Reactor simulations are performed with the new kinetic model using the CHEMKIN software [30]. Both experimental units are modelled as a plug flow reactor (PFR) using the measured temperature profiles for each experiment as input (c.f. Appendix D), which has been proven to be a valid assumption [31].

6.3. Results and discussion

6.3.1. *Ab initio* calculations

The thermal decomposition of the non-cyclic sulfur-containing compounds DMS, DMDS, DMSO, COS and CS_2 is governed by free radical chemistry. During pyrolysis of the pure compound, the formation of radicals is initiated by a homolytic bond scission. In case of a hydrocarbon matrix, the initial radicals are formed via hydrogen abstraction reaction by the large pool of hydrogen atoms and methyl radicals and to a lesser extent by a homolytic scission, depending on the bond strengths of the parent molecule. A bond dissociation energy (BDE) analysis of these sulfur-containing compounds can be used to gain insight into their relative thermal stability. The BDEs are a measure for the bond strengths and can thus be used to identify the weakest bonds for each compound. In Figure 6-1, the *ab initio* values calculated at the CBS-QB3 level of theory for the BDEs of DMSO, DMDS, DMS, COS and CS_2 are depicted. The BDE values for the analogous bonds in alkanes are included for comparison. The reported BDE values are in good agreement with other computational data available in literature [20, 32].

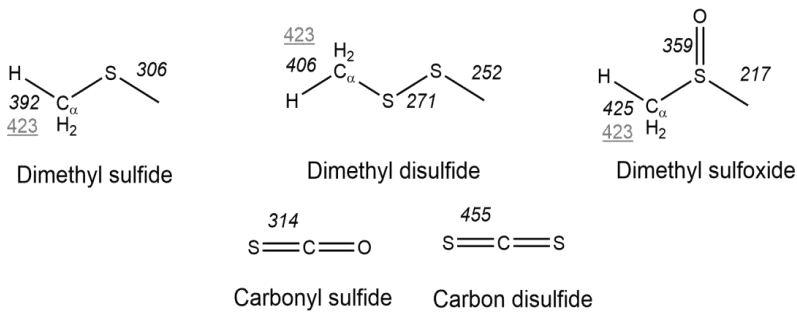

Figure 6-1: Bond dissociation energies [kJ mol^{-1}] for dimethyl sulfide (DMS), dimethyl disulfide (DMDS), dimethyl sulfoxide (DMSO), carbonyl sulfide (COS) and carbon disulfide (CS_2) and the analogous alkanes (grey) calculated at the CBS-QB3 level of theory.

The presence of a sulfur atom influences the BDEs of the nearby C_α-H, C_α-C and C_α-S bonds significantly, with C_α the carbon atom next to the sulfur atom. The weakest bonds in these sulfur-containing compounds are the single C-S bonds, i.e. a BDE of 306, 252 and 217 kJ mol^{-1} for DMS, DMDS and DMSO respectively. An adjacent sulfur atom decreases the BDE of the C-S bond with approximately 50 kJ mol^{-1} when comparing DMS and DMDS. This decrease can be explained by electronic effects, i.e. the lone pairs of the sulfur atom stabilize the formed radical and thus lower the corresponding BDE. The presence of a tetravalent sulfur atom in

DMSO even leads to a decrease of approximately 90 kJ mol^{-1} for the BDE of the C-S bond compared to DMS. The *ab initio* calculated value for the BDE of the S-S bond in DMDS is equal to 271 kJ mol^{-1}, which is in good agreement with the experimental value of 273 ± 4 kJ mol^{-1} reported by Nicovich et al. [33]. For the BDE of the C-S bond in DMDS an experimental value of 240 ± 6 kJ mol^{-1} has been reported [34].

The BDEs of the C_α-H bonds in DMS, DMDS and DMSO are equal to 392, 406 and 425 kJ mol^{-1} respectively. The presence of a bivalent sulfur atom in (di-)sulfides thus reduces the BDE of the C_α-H bond with approximately 30 kJ mol^{-1} compared to the BDE of a primary alkane C-H bond, i.e. 423 kJ mol^{-1}. On the contrary, the BDE of the C_α-H bond next to the tetravalent sulfur atom of the sulfoxide group is not influenced significantly.

The *ab initio* calculated BDE for the S=O bond in DMSO agrees well with the experimental BDE reported by Herron et al. [35], i.e. 364 kJ mol^{-1}. The BDEs of the double C=S bonds in both COS and CS_2 are much higher compared to the single C-S bonds, which corresponds to a much higher thermal stability of these sulfur-containing compounds. The *ab initio* calculated value for the BDE of the C=S bond in COS amounts to 314 kJ mol^{-1}, which is only 3 kJ mol^{-1} higher than the experimental value [36]. The C=S bond is significantly stronger in CS_2, i.e. an *ab initio* calculated value of 455 kJ mol^{-1}, which is in agreement with the experimental value of 441 ± 12 kJ mol^{-1} [36]. Taking into account the results of this BDE analysis, CS_2 seems to be the most thermally stable sulfur-containing compound, while DMSO has the lowest thermal stability due to the weak C-S bond.

In addition to the homolytic bond scission reactions as important initiating reactions, DMDS can also undergo an unimolecular elimination reaction as part of a plausible non-radical decomposition mechanism. A pressure dependent rate coefficient has been determined for this reaction using the RRKM theory with the MESMER program [37]. Argon is used as bath gas and the energy transfer probability is modeled using a single exponential energy transfer model, with a ΔE_{down} of 130 cm^{-1}. The rate coefficients have been fitted to Chebyshev polynomials over the temperature range 300 to 2000 K and pressure range 1 to 10^4 kPa. The high-pressure limit rate coefficients expressed in Arrhenius form are given by:

$$k_{DMDS,uni} = 2.60 \cdot 10^{13}\, exp\left(-\frac{282.3 \cdot 10^3}{T}\right)\ s^{-1} \qquad \text{(Eq. 6-1)}$$

The activation energy of this reaction leading to the formation of thioformaldehyde and methane thiol amounts to 282 kJ mol^{-1}. Although this value is close to the BDE of 271 kJ mol^{-1}

for the S-S bond, the pre-exponential factor is five orders of magnitude lower compared to the pre-exponential factor for the S-S bond scission as calculated by Vandeputte et al. [20].

6.3.2. Potential energy surfaces

To study the main decomposition pathways and product channels for COS, CS_2 and DMSO pyrolysis, the relevant potential energy surfaces have been constructed. The potential energy surfaces for the hydrogen addition to COS and CS_2 are shown in Figure 6-2. For the hydrogen addition to COS, there are three possibilities, i.e. addition to the carbon, sulfur or oxygen atom. The energetically most favorable pathway proceeds via hydrogen addition to the sulfur atom, followed by scission of the C-S bond leading the formation of CO and a thiyl radical. The hydrogen addition to the sulfur atom has the lowest reaction barrier i.e. 24 kJ mol^{-1} of both steps. Hydrogen addition to the oxygen atom does not only have a higher reaction barrier of 93 kJ mol^{-1}, but it also leads to the formation of the unstable products carbon monosulfide (CS) and a hydroxyl radical, for which the combined enthalpy is 250 kJ mol^{-1} higher than the reactants. Hydrogen addition to the carbon atom also has a higher reaction barrier compared to addition to the sulfur atom, i.e. 40 kJ mol^{-1}. The subsequent hydrogen shift from the carbon to the sulfur atom has a barrier of 115 kJ mol^{-1}, which is significantly higher than this first addition step. Note that according to Hadad et al. [38], it is energetically preferable to have a combination of a C=O and C-S bond rather than a C=S bond and a C-O bond in a stable molecule.

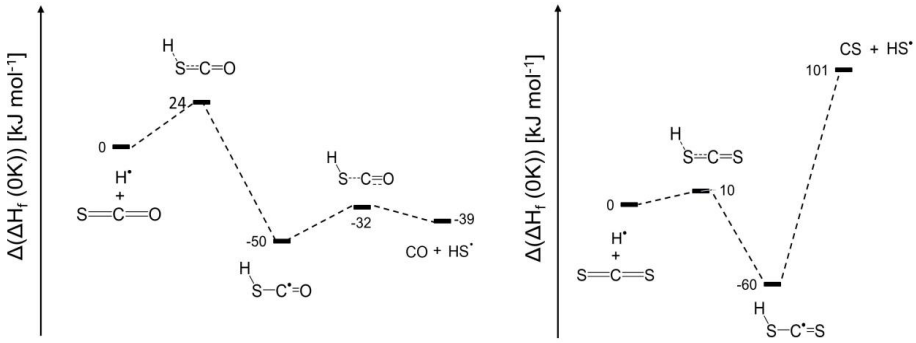

Figure 6-2: Potential energy surface for the reaction between a hydrogen atom and COS (left) and CS_2 (right). The values are CBS-QB3 calculated enthalpies of formation [kJ mol^{-1}] at 0 K relative to the enthalpy of formation of the reactants.

Formation of CO and the thiyl radical via the pathway initiated by hydrogen addition to the sulfur atom is thus the favored reaction pathway. For hydrogen addition to CS_2, addition to the sulfur atom also has the lowest reaction barrier, i.e 10 kJ mol^{-1}, compared to addition to the carbon atom (38 kJ mol^{-1}). Subsequent scission of the C-S bond leads to formation of CS and a

thiyl radical, for which the combined enthalpy is 101 kJ mol^{-1} higher than the reactants. No saddle point structure has been located for this reaction with the CBS-QB3 level of theory.

To gain insight into the decomposition of the methyl sulfinyl radical $CH_3S^{\cdot}{=}O$, i.e. the radical formed after C-S bond scission in DMSO, the potential energy surface has been constructed, c.f. Figure 6-3.

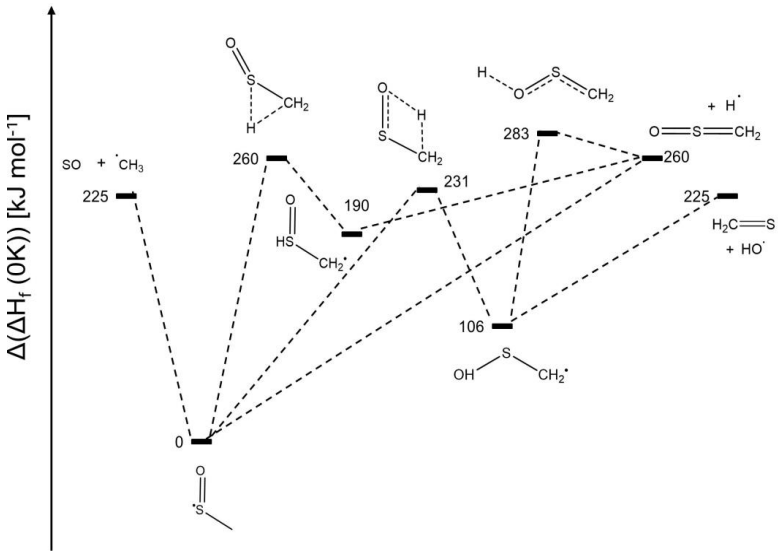

Figure 6-3: Selected part of the potential energy surface for the methyl sulfinyl radical $CH_3S^{\cdot}{=}O$, i.e. the radical formed after C-S bond scission in DMSO. The values are CBS-QB3 calculated enthalpies of formation [kJ mol^{-1}] at 0 K relative to the enthalpy of formation of $CH_3S^{\cdot}{=}O$.

One of the most simple reactions available for the sulfur-centered radical $CH_3S^{\cdot}{=}O$ is the direct formation of SO and a methyl radical via C-S bond scission. Despite the high BDE of the C-S bond, this reaction pathway has been proposed in the experimental study of Thyrion and Debecker [14]. Ramphal et al. [15] have confirmed the importance of this bond scission reaction in a recent study on the photodissociation of the $CH_3S^{\cdot}{=}O$ radical.

The first possible isomerization reaction is a hydrogen shift from the carbon to the sulfur atom, which has a reaction barrier of 260 kJ mol^{-1}. Scission of the S-H bond of the carbon-centered radical $^{\cdot}CH_2SH{=}O$ results in the formation of sulfine, i.e. $CH_2{=}S{=}O$, which corresponds to a reaction enthalpy of 70 kJ mol^{-1}. Another reaction pathway starting from $^{\cdot}CH_2SH{=}O$ proceeds via the migration of the oxygen atom to the carbon atom followed by either β-scission of the C-H bond resulting in the formation of HSCH=O and a hydrogen atom or β–scission of the C-S bond resulting in the formation of the thiyl radical and formaldehyde. As the enthalpy barrier

for the migration of the oxygen to the carbon atom is significantly higher compared to the reaction enthalpy of the S-H bond scission, i.e. 148 kJ mol^{-1}, this pathway is not taken into account.

The second possible isomerization reaction in which a hydrogen atom shifts from the carbon atom to the oxygen atom, proceeds via a four-membered cyclic transition state and has a reaction barrier of 231 kJ mol^{-1}. Subsequent scission of the O-H bond in the $^{\cdot}CH_2SOH$ radical leads to the formation of sulfine. Thioformaldehyde and a hydroxyl radical can be formed via the β-scission of the S-O bond of the $^{\cdot}CH_2SOH$ radical. No saddle point structure could be located for this reaction with the CBS-QB3 level of theory. Direct formation of sulfine via β-scission of the methyl sulfinyl radical is also possible with a reaction enthalpy of 260 kJ mol^{-1}.

In addition to the homolytic scission of the C-S bond of DMSO, hydrogen abstraction and radical addition to either the sulfur or oxygen atom can be important initiating reactions, when a radical pool has been established. Hydrogen abstraction by a hydrogen atom has a reaction barrier of 45 kJ mol^{-1}, c.f. Figure 6-4.

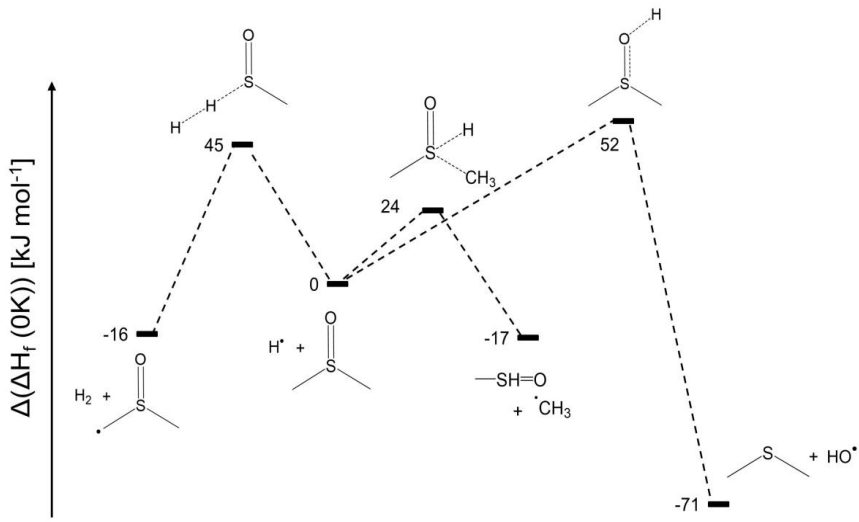

Figure 6-4: Potential energy surface for the reaction between a hydrogen atom and DMSO. The values are CBS-QB3 calculated enthalpies of formation at 0 K relative to the enthalpy of formation [kJ mol^{-1}] of the reactants, i.e. H + DMSO.

Similar to COS and CS_2, a hydrogen atom or methyl radical can add to the S=O bond of DMSO. The hydrogen addition on the oxygen atom combined with the S-O bond scission leads to the formation of DMS and a hydroxyl radical, with a reaction barrier of 52 kJ mol^{-1}. Alternatively, hydrogen addition on the sulfur atom results in the formation of a methyl radical and the sulfur-

containing species $CH_3SH{=}O$. This reaction has the lowest reaction barrier of all three reactions, i.e. 24 kJ mol^{-1}.

6.3.3. Assessment of the kinetic model

6.3.3.1. Dimethyl disulfide (DMDS)

A comparison between the experimental and simulated concentrations of the main sulfur-containing compounds for DMDS decomposition in both nitrogen and C_2H_6, is given in Figure 6-5. Almost full conversion of DMDS is reached at 773 K for combined pyrolysis with C_2H_6. For pyrolysis of DMDS in nitrogen this is reached at a higher temperature of 873 K. The model is able to capture this difference in reactivity caused by the presence of an initial hydrocarbon pool in the case of C_2H_6 steam cracking. For both pyrolysis in nitrogen as well as in C_2H_6, H_2S is the main sulfur-containing product over the complete temperature range. With increasing temperature the selectivity towards methane thiol decreases, in favor of the CS_2 selectivity.

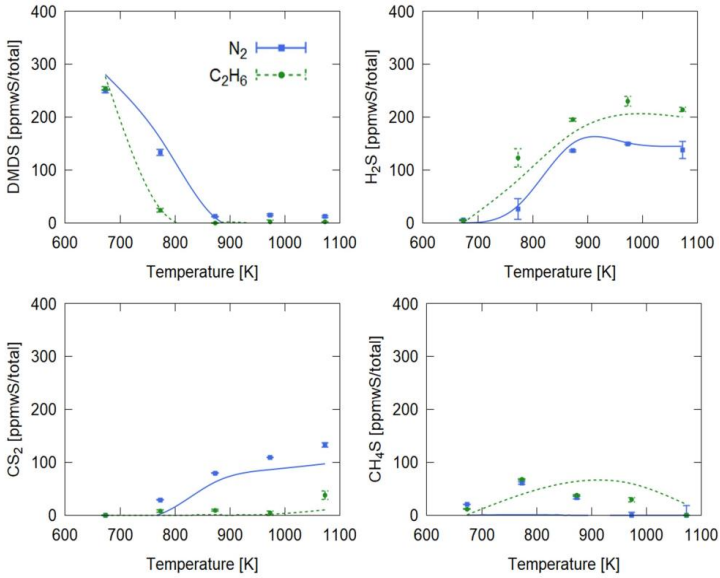

Figure 6-5: Experimental (points) and simulated (lines) concentrations of the main sulfur-containing compounds as a function of temperature [K] during the pyrolysis of DMDS in nitrogen (blue) and in a C_2H_6 matrix (green). Experimental conditions are a pressure of 120 kPa and a DMDS inlet concentration of 286 ppmwS/total.

Overall, a good agreement is obtained between experimental and simulation results for the main sulfur-containing products H_2S, CS_2 and CH_4S. A maximum in the H_2S yield is obtained at 973 K, with a higher selectivity towards H_2S in the case of pyrolysis with C_2H_6 compared to pyrolysis in nitrogen. For pyrolysis in nitrogen, CS_2 has an increasing yield as a function of

temperature over the complete temperature range. The CS_2 yield is significantly lower in the presence of C_2H_6, which is underpredicted by the model.

To gain more insight into the main reaction pathways governing DMDS decomposition and the influence of a hydrocarbon matrix, rate of production analyses have been performed. The results of this analysis for DMDS pyrolysis in nitrogen at a temperature of 873 K, which corresponds to a DMDS conversion of 98%, is shown in Figure 6-6.

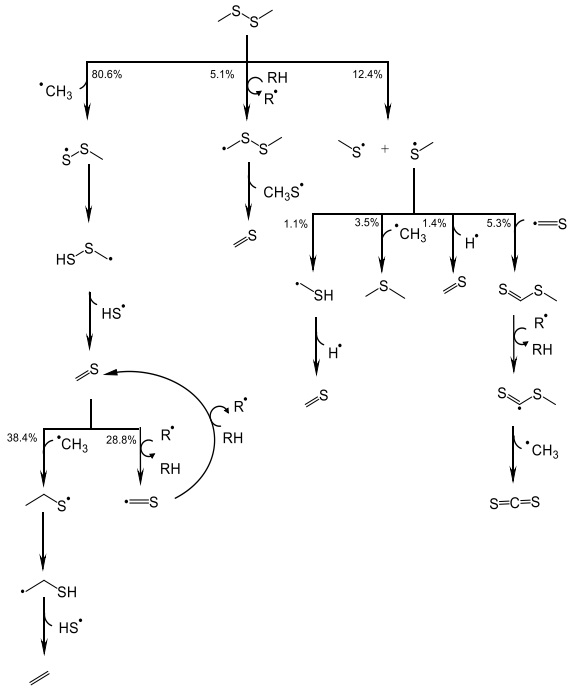

Figure 6-6: Rate of production analysis for the pyrolysis of DMDS at a temperature of 873 K, a reactor distance of 20 cm and initial DMDS mole fraction of 286 ppmwS/total. Percentages report the rate of production relative to the total decomposition of DMDS.

The contribution of the unimolecular elimination reaction of DMDS, forming thioformaldehyde (CH_2=S) and methane thiol, is negligible under the studied conditions. Decomposition of DMDS is initiated mainly by homolytic scission of the C-S bond (12.4%) and the S-S bond (80.6%). A small fraction of DMDS is converted by hydrogen abstraction, mainly by hydrogen and methyl radicals. The formed radical $^{\cdot}CH_2SSCH_3$ undergoes β-scission of the weak S-S bond, which leads to thioformaldehyde. The contribution of the unimolecular elimination of DMDS at these conditions is negligible. The sulfur-centered radical $CH_3SS^{\cdot}$ formed after C-S bond scission undergoes intramolecular hydrogen abstraction followed by β-scission leading to the formation of thioformaldehyde and a thiyl radical. Thioformaldehyde is an important

reactive intermediate in the decomposition of sulfide species. The pathway proceeding via addition of methyl radicals, obtained directly from C-S bond scission of DMDS, to thioformaldehyde further leads to the formation of ethylene and H_2S. A minor fraction of thioformaldehyde undergoes hydrogen abstraction after which it undergoes a recombination with a methane thiol radical to form $CH_3SC{=}S$ or it is converted back to thioformaldehyde. Hydrogen abstraction from the intermediate $CH_3SC{=}S$ followed by β-scission is the main CS_2 formation pathway. Pathways going via the methane thiol radical, formed after S-S bond scission in DMDS, can lead to the formation of dimethyl sulfide by recombination with a methyl radical or to methane thiol after hydrogen abstraction.

The reaction path analysis for the decomposition of DMDS during ethane steam cracking at 873 K, corresponding to complete conversion of DMDS, is shown in Figure 6-7.

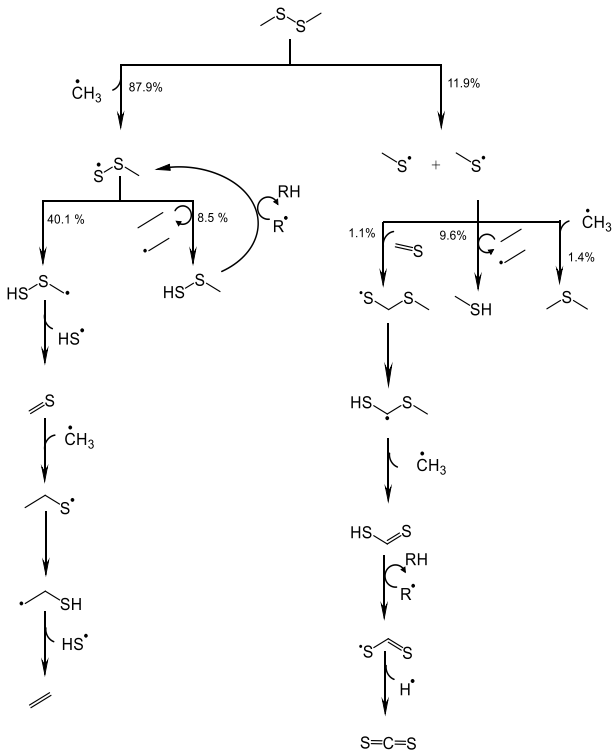

Figure 6-7: Rate of production analysis for the pyrolysis of DMDS at a temperature of 873 K, a reactor distance of 20 cm and initial DMDS mole fraction of 286 ppmwS/total. Percentages report the rate of production relative to the total decomposition of DMDS.

The decomposition of DMDS is still initiated via C-S and S-S bond scissions, in agreement with the low BDEs compared to hydrocarbons, see Section 6.3.1. Hydrogen abstraction from

C_2H_6 by the sulfur-centered radical $CH_3SS^{\cdot}$ now competes with intramolecular hydrogen abstraction, accounting for 8.5% of the decomposition rate. In contrast to the pure pyrolysis of DMDS, bimolecular reactions and more in particular hydrogen abstraction from ethane dominate for the methane thiol radical. Only a very small fraction of these radicals add to thioformaldehyde leading to the formation of CS_2.

6.3.3.2. Carbonyl sulfide (COS)

The pyrolysis of COS has been studied experimentally in both nitrogen and C_2H_6. With the absence of a hydrocarbon matrix, no decomposition of COS is observed below a temperature of 1173 K, which is the maximum temperature reached during the experiments. This low reactivity is to be expected taking into account the high BDEs of both the C=O and C=S double bonds. The experimental and simulated concentrations of the main sulfur-containing compounds for COS pyrolysis in a C_2H_6 matrix are shown in Figure 6-8. A good agreement is obtained between experimental and simulation results for the conversion of COS as well as the main sulfur-containing products H_2S. The model is also able to capture the trends for CS_2 and thiophene (C_4H_4S), both with increasing concentrations as a function of temperature. Note that these concentrations are significantly lower compared to H_2S, but the correct order of magnitude in ppmwS/HC is predicted by the model.

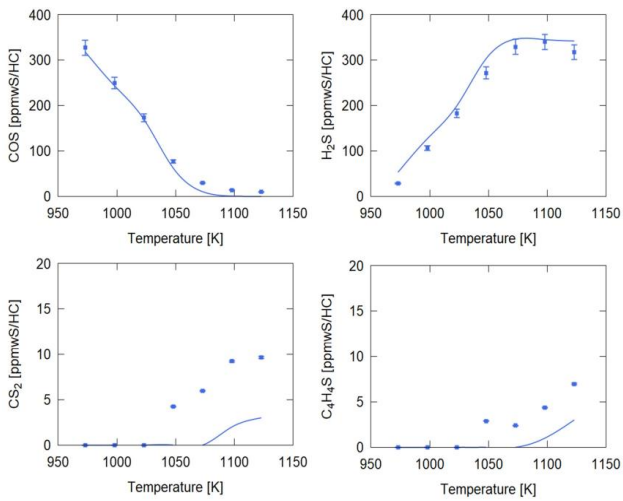

Figure 6-8: Experimental (symbols) and simulated (lines) concentrations of the main sulfur-containing products as a function of temperature [K] during the pyrolysis of COS in C_2H_6. Experimental conditions are a pressure of 150 kPa and a COS inlet concentration of 695 ppmwS/HC.

Figure 6-9 displays the experimental and simulated yields of C_2H_6, C_2H_4, CH_4, H_2 and CO for the pyrolysis of COS. A good agreement is obtained between both experimental and modeling

results. The conversion of C_2H_6 at a temperature of 1123 K amounts to 70%, with an ethylene yield of 53 wt%.

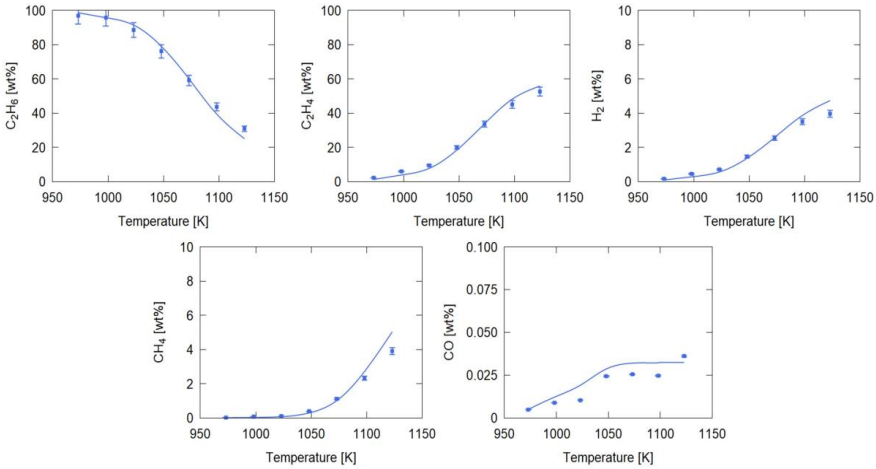

Figure 6-9: Experimental (symbol) and simulated (lines) concentrations of C_2H_6, C_2H_4, H_2, CH_4 and CO as a function of temperature [K] during the pyrolysis of COS in a C_2H_6 matrix. Experimental conditions are a pressure of 150 kPa and a COS inlet concentration of 695 ppmwS/HC.

The reaction path analysis for the pyrolysis of COS in a C_2H_6 matrix at a temperature of 1073 K, which corresponds to a COS conversion of 92%, is given in Figure 6-10. Hydrogen addition on the sulfur atom on COS followed by scission of the C-S bond leads to the formation of CO and a thiyl radical. This direct pathway is in agreement with the monotonous increase of H_2S and CO until complete conversion of COS is reached, i.e. at a temperature of approximately 1073 K. Due the availability of hydrocarbon species formed via pyrolysis of C_2H_6, hydrogen abstraction by the thiyl radical from hydrocarbons, mainly C_2H_4 and C_2H_6, dominates leading to formation of the main sulfur-containing product H_2S. A very small fraction of these thiyl radicals, i.e. less than 1.5% at 1073 K, undergoes an addition reaction to ethylene forming the intermediate carbon-centered radical $^{\cdot}CH_2CH_2SH$. Intramolecular hydrogen abstraction followed by β-scission leads to thioformaldehyde. After a hydrogen radical addition and abstraction reaction thioformaldehyde is mainly converted to methane thiol, which is one of the minor sulfur-containing products. Reaction between thioformaldehyde and the sulfur-centered methane thiol radical $CH_3S^{\cdot}$ can lead to CS_2 formation via a sequence of radical addition and hydrogen abstraction reactions. Due to the low concentration of these sulfur-containing radicals, in comparison due to the large pool of hydrocarbon species, these reactions between two sulfur-containing compounds are limited in the case of pyrolysis in a C_2H_6 matrix.

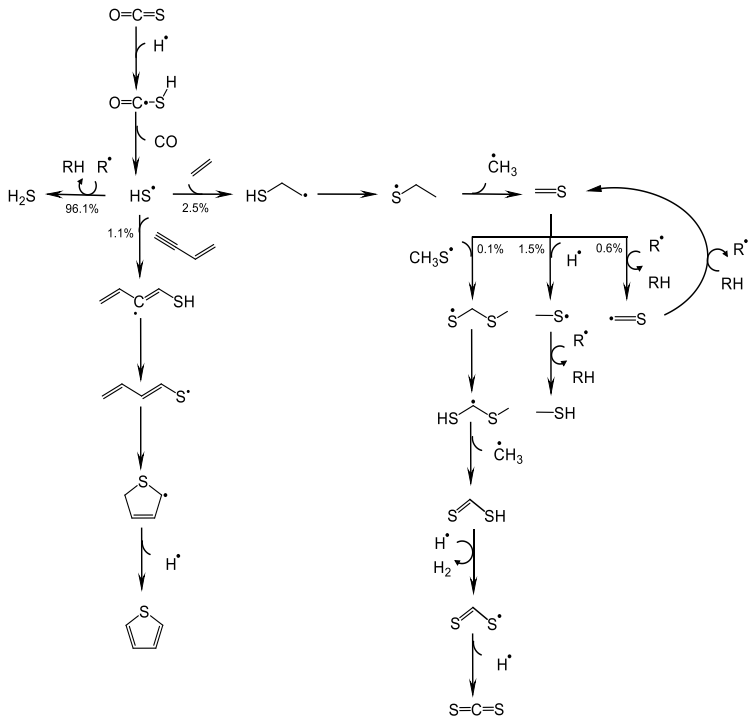

Figure 6-10: Rate of production analysis for the pyrolysis of COS in a C_2H_6 matrix at a temperature of 1073 K and a reactor distance of 50 cm. Percentages report the rate of production relative to the total decomposition of COS.

The thiyl radical can also react with unsaturated hydrocarbon species with at least four carbon atoms, such as butadiene and vinyl acetylene, to form the aromatic sulfur-containing compound thiophene. Hydrogen addition to vinyl acetylene followed by intramolecular hydrogen abstraction leads to the sulfur-centered thiobutadienyl radical CH_2=CHCH=CHS$^{\cdot}$. This radical can undergo an intramolecular radical addition to form a five ring structure, which is further converted to thiophene after C-H β-scission. Note that this also has been suggested as the main pathway for thiophene decomposition in hydrocarbon pyrolysis by Bajus et al. [2].

6.3.3.3. Heptane cracking with sulfur-containing compounds (CS_2, DMDS, DMS, DMSO)

The experimental and simulated mass fractions of the main sulfur-containing products for C_7H_{16} steam cracking in the pilot plant unit with respectively CS_2, DMDS, DMS and DMSO as additives are given in Table 6-3. Almost complete conversion is reached for DMDS, DMS and DMSO, while for CS_2 the experimentally observed conversion is equal to approximately 50%. The main sulfur-containing product is H_2S, with 78%, 95% and 79% of the detected sulfur equal

to H_2S for respectively CS_2, DMDS and DMS. In DMSO decomposition both H_2S and SO_2 are important sulfur-containing products, accounting for 45% and 49% of the detected sulfur. For all four sulfur-containing compounds, thiophene is formed as a minor sulfur-containing product, with yields in the same order of magnitude. Alkyl substituted thiophenes were also experimentally detected (with concentrations one order of magnitude lower then thiophene), but their formation is not accounted for in the new model.

Table 6-3: Experimental and simulated mass fractions [ppmwS/HC] of the main sulfur-containing products for the C_7H_{16} steam cracking experiments with a COT of 1123 K, a pressure of 170 kPa and with 842 ppmwS/HC of CS_2, 841 ppmwS/HC of DMDS, 826 ppmwS/HC of DMS, 821 ppmwS/HC of DMSO added to the feed.

	CS_2		DMDS		DMS		DMSO	
Yields [ppmwS/HC]	Exp.	Sim.	Exp.	Sim.	Exp.	Sim.	Exp.	Sim.
H_2S	317	301	672	710	619	669	344	298
CS_2	419	435	10	13	14	13	8	4
SO_2	-	0	-	0	-	0	370	471
DMS	-	0	1	11	26	27	-	0
DMDS	-	0	1	0	2	0	-	0
Thiophene	23	10	25	13	46	21	29	15

The new model is able to capture the main experimental trends, with a reasonable agreement between experimental and simulated yields for all sulfur-containing compounds taking into account the low concentrations of the sulfur-containing additives. Taking into account the high BDE of the C=S double bond, the decomposition of CS_2 at the studied COT of 1023 is initiated by addition of one of the main hydrocarbon radical species, i.e. a hydrogen or methyl radical. Hydrogen addition followed by α-scission of the weakened C-S bond leads to formation of the thiyl radical, which is further converted to H_2S by hydrogen abstraction from mainly C_7H_{16}, c.f. Figure 6-11. Due to the high endothermicity of this reaction, compared to the analogous reaction for COS decomposition, not all CS_2 is converted at the studied conditions, reflecting the high thermal stability of this sulfur-containing additive.

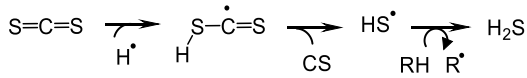

Figure 6-11: Main reaction pathway for CS_2 decomposition during C_7H_{16} steam cracking at a COT of 1073 K.

DMDS almost completely decomposes under the studied cracking conditions. The reaction pathways for formation of the main sulfur-containing products H_2S, CS_2 and DMS are similar to those shown in Figure 6-7 for decomposition of DMDS in a C_2H_6 matrix. It is clear that significantly larger sulfur-containing products can be formed via addition or recombination reactions in this case due to the substantial amounts of long-chain hydrocarbon species. More specifically the presence of substantial amounts of unsaturated hydrocarbon species with at least four carbon atoms leads to the formation of thiophene, and its corresponding alkyl homologues, with larger concentrations (on sulfur basis) compared to CS_2 for DMDS, DMS and DMSO decomposition.

The decomposition of DMS is mainly initiated by homolytic scission of the C-S bond resulting in the formation of the methane thiol radical. The reaction pathways for this radical are analogous to those in DMDS decomposition, as discussed in Section 6.3.3.1. The main decomposition pathway, c.f. Figure 6-12, proceeds via the reactive thioformaldehyde resulting in the formation of ethylene and a thiyl radical, which is converted to H_2S after hydrogen abstraction from C_7H_{16}.

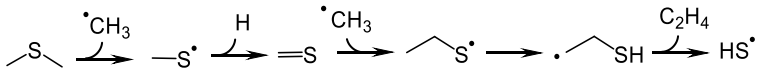

Figure 6-12: Main reaction pathway for DMS decomposition during C_7H_{16} steam cracking at a COT of 1073 K.

A rate of production analysis for decomposition of DMSO during C_7H_{16} cracking at 1073 K is given in Figure 6-13. Due to the weak BDE of the C-S bond, which is caused by electronic effects of the adjacent sulfoxide group, the decomposition of DMSO is mainly initiated via homolytic bond scission. Hydrogen abstraction from the C-H bond accounts only for a very small fraction of the decomposition (1.3%).

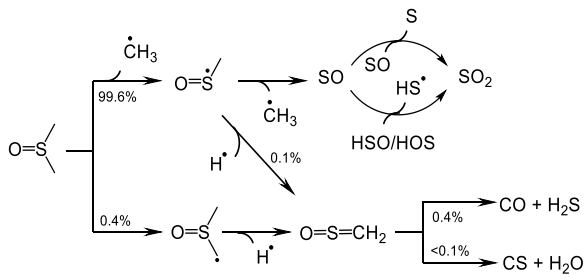

Figure 6-13: Rate of production analysis for the pyrolysis of DMSO at a COT of 1073 K, a reactor distance of 20 cm and initial DMSO mole fraction of 821 ppmwS/HC. Percentages report the rate of productions relative to the total decomposition of DMDO.

The sulfur-centered $CH_3S^{\cdot}$=O radical decomposes almost exclusively via C-S bond scission resulting in the formation of a methyl radical and SO. Only a minor fraction (<1%) undergoes C-H β-scission leading to formation of CH_2=S=O. According to Alzueta et al. [7], the decomposition of sulfine produces mainly CO and H_2S (R1), while a minor reaction pathway is the formation of carbon monosulfide (CS) and H_2O (R2). Because no rate coefficients are available in literature for these reactions, the rate coefficients are approximated based on analogy with the decomposition of formaldehyde oxide (CH_2OO).

$$CH_2SO \rightleftarrows CO + H_2S \quad \text{(R1)}$$

$$CH_2SO \rightleftarrows CS + H_2O \quad \text{(R2)}$$

Sulfine can also be formed by C-H bond β-scission of the carbon-centered radical formed via hydrogen abstraction from DMSO, but this pathway accounts for only 1.3% of the total decomposition rate. Radical addition of a thiyl radical to the intermediate CS followed by β-scission of the S-H bond leads to formation of the minor sulfur-containing product CS_2. SO_2 is a secondary product formed via reactions between the very reactive SO and other sulfur-containing species. The main reaction for SO_2 formation is via reaction between two SO species.

$$SO + SO \rightleftarrows SO_2 + S \quad \text{(R3)}$$

A minor reaction pathway for SO_2 formation proceeds via the HSO (R4) and HOS (R5) radical species, which are formed after hydrogen abstraction from the sulfur-containing compound HSOH. According to the submechanism of Alzueta et al. [7], formation of HSOH is possibly via reaction between S and H_2O. Abstraction by the thiyl radical, which is mainly formed via (R4) and (R5), from heptane leads to formation of H_2S.

$$SO + HSO \rightleftarrows HS^{\cdot} + SO_2 \quad \text{(R4)}$$

$$SO + HOS \rightleftarrows HS^{\cdot} + SO_2 \quad \text{(R5)}$$

$$HSOH \rightleftarrows S + H_2O \quad \text{(R6)}$$

6.4. Conclusions

The decomposition of five sulfur-containing compounds that can be present either as additives or feedstock impurities in the steam cracking process has been studied by combining first principles based kinetic modeling with experimental validation. These five compounds include dimethyl sulfide (DMDS), dimethyl disulfide (DMS), dimethyl sulfoxide (DMSO), carbonyl sulfide (COS) and carbon disulfide (CS_2). Both the influence of the sulfur-containing functional group as well as the presence of a hydrocarbon matrix on the decomposition chemistry and the pyrolysis products has been investigated. The automatic kinetic model generation tool Genesys has been used to generate a new kinetic model, with thermodynamic and kinetic data for the main species and reactions of the studied compounds obtained from *ab initio* calculations. The performance of the kinetic model has been tested against experimental data gathered in a tubular and pilot plant reactor at steam cracking conditions.

The model succeeds in capturing the main experimental trends in species concentrations, without any fitting of the model thermodynamic and kinetic parameters over the wide range of conditions. The weakening effect of the sulfur atoms on the bond strengths of the (di-)sulfide compounds DMDS and DMS leads to a high reactivity under the studied steam cracking conditions, with mainly homolytic scission as initiating reactions even in the case of a hydrocarbon matrix. The main sulfur-containing product is H_2S, while methane thiol and dimethyl sulfide and CS_2 are minor products. In the presence of hydrocarbons, the decomposition of both COS and CS_2 proceeds via hydrogen radical addition followed by β-scission leading to the direct formation of H_2S after hydrogen abstraction. While the conversion of COS is complete, CS_2 has a much higher thermal stability and is even formed as minor product in COS decomposition under steam cracking conditions. For DMSO composition, which has an even higher reactivity compared to DMDS, both SO_2 and H_2S are the dominant sulfur-containing products. For all compounds, the thiyl radical formed during decomposition can combine with saturated hydrocarbon species with at least four atoms, leading to the formation of thiophene.

6.5. References

[1] H. Zimmermann, R. Walzl, Ethylene, Ullmann's Encyclopedia of Industrial Chemistry, Wiley-VCH Verlag GmbH & Co. KGaA, 2000.

[2] M. Bajus, Sulfur compounds in hydrocarbon pyrolysis, Sulfur Reports 9 (1989) 25-66.

[3] N. Rahimi, R. Karimzadeh, S.M. Jazayeri, K.D. Nia, An empirical investigation of the influence of sulfur additives on the catalytic rate of coke deposition and CO formation in the steam cracking of LPG over Incoloy 600 and stainless steel, Chemical Engineering Journal 238 (2014) 210-218.

[4] I. Dhuyvetter, M.-F. Reyniers, G.F. Froment, G.B. Marin, D. Viennet, The Influence of Dimethyl Disulfide on Naphtha Steam Cracking, Industrial & Engineering Chemistry Research 40 (2001) 4353-4362.

[5] S.M. Jazayeri, R. Karimzadeh, Experimental Investigation of Initial Coke Formation over Stainless Steel, Chromium, and Iron in Thermal Cracking of Ethane with Hydrogen Sulfide as an Additive, Energy & Fuels 25 (2011) 4235-4247.

[6] N.M. Vandewiele, K.M. Van Geem, M.F. Reyniers, G.B. Marin, Genesys: Kinetic model construction using chemo-informatics, Chemical Engineering Journal 207 (2012) 526-538.

[7] M.U. Alzueta, R. Pernía, M. Abián, Á. Millera, R. Bilbao, CH3SH conversion in a tubular flow reactor. Experiments and kinetic modelling, Combustion and Flame 203 (2019) 23-30.

[8] S.W. Benson, F.R. Cruickshank, D.M. Golden, G.R. Haugen, H.E. O'Neal, A.S. Rodgers, R. Shaw, R. Walsh, Additivity rules for the estimation of thermochemical properties, Chemical Reviews 69 (1969) 279-324.

[9] M.K. Sabbe, M. Saeys, M.F. Reyniers, G.B. Marin, V. Van Speybroeck, M. Waroquier, Group additive values for the gas phase standard enthalpy of formation of hydrocarbons and hydrocarbon radicals, Journal of Physical Chemistry A 109 (2005) 7466-7480.

[10] M.K. Sabbe, F. De Vleeschouwer, M.-F. Reyniers, M. Waroquier, G.B. Marin, First Principles Based Group Additive Values for the Gas Phase Standard Entropy and Heat Capacity of Hydrocarbons and Hydrocarbon Radicals, The Journal of Physical Chemistry A 112 (2008) 12235-12251.

[11] P.D. Paraskevas, M.K. Sabbe, M.F. Reyniers, N. Papayannakos, G.B. Marin, Group additive values for the gas-phase standard enthalpy of formation, entropy and heat capacity of oxygenates, Chemistry 19 (2013) 16431-16452.

[12] A.G. Vandeputte, M.K. Sabbe, M.F. Reyniers, G.B. Marin, Modeling the gas-phase thermochemistry of organosulfur compounds, Chemistry 17 (2011) 7656-7673.

[13] J.A. Miller, S.J. Klippenstein, The H + C2H2 (+M) ⇄ C2H3 (+M) and H + C2H2 (+M) ⇄ C2H5 (+M) reactions: Electronic structure, variational transition-state theory, and solutions to a two-dimensional master equation, Physical Chemistry Chemical Physics 6 (2004) 1192-1202.

[14] M. Saeys, M.F. Reyniers, G.B. Marin, V. Van Speybroeck, M. Waroquier, Ab initio group contribution method for activation energies for radical additions, AIChE Journal 50 (2004) 426-444.

[15] M.K. Sabbe, A.G. Vandeputte, M.-F. Reyniers, M. Waroquier, G.B. Marin, Modeling the influence of resonance stabilization on the kinetics of hydrogen abstractions, Physical Chemistry Chemical Physics 12 (2010) 1278-1298.

[16] M.K. Sabbe, M.F. Reyniers, V. Van Speybroeck, M. Waroquier, G.B. Marin, Carbon-Centered Radical Addition and β-Scission Reactions: Modeling of Activation Energies and Pre-exponential Factors, Chemphyschem 9 (2008) 124-140.

[17] M.K. Sabbe, M.-F. Reyniers, M. Waroquier, G.B. Marin, Hydrogen Radical Additions to Unsaturated Hydrocarbons and the Reverse β-Scission Reactions: Modeling of Activation Energies and Pre-Exponential Factors, Chemphyschem 11 (2010) 195-210.

[18] P.D. Paraskevas, M.K. Sabbe, M.-F. Reyniers, G.B. Marin, N.G. Papayannakos, Group additive kinetic modeling for carbon-centered radical addition to oxygenates and β-scission of oxygenates, AIChE Journal 62 (2016) 802-814.

[19] A.G. Vandeputte, M.F. Reyniers, G.B. Marin, A theoretical study of the thermodynamics and kinetics of small organosulfur compounds, Theoretical Chemistry Accounts 123 (2009) 391-412.

[20] A.G. Vandeputte, M.-F. Reyniers, G.B. Marin, Theoretical study of the thermal decomposition of dimethyl disulfide, The Journal of Physical Chemistry A 114 (2010) 10531-10549.

[21] A.G. Vandeputte, M.-F. Reyniers, G.B. Marin, Kinetics of Homolytic Substitutions by Hydrogen Atoms at Thiols and Sulfides, Chemphyschem 14 (2013) 1703-1722.

[22] A.G. Vandeputte, M.K. Sabbe, M.-F. Reyniers, G.B. Marin, Kinetics of α hydrogen abstractions from thiols, sulfides and thiocarbonyl compounds, Physical Chemistry Chemical Physics 14 (2012) 12773-12793.

[23] A.G. Vandeputte, M.-F. Reyniers, G.B. Marin, Kinetic modeling of hydrogen abstractions involving sulfur radicals, Chemphyschem 14 (2013) 3751-3771.

[24] M.R. Harper, K.M. Van Geem, S.P. Pyl, G.B. Marin, W.H. Green, Comprehensive reaction mechanism for n-butanol pyrolysis and combustion, Combustion and Flame 158 (2011) 16-41.

[25] R. De Bruycker, J.M. Anthonykutty, J. Linnekoski, A. Harlin, J. Lehtonen, K.M. Van Geem, J. Räsänen, G.B. Marin, Assessing the Potential of Crude Tall Oil for the Production of Green-Base Chemicals: An Experimental and Kinetic Modeling Study, Industrial & Engineering Chemistry Research 53 (2014) 18430-18442.

[26] S.P. Pyl, C.M. Schietekat, K.M. Van Geem, M.-F. Reyniers, J. Vercammen, J. Beens, G.B. Marin, Rapeseed oil methyl ester pyrolysis: On-line product analysis using comprehensive two-dimensional gas chromatography, Journal of Chromatography A 1218 (2011) 3217-3223.

[27] K.M. Van Geem, S.P. Pyl, M.-F. Reyniers, J. Vercammen, J. Beens, G.B. Marin, On-line analysis of complex hydrocarbon mixtures using comprehensive two-dimensional gas chromatography, Journal of Chromatography A 1217 (2010) 6623-6633.

[28] N. Olahova, Influence of sulfur compounds on product yields and coke formation during steam cracking of hydrocarbons, 2018.

[29] N. Olahova, M.R. Djokic, R. Van de Vijver, N.D. Ristic, G.B. Marin, M.-F. Reyniers, K.M. Van Geem, Thermal decomposition of sulfur compounds and their role in coke formation during steam cracking of heptane, Chemical Engineering & Technology 39 (2016) 2096-2106.

[30] R.J. Kee, F.M. Rupley, J.A. Miller, M.E. Coltrin, J.F. Grcar, E. Meeks, H.K. Moffat, A.E. Lutz, G. Dixon-Lewis, M.D. Smooke, J. Warnatz, G.H. Evans, R.S. Larson, R.E. Mitchell, L.R. Petzold, W.C. Reynolds, M. Caracotsios, W.E. Stewart, P. Glarborg, C. Wang, O. Adigun, Chemkin-Pro 15112, Reaction Design: San Diego, CA, USA, (2011).

[31] K.M. Van Geem, M.-F. Reyniers, G.B. Marin, J. Song, W.H. Green, D.M. Matheu, Automatic reaction network generation using RMG for steam cracking of n-hexane, AIChE Journal 52 (2006) 718-730.

[32] L.-F. Zou, Y. Fu, K. Shen, Q.-X. Guo, Sulfur–sulfur bond dissociation enthalpies: A high-level ab initio study, Journal of Molecular Structure: THEOCHEM 807 (2007) 87-92.

[33] J.M. Nicovich, K.D. Kreutter, C.A. Van Dijk, P.H. Wine, Temperature-dependent kinetics studies of the reactions $Br(^2P_{3/2}) + H_2S$ <-> SH + HBr and $Br(^2P_{3/2}) + H_2S$ <-> CH_3S + HBr. Heats of formation of SH and CH_3S radicals, The Journal of Physical Chemistry 96 (1992) 2518-2528.

[34] S. Nourbakhsh, C.L. Liao, C.Y. Ng, A 193 nm laser photofragmentation time-of-flight mass spectrometric study of CH3SSCH3, SSCH3, and SCH3, The Journal of Chemical Physics 92 (1990) 6587-6593.

[35] J.T. Herron, Thermochemistry of Sulfoxides and Sulfones, Sulphones and Sulphoxides 1988, pp. 95-106.

[36] P.J. Lindstrom, W.G. Mallard, NIST Chemistry WebBook, NIST Standard Reference Database Number 69, National Institute of Standards and Technology, Gaithersburg MD.

[37] D.R. Glowacki, C.-H. Liang, C. Morley, M.J. Pilling, S.H. Robertson, MESMER: An Open-Source Master Equation Solver for Multi-Energy Well Reactions, The Journal of Physical Chemistry A 116 (2012) 9545-9560.

[38] C.M. Hadad, P.R. Rablen, K.B. Wiberg, C−O and C−S Bonds: Stability, Bond Dissociation Energies, and Resonance Stabilization, The Journal of Organic Chemistry 63 (1998) 8668-8681.

7

Conclusions and future outlook

7.1. Conclusions

The gradual shift from fossil to more sustainable and alternative feedstocks, driven by the increasingly strict environmental regulations and process economics primarily determined by the feedstock price, poses a challenge for the (petro)chemical industry. A common concern is the presence of substantial amounts of heteroatomic compounds (nitrogen, oxygen, sulfur) and their potential negative impact on the process, considering safety, operability and quality of the product streams. These alternative feedstocks do not only have a higher heteroatomic concentration, but also a different distribution of compounds, which raises the question whether the current global feedstock specifications are still valid. The pyrolysis and oxidation chemistry of the heteroatomic compounds encountered as feedstock impurities and process additives and the effect of a changing hydrocarbon matrix is in general poorly understood, and in some cases, even completely unknown. This clear and important knowledge gap has motivated the recent large interest in the thermochemical reactions of these heteroatomic compounds, ideally coming up with a predictive model that allows to estimate what is acceptable and what not under a certain set of conditions. In this PhD thesis, quantum chemistry calculations, kinetic modelling and experimental work are combined to improve the fundamental understanding of the pyrolysis and oxidation chemistry of nitrogen-, oxygen- and sulfur-containing model compounds present in renewable and alternative steam cracking feedstocks and energy carriers. With the microkinetic modeling approach accurate kinetic models are generated to describe the thermochemical reactions as well as the effect of a hydrocarbon matrix, for a number of well-chosen model compounds over a wide range of conditions.

7.1.1 Quantum chemical calculations

Theoretical calculations at the CBS-QB3 level of theory and approximation methods based on these calculations have been used to determine the thermodynamic and kinetic parameters of the studied heteroatomic compounds and their reactions. To improve the accuracy of the

standard enthalpy of formation obtained at CBS-QB3 level of theory, a new set of bond additive corrections has been derived from a dataset of 371 hydrocarbons and heteroatomic molecules. This correction scheme enables to predict the experimental value with "thermodynamic accuracy", i.e. a mean absolute deviation lower than 4 kJ mol^{-1}.

While for oxygen- and sulfur-containing compounds, a limited number of accurate group additivity schemes focusing on the most common functionalities and reaction families, is available, this is not yet the case for nitrogen-containing compounds. To tackle this issue, a consistent set of a total of 91 group additive values and three non-nearest-neighbor interactions has been determined to approximate the thermodynamic parameters from a dataset of CBS-QB3 calculations for 300 nitrogen-containing species. This dataset contains a wide range of functionalities, including amine, imine, nitrile, nitro, nitroso, nitrite, nitrate and azo functional groups, which are all relevant to describe the pyrolysis or oxidation of nitrogen-containing feedstock additives or impurities.

New group additivity schemes have also been determined to approximate the Arrhenius parameters of hydrogen abstraction reactions from C-H and N-H bonds by hydrogen atoms and nitrogen- and carbon-centered radicals. A comparison with available experimental studies shows that the employed methodology using the CBS-QB3 composite method leads to accurate rate coefficients for the studied reaction families, i.e. the rate coefficients are approximated within a factor of two of the experimental values. From a dataset of 316 high-pressure limit rate coefficients calculated at the CBS-QB3 level of theory, 76 group additive values have been determined. The introduction of 14 resonance corrections is required to account for the cross-interactions between conjugating systems on the two primary atoms in the reactive center, being either a carbon or nitrogen atom.

Aside from new reaction pathways involving the heteroatom-containing functional group, the presence of a heteroatom has a significant influence on the bond strengths of nearby C-H and C-C bonds. To study the main decomposition pathways and product channels for the small hazardous species such as NH_3, NO_x, SO_x and H_2S, the relevant potential energy surfaces have been constructed. For the species and reactions important to accurately describe the pyrolysis and oxidation of the model compounds, which have been identified both before and after the model simulations via combined rate of production and sensitivity analyses, *ab initio* calculations have been performed at the CBS-QB3 level of theory.

7.1.2 Kinetic modeling with Genesys for H, C, N, O and S containing molecules

The automatic kinetic model generator Genesys has been used for the kinetic model construction for most of the model compounds in this PhD thesis. While the same procedure as for hydrocarbons can be applied, the main challenges of kinetic model generation for heteroatomic compounds are the lack of accurate thermodynamic and kinetic data as well as the identification of all relevant elementary reactions. The data scarcity has been addressed with new *ab initio* calculations and group additivity schemes that enable a fast "on-the-fly" approximation procedure. The identification of the main reaction types as input to the kinetic model generator still relies on sufficient user's knowledge of the occurring chemistry. For the compounds studied in this PhD thesis, the kinetic model generation is based on the same reaction families as for hydrocarbons under pyrolysis and oxidation conditions, as well as additional reaction types important for these compounds such as inter- and intramolecular substitution and unimolecular elimination reactions. Aside from the majority of elementary reactions belonging to a particular reaction family, reaction networks often contain a limited set of reactions that are of a more complex nature. Without any information on the potential energy surface, automatically generating these reactions is difficult, especially in the case that the number of similar known reactions is low. Therefore, an a priori exploration of the potential energy surface has been performed to investigate for example the low-temperature oxidation pathways of the aliphatic amines as well as the interaction between hydrocarbon radicals and saturated sulfur-containing compounds.

In order to describe the reactions between small hydrocarbons (C_1-C_2) with nitrogen- and sulfur-containing species, including the formation and destruction of SO_x and NO_x, two literature mechanisms of Alzueta et al. and Glarborg et al. have been used to complement the kinetic model generated by Genesys. Care should be taken when using these literature mechanisms for simulating conditions different from those used for model validation. A large number of the reactions between small nitrogen or sulfur-containing compounds and the hydrocarbon radical pool that can become important in case of a hydrocarbon matrix, i.e. corresponding to steam cracking reactions, require a detailed re-evaluation of their kinetic parameters. These reactions are for example based on an analogy with the corresponding reactions of hydrocarbons and have not yet been correctly validated.

7.1.3 Experimental validation

Different experimental datasets covering both pyrolysis and oxidation over a wide range of conditions have been used to gain insight into the thermochemical reactions of different classes of nitrogen- and sulfur-containing compounds. New experimental data has been gathered for the pyrolysis and oxidation of the aliphatic amine compound diethylamine using two different experimental units, i.e. a jet-stirred and a tubular reactor. Combined with the limited literature data available for the analogous amines dimethyl- and ethylamine reported in shock tube and laminar premixed flame studies, the first-principles based kinetic model, which includes the thermodynamic and kinetic parameters approximated with the new group additivity schemes, have been validated. In-house experimental data for the well-known sulfur-containing impurities and additives, such as dimethyl disulfide and carbonyl sulfide, has been used to investigate the influence of a hydrocarbon matrix on the reactivity and product distribution. In general, the kinetic models succeed in predicting the main experimental trends and enable the identification of the dominant reaction pathways. However, as the experimental data available for these types of heteroatomic compounds is still very scarce, a more thorough model validation with additional experimental datasets covering a wide range of conditions and also involving a hydrocarbon matrix to have more emphasis on the interactions with the hydrocarbon radical pool, is required.

7.2. Future outlook

The data scarcity for heteroatomic compounds has been addressed in this PhD thesis by providing new group additivity schemes based on an extensive dataset of *ab initio* calculations. Determination of new group additivity values to cover a broader range of functional groups, containing for example more than two heteroatoms, and reaction types, such as β-scission/radical addition and intramolecular hydrogen abstraction, is required to enable modeling of more complex species. For cyclic structures, analogies with smaller sulfur- and nitrogen-containing compounds do not provide sufficient accuracy and values based on similar reactions of hydrocarbons cannot be used due to the significant influence of the presence and position of the heteroatom on for example the bond strengths of the compounds. The datasets presented in this PhD thesis for regression of the group additive values for nitrogen-containing compounds can easily be extended to include other species and reactions for which the thermodynamic and kinetic parameters are obtained with the same methodology. This will enable the relatively fast and straightforward determination of missing group additive values,

as the framework for the derivation of the group additivity scheme has already been set in place. Although the automation procedures implemented in Genesys minimize the user involvement required to perform *ab initio* calculations significantly, the nature of the heteroatom (nitrogen, oxygen or sulfur) can introduce several challenges concerning the stereochemistry, hindered rotor profiles and so on. This can be addressed with a number of improvements on the approximations used to obtain the thermodynamic and kinetic parameters. For example, multidimensional hindered rotor (instead of 1D) approximations can be used when several rotors are strongly coupled, which is often the case for heteroatomic compounds.

Over the past few years many advances have been made in the development of the automatic kinetic model generation software tool Genesys. With the knowledge gathered from the experimentally validated kinetic models presented in this PhD thesis, Genesys can now be used for the construction of accurate kinetic models for simple sulfur- and nitrogen-containing compounds under pyrolysis or oxidation conditions. The use of automation procedures developed for an efficient exploration of the potential energy surface can help to tackle the issue of identifying reactions of a more complex nature that cannot be neglected and should be included in the kinetic model. This combination could prove to be especially useful to investigate the chemistry of larger heteroatomic compounds, including cyclic structures, for which the pyrolysis and oxidation chemistry is still relatively unknown in general. In order to enlarge the application domain of the generated kinetic models, the pressure dependence of rate coefficients can be taken into account. Currently, only high-pressure limit rate coefficients can be calculated with Genesys and the fall-off region of the rate coefficients is neglected. The inclusion of pressure dependency would open up the use of this methodology to other applications, such as combustion and atmospheric chemistry, i.e. processes in which these heteroatomic compounds also play an important role.

The new kinetic model for the aliphatic amines shows a promising agreement with the limited experimental datasets. However, the reaction pathways need to be further verified in order to generate a widely applicable model able to describe the formation of the main products over a wide range of conditions. Further validation of the kinetic model can be performed with new experimental datasets with varying conversion, dilution etc. for a set of model compounds with different carbon chain length or branching degree of the nitrogen atom. This will aid to better assess the kinetics of the sensitive reactions, including the reactions between small nitrogen-containing compounds and hydrocarbons included in the literature mechanism. This also holds true for the decomposition of the sulfur-containing compounds studied in this PhD thesis.

Additional experiments and simulations are required to better understand the thermochemical reactions of the sulfur-containing additives and impurities over a wide range of conditions.

Appendices

Appendix A

Supporting information to Chapter 3

A.1. Development of bond additivity corrections (BACs)

A.1.1. Database for regression of BACs and performance of CBS-QB3/BAC

Table A-1: Training (T) and validation (V) reference data for regression of BACs: Experimental and *ab initio* calculated (with and without BACs) standard enthalpies of formation at 298 K and the corresponding deviations, expressed in kJ mol^{-1}. The experimental database entries are taken from ATcT [1], Pedley et al. [2] and the NIST database [3].

No.		InChI	$\Delta_f H^\circ_{exp}$	Ref	$\Delta_f H^\circ_{calc}$		$\Delta_f H^\circ_{calc} - \Delta_f H^\circ_{exp}$	
					CBS-QB3	CBS-QB3 + BAC	CBS-QB3	CBS-QB3 + BAC
1	T	InChI=1S/CH3O/c1-2/h1H3	21.53 ± 0.3	[1]	18.56	21.05	-2.97	-0.48
2	T	InChI=1S/C3H8/c1-3-2/h3H2,1-2H3	-105.03 ± 0.2	[1]	-100.67	-105.35	4.36	-0.32
3	T	InChI=1S/C4H10O/c1-2-3-4-5/h5H,2-4H2,1H3	-275.00 ± 0.4	[2]	-271.20	-274.10	3.80	0.90
4	T	InChI=1S/C4H8O/c1-4(2)3-5/h3-4H,1-2H3	-215.80 ± 0.9	[2]	-211.17	-213.14	4.63	2.66
5	T	InChI=1S/C4H10S/c1-3-4-5-2/h3-4H2,1-2H3	-82.30 ± 1.0	[2]	-80.55	-81.61	1.75	0.69
6	T	InChI=1S/HNO/c1-2/h1H	106.96 ± 0.1	[1]	104.11	105.62	-2.85	-1.34
7	T	InChI=1S/C4H10O2/c1-3-5-6-4-2/h3-4H2,1-2H3	-192.80 ± 2.5	[2]	-197.30	-193.83	-4.50	-1.03
8	T	InChI=1S/C5H10/c1-3-5-4-2/h3,5H,4H2,1-2H3/b5-3+	-31.90 ± 1.1	[2]	-21.42	-28.47	10.48	3.43
9	T	InChI=1S/C2H2O/c1-2-3/h1,3H	92.80 ± 1.5	[1]	94.14	96.27	1.34	3.47
10	T	InChI=1S/CH3N/c1-2/h2H,1H2	88.60 ± 0.6	[1]	90.00	88.55	1.40	-0.05
11	T	InChI=1S/C4H10S/c1-3-4(2)5/h4-5H,3H2,1-2H3	-96.90 ± 0.9	[2]	-96.90	-98.64	0.00	-1.74
12	T	InChI=1S/C5H10/c1-2-4-5-3-1/h1-5H2	-77.58 ± 0.4	[1]	-66.92	-75.08	10.66	2.50
13	T	InChI=1S/C6H12/c1-4-5-6(2)3/h2,4-5H2,1,3H3	-59.40 ± 1.3	[2]	-44.87	-53.56	14.53	5.84
14	T	InChI=1S/C5H6S/c1-5-3-2-4-6-5/h2-4H,1H3	84.35 ± 0.9	[3]	82.60	81.46	-1.75	-2.89
15	T	InChI=1S/C6H14/c1-5(2)6(3)4/h5-6H,1-4H3	-178.30 ± 1.0	[2]	-167.65	-177.22	10.65	1.08
16	T	InChI=1S/CH4O2/c1-3-2/h2H,1H3	-127.72 ± 0.8	[1]	-134.74	-130.04	-7.02	-2.32
17	T	InChI=1S/C9H12/c1-8(2)9-6-4-3-5-7-9/h3-8H,1-2H3	3.90 ± 1.1	[3]	13.43	1.40	9.53	-2.50
18	T	InChI=1S/CHO/c1-2/h1H	41.80 ± 0.1	[1]	41.21	44.58	-0.59	2.78
19	T	InChI=1S/C3H8S2/c1-3(5)2-4/h3-5H,2H2,1H3	-29.70 ± 1.3	[2]	-31.20	-26.74	-1.50	2.96
20	T	InChI=1S/C4H11N/c1-3-5-4-2/h5H,3-4H2,1-2H3	-72.50 ± 1.2	[2]	-63.20	-69.27	9.30	3.23
21	T	InChI=1S/C3H5NO/c1-5-3-2-4/h3H2,1H3	-35.65 ± 0.7	[3]	-37.73	-33.95	-2.08	1.70
22	T	InChI=1S/C7H16/c1-3-5-7-6-4-2/h3-7H2,1-2H3	-187.53 ± 0.5	[1]	-173.90	-185.10	13.63	2.43
23	T	InChI=1S/C4H9/c1-4(2)3/h1-3H3	50.30 ± 0.7	[1]	56.04	50.17	5.74	-0.13
24	T	InChI=1S/CH4O2/c2-1-3/h2-3H,1H2	-393.25 ± 1.1	[1]	-398.39	-392.98	-5.14	0.27
25	T	InChI=1S/C7H16/c1-6(2)5-7(3)4/h6-7H,5H2,1-4H3	-201.70 ± 1.1	[2]	-190.44	-201.64	11.26	0.06

26	T	InChI=1S/C2H4S/c1-2-3-1/h1-2H2	82.00	±	1.3	[2]	75.88	77.86	-6.12	-4.14
27	T	InChI=1S/C5H12O/c1-3-4-5(2)6/h5-6H,3-4H2,1-2H3	-312.70	±	1.7	[2]	-309.80	-314.33	2.90	-1.63
28	T	InChI=1S/CH4N/c1-2/h1-2H2	148.51	±	0.4	[1]	153.70	151.28	5.19	2.77
29	T	InChI=1S/C2H2O2/c3-1-2-4/h1-2H	-212.00	±	0.8	[2]	-218.68	-213.04	-6.68	-1.04
30	T	InChI=1S/C6H15N/c1-3-5-7-6-4-2/h7H,3-6H2,1-2H3	-116.10	±	0.5	[2]	-103.30	-112.64	12.80	3.46
31	T	InChI=1S/C4H8/c1-4-2-3-4/h4H,2-3H2,1H3	24.30	±	1.3	[1]	32.01	25.48	7.71	1.18
32	T	InChI=1S/C3H5N/c1-2-3-4/h2H2,1H3	51.50	±	0.6	[2]	60.80	57.50	9.30	6.00
33	T	InChI=1S/C6H14/c1-4-6(3)5-2/h6H,4-5H2,1-3H3	-172.10	±	1.0	[2]	-161.37	-170.94	10.73	1.16
34	T	InChI=1S/C5H6/c1-2-4-5-3-1/h1-4H,5H2	132.76	±	0.8	[1]	144.82	138.43	12.06	5.67
35	T	InChI=1S/C2H6S/c1-2-3/h3H,2H2,1H3	-46.30	±	0.6	[2]	-48.60	-47.08	-2.30	-0.78
36	T	InChI=1S/C8H10/c1-7-3-5-8(2)6-4-7/h3-6H,1-2H3	18.00	±	1.0	[2]	25.15	14.75	7.15	-3.25
37	T	InChI=1S/C6H10/c1-3-5-6-4-2/h1H,4-6H2,2H3	122.30	±	1.2	[3]	134.41	126.61	12.11	4.31
38	T	InChI=1S/C5H10O/c1-3-4-5(2)6/h3-4H2,1-2H3	-259.00	±	1.0	[2]	-255.27	-258.87	3.73	0.13
39	T	InChI=1S/C3H3/c1-2-3-1/h1H,2H2	523.53	±	0.7	[1]	530.08	526.51	6.55	2.98
40	T	InChI=1S/CHO2/c2-1-3/h(H,2,3)	-183.93	±	0.5	[1]	-186.63	-179.85	-2.70	4.08
41	T	InChI=1S/C3H8O/c1-2-3-4/h4H,2-3H2,1H3	-255.22	±	0.3	[1]	-254.24	-255.51	0.98	-0.29
42	T	InChI=1S/C2H6O2/c1-3-4-2/h1-2H3	-125.70	±	1.3	[2]	-131.72	-124.98	-6.02	0.72
43	T	InChI=1S/C3H6/c1-2-3-1/h1-3H2	53.65	±	0.5	[1]	59.96	55.07	6.31	1.42
44	T	InChI=1S/C4H4N2/c1-2-6-4-3-5-1/h1-4H	195.80	±	1.5	[3]	203.90	201.55	8.10	5.75
45	T	InChI=1S/C5H8/c1-3-5-4-2/h5H,1,4H2,2H3	140.70	±	0.7	[2]	150.22	144.05	9.52	3.35
46	T	InChI=1S/C5H10O/c1-4(2)5(3)6/h4H,1-3H3	-262.50	±	0.9	[2]	-259.52	-263.12	2.98	-0.62
47	T	InChI=1S/C5H12O2/c1-5(2,6-3)7-4/h1-4H3	-429.30	±	2.3	[2]	-440.70	-434.47	-11.40	-5.17
48	T	InChI=1S/C5H10/c1-4-5(2)3/h2,4H2,1,3H3	-35.30	±	1.0	[2]	-26.76	-33.81	8.54	1.49
49	T	InChI=1S/C2N2/c3-1-2-4	310.18	±	0.4	[1]	312.81	312.52	2.63	2.34
50	T	InChI=1S/C4H4O2/c5-4-2-1-3-6-4/h1-2H,3H2	-257.20	±	1.6	[2]	-262.14	-256.36	-4.94	0.84
51	T	InChI=1S/C8H18/c1-7(2,3)8(4,5)6/h1-6H3	-225.60	±	1.4	[2]	-218.02	-230.85	7.58	-5.25
52	T	InChI=1S/C2H3O/c1-2-3/h2H,1H2	15.62	±	0.8	[1]	13.82	15.56	-1.80	-0.06
53	T	InChI=1S/C6H12O2/c1-6(2,3)5(7)8-4/h1-4H3	-494.30	±	1.3	[2]	-492.50	-490.65	1.80	3.65
54	T	InChI=1S/C4H10S/c1-4(2,3)5/h5H,1-3H3	-109.60	±	0.9	[2]	-111.90	-113.64	-2.30	-4.04
55	T	InChI=1S/C3H6O/c1-3(2)4/h1-2H3	-216.14	±	0.3	[1]	-216.30	-216.64	-0.16	-0.50
56	T	InChI=1S/C6H12/c1-2-4-6-5-3-1/h1-6H2	-123.15	±	0.4	[1]	-113.01	-122.80	10.14	0.35
57	T	InChI=1S/C3H4/c1-3-2/h1-2H2	189.86	±	0.3	[1]	195.23	192.32	5.37	2.46
58	T	InChI=1S/C3H8S/c1-3(2)4/h3-4H,1-2H3	-76.20	±	0.7	[2]	-77.64	-77.75	-1.44	-1.55
59	T	InChI=1S/C3H8S/c1-3-4-2/h3H2,1-2H3	-59.60	±	1.2	[2]	-60.79	-60.22	-1.19	-0.62
60	T	InChI=1S/C2H6S/c1-3-2/h1-2H3	-37.50	±	0.6	[2]	-39.54	-37.34	-2.04	0.16
61	T	InChI=1S/C5H12O/c1-3-5-6-4-2/h3-5H2,1-2H3	-272.20	±	1.1	[2]	-271.34	-272.20	0.86	0.00
62	T	InChI=1S/C4H8/c1-3-4-2/h3-4H,1-2H3/b4-3-	-7.07	±	0.4	[1]	1.53	-3.89	8.60	3.18
63	T	InChI=1S/C2H6S2/c1-3-4-2/h1-2H3	-24.20	±	1.0	[2]	-29.03	-20.37	-4.83	3.83
64	T	InChI=1S/CH4S/c1-2/h2H,1H3	-22.90	±	0.7	[2]	-25.70	-22.54	-2.80	0.36
65	T	InChI=1S/C3H6O/c1-2-3-4/h3H,2H2,1H3	-185.60	±	0.6	[2]	-185.76	-186.10	-0.16	-0.50
66	T	InChI=1S/C4H10S2/c1-3-5-6-4-2/h3-4H2,1-2H3	-74.70	±	1.0	[2]	-75.90	-70.50	-1.20	4.20

67	T	InChI=1S/H3NO/c1-2/h2H,1H2	-43.61	±	0.5	[1]	-46.13	-46.08	-2.52	-2.47
68	T	InChI=1S/CH4N2O/c2-1(3)4/h(H4,2,3,4)	-235.50	±	1.2	[3]	-234.98	-234.47	0.52	1.03
69	T	InChI=1S/C5H12S/c1-3-4-5-6-2/h3-5H2,1-2H3	-102.20	±	1.1	[2]	-100.37	-103.06	1.83	-0.86
70	T	InChI=1S/CH2N/c1-2/h1-2H	272.22	±	0.7	[1]	274.42	273.41	2.20	1.19
71	T	InChI=1S/C5H10O/c1-2-3-4-5-6/h5H,2-4H2,1H3	-228.50	±	1.7	[2]	-222.35	-225.95	6.15	2.55
72	T	InChI=1S/CH4N2S/c2-1(3)4/h(H4,2,3,4)	22.90	±	1.6	[3]	15.92	17.59	-6.98	-5.31
73	T	InChI=1S/C4H8O/c1-3-4(2)5/h3H2,1-2H3	-238.70	±	0.5	[2]	-236.14	-238.11	2.56	0.59
74	T	InChI=1S/C3H6O2/c1-3(4)5-2/h1-2H3	-411.90	±	1.6	[2]	-417.58	-410.83	-5.68	1.07
75	T	InChI=1S/C3H6/c1-3-2/h3H,1H2,2H3	19.99	±	0.2	[1]	25.64	21.85	5.65	1.86
76	T	InChI=1S/C5H12O3/c1-5(6-2,7-3)8-4/h1-4H3	-572.40	±	2.3	[2]	-586.86	-573.55	-14.46	-1.15
77	T	InChI=1S/C2H4O/c1-2-3/h2-3H,1H2	-123.86	±	0.7	[1]	-123.11	-121.86	0.75	2.00
78	T	InChI=1S/C7H14O2/c1-3-5-6-7(8)9-4-2/h3-6H2,1-2H3	-506.90	±	2.8	[2]	-507.88	-507.66	-0.98	-0.76
79	T	InChI=1S/C6H14S/c1-3-5-7-6-4-2/h3-6H2,1-2H3	-125.30	±	0.9	[2]	-122.30	-126.62	3.00	-1.32
80	T	InChI=1S/C4H10S/c1-4(2)5-3/h4H,1-3H3	-90.50	±	0.8	[2]	-89.96	-91.02	0.54	-0.52
81	T	InChI=1S/C4H8O/c1-3-5-4-2/h3H,1,4H2,2H3	-140.80	±	0.9	[2]	-139.52	-137.86	1.28	2.94
82	T	InChI=1S/C4H8O/c1-2-3-4-5/h4H,2-3H2,1H3	-204.90	±	1.1	[2]	-203.69	-205.66	1.21	-0.76
83	T	InChI=1S/C2H4/c1-2/h1-2H2	52.45	±	0.1	[1]	55.86	53.70	3.41	1.25
84	T	InChI=1S/C7H10N2/c1-9(8)7-5-3-2-4-6-7/h2-6H,8H2,1H3	210.80	±	1.7	[3]	213.06	206.69	2.26	-4.11
85	T	InChI=1S/C2H3/c1-2/h1H,2H2	296.91	±	0.3	[1]	300.59	298.87	3.68	1.96
86	T	InChI=1S/C4H6O3/c1-3(5)7-4(2)6/h1-2H3	-572.50	±	1.5	[2]	-584.56	-575.10	-12.06	-2.60
87	T	InChI=1S/C4H4N2/c1-2-4-6-5-3-1/h1-4H	278.40	±	1.3	[3]	280.50	280.09	2.10	1.69
88	T	InChI=1S/C2H5/c1-2/h1H2,2H3	119.86	±	0.3	[1]	124.38	121.78	4.52	1.92
89	T	InChI=1S/C3H8O/c1-3(2)4/h3-4H,1-2H3	-272.87	±	0.3	[1]	-272.96	-274.23	-0.09	-1.36
90	T	InChI=1S/C4H2N2/c5-3-1-2-4-6/h1-2H/b2-1+	340.20	±	1.9	[2]	346.22	343.55	6.02	3.35
91	T	InChI=1S/C2H6O/c1-3-2/h1-2H3	-184.01	±	0.5	[1]	-188.28	-184.24	-4.27	-0.23
92	T	InChI=1S/C6H12/c1-5(2)6(3)4/h1-4H3	-68.20	±	1.1	[2]	-55.04	-63.73	13.16	4.47
93	T	InChI=1S/C2H5N/c1-2-3-1/h3H,1-2H2	123.40	±	1.9	[2]	130.50	127.47	7.10	4.07
94	T	InChI=1S/C9H12/c1-3-9-6-4-5-8(2)7-9/h4-7H,3H2,1-2H3	-1.90	±	1.2	[3]	6.92	-5.11	8.82	-3.21
95	T	InChI=1S/C3H9N/c1-2-3-4/h2-4H2,1H3	-70.20	±	0.4	[2]	-63.30	-69.43	6.90	0.77
96	T	InChI=1S/C6H12/c1-5(2)6(3)4/h6H,1H2,2-4H3	-62.60	±	1.3	[2]	-49.81	-58.50	12.79	4.10
97	T	InChI=1S/H2O/h1H2	-241.83	±	0.0	[1]	-242.99	-243.03	-1.16	-1.20
98	T	InChI=1S/C5H8/c1-3-5-4-2/h1H,4-5H2,2H3	144.30	±	2.1	[3]	154.31	148.14	10.01	3.84
99	T	InChI=1S/C4H10O/c1-3-4(2)5/h4-5H,3H2,1-2H3	-292.90	±	0.7	[2]	-290.50	-293.40	2.40	-0.50
100	T	InChI=1S/CH3O/c1-2/h2H,1H2	-16.56	±	0.3	[1]	-16.92	-14.48	-0.36	2.08
101	T	InChI=1S/C3H5/c1-3-2/h1H2,2H3	252.56	±	0.8	[1]	257.53	254.18	4.97	1.62
102	T	InChI=1S/C5H12S/c1-4-6-5(2)3/h5H,4H2,1-3H3	-117.20	±	2.4	[2]	-110.58	-113.27	6.62	3.93
103	T	InChI=1S/CH4O/c1-2/h2H,1H3	-200.71	±	0.2	[1]	-203.66	-201.66	-2.95	-0.95
104	T	InChI=1S/C5H12O/c1-3-4-5-6-2/h3-5H2,1-2H3	-258.10	±	1.2	[2]	-257.48	-258.34	0.62	-0.24
105	T	InChI=1S/C7H8O/c1-8-7-5-3-2-4-6-7/h2-6H,1H3	-72.30	±	1.2	[3]	-69.28	-70.97	3.02	1.33
106	T	InChI=1S/H2N2/c1-2/h1-2H	200.21	±	0.4	[1]	201.56	202.76	1.35	2.55
107	T	InChI=1S/C3H10N2/c1-3(5)2-4/h3H,2,4-5H2,1H3	-61.62	±	0.5	[2]	-51.40	-58.98	10.22	2.64

108	T	InChI=1S/C2H5NO/c1-2(3)4/h1H3,(H2,3,4)	-238.33	±	0.8	[3]	-236.93	-236.60	1.40	1.73
109	T	InChI=1S/C7H8S/c1-8-7-5-3-2-4-6-7/h2-6H,1H3	97.28	±	0.8	[3]	98.59	95.07	1.31	-2.21
110	T	InChI=1S/C6H14S/c1-2-3-4-5-6-7/h7H,2-6H2,1H3	-129.90	±	1.0	[2]	-123.24	-128.24	6.66	1.66
111	T	InChI=1S/C4H8O2/c1-3-6-4(2)5/h3H2,1-2H3	-444.10	±	0.6	[2]	-449.27	-444.15	-5.17	-0.05
112	T	InChI=1S/C4H4N2/c5-3-1-2-4-6/h1-2H2	209.70	±	0.7	[2]	217.54	213.99	7.84	4.29
113	T	InChI=1S/C3H5/c1-3-2/h1,3H,2H3	267.19	±	0.8	[1]	272.86	269.51	5.67	2.32
114	T	InChI=1S/C8H10/c1-7-4-3-5-8(2)6-7/h3-6H,1-2H3	17.20	±	0.8	[2]	25.31	14.91	8.11	-2.29
115	T	InChI=1S/CH2O3/c2-1(3)4/h(H2,2,3,4)	-612.96	±	0.8	[1]	-618.85	-609.10	-5.89	3.86
116	T	InChI=1S/C3H7/c1-3-2/h3H,1-2H3	88.86	±	0.6	[1]	93.39	89.16	4.53	0.30
117	T	InChI=1S/C8H18O/c1-2-3-4-5-6-7-8-9/h9H,2-8H2,1H3	-355.50	±	0.8	[2]	-346.70	-356.12	8.80	-0.62
118	T	InChI=1S/C5H8/c1-4-5(2)3/h4H,1-2H2,3H3	75.50	±	1.1	[2]	86.20	80.03	10.70	4.53
119	T	InChI=1S/C6H12/c1-3-5-6-4-2/h3,5H,4,6H2,1-2H3/b5-3+	-53.90	±	1.6	[2]	-40.55	-49.24	13.35	4.66
120	T	InChI=1S/CN/c1-2	440.00	±	0.2	[1]	446.10	446.51	6.10	6.51
121	T	InChI=1S/C6H12/c1-4-6(3)5-2/h3-5H2,1-2H3	-56.00	±	1.5	[2]	-43.94	-52.63	12.06	3.37
122	T	InChI=1S/C4H5N/c5-3-4-1-2-4/h4H,1-2H2	182.70	±	0.7	[3]	184.23	179.08	1.53	-3.62
123	T	InChI=1S/C6H14/c1-3-5-6-4-2/h3-6H2,1-2H3	-166.93	±	0.3	[1]	-155.50	-165.07	11.43	1.86
124	T	InChI=1S/C4H11N/c1-3-4(2)5/h4H,3,5H2,1-2H3	-104.90	±	1.0	[2]	-95.70	-103.46	9.20	1.44
125	T	InChI=1S/C5H12S/c1-2-3-4-5-6/h6H,2-5H2,1H3	-110.10	±	1.1	[2]	-104.79	-108.16	5.31	1.94
126	T	InChI=1S/C6H12/c1-4-5-6(2)3/h4,6H,1,5H2,2-3H3	-51.30	±	1.8	[2]	-38.04	-46.73	13.26	4.57
127	T	InChI=1S/C8H6S/c1-2-4-8-7(3-1)5-6-9-8/h1-6H	166.28	±	0.5	[3]	168.00	163.51	1.72	-2.77
128	T	InChI=1S/H2N/h1H2	186.00	±	0.1	[1]	188.50	188.50	2.50	2.50
129	T	InChI=1S/C4H10/c1-4(2)3/h4H,1-3H3	-134.78	±	0.3	[1]	-128.31	-134.62	6.47	0.16
130	T	InChI=1S/C7H8O/c8-6-7-4-2-1-3-5-7/h1-5,8H,6H2	-94.60	±	3.0	[2]	-91.24	-96.60	3.36	-2.00
131	T	InChI=1S/C4H11N/c1-2-3-4-5/h2-5H2,1H3	-92.00	±	1.2	[2]	-81.30	-89.06	10.70	2.94
132	T	InChI=1S/C6H6S/c7-6-4-2-1-3-5-6/h1-5,7H	112.40	±	0.9	[2]	111.90	109.33	-0.50	-3.07
133	T	InChI=1S/C7H16/c1-5-7(3,4)6-2/h5-6H2,1-4H3	-201.20	±	1.1	[2]	-188.54	-199.74	12.66	1.46
134	T	InChI=1S/C4H10O/c1-3-5-4-2/h3-4H2,1-2H3	-252.10	±	0.8	[2]	-251.71	-250.93	0.39	1.17
135	T	InChI=1S/C4H2/c1-3-4-2/h1-2H	460.05	±	0.8	[1]	467.43	464.66	7.38	4.61
136	T	InChI=1S/C6H14/c1-5-6(2,3)4/h5H2,1-4H3	-186.10	±	1.0	[2]	-176.88	-186.45	9.22	-0.35
137	T	InChI=1S/H2S/h1H2	-20.60	±	0.5	[3]	-25.31	-21.20	-4.71	-0.60
138	T	InChI=1S/C4H8O2/c1-2-3-4(5)6/h2-3H2,1H3,(H,5,6)	-475.80	±	4.1	[2]	-473.55	-472.11	2.25	3.69
139	T	InChI=1S/C3H5/c1-2-3-1/h1H,2-3H2	290.20	±	1.6	[1]	299.04	294.59	8.84	4.39
140	T	InChI=1S/C4H9/c1-3-4-2/h1,3-4H2,2H3	80.23	±	0.7	[1]	87.74	81.87	7.51	1.64
141	T	InChI=1S/C5H12S/c1-5(2)3-4-6/h5-6H,3-4H2,1-2H3	-114.90	±	1.2	[2]	-112.72	-116.09	2.18	-1.19
142	T	InChI=1S/C4H8/c1-3-4-2/h3H,1,4H2,2H3	-0.08	±	0.4	[1]	7.81	2.39	7.89	2.47
143	T	InChI=1S/C4H6/c1-4-2-3-4/h1-3H2	200.50	±	1.8	[1]	200.22	194.58	-0.28	-5.92
144	T	InChI=1S/CH4N/c1-2/h2H,1H3	177.10	±	1.7	[1]	181.00	179.11	3.90	2.01
145	T	InChI=1S/C5H8/c1-3-5-4-2/h3-5H,1H2,2H3/b5-4+	76.10	±	0.9	[2]	88.52	82.35	12.42	6.25
146	T	InChI=1S/C2H4O2/c1-2(3)4/h1H3,(H,3,4)	-432.50	±	3.0	[1]	-435.23	-430.52	-2.73	1.98
147	T	InChI=1S/C9H12/c1-3-9-7-5-4-6-8(9)2/h4-7H,3H2,1-2H3	1.20	±	1.2	[3]	9.25	-2.78	8.05	-3.98
148	T	InChI=1S/H4N2/c1-2/h1-2H2	97.68	±	0.5	[1]	100.02	99.27	2.34	1.59

149	T	InChI=1S/C4H8/c1-4(2)3/h1H2,2-3H3	-17.15	±	0.4	[1]	-9.35	-14.77	7.80	2.38
150	T	InChI=1S/C4H11N/c1-4(2)3-5/h4H,3,5H2,1-2H3	-98.70	±	0.5	[2]	-90.40	-98.16	8.30	0.54
151	T	InChI=1S/C8H18S2/c1-7(2,3)9-10-8(4,5)6/h1-6H3	-202.00	±	2.3	[2]	-205.10	-206.22	-3.10	-4.22
152	T	InChI=1S/C2H7N/c1-3-2/h3H,1-2H3	-18.60	±	0.5	[1]	-14.80	-17.61	3.80	0.99
153	T	InChI=1S/C4H7N/c1-2-3-4-5/h2-3H2,1H3	33.60	±	1.0	[2]	39.00	34.07	5.40	0.47
154	T	InChI=1S/C6H14O/c1-3-5-7-6-4-2/h3-6H2,1-2H3	-292.90	±	1.1	[2]	-291.26	-293.75	1.64	-0.85
155	T	InChI=1S/HNO2/c2-1-3/h(H,2,3)	-79.17	±	0.1	[1]	-83.44	-78.96	-4.27	0.21
156	T	InChI=1S/C5H8/c1-3-5-4-2/h3H2,1-2H3	128.90	±	2.1	[3]	137.44	131.27	8.54	2.37
157	T	InChI=1S/C6H14S/c1-3-5-6-7-4-2/h3-6H2,1-2H3	-127.10	±	2.4	[2]	-120.28	-124.60	6.82	2.50
158	T	InChI=1S/C7H16O/c1-6(2)8-7(3,4)5/h6H,1-5H3	-357.60	±	5.1	[2]	-354.95	-359.07	2.65	-1.47
159	T	InChI=1S/C2H2/c1-2/h1-2H	228.28	±	0.1	[1]	234.41	233.13	6.13	4.85
160	T	InChI=1S/C4H10S/c1-3-5-4-2/h3-4H2,1-2H3	-83.60	±	0.8	[2]	-82.18	-83.24	1.42	0.36
161	T	InChI=1S/C6H12O2/c1-3-5-6(7)8-4-2/h3-5H2,1-2H3	-485.00	±	1.0	[3]	-486.95	-485.10	-1.95	-0.10
162	T	InChI=1S/C6H10/c1-5-6(2,3)4/h1H,2-4H3	107.00	±	1.3	[3]	117.75	109.95	10.75	2.95
163	T	InChI=1S/C2HO/c1-2-3/h1H	177.97	±	0.6	[1]	179.48	182.10	1.51	4.13
164	T	InChI=1S/C2H5NO/c1-2-3-4/h2,4H,1H3	-22.55	±	0.3	[3]	-19.67	-19.78	2.88	2.77
165	T	InChI=1S/CH2O2/c1-2-3-1/h1H2	1.74	±	0.6	[1]	-6.18	1.97	-7.92	0.23
166	T	InChI=1S/C2H6/c1-2/h1-2H3	-83.91	±	0.1	[1]	-81.85	-84.89	2.06	-0.98
167	T	InChI=1S/C5H12/c1-4-5(2)3/h5H,4H2,1-3H3	-153.27	±	0.4	[1]	-145.24	-153.18	8.03	0.09
168	T	InChI=1S/CH5N/c1-2/h2H2,1H3	-21.10	±	0.3	[1]	-19.50	-22.36	1.60	-1.26
169	T	InChI=1S/C6H12O2/c1-3-4-5-6(7)8-2/h3-5H2,1-2H3	-471.20	±	0.9	[2]	-476.86	-475.01	-5.66	-3.81
170	T	InChI=1S/C6H14S/c1-3-4-5-6-7-2/h3-6H2,1-2H3	-121.90	±	2.4	[2]	-114.57	-118.89	7.33	3.01
171	T	InChI=1S/C6H12/c1-5-6(2,3)4/h5H,1H2,2-4H3	-60.50	±	1.3	[2]	-49.50	-58.19	11.00	2.31
172	T	InChI=1S/CH2O/c1-2/h1H2	-109.19	±	0.1	[1]	-113.53	-110.60	-4.34	-1.41
173	T	InChI=1S/C7H14O/c1-2-3-4-5-6-7-8/h7H,2-6H2,1H3	-263.80	±	4.0	[2]	-260.13	-266.99	3.67	-3.19
174	T	InChI=1S/C3H9N/c1-4(2)3/h1-3H3	-24.10	±	0.9	[1]	-24.30	-27.06	-0.20	-2.96
175	T	InChI=1S/N2O/c1-2-3-1	349.80	±	1.7	[1]	344.03	351.21	-5.77	1.41
176	T	InChI=1S/CH3O2/c1-3-2/h1H3	12.54	±	0.5	[1]	7.95	13.13	-4.59	0.59
177	T	InChI=1S/C6H6O/c7-6-4-2-1-3-5-6/h1-5,7H	-93.12	±	0.7	[1]	-88.30	-92.03	4.82	1.09
178	T	InChI=1S/C6H10/c1-3-5-6-4-2/h3-4H,1-2,5-6H2	83.79	±	0.4	[1]	97.51	89.71	13.72	5.92
179	T	InChI=1S/C2H3O/c1-2-3/h1H3	-9.97	±	0.4	[1]	-9.77	-8.03	0.20	1.94
180	T	InChI=1S/C5H8/c1-2-4-5-3-1/h1-2H,3-5H2	33.85	±	0.5	[1]	45.05	37.78	11.20	3.93
181	T	InChI=1S/CH4/h1H4	-74.52	±	0.1	[1]	-74.17	-75.58	0.35	-1.06
182	T	InChI=1S/C5H12S/c1-5(2,3)4-6/h6H,4H2,1-3H3	-129.00	±	1.0	[2]	-125.54	-128.91	3.46	0.09
183	T	InChI=1S/H3N/h1H3	-45.60	±	0.0	[1]	-43.90	-46.82	1.70	-1.22
184	T	InChI=1S/C10H14/c1-10(2,3)9-7-5-4-6-8-9/h4-8H,1-3H3	-22.70	±	1.4	[3]	-12.20	-25.86	10.50	-3.16
185	T	InChI=1S/C5H12S/c1-3-5(2)4-6/h5-6H,3-4H2,1-2H3	-115.10	±	1.0	[2]	-111.64	-115.01	3.46	0.09
186	T	InChI=1S/C5H12S/c1-5(2,3)6-4/h1-4H3	-121.30	±	0.8	[2]	-122.49	-125.18	-1.19	-3.88
187	T	InChI=1S/C4H6/c1-3-4-2/h4H,1H2,2H3	162.30	±	0.6	[2]	169.60	165.06	7.30	2.76
188	T	InChI=1S/C5H10O/c1-3-5(6)4-2/h3-4H2,1-2H3	-257.90	±	0.8	[2]	-255.75	-259.35	2.15	-1.45
189	T	InChI=1S/C8H18N2/c1-7(2,3)9-10-8(4,5)6/h1-6H3	-36.40	±	2.8	[3]	-32.63	-41.12	3.77	-4.72

190	T	InChI=1S/C7H14O/c1-5-6(8)7(2,3)4/h5H2,1-4H3	-313.70	±	1.4	[2]	-309.82	-316.68	3.88	-2.98
191	T	InChI=1S/C3H7/c1-3-2/h1,3H2,2H3	100.81	±	0.6	[1]	106.77	102.54	5.96	1.73
192	T	InChI=1S/C5H12S2/c6-4-2-1-3-5-7/h6-7H,1-5H2	-71.00	±	1.4	[2]	-67.70	-66.50	3.30	4.50
193	T	InChI=1S/C7H16/c1-6(2)7(3,4)5/h6H,1-5H3	-204.50	±	1.3	[2]	-195.70	-206.90	8.80	-2.40
194	T	InChI=1S/C8H18/c1-3-5-7-8-6-4-2/h3-8H2,1-2H3	-208.27	±	0.7	[1]	-193.66	-206.49	14.61	1.78
195	T	InChI=1S/C6H12/c1-6-4-2-3-5-6/h6H,2-5H2,1H3	-106.20	±	0.8	[1]	-96.10	-105.89	10.10	0.31
196	T	InChI=1S/C6H12O2/c1-2-3-4-5-6(7)8/h2-5H2,1H3,(H,7,8)	-511.90	±	2.3	[2]	-511.50	-513.32	0.40	-1.42
197	T	InChI=1S/CO2/c2-1-3	-393.48	±	0.0	[1]	-399.80	-392.53	-6.32	0.94
198	T	InChI=1S/C7H16/c1-4-6-7(3)5-2/h7H,4-6H2,1-3H3	-191.30	±	1.0	[2]	-179.87	-191.07	11.43	0.23
199	T	InChI=1S/C5H11N/c1-2-4-6-5-3-1/h6H,1-5H2	-47.15	±	0.6	[3]	-41.80	-49.72	5.35	-2.57
200	T	InChI=1S/C7H14O2/c1-2-3-4-5-6-7(8)9/h2-6H2,1H3,(H,8,9)	-536.20	±	2.1	[2]	-529.32	-532.77	6.88	3.43
201	T	InChI=1S/C6H12O/c1-4-6(7)5(2)3/h5H,4H2,1-3H3	-286.10	±	1.0	[2]	-281.87	-287.10	4.23	-1.00
202	T	InChI=1S/C6H10/c1-5(2)6(3)4/h1,3H2,2,4H3	45.10	±	1.1	[2]	56.75	48.95	11.65	3.85
203	T	InChI=1S/C4H5N/c1-2-4-5-3-1/h1-5H	108.30	±	0.5	[3]	113.09	108.56	4.79	0.26
204	T	InChI=1S/C5H12O/c1-2-3-4-5-6/h6H,2-5H2,1H3	-294.70	±	0.5	[2]	-290.70	-295.23	4.00	-0.53
205	T	InChI=1S/CS2/c2-1-3	117.10	±	0.8	[3]	108.49	115.33	-8.61	-1.77
206	T	InChI=1S/C6H12/c1-3-5-6-4-2/h5-6H,3-4H2,1-2H3/b6-5-	-47.60	±	1.3	[2]	-34.58	-43.27	13.02	4.33
207	T	InChI=1S/C6H5O/c7-6-4-2-1-3-5-6/h1-5H	56.08	±	0.9	[1]	58.00	54.76	1.92	-1.32
208	T	InChI=1S/C3H9N/c1-3(2)4/h3H,4H2,1-2H3	-83.80	±	0.6	[2]	-80.66	-86.79	3.14	-2.99
209	T	InChI=1S/C2H6S2/c3-1-2-4/h3-4H,1-2H2	-9.70	±	1.1	[2]	-15.80	-9.71	-6.10	-0.01
210	T	InChI=1S/C4H8/c1-3-4-2/h3-4H,1-2H3/b4-3+	-11.17	±	0.4	[1]	-3.56	-8.98	7.61	2.19
211	T	InChI=1S/C3H4/c1-3-2/h1H,2H3	185.74	±	0.3	[1]	191.97	189.06	6.23	3.32
212	T	InChI=1S/C5H10O2/c1-4(2)7-5(3)6/h4H,1-3H3	-481.70	±	0.8	[2]	-485.80	-482.32	-4.10	-0.62
213	T	InChI=1S/HO/h1H	37.49	±	0.0	[1]	37.33	37.77	-0.16	0.28
214	T	InChI=1S/C8H8/c1-2-8-6-4-3-5-7-8/h2-7H,1H2	148.33	±	0.6	[1]	159.50	149.98	11.17	1.65
215	T	InChI=1S/C2H3O/c1-2-3-1/h1H,2H2	164.50	±	1.4	[1]	165.05	169.31	0.55	4.81
216	T	InChI=1S/C4H6/c1-3-4-2/h1H,4H2,2H3	165.77	±	0.7	[1]	175.27	170.73	9.50	4.96
217	T	InChI=1S/C2H5O/c1-2-3/h2H2,1H3	-12.74	±	0.5	[1]	-13.26	-12.41	-0.52	0.33
218	T	InChI=1S/C6H10/c1-3-5-6-4-2/h3-4H2,1-2H3	105.40	±	1.9	[3]	119.78	111.98	14.38	6.58
219	T	InChI=1S/C5H8/c1-5-3-2-4-5/h1-4H2	121.50	±	0.7	[1]	131.92	124.65	10.42	3.15
220	T	InChI=1S/C6H12/c1-4-5-6(2)3/h4-6H,1-3H3/b5-4+	-61.50	±	1.4	[2]	-47.91	-56.60	13.59	4.90
221	T	InChI=1S/C2H2O/c1-2-3/h1H2	-48.57	±	0.1	[1]	-47.91	-45.73	0.66	2.84
222	T	InChI=1S/NO/c1-2	91.12	±	0.1	[1]	87.14	89.63	-3.98	-1.49
223	T	InChI=1S/C2H4O/c1-2-3/h2H,1H3	-165.45	±	0.3	[1]	-166.81	-165.51	-1.36	-0.06
224	T	InChI=1S/C5H10S/c1-3-5-6-4-2/h3H,1,4-5H2,2H3	17.80	±	2.8	[2]	19.23	17.42	1.43	-0.38
225	T	InChI=1S/H2O3/c1-3-2/h1-2H	-90.27	±	0.7	[1]	-99.27	-93.91	-9.00	-3.64
226	T	InChI=1S/C4H10O/c1-3-4-5-2/h3-4H2,1-2H3	-238.20	±	0.7	[2]	-240.35	-239.57	-2.15	-1.37
227	T	InChI=1S/C3H4O/c1-2-3-4/h2-3H,1H2	-65.40	±	1.0	[2]	-63.37	-62.82	2.03	2.58
228	T	InChI=1S/C4H10/c1-3-4-2/h3-4H2,1-2H3	-125.94	±	0.3	[1]	-118.94	-125.25	7.00	0.69
229	T	InChI=1S/C4H9N/c1-2-4-5-3-1/h5H,1-4H2	-3.40	±	1.0	[3]	2.93	-3.36	6.33	0.04
230	T	InChI=1S/C5H10/c1-4-5(2)3/h4H,1-3H3	-41.80	±	1.1	[2]	-32.27	-39.32	9.53	2.48

231	T	InChI=1S/CHN/c1-2/h1H	129.30	±	0.1	[1]	132.90	132.86	3.60	3.56
232	T	InChI=1S/C2H3O2/c1-4-2-3/h1H3	-157.70	±	2.1	[1]	-164.63	-155.81	-6.93	1.89
233	T	InChI=1S/C4H6/c1-3-4-2/h3-4H,1-2H2	110.57	±	0.4	[1]	119.56	115.02	8.99	4.45
234	T	InChI=1S/C5H10/c1-3-5-4-2/h3H,1,4-5H2,2H3	-21.30	±	1.0	[2]	-10.80	-17.85	10.50	3.45
235	T	InChI=1S/C9H12/c1-2-6-9-7-4-3-5-8-9/h3-5,7-8H,2,6H2,1H3	7.90	±	0.8	[2]	19.44	7.41	11.54	-0.49
236	T	InChI=1S/C5H12/c1-5(2,3)4/h1-4H3	-167.52	±	0.4	[1]	-161.70	-169.64	5.82	-2.12
237	T	InChI=1S/C5H12O2/c1-3-6-5-7-4-2/h3-5H2,1-2H3	-414.80	±	0.8	[2]	-423.86	-417.63	-9.06	-2.83
238	T	InChI=1S/C8H18S2/c1-7(2)5-9-10-6-8(3)4/h7-8H,5-6H2,1-4H3	-170.90	±	2.2	[2]	-175.60	-176.72	-4.70	-5.82
239	T	InChI=1S/C4H6/c1-2-4-3-1/h1-2H,3-4H2	159.74	±	0.9	[1]	170.30	164.66	10.56	4.92
240	T	InChI=1S/C5H8/c1-4-5(2)3/h1H2,2-3H3	129.10	±	0.6	[3]	137.80	131.63	8.70	2.53
241	T	InChI=1S/C7H14O/c1-5(2)7(8)6(3)4/h5-6H,1-4H3	-311.30	±	1.2	[2]	-306.80	-313.66	4.50	-2.36
242	T	InChI=1S/C3H6O2/c1-2-5-3-4/h3H,2H2,1H3	-398.00	±	0.6	[2]	-397.95	-391.20	0.05	6.80
243	T	InChI=1S/C8H18S2/c1-3-5-7-9-10-8-6-4-2/h3-8H2,1-2H3	-158.40	±	2.6	[2]	-156.40	-157.52	2.00	0.88
244	T	InChI=1S/C5H12O/c1-5(2)3-4-6/h5-6H,3-4H2,1-2H3	-301.30	±	1.4	[2]	-298.40	-302.93	2.90	-1.63
245	T	InChI=1S/C5H12/c1-3-5-4-2/h3-5H2,1-2H3	-146.34	±	0.3	[1]	-137.20	-145.14	9.14	1.20
246	T	InChI=1S/COS/c2-1-3	-138.41	±	1.0	[3]	-143.21	-136.15	-4.80	2.26
247	T	InChI=1S/C2H5O/c1-2-3/h3H,1-2H2	-26.06	±	0.6	[1]	-23.91	-23.10	2.15	2.96
248	T	InChI=1S/C4H10S/c1-4(2)3-5/h4-5H,3H2,1-2H3	-97.30	±	0.9	[2]	-96.00	-97.74	1.30	-0.44
249	T	InChI=1S/C2H3N/c1-2-3/h1H3	74.04	±	7.2	[2]	77.50	75.83	3.46	1.79
250	T	InChI=1S/C5H7N/c1-6-4-2-3-5-6/h2-5H,1H3	103.10	±	0.5	[3]	105.90	101.43	2.80	-1.67
251	T	InChI=1S/C5H12O/c1-4(2)5(3)6/h4-6H,1-3H3	-315.20	±	1.4	[2]	-316.30	-320.83	-1.10	-5.63
252	T	InChI=1S/C7H8/c1-7-5-3-2-4-6-7/h2-6H,1H3	50.01	±	0.3	[1]	57.82	49.05	7.81	-0.96
253	T	InChI=1S/C4H6O/c1-2-3-4-5/h2-4H,1H3/b3-2+	-100.70	±	1.0	[2]	-99.00	-100.08	1.70	0.62
254	T	InChI=1S/C8H16O2/c1-4-5-6-8(9)10-7(2)3/h7H,4-6H2,1-3H3	-544.90	±	3.2	[2]	-542.66	-544.07	2.24	0.83
255	T	InChI=1S/C5H12S/c1-4-5(2,3)6/h6H,4H2,1-3H3	-127.10	±	1.0	[2]	-128.07	-131.44	-0.97	-4.34
256	T	InChI=1S/C6H14S2/c1-3-5-7-8-6-4-2/h3-6H2,1-2H3	-117.30	±	1.1	[2]	-118.30	-116.16	-1.00	1.14
257	T	InChI=1S/C4H10O3/c1-5-4(6-2)7-3/h4H,1-3H3	-531.60	±	2.9	[2]	-543.47	-528.53	-11.87	3.07
258	T	InChI=1S/C5H12O/c1-3-5(2)4-6/h5-6H,3-4H2,1-2H3	-302.00	±	1.4	[2]	-296.50	-301.03	5.50	0.97
259	T	InChI=1S/C3H6O/c1-2-3-4/h2,4H,1,3H2	-124.50	±	1.8	[2]	-119.53	-119.91	4.97	4.59
260	T	InChI=1S/C5H12S/c1-3-5-6-4-2/h3-5H2,1-2H3	-104.70	±	0.8	[2]	-102.83	-105.52	1.87	-0.82
261	T	InChI=1S/C2H6OS/c1-4(2)3/h1-2H3	-150.50	±	1.5	[3]	-150.56	-153.33	-0.06	-2.83
262	T	InChI=1S/C4H6O2/c1-3-6-4(2)5/h3H,1H2,2H3	-314.90	±	0.6	[2]	-317.36	-311.36	-2.46	3.54
263	T	InChI=1S/C2H6N/c1-3-2/h1-2H3	156.30	±	1.5	[1]	160.95	159.11	4.65	2.81
264	T	InChI=1S/C5H10/c1-3-5-4-2/h3,5H,4H2,1-2H3/b5-3-	-27.60	±	1.0	[2]	-16.45	-23.50	11.15	4.10
265	T	InChI=1S/CH2O2/c2-1-3/h1H,(H,2,3)	-378.45	±	0.2	[1]	-383.35	-377.01	-4.90	1.44
266	T	InChI=1S/C8H6/c1-2-8-6-4-3-5-7-8/h1,3-7H	317.20	±	1.1	[1]	330.70	322.07	13.50	4.87
267	T	InChI=1S/C4H4S/c1-2-4-5-3-1/h1-4H	114.90	±	1.0	[3]	114.40	114.89	-0.50	-0.01
268	T	InChI=1S/C6H12O/c1-3-5-6-7-4-2/h4H,2-3,5-6H2,1H3	-184.50	±	2.7	[2]	-176.91	-178.51	7.59	5.99
269	T	InChI=1S/C6H14/c1-4-5-6(2)3/h6H,4-5H2,1-3H3	-174.80	±	1.0	[2]	-163.62	-173.19	11.18	1.61
270	T	InChI=1S/HO2/c1-2/h1H	12.26	±	0.2	[1]	9.32	12.46	-2.94	0.20
271	T	InChI=1S/C6H12/c1-3-5-6-4-2/h3H,1,4-6H2,2H3	-43.50	±	1.6	[2]	-29.18	-37.87	14.32	5.63

272	T	InChI=1S/C6H12O/c1-3-4-5-6(2)7/h3-5H2,1-2H3	-279.80	±	1.1	[2]	-274.52	-279.75	5.28	0.05
273	T	InChI=1S/CH3NO2/c1-4-2-3/h1H3	-64.42	±	0.9	[1]	-69.58	-63.06	-5.16	1.36
274	T	InChI=1S/C4H10O/c1-4(2)5-3/h4H,1-3H3	-252.00	±	1.0	[2]	-253.11	-252.33	-1.11	-0.33
275	T	InChI=1S/H2O2/c1-2/h1-2H	-135.46	±	0.1	[1]	-140.10	-137.44	-4.64	-1.99
276	T	InChI=1S/C2H4O2/c1-4-2-3/h2H,1H3	-357.80	±	0.6	[1]	-366.18	-357.80	-8.38	0.00
277	T	InChI=1S/C5H10O2/c1-3-5(6)7-4-2/h3-4H2,1-2H3	-463.60	±	0.8	[2]	-468.27	-464.79	-4.67	-1.19
278	T	InChI=1S/H2O4/c1-3-4-2/h1-2H	-44.00	±	2.4	[1]	-52.99	-44.94	-8.99	-0.94
279	T	InChI=1S/C4H4O/c1-2-4-5-3-1/h1-4H	-34.80	±	0.7	[2]	-32.37	-30.05	2.43	4.75
280	T	InChI=1S/C7H14/c1-3-5-7-6-4-2/h3H,1,4-7H2,2H3	-62.30	±	1.0	[2]	-47.52	-57.84	14.78	4.46
281	T	InChI=1S/C4H11N/c1-4(2,3)5/h5H2,1-3H3	-120.90	±	0.7	[2]	-115.70	-123.46	5.20	-2.56
282	T	InChI=1S/C5H8/c1-3-5-4-2/h3-5H,1H2,2H3/b5-4-	81.40	±	1.2	[3]	93.95	87.78	12.55	6.38
283	T	InChI=1S/C7H5N/c8-6-7-4-2-1-3-5-7/h1-5H	215.70	±	1.5	[2]	224.40	217.01	8.70	1.31
284	T	InChI=1S/C7H16/c1-4-7(5-2)6-3/h7H,4-6H2,1-3H3	-189.60	±	1.2	[2]	-175.60	-186.80	14.00	2.80
285	T	InChI=1S/C8H10/c1-7-5-3-4-6-8(7)2/h3-6H,1-2H3	19.10	±	1.1	[2]	26.54	16.14	7.44	-2.96
286	T	InChI=1S/C7H12O2/c1-3-5-6-7(8)9-4-2/h3H,1,4-6H2,2H3	-385.60	±	2.5	[2]	-379.67	-378.56	5.93	7.04
287	T	InChI=1S/C8H15N/c1-2-3-4-5-6-7-8-9/h2-7H2,1H3	-50.60	±	1.5	[3]	-36.55	-48.01	14.05	2.59
288	T	InChI=1S/C5H10O/c1-4-6-5(2)3/h4-5H,1H2,2-3H3	-173.80	±	2.3	[2]	-170.81	-170.78	2.99	3.02
289	T	InChI=1S/C4H10S/c1-2-3-4-5/h5H,2-4H2,1H3	-88.10	±	1.2	[2]	-86.20	-87.94	1.90	0.16
290	T	InChI=1S/C4H6O2/c1-3(5)4(2)6/h1-2H3	-326.44	±	0.7	[1]	-331.40	-329.03	-4.96	-2.59
291	T	InChI=1S/C3H8O/c1-3-4-2/h3H2,1-2H3	-216.40	±	0.7	[2]	-219.94	-217.53	-3.54	-1.13
292	T	InChI=1S/C7H16/c1-5-7(4)6(2)3/h6-7H,5H2,1-4H3	-198.90	±	1.5	[2]	-183.52	-194.72	15.38	4.18
293	T	InChI=1S/C6H8/c1-2-4-6-5-3-1/h1-4H,5-6H2	104.60	±	0.6	[1]	120.02	112.00	15.42	7.40
294	T	InChI=1S/C3H4N2/c1-2-4-5-3-1/h1-3H,(H,4,5)	179.40	±	0.8	[3]	178.14	177.94	-1.26	-1.46
295	T	InChI=1S/C5H4O2/c6-3-5-1-2-7-4-5/h1-4H	-151.90	±	1.1	[2]	-153.19	-148.16	-1.29	3.74
296	T	InChI=1S/C3H4/c1-2-3-1/h1-2H,3H2	283.82	±	0.6	[1]	290.50	286.49	6.68	2.67
297	T	InChI=1S/C4H9/c1-4(2)3/h4H,1H2,2-3H3	73.18	±	0.8	[1]	80.28	74.41	7.10	1.23
298	T	InChI=1S/C4H10O/c1-4(2)3-5/h4-5H,3H2,1-2H3	-283.90	±	0.9	[2]	-280.70	-283.60	3.20	0.30
299	T	InChI=1S/C2H8N2/c3-1-2-4/h1-4H2	-17.60	±	0.6	[2]	-14.41	-20.36	3.19	-2.76
300	T	InChI=1S/C4H6/c1-3-4-2/h1-2H3	146.00	±	0.6	[1]	154.87	150.33	8.87	4.33
301	T	InChI=1S/H2NO/c1-2/h1H2	64.52	±	0.9	[1]	60.36	60.90	-4.16	-3.62
302	T	InChI=1S/C5H12O/c1-3-5(6)4-2/h5-6H,3-4H2,1-2H3	-317.20	±	1.5	[2]	-308.40	-312.93	8.80	4.27
303	T	InChI=1S/C2H7N/c1-2-3/h2-3H2,1H3	-47.40	±	0.7	[2]	-45.30	-49.79	2.10	-2.39
304	T	InChI=1S/CH6N2/c1-3-2/h3H,2H2,1H3	94.60	±	0.6	[2]	97.00	96.30	2.40	1.70
305	T	InChI=1S/C2H6O2/c3-1-2-4/h3-4H,1-2H2	-389.43	±	0.5	[1]	-398.18	-394.40	-8.75	-4.97
306	T	InChI=1S/C2H6O/c1-2-3/h3H,2H2,1H3	-234.61	±	0.2	[1]	-235.10	-234.73	-0.49	-0.12
307	T	InChI=1S/C5H5N/c1-2-4-6-5-3-1/h1-5H	140.40	±	0.7	[2]	144.10	139.36	3.70	-1.04
308	T	InChI=1S/C7H13N/c1-2-3-4-5-6-7-8/h2-6H2,1H3	-31.00	±	1.3	[2]	-18.03	-27.85	12.97	3.15
309	T	InChI=1S/HO3/c1-3-2/h1H	23.33	±	0.1	[1]	24.33	30.17	1.00	6.84
310	T	InChI=1S/C5H9N/c1-5(2,3)4-6/h1-3H3	-2.50	±	0.8	[2]	2.93	-3.63	5.43	-1.13
311	T	InChI=1S/C6H5NO/c8-7-6-4-2-1-3-5-6/h1-5H	198.70	±	1.2	[1]	201.00	196.84	2.30	-1.86
312	T	InChI=1S/C5H8/c1-3-5-4-2/h3-4H,1-2H3	133.10	±	0.8	[2]	143.50	137.33	10.40	4.23

313	T	InChI=1S/C6H12/c1-4-6(3)5-2/h4,6H,1,5H2,2-3H3	-49.50	±	1.5	[2]	-37.58	-46.27	11.92	3.23
314	T	InChI=1S/C4H4O2/c1-3-2-4(5)6-3/h1-2H2	-190.20	±	0.5	[2]	-193.20	-187.42	-3.00	2.78
315	T	InChI=1S/C3H8S/c1-2-3-4/h4H,2-3H2,1H3	-67.90	±	0.7	[2]	-67.90	-68.01	0.00	-0.11
316	T	InChI=1S/C8H10/c1-2-8-6-4-3-5-7-8/h3-7H,2H2,1H3	29.72	±	0.6	[1]	39.27	28.87	9.55	-0.85
317	T	InChI=1S/C6H14O2/c1-3-7-5-6-8-4-2/h3-6H2,1-2H3	-408.20	±	1.0	[2]	-415.86	-411.26	-7.66	-3.06
318	T	InChI=1S/C4H8/c1-2-4-3-1/h1-4H2	27.63	±	0.4	[1]	34.44	27.91	6.81	0.28
319	T	InChI=1S/C8H19N/c1-3-5-7-9-8-6-4-2/h9H,3-8H2,1-2H3	-156.60	±	0.6	[2]	-139.59	-152.19	17.01	4.41
320	T	InChI=1S/C5H10O2/c1-2-3-4-5(6)7/h2-4H2,1H3,(H,6,7)	-491.90	±	3.0	[2]	-491.05	-491.24	0.85	0.66
321	T	InChI=1S/C6H12O/c1-5(7)6(2,3)4/h1-4H3	-290.70	±	1.0	[2]	-289.44	-294.67	1.26	-3.97
322	T	InChI=1S/C7H16/c1-5-6-7(2,3)4/h5-6H2,1-4H3	-205.90	±	1.5	[2]	-195.29	-206.49	10.61	-0.59
323	T	InChI=1S/C4H10O/c1-4(2,3)5/h5H,1-3H3	-312.50	±	0.8	[2]	-312.60	-315.50	-0.10	-3.00
324	T	InChI=1S/C3H6O2/c1-2-3(4)5/h2H2,1H3,(H,4,5)	-453.50	±	0.5	[2]	-454.40	-451.32	-0.90	2.18
325	T	InChI=1S/CH3/h1H3	146.37	±	0.1	[1]	151.78	150.81	5.41	4.44
326	T	InChI=1S/C5H8/c1-3-5-4-2/h3-4H,1-2,5H2	105.60	±	1.2	[2]	117.47	111.30	11.87	5.70
327	T	InChI=1S/C5H10O/c1-3-5-6-4-2/h4H,2-3,5H2,1H3	-161.60	±	2.3	[2]	-159.60	-159.57	2.00	2.03
328	T	InChI=1S/C6H6/c1-2-4-6-5-3-1/h1-6H	83.11	±	0.2	[1]	90.57	83.43	7.46	0.32
329	V	InChI=1S/C5H14N2/c1-6(2)5-7(3)4/h5H2,1-4H3	-17.70	±	1.8	[2]	-16.24	-20.34	1.46	-2.64
330	V	InChI=1S/C4H10OS/c1-3-6(5)4-2/h3-4H2,1-2H3	-205.00	±	2.0	[3]	-196.13	-202.17	8.87	2.83
331	V	InChI=1S/C2H4O/c1-2-3-1/h1-2H2	-52.54	±	0.4	[1]	-55.46	-51.64	-2.92	0.90
332	V	InChI=1S/C2H5O/c1-2-3/h2-3H,1H3	-55.59	±	0.7	[1]	-54.71	-53.90	0.88	1.69
333	V	InChI=1S/C6H12/c1-4-6(3)5-2/h4H,5H2,1-3H3/b6-4-	-62.30	±	1.5	[2]	-48.94	-57.63	13.36	4.67
334	V	InChI=1S/C5H11N/c6-5-3-1-2-4-5/h5H,1-4,6H2	-54.86	±	0.9	[3]	-44.98	-54.59	9.88	0.27
335	V	InChI=1S/H2NO/c1-2/h1-2H	94.80	±	0.9	[1]	93.02	94.04	-1.78	-0.76
336	V	InChI=1S/C2H3O2/c1-4-2-3/h2H,1H2	-156.80	±	1.7	[1]	-163.39	-154.57	-6.59	2.23
337	V	InChI=1S/C5H6S/c1-5-2-3-6-4-5/h2-4H,1H3	83.59	±	0.9	[3]	82.50	81.36	-1.09	-2.23
338	V	InChI=1S/C9H12/c1-3-9-6-4-8(2)5-7-9/h4-7H,3H2,1-2H3	-3.30	±	1.5	[3]	6.96	-5.07	10.26	-1.77
339	V	InChI=1S/C5H10O3/c1-3-7-5(6)8-4-2/h3-4H2,1-2H3	-640.00	±	0.8	[2]	-648.44	-637.87	-8.44	2.13
340	V	InChI=1S/CH3NO2/c1-2(3)4/h1H3	-74.75	±	0.5	[1]	-83.81	-79.76	-9.06	-5.01
341	V	InChI=1S/C4H7N/c1-4(2)3-5/h4H,1-2H3	24.30	±	1.3	[2]	34.90	29.97	10.60	5.67
342	V	InChI=1S/C3H6S/c1-2-4-3-1/h1-3H2	60.60	±	1.4	[2]	63.47	63.82	2.87	3.22
343	V	InChI=1S/C6H14O/c1-5(2)7-6(3)4/h5-6H,1-4H3	-319.20	±	1.6	[2]	-319.60	-322.09	-0.40	-2.89
344	V	InChI=1S/C4H9/c1-3-4-2/h3H,4H2,1-2H3	66.07	±	2.0	[1]	74.62	68.75	8.55	2.68
345	V	InChI=1S/C6H14O/c1-2-3-4-5-6-7/h7H,2-6H2,1H3	-315.80	±	0.6	[2]	-308.60	-314.76	7.20	1.04
346	V	InChI=1S/C4H10S2/c5-3-1-2-4-6/h5-6H,1-4H2	-50.40	±	1.8	[2]	-50.20	-47.37	0.20	3.03
347	V	InChI=1S/C6H12O/c1-3-5-6(7)4-2/h3-5H2,1-2H3	-278.30	±	0.9	[2]	-274.58	-279.81	3.72	-1.51
348	V	InChI=1S/C5H10/c1-4-5(2)3/h4-5H,1H2,2-3H3	-27.60	±	1.0	[2]	-18.44	-25.49	9.16	2.11
349	V	InChI=1S/C4H6O/c1-3-5-4-2/h3-4H,1-2H2	-13.60	±	1.0	[2]	-11.23	-8.69	2.37	4.91
350	V	InChI=1S/C5H12O/c1-5(2,3)6-4/h1-4H3	-283.50	±	1.1	[2]	-286.27	-287.13	-2.77	-3.63
351	V	InChI=1S/C7H6O2/c8-5-6-2-1-3-7(9)4-6/h1-5,9H	-213.70	±	1.0	[2]	-213.52	-214.54	0.18	-0.84
352	V	InChI=1S/C7H6O2/c8-7(9)6-4-2-1-3-5-6/h1-5H,(H,8,9)	-294.10	±	2.2	[2]	-296.69	-297.71	-2.59	-3.61
353	V	InChI=1S/C2H5NS/c1-2(3)4/h1H3,(H2,3,4)	12.70	±	1.2	[3]	9.70	11.19	-3.00	-1.51

354	V	InChI=1S/C6H10/c1-2-4-6-5-3-1/h1-2H,3-6H2	-5.00	±	0.7	[1]	6.74	-2.16	11.74	2.84
355	V	InChI=1S/C8H18/c1-7(2)6-8(3,4)5/h7H,6H2,1-5H3	-223.70	±	1.5	[1]	-214.35	-227.18	9.35	-3.48
356	V	InChI=1S/C7H8S/c8-6-7-4-2-1-3-5-7/h1-5,8H,6H2	93.10	±	1.1	[3]	95.56	91.36	2.46	-1.74
357	V	InChI=1S/C4H11NO/c1-3-5(6)4-2/h6H,3-4H2,1-2H3	-121.77	±	0.7	[3]	-121.28	-124.38	0.49	-2.61
358	V	InChI=1S/C7H14/c1-2-7-5-3-4-6-7/h7H,2-6H2,1H3	-127.10	±	1.1	[1]	-114.75	-126.17	12.35	0.93
359	V	InChI=1S/C5H10/c1-5(2)3-4-5/h3-4H2,1-2H3	-8.20	±	1.2	[1]	-2.06	-10.22	6.14	-2.02
360	V	InChI=1S/C7H16/c1-4-5-6-7(2)3/h7H,4-6H2,1-3H3	-194.60	±	1.0	[2]	-182.28	-193.48	12.32	1.12
361	V	InChI=1S/C3H4N2/c1-2-5-3-4-1/h1-3H,(H,4,5)	132.90	±	0.6	[3]	132.70	130.57	-0.20	-2.33
362	V	InChI=1S/NO2/c2-1-3	33.10	±	1.0	[3]	25.80	30.77	-7.30	-2.33
363	V	InChI=1S/C6H14S/c1-5-7-6(2,3)4/h5H2,1-4H3	-148.00	±	2.5	[2]	-142.85	-147.17	5.15	0.83
364	V	InChI=1S/C6H15N/c1-5(2)7-6(3)4/h5-7H,1-4H3	-136.30	±	0.5	[2]	-127.01	-136.35	9.29	-0.05
365	V	InChI=1S/CH5N3S/c2-1(5)4-3/h3H2,2H2,4H1	128.20	±	1.6	[3]	127.70	129.68	-0.50	1.48
366	V	InChI=1S/C5H12O/c1-4-5(2,3)6/h6H,4H2,1-3H3	-330.80	±	1.4	[2]	-329.00	-333.53	1.80	-2.73
367	V	InChI=1S/C6H12O2/c1-3-4-5-8-6(2)7/h3-5H2,1-2H3	-485.60	±	0.7	[2]	-486.63	-484.78	-1.03	0.82
368	V	InChI=1S/C5H12S/c1-4(2)5(3)6/h4-6H,1-3H3	-121.30	±	0.8	[2]	-119.58	-122.95	1.72	-1.65
369	V	InChI=1S/C2H6N/c1-3-2/h3H,1H2,2H3	151.10	±	1.0	[1]	156.33	153.96	5.23	2.86
370	V	InChI=1S/C5H8/c1-4-5(2)3/h1,5H,2-3H3	136.40	±	2.1	[3]	149.60	143.43	13.20	7.03
371	V	InChI=1S/C6H10/c1-3-5-6-4-2/h3,5H2,1-2H3	107.70	±	2.4	[3]	116.92	109.12	9.22	1.42

A.1.2. CBS-QB3 methodology: Comparison with values of Montgomery et al.

Table A-2: Deviations between the experimental standard enthalpies of formation at 298 K and (1) the CBS-QB3 calculated values as reported by Montgomery et al. [4], (2) the CBS-QB3 calculated values obtained in this work and (3) the corrected CBS-QB3 calculated values, i.e. including SOCs and BACs, expressed in kJ mol^{-1}.

No.	InChI	$\Delta_f H^\circ_{exp}$	$\Delta_f H^\circ_{calc} - \Delta_f H^\circ_{exp}$		
			CBS-QB3 Montgomery et al. [4]	CBS-QB3	CBS-QB3 + BAC
1	InChI=1S/C2H3/c1-2/h1H,2H2	299.57	1.26	3.68	1.96
2	InChI=1S/C3H4/c1-2-3-1/h1-2H,3H2	276.98	13.81	6.68	2.67
3	InChI=1S/C2H2/c1-2/h1-2H	228.03	6.69	6.13	4.85
4	InChI=1S/C4H6/c1-4-2-3-4/h1-3H2	200.41	0.00	-0.28	-5.92
5	InChI=1S/C3H4/c1-3-2/h1H,2H3	184.93	7.11	6.23	3.32
6	InChI=1S/H2N/h1H2	188.70	-0.42	2.50	2.50
7	InChI=1S/C4H6/c1-2-4-3-1/h1-2H,3-4H2	156.48	14.23	10.56	4.92
8	InChI=1S/C4H6/c1-3-4-2/h1-2H3	145.60	9.62	8.87	4.33
9	InChI=1S/C2H6OS/c1-4(2)3/h1-2H3	-151.46	2.93	-0.06	-2.83
10	InChI=1S/CH3/h1H3	146.44	2.51	2.41	2.06
11	InChI=1S/C5H5N/c1-2-4-6-5-3-1/h1-5H	140.58	4.18	3.70	-1.04
12	InChI=1S/CHN/c1-2/h1H	128.87	4.18	3.60	3.56
13	InChI=1S/C4H6/c1-3-4-2/h3-4H,1-2H2	110.04	10.04	8.99	4.45
14	InChI=1S/C4H4S/c1-2-4-5-3-1/h1-4H	115.06	1.67	-0.50	-0.01
15	InChI=1S/C4H5N/c1-2-4-5-3-1/h1-5H	108.37	5.02	4.79	0.26
16	InChI=1S/CS2/c2-1-3	117.15	-10.46	-8.61	-1.77
17	InChI=1S/C3H7/c1-3-2/h3H,1-2H3	89.96	5.02	4.53	0.30
18	InChI=1S/C6H6/c1-2-4-6-5-3-1/h1-6H	78.80	8.79	7.46	0.32
19	InChI=1S/C2H3N/c1-2-3/h1H3	75.31	2.51	3.46	1.79
20	InChI=1S/C3H6/c1-2-3-1/h1-3H2	53.14	7.11	6.31	1.42
21	InChI=1S/C4H9/c1-4(2)3/h1-3H3	51.46	5.02	5.74	-0.13
22	InChI=1S/C2H4/c1-2/h1-2H2	52.30	3.77	3.41	1.25
23	InChI=1S/HO/h1H	39.33	-1.26	-0.16	0.28
24	InChI=1S/C4H8/c1-2-4-3-1/h1-4H2	28.45	6.28	6.81	0.28
25	InChI=1S/NO2/c2-1-3	33.05	-5.86	-7.30	-2.33
26	InChI=1S/C3H6/c1-3-2/h3H,1H2,2H3	20.08	5.86	5.65	1.86
27	InChI=1S/CH3O/c1-2/h1H3	17.15	2.09	-2.97	-0.48
28	InChI=1S/C4H8/c1-4(2)3/h1H2,2-3H3	-16.74	7.53	7.80	2.38
29	InChI=1S/C2H5O/c1-2-3/h2H2,1H3	-15.48	2.93	-0.52	0.33
30	InChI=1S/C2H7N/c1-3-2/h3H,1-2H3	-18.41	3.35	3.80	0.99
31	InChI=1S/CH3O/c1-2/h2H,1H2	-17.15	1.26	-0.36	2.08
32	InChI=1S/CH5N/c1-2/h2H2,1H3	-23.01	3.35	1.60	-1.26
33	InChI=1S/H2S/h1H2	-20.50	-2.93	-4.71	-0.60
34	InChI=1S/CH4S/c1-2/h2H,1H3	-23.01	-0.84	-2.80	0.36
35	InChI=1S/C3H9N/c1-4(2)3/h1-3H3	-23.85	-1.67	-0.20	-2.96
36	InChI=1S/C4H4O/c1-2-4-5-3-1/h1-4H	-34.73	3.35	2.43	4.75
37	InChI=1S/C2H6S/c1-3-2/h1-2H3	-37.24	-0.84	-2.04	0.16

38	InChI=1S/H3N/h1H3	-46.02	2.09	1.70	-1.22
39	InChI=1S/C2H6S/c1-2-3/h3H,2H2,1H3	-46.44	1.26	-2.30	-0.78
40	InChI=1S/C2H2O/c1-2-3/h1H2	-47.70	0.42	0.66	2.84
41	InChI=1S/CH3NO2/c1-4-2-3/h1H3	-66.53	-6.28	-5.16	1.36
42	InChI=1S/CH4/h1H4	-74.48	0.42	0.35	-1.06
43	InChI=1S/CH3NO2/c1-2(3)4/h1H3	-74.48	-7.11	-9.06	-5.01
44	InChI=1S/C2H6/c1-2/h1-2H3	-83.68	1.67	2.06	-0.98
45	InChI=1S/CH2O/c1-2/h1H2	-108.78	-4.18	-4.34	-1.41
46	InChI=1S/C4H10/c1-3-4-2/h3-4H2,1-2H3	-125.52	5.02	7.00	0.69
47	InChI=1S/C4H10/c1-4(2)3/h4H,1-3H3	-134.31	5.02	6.47	0.16
48	InChI=1S/COS/c2-1-3	-138.49	-10.04	-4.80	2.26
49	InChI=1S/C2H4O/c1-2-3/h2H,1H3	-166.10	0.00	-1.36	-0.06
50	InChI=1S/C2H6O/c1-3-2/h1-2H3	-184.10	-3.77	-4.27	-0.23
51	InChI=1S/C3H6O/c1-3(2)4/h1-2H3	-217.15	0.00	-0.16	-0.50
52	InChI=1S/C2H2O2/c3-1-2-4/h1-2H	-212.13	-5.44	-6.68	-1.04
53	InChI=1S/C3H8O/c1-3-4-2/h3H2,1-2H3	-216.31	-4.60	-3.54	-1.13
54	InChI=1S/C2H5NO/c1-2(3)4/h1H3,(H2,3,4)	-238.49	3.35	1.40	1.73
55	InChI=1S/C2H6O/c1-2-3/h3H,2H2,1H3	-235.14	0.00	-0.49	-0.12
56	InChI=1S/H2O/h1H2	-241.84	-0.84	-1.16	-1.20
57	InChI=1S/C3H8O/c1-3(2)4/h3-4H,1-2H3	-272.80	0.42	-0.09	-1.36
58	InChI=1S/C2H4O2/c1-4-2-3/h2H,1H3	-355.64	-9.20	-8.38	0.00
59	InChI=1S/CH2O2/c2-1-3/h1H,(H,2,3)	-378.652	-3.77	-4.90	1.44
	Mean deviation (MD)		1.55	1.01	0.48
	Mean absolute deviation (MAD)		4.00	3.95	1.69
	Root mean squares deviation (RMS)		14.23	10.56	4.92
	Maximum absolute deviation (MAX)		5.43	4.88	2.25

A.2. Development of group additive values (GAVs)

A.2.1. CBS-QB3 methodology: Comparison with experimental entropies and heat capacities

Table A-3: Experimental and *ab initio* calculated (CBS-QB3) standard entropy and heat capacity at 298 K and the corresponding deviations, expressed in J mol^{-1} K^{-1}. The experimental values for the standard entropy and heat capacity are taken from Dean and Lange [5].

No	InChI	S°_{exp}	S°_{calc}	$S^{\circ}_{calc} - S^{\circ}_{exp}$	$C^{\circ}_{p,exp}$	$C^{\circ}_{p,calc}$	$C^{\circ}_{p,calc} - C^{\circ}_{p,exp}$
1	InChI=1S/H3N/h1H3	192.7	192.3	-0.4	37.2	35.0	-2.2
2	InChI=1S/CHN/c1-2/h1H	201.8	201.1	0.8	-	-	-
3	InChI=1S/HNO/c1-2/h1H	220.7	220.6	0.2	-	-	-
4	InChI=1S/H4N2/c1-2/h1-2H2	238.7	239.4	-0.7	-	-	-
5	InChI=1S/NO2/c2-1-3	240.0	239.8	0.2	-	-	-
6	InChI=1S/C2N2/c3-1-2-4	241.6	239.2	2.4	-	-	-
7	InChI=1S/CH5N/c1-2/h2H2,1H3	242.9	241.5	1.4	50.1	49.5	-0.6
8	InChI=1S/C2H3N/c1-2-3/h1H3	243.4	242.4	1.0	52.5	51.8	-0.7
9	InChI=1S/HNO2/c2-1-3/h(H,2,3)	249.4	248.2	1.2	0.0	0.0	0.0
10	InChI=1S/C2H5N/c1-2-3-1/h3H,1-2H2	250.6	244.1	6.5	52.6	50.7	-1.9
11	InChI=1S/C2H7N/c1-3-2/h3H,1-2H3	273.0	273.0	0.0	70.7	69.6	-1.1
12	InChI=1S/CH3NO2/c1-2(3)4/h1H3	275.0	275.3	-0.3	57.3	57.2	-0.1
13	InChI=1S/C2H7N/c1-2-3/h2-3H2,1H3	283.8	281.8	2.0	71.5	71.8	0.3
14	InChI=1S/CH3NO2/c1-4-2-3/h1H3	284.3	286.5	-2.2	63.2	64.3	1.1
15	InChI=1S/C3H9N/c1-4(2)3/h1-3H3	287.1	290.8	-3.7	-	-	-
16	InChI=1S/C3H9N/c1-3(2)4/h3H,4H2,1-2H3	312.2	311.9	0.3	97.5	95.5	-2.0
17	InChI=1S/C3H9N/c1-2-3-4/h2-4H2,1H3	325.1	322.5	2.6	91.2	95.3	4.1
18	InChI=1S/C4H7N/c1-2-3-4-5/h2-3H2,1H3	325.4	323.5	1.9	97.0	96.6	-0.4
19	InChI=1S/C4H11N/c1-4(2,3)5/h5H2,1-3H3	337.9	329.0	8.9	120.0	121.8	1.8
20	InChI=1S/C4H11N/c1-3-4(2)5/h4H,3,5H2,1-2H3	351.3	355.0	-3.7	117.2	121.3	4.1
21	InChI=1S/C4H11N/c1-3-5-4-2/h5H,3-4H2,1-2H3	352.2	346.1	6.1	115.7	123.5	7.8
22	InChI=1S/C4H11N/c1-2-3-4-5/h2-5H2,1H3	363.3	359.7	3.6	118.6	119.8	1.2
23	InChI=1S/C6H15N/c1-3-5-7-6-4-2/h7H,3-6H2,1-2H3	-	-	0.0	169.9	168.4	0.0
	Mean deviation (MD)			1.3			0.8
	Mean absolute deviation (MAD)			2.2			2.1
	Root mean squares deviation (RMS)			3.2			2.8
	Maximum absolute deviation (MAX)			8.9			7.8

A.2.2. Database for regression of GAVs

Table A-4: Training (T) and validation (V) data for regression of thermodynamic group additive values: Raw and BAC-corrected standard enthalpies of formation [kJ mol^{-1}] calculated at the CBS-QB3 level of theory, molecular and intrinsic standard entropy at 298 K [J mol^{-1} K^{-1}], total symmetry number and number of optical isomers and heat capacity values [J mol^{-1} K^{-1}] at 300 K, 400 K, 500 K, 600 K, 800 K, 1000 K and 1500 K.

No.		InChI	$\Delta_f H^\circ$	σ	n_{opt}	S°	S°_{int}	C_p°						
								300 K	400 K	500 K	600 K	800 K	1000 K	1500 K
1	T	InChI=1S/C2H2N/c1-2-3/h1,3H	397.7	1	1	255.1	255.1	58.7	65.5	70.7	74.9	81.3	86.3	94.6
2	T	InChI=1S/C2H2N/c1-2-3/h1H2	262.2	2	1	248.0	253.8	52.5	59.8	65.8	70.7	78.6	84.6	94.2
3	T	InChI=1S/C2H3N/c1-2-3/h1H,3H2	253.1	1	1	253.6	253.6	61.3	70.4	77.5	83.2	92.3	99.5	112.1
4	T	InChI=1S/C2H3N/c1-2-3/h1H3	77.5	3	1	242.4	251.5	51.8	60.7	69.0	76.3	88.3	97.6	112.4
5	T	InChI=1S/C2H3N/c1-2-3/h3H,1H2	190.5	1	1	249.9	249.9	55.0	65.5	74.1	81.1	91.9	100.0	113.2
6	T	InChI=1S/C2H4N/c1-2-3/h1,3H2	290.8	1	1	276.7	276.7	66.7	79.0	88.8	96.4	107.8	116.3	130.6
7	T	InChI=1S/C2H4N/c1-2-3/h1-2H,3H2	315.6	1	1	270.7	270.7	63.2	76.0	86.5	95.1	108.2	117.7	132.6
8	T	InChI=1S/C2H4N/c1-2-3/h2-3H,1H2	210.7	1	1	259.8	259.8	56.5	70.2	81.9	91.4	106.0	116.6	133.4
9	T	InChI=1S/C2H4N/c1-2-3/h2H,1H3	202.8	3	1	268.8	278.0	56.9	67.5	77.6	86.6	101.2	112.3	129.7
10	T	InChI=1S/C2H4N/c1-2-3/h3H,1H3	227.5	3	1	268.6	277.7	56.6	67.5	77.7	86.6	100.9	111.7	129.0
11	T	InChI=1S/C2H4N/c1-3-2/h1-2H2	233.6	8	1	245.2	262.4	59.1	71.9	83.1	92.4	106.8	117.5	134.2
12	T	InChI=1S/C2H4N/c1-3-2/h1H,2H3	270.1	3	1	268.3	277.5	56.2	66.6	76.7	85.7	100.4	111.7	129.3
13	T	InChI=1S/C2H5N/c1-2-3/h2-3H,1H3/b3-2+	45.7	3	1	263.4	272.6	58.7	71.6	84.0	95.1	113.0	126.6	148.1
14	T	InChI=1S/C2H5N/c1-2-3/h2H,1,3H2	58.7	1	1	268.8	268.8	62.5	77.2	90.0	100.8	117.6	130.1	150.0
15	T	InChI=1S/C2H5N/c1-3-2/h1H2,2H3	80.7	3	1	266.6	275.7	60.8	73.2	85.2	96.1	113.9	127.5	148.9
16	T	InChI=1S/C2H5NO/c1-2(3)4/h1H3,3H2	-236.9	3	1	296.2	305.4	73.9	89.7	103.7	115.6	134.3	148.2	170.4
17	T	InChI=1S/C2H5NO/c1-2-3-4/h2H2,1H3	43.5	3	1	305.3	314.4	75.8	88.8	101.8	113.4	132.3	146.5	168.7
18	T	InChI=1S/C2H5NO/c1-3-2-4/h2H,1H3,3H1	-192.0	3	2	296.8	300.2	68.2	83.6	98.2	111.1	131.7	147.0	170.6
19	T	InChI=1S/C2H5NO2/c1-2-5-3-4/h2H2,1H3	-104.1	3	1	331.5	340.6	89.7	106.1	121.6	134.9	155.8	171.2	194.5
20	T	InChI=1S/C2H6N/c1-2-3/h2H,3H2,1H3	122.0	3	1	286.6	295.8	72.1	86.8	100.0	111.5	129.8	143.8	166.4
21	T	InChI=1S/C2H6N/c1-2-3/h3H,2H2,1H3	155.4	3	1	286.8	295.9	67.8	82.2	95.8	107.7	127.0	141.8	165.5
22	T	InChI=1S/C2H6N/c1-3-2/h1-2H3	161.0	18	1	281.3	305.3	60.7	75.1	89.5	102.5	123.7	139.8	164.9
23	T	InChI=1S/C2H6N/c1-3-2/h3H,1H2,2H3	156.3	6	2	285.2	294.3	72.1	86.4	99.4	110.8	129.3	143.6	166.8
24	T	InChI=1S/C2H6N2/c1-2(3)4/h1,3-4H2	51.3	2	1	280.9	286.7	89.4	114.8	134.1	147.5	164.3	175.1	192.9
25	T	InChI=1S/C2H6N2/c1-3-4-2/h1-2H3	156.2	18	1	288.8	312.9	78.4	93.8	108.9	122.4	144.6	161.5	187.8

26	T	InChI=1S/C2H6NO/c1-2-3-4/h3H,2H2,1H3	16.8	3	2	320.4	323.8	79.0	95.7	111.4	124.9	146.5	162.7	188.2
27	T	InChI=1S/C2H6NO/c1-2-3-4/h4H,2H2,1H3	42.7	3	1	311.3	320.4	80.5	97.7	113.4	126.8	147.8	163.5	188.4
28	T	InChI=1S/C2H6NO/c1-3(2)4/h1-2H3	23.7	9	1	306.2	324.5	78.5	93.6	108.7	122.4	144.6	161.5	187.8
29	T	InChI=1S/C2H7N/c1-2-3/h2-3H2,1H3	-45.3	3	1	281.8	290.9	71.8	88.6	104.2	117.7	139.6	156.4	183.7
30	T	InChI=1S/C2H7N/c1-3-2/h3H,1-2H3	-14.8	9	1	273.0	291.3	69.6	86.7	102.9	117.0	139.7	157.0	184.7
31	T	InChI=1S/C2H7NO/c1-2-3-4/h3-4H,2H2,1H3	-78.8	3	1	306.7	315.9	86.7	108.2	127.5	143.6	167.6	184.4	209.5
32	T	InChI=1S/C2H7NO/c1-3(2)4/h4H,1-2H3	-67.7	9	1	296.7	315.0	89.6	111.0	129.5	144.6	167.2	183.4	208.6
33	T	InChI=1S/C2H8N2/c1-2(3)4/h2H,3-4H2,1H3	-39.9	3	1	313.9	323.1	92.9	115.9	135.7	151.9	176.4	194.7	224.4
34	T	InChI=1S/C2H8N2/c1-2-4-3/h4H,2-3H2,1H3	70.5	3	2	316.1	319.5	97.0	118.3	136.6	152.0	176.5	195.2	225.7
35	T	InChI=1S/C2H8N2/c1-3-4-2/h3-4H,1-2H3	97.6	18	4	307.6	320.1	91.6	113.9	133.9	150.7	177.0	196.4	226.8
36	T	InChI=1S/C2H8N2/c1-4(2)3/h3H2,1-2H3	84.2	9	1	302.8	321.0	90.6	113.8	134.4	151.4	177.5	196.8	227.0
37	T	InChI=1S/C2H8N2/c1-4-2-3/h4H,2-3H2,1H3	4.1	3	2	325.3	328.6	95.3	114.5	132.5	148.2	173.5	192.8	223.9
38	T	InChI=1S/C3H10N2/c1-2-3(4)5/h3H,2,4-5H2,1H3	-58.0	3	1	351.6	360.8	117.7	145.8	170.6	191.3	223.1	246.5	284.2
39	T	InChI=1S/C3H10N2/c1-3(2)5-4/h3,5H,4H2,1-2H3	37.3	9	2	343.5	356.0	124.0	151.3	174.8	194.5	225.3	248.6	286.1
40	T	InChI=1S/C3H10N2/c1-3(4)5-2/h3,5H,4H2,1-2H3/t3-/m1/s1	-33.0	9	2	348.4	360.9	118.9	146.2	170.6	191.2	223.0	246.8	284.8
41	T	InChI=1S/C3H10N2/c1-3-5(2)4/h3-4H2,1-2H3	58.8	9	2	346.1	358.6	117.1	145.0	170.2	191.5	224.5	248.9	287.1
42	T	InChI=1S/C3H10N2/c1-5(2)3-4/h3-4H2,1-2H3	-4.3	9	1	341.6	359.8	115.0	143.1	168.7	190.4	223.9	248.5	286.7
43	T	InChI=1S/C3H3N/c1-2-3-4/h1,3-4H/b4-3+	334.7	1	1	275.5	275.5	66.4	79.1	89.5	98.0	111.1	120.7	135.9
44	T	InChI=1S/C3H4N/c1-2-3-4/h2-3H,1H2	306.2	1	1	284.0	284.0	72.6	89.8	103.4	113.9	129.0	139.6	155.8
45	T	InChI=1S/C3H4N/c1-2-3-4/h2H,1H3	228.1	3	1	294.2	303.3	68.6	82.0	94.0	104.4	120.9	133.2	152.4
46	T	InChI=1S/C3H4N/c1-2-3-4/h4H,1H3	357.7	3	1	305.6	314.7	77.7	90.0	101.1	110.8	126.4	138.2	156.7
47	T	InChI=1S/C3H4N/c1-3-4-2/h1H,2H3	392.8	3	1	297.4	306.5	73.6	86.5	97.8	107.6	123.0	134.6	152.9
48	T	InChI=1S/C3H5N/c1-2-3-4/h2,4H,1H3	171.6	3	1	288.4	297.5	76.0	90.9	104.5	116.2	135.0	149.2	171.6
49	T	InChI=1S/C3H5N/c1-2-3-4/h2-4H,1H2/b4-3-	145.5	1	1	278.0	278.0	72.5	92.2	108.8	122.2	141.7	155.3	175.6
50	T	InChI=1S/C3H5N/c1-2-3-4/h2H2,1H3	60.8	3	1	285.2	294.4	72.9	88.6	102.5	114.5	133.8	148.5	171.5
51	T	InChI=1S/C3H5N/c1-2-3-4/h4H2,1H3	219.2	1	1	308.9	308.9	82.0	96.0	108.7	119.8	137.8	151.7	174.3
52	T	InChI=1S/C3H5N/c1-3-4-2/h1,4H,2H3	262.0	3	2	297.7	301.1	80.1	94.4	107.0	117.8	135.4	148.9	170.9
53	T	InChI=1S/C3H5N/c1-3-4-2/h1H2,2H3	191.0	3	1	289.5	298.6	74.7	89.8	103.6	115.4	134.5	148.9	171.6
54	T	InChI=1S/C3H5N/c1-3-4-2/h3H,1-2H2	171.3	1	1	288.2	288.2	79.4	97.3	111.8	123.3	140.7	153.6	174.1
55	T	InChI=1S/C3H6N/c1-2-3-4/h2,4H,1,3H2	269.2	1	1	314.5	314.5	80.5	98.4	114.4	127.8	148.8	164.5	189.2
56	T	InChI=1S/C3H6N/c1-2-3-4/h2-3H,1,4H2	171.9	2	1	294.8	300.6	82.9	102.4	118.9	132.5	153.3	168.6	193.1
57	T	InChI=1S/C3H6N/c1-2-3-4/h2-4H,1H3	178.3	3	1	298.0	307.1	76.7	95.0	111.9	126.3	149.0	165.8	191.9

58	T	InChI=1S/C3H6N/c1-2-3-4/h3-4H,1-2H2/b4-3+	238.4	2	1	316.0	321.8	84.9	100.4	115.1	127.9	148.4	164.0	188.8
59	T	InChI=1S/C3H6N/c1-2-3-4/h4H,2H2,1H3	209.4	3	1	314.2	323.4	79.1	95.7	111.2	124.6	146.0	162.2	187.9
60	T	InChI=1S/C3H6N/c1-3(2)4/h1-2H3	163.5	18	1	299.1	323.1	80.2	95.7	110.6	123.9	145.5	162.0	188.0
61	T	InChI=1S/C3H6N/c1-3(2)4/h4H,1H2,2H3	174.2	6	1	299.1	314.0	77.8	97.4	114.5	128.8	150.9	167.3	192.4
62	T	InChI=1S/C3H6N/c1-3-4-2/h1,3-4H,2H3	317.5	3	2	311.3	314.7	87.7	104.8	120.1	133.2	153.8	169.0	192.3
63	T	InChI=1S/C3H6N/c1-3-4-2/h2H,3H2,1H3	244.7	3	1	312.7	321.8	80.7	97.1	112.5	125.8	147.2	163.4	188.9
64	T	InChI=1S/C3H6N/c1-3-4-2/h3-4H,1-2H2	229.4	2	1	306.9	312.7	86.3	104.2	119.7	132.7	153.1	168.4	192.4
65	T	InChI=1S/C3H6N/c1-3-4-2/h3H,1H2,2H3	199.3	3	1	295.9	305.0	78.0	96.2	112.9	127.3	149.8	166.5	192.5
66	T	InChI=1S/C3H6N/c1-3-4-2/h3H,2H2,1H3	192.4	6	1	294.4	309.3	79.1	97.2	113.8	127.9	150.3	166.9	192.8
67	T	InChI=1S/C3H6N/c1-3-4-2/h4H,1H2,2H3	295.2	3	2	318.3	321.7	79.9	96.6	112.0	125.3	146.5	162.4	187.8
68	T	InChI=1S/C3H7N/c1-2-3-4/h2-3H,4H2,1H3/b3-2+	36.8	3	1	302.8	312.0	86.8	106.3	124.0	139.2	163.0	180.7	208.7
69	T	InChI=1S/C3H7N/c1-2-3-4/h2H,1,3-4H2	65.0	1	1	304.4	304.4	88.5	109.6	127.0	141.3	163.5	180.3	207.9
70	T	InChI=1S/C3H7N/c1-2-3-4/h3-4H,2H2,1H3/b4-3+	27.5	3	1	307.3	316.4	80.1	99.5	117.6	133.4	158.5	177.5	207.3
71	T	InChI=1S/C3H7N/c1-3(2)4/h1,4H2,2H3	21.9	3	1	298.7	307.9	86.4	107.3	125.4	140.6	164.5	182.3	210.1
72	T	InChI=1S/C3H7N/c1-3(2)4/h4H,1-2H3	4.9	9	1	299.6	317.8	80.6	99.1	116.7	132.2	157.4	176.4	206.6
73	T	InChI=1S/C3H7N/c1-3-4-2/h2-3H2,1H3	55.9	3	1	298.6	307.7	84.6	104.1	121.7	137.0	161.3	179.8	208.8
74	T	InChI=1S/C3H7N/c1-3-4-2/h3-4H,1H2,2H3	61.4	3	2	298.6	301.9	83.6	103.6	121.7	137.3	162.0	180.6	210.4
75	T	InChI=1S/C3H7N/c1-3-4-2/h3H,1-2H3/b4-3+	38.3	9	1	297.5	315.8	82.1	99.8	117.1	132.6	158.0	177.3	207.5
76	T	InChI=1S/C3H7NO/c1-2-3(4)5/h2H2,1H3,4H2	-256.1	3	1	336.6	345.8	99.2	119.5	138.1	154.1	179.7	198.9	229.5
77	T	InChI=1S/C3H7NO/c1-2-3-4-5/h2-3H2,1H3	25.5	3	1	342.4	351.5	96.2	117.0	136.1	152.6	178.8	198.2	228.5
78	T	InChI=1S/C3H7NO/c1-3(2)4-5/h3H,1-2H3	11.2	3	1	333.2	342.3	98.5	118.1	136.3	152.2	177.9	197.3	227.7
79	T	InChI=1S/C3H7NO/c1-3(5)4-2/h1-2H3,4H1	-237.2	9	2	327.2	339.7	89.2	110.7	130.8	148.3	176.1	196.7	228.9
80	T	InChI=1S/C3H7NO/c1-4(2)3-5/h3H,1-2H3	-196.9	9	1	324.4	342.6	93.4	112.6	131.6	148.7	176.7	197.7	230.2
81	T	InChI=1S/C3H7NO2/c1-2-3-4(5)6/h2-3H2,1H3	-132.6	6	1	354.9	369.8	103.2	128.0	150.2	169.0	198.0	219.1	251.3
82	T	InChI=1S/C3H7NO2/c1-2-3-6-4-5/h2-3H2,1H3	-122.9	3	1	359.1	368.2	108.9	132.9	154.6	172.9	201.5	222.3	254.0
83	T	InChI=1S/C3H7NO2/c1-3(2)4(5)6/h3H,1-2H3	-147.2	18	1	346.8	370.8	104.9	129.4	151.2	169.6	198.1	219.0	250.9
84	T	InChI=1S/C3H7NO2/c1-3(2)6-4-5/h3H,1-2H3	-139.4	9	1	348.4	366.6	116.5	141.2	161.7	178.4	204.3	223.4	253.3
85	T	InChI=1S/C3H8N/c1-2-3-4/h1-4H2	143.1	2	1	335.0	340.7	93.0	114.2	133.1	149.2	174.4	193.5	224.4
86	T	InChI=1S/C3H8N/c1-2-3-4/h2H,3-4H2,1H3	133.1	3	1	334.5	343.6	92.0	111.7	130.1	146.2	172.0	191.8	223.7
87	T	InChI=1S/C3H8N/c1-2-3-4/h3H,2,4H2,1H3	104.5	3	1	325.9	335.0	93.4	114.7	133.5	149.6	174.9	194.2	225.1
88	T	InChI=1S/C3H8N/c1-2-3-4/h4H,2-3H2,1H3	140.5	3	1	327.2	336.3	90.6	111.1	130.2	146.8	173.3	193.3	225.0
89	T	InChI=1S/C3H8N/c1-3(2)4/h3-4H,1-2H3	125.2	9	1	318.5	336.7	91.6	112.9	131.9	148.1	173.9	193.5	224.9

90	T	InChI=1S/C3H8N/c1-3(2)4/h4H2,1-2H3	77.5	18	1	316.6	340.6	97.0	115.8	133.2	148.5	173.6	193.0	224.5
91	T	InChI=1S/C3H8N/c1-3-4-2/h3H2,1-2H3	134.9	9	2	323.0	335.5	88.1	107.8	126.9	143.8	171.2	192.0	224.7
92	T	InChI=1S/C3H8N/c1-3-4-2/h4H,1,3H2,2H3	169.4	6	2	325.6	334.7	98.3	117.5	135.4	150.9	176.0	195.2	226.0
93	T	InChI=1S/C3H8N/c1-3-4-2/h4H,2-3H2,1H3	131.8	9	2	324.4	336.9	96.8	116.8	134.9	150.4	175.5	194.8	225.8
94	T	InChI=1S/C3H8N2/c1-2-3(4)5/h2-3H,1,4-5H2	74.2	1	1	338.3	338.3	111.1	136.7	157.5	174.0	198.7	217.2	247.6
95	T	InChI=1S/C3H8N2/c1-3(4)5-2/h5H,1,4H2,2H3	54.6	3	2	322.4	325.7	108.3	138.9	164.6	184.4	211.3	228.6	254.4
96	T	InChI=1S/C3H8N2/c1-3-5-4-2/h3H2,1-2H3	131.1	9	1	334.6	352.9	101.1	122.7	143.1	161.2	190.4	212.4	247.0
97	T	InChI=1S/C3H8NO/c1-3(2)4-5/h3,5H,1-2H3	11.9	9	1	341.0	359.2	107.4	130.8	151.3	168.5	195.5	215.8	248.0
98	T	InChI=1S/C3H8NO/c1-3(2)4-5/h3-4H,1-2H3	-16.3	9	2	349.8	362.3	103.9	126.4	146.9	164.6	192.8	214.1	247.5
99	T	InChI=1S/C3H8NO/c1-3-4(2)5/h3H2,1-2H3	-3.1	9	2	350.3	362.8	102.0	123.1	143.5	161.6	190.8	212.8	247.2
100	T	InChI=1S/C3H9N/c1-2-3-4/h2-4H2,1H3	-63.3	3	1	322.5	331.7	95.3	117.9	138.8	156.8	185.8	207.8	243.2
101	T	InChI=1S/C3H9N/c1-3(2)4/h3H,4H2,1-2H3	-80.7	9	1	311.9	330.2	95.5	119.5	140.8	158.7	187.1	208.7	243.6
102	T	InChI=1S/C3H9N/c1-3-4-2/h4H,3H2,1-2H3	-40.7	9	2	315.0	327.5	96.4	118.4	139.0	157.1	186.5	208.9	244.5
103	T	InChI=1S/C3H9N/c1-4(2)3/h1-3H3	-24.3	81	1	290.8	327.3	91.3	115.5	138.2	157.7	188.4	211.1	246.4
104	T	InChI=1S/C3H9NO/c1-3(2)4-5/h3-5H,1-2H3	-112.2	9	1	334.3	352.6	112.7	140.0	164.5	184.8	215.4	236.9	269.5
105	T	InChI=1S/C3H9NO/c1-3-4(2)5/h5H,3H2,1-2H3	-94.6	9	2	336.5	349.0	118.0	144.9	168.0	186.9	215.8	236.8	269.3
106	T	InChI=1S/C4H10N/c1-2-3-4-5/h2H,3-5H2,1H3	112.8	3	1	374.6	383.8	113.1	139.3	163.7	184.7	218.1	243.3	283.3
107	T	InChI=1S/C4H10N/c1-2-3-4-5/h3H,2,4-5H2,1H3	116.0	3	1	377.9	387.0	110.9	138.1	162.7	183.7	217.0	242.2	282.5
108	T	InChI=1S/C4H10N/c1-2-3-4-5/h4H,2-3,5H2,1H3	86.1	3	1	364.5	373.6	118.0	145.0	169.1	189.7	222.1	246.6	285.4
109	T	InChI=1S/C4H10N/c1-3-4(2)5/h3,5H2,1-2H3	61.4	9	1	364.1	382.3	115.9	142.1	165.8	186.3	219.1	244.0	283.7
110	T	InChI=1S/C4H10N/c1-3-5-4-2/h3,5H,4H2,1-2H3	99.1	9	2	363.9	376.4	125.4	147.9	169.9	189.5	221.6	246.1	285.3
111	T	InChI=1S/C4H10N/c1-3-5-4-2/h3-4H2,1-2H3	108.8	18	1	355.2	379.2	114.7	140.4	164.4	185.3	219.0	244.6	284.8
112	T	InChI=1S/C4H10N/c1-3-5-4-2/h5H,1,3-4H2,2H3	143.3	6	2	364.2	373.4	124.6	148.5	170.9	190.6	222.6	246.9	285.8
113	T	InChI=1S/C4H10N/c1-4(2)3-5/h4-5H,3H2,1-2H3	108.2	9	1	352.0	370.3	117.5	144.3	168.7	189.4	222.1	246.7	285.6
114	T	InChI=1S/C4H10N2/c1-3-4(5)6-2/h3-4,6H,1,5H2,2H3/t4-/m1/s1	75.5	3	2	364.6	368.0	138.0	174.5	203.6	225.4	255.6	277.0	311.6
115	T	InChI=1S/C4H10N2/c1-3-5-6-4-2/h3-4H2,1-2H3	105.7	18	1	372.5	396.5	124.0	151.7	177.4	199.9	236.1	263.4	306.1
116	T	InChI=1S/C4H11N/c1-2-3-4-5/h2-5H2,1H3	-81.3	3	1	359.8	368.9	119.8	147.4	173.3	195.8	231.9	259.3	302.9
117	T	InChI=1S/C4H11N/c1-3-4(2)5/h4H,3,5H2,1-2H3/t4-/m1/s1	-95.7	9	2	355.0	367.5	121.3	150.2	176.3	198.5	233.8	260.5	303.4
118	T	InChI=1S/C4H11N/c1-3-5-4-2/h5H,3-4H2,1-2H3	-63.2	9	1	346.1	364.4	123.5	150.3	175.5	197.6	233.5	261.0	304.4
119	T	InChI=1S/C4H11N/c1-4(2)3-5/h4H,3,5H2,1-2H3	-90.4	9	1	349.7	368.0	119.3	148.4	175.0	197.6	233.5	260.5	303.5
120	T	InChI=1S/C4H11N/c1-4(2)5-3/h4-5H,1-3H3	-72.7	27	2	344.6	366.2	119.6	148.6	174.9	197.5	233.6	260.9	304.2
121	T	InChI=1S/C4H11N/c1-4(2,3)5/h5H2,1-3H3	-115.7	81	1	329.0	365.6	121.8	152.8	179.5	201.6	236.0	262.1	304.0

122	T	InChI=1S/C4H11N/c1-4-5(2)3/h4H2,1-3H3	-46.9	27	1	340.4	367.8	115.2	144.7	172.1	195.9	233.6	261.8	305.6
123	T	InChI=1S/C4H11NO/c1-3-5(6)4-2/h6H,3-4H2,1-2H3	-121.3	9	1	363.2	381.5	146.7	179.1	206.5	229.3	264.4	290.2	330.2
124	T	InChI=1S/C4H12N2/c1-4-6(3)5-2/h5H,4H2,1-3H3	61.7	27	4	375.3	391.2	138.1	170.6	200.5	226.4	267.7	298.8	347.4
125	T	InChI=1S/C4H3N/c1-2-3-4-5/h1H3	328.1	3	1	289.7	298.8	80.6	93.5	104.6	114.1	129.5	141.0	158.8
126	T	InChI=1S/C4H4N/c1-2-3-4-5/h2-3H,1H2	292.5	1	1	305.4	305.4	83.2	101.0	115.9	128.0	146.3	159.5	179.8
127	T	InChI=1S/C4H4N/c1-3-5-4-2/h1,4H,2H2	459.3	1	1	304.0	304.0	91.4	110.2	124.5	135.7	152.3	164.2	181.9
128	T	InChI=1S/C4H5N/c1-2-3-4-5/h2-3H,1H3/b3-2+	157.8	3	1	308.0	317.2	86.3	103.7	119.3	132.7	154.0	170.0	194.6
129	T	InChI=1S/C4H5N/c1-2-3-4-5/h2H,1,3H2	174.3	1	1	318.6	318.6	85.3	103.7	119.7	133.3	154.5	170.3	194.7
130	T	InChI=1S/C4H5N/c1-2-3-4-5/h4-5H,1H3/b5-4+	290.3	3	1	323.1	332.2	88.4	105.7	121.6	135.2	156.9	173.1	198.1
131	T	InChI=1S/C4H5N/c1-3-5-4-2/h1,4-5H,2H2	345.3	1	2	330.0	324.3	97.4	115.2	130.1	142.4	161.3	175.2	197.2
132	T	InChI=1S/C4H5N/c1-4(2)3-5/h1H2,2H3	158.5	3	1	307.0	316.2	86.7	104.6	120.2	133.4	154.4	170.1	194.6
133	T	InChI=1S/C4H6N/c1-2-3-4-5/h3H,2H2,1H3	209.6	3	1	335.0	344.2	90.1	110.2	127.9	142.9	166.6	184.2	211.5
134	T	InChI=1S/C4H6N/c1-3-4-5-2/h3H,2H2,1H3	343.6	3	1	331.3	340.4	96.9	116.9	134.5	149.4	172.4	189.2	214.8
135	T	InChI=1S/C4H6N/c1-3-5-4-2/h1H,4H2,2H3	365.7	3	1	336.7	345.8	95.5	114.9	131.9	146.3	168.9	185.8	212.2
136	T	InChI=1S/C4H6N/c1-3-5-4-2/h3-4H,1-2H2	262.6	2	1	299.1	304.8	91.3	118.5	142.7	162.2	189.1	205.4	225.7
137	T	InChI=1S/C4H6N/c1-3-5-4-2/h4H,1H2,2H3	324.9	3	1	330.2	339.3	95.7	116.2	134.1	149.2	172.7	189.8	215.7
138	T	InChI=1S/C4H6N/c1-4(2)3-5/h1-2H3	190.0	18	1	326.6	350.6	88.7	107.2	124.5	139.7	164.2	182.5	210.7
139	T	InChI=1S/C4H7N/c1-2-3-4-5/h2,5H2,1H3	201.4	3	1	331.7	340.8	102.8	124.1	142.7	158.6	183.8	202.9	233.6
140	T	InChI=1S/C4H7N/c1-2-3-4-5/h2-3H2,1H3	39.0	3	1	323.5	332.6	96.6	118.4	137.9	154.4	180.7	200.4	231.3
141	T	InChI=1S/C4H7N/c1-2-3-4-5/h2-5H,1H3/b3-2+,5-4-	121.4	3	1	314.3	323.4	95.9	118.8	139.1	156.3	183.1	202.7	232.8
142	T	InChI=1S/C4H7N/c1-3-4-5-2/h3-4H,1H2,2H3/b5-4-	136.7	3	1	312.4	321.5	96.3	120.6	141.9	159.6	186.6	206.0	235.1
143	T	InChI=1S/C4H7N/c1-3-4-5-2/h3-4H,2H2,1H3/b4-3+	140.8	3	1	312.5	321.6	96.9	122.0	143.7	161.3	187.1	205.4	233.9
144	T	InChI=1S/C4H7N/c1-3-5-4-2/h1,4H2,2H3	164.2	3	1	329.2	338.3	96.6	118.6	138.1	154.7	180.8	200.3	231.1
145	T	InChI=1S/C4H7N/c1-3-5-4-2/h1,5H,4H2,2H3	234.6	3	2	339.2	342.5	102.8	124.0	142.3	157.7	182.2	200.8	230.6
146	T	InChI=1S/C4H7N/c1-3-5-4-2/h3-4H,1H2,2H3/b5-4-	127.6	3	1	316.4	325.5	99.8	123.3	143.1	159.3	184.4	203.1	232.5
147	T	InChI=1S/C4H7N/c1-3-5-4-2/h3-5H,1-2H2	146.6	2	1	319.1	324.9	108.7	131.2	150.1	166.1	191.2	209.8	238.2
148	T	InChI=1S/C4H7N/c1-4(2)3-5/h4H,1-2H3	34.9	9	1	315.3	333.5	97.3	119.4	138.7	155.1	181.0	200.4	231.2
149	T	InChI=1S/C4H7N/c1-4(2)5-3/h1,3H2,2H3	139.6	3	1	322.5	331.6	95.6	118.3	138.2	155.0	181.3	200.9	231.4
150	T	InChI=1S/C4H8N/c1-3-4(2)5/h3H,1,5H2,2H3	128.6	6	1	329.5	344.4	107.0	131.6	153.0	171.1	199.3	220.3	253.1
151	T	InChI=1S/C4H8N/c1-3-4-5-2/h3-5H,1H2,2H3	171.7	6	2	335.6	344.7	102.4	126.8	148.9	167.6	197.1	219.1	253.7
152	T	InChI=1S/C4H8N/c1-3-4-5-2/h4H,2-3H2,1H3	174.0	6	1	346.5	361.4	101.7	126.0	148.0	166.9	196.8	218.8	252.4
153	T	InChI=1S/C4H8N/c1-3-5-4-2/h5H,1,4H2,2H3	268.7	3	2	348.5	351.9	106.7	131.7	153.5	171.3	198.2	218.0	249.3

154	T	InChI=1S/C4H8N/c1-4(2)3-5/h3,5H,1-2H3	134.7	18	1	325.7	349.8	98.4	121.8	143.8	162.8	193.0	215.5	250.4
155	T	InChI=1S/C4H8N/c1-4(2)3-5/h3H,1,5H2,2H3	139.2	6	1	332.2	347.1	104.7	130.1	152.1	170.4	198.8	219.8	252.7
156	T	InChI=1S/C4H8N/c1-4(2)3-5/h4-5H,1-2H3	184.2	9	1	338.1	356.4	101.7	125.7	146.9	164.8	193.0	214.2	247.6
157	T	InChI=1S/C4H8N/c1-4(2)5-3/h1H2,2-3H3	169.1	9	1	333.1	351.4	95.4	120.8	143.6	163.0	193.4	215.8	250.7
158	T	InChI=1S/C4H8N/c1-4(2)5-3/h3H2,1-2H3	156.7	36	1	335.9	365.7	101.6	124.8	146.3	164.9	194.6	216.7	251.2
159	T	InChI=1S/C4H8N/c1-4-5(2)3/h1H2,2-3H3	289.7	9	1	345.7	364.0	103.4	126.1	147.9	166.7	196.1	217.3	249.8
160	T	InChI=1S/C4H9N/c1-2-3-4-5/h2-3H,4-5H2,1H3/b3-2+	34.7	3	1	346.6	355.7	109.7	134.9	157.3	176.3	206.4	229.3	266.1
161	T	InChI=1S/C4H9N/c1-2-3-4-5/h3-4H,2,5H2,1H3/b4-3+	18.2	3	1	340.2	349.4	109.9	136.0	159.4	179.2	210.2	233.1	268.9
162	T	InChI=1S/C4H9N/c1-3-4(2)5/h2-3,5H2,1H3	5.4	3	1	338.0	347.1	108.1	135.7	159.7	179.8	210.9	233.8	269.5
163	T	InChI=1S/C4H9N/c1-3-4(2)5/h3-4H,1,5H2,2H3/t4-/m0/s1	30.7	3	2	339.2	342.6	113.1	141.0	164.0	182.7	211.4	232.9	267.8
164	T	InChI=1S/C4H9N/c1-3-4-5-2/h3,5H,1,4H2,2H3	69.4	3	2	337.9	341.3	110.9	137.6	160.8	180.1	210.3	232.8	268.6
165	T	InChI=1S/C4H9N/c1-3-4-5-2/h4H,3H2,1-2H3/b5-4+	20.0	9	1	340.4	358.6	104.2	127.7	150.2	170.3	202.9	227.7	266.5
166	T	InChI=1S/C4H9N/c1-3-5-4-2/h3,5H,1,4H2,2H3	36.6	3	2	343.0	346.3	110.4	135.5	158.7	178.8	210.9	234.8	271.6
167	T	InChI=1S/C4H9N/c1-3-5-4-2/h3H,4H2,1-2H3/b5-3+	12.3	9	1	334.2	352.4	105.1	130.4	153.5	173.5	205.5	229.7	267.4
168	T	InChI=1S/C4H9N/c1-4(2)3-5/h1,3,5H2,2H3	29.7	3	1	341.7	350.9	114.0	137.1	158.5	177.1	206.9	229.7	266.3
169	T	InChI=1S/C4H9N/c1-4(2)3-5/h3-5H,1-2H3/b5-3+	1.6	9	1	335.1	353.3	104.5	130.0	153.2	173.1	204.9	228.9	266.6
170	T	InChI=1S/C4H9N/c1-4(2)3-5/h3H,5H2,1-2H3	5.6	9	1	336.7	355.0	107.8	133.3	156.2	175.7	206.6	229.7	266.6
171	T	InChI=1S/C4H9N/c1-4(2)5-3/h1-3H3	10.1	27	1	336.2	363.6	97.8	122.5	146.0	166.8	200.3	225.7	265.2
172	T	InChI=1S/C4H9N/c1-4(2)5-3/h5H,1H2,2-3H3	23.4	9	2	332.1	344.6	109.9	136.7	160.2	180.1	211.6	235.0	271.1
173	T	InChI=1S/C4H9N/c1-4-5(2)3/h4H,1H2,2-3H3	58.8	9	1	336.2	354.4	104.7	129.5	153.0	173.8	207.2	232.3	270.5
174	T	InChI=1S/C4H9NO/c1-2-3-4(5)6/h2-3H2,1H3,5H2	-275.3	3	1	371.9	381.1	123.8	150.9	175.0	195.5	227.9	251.9	289.9
175	T	InChI=1S/C4H9NO/c1-3(2)4(5)6/h3H,1-2H3,5H2	-281.0	9	1	364.8	383.0	125.6	151.9	175.4	195.5	227.3	251.2	289.2
176	T	InChI=1S/C4H9NO/c1-3-4(2)5-6/h4H,3H2,1-2H3/t4-/m1/s1	-7.2	9	2	375.7	388.2	126.1	150.4	173.2	193.2	225.4	249.6	287.7
177	T	InChI=1S/C4H9NO/c1-3-5-4(2)6/h3H2,1-2H3,5H1	-264.1	9	2	370.3	382.8	112.2	141.0	167.0	189.3	224.2	249.8	289.5
178	T	InChI=1S/C4H9NO/c1-4(2)3-5-6/h4H,3H2,1-2H3	-1.2	9	1	368.2	386.4	121.3	148.6	173.2	194.1	226.8	251.1	288.7
179	T	InChI=1S/C4H9NO/c1-4(6)5(2)3/h1-3H3	-231.1	27	1	358.6	386.0	112.5	137.8	162.4	184.4	220.1	246.8	288.1
180	T	InChI=1S/C4H9NO2/c1-2-3-4-5(6)7/h2-4H2,1H3	-151.5	6	1	392.6	407.5	128.8	158.5	185.4	208.4	244.4	270.7	310.8
181	T	InChI=1S/C4H9NO2/c1-3-4(2)5(6)7/h4H,3H2,1-2H3/t4-/m1/s1	-168.5	18	2	387.3	405.6	132.9	162.3	188.6	211.0	245.9	271.6	310.9
182	T	InChI=1S/C4H9NO2/c1-3-4(2)7-5-6/h4H,3H2,1-2H3/t4-/m1/s1	-159.7	9	2	391.3	403.8	142.3	172.6	198.4	219.7	252.4	276.3	313.6
183	T	InChI=1S/C4H9NO2/c1-4(2)3-5(6)7/h4H,3H2,1-2H3	-161.0	18	1	384.8	408.8	129.3	159.9	187.2	210.1	245.6	271.5	310.9
184	T	InChI=1S/C4H9NO2/c1-4(2)3-7-5-6/h4H,3H2,1-2H3	-150.2	9	1	389.0	407.2	134.7	164.8	191.9	214.7	249.9	275.5	314.5
185	T	InChI=1S/C5H10N/c1-3-4-5(2)6/h3-4H,6H2,1-2H3	101.8	9	1	371.7	390.0	127.5	156.7	183.4	206.4	242.7	269.6	311.5

186	T	InChI=1S/C5H10N/c1-3-5(2)4-6/h4,6H,3H2,1-2H3	117.3	9	1	369.4	387.6	121.4	151.8	179.4	202.9	239.9	267.4	310.1
187	T	InChI=1S/C5H10N/c1-4-5(2)6-3/h4,6H,1H2,2-3H3	138.6	18	2	370.4	388.6	126.1	155.4	182.0	204.9	241.2	268.3	310.7
188	T	InChI=1S/C5H10N/c1-4-6-5(2)3/h2,4H2,1,3H3	143.7	18	1	367.4	391.5	123.6	154.3	182.0	205.6	242.8	270.2	312.5
189	T	InChI=1S/C5H10N/c1-4-6-5(2)3/h4H,1-3H3	117.5	54	1	364.1	397.2	121.8	151.4	179.9	204.9	244.0	272.0	312.8
190	T	InChI=1S/C5H10N/c1-5(2)4-6-3/h4H,1-3H3	125.2	54	1	360.4	393.6	120.6	148.2	175.0	198.7	236.9	265.5	309.6
191	T	InChI=1S/C5H11N/c1-2-3-4-5-6/h3-4H,2,5-6H2,1H3/b4-3+	16.8	3	1	383.3	392.5	135.5	166.8	194.1	217.1	253.7	281.4	325.9
192	T	InChI=1S/C5H11N/c1-3-4-5-6-2/h3-4,6H,5H2,1-2H3/b4-3+	38.9	9	2	373.1	385.6	135.0	165.8	193.5	217.2	254.7	282.8	327.4
193	T	InChI=1S/C5H11N/c1-3-5(2)4-6/h4-6H,3H2,1-2H3	-15.9	9	2	377.3	389.8	132.3	162.2	189.8	213.8	252.1	281.0	326.5
194	T	InChI=1S/C5H11N/c1-3-5(2)4-6/h4H,3,6H2,1-2H3/b5-4-	-11.7	9	1	374.3	392.5	130.4	162.1	190.6	214.8	252.9	281.3	326.2
195	T	InChI=1S/C5H11N/c1-3-5-6-4-2/h3,6H,1,4-5H2,2H3	43.1	3	2	375.9	379.3	138.1	169.5	197.1	220.5	257.2	284.8	328.5
196	T	InChI=1S/C5H11N/c1-4(2)5(3)6/h5H,1,6H2,2-3H3/t5-/m1/s1	-2.8	9	2	374.0	386.5	134.9	168.5	196.9	220.2	256.3	283.4	326.6
197	T	InChI=1S/C5H11N/c1-4-5(2)6-3/h4-6H,1H2,2-3H3/t5-/m0/s1	38.9	9	4	374.9	381.6	133.7	166.7	195.7	219.8	257.2	284.9	328.4
198	T	InChI=1S/C5H11N/c1-4-5(2)6-3/h4H2,1-3H3/b6-5+	-10.1	27	1	376.9	404.3	122.7	152.0	180.3	205.4	246.0	276.7	324.5
199	T	InChI=1S/C5H11N/c1-4-5(2,3)6/h4H,1,6H2,2-3H3	-3.3	9	1	365.0	383.2	137.2	169.9	198.0	221.2	257.1	283.9	327.1
200	T	InChI=1S/C5H11N/c1-4-6(3)5-2/h4H,1,5H2,2-3H3	34.8	9	2	366.6	379.1	131.9	162.7	190.9	215.4	254.4	283.8	329.9
201	T	InChI=1S/C5H11N/c1-4-6-5(2)3/h4H2,1-3H3	-19.4	27	1	374.6	402.0	121.5	152.7	182.1	207.7	248.8	279.5	326.7
202	T	InChI=1S/C5H11N/c1-4-6-5(2)3/h6H,2,4H2,1,3H3	-2.1	9	2	368.7	381.2	136.6	168.5	196.8	220.9	259.2	287.8	331.8
203	T	InChI=1S/C5H11N/c1-5(2)4-6-3/h4,6H,1-3H3	13.7	27	2	370.4	392.1	129.4	161.0	190.1	215.1	254.1	282.8	327.6
204	T	InChI=1S/C5H11NO/c1-3-5(4-2)6-7/h5H,3-4H2,1-2H3	-26.3	9	1	402.3	420.5	156.8	185.8	212.5	235.9	273.8	302.5	347.9
205	T	InChI=1S/C5H11NO/c1-4-5(7)6(2)3/h4H2,1-3H3	-250.1	27	1	391.5	418.9	139.6	169.3	198.4	224.5	267.1	299.1	348.5
206	T	InChI=1S/C5H11NO/c1-5(2,3)4(6)7/h1-3H3,6H2	-310.7	81	1	381.0	417.5	146.2	181.4	211.7	236.8	275.6	304.3	349.3
207	T	InChI=1S/C5H11NO2/c1-3-5(4-2)6(7)8/h5H,3-4H2,1-2H3	-190.2	18	1	414.7	438.7	159.9	194.6	226.1	252.9	294.6	325.0	371.5
208	T	InChI=1S/C5H11NO2/c1-5(2,3)4-6(7)8/h4H2,1-3H3	-191.4	16	1	400.2	442.5	155.3	192.3	225.0	252.2	294.1	324.5	370.6
209	T	InChI=1S/C5H12N/c1-4-5(2)6-3/h6H,4H2,1-3H3	76.1	27	1	391.0	418.4	140.2	170.8	199.8	225.2	265.8	296.4	344.4
210	T	InChI=1S/C5H12N2/c1-3-5-7-6-4-2/h3-5H2,1-2H3	86.7	9	1	418.7	436.9	147.1	181.3	212.7	239.8	283.0	315.4	365.8
211	T	InChI=1S/C5H13N/c1-2-3-4-5-6/h2-6H2,1H3	-99.5	3	1	397.3	406.4	145.3	177.6	208.3	235.1	278.2	310.8	362.6
212	T	InChI=1S/C5H13N/c1-3-4-5(2)6/h5H,3-4,6H2,1-2H3/t5-/m1/s1	-116.0	9	2	392.4	404.9	146.0	180.8	211.8	238.3	280.4	312.4	363.2
213	T	InChI=1S/C5H13N/c1-3-5(6)4-2/h5H,3-4,6H2,1-2H3	-113.1	9	1	386.5	404.8	147.9	181.1	211.6	238.1	280.2	312.2	363.1
214	T	InChI=1S/C5H13N/c1-4-5(2,3)6/h4,6H2,1-3H3	-130.5	27	1	375.5	402.9	144.4	181.0	213.1	239.9	281.9	313.3	363.5
215	T	InChI=1S/C5H13N/c1-4-6-5(2)3/h5-6H,4H2,1-3H3	-98.6	27	2	382.6	404.2	145.1	180.2	211.5	238.4	281.3	313.6	364.6
216	T	InChI=1S/C5H13N/c1-5(2,3)6-4/h6H,1-4H3	-102.7	24	2	359.9	399.8	142.2	179.0	211.3	238.4	281.0	312.9	363.6
217	T	InChI=1S/C5H4N/c1-3-5-6-4-2/h2H,1H3	625.7	3	1	354.1	363.2	106.6	123.9	138.1	150.0	168.6	182.4	203.5

218	T	InChI=1S/C5H6N/c1-2-3-4-5-6/h2-4H,1H3	257.9	3	1	343.8	353.0	104.6	127.0	146.9	163.7	189.8	209.0	238.4
219	T	InChI=1S/C5H6N/c1-3-5(2)4-6/h3H,2H2,1H3	276.1	6	1	334.7	349.6	106.2	129.4	149.2	165.6	191.0	209.6	238.5
220	T	InChI=1S/C5H6N/c1-3-5-6-4-2/h4H,2H2,1H3	421.1	3	1	352.8	361.9	112.1	135.8	155.7	172.3	197.9	216.4	243.9
221	T	InChI=1S/C5H6N/c1-4-6-5(2)3/h1H,2H2,3H3	421.3	3	1	353.2	362.3	125.1	148.8	167.5	182.6	205.8	222.7	248.4
222	T	InChI=1S/C5H7N/c1-2-3-4-5-6/h2-3H,4H2,1H3/b3-2+	142.1	3	1	354.7	363.8	108.3	131.4	152.2	170.2	198.9	220.3	253.5
223	T	InChI=1S/C5H7N/c1-3-4-5-6-2/h5H,1-2H3/b6-5+	284.2	9	1	365.5	383.7	108.7	131.4	152.6	171.1	200.8	223.0	257.0
224	T	InChI=1S/C5H7N/c1-3-5(2)4-6/h2-3H2,1H3	138.6	3	1	346.7	355.9	109.4	133.8	154.9	172.7	200.7	221.5	254.0
225	T	InChI=1S/C5H7N/c1-3-5(2)4-6/h3H,1-2H3/b5-3-	121.9	9	1	341.4	359.7	109.2	131.5	151.9	169.6	198.3	219.8	253.2
226	T	InChI=1S/C5H7N/c1-3-5-6-4-2/h2-3,5-6H,1H3/b5-3+	321.2	3	2	366.0	369.4	118.5	141.6	161.8	178.8	205.3	224.9	255.5
227	T	InChI=1S/C5H7N/c1-4-6-5(2)3/h1,6H,2H2,3H3	306.1	3	2	356.8	360.2	119.3	143.5	163.9	180.9	207.4	226.9	257.2
228	T	InChI=1S/C5H7N/c1-5(2)3-4-6/h1,3H2,2H3	137.1	3	1	347.8	356.9	108.7	132.7	153.7	171.5	199.8	220.9	253.7
229	T	InChI=1S/C5H7N/c1-5(2)3-4-6/h3H,1-2H3	116.1	9	1	341.6	359.8	109.5	131.9	152.3	170.1	198.6	220.0	253.3
230	T	InChI=1S/C5H8N/c1-3-5(2)4-6/h3H2,1-2H3	170.1	9	1	373.4	391.7	110.8	135.7	158.6	178.3	209.9	233.5	270.0
231	T	InChI=1S/C5H8N/c1-3-5-6-4-2/h3-4H,1-2H3	302.6	9	1	369.9	388.1	114.9	140.6	163.9	184.0	215.6	238.8	273.9
232	T	InChI=1S/C5H8N/c1-4-6-5(2)3/h1,5H,2-3H3	333.1	3	1	373.7	382.8	123.2	148.1	169.8	188.1	216.7	238.2	271.9
233	T	InChI=1S/C5H8N/c1-4-6-5(2)3/h4H,1-2H2,3H3	234.0	12	1	329.8	350.5	121.7	152.8	178.5	199.7	231.3	252.6	281.8
234	T	InChI=1S/C5H8N/c1-5(2)3-4-6/h5-6H,1-2H3	313.4	9	1	368.2	386.4	123.2	148.9	171.3	190.1	219.5	241.3	275.7
235	T	InChI=1S/C5H9N/c1-3-5(2)4-6/h5H,3H2,1-2H3/t5-/m0/s1	14.4	9	2	359.5	372.0	122.9	149.9	174.2	194.9	227.7	252.3	291.0
236	T	InChI=1S/C5H9N/c1-3-5(6)4-2/h3-5H,1-2,6H2	142.2	1	1	361.4	361.4	130.9	159.6	183.3	202.6	232.5	254.9	291.1
237	T	InChI=1S/C5H9N/c1-3-5-6-4-2/h3,5H,1,4H2,2H3/b6-5-	110.5	3	1	349.3	358.4	119.6	151.3	178.4	200.6	234.1	258.3	294.9
238	T	InChI=1S/C5H9N/c1-3-5-6-4-2/h3-6H,2H2,1H3/b5-3+	124.0	3	2	364.7	368.1	129.9	157.0	181.0	201.7	234.6	258.9	296.2
239	T	InChI=1S/C5H9N/c1-4-6-5(2)3/h1,5-6H,2-3H3	199.3	9	2	358.9	371.4	128.5	156.1	179.6	199.2	230.0	253.3	290.6
240	T	InChI=1S/C5H9N/c1-4-6-5(2)3/h4,6H,1-2H2,3H3	111.2	3	2	357.4	360.8	126.3	155.4	181.0	202.3	235.0	258.7	294.9
241	T	InChI=1S/C5H9N/c1-4-6-5(2)3/h4H,2H2,1,3H3/b6-4-	94.7	9	1	357.7	375.9	119.7	146.8	171.3	192.3	225.8	250.9	290.1
242	T	InChI=1S/C5H9N/c1-5(2)3-4-6/h3-4,6H,1-2H3/b6-4-	84.1	9	1	347.7	366.0	120.8	148.0	172.7	194.0	227.9	253.1	291.8
243	T	InChI=1S/C5H9N/c1-5(2,3)4-6/h1-3H3	2.9	81	1	331.8	368.3	123.7	152.4	177.0	197.6	229.6	253.6	291.5
244	T	InChI=1S/C6H11N/c1-3-5-6(7)4-2/h3-6H,2,7H2,1H3/b5-3-/t6-/m0/s1	117.8	3	2	402.5	405.9	150.7	184.6	214.1	238.7	276.9	305.2	350.0
245	T	InChI=1S/C6H11N/c1-3-6(2)4-5-7/h4-5,7H,3H2,1-2H3/b6-4+,7-5+	67.3	9	1	383.7	401.9	141.6	175.9	207.0	233.5	274.9	305.3	351.8
246	T	InChI=1S/C6H11N/c1-3-6(4-2)5-7/h6H,3-4H2,1-2H3	-6.0	9	1	390.3	408.5	149.2	181.0	210.0	234.9	274.6	304.3	350.8
247	T	InChI=1S/C6H11N/c1-4-6(2,3)5-7/h4H2,1-3H3	-16.2	27	1	380.5	407.9	147.5	182.0	211.9	236.9	276.1	305.3	351.2
248	T	InChI=1S/C6H11N/c1-4-6(5-2)7-3/h4-7H,1-2H2,3H3	147.1	3	1	385.1	394.2	150.9	189.0	220.2	245.1	282.5	309.8	353.0
249	T	InChI=1S/C6H11N/c1-5(2)7-6(3)4/h7H,1,3H2,2,4H3	83.4	9	1	394.0	412.3	150.4	184.5	213.7	238.3	276.5	305.0	349.9

250	T	InChI=1S/C6H11N/c1-6(2)4-5-7-3/h4-5H,1-3H3/b7-5-	75.4	27	1	383.7	411.1	144.7	176.6	206.0	231.8	273.1	304.0	351.3
251	T	InChI=1S/C6H11NO2/c1-3-5-6(4-2)9-7-8/h3,6H,1,4-5H2,2H3/t6-/m0/s1	-71.1	3	2	459.5	462.9	178.9	218.6	252.7	280.5	322.3	352.1	397.3
252	T	InChI=1S/C6H13N/c1-5-6(2,3)7-4/h5,7H,1H2,2-4H3	7.7	27	2	396.3	418.0	163.4	201.3	234.5	262.2	305.1	337.1	387.9
253	T	InChI=1S/C6H13N/c1-5-7(4)6(2)3/h5-6H,1H2,2-4H3	6.2	27	2	393.8	415.4	155.5	194.2	228.3	257.1	302.5	336.4	389.7
254	T	InChI=1S/C6H13NO/c1-4-5-6(8)7(2)3/h4-5H2,1-3H3	-269.6	27	1	426.3	453.7	163.6	200.0	234.8	265.6	315.0	352.0	409.0
255	T	InChI=1S/C6H13NO/c1-4-7(5-2)6(3)8/h4-5H2,1-3H3	-284.3	27	1	421.0	448.4	167.1	206.2	241.8	272.2	320.1	355.6	410.5
256	T	InChI=1S/C6H15N/c1-3-5-7-6-4-2/h7H,3-6H2,1-2H3	-103.3	9	1	427.4	445.7	168.4	206.6	242.7	274.3	325.1	363.4	423.5
257	T	InChI=1S/C6H15N/c1-4-7(5-2)6-3/h4-6H2,1-3H3	-86.8	81	1	402.8	439.3	170.4	206.3	241.8	273.8	325.8	365.0	425.6
258	T	InChI=1S/C6H15N/c1-5(2)7-6(3)4/h5-7H,1-4H3	-127.0	81	1	407.4	443.9	168.7	210.7	248.5	280.6	330.6	367.6	424.9
259	T	InChI=1S/C6H6N/c1-3-5-7-6-4-2/h1-2H3	585.6	18	1	401.7	425.7	127.4	149.5	169.3	186.5	214.1	234.5	265.7
260	T	InChI=1S/C6H7N/c1-6(2)4-3-5-7/h6H,1-2H3	284.1	9	1	362.1	380.3	126.0	152.2	174.5	193.0	222.2	243.9	277.6
261	T	InChI=1S/C6H8N/c1-3-4-6(2)5-7/h3H,1,4H2,2H3	282.9	3	1	396.3	405.4	130.2	155.3	178.8	199.3	231.8	256.0	293.3
262	T	InChI=1S/C6H8N/c1-6(2)4-3-5-7/h3-4H,1-2H3	222.3	18	1	370.7	394.7	125.2	153.1	178.2	199.7	233.5	258.5	296.8
263	T	InChI=1S/C6H9N/c1-3-6(2)4-5-7/h4H,3H2,1-2H3/b6-4+	99.1	9	1	377.2	395.5	131.6	161.3	187.5	209.8	245.2	271.6	312.8
264	T	InChI=1S/C7H11N/c1-3-5-7(4-2)6-8/h3,7H,1,4-5H2,2H3/t7-/m1/s1	104.4	3	2	422.3	425.7	162.0	197.3	228.4	254.7	295.9	326.5	374.1
265	T	InChI=1S/C7H11N/c1-4-5-7(2,3)6-8/h4H,1,5H2,2-3H3	92.6	9	1	401.2	419.5	166.6	203.0	234.2	260.1	300.0	329.4	375.5
266	T	InChI=1S/C7H13N/c1-4-5-7(2,3)6-8/h4-5H2,1-3H3	-35.3	27	1	412.4	439.8	175.2	216.4	250.8	279.5	324.5	358.3	411.6
267	T	InChI=1S/C7H14N/c1-4-7(3)6-8-5-2/h6H,4-5H2,1-3H3	81.1	27	1	437.9	465.3	165.1	207.1	245.5	278.3	330.3	368.9	428.7
268	T	InChI=1S/C7H17N/c1-4-5-8-6-7(2)3/h7-8H,4-6H2,1-3H3	-130.0	27	2	466.2	487.9	194.1	239.9	281.8	317.7	374.8	417.6	484.1
269	T	InChI=1S/C8H19N/c1-3-5-7-9-8-6-4-2/h9H,3-8H2,1-2H3	-139.6	9	1	513.6	531.9	220.3	267.8	313.3	353.4	417.9	466.6	542.8
270	T	InChI=1S/CH2N/c1-2/h1-2H	274.4	1	1	228.4	228.4	38.2	43.0	47.5	51.5	57.8	62.8	70.9
271	T	InChI=1S/CH2N/c1-2/h1H2	239.3	1	1	224.0	224.0	37.6	42.3	46.9	51.0	57.9	63.2	71.6
272	T	InChI=1S/CH3N/c1-2/h2H,1H2	90.0	1	1	227.0	227.0	37.8	44.3	51.2	57.6	68.2	76.3	89.3
273	T	InChI=1S/CH3NO/c1-2-3/h1H3	68.6	3	1	260.3	269.4	52.1	60.4	68.5	75.8	87.5	96.3	110.0
274	T	InChI=1S/CH3NO2/c1-2(3)4/h1H3	-83.8	6	1	275.3	290.2	57.2	69.7	81.1	90.8	105.8	116.5	132.4
275	T	InChI=1S/CH3NO2/c1-4-2-3/h1H3	-69.6	3	1	286.5	295.7	64.3	74.9	84.9	93.7	107.6	117.8	133.2
276	T	InChI=1S/CH4N/c1-2/h1-2H2	153.7	2	1	246.0	251.7	51.0	60.1	67.9	74.5	84.9	93.1	107.0
277	T	InChI=1S/CH4N/c1-2/h2H,1H3	181.0	3	1	245.7	254.8	45.4	53.4	61.5	68.9	81.2	90.7	106.3
278	T	InChI=1S/CH4NO/c1-2-3/h2H,1H3	43.6	3	2	279.2	282.6	56.1	66.2	76.3	85.3	100.0	111.2	128.7
279	T	InChI=1S/CH4NO/c1-2-3/h3H,1H3	67.4	3	1	272.2	281.3	57.7	68.6	78.9	87.8	101.9	112.4	129.1
280	T	InChI=1S/CH5N/c1-2/h2H2,1H3	-19.5	3	1	241.5	250.6	49.5	59.4	69.2	78.0	92.8	104.6	124.1
281	T	InChI=1S/CH6N2/c1-3-2/h3H,2H2,1H3	97.0	3	2	278.6	282.0	72.8	88.1	101.2	112.2	129.8	143.4	165.9

282	V	InChI=1S/C3H8N2/c1-2-3(4)5/h2H,4-5H2,1H3	31.2	3	1	325.1	334.2	112.4	142.0	165.0	182.0	205.3	221.9	249.7
283	V	InChI=1S/C4H10N/c1-2-3-4-5/h5H,2-4H2,1H3	122.1	3	1	366.4	375.6	115.6	141.1	165.2	186.1	219.6	244.8	284.7
284	V	InChI=1S/C4H10N2/c1-2-3-6-4-5/h2,6H,1,3-5H2	88.2	1	2	384.9	379.2	136.4	165.4	190.8	212.0	244.7	269.1	308.1
285	V	InChI=1S/C4H10NO/c1-3-5(6)4-2/h3-4H2,1-2H3	-29.7	9	1	381.9	400.2	125.6	153.1	179.0	201.5	237.6	264.6	306.9
286	V	InChI=1S/C4H8N/c1-3-4(2)5/h5H,2-3H2,1H3	157.7	6	1	331.1	346.0	99.4	125.6	148.2	167.0	196.0	217.4	251.1
287	V	InChI=1S/C5H10N/c1-5(2)4-6-3/h4-5H,3H2,1-2H3	148.4	18	1	373.7	397.8	126.4	157.2	184.6	207.8	244.1	270.9	312.1
288	V	InChI=1S/C5H11N/c1-3-4-5(2)6/h4H,3,6H2,1-2H3/b5-4-	-21.5	9	1	373.1	391.3	128.4	161.8	191.3	216.2	254.9	283.4	327.8
289	V	InChI=1S/C5H11N/c1-3-5-6-4-2/h5H,3-4H2,1-2H3/b6-5-	-4.0	9	1	375.3	393.6	127.3	158.6	187.2	211.7	250.9	280.4	326.5
290	V	InChI=1S/C5H11NO2/c1-3-5(4-2)8-6-7/h5H,3-4H2,1-2H3	-180.1	9	1	420.8	439.1	167.6	203.5	234.9	260.9	300.5	329.3	373.9
291	V	InChI=1S/C5H12N2/c1-3-4-5(6)7-2/h3-5,7H,6H2,1-2H3/b4-3+/t5-/m1/s1	45.4	9	2	400.7	413.2	158.9	199.0	233.5	260.8	300.2	327.8	371.0
292	V	InChI=1S/C5H12N2/c1-3-4-5-7-6-2/h3-5H2,1-2H3	93.4	9	1	412.6	430.9	150.1	183.3	214.1	240.9	283.9	316.3	366.6
293	V	InChI=1S/C5H8N/c1-5(2)3-4-6/h3,5H,1-2H3	183.2	9	1	364.1	382.4	114.8	141.3	164.3	183.6	213.8	236.2	271.2
294	V	InChI=1S/C6H11N/c1-4-5-7-6(2)3/h5H,2,4H2,1,3H3/b7-5+	75.9	9	1	400.8	419.0	141.9	174.6	204.4	230.0	270.7	301.3	349.0
295	V	InChI=1S/C6H13N/c1-4-5-6(2,3)7/h4-5H,7H2,1-3H3/b5-4+	-33.3	27	1	402.3	429.7	159.4	197.0	230.0	257.8	301.3	333.9	386.0
296	V	InChI=1S/C6H13NO/c1-4-6(8)7(3)5-2/h4-5H2,1-3H3	-278.3	27	2	438.4	460.1	162.5	200.3	235.6	266.5	315.9	352.6	409.2
297	V	InChI=1S/C6H13NO2/c1-4-6(2,3)5-7(8)9/h4-5H2,1-3H3	-206.6	54	1	440.3	473.5	185.2	227.5	264.3	295.1	342.6	377.3	430.4
298	V	InChI=1S/C6H14N/c1-4-6(2,3)5-7/h5H,4,7H2,1-3H3	31.1	27	1	414.9	442.3	170.1	210.7	245.2	273.8	318.4	351.8	405.0
299	V	InChI=1S/C6H15N/c1-4-6(2,3)5-7/h4-5,7H2,1-3H3	-138.8	27	1	411.4	438.8	170.3	212.4	249.6	280.7	329.3	365.7	423.5
300	V	InChI=1S/C6H8N2/c7-5-3-1-2-4-6-8/h1-4H2	166.8	2	1	405.7	411.5	150.2	178.3	202.6	223.2	255.9	280.5	318.5

A.2.3. Differences between CBS-QB3 and GA approximated thermodynamic properties

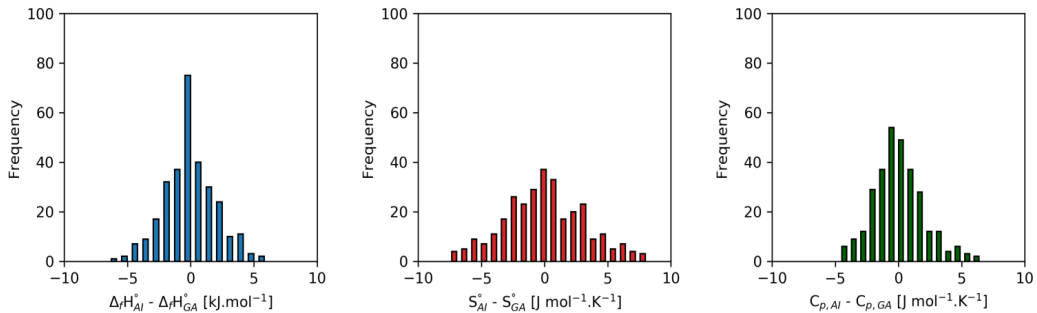

Figure A-1: Distribution of the differences between *ab initio* calculated (AI) and group additive approximated values (GA) for the (a) enthalpy of formation [kJ mol^{-1}], (b) entropy and (c) heat capacity [J mol^{-1} K^{-1}].

Table A-5: Differences between the *ab initio* calculated (AI) and group additive approximated (GA) values for the standard enthalpy of formation [kJ mol^{-1}] and intrinsic standard entropy [J mol^{-1} K^{-1}] at 298 K and the heat capacities [J mol^{-1} K^{-1}] at different temperatures for all 300 molecules. The GA approximations obtained with the final set of GAVs is used.

No.		InChI	$\Delta = AI - GA$								
			$\Delta_f H^\circ$	S°_{int}	C_p°						
					300 K	400 K	500 K	600 K	800 K	1000 K	1500 K
1	T	InChI=1S/C2H2N/c1-2-3/h1,3H	1.0	-2.7	-1.4	-1.5	-1.7	-1.9	-2.2	-2.4	-2.7
2	T	InChI=1S/C2H2N/c1-2-3/h1H2	0.0	0.0	0.0	0.0	0.0	0.0	0.0	0.0	0.0
3	T	InChI=1S/C2H3N/c1-2-3/h1H,3H2	-3.1	0.5	-2.4	-2.2	-2.2	-2.3	-2.5	-2.7	-2.8
4	T	InChI=1S/C2H3N/c1-2-3/h1H3	0.0	0.0	0.0	0.0	0.0	0.0	0.0	0.0	0.0
5	T	InChI=1S/C2H3N/c1-2-3/h3H,1H2	-6.5	-2.7	1.9	2.3	2.3	2.1	1.6	1.2	0.7
6	T	InChI=1S/C2H4N/c1-2-3/h1,3H2	-1.2	-2.1	4.7	4.4	3.8	3.2	2.3	1.9	1.3
7	T	InChI=1S/C2H4N/c1-2-3/h1-2H,3H2	3.8	0.4	-0.7	-0.5	-0.2	0.1	0.5	0.6	0.4
8	T	InChI=1S/C2H4N/c1-2-3/h2-3H,1H2	0.4	-3.9	1.7	1.8	1.6	1.3	0.8	0.5	0.2
9	T	InChI=1S/C2H4N/c1-2-3/h2H,1H3	0.7	3.9	-1.5	-1.5	-1.4	-1.2	-0.8	-0.6	-0.3
10	T	InChI=1S/C2H4N/c1-2-3/h3H,1H3	-0.4	-0.5	0.7	0.6	0.5	0.4	0.1	0.0	0.0

11	T	InChI=1S/C2H4N/c1-3-2/h1-2H2	0.0	0.0	0.0	0.0	0.0	0.0	0.0	0.0	0.0
12	T	InChI=1S/C2H4N/c1-3-2/h1H,2H3	0.9	-2.0	-2.0	-1.2	-0.8	-0.6	-0.3	-0.3	-0.2
13	T	InChI=1S/C2H5N/c1-2-3/h2-3H,1H3/b3-2+	-0.2	2.2	-0.9	-0.7	-0.5	-0.5	-0.5	-0.5	-0.3
14	T	InChI=1S/C2H5N/c1-2-3/h2H,1,3H2	-2.8	4.1	-1.5	-1.7	-1.7	-1.6	-1.4	-1.1	-0.8
15	T	InChI=1S/C2H5N/c1-3-2/h1H2,2H3	0.2	2.4	0.2	0.5	0.6	0.6	0.6	0.5	0.2
16	T	InChI=1S/C2H5NO/c1-2(3)4/h1H3,3H2	-0.3	-1.9	0.2	1.0	1.5	1.6	1.1	0.6	0.0
17	T	InChI=1S/C2H5NO/c1-2-3-4/h2H2,1H3	-0.9	3.2	2.5	1.1	0.4	0.0	-0.1	-0.1	0.1
18	T	InChI=1S/C2H5NO/c1-3-2-4/h2H,1H3,3H1	4.2	-2.3	-0.3	0.0	0.2	0.3	0.4	0.4	0.3
19	T	InChI=1S/C2H5NO2/c1-2-5-3-4/h2H2,1H3	-0.1	8.2	3.1	1.9	1.2	0.7	0.3	0.2	0.1
20	T	InChI=1S/C2H6N/c1-2-3/h2H,3H2,1H3	-0.4	-0.9	0.6	0.3	0.4	0.6	0.9	1.0	0.9
21	T	InChI=1S/C2H6N/c1-2-3/h3H,2H2,1H3	-2.0	0.5	0.6	0.4	0.2	0.1	0.0	0.0	0.0
22	T	InChI=1S/C2H6N/c1-3-2/h1-2H3	-0.1	2.7	-1.5	-1.3	-1.1	-0.8	-0.4	-0.2	0.1
23	T	InChI=1S/C2H6N/c1-3-2/h3H,1H2,2H3	-0.4	-1.1	-0.4	-0.4	-0.5	-0.4	-0.2	0.0	0.3
24	T	InChI=1S/C2H6N2/c1-2(3)4/h1,3-4H2	-2.2	0.1	-0.2	0.1	0.3	0.4	0.2	0.1	0.0
25	T	InChI=1S/C2H6N2/c1-3-4-2/h1-2H3	-0.1	1.6	0.1	-0.1	-0.2	-0.2	-0.1	-0.1	-0.1
26	T	InChI=1S/C2H6NO/c1-2-3-4/h3H,2H2,1H3	1.1	-0.4	0.8	1.6	1.7	1.5	0.9	0.6	0.2
27	T	InChI=1S/C2H6NO/c1-2-3-4/h4H,2H2,1H3	0.1	0.2	-1.8	-1.4	-1.1	-0.8	-0.5	-0.3	-0.2
28	T	InChI=1S/C2H6NO/c1-3(2)4/h1-2H3	-0.5	0.9	0.1	-0.4	-0.4	-0.3	0.1	0.3	0.3
29	T	InChI=1S/C2H7N/c1-2-3/h2-3H2,1H3	-0.1	1.2	0.1	-0.1	-0.1	-0.1	-0.1	-0.1	-0.1
30	T	InChI=1S/C2H7N/c1-3-2/h3H,1-2H3	-1.7	1.0	-0.6	0.0	0.3	0.3	0.2	0.1	0.1
31	T	InChI=1S/C2H7NO/c1-2-3-4/h3-4H,2H2,1H3	-0.9	2.7	-3.7	-3.5	-2.9	-2.2	-1.3	-0.7	-0.3
32	T	InChI=1S/C2H7NO/c1-3(2)4/h4H,1-2H3	1.7	2.4	-1.0	-0.6	-0.4	-0.4	-0.6	-0.8	-0.6
33	T	InChI=1S/C2H8N2/c1-2(3)4/h2H,3-4H2,1H3	-0.6	0.8	-0.5	-0.2	-0.1	0.0	0.1	0.1	0.0
34	T	InChI=1S/C2H8N2/c1-2-4-3/h4H,2-3H2,1H3	0.5	-0.2	-1.1	-1.1	-1.2	-1.2	-1.0	-0.8	-0.3
35	T	InChI=1S/C2H8N2/c1-3-4-2/h3-4H,1-2H3	-0.8	2.1	-0.9	0.1	0.9	1.4	1.4	1.1	0.2
36	T	InChI=1S/C2H8N2/c1-4(2)3/h3H2,1-2H3	-0.8	1.0	-0.9	0.1	0.7	0.9	0.8	0.6	0.0
37	T	InChI=1S/C2H8N2/c1-4-2-3/h4H,2-3H2,1H3	-1.3	3.1	0.3	-0.2	-0.5	-0.7	-0.8	-0.7	-0.4
38	T	InChI=1S/C3H10N2/c1-2-3(4)5/h3H,2,4-5H2,1H3	0.2	-1.4	-0.9	-0.6	-0.2	0.0	0.3	0.3	0.2
39	T	InChI=1S/C3H10N2/c1-3(2)5-4/h3,5H,4H2,1-2H3	-0.6	-1.6	1.7	0.8	0.4	0.3	0.2	0.2	0.3
40	T	InChI=1S/C3H10N2/c1-3(4)5-2/h3,5H,4H2,1-2H3/t3-/m1/s1	0.4	0.6	1.4	0.8	0.3	-0.1	-0.3	-0.4	-0.2
41	T	InChI=1S/C3H10N2/c1-3-5(2)4/h3-4H2,1-2H3	0.0	1.1	0.0	0.0	0.2	0.4	0.6	0.5	0.2
42	T	InChI=1S/C3H10N2/c1-5(2)3-4/h3-4H2,1-2H3	1.3	-2.4	0.0	0.1	0.2	0.4	0.5	0.6	0.4

43	T	InChI=1S/C3H3N/c1-2-3-4/h1,3-4H/b4-3+	2.8	-5.6	-2.6	-2.4	-2.4	-2.4	-2.5	-2.6	-2.7
44	T	InChI=1S/C3H4N/c1-2-3-4/h2-3H,1H2	3.3	1.5	0.7	1.7	1.8	1.5	0.7	0.1	-0.3
45	T	InChI=1S/C3H4N/c1-2-3-4/h2H,1H3	-0.7	-0.4	1.9	1.2	0.9	0.8	0.7	0.7	0.6
46	T	InChI=1S/C3H4N/c1-2-3-4/h4H,1H3	0.5	6.3	0.5	0.6	0.7	0.9	1.1	1.2	1.4
47	T	InChI=1S/C3H4N/c1-3-4-2/h1H,2H3	0.7	-1.0	1.4	1.3	1.1	1.0	0.8	0.7	0.5
48	T	InChI=1S/C3H5N/c1-2-3-4/h2,4H,1H3	3.9	0.5	0.1	0.1	0.2	0.2	0.2	0.2	0.2
49	T	InChI=1S/C3H5N/c1-2-3-4/h2-4H,1H2/b4-3-	-1.2	-0.8	-0.6	0.8	1.6	1.9	1.9	1.6	1.0
50	T	InChI=1S/C3H5N/c1-2-3-4/h2H2,1H3	0.4	1.2	-1.1	-1.4	-1.3	-1.1	-0.7	-0.5	-0.2
51	T	InChI=1S/C3H5N/c1-2-3-4/h4H2,1H3	2.5	5.1	1.2	1.0	1.0	1.0	1.1	1.2	1.3
52	T	InChI=1S/C3H5N/c1-3-4-2/h1,4H,2H3	1.9	0.3	1.4	0.8	0.4	0.2	0.2	0.2	0.2
53	T	InChI=1S/C3H5N/c1-3-4-2/h1H2,2H3	1.7	-0.7	-0.6	-0.4	-0.4	-0.3	-0.3	-0.2	-0.2
54	T	InChI=1S/C3H5N/c1-3-4-2/h3H,1-2H2	0.8	5.8	2.0	1.2	0.4	-0.1	-0.3	-0.3	-0.1
55	T	InChI=1S/C3H6N/c1-2-3-4/h2,4H,1,3H2	2.8	2.1	-2.8	-2.7	-2.4	-1.9	-1.1	-0.6	-0.1
56	T	InChI=1S/C3H6N/c1-2-3-4/h2-3H,1,4H2	1.9	-4.8	3.0	3.0	2.6	2.2	1.4	0.8	0.0
57	T	InChI=1S/C3H6N/c1-2-3-4/h2-4H,1H3	-2.8	-0.9	-0.9	-1.0	-0.9	-0.8	-0.6	-0.4	-0.2
58	T	InChI=1S/C3H6N/c1-2-3-4/h3-4H,1-2H2/b4-3+	0.2	-2.7	4.0	3.0	2.4	2.0	1.4	1.1	0.7
59	T	InChI=1S/C3H6N/c1-2-3-4/h4H,2H2,1H3	-0.4	2.8	-0.2	-0.3	-0.3	-0.3	-0.2	-0.1	0.0
60	T	InChI=1S/C3H6N/c1-3(2)4/h1-2H3	1.2	0.8	0.4	-0.1	-0.3	-0.3	-0.2	-0.1	-0.1
61	T	InChI=1S/C3H6N/c1-3(2)4/h4H,1H2,2H3	0.8	7.3	-0.2	-0.3	-0.2	-0.1	0.2	0.4	0.3
62	T	InChI=1S/C3H6N/c1-3-4-2/h1,3-4H,2H3	4.1	4.5	3.0	2.3	1.8	1.4	0.8	0.4	-0.3
63	T	InChI=1S/C3H6N/c1-3-4-2/h2H,3H2,1H3	1.5	6.4	-0.2	-1.0	-1.3	-1.3	-1.1	-1.0	-0.6
64	T	InChI=1S/C3H6N/c1-3-4-2/h3-4H,1-2H2	-3.6	2.9	-0.7	-0.8	-0.9	-1.0	-1.1	-1.1	-0.8
65	T	InChI=1S/C3H6N/c1-3-4-2/h3H,1H2,2H3	2.5	-1.6	1.0	1.1	0.9	0.7	0.2	-0.1	-0.4
66	T	InChI=1S/C3H6N/c1-3-4-2/h3H,2H2,1H3	-1.0	-7.3	1.2	0.8	0.6	0.4	0.1	0.0	0.3
67	T	InChI=1S/C3H6N/c1-3-4-2/h4H,1H2,2H3	1.6	3.0	-2.9	-4.0	-4.6	-4.8	-4.3	-3.4	-1.9
68	T	InChI=1S/C3H7N/c1-2-3-4/h2-3H,4H2,1H3/b3-2+	4.6	2.9	0.1	-0.2	-0.2	-0.2	-0.4	-0.6	-0.9
69	T	InChI=1S/C3H7N/c1-2-3-4/h2H,1,3-4H2	1.1	-2.2	0.7	1.5	1.5	1.3	0.9	0.6	0.3
70	T	InChI=1S/C3H7N/c1-2-3-4/h3-4H,2H2,1H3/b4-3+	-0.2	3.7	-2.9	-1.9	-1.2	-0.8	-0.4	-0.2	0.0
71	T	InChI=1S/C3H7N/c1-3(2)4/h1,4H2,2H3	-2.6	0.2	-0.8	-0.9	-0.8	-0.5	-0.1	0.2	0.4
72	T	InChI=1S/C3H7N/c1-3(2)4/h4H,1-2H3	-1.2	-0.8	-0.4	0.1	0.3	0.3	0.2	0.1	0.1
73	T	InChI=1S/C3H7N/c1-3-4-2/h2-3H2,1H3	1.3	-1.5	1.3	1.1	0.8	0.6	0.4	0.3	0.0
74	T	InChI=1S/C3H7N/c1-3-4-2/h3-4H,1H2,2H3	-1.8	-2.6	-1.1	-1.2	-1.6	-1.9	-2.2	-2.1	-0.9

75	T	InChI=1S/C3H7N/c1-3-4-2/h3H,1-2H3/b4-3-	0.2	-1.3	0.4	0.5	0.5	0.3	0.1	-0.1	-0.2
76	T	InChI=1S/C3H7NO/c1-2-3(4)5/h2H2,1H3,4H2	-1.2	6.9	-1.4	-3.6	-5.0	-5.3	-4.7	-3.7	-1.8
77	T	InChI=1S/C3H7NO/c1-2-3-4-5/h2-3H2,1H3	0.0	0.4	-2.3	-1.0	-0.4	-0.2	-0.1	0.0	0.1
78	T	InChI=1S/C3H7NO/c1-3(2)4-5/h3H,1-2H3	-0.2	-1.5	-3.5	-3.1	-2.6	-2.1	-1.3	-0.9	-0.3
79	T	InChI=1S/C3H7NO/c1-3(5)4-2/h1-2H3,4H1	-1.7	-1.7	1.4	0.5	-0.1	-0.4	-0.6	-0.6	-0.5
80	T	InChI=1S/C3H7NO/c1-4(2)3-5/h3H,1-2H3	-4.2	2.3	0.3	0.0	-0.2	-0.3	-0.4	-0.4	-0.3
81	T	InChI=1S/C3H7NO2/c1-2-3-4(5)6/h2-3H2,1H3	-0.4	-0.2	-3.9	-2.3	-1.4	-0.8	-0.2	0.1	0.6
82	T	InChI=1S/C3H7NO2/c1-2-3-6-4-5/h2-3H2,1H3	-0.1	-4.1	-2.8	-1.5	-0.9	-0.6	-0.4	-0.3	-0.1
83	T	InChI=1S/C3H7NO2/c1-3(2)4(5)6/h3H,1-2H3	2.6	5.7	-2.5	-2.4	-2.3	-2.1	-1.7	-1.2	-0.5
84	T	InChI=1S/C3H7NO2/c1-3(2)6-4-5/h3H,1-2H3	2.2	4.3	-2.6	-3.5	-4.3	-4.7	-4.6	-4.1	-3.0
85	T	InChI=1S/C3H8N/c1-2-3-4/h1-4H2	-3.3	-0.7	-1.8	-0.8	-0.2	0.1	0.2	0.1	0.1
86	T	InChI=1S/C3H8N/c1-2-3-4/h2H,3-4H2,1H3	-0.2	-2.6	1.7	1.7	1.5	1.3	0.9	0.6	0.3
87	T	InChI=1S/C3H8N/c1-2-3-4/h3H,2,4H2,1H3	1.0	-1.5	-3.2	-2.0	-1.2	-0.7	-0.4	-0.2	-0.1
88	T	InChI=1S/C3H8N/c1-2-3-4/h4H,2-3H2,1H3	2.0	1.0	-1.8	-0.9	-0.5	-0.3	-0.2	-0.2	-0.1
89	T	InChI=1S/C3H8N/c1-3(2)4/h3-4H,1-2H3	-0.1	3.4	0.1	0.0	-0.3	-0.5	-0.7	-0.6	-0.4
90	T	InChI=1S/C3H8N/c1-3(2)4/h4H2,1-2H3	-3.6	-0.1	3.5	2.3	1.4	0.8	0.3	0.1	0.0
91	T	InChI=1S/C3H8N/c1-3-4-2/h3H2,1-2H3	0.0	-4.5	0.3	0.1	0.0	-0.1	-0.1	-0.1	-0.1
92	T	InChI=1S/C3H8N/c1-3-4-2/h4H,1,3H2,2H3	-1.7	-4.7	4.6	3.4	2.5	1.9	1.2	0.9	0.6
93	T	InChI=1S/C3H8N/c1-3-4-2/h4H,2-3H2,1H3	1.2	4.0	-1.4	-1.3	-1.3	-1.3	-1.1	-1.0	-0.7
94	T	InChI=1S/C3H8N2/c1-2-3(4)5/h2-3H,1,4-5H2	3.4	5.2	-1.2	-4.6	-6.8	-7.5	-6.7	-5.0	-2.4
95	T	InChI=1S/C3H8N2/c1-3(4)5-2/h5H,1,4H2,2H3	-0.5	-0.8	-2.0	-1.8	-0.8	0.5	1.9	2.1	1.0
96	T	InChI=1S/C3H8N2/c1-3-5-4-2/h3H2,1-2H3	0.1	-0.7	0.6	0.0	-0.2	-0.3	-0.2	-0.2	-0.1
97	T	InChI=1S/C3H8NO/c1-3(2)4-5/h3,5H,1-2H3	1.3	1.2	0.8	0.6	0.3	0.0	-0.3	-0.4	-0.4
98	T	InChI=1S/C3H8NO/c1-3(2)4-5/h3-4H,1-2H3	0.2	0.3	1.4	1.2	0.7	0.2	-0.3	-0.5	-0.4
99	T	InChI=1S/C3H8NO/c1-3-4(2)5/h3H2,1-2H3	-1.1	1.8	-1.9	-2.2	-2.0	-1.6	-1.0	-0.6	-0.2
100	T	InChI=1S/C3H9N/c1-2-3-4/h2-4H2,1H3	0.7	2.1	-1.6	-1.1	-0.7	-0.5	-0.4	-0.4	-0.3
101	T	InChI=1S/C3H9N/c1-3(2)4/h3H,4H2,1-2H3	-3.4	2.6	-0.5	-0.3	-0.2	-0.2	-0.2	-0.2	0.0
102	T	InChI=1S/C3H9N/c1-3-4-2/h4H,3H2,1-2H3	-1.4	-0.2	0.6	0.3	0.1	-0.1	-0.2	-0.2	0.0
103	T	InChI=1S/C3H9N/c1-4(2)3/h1-3H3	-0.2	0.4	1.1	0.4	0.1	0.0	-0.1	-0.1	-0.1
104	T	InChI=1S/C3H9NO/c1-3(2)4-5/h3-5H,1-2H3	-2.2	1.6	-2.0	-2.7	-2.5	-1.9	-1.0	-0.5	-0.1
105	T	InChI=1S/C3H9NO/c1-3-4(2)5/h5H,3H2,1-2H3	0.9	-1.0	1.8	2.0	1.7	1.4	0.8	0.4	0.1
106	T	InChI=1S/C4H10N/c1-2-3-4-5/h2H,3-5H2,1H3	-1.7	-2.4	-2.4	-0.9	0.0	0.4	0.6	0.4	0.2

107	T	InChI=1S/C4H10N/c1-2-3-4-5/h3H,2,4-5H2,1H3	1.6	0.8	-4.5	-2.1	-1.0	-0.6	-0.5	-0.6	-0.6
108	T	InChI=1S/C4H10N/c1-2-3-4-5/h4H,2-3,5H2,1H3	1.4	-2.8	-3.8	-1.9	-0.7	-0.1	0.4	0.6	0.5
109	T	InChI=1S/C4H10N/c1-3-4(2)5/h3,5H2,1-2H3	-4.4	0.1	-0.9	-0.1	0.3	0.6	0.7	0.7	0.5
110	T	InChI=1S/C4H10N/c1-3-5-4-2/h3,5H,4H2,1-2H3	-3.0	4.4	4.2	0.9	-0.6	-1.2	-1.5	-1.4	-0.9
111	T	InChI=1S/C4H10N/c1-3-5-4-2/h3-4H2,1-2H3	0.1	1.8	1.2	1.3	1.1	0.9	0.5	0.3	0.0
112	T	InChI=1S/C4H10N/c1-3-5-4-2/h5H,1,3-4H2,2H3	-1.7	-3.5	5.4	3.1	1.7	1.0	0.5	0.4	0.4
113	T	InChI=1S/C4H10N/c1-4(2)3-5/h4-5H,3H2,1-2H3	-2.6	-4.1	2.0	1.5	1.4	1.2	0.9	0.6	0.0
114	T	InChI=1S/C4H10N2/c1-3-4(5)6-2/h3-4,6H,1,5H2,2H3/t4-/m1/s1	-1.3	-3.1	1.6	3.9	4.7	4.5	3.3	2.2	0.9
115	T	InChI=1S/C4H10N2/c1-3-5-6-4-2/h3-4H2,1-2H3	0.0	0.5	1.1	0.2	-0.2	-0.3	-0.3	-0.2	0.0
116	T	InChI=1S/C4H11N/c1-2-3-4-5/h2-5H2,1H3	1.6	-0.6	-2.3	-1.7	-1.3	-1.0	-0.7	-0.5	-0.3
117	T	InChI=1S/C4H11N/c1-3-4(2)5/h4H,3,5H2,1-2H3/t4-/m1/s1	0.4	0.1	0.1	0.2	0.2	0.2	0.1	0.0	0.0
118	T	InChI=1S/C4H11N/c1-3-5-4-2/h5H,3-4H2,1-2H3	2.4	-0.7	2.0	0.9	0.2	-0.2	-0.4	-0.3	-0.1
119	T	InChI=1S/C4H11N/c1-4(2)3-5/h4H,3,5H2,1-2H3	1.3	-0.6	-0.7	-1.3	-1.1	-0.9	-0.5	-0.4	-0.4
120	T	InChI=1S/C4H11N/c1-4(2)5-3/h4-5H,1-3H3	-1.3	0.7	-0.5	-0.6	-0.7	-0.7	-0.7	-0.5	-0.2
121	T	InChI=1S/C4H11N/c1-4(2,3)5/h5H2,1-3H3	-3.7	2.1	2.1	1.7	1.4	1.2	0.9	0.7	0.4
122	T	InChI=1S/C4H11N/c1-4-5(2)3/h4H2,1-3H3	-1.7	3.0	-1.6	-0.7	-0.5	-0.5	-0.6	-0.6	-0.5
123	T	InChI=1S/C4H11NO/c1-3-5(6)4-2/h6H,3-4H2,1-2H3	0.5	-5.8	4.9	4.8	3.9	3.2	2.2	1.6	1.0
124	T	InChI=1S/C4H12N2/c1-4-6(3)5-2/h5H,4H2,1-3H3	0.8	-2.1	0.9	-0.1	-0.9	-1.4	-1.4	-1.1	-0.2
125	T	InChI=1S/C4H3N/c1-2-3-4-5/h1H3	0.9	0.0	-0.2	-0.1	0.0	0.1	0.2	0.2	0.1
126	T	InChI=1S/C4H4N/c1-2-3-4-5/h2-3H,1H2	4.4	-3.3	2.7	3.0	2.7	2.2	1.5	1.1	0.5
127	T	InChI=1S/C4H4N/c1-3-5-4-2/h1,4H,2H2	-0.1	-7.5	-4.7	-4.2	-3.9	-3.9	-3.9	-3.9	-3.9
128	T	InChI=1S/C4H5N/c1-2-3-4-5/h2-3H,1H3/b3-2+	5.7	-0.8	1.9	2.0	1.8	1.4	1.0	0.7	0.4
129	T	InChI=1S/C4H5N/c1-2-3-4-5/h2H,1,3H2	2.4	-0.3	0.8	0.9	0.8	0.6	0.4	0.3	0.2
130	T	InChI=1S/C4H5N/c1-2-3-4-5/h4-5H,1H3/b5-4+	-2.2	0.4	2.3	1.9	1.7	1.6	1.5	1.5	1.5
131	T	InChI=1S/C4H5N/c1-3-5-4-2/h1,4-5H,2H2	-1.0	2.1	1.0	0.7	0.5	0.3	0.0	-0.1	-0.2
132	T	InChI=1S/C4H5N/c1-4(2)3-5/h1H2,2H3	2.2	1.4	-0.4	-0.4	-0.3	-0.3	-0.2	-0.2	-0.1
133	T	InChI=1S/C4H6N/c1-2-3-4-5/h3H,2H2,1H3	-0.3	0.6	-1.7	-0.8	-0.3	-0.1	0.0	0.0	0.1
134	T	InChI=1S/C4H6N/c1-3-4-5-2/h3H,2H2,1H3	1.3	-1.2	0.9	1.0	0.9	0.7	0.4	0.1	-0.3
135	T	InChI=1S/C4H6N/c1-3-5-4-2/h1H,4H2,2H3	-0.1	0.9	-2.4	-1.7	-1.2	-0.9	-0.5	-0.4	-0.2
136	T	InChI=1S/C4H6N/c1-3-5-4-2/h3-4H,1-2H2	-4.2	-1.3	-3.6	-2.5	-0.7	0.6	1.7	1.8	1.4
137	T	InChI=1S/C4H6N/c1-3-5-4-2/h4H,1H2,2H3	-4.1	-1.6	1.3	1.1	0.9	0.7	0.6	0.5	0.5
138	T	InChI=1S/C4H6N/c1-4(2)3-5/h1-2H3	-0.2	2.5	-0.8	-0.7	-0.6	-0.4	-0.1	0.0	0.2

139	T	InChI=1S/C4H7N/c1-2-3-4-5/h2,5H2,1H3	0.7	-5.7	1.1	1.2	1.2	1.3	1.4	1.4	1.4
140	T	InChI=1S/C4H7N/c1-2-3-4-5/h2-3H2,1H3	-2.5	-0.5	-2.6	-1.8	-1.1	-0.6	-0.3	-0.2	-0.2
141	T	InChI=1S/C4H7N/c1-2-3-4-5/h2-5H,1H3/b3-2+,5-4-	4.0	0.3	0.0	-0.2	-0.6	-1.0	-1.1	-1.0	-0.7
142	T	InChI=1S/C4H7N/c1-3-4-5-2/h3-4H,1H2,2H3/b5-4-	-2.3	-4.0	1.1	2.2	2.6	2.7	2.4	2.0	1.2
143	T	InChI=1S/C4H7N/c1-3-4-5-2/h3-4H,2H2,1H3/b4-3+	-0.4	-5.1	-3.3	-1.7	-0.1	0.9	1.6	1.4	0.8
144	T	InChI=1S/C4H7N/c1-3-5-4-2/h1,4H2,2H3	0.9	3.0	-1.4	-2.0	-2.1	-2.0	-1.6	-1.2	-0.7
145	T	InChI=1S/C4H7N/c1-3-5-4-2/h1,5H,4H2,2H3	0.6	4.4	-1.4	-0.9	-0.6	-0.4	-0.2	-0.2	-0.2
146	T	InChI=1S/C4H7N/c1-3-5-4-2/h3-4H,1H2,2H3/b5-4-	-0.4	-0.7	1.2	0.5	-0.3	-0.9	-1.2	-1.2	-0.7
147	T	InChI=1S/C4H7N/c1-3-5-4-2/h3-5H,1-2H2	-4.7	1.7	3.1	3.1	2.6	2.3	2.2	2.3	2.3
148	T	InChI=1S/C4H7N/c1-4(2)3-5/h4H,1-2H3	2.0	4.3	-1.4	-1.3	-1.2	-1.0	-0.8	-0.6	-0.2
149	T	InChI=1S/C4H7N/c1-4(2)5-3/h1,3H2,2H3	1.9	-0.6	-1.5	-0.8	-0.3	-0.1	0.2	0.3	0.2
150	T	InChI=1S/C4H8N/c1-3-4(2)5/h3H,1,5H2,2H3	-2.2	-2.5	2.4	2.6	2.5	2.4	2.0	1.8	1.2
151	T	InChI=1S/C4H8N/c1-3-4-5-2/h3-5H,1H2,2H3	-4.2	1.4	-1.6	-1.9	-2.1	-2.1	-1.8	-1.3	-0.1
152	T	InChI=1S/C4H8N/c1-3-4-5-2/h4H,2-3H2,1H3	-0.6	5.0	-1.4	-0.6	-0.3	0.0	0.2	0.3	0.2
153	T	InChI=1S/C4H8N/c1-3-5-4-2/h5H,1,4H2,2H3	1.3	-4.2	-1.7	-0.1	0.6	0.7	0.3	-0.1	-0.4
154	T	InChI=1S/C4H8N/c1-4(2)3-5/h3,5H,1-2H3	1.2	3.4	0.9	0.5	0.2	0.0	-0.1	-0.1	0.0
155	T	InChI=1S/C4H8N/c1-4(2)3-5/h3H,1,5H2,2H3	2.3	3.4	-1.3	-1.1	-0.6	-0.1	0.4	0.5	0.1
156	T	InChI=1S/C4H8N/c1-4(2)3-5/h4-5H,1-2H3	0.8	-2.3	-0.6	-0.3	-0.2	-0.1	0.0	0.1	0.1
157	T	InChI=1S/C4H8N/c1-4(2)5-3/h1H2,2-3H3	-1.6	-0.5	-1.8	-1.6	-1.5	-1.4	-1.2	-1.0	-0.7
158	T	InChI=1S/C4H8N/c1-4(2)5-3/h3H2,1-2H3	-1.6	6.1	0.5	0.0	-0.8	-1.6	-2.4	-2.5	-1.3
159	T	InChI=1S/C4H8N/c1-4-5(2)3/h1H2,2-3H3	-1.7	3.3	-0.2	-0.3	0.2	0.9	1.7	1.7	0.9
160	T	InChI=1S/C4H9N/c1-2-3-4-5/h2-3H,4-5H2,1H3/b3-2+	0.1	4.8	-0.8	-0.7	-0.7	-0.7	-0.6	-0.5	-0.3
161	T	InChI=1S/C4H9N/c1-2-3-4-5/h3-4H,2,5H2,1H3/b4-3+	3.3	-1.6	1.2	1.2	1.3	1.3	1.1	0.8	0.1
162	T	InChI=1S/C4H9N/c1-3-4(2)5/h2-3,5H2,1H3	-1.9	-2.5	-1.1	-0.9	-0.4	0.1	0.7	0.9	0.7
163	T	InChI=1S/C4H9N/c1-3-4(2)5/h3-4H,1,5H2,2H3/t4-/m0/s1	-0.6	-2.2	2.6	2.6	2.1	1.6	0.9	0.5	0.3
164	T	InChI=1S/C4H9N/c1-3-4-5-2/h3,5H,1,4H2,2H3	-0.3	-3.3	-1.0	0.2	0.7	0.8	0.7	0.5	0.3
165	T	InChI=1S/C4H9N/c1-3-4-5-2/h4H,3H2,1-2H3/b5-4-	0.0	-0.8	-1.0	-0.8	-0.7	-0.6	-0.4	-0.3	-0.1
166	T	InChI=1S/C4H9N/c1-3-5-4-2/h3,5H,1,4H2,2H3	-0.4	4.3	0.2	-0.7	-1.0	-1.0	-0.6	-0.1	0.4
167	T	InChI=1S/C4H9N/c1-3-5-4-2/h3H,4H2,1-2H3/b5-3-	0.2	-0.6	0.6	0.8	0.7	0.4	0.0	-0.2	-0.3
168	T	InChI=1S/C4H9N/c1-4(2)3-5/h1,3,5H2,2H3	-1.1	5.8	0.1	-2.7	-3.3	-3.1	-2.2	-1.5	-0.7
169	T	InChI=1S/C4H9N/c1-4(2)3-5/h3-5H,1-2H3/b5-3+	0.4	2.5	-1.5	-1.4	-1.2	-1.1	-0.8	-0.6	-0.3
170	T	InChI=1S/C4H9N/c1-4(2)3-5/h3H,5H2,1-2H3	-2.1	2.4	-0.5	-0.7	-1.0	-1.1	-1.0	-0.8	-0.3

171	T	InChI=1S/C4H9N/c1-4(2)5-3/h1-3H3	1.9	-0.2	-0.8	-0.1	0.0	-0.1	-0.4	-0.6	-0.6
172	T	InChI=1S/C4H9N/c1-4(2)5-3/h5H,1H2,2-3H3	-2.8	-2.9	1.9	2.5	2.4	2.2	1.8	1.5	0.9
173	T	InChI=1S/C4H9N/c1-4-5(2)3/h4H,1H2,2-3H3	-2.0	7.9	-0.8	-1.2	-1.4	-1.2	-0.7	-0.2	0.1
174	T	InChI=1S/C4H9NO/c1-2-3-4(5)6/h2-3H2,1H3,5H2	-1.5	2.3	-1.9	-2.5	-3.1	-3.3	-2.9	-2.3	-1.0
175	T	InChI=1S/C4H9NO/c1-3(2)4(5)6/h3H,1-2H3,5H2	0.7	-4.1	3.2	3.5	3.7	3.6	2.9	2.1	1.0
176	T	InChI=1S/C4H9NO/c1-3-4(2)5-6/h4H,3H2,1-2H3/t4-/m1/s1	0.2	4.5	-1.0	-1.1	-0.8	-0.6	-0.3	-0.2	-0.1
177	T	InChI=1S/C4H9NO/c1-3-5-4(2)6/h3H2,1-2H3,5H1	-2.4	4.0	-1.2	-0.5	-0.1	0.1	0.2	0.2	0.2
178	T	InChI=1S/C4H9NO/c1-4(2)3-5-6/h4H,3H2,1-2H3	0.9	-3.7	-0.2	-0.1	0.0	0.1	0.2	0.1	-0.1
179	T	InChI=1S/C4H9NO/c1-4(6)5(2)3/h1-3H3	1.0	6.8	-0.3	-1.8	-2.5	-2.7	-2.6	-2.3	-1.7
180	T	InChI=1S/C4H9NO2/c1-2-3-4-5(6)7/h2-4H2,1H3	-0.4	-2.4	-3.5	-2.1	-1.2	-0.8	-0.3	0.0	0.5
181	T	InChI=1S/C4H9NO2/c1-3-4(2)5(6)7/h4H,3H2,1-2H3/t4-/m1/s1	0.1	0.5	0.4	0.2	0.0	-0.2	-0.3	-0.3	-0.2
182	T	InChI=1S/C4H9NO2/c1-3-4(2)7-5-6/h4H,3H2,1-2H3/t4-/m1/s1	0.7	1.5	-2.0	-2.3	-2.7	-2.9	-2.9	-2.8	-2.4
183	T	InChI=1S/C4H9NO2/c1-4(2)3-5(6)7/h4H,3H2,1-2H3	-1.0	-0.2	-0.9	-1.2	-1.0	-0.8	-0.4	-0.3	-0.1
184	T	InChI=1S/C4H9NO2/c1-4(2)3-7-5-6/h4H,3H2,1-2H3	0.2	-4.1	-0.2	-0.4	-0.2	-0.1	0.1	0.1	0.0
185	T	InChI=1S/C5H10N/c1-3-4-5(2)6/h3-4H,6H2,1-2H3	0.3	-1.3	0.1	0.2	0.5	0.7	1.0	1.0	0.7
186	T	InChI=1S/C5H10N/c1-3-5(2)4-6/h4,6H,3H2,1-2H3	-0.9	-0.3	0.6	1.7	2.1	2.1	1.8	1.5	0.9
187	T	InChI=1S/C5H10N/c1-4-5(2)6-3/h4,6H,1H2,2-3H3	1.9	3.8	-2.6	-2.8	-3.0	-3.1	-3.0	-2.7	-1.9
188	T	InChI=1S/C5H10N/c1-4-6-5(2)3/h2,4H2,1,3H3	-0.8	2.2	0.8	0.5	0.6	0.7	1.0	1.1	1.1
189	T	InChI=1S/C5H10N/c1-4-6-5(2)3/h4H,1-3H3	1.6	-6.1	-0.5	0.0	0.8	1.6	2.4	2.5	1.3
190	T	InChI=1S/C5H10N/c1-5(2)4-6-3/h4H,1-3H3	-0.5	0.5	1.0	-0.3	-0.7	-0.7	-0.6	-0.4	-0.1
191	T	InChI=1S/C5H11N/c1-2-3-4-5-6/h3-4H,2,5-6H2,1H3/b4-3+	-0.5	-0.4	3.0	2.8	2.2	1.7	1.0	0.6	0.3
192	T	InChI=1S/C5H11N/c1-3-4-5-6-2/h3-4,6H,5H2,1-2H3/b4-3+	-1.5	-3.3	0.3	0.8	0.9	0.9	0.6	0.4	0.2
193	T	InChI=1S/C5H11N/c1-3-5(2)4-6/h4-6H,3H2,1-2H3	-4.1	0.5	2.9	2.8	2.5	2.2	1.5	1.1	0.6
194	T	InChI=1S/C5H11N/c1-3-5(2)4-6/h4H,3,6H2,1-2H3/b5-4-	-2.2	-2.0	0.1	-0.2	-0.4	-0.4	-0.3	-0.1	0.1
195	T	InChI=1S/C5H11N/c1-3-5-6-4-2/h3,6H,1,4-5H2,2H3	-0.4	-2.7	0.7	0.8	0.7	0.6	0.4	0.3	0.2
196	T	InChI=1S/C5H11N/c1-4(2)5(3)6/h5H,1,6H2,2-3H3/t5-/m1/s1	-1.1	3.3	-1.7	-1.6	-1.3	-1.0	-0.6	-0.5	-0.4
197	T	InChI=1S/C5H11N/c1-4-5(2)6-3/h4-6H,1H2,2-3H3/t5-/m0/s1	1.7	-1.1	-0.9	-0.9	-0.8	-0.6	-0.3	-0.1	0.1
198	T	InChI=1S/C5H11N/c1-4-5(2)6-3/h4H2,1-3H3/b6-5+	-0.2	-1.9	0.6	0.3	0.1	0.0	-0.1	-0.2	-0.2
199	T	InChI=1S/C5H11N/c1-4-5(2,3)6/h4H,1,6H2,2-3H3	-1.4	0.4	-0.5	-0.5	-0.5	-0.4	-0.3	-0.2	0.0
200	T	InChI=1S/C5H11N/c1-4-6(3)5-2/h4H,1,5H2,2-3H3	0.1	-4.9	0.8	0.6	0.2	-0.2	-0.7	-0.9	-0.5
201	T	InChI=1S/C5H11N/c1-4-6-5(2)3/h4H2,1-3H3	-1.7	2.2	0.1	-0.2	-0.1	0.1	0.5	0.8	0.9
202	T	InChI=1S/C5H11N/c1-4-6-5(2)3/h6H,2,4H2,1,3H3	-2.1	-3.8	3.0	3.0	2.7	2.4	2.1	2.0	1.7

203	T	InChI=1S/C5H11N/c1-5(2)4-6-3/h4,6H,1-3H3	4.3	-0.4	0.4	1.0	1.4	1.5	1.3	0.9	0.2
204	T	InChI=1S/C5H11NO/c1-3-5(4-2)6-7/h5H,3-4H2,1-2H3	0.0	-3.0	4.5	4.2	3.4	2.7	1.7	1.1	0.4
205	T	InChI=1S/C5H11NO/c1-4-5(7)6(2)3/h4H2,1-3H3	1.9	-0.7	0.2	-0.8	-1.3	-1.4	-1.0	-0.7	-0.1
206	T	InChI=1S/C5H11NO/c1-5(2,3)4(6)7/h1-3H3,6H2	2.3	-3.2	-0.1	1.6	2.9	3.5	3.6	3.2	1.9
207	T	InChI=1S/C5H11NO2/c1-3-5(4-2)6(7)8/h5H,3-4H2,1-2H3	-2.7	-6.2	2.1	2.3	2.4	2.3	2.0	1.5	0.7
208	T	InChI=1S/C5H11NO2/c1-5(2,3)4-6(7)8/h4H2,1-3H3	-1.0	5.8	1.8	0.3	-0.3	-0.5	-0.6	-0.5	-0.5
209	T	InChI=1S/C5H12N/c1-4-5(2)6-3/h6H,4H2,1-3H3	4.4	-1.7	-0.7	-0.7	-0.3	0.1	0.4	0.5	0.5
210	T	InChI=1S/C5H12N2/c1-3-5-7-6-4-2/h3-5H2,1-2H3	-0.1	1.1	-1.0	-0.4	0.0	0.1	0.2	0.1	0.0
211	T	InChI=1S/C5H13N/c1-2-3-4-5-6/h2-6H2,1H3	2.3	-3.0	-2.0	-1.8	-1.4	-1.1	-0.8	-0.6	-0.3
212	T	InChI=1S/C5H13N/c1-3-4-5(2)6/h5H,3-4,6H2,1-2H3/t5-/m1/s1	-1.0	-2.4	-0.3	0.5	0.6	0.5	0.3	0.2	0.2
213	T	InChI=1S/C5H13N/c1-3-5(6)4-2/h5H,3-4,6H2,1-2H3	1.9	-2.6	1.5	0.8	0.5	0.3	0.1	0.0	0.0
214	T	InChI=1S/C5H13N/c1-4-5(2,3)6/h4,6H2,1-3H3	0.3	-0.4	-0.5	-0.3	-0.1	0.1	0.3	0.3	0.2
215	T	InChI=1S/C5H13N/c1-4-6-5(2)3/h5-6H,4H2,1-3H3	-1.0	1.3	-0.6	-0.3	-0.3	-0.4	-0.2	0.0	0.3
216	T	InChI=1S/C5H13N/c1-5(2,3)6-4/h6H,1-4H3	3.4	-1.6	-1.6	-1.4	-1.4	-1.3	-1.2	-1.0	-0.6
217	T	InChI=1S/C5H4N/c1-3-5-6-4-2/h2H,1H3	0.3	-5.9	-1.8	-1.6	-1.6	-1.7	-1.8	-1.9	-2.1
218	T	InChI=1S/C5H6N/c1-2-3-4-5-6/h2-4H,1H3	-0.9	-0.1	1.4	1.4	1.2	1.0	0.6	0.5	0.3
219	T	InChI=1S/C5H6N/c1-3-5(2)4-6/h3H,2H2,1H3	3.4	-1.2	0.8	1.0	0.9	0.8	0.7	0.5	0.4
220	T	InChI=1S/C5H6N/c1-3-5-6-4-2/h4H,2H2,1H3	1.1	-0.3	-1.1	-0.9	-0.7	-0.4	-0.1	0.0	0.1
221	T	InChI=1S/C5H6N/c1-4-6-5(2)3/h1H,2H2,3H3	-1.1	7.9	5.7	5.1	4.6	4.3	4.0	3.8	3.8
222	T	InChI=1S/C5H7N/c1-2-3-4-5-6/h2-3H,4H2,1H3/b3-2+	-0.6	0.6	1.0	1.0	0.8	0.6	0.4	0.2	0.1
223	T	InChI=1S/C5H7N/c1-3-4-5-6-2/h5H,1-2H3/b6-5+	-0.6	5.2	0.3	0.5	0.7	0.8	1.0	1.1	1.2
224	T	InChI=1S/C5H7N/c1-3-5(2)4-6/h2-3H2,1H3	-0.5	-0.8	0.3	0.5	0.5	0.5	0.4	0.3	0.1
225	T	InChI=1S/C5H7N/c1-3-5(2)4-6/h3H,1-2H3/b5-3-	-5.1	0.6	-0.7	-1.1	-1.1	-1.1	-0.8	-0.6	-0.4
226	T	InChI=1S/C5H7N/c1-3-5-6-4-2/h2-3,5-6H,1H3/b5-3+	4.2	2.8	-0.6	-0.4	-0.3	-0.3	-0.5	-0.6	-0.7
227	T	InChI=1S/C5H7N/c1-4-6-5(2)3/h1,6H,2H2,3H3	-3.2	-4.9	-0.4	-0.3	-0.2	0.0	0.4	0.7	0.9
228	T	InChI=1S/C5H7N/c1-5(2)3-4-6/h1,3H2,2H3	-1.8	-0.3	-1.8	-1.8	-1.6	-1.3	-0.8	-0.5	-0.3
229	T	InChI=1S/C5H7N/c1-5(2)3-4-6/h3H,1-2H3	-2.9	3.5	-1.1	-1.5	-1.5	-1.4	-1.0	-0.7	-0.4
230	T	InChI=1S/C5H8N/c1-3-5(2)4-6/h3H2,1-2H3	-1.3	3.7	-3.9	-2.4	-1.7	-1.3	-0.8	-0.6	-0.3
231	T	InChI=1S/C5H8N/c1-3-5-6-4-2/h3-4H,1-2H3	2.8	2.8	-2.2	-2.1	-1.8	-1.5	-1.0	-0.7	-0.2
232	T	InChI=1S/C5H8N/c1-4-6-5(2)3/h1,5H,2-3H3	-0.6	0.1	1.0	0.4	0.1	-0.1	-0.3	-0.3	-0.3
233	T	InChI=1S/C5H8N/c1-4-6-5(2)3/h4H,1-2H2,3H3	4.2	1.3	3.6	2.5	0.7	-0.6	-1.7	-1.8	-1.4
234	T	InChI=1S/C5H8N/c1-5(2)3-4-6/h5-6H,1-2H3	-1.5	-3.6	0.9	0.9	1.0	1.0	1.1	1.2	1.3

235	T	InChI=1S/C5H9N/c1-3-5(2)4-6/h5H,3H2,1-2H3/t5-/m0/s1	0.3	2.9	-0.9	-0.9	-0.8	-0.7	-0.5	-0.3	-0.2
236	T	InChI=1S/C5H9N/c1-3-5(6)4-2/h3-5H,1-2,6H2	-1.3	1.7	2.4	0.9	-0.2	-0.8	-1.0	-0.8	-0.4
237	T	InChI=1S/C5H9N/c1-3-5-6-4-2/h3,5H,1,4H2,2H3/b6-5-	-2.5	-3.1	1.6	2.5	2.9	2.8	2.3	1.8	1.1
238	T	InChI=1S/C5H9N/c1-3-5-6-4-2/h3-6H,2H2,1H3/b5-3+	1.9	0.6	1.5	1.3	1.0	1.0	1.2	1.4	1.4
239	T	InChI=1S/C5H9N/c1-4-6-5(2)3/h1,5-6H,2-3H3	-2.5	-4.7	-0.1	0.1	0.2	0.1	0.1	0.0	0.0
240	T	InChI=1S/C5H9N/c1-4-6-5(2)3/h4,6H,1-2H2,3H3	-3.2	-5.4	-2.7	-2.1	-1.0	-0.2	0.4	0.4	0.1
241	T	InChI=1S/C5H9N/c1-4-6-5(2)3/h4H,2H2,1,3H3/b6-4-	-0.6	-0.1	1.4	1.0	0.7	0.5	0.2	0.0	-0.1
242	T	InChI=1S/C5H9N/c1-5(2)3-4-6/h3-4,6H,1-2H3/b6-4-	-0.3	4.5	-1.2	-2.7	-3.3	-3.3	-2.8	-2.1	-1.1
243	T	InChI=1S/C5H9N/c1-5(2,3)4-6/h1-3H3	0.6	5.2	-1.7	-2.3	-2.3	-2.0	-1.5	-1.1	-0.5
244	T	InChI=1S/C6H11N/c1-3-5-6(7)4-2/h3-6H,2,7H2,1H3/b5-3-/t6-/m0/s1	3.6	1.8	-0.6	-1.8	-1.9	-1.6	-1.0	-0.7	-0.4
245	T	InChI=1S/C6H11N/c1-3-6(2)4-5-7/h4-5,7H,3H2,1-2H3/b6-4+,7-5+	0.2	-1.5	-2.3	-3.1	-2.9	-2.3	-1.4	-0.9	-0.3
246	T	InChI=1S/C6H11N/c1-3-6(4-2)5-7/h6H,3-4H2,1-2H3	-1.3	-0.4	0.2	0.0	-0.1	-0.1	0.0	0.0	0.0
247	T	InChI=1S/C6H11N/c1-4-6(2,3)5-7/h4H2,1-3H3	0.3	4.9	-3.0	-3.0	-2.5	-2.1	-1.4	-1.0	-0.5
248	T	InChI=1S/C6H11N/c1-4-6(5-2)7-3/h4-7H,1-2H2,3H3	-2.3	-3.5	-1.7	0.9	2.1	2.4	2.0	1.5	0.8
249	T	InChI=1S/C6H11N/c1-5(2)7-6(3)4/h7H,1,3H2,2,4H3	6.0	3.1	-1.9	-2.3	-2.7	-3.0	-3.8	-4.1	-3.8
250	T	InChI=1S/C6H11N/c1-6(2)4-5-7-3/h4-5H,1-3H3/b7-5-	-1.2	2.9	0.6	-1.2	-2.0	-2.3	-2.0	-1.6	-0.9
251	T	InChI=1S/C6H11NO2/c1-3-5-6(4-2)9-7-8/h3,6H,1,4-5H2,2H3/t6-/m0/s1	-2.0	-2.8	6.6	7.6	8.3	8.7	8.7	8.3	7.0
252	T	InChI=1S/C6H13N/c1-5-6(2,3)7-4/h5,7H,1H2,2-4H3	3.6	-2.8	1.6	1.6	1.4	1.2	0.8	0.5	0.1
253	T	InChI=1S/C6H13N/c1-5-7(4)6(2)3/h5-6H,1H2,2-4H3	3.6	-6.4	0.1	1.0	1.0	0.5	-0.2	-0.6	-0.5
254	T	InChI=1S/C6H13NO/c1-4-5-6(8)7(2)3/h4-5H2,1-3H3	1.3	-5.8	-0.9	-0.3	0.1	0.3	0.5	0.6	0.7
255	T	InChI=1S/C6H13NO/c1-4-7(5-2)6(3)8/h4-5H2,1-3H3	0.2	-5.6	3.1	4.0	4.2	4.0	3.0	2.1	0.7
256	T	InChI=1S/C6H15N/c1-3-5-7-6-4-2/h7H,3-6H2,1-2H3	0.0	0.8	-3.4	-3.2	-2.8	-2.4	-1.7	-1.1	-0.4
257	T	InChI=1S/C6H15N/c1-4-7(5-2)6-3/h4-6H2,1-3H3	0.6	-1.0	0.5	0.2	0.2	0.2	0.2	0.2	0.2
258	T	InChI=1S/C6H15N/c1-5(2)7-6(3)4/h5-7H,1-4H3	2.7	3.2	-1.3	-0.9	0.0	0.8	1.6	1.6	0.7
259	T	InChI=1S/C6H6N/c1-3-5-7-6-4-2/h1-2H3	-0.3	5.9	1.8	1.6	1.6	1.7	1.8	1.9	2.1
260	T	InChI=1S/C6H7N/c1-6(2)4-3-5-7/h6H,1-2H3	-0.9	0.0	0.2	0.1	-0.1	-0.1	-0.2	-0.2	-0.1
261	T	InChI=1S/C6H8N/c1-3-4-6(2)5-7/h3H,1,4H2,2H3	1.4	-6.1	4.7	3.2	2.3	1.7	1.0	0.6	0.1
262	T	InChI=1S/C6H8N/c1-6(2)4-3-5-7/h3-4H,1-2H3	-3.5	3.3	-4.1	-4.3	-3.8	-3.2	-2.2	-1.5	-0.8
263	T	InChI=1S/C6H9N/c1-3-6(2)4-5-7/h4H,3H2,1-2H3/b6-4+	-2.7	-2.7	-0.9	-0.5	-0.2	-0.1	0.0	0.0	-0.1
264	T	InChI=1S/C7H11N/c1-3-5-7(4-2)6-8/h3,7H,1,4-5H2,2H3/t7-/m1/s1	-1.0	-6.8	2.1	2.2	2.0	1.8	1.3	0.9	0.4
265	T	InChI=1S/C7H11N/c1-4-5-7(2,3)6-8/h4H,1,5H2,2-3H3	-1.0	-7.0	5.2	4.0	3.5	3.1	2.4	1.8	0.8
266	T	InChI=1S/C7H13N/c1-4-5-7(2,3)6-8/h4-5H2,1-3H3	0.1	-3.1	-0.5	1.2	1.3	1.0	0.5	0.3	0.2

267	T	InChI=1S/C7H14N/c1-4-7(3)6-8-5-2/h6H,4-5H2,1-3H3	-3.4	-5.3	-0.6	-0.4	-0.2	0.0	0.2	0.2	0.2
268	T	InChI=1S/C7H17N/c1-4-5-8-6-7(2)3/h7-8H,4-6H2,1-3H3	0.9	4.0	-0.8	-0.6	-0.4	-0.1	0.2	0.3	-0.3
269	T	InChI=1S/C8H19N/c1-3-5-7-9-8-6-4-2/h9H,3-8H2,1-2H3	1.4	7.3	-1.9	-2.4	-2.4	-2.2	-1.7	-1.1	-0.5
270	T	InChI=1S/CH2N/c1-2/h1-2H	-2.4	-4.3	2.1	2.3	2.1	1.9	1.5	1.2	0.8
271	T	InChI=1S/CH2N/c1-2/h1H2	-5.2	-6.3	0.4	-0.1	-0.1	0.0	0.4	0.6	0.6
272	T	InChI=1S/CH3N/c1-2/h2H,1H2	1.7	0.4	-0.6	-1.2	-1.3	-1.2	-0.7	-0.4	-0.2
273	T	InChI=1S/CH3NO/c1-2-3/h1H3	0.0	0.0	0.0	0.0	0.0	0.0	0.0	0.0	0.0
274	T	InChI=1S/CH3NO2/c1-2(3)4/h1H3	0.0	0.0	0.0	0.0	0.0	0.0	0.0	0.0	0.0
275	T	InChI=1S/CH3NO2/c1-4-2-3/h1H3	0.0	0.0	0.0	0.0	0.0	0.0	0.0	0.0	0.0
276	T	InChI=1S/CH4N/c1-2/h1-2H2	2.8	-5.8	2.6	2.6	2.7	2.7	2.4	2.0	1.2
277	T	InChI=1S/CH4N/c1-2/h2H,1H3	-2.5	-3.2	3.8	2.9	2.2	1.8	1.3	1.1	0.8
278	T	InChI=1S/CH4NO/c1-2-3/h2H,1H3	1.8	-4.2	3.5	3.5	3.0	2.4	1.6	1.2	0.7
279	T	InChI=1S/CH4NO/c1-2-3/h3H,1H3	-1.5	-1.5	1.0	0.8	0.8	0.8	0.8	0.7	0.5
280	T	InChI=1S/CH5N/c1-2/h2H2,1H3	-0.5	-1.7	3.4	2.0	1.1	0.7	0.3	0.2	0.2
281	T	InChI=1S/CH6N2/c1-3-2/h3H,2H2,1H3	0.8	-0.3	0.3	0.1	-0.2	-0.4	-0.5	-0.5	-0.1
282	V	InChI=1S/C3H8N2/c1-2-3(4)5/h2H,4-5H2,1H3	-1.6	-1.9	4.5	3.8	2.1	0.6	-0.9	-0.9	0.1
283	V	InChI=1S/C4H10N/c1-2-3-4-5/h5H,2-4H2,1H3	2.5	0.3	-2.0	-1.1	-0.6	-0.4	-0.3	-0.2	-0.2
284	V	InChI=1S/C4H10N2/c1-2-3-6-4-5/h2,6H,1,3-5H2	-0.1	-0.7	-0.2	0.1	0.3	0.4	0.3	0.2	0.0
285	V	InChI=1S/C4H10NO/c1-3-5(6)4-2/h3-4H2,1-2H3	-1.5	1.7	-4.0	-3.6	-2.9	-2.3	-1.4	-1.0	-0.5
286	V	InChI=1S/C4H8N/c1-3-4(2)5/h5H,2-3H2,1H3	1.6	-2.5	-0.6	-0.5	-0.4	-0.4	-0.4	-0.4	-0.2
287	V	InChI=1S/C5H10N/c1-5(2)4-6-3/h4-5H,3H2,1-2H3	1.6	2.3	0.2	-0.2	-0.3	-0.4	-0.3	-0.3	-0.5
288	V	InChI=1S/C5H11N/c1-3-4-5(2)6/h4H,3,6H2,1-2H3/b5-4-	0.5	-2.6	-3.6	-2.4	-1.2	-0.4	0.3	0.3	0.1
289	V	InChI=1S/C5H11N/c1-3-5-6-4-2/h5H,3-4H2,1-2H3/b6-5-	1.9	-1.8	-0.6	-0.1	0.0	0.1	0.0	-0.1	-0.1
290	V	InChI=1S/C5H11NO2/c1-3-5(4-2)8-6-7/h5H,3-4H2,1-2H3	-0.9	-3.0	-1.9	-1.7	-1.3	-1.1	-1.2	-1.5	-1.7
291	V	InChI=1S/C5H12N2/c1-3-4-5(6)7-2/h3-5,7H,6H2,1-2H3/b4-3+/t5-/m1/s1	-2.1	-2.1	-0.4	0.8	2.1	3.0	3.4	2.9	1.5
292	V	InChI=1S/C5H12N2/c1-3-4-5-7-6-2/h3-5H2,1-2H3	0.2	-2.5	-0.8	0.2	0.6	0.6	0.5	0.4	0.2
293	V	InChI=1S/C5H8N/c1-5(2)3-4-6/h3,5H,1-2H3	1.0	-0.2	-0.1	-0.5	-0.6	-0.6	-0.6	-0.7	-0.6
294	V	InChI=1S/C6H11N/c1-4-5-7-6(2)3/h5H,2,4H2,1,3H3/b7-5+	-1.3	0.7	0.1	-0.2	-0.4	-0.4	-0.4	-0.2	-0.1
295	V	InChI=1S/C6H13N/c1-4-5-6(2,3)7/h4-5H,7H2,1-3H3/b5-4+	-2.2	2.5	-1.1	-1.0	-0.9	-0.8	-0.5	-0.3	-0.1
296	V	InChI=1S/C6H13NO/c1-4-6(8)7(3)5-2/h4-5H2,1-3H3	-0.1	3.1	-2.4	-1.1	-0.4	0.1	0.6	0.7	0.7
297	V	InChI=1S/C6H13NO2/c1-4-6(2,3)5-7(8)9/h4-5H2,1-3H3	2.7	-3.1	6.6	5.2	3.9	2.9	1.5	0.7	-0.5
298	V	InChI=1S/C6H14N/c1-4-6(2,3)5-7/h5H,4,7H2,1-3H3	-2.6	2.3	2.6	3.1	2.6	1.9	0.8	0.2	-0.2

299	V	InChI=1S/C6H15N/c1-4-6(2,3)5-7/h4-5,7H2,1-3H3	2.3	2.6	1.8	1.6	1.3	0.9	0.4	0.0	-0.3
300	V	InChI=1S/C6H8N2/c7-5-3-1-2-4-6-8/h1-4H2	1.1	-0.3	1.8	1.6	1.2	0.8	0.5	0.3	0.2

A.2.4. Comparison with previously derived GAVs of Benson et al.

Table A-6: Differences between group additive values for the standard enthalpy of formation [kJ mol^{-1}], the entropy and heat capacity [J mol^{-1} K^{-1}] for nitrogen-containing compounds obtained in this work and reported by Benson et al. [6] for all groups in common.

Group	GAV (current work) – GAV(literature)								
	$\Delta_f H^\circ$	S°	C_p°						
	298 K	298 K	300 K	400 K	500 K	600 K	800 K	1000 K	1500 K
C-(C)(N)(H)$_2$	-0.2	-3.6	3.7	2.5	1.7	1.3	0.8	0.6	
C-(C)(CN)(H)$_2$	3.9	-2.2	2.6	2.1	0.8	-0.2	-1.1	-0.7	
C-(C)(N$_A$)(H)$_2$	-3.9	1.3	-	-	-	-	-	-	-
C-(N)$_2$(H)$_2$	3.7	-	-	-	-	-	-	-	-
C-(C)$_2$(N)(H)	3.1	-3.0	5.5	4.2	2.7	2.6	1.5	1.2	-
C-(C)$_2$(CN)(H)	4.0	-8.0	2.7	3.9	4.4	3.9	2.9	2.2	-
C-(C)$_3$(N)	1.3	-0.5	5.5	4.4	3.0	2.2	0.6	0.4	-
C$_d$-(CN)(H)	-7.2	4.8	0.0	-0.8	-1.3	-1.2	-1.0	0.3	-
C$_t$-(CN)	-21.3	-3.0	-1.0	-0.8	-1.0	-0.9	-0.7	-0.6	-0.6
CO-(C)(N)	15.8	-10.6	-1.9	0.3	1.0	2.1	-1.3	-5.1	
C-(C)(NO)(H)$_2$	8.8	-	-	-	-	-	-	-	-
C-(C)$_2$(NO)(H)	4.1	-	-	-	-	-	-	-	-
C-(C)(NO$_2$)(H)$_2$	-2.1	0.4	-	-	-	-	-	-	-
C-(C)$_2$(NO$_2$)(H)	5.8	-1.8	-	-	-	-	-	-	-
N-(CO)(H)$_2$	-10.0	19.6	11.2	6.9	3.6	1.4	-0.7	-1.6	-
N-(C)(CO)(H)	-9.7	-	-	-	-	-	-	-	-
N-(C)(H)$_2$	1.1	0.8	-2.8	-1.6	-0.8	-0.3	-0.1	0.0	0.1
N-(C)$_2$(H)	5.6	-1.5	2.7	1.3	0.6	0.3	0.0	-0.3	0.0
N-(C)$_3$	0.0	1.6	0.7	0.6	0.7	1.1	1.5	1.9	2.4
N-(N)(H)$_2$	-1.4	1.4	0.7	0.3	-0.3	-0.8	-1.5	-2.0	-2.5
N-(C)(N)(H)	4.1	-8.4	1.1	0.8	1.1	1.5	1.9	2.4	3.4
N-(C)$_2$(N)	1.2	0.2	-	-	-	-	-	-	-
N$_I$-(C)	7.9	-	-	-	-	-	-	-	-
N$_A$-(C)	-14.1	-	-	-	-	-	-	-	-

A.2.5. Comparison with previously derived GAVs of Holmes and Aubry

Table A-7: Differences between group additive values and pairs of linear dependent for the standard enthalpy of formation [kJ mol^{-1}] for nitrogen-containing compounds obtained in this work and reported by Holmes and Aubry [7] for all groups in common.

Group	GAV (current work) – GAV (literature)	Pairs of linear dependent groups	GAVs (current work) – GAVs (literature)
	$\Delta_f H^\circ$		$\Delta_f H^\circ$
C-(C)(N)(H)$_2$	-4.8	C-(CN)(C)(H)$_2$+CN-(C)	4.1
C-(C)(CN)(H)$_2$	124.1	C-(CN)(C$_d$)(H)$_2$+CN-(C$_d$)	9.1
C-(C$_d$)(CN)(H)$_2$	124.1	N-(CO)(H)$_2$+CO-(N)(C)	2.1
C-(C)$_2$(N)(H)	-0.6	N-(C)(CO)(H)+CO-(N)(C)	6.4
C-(C)$_3$(N)	0.9		
C$_d$-(C)(N)	0.4		
C$_I$-(C)(H)	26		
C$_I$ -(Cd)(H)	3.0		
C$_I$-(C)$_2$	3.5		
N-(CO)(H)$_2$	39		
N-(C)(CO)(H)	-8.1		
N-(C)$_2$(CO)	1.0		
N-(C)(H)$_2$	3.1		
N-(C)$_2$(H)	5.0		
N-(C)$_3$	0.0		
N-(C)(C$_d$)(H)	-3.2		
N-(C$_d$)$_2$(H)	-1.6		
N$_I$-(H)	-2.3		
N$_I$-(C)	1.0		
N$_I$-(C$_d$)	-12.9		

A.2.6. Comparison with previously derived GAVs of Ashcraft et al.

Table A-8: Differences between group additive values and pairs of linear dependent groups for the standard enthalpy of formation [kJ mol^{-1}], the entropy and heat capacity [J mol^{-1} K^{-1}] for nitrogen-containing compounds obtained in this work and reported by Ashcraft et al. [8] for all groups in common.

Group	GAV (current work) – GAV(literature)								
	$\Delta_f H^\circ$	S°	C_p°						
	298 K	298 K	300 K	400 K	500 K	600 K	800 K	1000 K	1500 K
C-(C)(N)(H)$_2$	-0.2	-3.6	3.5	2.5	1.6	1.2	0.7	0.7	-1.9
C-(C)(C$_I$)(H)$_2$	1.6	0.1	0.5	0.3	0.3	0.1	-0.2	-0.4	-0.1
C-(C)(CN)(H)$_2$	2.3	-0.5	1.7	1.7	1.6	1.4	1.0	1.0	1.1
C-(C)(N$_A$)(H)$_2$	-3.9	3.0	0.2	-0.1	-0.5	-0.5	-0.7	-0.5	-0.3
C-(C)$_2$(C$_I$)(H)	1.8	0.2	0.6	0.2	0.2	0.5	0.1	0.5	0.6
C-(C)$_3$(CN)	4.2	-6.0	2.8	3.3	3.6	3.9	3.2	3.3	3.2
C$_d$-(C)(N)	26.7	0.9	-1.7	-3.5	-3.9	-3.8	-3.3	-2.3	-
C$_d$-(C)(CN)	-2.7	-3.1	3.1	2.9	2.6	2.7	2.2	1.8	1.3
C$_I$-(C)(H)	10.1	-6.2	-5.6	-5.5	-5.7	-6.1	-6.3	-7.2	-
C$_I$-(C)$_2$	1.6	-54.9	-1.5	-1.8	-2.6	-3.2	-4.4	-5.0	-6.0
C-(C)(NO)(H)$_2$	-0.9	-1.4	-1.0	-0.9	-0.4	-0.4	0.1	0.3	0.2
C-(C)$_2$(NO)(H)	-0.9	-7.2	5.2	4.5	3.9	3.4	2.5	2.3	1.9
C-(C)(NO$_2$)(H)$_2$	-3.4	-1.7	3.0	2.2	1.7	1.5	1.1	0.7	0.2
C-(C)$_2$(NO$_2$)(H)	-2.2	-4.3	0.6	0.9	1.4	1.9	2.1	2.1	1.8
N-(C$_d$)(H)$_2$	-27.0	-0.6	2.0	2.4	2.0	1.8	1.7	1.4	1.2
N-(C)(C$_d$)(H)	-26.2	0.0	-2.7	-1.8	-0.9	0.5	1.7	2.5	2.8
N-(N)(H)$_2$	-1.4	1.5	0.7	0.2	-0.2	-0.9	-1.4	-1.9	-2.5
N-(C)(N)(H)	4.1	-8.3	1.2	0.8	1.1	1.5	1.9	2.4	3.4
N-(C)$_2$(N)	11.2	3.1	-0.2	-1.5	-2.0	-1.7	-0.7	0.6	1.7
N$_I$-(H)	-6.5	55.1	5.2	5.0	5.4	5.9	6.6	7.2	8.0
N$_I$-(C)	7.9	56.7	6.6	5.7	6.4	7.0	8.3	8.7	9.7
N$_A$-(C)	8.9	-1.7	-0.1	0.1	0.8	1.1	1.2	1.0	1.1
Pairs of linear dependent GAVs									
N-(C$_d$)(H)$_2$ + C$_d$-(C)(N)	-0.3	-0.6	2.0	2.4	2.0	1.8	1.7	1.4	1.2
N-(C$_d$)(C)(H) + C$_d$-(C)(N)	0.5	0.0	-2.7	-1.8	-0.9	0.5	1.7	2.5	2.8

A.3. References

[1] B. Ruscic, D.H. Bross, Active Thermochemical Tables (ATcT) values based on ver. 1.122d of the Thermochemical Network (2018); available at ATcT.anl.gov.

[2] J. Pedley, R.D. Naylor, S.P. Kirby, Thermochemical data of organic compounds, springer Netherlands, 1986.

[3] P.J. Lindstrom, W.G. Mallard, NIST Chemistry WebBook, NIST Standard Reference Database Number 69, National Institute of Standards and Technology, Gaithersburg MD.

[4] J.A. Montgomery, M.J. Frisch, J.W. Ochterski, G.A. Petersson, A complete basis set model chemistry. VII. Use of the minimum population localization method, The Journal of Chemical Physics 112 (2000) 6532-6542.

[5] J.A. Dean, N.A. Lange, Lange's Handbook of Chemistry, McGraw-Hill, 1999.

[6] S.W. Benson, F.R. Cruickshank, D.M. Golden, G.R. Haugen, H.E. O'Neal, A.S. Rodgers, R. Shaw, R. Walsh, Additivity rules for the estimation of thermochemical properties, Chemical Reviews 69 (1969) 279-324.

[7] J.L. Holmes, C. Aubry, Group Additivity Values for Estimating the Enthalpy of Formation of Organic Compounds: An Update and Reappraisal. 2. C, H, N, O, S, and Halogens, The Journal of Physical Chemistry A 116 (2012) 7196-7209.

[8] R.W. Ashcraft, W.H. Green, Thermochemical Properties and Group Values for Nitrogen-Containing Molecules, The Journal of Physical Chemistry A 112 (2008) 9144-9152.

Appendix B

Supporting information to Chapter 4

B.1. CBS-QB3 methodology: Experimental validation

Table B-1: Experimental validation of the CBS-QB3 methodology: Source and kinetic parameters for the modified Arrhenius expression, i.e. $k=A\cdot T^n\cdot exp(-E_a/RT)$. The pre-exponential factor is expressed in $m^3\ mol^{-1}\ s^{-1}$ and E_a is expressed in kJ mol^{-1}.

No.	Reaction	Ref	Temperature [K]	*A*	*n*	E_a
1	H + NH_3 ↔ H_2 + $^{\bullet}NH_2$	[1]	490 – 960	7.29E+07	0.0	57.5
		[2]	524 - 714	4.00E+06	0.0	41.8
		[3]	863 - 963	4.09E+07	0.0	57.3
		[4]	673 – 1000	8.07E+07	0.0	60.9
		[5]	500 - 1800	6.36E-01	2.39	42.6
		[6]	908 - 1780	3.44E+08	0.0	67.1
2	$^{\bullet}NH_2$ + CH_4 ↔ NH_3 + $^{\bullet}CH_3$	[7]	300 - 520	4.94E+05	0.0	43.9
		[8]	743 - 1020	4.70E+06	0.0	38.9
		[9]	1500 – 2100	1.20E+07	0.0	63.4
		[10]	1591 – 2084	7.05E+07	0.0	71.3
3	$^{\bullet}NH_2$ + ↔ NH_3 +	[7]	300 - 520	3.70E+05	0.0	29.9
		[11]	600 – 970	9.70E+06	0.0	44.4
		[9]	1500 – 2100	9.70E+06	0.0	48.0
4	$^{\bullet}CH_3$ + —NH_2 ↔ CH_4 + $^{\bullet}$—NH_2	[12]	380 - 450	9.76E+04	0.0	36.4
5	$^{\bullet}CH_3$ + —NH_2 ↔ CH_4 + —$NH^{\bullet}$	[12]	380 - 450	3.55E+03	0.0	23.9
6	$^{\bullet}CH_3$ + ↔ CH_4 +	[13]	400 - 450	6.31E+10	0.0	26.8
7	$^{\bullet}CH_3$ + ↔ CH_4 +	[14]	380 – 450	1.50E+05	0.0	33.9
8	$^{\bullet}CH_3$ + ↔ CH_4 +	[14]	380 - 450	7.59E+03	0.0	27.1

B.2. H-H-N hydrogen abstractions

B.2.1. Single-event Arrhenius parameters for reference reaction

Table B-2: Intrinsic Arrhenius parameters over the temperature range 300-1800 K for the reference reaction of H-H-N hydrogen abstraction reactions, i.e. H· + NH_3 → H_2 + ·NH_2. The single-event pre-exponential factor is expressed in m^3 mol^{-1} s^{-1} and E_a is expressed in kJ mol^{-1}.

Temperature [K]	Forward		Reverse	
	$log\tilde{A}$	E_a	$log\tilde{A}$	E_a
300	7.124	57.7	6.048	48.2
400	7.203	58.2	6.040	48.1
500	7.249	58.5	6.069	48.3
600	7.355	59.6	6.140	49.0
700	7.462	60.9	6.235	50.1
800	7.563	62.3	6.339	51.6
900	7.658	63.8	6.444	53.2
1000	7.746	65.4	6.545	55.1
1100	7.826	67.0	6.642	57.0
1200	7.900	68.6	6.733	59.0
1300	7.967	70.2	6.818	61.0
1400	8.030	71.8	6.896	63.0
1500	8.087	73.4	6.969	65.0
1600	8.140	75.0	7.037	67.0
1700	8.190	76.5	7.100	69.0
1800	8.236	78.1	7.158	71.0

B.2.2. Rate coefficients in the temperature range 300-1800 K

Table B-3: Rate coefficients [m^3 mol^{-1} s^{-1}] in the temperature range 300-1800 K for the reactions presented in Table B-4. The rate coefficients do not include tunneling contributions.

No.		300 K	400 K	500 K	600 K	700 K	800 K	900 K	1000 K	1100 K	1200 K	1300 K	1400 K	1500 K	1600 K	1700 K	1800 K
1	→	3.6E-03	1.2E+00	3.9E+01	4.2E+02	2.4E+03	9.1E+03	2.6E+04	6.3E+04	1.3E+05	2.4E+05	4.2E+05	6.7E+05	1.0E+06	1.5E+06	2.1E+06	2.8E+06
1	←	1.9E-02	2.3E+00	4.1E+01	2.9E+02	1.2E+03	3.6E+03	8.8E+03	1.8E+04	3.4E+04	5.8E+04	9.2E+04	1.4E+05	2.0E+05	2.8E+05	3.8E+05	5.0E+05
2	→	2.1E+00	1.2E+02	1.5E+03	7.9E+03	2.8E+04	7.3E+04	1.6E+05	3.0E+05	5.2E+05	8.2E+05	1.2E+06	1.8E+06	2.4E+06	3.2E+06	4.2E+06	5.3E+06
2	←	2.5E-05	1.3E-02	5.9E-01	7.8E+00	5.1E+01	2.1E+02	6.8E+02	1.7E+03	3.9E+03	7.6E+03	1.4E+04	2.3E+04	3.7E+04	5.6E+04	8.2E+04	1.2E+05
3	→	1.8E+04	9.2E+04	2.7E+05	5.7E+05	1.0E+06	1.6E+06	2.4E+06	3.3E+06	4.4E+06	5.7E+06	7.1E+06	8.7E+06	1.0E+07	1.2E+07	1.5E+07	1.7E+07
3	←	6.1E-10	4.9E-06	1.1E-03	4.2E-02	5.9E-01	4.4E+00	2.2E+01	7.9E+01	2.3E+02	5.8E+02	1.3E+03	2.6E+03	4.8E+03	8.2E+03	1.3E+04	2.1E+04
4	→	3.3E+00	1.3E+02	1.2E+03	6.0E+03	2.0E+04	4.9E+04	1.0E+05	1.9E+05	3.3E+05	5.1E+05	7.7E+05	1.1E+06	1.5E+06	2.0E+06	2.6E+06	3.3E+06
4	←	1.1E-13	5.4E-09	3.8E-06	3.2E-04	8.0E-03	9.4E-02	6.6E-01	3.2E+00	1.2E+01	3.7E+01	9.8E+01	2.3E+02	4.8E+02	9.2E+02	1.7E+03	2.8E+03
5	→	1.5E+01	5.1E+02	4.4E+03	1.9E+04	5.8E+04	1.4E+05	2.7E+05	4.8E+05	7.7E+05	1.2E+06	1.7E+06	2.3E+06	3.1E+06	4.1E+06	5.2E+06	6.4E+06
5	←	4.6E-14	3.9E-09	3.6E-06	3.5E-04	9.6E-03	1.2E-01	8.7E-01	4.4E+00	1.7E+01	5.2E+01	1.4E+02	3.2E+02	6.9E+02	1.3E+03	2.4E+03	4.2E+03
6	→	2.4E+02	4.0E+03	2.2E+04	7.4E+04	1.8E+05	3.6E+05	6.4E+05	1.0E+06	1.5E+06	2.2E+06	2.9E+06	3.8E+06	4.9E+06	6.1E+06	7.5E+06	9.0E+06
6	←	8.7E-08	1.6E-04	1.6E-02	3.6E-01	3.5E+00	2.0E+01	8.2E+01	2.6E+02	6.8E+02	1.5E+03	3.1E+03	5.9E+03	1.0E+04	1.7E+04	2.6E+04	4.0E+04
7	→	3.4E+01	6.6E+02	4.2E+03	1.5E+04	4.1E+04	8.8E+04	1.7E+05	2.8E+05	4.4E+05	6.5E+05	9.2E+05	1.3E+06	1.6E+06	2.1E+06	2.6E+06	3.3E+06
7	←	2.2E-14	2.2E-09	2.4E-06	2.7E-04	8.6E-03	1.2E-01	9.7E-01	5.3E+00	2.2E+01	7.4E+01	2.1E+02	5.2E+02	1.1E+03	2.3E+03	4.4E+03	7.8E+03
8	→	9.4E-01	4.8E+01	5.2E+02	2.6E+03	8.4E+03	2.1E+04	4.3E+04	7.8E+04	1.3E+05	2.0E+05	2.9E+05	4.0E+05	5.3E+05	6.9E+05	8.7E+05	1.1E+06
8	←	7.9E-19	1.9E-12	1.3E-08	4.9E-06	3.4E-04	8.4E-03	1.0E-01	7.5E-01	3.9E+00	1.6E+01	5.0E+01	1.4E+02	3.3E+02	7.3E+02	1.5E+03	2.7E+03
9	→	2.6E+02	3.5E+03	1.8E+04	5.4E+04	1.3E+05	2.4E+05	4.2E+05	6.7E+05	9.8E+05	1.4E+06	1.9E+06	2.5E+06	3.1E+06	3.9E+06	4.8E+06	5.7E+06
9	←	3.9E-15	5.2E-10	6.6E-07	8.1E-05	2.6E-03	3.8E-02	3.0E-01	1.7E+00	6.9E+00	2.3E+01	6.4E+01	1.6E+02	3.5E+02	7.0E+02	1.3E+03	2.3E+03
10	→	3.9E+00	1.9E+02	2.1E+03	1.1E+04	3.7E+04	9.4E+04	2.0E+05	3.7E+05	6.3E+05	9.9E+05	1.5E+06	2.1E+06	2.9E+06	3.8E+06	4.9E+06	6.2E+06
10	←	4.5E-05	2.0E-02	8.4E-01	1.0E+01	6.5E+01	2.7E+02	8.2E+02	2.1E+03	4.6E+03	9.0E+03	1.6E+04	2.7E+04	4.3E+04	6.4E+04	9.4E+04	1.3E+05
11	→	1.2E+00	7.9E+01	1.0E+03	5.8E+03	2.1E+04	5.7E+04	1.3E+05	2.5E+05	4.3E+05	6.9E+05	1.0E+06	1.5E+06	2.1E+06	2.8E+06	3.7E+06	4.7E+06
11	←	9.6E-05	3.3E-02	1.2E+00	1.3E+01	7.6E+01	3.0E+02	8.9E+02	2.2E+03	4.7E+03	9.0E+03	1.6E+04	2.6E+04	4.1E+04	6.2E+04	8.9E+04	1.2E+05
12	→	3.5E+00	1.8E+02	2.0E+03	1.0E+04	3.5E+04	9.1E+04	1.9E+05	3.7E+05	6.2E+05	9.9E+05	1.5E+06	2.1E+06	2.9E+06	3.8E+06	5.0E+06	6.3E+06
12	←	2.6E-05	1.4E-02	6.4E-01	8.5E+00	5.6E+01	2.4E+02	7.6E+02	2.0E+03	4.4E+03	8.7E+03	1.6E+04	2.7E+04	4.3E+04	6.5E+04	9.5E+04	1.3E+05
13	→	9.4E+03	5.7E+04	1.8E+05	4.0E+05	7.5E+05	1.2E+06	1.9E+06	2.6E+06	3.6E+06	4.7E+06	5.9E+06	7.4E+06	9.0E+06	1.1E+07	1.3E+07	1.5E+07
13	←	2.8E-09	1.2E-05	1.8E-03	5.5E-02	6.5E-01	4.3E+00	1.9E+01	6.6E+01	1.8E+02	4.4E+02	9.5E+02	1.8E+03	3.3E+03	5.6E+03	8.9E+03	1.4E+04
14	→	3.5E+03	2.7E+04	9.6E+04	2.4E+05	4.7E+05	8.1E+05	1.3E+06	1.9E+06	2.6E+06	3.4E+06	4.5E+06	5.6E+06	6.9E+06	8.4E+06	1.0E+07	1.2E+07

14	←	3.7E-09	1.7E-05	2.8E-03	8.6E-02	1.0E+00	7.0E+00	3.2E+01	1.1E+02	3.1E+02	7.4E+02	1.6E+03	3.1E+03	5.6E+03	9.5E+03	1.5E+04	2.4E+04
15	→	3.2E+01	7.5E+02	5.3E+03	2.1E+04	5.7E+04	1.3E+05	2.5E+05	4.2E+05	6.8E+05	1.0E+06	1.5E+06	2.0E+06	2.7E+06	3.5E+06	4.5E+06	5.5E+06
15	←	2.4E-12	6.7E-08	3.3E-05	2.2E-03	4.7E-02	4.9E-01	3.2E+00	1.5E+01	5.2E+01	1.5E+02	3.9E+02	8.9E+02	1.8E+03	3.5E+03	6.2E+03	1.0E+04
16	→	5.5E+02	6.9E+03	3.3E+04	9.8E+04	2.2E+05	4.2E+05	7.0E+05	1.1E+06	1.6E+06	2.2E+06	3.0E+06	3.9E+06	4.9E+06	6.1E+06	7.4E+06	8.9E+06
16	←	1.5E-14	2.3E-09	3.2E-06	4.1E-04	1.4E-02	2.1E-01	1.7E+00	9.8E+00	4.1E+01	1.4E+02	4.0E+02	9.9E+02	2.2E+03	4.5E+03	8.5E+03	1.5E+04
17	→	4.3E+01	8.9E+02	5.7E+03	2.1E+04	5.4E+04	1.1E+05	2.1E+05	3.5E+05	5.3E+05	7.7E+05	1.1E+06	1.4E+06	1.9E+06	2.4E+06	2.9E+06	3.6E+06
17	←	2.0E-14	1.9E-09	1.9E-06	2.0E-04	5.7E-03	7.4E-02	5.5E-01	2.8E+00	1.1E+01	3.5E+01	9.4E+01	2.2E+02	4.8E+02	9.4E+02	1.7E+03	3.0E+03
18	→	1.4E+02	2.8E+03	1.8E+04	6.4E+04	1.7E+05	3.5E+05	6.4E+05	1.1E+06	1.6E+06	2.3E+06	3.2E+06	4.3E+06	5.6E+06	7.1E+06	8.8E+06	1.1E+07
18	←	1.1E-13	1.0E-08	1.1E-05	1.1E-03	3.2E-02	4.2E-01	3.1E+00	1.6E+01	6.3E+01	2.0E+02	5.4E+02	1.3E+03	2.7E+03	5.4E+03	9.9E+03	1.7E+04
19	→	5.9E+01	1.3E+03	9.0E+03	3.4E+04	9.1E+04	2.0E+05	3.6E+05	6.1E+05	9.4E+05	1.4E+06	1.9E+06	2.6E+06	3.4E+06	4.3E+06	5.3E+06	6.5E+06
19	←	2.0E-08	5.1E-05	6.1E-03	1.6E-01	1.7E+00	1.0E+01	4.4E+01	1.5E+02	3.9E+02	9.2E+02	1.9E+03	3.7E+03	6.5E+03	1.1E+04	1.7E+04	2.6E+04
20	→	2.9E+02	4.2E+03	2.1E+04	6.6E+04	1.5E+05	2.9E+05	5.0E+05	7.8E+05	1.1E+06	1.6E+06	2.1E+06	2.7E+06	3.4E+06	4.2E+06	5.1E+06	6.1E+06
20	←	9.9E-08	1.6E-04	1.5E-02	3.1E-01	2.8E+00	1.5E+01	5.9E+01	1.8E+02	4.6E+02	1.0E+03	2.0E+03	3.7E+03	6.3E+03	1.0E+04	1.6E+04	2.3E+04
21	→	1.9E+02	2.6E+03	1.3E+04	4.0E+04	9.3E+04	1.8E+05	3.1E+05	5.0E+05	7.4E+05	1.1E+06	1.4E+06	1.9E+06	2.5E+06	3.1E+06	3.8E+06	4.6E+06
21	←	3.6E-12	6.7E-08	2.6E-05	1.5E-03	2.8E-02	2.7E-01	1.7E+00	7.3E+00	2.5E+01	7.3E+01	1.8E+02	4.0E+02	8.2E+02	1.5E+03	2.7E+03	4.5E+03
22	→	2.6E-02	3.9E+00	8.3E+01	6.7E+02	3.1E+03	1.0E+04	2.7E+04	5.8E+04	1.1E+05	1.9E+05	3.1E+05	4.8E+05	6.9E+05	9.6E+05	1.3E+06	1.7E+06
22	←	1.3E-18	2.3E-12	1.3E-08	4.0E-06	2.5E-04	5.8E-03	6.7E-02	4.8E-01	2.4E+00	9.6E+00	3.1E+01	8.4E+01	2.0E+02	4.4E+02	8.8E+02	1.6E+03
23	→	1.6E+02	2.2E+03	1.1E+04	3.4E+04	8.0E+04	1.6E+05	2.7E+05	4.2E+05	6.2E+05	8.8E+05	1.2E+06	1.5E+06	2.0E+06	2.5E+06	3.0E+06	3.6E+06
23	←	3.8E-15	5.0E-10	6.2E-07	7.6E-05	2.5E-03	3.5E-02	2.9E-01	1.6E+00	6.5E+00	2.2E+01	6.1E+01	1.5E+02	3.3E+02	6.7E+02	1.3E+03	2.2E+03
24	→	1.3E+01	3.9E+02	3.2E+03	1.4E+04	4.1E+04	9.6E+04	1.9E+05	3.4E+05	5.5E+05	8.4E+05	1.2E+06	1.7E+06	2.2E+06	2.9E+06	3.6E+06	4.4E+06
24	←	3.0E-16	9.3E-11	1.9E-07	3.3E-05	1.3E-03	2.2E-02	2.1E-01	1.2E+00	5.5E+00	1.9E+01	5.7E+01	1.4E+02	3.3E+02	6.8E+02	1.3E+03	2.3E+03
25	→	1.7E+02	2.3E+03	1.2E+04	3.5E+04	8.2E+04	1.6E+05	2.8E+05	4.4E+05	6.5E+05	9.3E+05	1.3E+06	1.7E+06	2.1E+06	2.7E+06	3.3E+06	4.0E+06
25	←	1.1E-12	3.6E-08	2.0E-05	1.4E-03	3.1E-02	3.4E-01	2.3E+00	1.1E+01	3.9E+01	1.2E+02	3.1E+02	7.1E+02	1.5E+03	2.9E+03	5.2E+03	8.8E+03
26	→	1.7E+02	2.5E+03	1.3E+04	4.1E+04	9.7E+04	1.9E+05	3.3E+05	5.3E+05	7.8E+05	1.1E+06	1.5E+06	2.0E+06	2.5E+06	3.2E+06	3.9E+06	4.7E+06
26	←	8.5E-15	9.0E-10	9.8E-07	1.1E-04	3.3E-03	4.5E-02	3.5E-01	1.9E+00	7.6E+00	2.5E+01	6.9E+01	1.7E+02	3.6E+02	7.3E+02	1.4E+03	2.4E+03

B.2.3. Arrhenius parameters regressed at 1000 K

Table B-4: Standard reaction enthalpy [kJ mol^{-1}], pre-exponential factor [m^3 mol^{-1} s^{-1}], activation energy [kJ mol^{-1}] and rate coefficient [m^3 mol^{-1} s^{-1}] at 1000 K for 25 H-H-N hydrogen abstraction reactions in the training (T) and validation dataset (V). The Arrhenius parameters exclude tunneling.

No.		Reaction	ΔH_r°	Forward			Reverse		
				$logA$	E_a	k_{for}	$logA$	E_a	k_{rev}
1	T	H• + NH_3 ↔ H_2 + NH_2•	12.4	8.223	65.4	6.3E+04	7.147	55.1	1.8E+04
2	T	H• + —NH_2 ↔ H_2 + —NH•	-21.3	8.010	48.3	3.0E+05	6.972	71.2	1.7E+03
3	T	H• + =NH ↔ H_2 + =N•	-72.5	7.835	25.0	3.3E+06	6.998	97.5	7.9E+01
4	T	+ ↔ H_2 +	-69.8	7.742	46.9	1.9E+05	6.749	119.3	3.2E+00
5	T	H• + ↔ H_2 +	-77.2	7.933	43.0	4.8E+05	6.982	121.2	4.4E+00
6	T	H• + ↔ H_2 +	-46.1	7.872	35.5	1.0E+06	6.937	86.4	2.6E+02
7	T	H• + ↔ H_2 +	-81.2	7.540	39.9	2.8E+05	7.429	128.1	5.3E+00
8	T	H• + ↔ H_2 +	-105.9	7.241	44.9	7.8E+04	7.720	150.1	7.5E-01
9	T	H• + ↔ H_2 +	-91.1	7.636	34.5	6.7E+05	6.915	127.9	1.7E+00
10	V	H• + ↔ H_2 +	-21.1	8.032	46.9	3.7E+05	6.992	70.1	2.1E+03
11	V	H• + ↔ H_2 +	-15.9	7.992	49.7	2.5E+05	6.899	67.9	2.2E+03
12	V	H• + ↔ H_2 +	-23.1	8.060	47.6	3.7E+05	7.049	71.7	2.0E+03
13	V	H• + ↔ H_2 +	-64.7	7.820	26.6	2.6E+06	6.656	92.4	6.6E+01
14	V	H• + ↔ H_2 +	-63.3	7.786	28.9	1.9E+06	6.908	93.1	1.1E+02
15	V	H• + ↔ H_2 +	-69.6	7.810	41.6	4.2E+05	7.157	114.5	1.5E+01
16	V	H• + ↔ H_2 +	-90.1	7.786	33.3	1.1E+06	7.782	129.8	9.8E+00
17	V	H• + ↔ H_2 +	-83.4	7.539	38.1	3.5E+05	6.885	122.9	2.8E+00
18	V	H• + ↔ H_2 +	-82.8	8.007	37.9	1.1E+06	7.650	123.1	1.6E+01
19	V	H• + ↔ H_2 +	-46.3	7.826	38.9	6.1E+05	6.845	89.4	1.5E+02
20	V	H• + ↔ H_2 +	-49.9	7.651	33.5	7.8E+05	6.630	83.6	1.8E+02
21	V	H• + ↔ H_2 +	-76.1	7.545	35.2	5.0E+05	6.689	111.3	7.3E+00
22	V	H• + ↔ H_2 +	-99.1	7.824	58.5	5.8E+04	7.412	147.9	4.8E-01
23	V	H• + ↔ H_2 +	-90.7	7.434	34.5	4.2E+05	6.897	128.1	1.6E+00
24	V	H• + ↔ H_2 +	-86.0	7.786	43.0	3.4E+05	7.143	134.8	1.2E+00
25	V	H• + ↔ H_2 +	-76.1	7.485	35.1	4.4E+05	7.144	116.8	1.1E+01
26	V	H• + ↔ H_2 +	-88.0	7.564	35.1	5.3E+05	6.861	125.9	1.9E+00

B.2.4. Reaction path degeneracy

Table B-5: External and internal symmetry numbers, number of optical isomers and number of single events n_e for all H-H-N hydrogen abstractions of Table B-4.

No.		Reactant 1 R·			Reactant 2 RH			Transition state			Reaction path degeneracy
		σ_{ext}	σ_{int}	n_{opt}	σ_{ext}	σ_{int}	n_{opt}	σ_{ext}	σ_{int}	n_{opt}	n_e
1	→	1	1	1	3	1	1	1	1	1	3
1	←	2	1	1	1	1	3	1	1	1	4
2	←	1	1	1	1	3	1	1	3	2	2
2	→	2	1	1	1	1	2	1	3	2	4
3	←	1	1	1	1	1	1	1	1	1	1
3	→	2	1	1	2	1	1	1	1	1	4
4	←	1	1	1	1	1	1	1	1	2	2
4	→	2	1	1	1	1	2	1	1	2	4
5	←	1	1	1	1	1	1	1	1	1	1
5	→	2	1	1	1	1	1	1	1	1	2
6	←	1	1	1	1	9	1	1	9	1	1
6	→	2	1	1	9	1	1	1	9	1	4
7	←	1	1	1	1	3	2	1	3	2	1
7	→	2	1	1	3	1	1	1	3	2	4
8	←	1	1	1	1	1	1	1	1	1	1
8	→	2	1	1	2	1	1	1	1	1	4
9	←	1	1	1	1	3	2	1	3	2	1
9	→	2	1	1	3	1	1	1	3	2	4
10	←	1	1	1	1	3	1	1	3	2	2
10	→	2	1	1	3	1	2	1	3	2	4
11	←	1	1	1	1	9	1	1	9	2	2
11	→	2	1	1	9	1	2	1	9	2	4
12	←	1	1	1	1	9	1	1	9	2	2
12	→	2	1	1	9	1	2	1	9	2	4
13	←	1	1	1	1	3	1	1	3	1	1
13	→	2	1	1	3	1	1	1	3	1	2
14	←	1	1	1	1	9	1	1	9	1	1
14	→	2	1	1	9	1	1	1	9	1	2
15	←	1	1	1	1	3	1	1	3	2	2
15	→	2	1	1	6	1	2	1	3	2	8
16	←	1	1	1	1	9	1	1	9	2	2
16	→	2	1	1	9	1	2	1	9	2	8
17	←	1	1	1	1	3	1	1	3	2	2
17	→	2	1	1	3	1	2	1	3	2	4
18	←	1	1	1	1	9	1	1	9	2	2
18	→	2	1	1	9	1	2	1	9	2	4
19	←	1	1	1	1	9	2	1	9	2	1
19	→	2	1	1	9	1	1	1	9	2	4
20	←	1	1	1	1	9	1	1	9	1	1
20	→	2	1	1	9	1	1	1	9	1	4
21	←	1	1	1	1	9	2	1	9	2	1
21	→	2	1	1	9	1	1	1	9	2	4
22	←	1	1	1	1	3	2	1	3	2	1
22	→	2	1	1	3	1	1	1	3	2	4
23	←	1	1	1	1	3	2	1	3	2	1
23	→	2	1	1	3	1	1	1	3	2	4
24	→	1	1	1	1	3	2	1	3	2	1
24	←	2	1	1	3	1	1	1	3	2	4
25	→	1	1	1	1	9	2	1	9	2	1
25	←	2	1	1	9	1	1	1	9	2	4
26	→	1	1	1	1	9	2	1	9	2	1
26	←	2	1	1	9	1	1	1	9	2	4

B.2.5. Group additive values between 300 and 1800 K

Table B-6: Primary group additive values ΔGAV°s between 300 and 1800 K for abstraction of a hydrogen atom from N-H by a hydrogen atom, deduced from the combined training and test set. For the reference reaction, the single-event pre-exponential factor is expressed in m^3 mol^{-1} s^{-1} and E_a is expressed in kJ mol^{-1}.

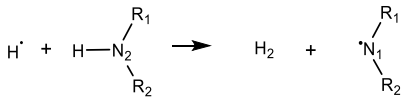

		300 K				400 K				500 K				600 K			
		ΔGAV°(N_1)		ΔGAV°(N_2)		ΔGAV°(N_1)		ΔGAV°(N_2)		ΔGAV°(N_1)		ΔGAV°(N_2)		ΔGAV°(N_1)		ΔGAV°(N_2)	
No.	**Group**	$log\tilde{A}$	E_a	$log\tilde{A}$	E_a	$log\tilde{A}$	E_a	$log\tilde{A}$	E_a	$log\tilde{A}$	E_a	$log\tilde{A}$	E_a	$log\tilde{A}$	E_a	$log\tilde{A}$	E_a
	Reference:	7.124	57.7	6.048	48.2	7.203	58.2	6.040	48.1	7.249	58.5	6.069	48.3	7.355	59.6	6.140	49.0
1	**N_i-(C)(H)**	-0.374	13.1	-0.094	-17.9	-0.302	13.6	-0.055	-17.6	-0.283	13.7	-0.048	-17.5	-0.242	14.1	-0.035	-17.4
2	**$N_{i,I}$**	-0.250	37.6	-0.062	-39.7	-0.195	38.0	-0.002	-39.3	-0.181	38.1	0.011	-39.2	-0.150	38.4	0.038	-38.9
3	**N_i-(C_d)(H)**	-0.476	61.3	-0.444	-26.8	-0.335	62.2	-0.400	-26.5	-0.293	62.6	-0.385	-26.4	-0.199	63.5	-0.353	-26.1
4	**N_i-(C_t)(H)**	-0.011	66.0	-0.150	-26.0	0.038	66.3	-0.134	-25.9	0.051	66.4	-0.132	-25.8	0.079	66.7	-0.127	-25.8
5	**N_i-$(C)_2$**	-0.745	27.3	0.007	-29.5	-0.599	28.3	0.046	-29.2	-0.562	28.6	0.049	-29.2	-0.481	29.4	0.055	-29.1
6	**N_i-(C_d)(C)**	-0.632	57.3	-0.361	-30.4	-0.489	58.3	-0.349	-30.4	-0.440	58.6	-0.341	-30.3	-0.330	59.7	-0.319	-30.1
7	**N_i-$(C_d)_2$**	0.303	90.3	-0.159	-16.8	0.378	90.9	-0.140	-16.6	0.386	90.9	-0.134	-16.6	0.398	91.0	-0.122	-16.5
8	**N_i-(C_t)(C)**	-0.597	68.7	-0.308	-31.8	-0.485	69.4	-0.268	-31.5	-0.453	69.7	-0.258	-31.4	-0.382	70.4	-0.237	-31.2

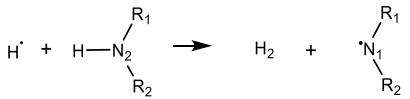

		700 K				800 K				900 K				1000 K			
		ΔGAV°(N_1)		ΔGAV°(N_2)		ΔGAV°(N_1)		ΔGAV°(N_2)		ΔGAV°(N_1)		ΔGAV°(N_2)		ΔGAV°(N_1)		ΔGAV°(N_2)	
No.	**Group**	$log\tilde{A}$	E_a	$log\tilde{A}$	E_a	$log\tilde{A}$	E_a	$log\tilde{A}$	E_a	$log\tilde{A}$	E_a	$log\tilde{A}$	E_a	$log\tilde{A}$	E_a	$log\tilde{A}$	E_a
	Reference:	7.462	60.9	6.235	50.1	7.563	62.3	6.339	51.6	7.658	63.8	6.444	53.2	7.746	65.4	6.545	55.1
1	**N_i-(C)(H)**	-0.214	14.5	-0.030	-17.4	-0.195	14.8	-0.025	-17.3	-0.181	15.0	-0.024	-17.2	-0.169	15.2	-0.024	-17.2
2	**$N_{i,I}$**	-0.129	38.6	0.052	-38.8	-0.114	38.9	0.061	-38.6	-0.102	39.1	0.065	-38.6	-0.092	39.2	0.068	-38.5
3	**N_i-(C_d)(H)**	-0.132	64.3	-0.326	-25.7	-0.083	65.1	-0.302	-25.4	-0.047	65.6	-0.283	-25.1	-0.018	66.1	-0.268	-24.8
4	**N_i-(C_t)(H)**	0.097	66.9	-0.125	-25.8	0.109	67.1	-0.122	-25.7	0.118	67.2	-0.121	-25.7	0.126	67.4	-0.120	-25.7
5	**N_i-(C)$_2$**	-0.428	30.1	0.052	-29.1	-0.391	30.6	0.049	-29.2	-0.364	31.0	0.043	-29.3	-0.343	31.4	0.037	-29.4
6	**N_i-(C_d)(C)**	-0.241	60.8	-0.293	-29.8	-0.167	61.8	-0.266	-29.4	-0.108	62.8	-0.242	-29.0	-0.060	63.6	-0.223	-28.7
7	**N_i-(C_d)$_2$**	0.383	90.9	-0.117	-16.4	0.352	90.4	-0.115	-16.4	0.315	89.9	-0.120	-16.5	0.278	89.2	-0.129	-16.6
8	**N_i-(C_t)(C)**	-0.334	71.0	-0.223	-31.0	-0.300	71.5	-0.213	-30.9	-0.275	71.9	-0.206	-30.8	-0.256	72.2	-0.201	-30.7

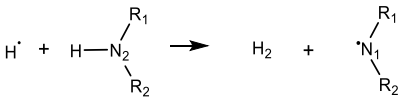

		1100 K				1200 K				1300 K				1400 K			
		ΔGAV°(N_1)		ΔGAV°(N_2)		ΔGAV°(N_1)		ΔGAV°(N_2)		ΔGAV°(N_1)		ΔGAV°(N_2)		ΔGAV°(N_1)		ΔGAV°(N_2)	
No.	Group	$log\tilde{A}$	E_a	$log\tilde{A}$	E_a	$log\tilde{A}$	E_a	$log\tilde{A}$	E_a	$log\tilde{A}$	E_a	$log\tilde{A}$	E_a	$log\tilde{A}$	E_a	$log\tilde{A}$	E_a
	Reference:	7.826	67.0	6.642	57.0	7.900	68.6	6.733	59.0	7.967	70.2	6.818	61.0	8.030	71.8	6.896	63.0
1	**N_i-(C)(H)**	-0.374	13.1	-0.094	-17.9	-0.302	13.6	-0.055	-17.6	-0.283	13.7	-0.048	-17.5	-0.242	14.1	-0.035	-17.4
2	**$N_{i,1}$**	-0.250	37.6	-0.062	-39.7	-0.195	38.0	-0.002	-39.3	-0.181	38.1	0.011	-39.2	-0.150	38.4	0.038	-38.9
3	**N_i-(C_d)(H)**	-0.476	61.3	-0.444	-26.8	-0.335	62.2	-0.400	-26.5	-0.293	62.6	-0.385	-26.4	-0.199	63.5	-0.353	-26.1
4	**N_i-(C_t)(H)**	-0.011	66.0	-0.150	-26.0	0.038	66.3	-0.134	-25.9	0.051	66.4	-0.132	-25.8	0.079	66.7	-0.127	-25.8
5	**N_i-(C)$_2$**	-0.745	27.3	0.007	-29.5	-0.599	28.3	0.046	-29.2	-0.562	28.6	0.049	-29.2	-0.481	29.4	0.055	-29.1
6	**N_i-(C_d)(C)**	-0.632	57.3	-0.361	-30.4	-0.489	58.3	-0.349	-30.4	-0.440	58.6	-0.341	-30.3	-0.330	59.7	-0.319	-30.1
7	**N_i-(C_d)$_2$**	0.303	90.3	-0.159	-16.8	0.378	90.9	-0.140	-16.6	0.386	90.9	-0.134	-16.6	0.398	91.0	-0.122	-16.5
8	**N_i-(C_t)(C)**	-0.597	68.7	-0.308	-31.8	-0.485	69.4	-0.268	-31.5	-0.453	69.7	-0.258	-31.4	-0.382	70.4	-0.237	-31.2

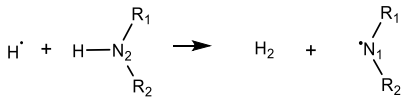

		1500 K				1600 K				1700 K				1800 K			
		ΔGAV°(N_1)		ΔGAV°(N_2)		ΔGAV°(N_1)		ΔGAV°(N_2)		ΔGAV°(N_1)		ΔGAV°(N_2)		ΔGAV°(N_1)		ΔGAV°(N_2)	
No.	Group	$log\tilde{A}$	E_a	$log\tilde{A}$	E_a	$log\tilde{A}$	E_a	$log\tilde{A}$	E_a	$log\tilde{A}$	E_a	$log\tilde{A}$	E_a	$log\tilde{A}$	E_a	$log\tilde{A}$	E_a
	Reference:	8.087	73.4	6.969	65.0	8.140	75.0	7.037	67.0	8.190	76.5	7.100	69.0	8.236	78.1	7.158	71.0
1	**N_i-(C)(H)**	-0.139	15.9	-0.024	-17.3	-0.137	16.0	-0.024	-17.3	-0.134	16.0	-0.025	-17.3	-0.132	16.1	-0.025	-17.3
2	**$N_{i,1}$**	-0.066	39.8	0.068	-38.5	-0.063	40.0	0.068	-38.5	-0.060	40.0	0.066	-38.6	-0.058	40.1	0.066	-38.6
3	**N_i-(C_d)(H)**	0.039	67.4	-0.220	-23.7	0.042	67.5	-0.215	-23.5	0.043	67.6	-0.210	-23.4	0.043	67.6	-0.207	-23.3
4	**N_i-(C_t)(H)**	0.144	67.8	-0.116	-25.6	0.145	67.8	-0.116	-25.6	0.146	67.9	-0.116	-25.6	0.148	67.9	-0.116	-25.6
5	**N_i-(C)$_2$**	-0.290	32.6	0.015	-29.9	-0.285	32.8	0.012	-30.0	-0.281	32.9	0.008	-30.1	-0.277	33.0	0.005	-30.2
6	**N_i-(C_d)(C)**	0.054	66.3	-0.180	-27.7	0.062	66.5	-0.178	-27.6	0.068	66.7	-0.178	-27.6	0.071	66.8	-0.178	-27.6
7	**N_i-(C_d)$_2$**	0.134	85.9	-0.185	-17.9	0.115	85.3	-0.196	-18.2	0.099	84.8	-0.206	-18.6	0.085	84.3	-0.216	-18.9
8	**N_i-(C_t)(C)**	-0.208	73.3	-0.191	-30.4	-0.204	73.4	-0.190	-30.4	-0.200	73.6	-0.190	-30.4	-0.196	73.7	-0.190	-30.4

B.2.6. Tunneling coefficients

Table B-7: Tunneling coefficients [-] for all reactions from Table B-4 over the temperature range 300-1800 K.

No.	κ(T)															
	300	**400**	**500**	**600**	**700**	**800**	**900**	**1000**	**1100**	**1200**	**1300**	**1400**	**1500**	**1600**	**1700**	**1800**
1	4.3	2.1	1.6	1.4	1.3	1.2	1.2	1.1	1.1	1.1	1.1	1.1	1.1	1.1	1.1	1.0
2	8.4	3.0	2.0	1.6	1.4	1.3	1.2	1.2	1.2	1.1	1.1	1.1	1.1	1.1	1.1	1.1
3	1.3	1.2	1.1	1.1	1.1	1.0	1.0	1.0	1.0	1.0	1.0	1.0	1.0	1.0	1.0	1.0
4	12.6	3.7	2.3	1.8	1.5	1.4	1.3	1.2	1.2	1.2	1.1	1.1	1.1	1.1	1.1	1.1
5	9.4	3.2	2.1	1.6	1.4	1.3	1.3	1.2	1.2	1.1	1.1	1.1	1.1	1.1	1.1	1.1
6	6.2	2.7	1.9	1.6	1.4	1.3	1.2	1.2	1.1	1.1	1.1	1.1	1.1	1.1	1.1	1.1
7	9.2	3.3	2.1	1.7	1.5	1.3	1.3	1.2	1.2	1.1	1.1	1.1	1.1	1.1	1.1	1.1
8	11.9	3.5	2.2	1.7	1.5	1.4	1.3	1.2	1.2	1.1	1.1	1.1	1.1	1.1	1.1	1.1
9	4.2	2.2	1.6	1.4	1.3	1.2	1.2	1.1	1.1	1.1	1.1	1.1	1.1	1.1	1.1	1.0
10	8.6	3.0	2.0	1.6	1.4	1.3	1.3	1.2	1.2	1.1	1.1	1.1	1.1	1.1	1.1	1.1
11	8.5	3.0	2.0	1.6	1.4	1.3	1.3	1.2	1.2	1.1	1.1	1.1	1.1	1.1	1.1	1.1
12	8.8	3.1	2.0	1.6	1.4	1.3	1.3	1.2	1.2	1.1	1.1	1.1	1.1	1.1	1.1	1.1
13	1.7	1.4	1.2	1.1	1.1	1.1	1.1	1.1	1.1	1.0	1.0	1.0	1.0	1.0	1.0	1.0
14	2.4	1.6	1.4	1.3	1.2	1.1	1.1	1.1	1.1	1.1	1.1	1.1	1.0	1.0	1.0	1.0
15	9.0	3.2	2.1	1.7	1.4	1.3	1.3	1.2	1.2	1.1	1.1	1.1	1.1	1.1	1.1	1.1
16	2.7	1.7	1.4	1.3	1.2	1.1	1.1	1.1	1.1	1.1	1.1	1.1	1.0	1.0	1.0	1.0
17	4.2	2.1	1.6	1.4	1.3	1.2	1.2	1.1	1.1	1.1	1.1	1.1	1.1	1.1	1.1	1.0
18	4.1	2.1	1.6	1.4	1.3	1.2	1.2	1.1	1.1	1.1	1.1	1.1	1.1	1.1	1.1	1.0
19	6.3	2.7	1.9	1.5	1.4	1.3	1.2	1.2	1.1	1.1	1.1	1.1	1.1	1.1	1.1	1.1
20	6.3	2.7	1.9	1.6	1.4	1.3	1.2	1.2	1.1	1.1	1.1	1.1	1.1	1.1	1.1	1.1
21	7.3	3.0	2.0	1.6	1.4	1.3	1.3	1.2	1.2	1.1	1.1	1.1	1.1	1.1	1.1	1.1
22	25.6	5.3	2.8	2.0	1.7	1.5	1.4	1.3	1.2	1.2	1.2	1.1	1.1	1.1	1.1	1.1
23	4.1	2.1	1.6	1.4	1.3	1.2	1.2	1.1	1.1	1.1	1.1	1.1	1.1	1.1	1.1	1.0
24	22.3	5.1	2.7	2.0	1.7	1.5	1.4	1.3	1.2	1.2	1.2	1.1	1.1	1.1	1.1	1.1
25	8.4	3.2	2.1	1.7	1.5	1.3	1.3	1.2	1.2	1.1	1.1	1.1	1.1	1.1	1.1	1.1

B.3. N-H-N hydrogen abstractions

B.3.1. Single-event Arrhenius parameters for reference reaction

Table B-8: Intrinsic Arrhenius parameters over the temperature range 300-1800 K for the reference reaction of H-H-N hydrogen abstraction reactions, i.e. $^{\cdot}NH_2 + NH_3 \rightarrow NH_3 + {}^{\cdot}NH_2$. The single-event pre-exponential factor is expressed in $m^3\ mol^{-1}\ s^{-1}$ and E_a is expressed in $kJ\ mol^{-1}$.

Temperature [K]	$log\tilde{A}$	E_a
300	5.067	44.6
400	5.292	46.2
500	5.398	46.9
600	5.635	49.3
700	5.849	51.9
800	6.041	54.6
900	6.210	57.3
1000	6.361	60.0
1100	6.497	62.7
1200	6.619	65.4
1300	6.729	68.0
1400	6.830	70.6
1500	6.922	73.2
1600	7.008	75.7
1700	7.087	78.2
1800	7.161	80.6

B.3.2. Rate coefficients in the temperature range 300-1800 K

Table B-9: Rate coefficients [m^3 mol^{-1} s^{-1}] in the temperature range 300-1800 K for the reactions presented in Table B-10. The rate coefficients do not include tunneling contributions.

No.		300 K	400 K	500 K	600 K	700 K	800 K	900 K	1000 K	1100 K	1200 K	1300 K	1400 K	1500 K	1600 K	1700 K	1800 K
1	→	5.5E-03	5.1E-01	8.5E+00	6.1E+01	2.7E+02	8.6E+02	2.2E+03	4.9E+03	9.6E+03	1.7E+04	2.9E+04	4.6E+04	7.0E+04	1.0E+05	1.4E+05	2.0E+05
1	←	5.5E-03	5.1E-01	8.5E+00	6.1E+01	2.7E+02	8.6E+02	2.2E+03	4.9E+03	9.6E+03	1.7E+04	2.9E+04	4.6E+04	7.0E+04	1.0E+05	1.4E+05	2.0E+05
2	→	5.1E+00	9.4E+01	6.1E+02	2.3E+03	6.4E+03	1.4E+04	2.8E+04	5.0E+04	8.3E+04	1.3E+05	1.9E+05	2.7E+05	3.7E+05	5.0E+05	6.5E+05	8.3E+05
2	←	1.2E-05	5.3E-03	2.4E-01	3.3E+00	2.3E+01	1.1E+02	3.7E+02	1.0E+03	2.4E+03	5.0E+03	9.6E+03	1.7E+04	2.9E+04	4.5E+04	6.9E+04	1.0E+05
3	→	7.4E+00	9.8E+01	5.3E+02	1.8E+03	4.7E+03	1.0E+04	2.0E+04	3.5E+04	5.7E+04	8.8E+04	1.3E+05	1.9E+05	2.6E+05	3.4E+05	4.5E+05	5.8E+05
3	←	1.6E-13	7.6E-09	5.8E-06	5.4E-04	1.5E-02	1.9E-01	1.5E+00	8.1E+00	3.3E+01	1.1E+02	3.1E+02	7.6E+02	1.7E+03	3.5E+03	6.6E+03	1.2E+04
4	→	3.5E+01	3.4E+02	1.5E+03	4.3E+03	1.0E+04	2.0E+04	3.6E+04	5.9E+04	9.2E+04	1.3E+05	1.9E+05	2.6E+05	3.5E+05	4.5E+05	5.8E+05	7.3E+05
4	←	2.1E-14	1.3E-09	1.1E-06	1.2E-04	3.4E-03	4.5E-02	3.5E-01	1.9E+00	7.6E+00	2.5E+01	7.1E+01	1.7E+02	3.9E+02	7.9E+02	1.5E+03	2.6E+03
5	→	5.4E+02	2.8E+03	8.8E+03	2.0E+04	4.0E+04	7.0E+04	1.1E+05	1.7E+05	2.4E+05	3.3E+05	4.5E+05	5.9E+05	7.5E+05	9.4E+05	1.2E+06	1.4E+06
5	←	3.7E-08	5.9E-05	5.9E-03	1.4E-01	1.5E+00	9.7E+00	4.3E+01	1.5E+02	4.1E+02	1.0E+03	2.2E+03	4.3E+03	7.9E+03	1.4E+04	2.2E+04	3.5E+04
6	→	2.3E+02	1.2E+03	3.8E+03	9.2E+03	1.9E+04	3.4E+04	5.6E+04	8.8E+04	1.3E+05	1.9E+05	2.6E+05	3.4E+05	4.5E+05	5.8E+05	7.3E+05	9.0E+05
6	←	2.7E-14	2.0E-09	2.1E-06	2.4E-04	7.9E-03	1.2E-01	9.9E-01	5.8E+00	2.5E+01	8.9E+01	2.6E+02	6.8E+02	1.6E+03	3.3E+03	6.6E+03	1.2E+04
7	→	1.0E+01	1.5E+02	8.1E+02	2.7E+03	6.6E+03	1.4E+04	2.5E+04	4.2E+04	6.5E+04	9.7E+04	1.4E+05	1.9E+05	2.5E+05	3.3E+05	4.2E+05	5.3E+05
7	←	1.7E-18	3.0E-12	2.0E-08	7.4E-06	5.3E-04	1.4E-02	1.8E-01	1.4E+00	7.6E+00	3.2E+01	1.1E+02	3.2E+02	8.0E+02	1.8E+03	3.8E+03	7.4E+03
8	→	2.0E+03	6.9E+03	1.7E+04	3.3E+04	5.7E+04	9.1E+04	1.4E+05	2.0E+05	2.8E+05	3.7E+05	4.9E+05	6.3E+05	7.9E+05	9.8E+05	1.2E+06	1.4E+06
8	←	5.7E-15	5.3E-10	5.9E-07	7.2E-05	2.4E-03	3.5E-02	3.0E-01	1.7E+00	7.5E+00	2.6E+01	7.6E+01	1.9E+02	4.4E+02	9.3E+02	1.8E+03	3.3E+03
9	→	3.2E-02	1.3E+00	1.5E+01	8.3E+01	3.0E+02	8.6E+02	2.0E+03	4.2E+03	7.8E+03	1.4E+04	2.2E+04	3.4E+04	5.0E+04	7.2E+04	9.9E+04	1.3E+05
9	←	3.1E-10	1.9E-06	4.2E-04	1.7E-02	2.6E-01	2.2E+00	1.2E+01	4.8E+01	1.6E+02	4.3E+02	1.0E+03	2.2E+03	4.3E+03	7.9E+03	1.4E+04	2.3E+04
10	→	2.4E+00	3.5E+01	2.0E+02	6.9E+02	1.8E+03	4.0E+03	7.7E+03	1.3E+04	2.2E+04	3.4E+04	5.0E+04	7.0E+04	9.7E+04	1.3E+05	1.7E+05	2.2E+05
10	←	6.3E-10	2.4E-06	3.9E-04	1.3E-02	1.6E-01	1.2E+00	5.8E+00	2.1E+01	6.3E+01	1.6E+02	3.6E+02	7.4E+02	1.4E+03	2.5E+03	4.1E+03	6.5E+03
11	→	5.4E-04	7.7E-02	1.7E+00	1.5E+01	7.4E+01	2.6E+02	7.1E+02	1.7E+03	3.4E+03	6.2E+03	1.1E+04	1.7E+04	2.6E+04	3.9E+04	5.5E+04	7.6E+04
11	←	5.5E+00	5.9E+01	2.9E+02	9.7E+02	2.5E+03	5.3E+03	1.0E+04	1.7E+04	2.8E+04	4.3E+04	6.3E+04	8.9E+04	1.2E+05	1.6E+05	2.1E+05	2.7E+05
12	→	1.4E-03	1.5E-01	2.9E+00	2.3E+01	1.1E+02	3.9E+02	1.1E+03	2.5E+03	5.3E+03	1.0E+04	1.8E+04	2.9E+04	4.6E+04	6.9E+04	9.9E+04	1.4E+05
12	←	3.9E-05	7.6E-03	2.1E-01	2.1E+00	1.2E+01	4.6E+01	1.4E+02	3.5E+02	7.7E+02	1.5E+03	2.8E+03	4.7E+03	7.6E+03	1.2E+04	1.7E+04	2.5E+04
13	→	1.0E-03	1.1E-01	2.2E+00	1.7E+01	7.9E+01	2.6E+02	7.0E+02	1.6E+03	3.2E+03	5.8E+03	9.8E+03	1.6E+04	2.4E+04	3.5E+04	4.9E+04	6.7E+04
13	←	5.7E-06	2.5E-03	1.1E-01	1.5E+00	1.0E+01	4.8E+01	1.6E+02	4.5E+02	1.1E+03	2.2E+03	4.2E+03	7.5E+03	1.3E+04	2.0E+04	3.0E+04	4.4E+04
14	→	1.1E-03	1.5E-01	3.2E+00	2.8E+01	1.4E+02	5.0E+02	1.4E+03	3.3E+03	6.9E+03	1.3E+04	2.3E+04	3.7E+04	5.8E+04	8.7E+04	1.3E+05	1.8E+05

14	←	1.1E-03	1.5E-01	3.2E+00	2.8E+01	1.4E+02	5.0E+02	1.4E+03	3.3E+03	6.9E+03	1.3E+04	2.3E+04	3.7E+04	5.8E+04	8.7E+04	1.3E+05	1.8E+05
15	→	8.7E-03	6.0E-01	8.6E+00	5.6E+01	2.3E+02	6.9E+02	1.7E+03	3.6E+03	6.9E+03	1.2E+04	2.0E+04	3.1E+04	4.6E+04	6.6E+04	9.1E+04	1.2E+05
15	←	8.7E-03	6.0E-01	8.6E+00	5.6E+01	2.3E+02	6.9E+02	1.7E+03	3.6E+03	6.9E+03	1.2E+04	2.0E+04	3.1E+04	4.6E+04	6.6E+04	9.1E+04	1.2E+05
16	→	7.8E+01	5.6E+02	2.1E+03	5.6E+03	1.2E+04	2.2E+04	3.8E+04	6.1E+04	9.1E+04	1.3E+05	1.8E+05	2.4E+05	3.2E+05	4.1E+05	5.1E+05	6.4E+05
16	←	2.3E-07	2.7E-04	2.1E-02	4.2E-01	3.8E+00	2.1E+01	8.1E+01	2.5E+02	6.4E+02	1.5E+03	2.9E+03	5.5E+03	9.5E+03	1.6E+04	2.4E+04	3.7E+04
17	→	1.3E+01	1.6E+02	8.3E+02	2.8E+03	7.0E+03	1.5E+04	2.7E+04	4.7E+04	7.4E+04	1.1E+05	1.6E+05	2.2E+05	3.0E+05	4.0E+05	5.1E+05	6.4E+05
17	←	3.9E-04	5.9E-02	1.4E+00	1.3E+01	7.3E+01	2.8E+02	8.2E+02	2.0E+03	4.4E+03	8.6E+03	1.5E+04	2.6E+04	4.1E+04	6.3E+04	9.2E+04	1.3E+05
18	→	2.2E+00	2.6E+01	1.3E+02	4.3E+02	1.1E+03	2.4E+03	4.5E+03	7.9E+03	1.3E+04	2.0E+04	2.9E+04	4.1E+04	5.7E+04	7.6E+04	1.0E+05	1.3E+05
18	←	1.2E-10	7.7E-07	1.8E-04	7.9E-03	1.3E-01	1.1E+00	6.2E+00	2.6E+01	8.6E+01	2.4E+02	5.9E+02	1.3E+03	2.6E+03	4.9E+03	8.5E+03	1.4E+04
19	→	6.2E+00	5.5E+01	2.3E+02	6.7E+02	1.5E+03	3.1E+03	5.5E+03	9.0E+03	1.4E+04	2.1E+04	3.0E+04	4.1E+04	5.5E+04	7.1E+04	9.1E+04	1.2E+05
19	←	4.4E-13	2.0E-08	1.4E-05	1.3E-03	3.4E-02	4.2E-01	3.0E+00	1.5E+01	5.7E+01	1.8E+02	4.6E+02	1.1E+03	2.3E+03	4.4E+03	7.9E+03	1.3E+04
20	→	9.2E+01	6.2E+02	2.2E+03	5.7E+03	1.2E+04	2.2E+04	3.8E+04	5.9E+04	8.8E+04	1.3E+05	1.7E+05	2.3E+05	3.0E+05	3.9E+05	4.9E+05	6.1E+05
20	←	1.1E-10	8.4E-07	2.0E-04	8.7E-03	1.4E-01	1.2E+00	6.3E+00	2.6E+01	8.2E+01	2.2E+02	5.3E+02	1.1E+03	2.2E+03	4.1E+03	7.0E+03	1.1E+04
21	→	2.1E-02	1.1E+00	1.3E+01	7.7E+01	2.9E+02	8.5E+02	2.0E+03	4.2E+03	7.8E+03	1.3E+04	2.2E+04	3.3E+04	4.9E+04	6.9E+04	9.5E+04	1.3E+05
21	←	2.1E-02	1.1E+00	1.3E+01	7.7E+01	2.9E+02	8.5E+02	2.0E+03	4.2E+03	7.8E+03	1.3E+04	2.2E+04	3.3E+04	4.9E+04	6.9E+04	9.5E+04	1.3E+05
22	→	1.1E-03	1.0E-01	1.7E+00	1.3E+01	5.8E+01	1.9E+02	4.9E+02	1.1E+03	2.2E+03	3.9E+03	6.6E+03	1.1E+04	1.6E+04	2.3E+04	3.3E+04	4.5E+04
22	←	3.7E-03	2.9E-01	4.8E+00	3.5E+01	1.6E+02	5.1E+02	1.4E+03	3.1E+03	6.1E+03	1.1E+04	1.9E+04	3.0E+04	4.6E+04	6.8E+04	9.6E+04	1.3E+05
23	→	2.9E-02	1.3E+00	1.5E+01	8.5E+01	3.2E+02	9.3E+02	2.2E+03	4.7E+03	8.9E+03	1.6E+04	2.5E+04	3.9E+04	5.9E+04	8.4E+04	1.2E+05	1.6E+05
23	←	2.6E-03	1.8E-01	2.9E+00	2.1E+01	9.2E+01	3.0E+02	8.0E+02	1.8E+03	3.6E+03	6.7E+03	1.1E+04	1.8E+04	2.8E+04	4.2E+04	6.0E+04	8.2E+04
24	→	1.2E-02	5.9E-01	7.2E+00	4.2E+01	1.6E+02	4.6E+02	1.1E+03	2.3E+03	4.2E+03	7.2E+03	1.2E+04	1.8E+04	2.6E+04	3.7E+04	5.1E+04	6.8E+04
24	←	2.1E-04	3.7E-02	9.9E-01	1.0E+01	5.8E+01	2.3E+02	7.0E+02	1.8E+03	4.0E+03	7.9E+03	1.4E+04	2.5E+04	4.0E+04	6.2E+04	9.2E+04	1.3E+05
25	→	2.3E-03	1.2E-01	1.4E+00	8.3E+00	3.2E+01	9.6E+01	2.3E+02	5.0E+02	9.6E+02	1.7E+03	2.8E+03	4.4E+03	6.7E+03	9.7E+03	1.4E+04	1.9E+04
25	←	5.7E-08	8.6E-05	8.6E-03	2.1E-01	2.3E+00	1.4E+01	6.1E+01	2.0E+02	5.5E+02	1.3E+03	2.7E+03	5.2E+03	9.3E+03	1.6E+04	2.5E+04	3.8E+04
26	→	1.1E+00	1.6E+01	9.7E+01	3.6E+02	1.0E+03	2.3E+03	4.6E+03	8.2E+03	1.4E+04	2.2E+04	3.2E+04	4.7E+04	6.5E+04	8.8E+04	1.2E+05	1.5E+05
26	←	4.6E-04	4.6E-02	8.8E-01	7.3E+00	3.6E+01	1.3E+02	3.6E+02	8.6E+02	1.8E+03	3.5E+03	6.1E+03	1.0E+04	1.6E+04	2.4E+04	3.5E+04	4.9E+04
27	→	1.7E-04	1.9E-02	3.4E-01	2.5E+00	1.1E+01	3.2E+01	7.8E+01	1.6E+02	3.0E+02	5.0E+02	7.9E+02	1.2E+03	1.7E+03	2.2E+03	3.0E+03	3.8E+03
27	←	1.7E-04	1.9E-02	3.4E-01	2.5E+00	1.1E+01	3.2E+01	7.8E+01	1.6E+02	3.0E+02	5.0E+02	7.9E+02	1.2E+03	1.7E+03	2.2E+03	3.0E+03	3.8E+03
28	→	4.5E-06	2.8E-03	1.5E-01	2.4E+00	1.9E+01	9.1E+01	3.2E+02	9.2E+02	2.2E+03	4.8E+03	9.2E+03	1.7E+04	2.8E+04	4.4E+04	6.7E+04	9.9E+04
28	←	1.4E-02	7.4E-01	9.4E+00	5.7E+01	2.3E+02	6.7E+02	1.6E+03	3.5E+03	6.6E+03	1.2E+04	1.9E+04	3.0E+04	4.4E+04	6.4E+04	8.9E+04	1.2E+05
29	→	1.2E-04	1.4E-02	2.7E-01	2.1E+00	1.0E+01	3.4E+01	9.2E+01	2.1E+02	4.2E+02	7.8E+02	1.3E+03	2.1E+03	3.3E+03	4.8E+03	6.8E+03	9.4E+03
29	←	9.1E-10	3.6E-06	6.0E-04	2.0E-02	2.6E-01	1.8E+00	8.6E+00	3.0E+01	8.6E+01	2.1E+02	4.5E+02	8.7E+02	1.6E+03	2.6E+03	4.3E+03	6.5E+03
30	→	1.0E-02	6.5E-01	9.0E+00	5.8E+01	2.4E+02	7.3E+02	1.8E+03	3.9E+03	7.6E+03	1.4E+04	2.2E+04	3.5E+04	5.3E+04	7.7E+04	1.1E+05	1.5E+05

30	←	1.3E-06	6.3E-04	3.0E-02	4.3E-01	3.1E+00	1.5E+01	5.2E+01	1.5E+02	3.6E+02	7.6E+02	1.5E+03	2.7E+03	4.5E+03	7.2E+03	1.1E+04	1.6E+04
31	→	2.4E-05	7.7E-03	2.7E-01	3.2E+00	2.0E+01	8.1E+01	2.5E+02	6.5E+02	1.4E+03	2.9E+03	5.2E+03	8.9E+03	1.4E+04	2.2E+04	3.2E+04	4.5E+04
31	←	2.8E+00	4.0E+01	2.3E+02	8.5E+02	2.3E+03	5.1E+03	1.0E+04	1.8E+04	3.0E+04	4.6E+04	6.9E+04	9.8E+04	1.4E+05	1.8E+05	2.4E+05	3.1E+05
32	→	3.5E-03	2.3E-01	3.2E+00	2.0E+01	8.1E+01	2.4E+02	5.8E+02	1.2E+03	2.3E+03	4.0E+03	6.5E+03	1.0E+04	1.5E+04	2.1E+04	2.9E+04	3.9E+04
32	←	7.2E-04	1.0E-01	2.2E+00	2.0E+01	1.0E+02	3.7E+02	1.1E+03	2.5E+03	5.4E+03	1.0E+04	1.8E+04	3.0E+04	4.7E+04	7.1E+04	1.0E+05	1.4E+05
33	→	5.6E-02	1.4E+00	1.1E+01	5.0E+01	1.6E+02	4.2E+02	9.2E+02	1.8E+03	3.2E+03	5.4E+03	8.5E+03	1.3E+04	1.9E+04	2.6E+04	3.6E+04	4.7E+04
33	←	1.5E-05	7.0E-03	3.5E-01	5.3E+00	4.0E+01	1.9E+02	6.7E+02	1.9E+03	4.5E+03	9.6E+03	1.8E+04	3.2E+04	5.3E+04	8.4E+04	1.3E+05	1.8E+05
34	→	3.6E-04	6.3E-02	1.6E+00	1.5E+01	8.1E+01	3.0E+02	8.7E+02	2.1E+03	4.5E+03	8.7E+03	1.5E+04	2.5E+04	4.0E+04	6.0E+04	8.7E+04	1.2E+05
34	←	1.7E-06	1.2E-03	7.3E-02	1.2E+00	1.0E+01	5.2E+01	2.0E+02	5.8E+02	1.5E+03	3.2E+03	6.4E+03	1.2E+04	2.0E+04	3.3E+04	5.1E+04	7.7E+04
35	→	1.3E-01	2.8E+00	2.2E+01	9.7E+01	3.0E+02	7.5E+02	1.6E+03	3.1E+03	5.3E+03	8.6E+03	1.3E+04	2.0E+04	2.8E+04	3.8E+04	5.1E+04	6.7E+04
35	←	1.3E-01	2.8E+00	2.2E+01	9.7E+01	3.0E+02	7.5E+02	1.6E+03	3.1E+03	5.3E+03	8.6E+03	1.3E+04	2.0E+04	2.8E+04	3.8E+04	5.1E+04	6.7E+04
36	→	3.4E-01	7.2E+00	5.3E+01	2.3E+02	7.1E+02	1.8E+03	3.7E+03	7.1E+03	1.2E+04	2.0E+04	3.1E+04	4.6E+04	6.5E+04	9.0E+04	1.2E+05	1.6E+05
36	←	5.9E-07	5.8E-04	4.3E-02	8.5E-01	7.7E+00	4.3E+01	1.7E+02	5.3E+02	1.4E+03	3.2E+03	6.5E+03	1.2E+04	2.2E+04	3.6E+04	5.7E+04	8.6E+04
37	→	9.3E-01	1.3E+01	6.9E+01	2.4E+02	6.4E+02	1.4E+03	2.7E+03	4.8E+03	7.8E+03	1.2E+04	1.8E+04	2.5E+04	3.5E+04	4.7E+04	6.1E+04	7.8E+04
37	←	2.2E-09	1.2E-05	2.5E-03	9.5E-02	1.3E+00	1.0E+01	5.0E+01	1.8E+02	5.3E+02	1.3E+03	2.9E+03	5.7E+03	1.0E+04	1.8E+04	2.9E+04	4.5E+04
38	→	9.4E+01	4.7E+02	1.5E+03	3.5E+03	7.2E+03	1.3E+04	2.2E+04	3.4E+04	5.0E+04	7.1E+04	9.8E+04	1.3E+05	1.7E+05	2.2E+05	2.8E+05	3.4E+05
38	←	3.9E-06	1.7E-03	7.9E-02	1.1E+00	7.9E+00	3.6E+01	1.2E+02	3.4E+02	7.9E+02	1.7E+03	3.1E+03	5.5E+03	9.2E+03	1.4E+04	2.2E+04	3.2E+04
39	→	1.7E-03	1.1E-01	1.5E+00	9.5E+00	3.7E+01	1.1E+02	2.7E+02	5.6E+02	1.1E+03	1.8E+03	3.0E+03	4.6E+03	6.7E+03	9.5E+03	1.3E+04	1.7E+04
39	←	1.7E-03	1.1E-01	1.5E+00	9.5E+00	3.7E+01	1.1E+02	2.7E+02	5.6E+02	1.1E+03	1.8E+03	3.0E+03	4.6E+03	6.7E+03	9.5E+03	1.3E+04	1.7E+04
40	→	3.7E-04	3.7E-02	6.9E-01	5.4E+00	2.6E+01	8.8E+01	2.4E+02	5.5E+02	1.1E+03	2.1E+03	3.6E+03	5.8E+03	9.0E+03	1.3E+04	1.9E+04	2.6E+04
40	←	4.9E-07	4.4E-04	3.1E-02	5.8E-01	5.0E+00	2.6E+01	9.6E+01	2.8E+02	6.8E+02	1.5E+03	2.8E+03	4.9E+03	8.2E+03	1.3E+04	1.9E+04	2.8E+04
41	→	5.0E-03	4.3E-01	7.3E+00	5.2E+01	2.3E+02	7.3E+02	1.9E+03	4.2E+03	8.2E+03	1.5E+04	2.5E+04	3.9E+04	5.9E+04	8.6E+04	1.2E+05	1.7E+05
41	←	1.2E-04	2.0E-02	4.8E-01	4.4E+00	2.3E+01	8.3E+01	2.3E+02	5.5E+02	1.2E+03	2.2E+03	3.8E+03	6.1E+03	9.5E+03	1.4E+04	2.0E+04	2.8E+04
42	→	4.5E+00	4.1E+01	1.9E+02	6.2E+02	1.6E+03	3.4E+03	6.5E+03	1.1E+04	1.8E+04	2.7E+04	4.0E+04	5.5E+04	7.5E+04	9.9E+04	1.3E+05	1.6E+05
42	←	4.5E+00	4.1E+01	1.9E+02	6.2E+02	1.6E+03	3.4E+03	6.5E+03	1.1E+04	1.8E+04	2.7E+04	4.0E+04	5.5E+04	7.5E+04	9.9E+04	1.3E+05	1.6E+05
43	→	1.2E-02	1.5E+00	3.1E+01	2.5E+02	1.2E+03	3.9E+03	1.0E+04	2.2E+04	4.2E+04	7.4E+04	1.2E+05	1.8E+05	2.7E+05	3.8E+05	5.1E+05	6.8E+05
43	←	2.2E-01	5.8E+00	4.6E+01	2.0E+02	6.0E+02	1.5E+03	3.1E+03	5.7E+03	9.7E+03	1.6E+04	2.3E+04	3.4E+04	4.8E+04	6.4E+04	8.5E+04	1.1E+05
44	→	2.9E-02	1.4E+00	1.6E+01	8.9E+01	3.3E+02	9.3E+02	2.2E+03	4.4E+03	8.2E+03	1.4E+04	2.2E+04	3.4E+04	4.9E+04	6.9E+04	9.4E+04	1.3E+05
44	←	2.9E-02	1.4E+00	1.6E+01	8.9E+01	3.3E+02	9.3E+02	2.2E+03	4.4E+03	8.2E+03	1.4E+04	2.2E+04	3.4E+04	4.9E+04	6.9E+04	9.4E+04	1.3E+05
45	→	3.2E+03	1.1E+04	2.7E+04	5.2E+04	8.9E+04	1.4E+05	2.1E+05	3.0E+05	4.1E+05	5.4E+05	7.0E+05	8.9E+05	1.1E+06	1.4E+06	1.7E+06	2.0E+06
45	←	2.1E-11	3.1E-07	1.1E-04	5.7E-03	1.0E-01	9.7E-01	5.7E+00	2.5E+01	8.3E+01	2.4E+02	5.8E+02	1.3E+03	2.6E+03	4.8E+03	8.3E+03	1.4E+04

B.3.3. Arrhenius parameters regressed at 1000 K

Table B-10: Standard reaction enthalpy [kJ mol^{-1}], pre-exponential factor [m^3 mol^{-1} s^{-1}], activation energy [kJ mol^{-1}] and rate coefficient [m^3 mol^{-1} s^{-1}] at 1000 K for all N-H-N hydrogen abstraction reactions in the training (T) and validation dataset (V). The Arrhenius parameters exclude tunneling.

No.		Reaction	ΔH_r°	Forward			Reverse		
				$logA$	E_a	k_{for}	$logA$	E_a	k_{rev}
1	T	·NH$_2$ + NH$_3$ ↔ NH$_3$ + ·NH$_2$	0.0	6.838	60.0	4.9E+03	6.838	60.0	4.9E+03
2	T	·NH$_2$ + —NH$_2$ ↔ NH$_3$ + —NH·	-33.8	6.995	43.6	5.0E+04	7.033	76.8	1.0E+03
3	T	·NH$_2$ + 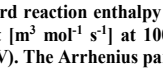 ↔ NH$_3$ + 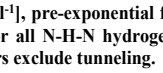	-82.3	6.791	42.8	3.5E+04	7.513	126.2	8.1E+00
4	T	·NH$_2$ + 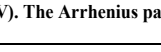 ↔ NH$_3$ + 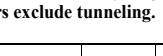	-89.7	6.765	37.9	5.9E+04	6.889	126.4	1.9E+00
5	T	·NH$_2$ + ↔ NH$_3$ + 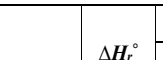	-58.5	6.871	31.2	1.7E+05	7.011	92.5	1.5E+02
6	T	·NH$_2$ + 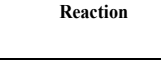 ↔ NH$_3$ + 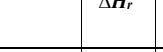	-93.6	6.730	33.9	8.8E+04	7.695	132.4	5.8E+00
7	T	·NH$_2$ + 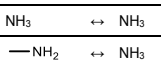 ↔ NH$_3$ +	-118.3	6.674	39.1	4.2E+04	8.228	154.7	1.4E+00
8	T	·NH$_2$ + 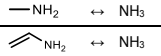 ↔ NH$_3$ + 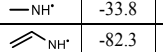	-103.5	6.770	27.9	2.0E+05	7.125	131.6	1.7E+00
9	T	—NH· + 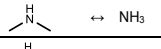 ↔ —NH$_2$ + 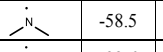	-48.5	6.504	54.9	4.2E+03	7.189	105.1	4.8E+01
10	T	—NH· + 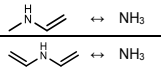 ↔ —NH$_2$ + 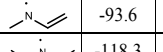	-55.9	6.369	42.6	1.3E+04	6.456	97.9	2.1E+01
11	T	═N· + 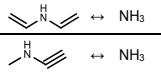 ↔ ═NH + 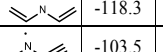	26.4	6.540	63.4	1.7E+03	6.441	41.8	1.7E+04
12	T	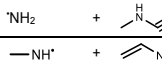 + 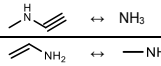 ↔ 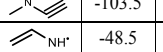 + 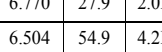	-7.4	6.806	64.8	2.5E+03	6.209	69.9	3.5E+02
13	T	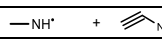 + 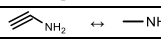 ↔ 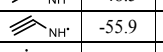 + 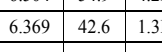	-11.4	6.425	61.5	1.6E+03	6.667	76.6	4.5E+02
14	T	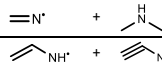 + 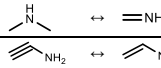 ↔ 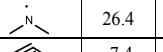 + 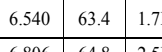	0.0	6.931	65.1	3.3E+03	6.931	65.1	3.3E+03
15	V	—NH· + —NH$_2$ ↔ —NH$_2$ + —NH·	0.0	6.554	57.1	3.6E+03	6.554	57.1	3.6E+03
16	V	—NH· + ═NH ↔ —NH$_2$ + ═N·	-51.2	6.627	35.0	6.1E+04	6.829	84.6	2.5E+02
17	V	—NH· + 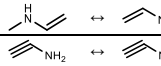 ↔ —NH$_2$ + 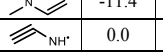	-24.8	6.791	40.4	4.7E+04	6.894	68.4	2.0E+03
18	V	—NH· + 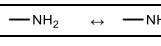 ↔ —NH$_2$ + 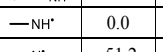	-59.9	6.119	42.2	7.9E+03	7.046	107.5	2.6E+01
19	V	—NH· + 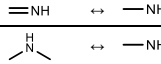 ↔ —NH$_2$ + 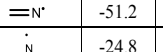	-84.6	5.963	38.2	9.0E+03	7.480	120.5	1.5E+01
20	V	—NH· + 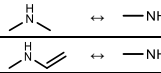 ↔ —NH$_2$ + 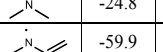	-69.7	6.587	34.5	5.9E+04	6.905	105.0	2.6E+01
21	V	═N· + ═NH ↔ ═NH + ═N·	0.0	6.507	55.0	4.2E+03	6.507	55.0	4.2E+03
22	V	═N· + 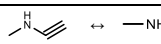 ↔ ═NH + 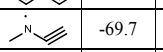	2.7	6.220	60.7	1.1E+03	6.703	61.3	3.1E+03
23	V	═N· + 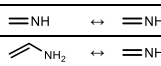 ↔ ═NH + 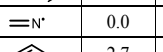	-4.7	6.616	56.0	4.7E+03	6.501	61.8	1.8E+03
24	V	═N· + 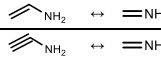 ↔ ═NH + 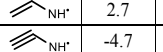	-8.7	6.229	54.8	2.3E+03	6.954	70.6	1.8E+03
25	V	═N· + 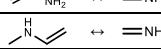 ↔ ═NH + 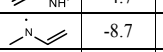	-33.4	5.707	57.3	5.0E+02	7.022	90.1	2.0E+02
26	V	═N· + 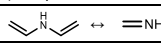 ↔ ═NH + 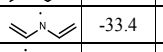	-18.6	6.268	44.8	8.2E+03	6.384	65.7	8.6E+02
27	V	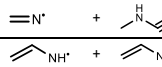 + 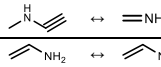 ↔ 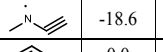 + 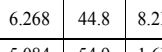	0.0	5.084	54.9	1.6E+02	5.084	54.9	1.6E+02
28	V	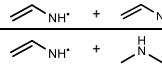 + 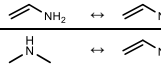 ↔ 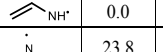 + 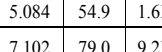	23.8	7.102	79.0	9.2E+02	6.520	56.8	3.5E+03
29	V	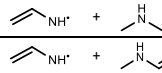 + 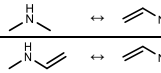 ↔ 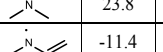 + 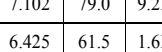	-11.4	6.425	61.5	1.6E+03	6.667	76.6	4.5E+02
30	V	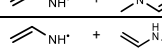 + 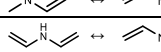 ↔ 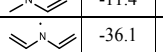 + 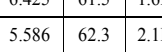	-36.1	5.586	62.3	2.1E+02	6.418	94.4	3.0E+01
31	V	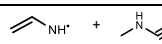 + 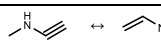 ↔ 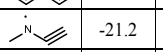 + 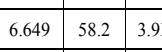	-21.2	6.649	58.2	3.9E+03	6.282	78.5	1.5E+02
32	V	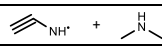 + 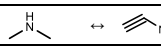 ↔ 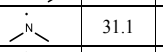 + 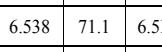	31.1	6.538	71.1	6.5E+02	6.554	43.8	1.8E+04
33	V	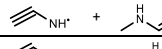 + 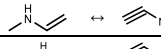 ↔ 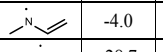 + 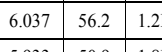	-4.0	6.037	56.2	1.2E+03	6.877	66.2	2.5E+03
34	V	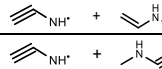 + 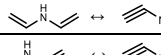 ↔ 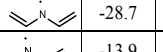 + 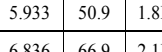	-28.7	5.933	50.9	1.8E+03	7.362	78.0	1.9E+03
35	V	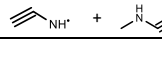 + 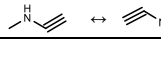 ↔ 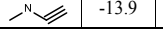 + 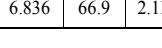	-13.9	6.836	66.9	2.1E+03	7.067	82.1	5.8E+02

36	V	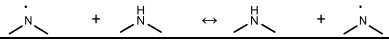	0.0	6.036	48.6	3.1E+03	6.036	48.6	3.1E+03
37	V	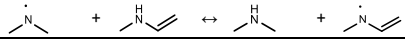	-35.1	6.402	48.6	7.1E+03	7.226	85.9	5.3E+02
38	V	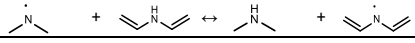	-59.8	5.935	42.9	4.8E+03	7.349	97.3	1.8E+02
39	V	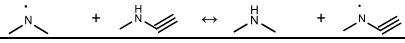	-45.0	6.313	33.9	3.4E+04	6.527	76.3	3.4E+02
40	V	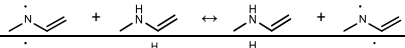	0.0	5.681	55.9	5.6E+02	5.681	55.9	5.6E+02
41	V	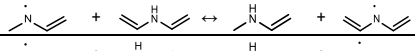	-24.7	6.058	63.2	5.5E+02	6.647	80.2	2.8E+02
42	V	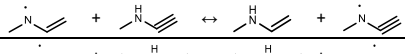	-9.9	6.767	60.0	4.2E+03	6.158	65.1	5.5E+02
43	V	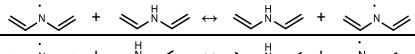	0.0	6.232	41.5	1.1E+04	6.232	41.5	1.1E+04
44	V	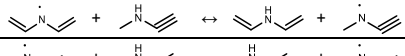	14.8	7.422	58.9	2.2E+04	6.223	47.0	5.7E+03
45	V	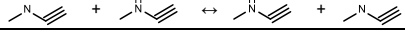	0.0	6.475	53.9	4.4E+03	6.475	53.9	4.4E+03

B.3.4. Reaction path degeneracy

Table B-11: External and internal symmetry numbers, number of optical isomers and number of single events n_e for all H-H-N hydrogen abstractions of Table B-10.

No.		Reactant 1 R·			Reactant 2 RH			Transition state			Reaction path degeneracy
		σ_{ext}	σ_{int}	n_{opt}	σ_{ext}	σ_{int}	n_{opt}	σ_{ext}	σ_{int}	n_{opt}	n_e
1	→	2	1	1	3	1	1	2	1	1	3
1	←	3	1	1	2	1	1	2	1	1	3
2	←	2	1	1	1	3	1	1	3	2	4
2	→	3	1	1	3	1	1	1	3	2	6
3	←	2	1	1	1	1	1	1	1	2	4
3	→	3	1	1	1	1	1	1	1	2	6
4	←	2	1	1	1	1	1	1	1	1	2
4	→	3	1	1	1	1	1	1	1	1	3
5	←	2	1	1	1	9	1	1	9	1	2
5	→	3	1	1	2	9	1	1	9	1	6
6	←	2	1	1	1	3	2	1	3	2	2
6	→	3	1	1	1	3	1	1	3	2	6
7	←	2	1	1	1	1	1	1	1	1	2
7	→	3	1	1	1	2	1	1	1	1	6
8	←	2	1	1	1	3	2	1	3	2	2
8	→	3	1	1	1	3	1	1	3	2	6
9	←	3	1	1	1	1	1	1	3	2	2
9	→	1	3	1	1	1	1	1	3	2	2
10	←	3	1	1	1	1	1	1	3	2	2
10	→	1	3	1	1	1	1	1	3	2	2
11	←	1	2	1	1	9	1	1	9	1	2
11	→	1	1	1	2	9	1	1	9	1	2
12	←	1	1	1	1	1	1	1	1	4	4
12	→	1	1	1	1	1	1	1	1	4	4
13	←	1	1	1	1	3	2	1	3	4	2
13	→	1	1	1	1	3	1	1	3	4	4
14	←	1	1	1	1	1	1	2	1	4	2
14	→	1	1	1	1	1	1	2	1	4	2
15	←	3	1	1	1	3	1	2	9	4	2
15	→	1	3	1	3	1	1	2	9	4	2
16	←	3	1	1	1	1	1	1	3	2	2
16	→	1	3	1	1	2	1	1	3	2	4
17	←	3	1	1	1	9	1	1	27	4	4
17	→	1	3	1	2	9	1	1	27	4	8
18	←	3	1	1	1	3	2	1	9	4	2
18	→	1	3	1	1	3	1	1	9	4	4
19	←	3	1	1	1	1	1	1	3	2	2
19	→	1	3	1	1	2	1	1	3	2	4
20	←	3	1	1	1	3	2	1	9	4	2
20	→	1	3	1	1	3	1	1	9	4	4
21	←	1	2	1	1	1	1	2	1	1	1
21	→	1	1	1	1	2	1	2	1	1	1
22	←	1	2	1	1	1	1	1	1	2	4
22	→	1	1	1	1	1	1	1	1	2	2
23	←	1	2	1	1	1	1	1	1	2	4
23	→	1	1	1	1	1	1	1	1	2	2
24	→	1	2	1	1	3	2	1	3	2	2
24	←	1	1	1	1	3	1	1	3	2	2
25	→	1	2	1	1	1	1	1	1	1	2
25	←	1	1	1	1	2	1	1	1	1	2
26	→	1	2	1	1	3	2	1	3	2	2
26	←	1	1	1	1	3	1	1	3	2	2

27	→	1	1	1	1	1	1	2	1	4	2
27	←	1	1	1	1	1	1	2	1	4	2
28	→	1	1	1	1	9	1	1	9	4	4
28	←	1	1	1	2	9	1	1	9	4	8
29	→	1	1	1	1	3	2	1	3	4	2
29	←	1	1	1	1	3	1	1	3	4	4
30	→	1	1	1	1	1	1	1	1	2	2
30	←	1	1	1	1	2	1	1	1	2	4
31	→	1	1	1	1	3	2	1	3	4	2
31	←	1	1	1	1	3	1	1	3	4	4
32	→	1	1	1	1	9	1	1	9	2	2
32	←	1	1	1	2	9	1	1	9	2	4
33	→	1	1	1	1	3	2	1	3	4	2
33	←	1	1	1	1	3	1	1	3	4	4
34	→	1	1	1	1	1	1	1	1	2	2
34	←	1	1	1	1	2	1	1	1	2	4
35	→	1	1	1	1	3	2	1	3	4	2
35	←	1	1	1	1	3	1	1	3	4	4
36	→	2	9	1	1	9	1	2	81	1	1
36	←	1	9	1	2	9	1	2	81	1	1
37	→	2	9	1	1	3	2	1	27	2	2
37	←	1	9	1	1	3	1	1	27	2	2
38	→	2	9	1	1	1	1	1	9	1	2
38	←	1	9	1	1	2	1	1	9	1	2
39	→	2	9	1	1	3	2	1	27	2	2
39	←	1	9	1	1	3	1	1	27	2	2
40	→	1	3	1	1	3	2	2	9	4	1
40	←	1	3	2	1	3	1	2	9	4	1
41	→	1	3	1	1	1	1	1	3	2	2
41	←	1	3	2	1	2	1	1	3	2	2
42	→	1	3	1	1	3	2	1	9	4	2
42	←	1	3	2	1	3	1	1	9	4	2
43	→	1	2	1	1	3	2	1	3	2	2
43	←	1	1	1	1	3	1	1	3	2	2
44	→	1	3	1	1	3	2	2	9	4	1
44	←	1	3	2	1	3	1	2	9	4	1
45	→	1	2	1	1	1	1	2	1	1	1
45	←	1	1	1	1	2	1	2	1	1	1

B.3.5. Group additive values between 300 and 1800 K

Table B-12: Primary group additive values ΔGAV°s between 300 and 1800 K for abstraction of a hydrogen atom from N-H by a nitrogen-centered radical, deduced from the combined training and test set. For the reference reaction, the single-event pre-exponential factor is expressed in m^3 mol^{-1} s^{-1} and E_a is expressed in kJ mol^{-1}.

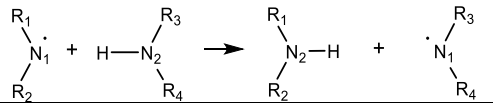

		300 K				400 K				500 K				600 K			
		ΔGAV°(N_1)		ΔGAV°(N_2)		ΔGAV°(N_1)		ΔGAV°(N_2)		ΔGAV°(N_1)		ΔGAV°(N_2)		ΔGAV°(N_1)		ΔGAV°(N_2)	
No.	**Group**	$log\tilde{A}$	E_a	$log\tilde{A}$	E_a	$log\tilde{A}$	E_a	$log\tilde{A}$	E_a	$log\tilde{A}$	E_a	$log\tilde{A}$	E_a	$log\tilde{A}$	E_a	$log\tilde{A}$	E_a
	Reference:	5.067	44.6	5.067	44.6	5.292	46.2	5.292	46.2	5.398	46.9	5.398	46.9	5.635	49.3	5.635	49.3
1	**N_i-(C)(H)**	-0.260	16.5	0.004	-15.4	-0.190	17.0	0.036	-15.2	-0.175	17.1	0.038	-15.2	-0.145	17.4	0.042	-15.1
2	**$N_{i,1}$**	-0.277	32.5	-0.072	-50.6	-0.221	32.9	0.000	-50.1	-0.211	32.9	0.015	-49.9	-0.190	33.2	0.045	-49.6
3	**N_i-(C_d)(H)**	-0.209	54.6	-0.553	-26.8	-0.122	55.2	-0.538	-26.7	-0.112	55.3	-0.548	-26.8	-0.093	55.5	-0.569	-27.0
4	**N_i-(C_t)(H)**	-0.387	55.5	-0.263	-32.2	-0.293	56.2	-0.189	-31.7	-0.267	56.4	-0.171	-31.6	-0.212	57.0	-0.132	-31.2
5	**N_i-(C)$_2$**	-0.703	22.9	0.054	-33.8	-0.528	24.1	0.116	-33.3	-0.487	24.4	0.116	-33.3	-0.400	25.3	0.117	-33.3
6	**N_i-(C_d)(C)**	-0.188	59.9	-0.332	-35.0	-0.049	60.9	-0.302	-34.7	-0.021	61.1	-0.306	-34.8	0.040	61.8	-0.313	-34.8
7	**N_i-(C_d)$_2$**	0.372	84.6	-0.636	-31.7	0.596	86.2	-0.590	-31.4	0.622	86.4	-0.584	-31.3	0.672	86.9	-0.568	-31.1
8	**N_i-(C_t)(C)**	-0.478	62.2	-0.151	-39.4	-0.335	63.2	-0.078	-38.9	-0.302	63.4	-0.065	-38.8	-0.230	64.2	-0.036	-38.5

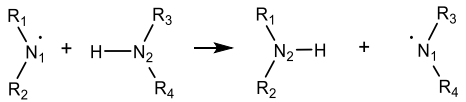

		700 K				800 K				900 K				1000 K			
		ΔGAV°(N_1)		ΔGAV°(N_2)		ΔGAV°(N_1)		ΔGAV°(N_2)		ΔGAV°(N_1)		ΔGAV°(N_2)		ΔGAV°(N_1)		ΔGAV°(N_2)	
No.	**Group**	$log\tilde{A}$	E_a	$log\tilde{A}$	E_a	$log\tilde{A}$	E_a	$log\tilde{A}$	E_a	$log\tilde{A}$	E_a	$log\tilde{A}$	E_a	$log\tilde{A}$	E_a	$log\tilde{A}$	E_a
	Reference:	5.849	51.9	5.849	51.9	6.041	54.6	6.041	54.6	6.210	57.3	6.210	57.3	6.361	60.0	6.361	60.0
1	**N_i-(C)(H)**	-0.127	17.6	0.042	-15.1	-0.116	17.8	0.039	-15.1	-0.108	17.9	0.038	-15.2	-0.102	18.0	0.037	-15.2
2	**$N_{i,I}$**	-0.178	33.3	0.061	-49.4	-0.172	33.4	0.068	-49.3	-0.168	33.4	0.072	-49.2	-0.164	33.5	0.074	-49.2
3	**N_i-(C_d)(H)**	-0.091	55.5	-0.594	-27.3	-0.095	55.4	-0.617	-27.6	-0.100	55.3	-0.636	-27.9	-0.105	55.2	-0.652	-28.2
4	**N_i-(C_t)(H)**	-0.176	57.3	-0.107	-30.9	-0.152	57.7	-0.091	-30.6	-0.134	58.0	-0.079	-30.4	-0.122	58.2	-0.070	-30.3
5	**N_i-$(C)_2$**	-0.347	25.9	0.104	-33.5	-0.314	26.4	0.089	-33.7	-0.290	26.8	0.076	-33.9	-0.273	27.1	0.064	-34.1
6	**N_i-(C_d)(C)**	0.077	62.2	-0.325	-35.0	0.101	62.5	-0.337	-35.1	0.119	62.8	-0.346	-35.3	0.134	63.1	-0.353	-35.4
7	**N_i-$(C_d)_2$**	0.662	86.8	-0.557	-31.0	0.627	86.3	-0.547	-30.9	0.586	85.6	-0.538	-30.8	0.547	84.9	-0.530	-30.6
8	**N_i-(C_t)(C)**	-0.185	64.7	-0.019	-38.3	-0.157	65.1	-0.011	-38.2	-0.138	65.4	-0.005	-38.1	-0.123	65.7	-0.002	-38.0

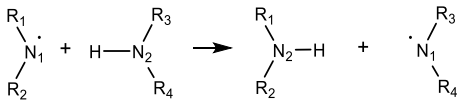

		1100 K				1200 K				1300 K				1400 K			
		ΔGAV°(N_1)		ΔGAV°(N_2)		ΔGAV°(N_1)		ΔGAV°(N_2)		ΔGAV°(N_1)		ΔGAV°(N_2)		ΔGAV°(N_1)		ΔGAV°(N_2)	
No.	**Group**	$log\tilde{A}$	E_a	$log\tilde{A}$	E_a	$log\tilde{A}$	E_a	$log\tilde{A}$	E_a	$log\tilde{A}$	E_a	$log\tilde{A}$	E_a	$log\tilde{A}$	E_a	$log\tilde{A}$	E_a
	Reference:	6.497	62.7	6.497	62.7	6.619	65.4	6.619	65.4	6.729	68.0	6.729	68.0	6.830	70.6	6.830	70.6
1	**N_i-(C)(H)**	-0.098	18.1	0.036	-15.2	-0.093	18.2	0.035	-15.2	-0.090	18.3	0.035	-15.2	-0.087	18.4	0.034	-15.3
2	**$N_{i,I}$**	-0.162	33.6	0.074	-49.2	-0.159	33.6	0.074	-49.2	-0.157	33.6	0.074	-49.2	-0.155	33.7	0.073	-49.2
3	**N_i-(C_d)(H)**	-0.111	55.1	-0.665	-28.4	-0.117	55.0	-0.676	-28.7	-0.122	54.9	-0.685	-28.9	-0.128	54.7	-0.693	-29.1
4	**N_i-(C_t)(H)**	-0.112	58.4	-0.063	-30.1	-0.104	58.6	-0.058	-30.0	-0.096	58.8	-0.052	-29.9	-0.090	58.9	-0.047	-29.8
5	**N_i-(C)$_2$**	-0.260	27.4	0.054	-34.3	-0.249	27.6	0.046	-34.4	-0.240	27.9	0.039	-34.6	-0.233	28.0	0.033	-34.8
6	**N_i-(C_d)(C)**	0.145	63.3	-0.360	-35.5	0.155	63.5	-0.364	-35.6	0.163	63.7	-0.368	-35.7	0.170	63.9	-0.371	-35.8
7	**N_i-(C_d)$_2$**	0.511	84.2	-0.525	-30.5	0.482	83.6	-0.520	-30.4	0.457	83.1	-0.515	-30.2	0.437	82.5	-0.512	-30.2
8	**N_i-(C_t)(C)**	-0.113	65.9	0.001	-38.0	-0.105	66.1	0.002	-37.9	-0.098	66.2	0.005	-37.9	-0.093	66.3	0.005	-37.9

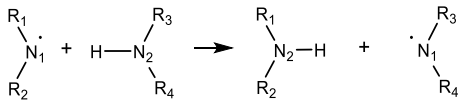

		1500 K				1600 K				1700 K				1800 K			
		ΔGAV°(N_1)		ΔGAV°(N_2)		ΔGAV°(N_1)		ΔGAV°(N_2)		ΔGAV°(N_1)		ΔGAV°(N_2)		ΔGAV°(N_1)		ΔGAV°(N_2)	
No.	**Group**	$log\tilde{A}$	E_a	$log\tilde{A}$	E_a	$log\tilde{A}$	E_a	$log\tilde{A}$	E_a	$log\tilde{A}$	E_a	$log\tilde{A}$	E_a	$log\tilde{A}$	E_a	$log\tilde{A}$	E_a
	Reference:	6.922	73.2	6.922	73.2	7.008	75.7	7.008	75.7	7.087	78.2	7.087	78.2	7.161	80.6	7.161	80.6
1	**N_i-(C)(H)**	-0.084	18.4	0.034	-15.2	-0.082	18.5	0.034	-15.3	-0.080	18.6	0.034	-15.3	-0.079	18.6	0.034	-15.3
2	**$N_{i,1}$**	-0.154	33.8	0.073	-49.3	-0.153	33.8	0.072	-49.3	-0.151	33.8	0.072	-49.3	-0.150	33.9	0.071	-49.3
3	**N_i-(C_d)(H)**	-0.133	54.6	-0.699	-29.3	-0.139	54.4	-0.705	-29.5	-0.144	54.3	-0.709	-29.6	-0.150	54.1	-0.714	-29.7
4	**N_i-(C_t)(H)**	-0.085	59.1	-0.043	-29.7	-0.080	59.2	-0.040	-29.6	-0.076	59.4	-0.036	-29.5	-0.072	59.5	-0.033	-29.4
5	**N_i-(C)$_2$**	-0.228	28.2	0.029	-34.9	-0.223	28.3	0.025	-35.0	-0.219	28.4	0.021	-35.1	-0.216	28.6	0.018	-35.2
6	**N_i-(C_d)(C)**	0.176	64.1	-0.372	-35.9	0.179	64.2	-0.374	-35.9	0.183	64.3	-0.375	-35.9	0.185	64.3	-0.377	-36.0
7	**N_i-(C_d)$_2$**	0.421	82.1	-0.509	-30.1	0.407	81.6	-0.508	-30.1	0.396	81.3	-0.507	-30.0	0.387	81.0	-0.507	-30.0
8	**N_i-(C_t)(C)**	-0.088	66.5	0.006	-37.8	-0.085	66.6	0.006	-37.9	-0.082	66.7	0.007	-37.8	-0.079	66.8	0.007	-37.8

B.3.6. Tunneling coefficients

Table B-13: Tunneling coefficients for all reactions from Table B-10 over the temperature range 300-1800 K.

No.	κ(T)															
	300	**400**	**500**	**600**	**700**	**800**	**900**	**1000**	**1100**	**1200**	**1300**	**1400**	**1500**	**1600**	**1700**	**1800**
1	19.7	4.6	2.6	1.9	1.6	1.5	1.4	1.3	1.2	1.2	1.2	1.1	1.1	1.1	1.1	1.1
2	11.6	3.8	2.4	1.8	1.6	1.4	1.3	1.3	1.2	1.2	1.2	1.1	1.1	1.1	1.1	1.1
3	7.4	3.0	2.0	1.6	1.4	1.3	1.3	1.2	1.2	1.1	1.1	1.1	1.1	1.1	1.1	1.1
4	4.9	2.4	1.8	1.5	1.3	1.3	1.2	1.2	1.1	1.1	1.1	1.1	1.1	1.1	1.1	1.1
5	4.4	2.4	1.8	1.5	1.4	1.3	1.2	1.2	1.1	1.1	1.1	1.1	1.1	1.1	1.1	1.1
6	5.2	2.6	1.9	1.6	1.4	1.3	1.2	1.2	1.2	1.1	1.1	1.1	1.1	1.1	1.1	1.1
7	9.7	3.5	2.2	1.7	1.5	1.4	1.3	1.2	1.2	1.2	1.1	1.1	1.1	1.1	1.1	1.1
8	2.6	1.7	1.4	1.3	1.2	1.2	1.1	1.1	1.1	1.1	1.1	1.1	1.0	1.0	1.0	1.0
9	23.8	5.5	2.9	2.1	1.7	1.5	1.4	1.3	1.3	1.2	1.2	1.2	1.1	1.1	1.1	1.1
10	16.1	4.8	2.8	2.1	1.7	1.5	1.4	1.3	1.3	1.2	1.2	1.2	1.1	1.1	1.1	1.1
11	10.9	4.1	2.5	2.0	1.7	1.5	1.4	1.3	1.3	1.2	1.2	1.2	1.1	1.1	1.1	1.1
12	35.6	6.4	3.2	2.2	1.8	1.6	1.4	1.3	1.3	1.2	1.2	1.2	1.2	1.1	1.1	1.1
13	42.5	6.9	3.3	2.3	1.8	1.6	1.5	1.4	1.3	1.2	1.2	1.2	1.2	1.1	1.1	1.1
14	43.6	7.1	3.4	2.3	1.9	1.6	1.5	1.4	1.3	1.3	1.2	1.2	1.2	1.1	1.1	1.1
15	25.9	5.7	3.0	2.2	1.8	1.6	1.4	1.3	1.3	1.2	1.2	1.2	1.2	1.1	1.1	1.1
16	8.0	3.4	2.3	1.8	1.6	1.4	1.3	1.3	1.2	1.2	1.2	1.1	1.1	1.1	1.1	1.1
17	13.3	4.5	2.7	2.0	1.7	1.5	1.4	1.3	1.3	1.2	1.2	1.2	1.2	1.1	1.1	1.1
18	10.4	3.8	2.4	1.9	1.6	1.4	1.3	1.3	1.2	1.2	1.2	1.1	1.1	1.1	1.1	1.1
19	9.5	3.8	2.4	1.9	1.6	1.5	1.4	1.3	1.2	1.2	1.2	1.1	1.1	1.1	1.1	1.1
20	7.4	3.3	2.3	1.8	1.6	1.4	1.3	1.3	1.2	1.2	1.2	1.1	1.1	1.1	1.1	1.1
21	25.8	5.8	3.1	2.2	1.8	1.6	1.4	1.4	1.3	1.2	1.2	1.2	1.2	1.1	1.1	1.1
22	28.4	6.0	3.1	2.2	1.8	1.6	1.4	1.4	1.3	1.2	1.2	1.2	1.2	1.1	1.1	1.1
23	24.6	5.6	3.0	2.2	1.8	1.6	1.4	1.3	1.3	1.2	1.2	1.2	1.2	1.1	1.1	1.1
24	27.8	5.9	3.1	2.2	1.8	1.6	1.4	1.3	1.3	1.2	1.2	1.2	1.2	1.1	1.1	1.1
25	50.6	8.3	3.8	2.5	2.0	1.7	1.5	1.4	1.3	1.3	1.2	1.2	1.2	1.2	1.1	1.1
26	17.3	5.2	2.9	2.2	1.8	1.6	1.5	1.4	1.3	1.3	1.2	1.2	1.2	1.1	1.1	1.1
27	54.5	7.6	3.5	2.3	1.9	1.6	1.5	1.4	1.3	1.3	1.2	1.2	1.2	1.1	1.1	1.1
28	34.3	6.6	3.3	2.3	1.8	1.6	1.5	1.4	1.3	1.2	1.2	1.2	1.2	1.1	1.1	1.1
29	52.8	7.7	3.5	2.4	1.9	1.6	1.5	1.4	1.3	1.3	1.2	1.2	1.2	1.1	1.1	1.1
30	36.1	6.7	3.3	2.3	1.8	1.6	1.5	1.4	1.3	1.3	1.2	1.2	1.2	1.1	1.1	1.1
31	15.1	4.8	2.8	2.1	1.7	1.5	1.4	1.3	1.3	1.2	1.2	1.2	1.2	1.1	1.1	1.1
32	28.8	5.9	3.1	2.2	1.8	1.6	1.4	1.3	1.3	1.2	1.2	1.2	1.2	1.1	1.1	1.1
33	23.9	5.9	3.1	2.2	1.8	1.6	1.5	1.4	1.3	1.3	1.2	1.2	1.2	1.1	1.1	1.1
34	58.4	7.7	3.5	2.3	1.9	1.6	1.5	1.4	1.3	1.3	1.2	1.2	1.2	1.1	1.1	1.1
35	18.5	5.5	3.1	2.3	1.9	1.6	1.5	1.4	1.3	1.3	1.2	1.2	1.2	1.2	1.2	1.1
36	23.6	6.0	3.2	2.3	1.8	1.6	1.5	1.4	1.3	1.3	1.2	1.2	1.2	1.1	1.1	1.1
37	18.5	5.6	3.1	2.3	1.9	1.6	1.5	1.4	1.3	1.3	1.2	1.2	1.2	1.2	1.1	1.1
38	6.0	3.1	2.2	1.8	1.6	1.4	1.3	1.3	1.2	1.2	1.2	1.2	1.1	1.1	1.1	1.1
39	31.5	6.5	3.3	2.3	1.9	1.6	1.5	1.4	1.3	1.3	1.2	1.2	1.2	1.2	1.1	1.1
40	57.1	8.4	3.7	2.5	2.0	1.7	1.5	1.4	1.3	1.3	1.2	1.2	1.2	1.2	1.1	1.1
41	44.7	7.5	3.5	2.4	1.9	1.6	1.5	1.4	1.3	1.3	1.2	1.2	1.2	1.2	1.1	1.1
42	17.9	6.1	3.5	2.5	2.1	1.8	1.6	1.5	1.4	1.4	1.3	1.3	1.2	1.2	1.2	1.2
43	40.0	7.6	3.6	2.5	2.0	1.7	1.5	1.4	1.3	1.3	1.2	1.2	1.2	1.2	1.1	1.1
44	31.4	6.8	3.5	2.4	1.9	1.7	1.5	1.4	1.3	1.3	1.2	1.2	1.2	1.2	1.1	1.1
45	2.1	1.5	1.3	1.2	1.2	1.1	1.1	1.1	1.1	1.1	1.0	1.0	1.0	1.0	1.0	1.0

B.4. C-H-N hydrogen abstractions

B.4.1. Single-event Arrhenius parameters for reference reaction

Table B-14: Intrinsic Arrhenius parameters over the temperature range 300-1800 K for the reference reaction of H-H-N hydrogen abstraction reactions, i.e. .e. $^{\cdot}CH_3 + CH_3NH_2 \rightarrow CH_4 + CH_3NH^{\cdot}$. The single-event pre-exponential factor is expressed in $m^3\ mol^{-1}\ s^{-1}$ and E_a is expressed in kJ mol^{-1}.

Temperature [K]	Forward		Reverse	
	$log\tilde{A}$	E_a	$log\tilde{A}$	E_a
300	5.149	48.1	5.471	70.7
400	5.315	49.3	5.671	72.6
500	5.395	49.8	5.767	73.4
600	5.575	51.7	5.984	76.0
700	5.747	53.7	6.183	78.8
800	5.908	56.0	6.361	81.5
900	6.056	58.4	6.520	84.2
1000	6.192	60.8	6.662	86.9
1100	6.316	63.3	6.789	89.5
1200	6.430	65.8	6.904	92.1
1300	6.535	68.2	7.008	94.6
1400	6.632	70.7	7.103	97.1
1500	6.721	73.2	7.190	99.6
1600	6.803	75.6	7.271	102.0
1700	6.880	78.1	7.346	104.4
1800	6.953	80.5	7.416	106.8

B.4.2. Rate coefficients in the temperature range 300-1800 K

Table B-15: Rate coefficients [m^3 mol^{-1} s^{-1}] in the temperature range 300-1800 K for the reactions presented in Table B-16. The rate coefficients do not include tunneling contributions.

No.		300 K	400 K	500 K	600 K	700 K	800 K	900 K	1000 K	1100 K	1200 K	1300 K	1400 K	1500 K	1600 K	1700 K	1800 K
1	→	9.1E-06	5.3E-03	2.6E-01	3.7E+00	2.6E+01	1.2E+02	4.0E+02	1.1E+03	2.5E+03	5.2E+03	9.9E+03	1.7E+04	2.8E+04	4.5E+04	6.7E+04	9.7E+04
1	←	8.3E-04	2.0E-01	5.8E+00	5.9E+01	3.4E+02	1.3E+03	3.9E+03	9.6E+03	2.1E+04	4.0E+04	7.2E+04	1.2E+05	1.9E+05	2.9E+05	4.2E+05	5.8E+05
2	→	2.2E-03	2.9E-01	5.7E+00	4.5E+01	2.1E+02	6.9E+02	1.8E+03	4.0E+03	8.0E+03	1.4E+04	2.4E+04	3.9E+04	5.9E+04	8.5E+04	1.2E+05	1.6E+05
2	←	4.6E-07	5.9E-04	4.9E-02	1.0E+00	9.7E+00	5.6E+01	2.3E+02	7.1E+02	1.9E+03	4.3E+03	9.0E+03	1.7E+04	3.0E+04	5.0E+04	7.8E+04	1.2E+05
3	→	9.8E+00	1.4E+02	7.3E+02	2.4E+03	6.0E+03	1.2E+04	2.3E+04	3.9E+04	6.1E+04	9.1E+04	1.3E+05	1.8E+05	2.4E+05	3.2E+05	4.1E+05	5.1E+05
3	←	6.0E-12	1.4E-07	6.3E-05	4.2E-03	8.9E-02	9.4E-01	6.1E+00	2.8E+01	1.0E+02	3.0E+02	7.8E+02	1.8E+03	3.7E+03	7.1E+03	1.3E+04	2.1E+04
4	→	5.8E-03	4.5E-01	6.7E+00	4.4E+01	1.8E+02	5.6E+02	1.4E+03	3.0E+03	5.8E+03	1.0E+04	1.7E+04	2.6E+04	3.9E+04	5.7E+04	7.9E+04	1.1E+05
4	←	1.2E-14	1.3E-09	1.6E-06	2.1E-04	7.5E-03	1.2E-01	1.0E+00	6.1E+00	2.7E+01	9.6E+01	2.9E+02	7.5E+02	1.7E+03	3.7E+03	7.1E+03	1.3E+04
5	→	2.5E-01	1.0E+01	1.0E+02	5.1E+02	1.7E+03	4.4E+03	9.6E+03	1.8E+04	3.2E+04	5.3E+04	8.2E+04	1.2E+05	1.7E+05	2.4E+05	3.2E+05	4.1E+05
5	←	1.4E-14	1.5E-09	1.8E-06	2.2E-04	7.3E-03	1.1E-01	9.1E-01	5.2E+00	2.2E+01	7.6E+01	2.2E+02	5.6E+02	1.3E+03	2.6E+03	5.0E+03	9.0E+03
6	→	3.4E-01	1.1E+01	1.0E+02	4.7E+02	1.5E+03	3.8E+03	8.0E+03	1.5E+04	2.6E+04	4.1E+04	6.3E+04	9.1E+04	1.3E+05	1.7E+05	2.3E+05	3.0E+05
6	←	2.1E-09	8.6E-06	1.5E-03	5.3E-02	7.5E-01	5.8E+00	3.0E+01	1.2E+02	3.6E+02	9.5E+02	2.2E+03	4.6E+03	8.9E+03	1.6E+04	2.7E+04	4.4E+04
7	→	1.1E-01	3.9E+00	3.7E+01	1.8E+02	6.2E+02	1.6E+03	3.6E+03	7.1E+03	1.3E+04	2.1E+04	3.3E+04	4.9E+04	7.0E+04	9.7E+04	1.3E+05	1.7E+05
7	←	1.2E-15	2.4E-10	4.5E-07	7.7E-05	3.4E-03	6.1E-02	6.2E-01	4.1E+00	2.0E+01	7.6E+01	2.4E+02	6.7E+02	1.6E+03	3.6E+03	7.3E+03	1.4E+04
8	→	8.3E-03	5.1E-01	6.3E+00	3.6E+01	1.3E+02	3.6E+02	8.3E+02	1.6E+03	2.9E+03	4.9E+03	7.6E+03	1.1E+04	1.6E+04	2.2E+04	3.0E+04	3.9E+04
8	←	1.2E-19	3.7E-13	3.4E-09	1.6E-06	1.4E-04	4.0E-03	5.7E-02	4.8E-01	2.8E+00	1.2E+01	4.4E+01	1.3E+02	3.4E+02	7.9E+02	1.7E+03	3.3E+03
9	→	3.8E+00	6.2E+01	3.6E+02	1.3E+03	3.3E+03	7.2E+03	1.4E+04	2.3E+04	3.7E+04	5.6E+04	8.2E+04	1.1E+05	1.5E+05	2.0E+05	2.6E+05	3.3E+05
9	←	9.8E-16	1.7E-10	2.9E-07	4.5E-05	1.8E-03	3.0E-02	2.9E-01	1.8E+00	8.2E+00	3.0E+01	9.2E+01	2.4E+02	5.7E+02	1.2E+03	2.4E+03	4.5E+03
10	→	5.5E-14	6.2E-09	7.3E-06	9.0E-04	3.0E-02	4.3E-01	3.6E+00	2.1E+01	8.8E+01	3.0E+02	8.7E+02	2.2E+03	5.0E+03	1.0E+04	2.0E+04	3.5E+04
10	←	3.1E+00	6.5E+01	4.6E+02	1.9E+03	5.4E+03	1.3E+04	2.7E+04	4.9E+04	8.4E+04	1.3E+05	2.0E+05	3.0E+05	4.2E+05	5.7E+05	7.6E+05	9.9E+05
11	→	4.9E-07	4.4E-04	2.9E-02	5.3E-01	4.5E+00	2.4E+01	9.2E+01	2.8E+02	7.1E+02	1.6E+03	3.2E+03	6.0E+03	1.1E+04	1.7E+04	2.7E+04	4.1E+04
11	←	2.9E-02	1.7E+00	2.3E+01	1.5E+02	6.3E+02	2.0E+03	5.0E+03	1.1E+04	2.2E+04	3.9E+04	6.7E+04	1.1E+05	1.6E+05	2.4E+05	3.4E+05	4.6E+05
12	→	1.7E+01	2.0E+02	1.0E+03	3.2E+03	7.7E+03	1.6E+04	2.9E+04	4.8E+04	7.5E+04	1.1E+05	1.6E+05	2.2E+05	2.9E+05	3.8E+05	4.8E+05	6.1E+05
12	←	1.2E-06	1.2E-03	9.0E-02	1.8E+00	1.6E+01	8.7E+01	3.4E+02	1.1E+03	2.7E+03	6.2E+03	1.3E+04	2.4E+04	4.1E+04	6.8E+04	1.1E+05	1.6E+05
13	→	8.5E-05	1.7E-02	4.8E-01	4.9E+00	2.7E+01	1.0E+02	3.1E+02	7.7E+02	1.7E+03	3.2E+03	5.8E+03	9.7E+03	1.5E+04	2.3E+04	3.4E+04	4.8E+04
13	←	3.1E-05	1.3E-02	5.8E-01	7.9E+00	5.5E+01	2.5E+02	8.5E+02	2.3E+03	5.5E+03	1.1E+04	2.2E+04	3.8E+04	6.3E+04	9.9E+04	1.5E+05	2.2E+05
14	→	7.0E-05	1.7E-02	5.1E-01	5.6E+00	3.3E+01	1.4E+02	4.2E+02	1.1E+03	2.4E+03	4.8E+03	8.7E+03	1.5E+04	2.4E+04	3.7E+04	5.5E+04	7.9E+04

14	←	5.2E-03	6.3E-01	1.3E+01	1.0E+02	5.0E+02	1.7E+03	4.6E+03	1.0E+04	2.1E+04	3.9E+04	6.6E+04	1.1E+05	1.6E+05	2.4E+05	3.4E+05	4.6E+05
15	→	2.7E+00	4.4E+01	2.7E+02	9.8E+02	2.6E+03	5.9E+03	1.1E+04	2.0E+04	3.3E+04	5.0E+04	7.4E+04	1.0E+05	1.4E+05	1.9E+05	2.5E+05	3.2E+05
15	←	1.4E-05	5.3E-03	2.2E-01	2.9E+00	1.9E+01	8.5E+01	2.8E+02	7.6E+02	1.7E+03	3.6E+03	6.7E+03	1.2E+04	1.9E+04	3.0E+04	4.5E+04	6.5E+04
16	→	1.4E-10	1.7E-06	5.2E-04	2.6E-02	4.6E-01	4.2E+00	2.4E+01	1.0E+02	3.4E+02	9.5E+02	2.3E+03	5.0E+03	1.0E+04	1.9E+04	3.2E+04	5.3E+04
16	←	1.8E-02	9.9E-01	1.3E+01	7.7E+01	3.1E+02	9.1E+02	2.3E+03	4.8E+03	9.3E+03	1.7E+04	2.7E+04	4.3E+04	6.5E+04	9.4E+04	1.3E+05	1.8E+05
17	→	4.2E-06	4.5E-03	3.4E-01	6.5E+00	5.8E+01	3.1E+02	1.2E+03	3.8E+03	9.7E+03	2.2E+04	4.4E+04	8.3E+04	1.4E+05	2.4E+05	3.7E+05	5.6E+05
17	←	1.4E-07	1.9E-04	1.6E-02	3.6E-01	3.5E+00	2.1E+01	8.6E+01	2.8E+02	7.7E+02	1.8E+03	3.8E+03	7.4E+03	1.3E+04	2.3E+04	3.7E+04	5.7E+04
18	→	1.5E-06	1.7E-03	1.3E-01	2.6E+00	2.3E+01	1.3E+02	5.0E+02	1.5E+03	3.9E+03	8.8E+03	1.8E+04	3.3E+04	5.8E+04	9.5E+04	1.5E+05	2.2E+05
18	←	9.9E-09	3.1E-05	4.5E-03	1.4E-01	1.8E+00	1.3E+01	6.3E+01	2.4E+02	7.2E+02	1.9E+03	4.3E+03	8.9E+03	1.7E+04	3.1E+04	5.2E+04	8.4E+04
19	→	1.1E-06	7.3E-04	4.2E-02	7.0E-01	5.6E+00	2.8E+01	1.1E+02	3.1E+02	7.8E+02	1.7E+03	3.4E+03	6.3E+03	1.1E+04	1.8E+04	2.7E+04	4.1E+04
19	←	7.0E-01	1.7E+01	1.4E+02	6.4E+02	2.1E+03	5.3E+03	1.2E+04	2.3E+04	4.0E+04	6.7E+04	1.1E+05	1.6E+05	2.3E+05	3.2E+05	4.3E+05	5.7E+05
20	→	1.9E-03	1.3E-01	2.0E+00	1.3E+01	5.7E+01	1.8E+02	4.8E+02	1.1E+03	2.2E+03	4.1E+03	7.0E+03	1.1E+04	1.8E+04	2.7E+04	3.9E+04	5.4E+04
20	←	1.2E-05	4.4E-03	1.8E-01	2.5E+00	1.8E+01	8.6E+01	3.1E+02	9.0E+02	2.3E+03	5.0E+03	1.0E+04	1.9E+04	3.2E+04	5.3E+04	8.4E+04	1.3E+05
21	→	2.5E+00	3.0E+01	1.6E+02	5.3E+02	1.4E+03	2.9E+03	5.7E+03	1.0E+04	1.7E+04	2.6E+04	3.9E+04	5.6E+04	7.9E+04	1.1E+05	1.4E+05	1.9E+05
21	←	4.1E-04	5.0E-02	1.0E+00	8.9E+00	4.5E+01	1.6E+02	4.7E+02	1.2E+03	2.5E+03	4.8E+03	8.7E+03	1.5E+04	2.4E+04	3.7E+04	5.4E+04	7.8E+04
22	→	7.7E-09	2.1E-05	2.7E-03	7.5E-02	8.7E-01	5.8E+00	2.6E+01	9.1E+01	2.6E+02	6.3E+02	1.4E+03	2.7E+03	5.0E+03	8.5E+03	1.4E+04	2.1E+04
22	←	4.4E-03	3.4E-01	5.5E+00	3.9E+01	1.7E+02	5.6E+02	1.5E+03	3.3E+03	6.7E+03	1.2E+04	2.1E+04	3.4E+04	5.2E+04	7.6E+04	1.1E+05	1.5E+05
23	→	7.7E-08	8.5E-05	6.5E-03	1.3E-01	1.2E+00	6.6E+00	2.6E+01	8.3E+01	2.2E+02	5.0E+02	1.0E+03	1.9E+03	3.4E+03	5.7E+03	9.0E+03	1.4E+04
23	←	4.3E-10	2.0E-06	3.7E-04	1.4E-02	2.0E-01	1.6E+00	8.7E+00	3.5E+01	1.1E+02	3.0E+02	7.2E+02	1.6E+03	3.1E+03	5.6E+03	9.7E+03	1.6E+04
24	→	1.6E-05	7.8E-03	3.6E-01	5.1E+00	3.6E+01	1.7E+02	5.7E+02	1.6E+03	3.7E+03	7.7E+03	1.5E+04	2.6E+04	4.3E+04	6.8E+04	1.0E+05	1.5E+05
24	←	2.4E-09	9.2E-06	1.5E-03	4.9E-02	6.5E-01	4.8E+00	2.4E+01	9.0E+01	2.8E+02	7.1E+02	1.6E+03	3.4E+03	6.5E+03	1.2E+04	1.9E+04	3.1E+04
25	→	2.3E-10	2.4E-06	7.2E-04	3.5E-02	5.9E-01	5.2E+00	2.9E+01	1.2E+02	3.9E+02	1.1E+03	2.5E+03	5.4E+03	1.0E+04	1.9E+04	3.2E+04	5.2E+04
25	←	2.0E-03	1.8E-01	3.2E+00	2.4E+01	1.1E+02	3.7E+02	9.7E+02	2.2E+03	4.4E+03	8.1E+03	1.4E+04	2.2E+04	3.4E+04	5.0E+04	7.0E+04	9.7E+04
26	→	9.4E-07	1.7E-03	1.7E-01	3.9E+00	3.9E+01	2.3E+02	9.6E+02	3.1E+03	8.1E+03	1.9E+04	3.9E+04	7.3E+04	1.3E+05	2.1E+05	3.3E+05	5.1E+05
26	←	2.1E-09	8.9E-06	1.5E-03	5.0E-02	6.7E-01	4.9E+00	2.4E+01	8.9E+01	2.7E+02	6.9E+02	1.6E+03	3.2E+03	6.0E+03	1.1E+04	1.8E+04	2.8E+04
27	→	4.5E-05	1.2E-02	4.1E-01	4.6E+00	2.8E+01	1.1E+02	3.5E+02	9.1E+02	2.0E+03	4.1E+03	7.4E+03	1.3E+04	2.0E+04	3.1E+04	4.7E+04	6.7E+04
27	←	8.8E-02	3.8E+00	4.1E+01	2.3E+02	8.1E+02	2.3E+03	5.2E+03	1.0E+04	1.9E+04	3.2E+04	5.1E+04	7.7E+04	1.1E+05	1.6E+05	2.1E+05	2.8E+05
28	→	2.2E-09	8.5E-06	1.4E-03	4.4E-02	5.7E-01	4.1E+00	2.0E+01	7.1E+01	2.1E+02	5.3E+02	1.2E+03	2.4E+03	4.5E+03	7.8E+03	1.3E+04	2.0E+04
28	←	4.9E-10	2.0E-06	3.4E-04	1.2E-02	1.7E-01	1.3E+00	6.8E+00	2.7E+01	8.3E+01	2.2E+02	5.2E+02	1.1E+03	2.1E+03	3.8E+03	6.5E+03	1.1E+04
29	→	2.6E-05	9.9E-03	3.9E-01	4.9E+00	3.2E+01	1.4E+02	4.5E+02	1.2E+03	2.7E+03	5.5E+03	1.0E+04	1.8E+04	2.9E+04	4.5E+04	6.7E+04	9.7E+04
29	←	1.1E-02	8.9E-01	1.4E+01	9.7E+01	4.2E+02	1.3E+03	3.4E+03	7.4E+03	1.4E+04	2.6E+04	4.3E+04	6.8E+04	1.0E+05	1.5E+05	2.1E+05	2.8E+05
30	→	4.2E-10	2.1E-06	4.0E-04	1.5E-02	2.1E-01	1.6E+00	8.3E+00	3.2E+01	1.0E+02	2.7E+02	6.2E+02	1.3E+03	2.5E+03	4.6E+03	7.8E+03	1.3E+04

30	←	1.1E+01	1.5E+02	8.3E+02	2.9E+03	7.8E+03	1.8E+04	3.5E+04	6.3E+04	1.1E+05	1.7E+05	2.5E+05	3.6E+05	5.1E+05	6.9E+05	9.2E+05	1.2E+06
31	→	6.2E-07	5.9E-04	4.1E-02	7.3E-01	6.2E+00	3.2E+01	1.2E+02	3.6E+02	9.1E+02	2.0E+03	4.0E+03	7.4E+03	1.3E+04	2.1E+04	3.2E+04	4.8E+04
31	←	1.5E-01	1.1E+01	1.5E+02	9.6E+02	3.9E+03	1.1E+04	2.8E+04	5.8E+04	1.1E+05	1.9E+05	3.1E+05	4.7E+05	7.0E+05	9.9E+05	1.4E+06	1.8E+06
32	→	1.9E-07	2.2E-04	1.8E-02	3.7E-01	3.5E+00	2.0E+01	7.9E+01	2.5E+02	6.7E+02	1.5E+03	3.2E+03	6.1E+03	1.1E+04	1.8E+04	2.8E+04	4.3E+04
32	←	6.1E+00	1.5E+02	1.1E+03	4.8E+03	1.4E+04	3.3E+04	6.7E+04	1.2E+05	2.0E+05	3.2E+05	4.8E+05	6.8E+05	9.4E+05	1.3E+06	1.7E+06	2.1E+06
33	→	3.7E-02	2.4E+00	3.3E+01	2.0E+02	7.9E+02	2.3E+03	5.5E+03	1.2E+04	2.2E+04	3.7E+04	6.0E+04	9.3E+04	1.4E+05	1.9E+05	2.7E+05	3.6E+05
33	←	1.1E-03	2.6E-01	7.6E+00	7.8E+01	4.4E+02	1.7E+03	5.1E+03	1.3E+04	2.7E+04	5.3E+04	9.5E+04	1.6E+05	2.5E+05	3.8E+05	5.6E+05	7.8E+05
34	→	7.6E-03	6.6E-01	1.1E+01	7.6E+01	3.3E+02	1.0E+03	2.6E+03	5.7E+03	1.1E+04	2.0E+04	3.3E+04	5.3E+04	7.9E+04	1.1E+05	1.6E+05	2.2E+05
34	←	1.7E-02	1.4E+00	2.2E+01	1.5E+02	6.5E+02	2.0E+03	5.0E+03	1.1E+04	2.1E+04	3.6E+04	6.0E+04	9.3E+04	1.4E+05	2.0E+05	2.8E+05	3.7E+05
35	→	2.1E-02	8.2E-01	8.9E+00	5.0E+01	1.9E+02	5.4E+02	1.3E+03	2.7E+03	5.1E+03	9.0E+03	1.5E+04	2.3E+04	3.4E+04	4.9E+04	6.9E+04	9.3E+04
35	←	9.0E-08	1.0E-04	8.9E-03	2.0E-01	2.1E+00	1.3E+01	5.7E+01	1.9E+02	5.4E+02	1.3E+03	2.9E+03	5.7E+03	1.0E+04	1.8E+04	2.9E+04	4.6E+04
36	→	1.1E+00	2.6E+01	1.9E+02	8.1E+02	2.4E+03	5.8E+03	1.2E+04	2.2E+04	3.7E+04	5.9E+04	9.0E+04	1.3E+05	1.8E+05	2.5E+05	3.3E+05	4.2E+05
36	←	1.5E-06	1.1E-03	7.0E-02	1.2E+00	9.9E+00	5.1E+01	1.9E+02	5.6E+02	1.4E+03	3.1E+03	6.1E+03	1.1E+04	1.9E+04	3.1E+04	4.8E+04	7.1E+04
37	→	7.1E-03	6.0E-01	9.7E+00	6.8E+01	2.9E+02	9.0E+02	2.3E+03	4.9E+03	9.5E+03	1.7E+04	2.8E+04	4.3E+04	6.4E+04	9.3E+04	1.3E+05	1.7E+05
37	←	9.4E-05	2.0E-02	5.9E-01	6.5E+00	3.9E+01	1.6E+02	5.1E+02	1.3E+03	3.0E+03	6.0E+03	1.1E+04	1.9E+04	3.1E+04	4.8E+04	7.2E+04	1.0E+05
38	→	8.0E-02	3.6E+00	4.0E+01	2.1E+02	7.4E+02	2.0E+03	4.5E+03	9.0E+03	1.6E+04	2.7E+04	4.3E+04	6.5E+04	9.4E+04	1.3E+05	1.8E+05	2.4E+05
38	←	2.7E-15	4.6E-10	7.5E-07	1.2E-04	4.9E-03	8.5E-02	8.2E-01	5.2E+00	2.5E+01	9.2E+01	2.9E+02	7.7E+02	1.8E+03	4.0E+03	8.0E+03	1.5E+04
39	→	4.7E-02	1.9E+00	2.0E+01	1.0E+02	3.7E+02	1.0E+03	2.3E+03	4.7E+03	8.5E+03	1.4E+04	2.3E+04	3.5E+04	5.0E+04	7.1E+04	9.7E+04	1.3E+05
39	←	8.1E-06	3.6E-03	1.6E-01	2.3E+00	1.6E+01	7.7E+01	2.7E+02	7.6E+02	1.8E+03	3.9E+03	7.6E+03	1.4E+04	2.3E+04	3.7E+04	5.7E+04	8.5E+04
40	→	3.4E-01	6.0E+00	3.8E+01	1.5E+02	4.1E+02	9.3E+02	1.9E+03	3.3E+03	5.6E+03	8.8E+03	1.3E+04	1.9E+04	2.7E+04	3.6E+04	4.8E+04	6.2E+04
40	←	5.2E-06	1.6E-03	6.1E-02	7.7E-01	5.1E+00	2.3E+01	7.6E+01	2.1E+02	4.9E+02	1.0E+03	2.0E+03	3.5E+03	5.9E+03	9.4E+03	1.4E+04	2.1E+04
41	→	2.1E-04	3.2E-02	7.5E-01	6.9E+00	3.6E+01	1.3E+02	3.8E+02	9.2E+02	1.9E+03	3.7E+03	6.6E+03	1.1E+04	1.7E+04	2.6E+04	3.7E+04	5.2E+04
41	←	3.6E-04	4.6E-02	1.0E+00	9.6E+00	5.3E+01	2.0E+02	6.2E+02	1.6E+03	3.5E+03	7.0E+03	1.3E+04	2.2E+04	3.6E+04	5.6E+04	8.4E+04	1.2E+05
42	→	7.4E+00	6.3E+01	2.6E+02	7.4E+02	1.7E+03	3.3E+03	5.7E+03	9.4E+03	1.4E+04	2.1E+04	3.0E+04	4.1E+04	5.4E+04	7.1E+04	9.1E+04	1.1E+05
42	←	5.4E-07	3.3E-04	1.9E-02	3.2E-01	2.7E+00	1.4E+01	5.3E+01	1.6E+02	4.1E+02	9.2E+02	1.9E+03	3.5E+03	6.1E+03	1.0E+04	1.6E+04	2.4E+04
43	→	3.1E-02	1.1E+00	1.0E+01	4.9E+01	1.6E+02	4.2E+02	9.1E+02	1.8E+03	3.1E+03	5.1E+03	7.9E+03	1.2E+04	1.7E+04	2.3E+04	3.1E+04	4.1E+04
43	←	3.2E-05	9.9E-03	3.5E-01	4.1E+00	2.5E+01	1.1E+02	3.3E+02	8.6E+02	1.9E+03	3.9E+03	7.1E+03	1.2E+04	2.0E+04	3.1E+04	4.6E+04	6.6E+04
44	→	2.7E-02	1.2E+00	1.3E+01	7.2E+01	2.6E+02	7.1E+02	1.6E+03	3.3E+03	6.1E+03	1.0E+04	1.7E+04	2.5E+04	3.7E+04	5.2E+04	7.1E+04	9.6E+04
44	←	6.5E-05	1.8E-02	5.9E-01	6.6E+00	4.0E+01	1.6E+02	5.0E+02	1.3E+03	2.9E+03	5.7E+03	1.0E+04	1.8E+04	2.9E+04	4.4E+04	6.5E+04	9.3E+04
45	→	1.8E-01	4.5E+00	3.6E+01	1.6E+02	4.8E+02	1.2E+03	2.5E+03	4.7E+03	8.1E+03	1.3E+04	2.0E+04	3.0E+04	4.2E+04	5.8E+04	7.8E+04	1.0E+05
45	←	3.8E-05	9.7E-03	3.1E-01	3.5E+00	2.1E+01	8.7E+01	2.7E+02	7.0E+02	1.6E+03	3.1E+03	5.8E+03	9.9E+03	1.6E+04	2.5E+04	3.6E+04	5.2E+04
46	→	4.7E-05	1.0E-02	3.1E-01	3.2E+00	1.8E+01	7.1E+01	2.1E+02	5.4E+02	1.2E+03	2.3E+03	4.2E+03	7.1E+03	1.1E+04	1.7E+04	2.6E+04	3.6E+04

46	←	1.2E-03	1.2E-01	2.3E+00	1.9E+01	9.3E+01	3.3E+02	9.2E+02	2.2E+03	4.6E+03	8.8E+03	1.6E+04	2.6E+04	4.1E+04	6.1E+04	8.9E+04	1.3E+05
47	→	2.4E-01	3.6E+00	2.1E+01	7.5E+01	2.0E+02	4.6E+02	9.1E+02	1.6E+03	2.7E+03	4.3E+03	6.4E+03	9.2E+03	1.3E+04	1.7E+04	2.3E+04	2.9E+04
47	←	1.4E-08	4.0E-05	5.7E-03	1.8E-01	2.2E+00	1.5E+01	7.2E+01	2.5E+02	7.3E+02	1.8E+03	3.9E+03	7.6E+03	1.4E+04	2.3E+04	3.8E+04	5.8E+04
48	→	8.4E-02	3.7E+00	4.0E+01	2.2E+02	7.7E+02	2.1E+03	4.7E+03	9.4E+03	1.7E+04	2.9E+04	4.5E+04	6.8E+04	9.8E+04	1.4E+05	1.9E+05	2.5E+05
48	←	2.0E-06	1.3E-03	7.6E-02	1.3E+00	1.0E+01	5.1E+01	1.9E+02	5.6E+02	1.4E+03	3.1E+03	6.3E+03	1.2E+04	2.0E+04	3.3E+04	5.1E+04	7.7E+04
49	→	1.1E-01	3.5E+00	3.2E+01	1.5E+02	5.1E+02	1.3E+03	2.9E+03	5.7E+03	1.0E+04	1.7E+04	2.6E+04	3.8E+04	5.5E+04	7.6E+04	1.0E+05	1.3E+05
49	←	3.1E-07	2.4E-04	1.6E-02	3.1E-01	2.7E+00	1.5E+01	6.0E+01	1.9E+02	5.0E+02	1.2E+03	2.4E+03	4.6E+03	8.1E+03	1.4E+04	2.2E+04	3.3E+04
50	→	9.0E-05	2.1E-02	6.1E-01	6.4E+00	3.6E+01	1.4E+02	4.2E+02	1.0E+03	2.2E+03	4.3E+03	7.7E+03	1.3E+04	2.0E+04	3.0E+04	4.4E+04	6.1E+04
50	←	2.2E-05	5.7E-03	2.0E-01	2.4E+00	1.6E+01	7.0E+01	2.4E+02	6.5E+02	1.5E+03	3.3E+03	6.3E+03	1.1E+04	1.9E+04	3.0E+04	4.6E+04	6.8E+04
51	→	1.1E+03	4.1E+03	1.1E+04	2.1E+04	3.8E+04	6.1E+04	9.2E+04	1.3E+05	1.8E+05	2.4E+05	3.2E+05	4.1E+05	5.1E+05	6.2E+05	7.6E+05	9.1E+05
51	←	2.2E-09	9.1E-06	1.6E-03	5.8E-02	8.1E-01	6.3E+00	3.3E+01	1.3E+02	4.0E+02	1.0E+03	2.4E+03	5.1E+03	9.9E+03	1.8E+04	3.0E+04	4.9E+04
52	→	6.1E+02	2.0E+03	4.8E+03	9.4E+03	1.7E+04	2.7E+04	4.1E+04	6.0E+04	8.3E+04	1.1E+05	1.5E+05	1.9E+05	2.4E+05	3.0E+05	3.7E+05	4.5E+05
52	←	2.2E-15	3.7E-10	6.0E-07	9.5E-05	3.9E-03	6.8E-02	6.7E-01	4.3E+00	2.0E+01	7.7E+01	2.4E+02	6.6E+02	1.6E+03	3.5E+03	7.0E+03	1.3E+04
53	→	2.8E-08	6.8E-05	8.1E-03	2.1E-01	2.3E+00	1.5E+01	6.6E+01	2.2E+02	6.3E+02	1.5E+03	3.2E+03	6.4E+03	1.2E+04	2.0E+04	3.2E+04	5.0E+04
53	←	5.5E+00	1.1E+02	7.4E+02	2.9E+03	8.3E+03	1.9E+04	3.8E+04	6.9E+04	1.2E+05	1.8E+05	2.7E+05	3.8E+05	5.3E+05	7.1E+05	9.3E+05	1.2E+06
54	→	9.9E-10	4.2E-06	7.2E-04	2.5E-02	3.4E-01	2.6E+00	1.3E+01	5.1E+01	1.6E+02	4.1E+02	9.6E+02	2.0E+03	3.9E+03	6.9E+03	1.2E+04	1.9E+04
54	←	2.8E+02	1.8E+03	6.2E+03	1.6E+04	3.4E+04	6.5E+04	1.1E+05	1.8E+05	2.8E+05	4.1E+05	5.8E+05	7.9E+05	1.1E+06	1.4E+06	1.7E+06	2.2E+06
55	→	2.0E-10	1.3E-06	2.9E-04	1.2E-02	1.8E-01	1.5E+00	8.2E+00	3.3E+01	1.1E+02	3.0E+02	7.1E+02	1.5E+03	3.0E+03	5.6E+03	9.6E+03	1.6E+04
55	←	7.2E+01	7.1E+02	3.2E+03	9.9E+03	2.4E+04	5.0E+04	9.2E+04	1.6E+05	2.5E+05	3.7E+05	5.4E+05	7.6E+05	1.0E+06	1.4E+06	1.8E+06	2.2E+06
56	→	6.1E-10	3.3E-06	6.5E-04	2.4E-02	3.5E-01	2.7E+00	1.4E+01	5.3E+01	1.6E+02	4.3E+02	1.0E+03	2.1E+03	4.0E+03	7.1E+03	1.2E+04	1.9E+04
56	←	2.8E+00	5.9E+01	4.3E+02	1.8E+03	5.6E+03	1.4E+04	3.0E+04	5.6E+04	9.8E+04	1.6E+05	2.5E+05	3.7E+05	5.3E+05	7.3E+05	9.9E+05	1.3E+06
57	→	1.4E-06	1.0E-03	6.0E-02	9.7E-01	7.7E+00	3.8E+01	1.4E+02	4.0E+02	9.9E+02	2.2E+03	4.3E+03	7.7E+03	1.3E+04	2.1E+04	3.3E+04	4.9E+04
57	←	2.3E-01	1.4E+01	1.8E+02	1.1E+03	4.3E+03	1.2E+04	2.9E+04	6.1E+04	1.1E+05	2.0E+05	3.1E+05	4.8E+05	7.0E+05	9.9E+05	1.4E+06	1.8E+06
58	→	7.8E-01	1.5E+01	1.1E+02	4.3E+02	1.3E+03	3.0E+03	6.3E+03	1.2E+04	2.0E+04	3.2E+04	4.8E+04	7.0E+04	9.8E+04	1.3E+05	1.8E+05	2.3E+05
58	←	1.7E-07	2.8E-04	2.7E-02	6.0E-01	6.0E+00	3.5E+01	1.5E+02	4.7E+02	1.2E+03	2.9E+03	5.9E+03	1.1E+04	2.0E+04	3.3E+04	5.2E+04	7.8E+04
59	→	9.7E-03	4.9E-01	6.0E+00	3.6E+01	1.4E+02	4.1E+02	9.8E+02	2.0E+03	3.8E+03	6.7E+03	1.1E+04	1.7E+04	2.5E+04	3.5E+04	4.9E+04	6.5E+04
59	←	2.2E-05	6.8E-03	2.6E-01	3.3E+00	2.2E+01	9.6E+01	3.2E+02	8.6E+02	2.0E+03	4.2E+03	7.9E+03	1.4E+04	2.3E+04	3.6E+04	5.4E+04	7.8E+04
60	→	2.2E-01	6.4E+00	5.5E+01	2.6E+02	8.3E+02	2.1E+03	4.5E+03	8.7E+03	1.5E+04	2.5E+04	3.8E+04	5.7E+04	8.1E+04	1.1E+05	1.5E+05	2.0E+05
60	←	4.3E-09	1.7E-05	2.7E-03	8.8E-02	1.1E+00	7.9E+00	3.7E+01	1.3E+02	3.9E+02	9.7E+02	2.1E+03	4.2E+03	7.8E+03	1.4E+04	2.2E+04	3.5E+04
61	→	4.0E+00	4.4E+01	2.2E+02	6.9E+02	1.7E+03	3.6E+03	6.7E+03	1.1E+04	1.8E+04	2.8E+04	4.0E+04	5.6E+04	7.5E+04	9.9E+04	1.3E+05	1.6E+05
61	←	3.7E-10	2.3E-06	4.9E-04	2.0E-02	2.9E-01	2.4E+00	1.2E+01	4.8E+01	1.5E+02	4.0E+02	9.3E+02	1.9E+03	3.7E+03	6.6E+03	1.1E+04	1.8E+04
62	→	9.5E+03	2.0E+04	3.5E+04	5.7E+04	8.6E+04	1.2E+05	1.7E+05	2.3E+05	3.1E+05	4.0E+05	5.0E+05	6.2E+05	7.6E+05	9.2E+05	1.1E+06	1.3E+06

62	←	1.4E-10	1.1E-06	2.9E-04	1.3E-02	2.0E-01	1.7E+00	9.1E+00	3.6E+01	1.2E+02	3.1E+02	7.4E+02	1.6E+03	3.0E+03	5.5E+03	9.4E+03	1.5E+04
63	→	5.2E+02	2.1E+03	5.7E+03	1.2E+04	2.2E+04	3.7E+04	5.7E+04	8.3E+04	1.2E+05	1.6E+05	2.1E+05	2.7E+05	3.4E+05	4.2E+05	5.2E+05	6.2E+05
63	←	8.0E-08	9.5E-05	8.0E-03	1.7E-01	1.7E+00	1.0E+01	4.2E+01	1.4E+02	3.7E+02	8.7E+02	1.8E+03	3.5E+03	6.3E+03	1.1E+04	1.7E+04	2.6E+04
64	→	1.4E+04	2.4E+04	3.8E+04	5.6E+04	8.0E+04	1.1E+05	1.5E+05	1.9E+05	2.5E+05	3.1E+05	3.8E+05	4.7E+05	5.7E+05	6.7E+05	8.0E+05	9.3E+05
64	←	9.0E-14	3.9E-09	2.8E-06	2.5E-04	6.6E-03	8.2E-02	6.1E-01	3.1E+00	1.2E+01	3.9E+01	1.1E+02	2.6E+02	5.6E+02	1.1E+03	2.1E+03	3.6E+03
65	→	2.5E-05	1.1E-02	4.7E-01	6.6E+00	4.7E+01	2.2E+02	7.6E+02	2.1E+03	5.2E+03	1.1E+04	2.1E+04	3.8E+04	6.4E+04	1.0E+05	1.6E+05	2.3E+05
65	←	9.6E-06	3.1E-03	1.2E-01	1.5E+00	1.0E+01	4.5E+01	1.5E+02	4.2E+02	1.0E+03	2.1E+03	4.1E+03	7.3E+03	1.2E+04	2.0E+04	3.1E+04	4.5E+04
66	→	1.1E-07	2.0E-04	2.1E-02	4.8E-01	4.9E+00	3.0E+01	1.2E+02	4.0E+02	1.1E+03	2.5E+03	5.3E+03	1.0E+04	1.8E+04	3.0E+04	4.8E+04	7.3E+04
66	←	4.4E-04	4.4E-02	8.6E-01	7.0E+00	3.5E+01	1.2E+02	3.5E+02	8.3E+02	1.8E+03	3.4E+03	6.0E+03	1.0E+04	1.6E+04	2.4E+04	3.6E+04	5.0E+04
67	→	3.7E-09	1.3E-05	1.8E-03	5.5E-02	6.7E-01	4.7E+00	2.2E+01	8.1E+01	2.4E+02	6.2E+02	1.4E+03	2.9E+03	5.6E+03	9.9E+03	1.7E+04	2.7E+04
67	←	2.3E+03	1.1E+04	2.9E+04	6.1E+04	1.1E+05	1.9E+05	2.9E+05	4.4E+05	6.3E+05	8.8E+05	1.2E+06	1.6E+06	2.0E+06	2.6E+06	3.2E+06	4.0E+06
68	→	1.3E+00	2.5E+01	1.6E+02	6.2E+02	1.7E+03	3.9E+03	7.8E+03	1.4E+04	2.3E+04	3.6E+04	5.4E+04	7.6E+04	1.1E+05	1.4E+05	1.9E+05	2.4E+05
68	←	2.2E-09	1.2E-05	2.4E-03	8.9E-02	1.3E+00	9.6E+00	4.9E+01	1.9E+02	5.7E+02	1.5E+03	3.4E+03	7.0E+03	1.3E+04	2.4E+04	4.0E+04	6.3E+04
69	→	2.3E-01	8.0E+00	7.4E+01	3.5E+02	1.2E+03	2.9E+03	6.4E+03	1.2E+04	2.1E+04	3.5E+04	5.3E+04	7.8E+04	1.1E+05	1.5E+05	2.0E+05	2.7E+05
69	←	3.3E-11	5.6E-07	2.1E-04	1.2E-02	2.4E-01	2.3E+00	1.4E+01	6.2E+01	2.1E+02	6.1E+02	1.5E+03	3.3E+03	6.8E+03	1.3E+04	2.2E+04	3.7E+04
70	→	4.2E-02	1.5E+00	1.5E+01	7.6E+01	2.6E+02	7.0E+02	1.6E+03	3.1E+03	5.6E+03	9.4E+03	1.5E+04	2.2E+04	3.2E+04	4.5E+04	6.1E+04	8.0E+04
70	←	1.7E-12	6.2E-08	3.9E-05	3.2E-03	8.1E-02	9.7E-01	7.0E+00	3.5E+01	1.3E+02	4.2E+02	1.1E+03	2.6E+03	5.6E+03	1.1E+04	2.0E+04	3.5E+04
71	→	2.6E+00	3.8E+01	2.1E+02	7.2E+02	1.9E+03	4.0E+03	7.5E+03	1.3E+04	2.1E+04	3.1E+04	4.5E+04	6.3E+04	8.6E+04	1.1E+05	1.5E+05	1.9E+05
71	←	1.8E-12	5.1E-08	2.8E-05	2.1E-03	4.8E-02	5.4E-01	3.7E+00	1.8E+01	6.7E+01	2.1E+02	5.4E+02	1.3E+03	2.6E+03	5.1E+03	9.3E+03	1.6E+04
72	→	5.7E+01	3.9E+02	1.3E+03	3.3E+03	6.6E+03	1.2E+04	1.9E+04	2.9E+04	4.1E+04	5.7E+04	7.6E+04	9.8E+04	1.2E+05	1.6E+05	1.9E+05	2.3E+05
72	←	2.8E-19	8.2E-13	7.4E-09	3.5E-06	3.0E-04	8.8E-03	1.2E-01	1.1E+00	6.1E+00	2.7E+01	9.5E+01	2.8E+02	7.3E+02	1.7E+03	3.6E+03	7.1E+03
73	→	6.5E-03	2.2E-01	2.1E+00	1.0E+01	3.5E+01	9.3E+01	2.1E+02	4.3E+02	7.8E+02	1.3E+03	2.1E+03	3.3E+03	4.8E+03	6.8E+03	9.4E+03	1.3E+04
73	←	2.7E-11	3.1E-07	1.0E-04	5.7E-03	1.1E-01	1.0E+00	6.3E+00	2.8E+01	9.6E+01	2.8E+02	6.9E+02	1.5E+03	3.1E+03	5.8E+03	1.0E+04	1.7E+04
74	→	9.6E-05	3.7E-02	1.5E+00	1.9E+01	1.2E+02	5.3E+02	1.7E+03	4.6E+03	1.0E+04	2.1E+04	4.0E+04	7.0E+04	1.1E+05	1.8E+05	2.7E+05	3.8E+05
74	←	1.5E-08	3.0E-05	3.3E-03	8.4E-02	9.3E-01	6.0E+00	2.7E+01	9.4E+01	2.7E+02	6.6E+02	1.5E+03	2.9E+03	5.4E+03	9.4E+03	1.5E+04	2.4E+04
75	→	3.2E-12	8.0E-08	3.9E-05	2.6E-03	5.7E-02	6.0E-01	3.9E+00	1.8E+01	6.5E+01	1.9E+02	4.9E+02	1.1E+03	2.3E+03	4.4E+03	7.8E+03	1.3E+04
75	←	8.2E-01	2.4E+01	2.1E+02	9.6E+02	3.1E+03	7.9E+03	1.7E+04	3.3E+04	5.8E+04	9.5E+04	1.5E+05	2.2E+05	3.1E+05	4.3E+05	5.8E+05	7.6E+05
76	→	1.3E-08	3.4E-05	4.4E-03	1.2E-01	1.4E+00	9.1E+00	4.1E+01	1.4E+02	4.1E+02	9.9E+02	2.2E+03	4.3E+03	7.9E+03	1.4E+04	2.2E+04	3.5E+04
76	←	1.1E+01	1.9E+02	1.1E+03	4.1E+03	1.1E+04	2.4E+04	4.7E+04	8.1E+04	1.3E+05	2.0E+05	2.9E+05	4.1E+05	5.6E+05	7.4E+05	9.6E+05	1.2E+06
77	→	1.9E-13	1.6E-08	1.6E-05	1.7E-03	4.9E-02	6.5E-01	5.0E+00	2.7E+01	1.1E+02	3.5E+02	9.5E+02	2.3E+03	5.0E+03	1.0E+04	1.9E+04	3.2E+04
77	←	7.4E-01	2.1E+01	1.8E+02	8.0E+02	2.5E+03	6.2E+03	1.3E+04	2.4E+04	4.2E+04	6.8E+04	1.0E+05	1.5E+05	2.1E+05	2.9E+05	3.8E+05	5.0E+05
78	→	1.6E-03	1.6E-01	3.2E+00	2.6E+01	1.3E+02	4.4E+02	1.2E+03	2.9E+03	5.9E+03	1.1E+04	1.9E+04	3.2E+04	5.0E+04	7.4E+04	1.1E+05	1.5E+05

78	←	2.6E-06	1.3E-03	6.6E-02	1.0E+00	7.9E+00	3.9E+01	1.5E+02	4.3E+02	1.1E+03	2.4E+03	4.8E+03	8.9E+03	1.5E+04	2.5E+04	4.0E+04	6.0E+04
79	→	1.2E-05	4.0E-03	1.5E-01	1.8E+00	1.1E+01	4.8E+01	1.5E+02	4.0E+02	9.0E+02	1.8E+03	3.3E+03	5.7E+03	9.1E+03	1.4E+04	2.1E+04	3.0E+04
79	←	2.1E-04	2.5E-02	5.2E-01	4.6E+00	2.4E+01	8.8E+01	2.6E+02	6.3E+02	1.4E+03	2.7E+03	4.8E+03	8.1E+03	1.3E+04	2.0E+04	2.9E+04	4.2E+04
80	→	1.2E-03	1.4E-01	2.9E+00	2.4E+01	1.2E+02	4.0E+02	1.1E+03	2.5E+03	5.1E+03	9.5E+03	1.6E+04	2.6E+04	4.1E+04	6.0E+04	8.6E+04	1.2E+05
80	←	8.3E-10	3.3E-06	5.5E-04	1.9E-02	2.6E-01	2.0E+00	1.0E+01	4.0E+01	1.2E+02	3.3E+02	7.6E+02	1.6E+03	3.1E+03	5.6E+03	9.6E+03	1.6E+04
81	→	2.6E-05	1.1E-02	4.8E-01	6.8E+00	4.9E+01	2.3E+02	8.1E+02	2.3E+03	5.6E+03	1.2E+04	2.3E+04	4.2E+04	7.0E+04	1.1E+05	1.7E+05	2.5E+05
81	←	6.7E-07	3.9E-04	2.2E-02	3.6E-01	2.9E+00	1.5E+01	5.8E+01	1.8E+02	4.5E+02	1.0E+03	2.1E+03	3.9E+03	6.8E+03	1.1E+04	1.8E+04	2.7E+04
82	→	2.0E-07	3.0E-04	2.7E-02	6.0E-01	5.8E+00	3.4E+01	1.4E+02	4.3E+02	1.1E+03	2.6E+03	5.3E+03	1.0E+04	1.7E+04	2.9E+04	4.5E+04	6.7E+04
82	←	5.3E-05	8.4E-03	2.1E-01	2.1E+00	1.2E+01	4.5E+01	1.4E+02	3.5E+02	7.7E+02	1.5E+03	2.8E+03	4.8E+03	7.7E+03	1.2E+04	1.8E+04	2.5E+04
83	→	2.9E+00	4.7E+01	2.9E+02	1.1E+03	2.9E+03	6.6E+03	1.3E+04	2.3E+04	3.8E+04	5.9E+04	8.8E+04	1.3E+05	1.7E+05	2.3E+05	3.0E+05	3.9E+05
83	←	1.7E-05	7.0E-03	3.0E-01	4.0E+00	2.7E+01	1.2E+02	4.0E+02	1.1E+03	2.5E+03	5.2E+03	9.8E+03	1.7E+04	2.8E+04	4.4E+04	6.6E+04	9.5E+04
84	→	3.3E-08	1.0E-04	1.5E-02	4.4E-01	5.3E+00	3.6E+01	1.7E+02	6.0E+02	1.7E+03	4.4E+03	9.7E+03	1.9E+04	3.6E+04	6.3E+04	1.0E+05	1.7E+05
84	←	4.1E-08	8.7E-05	1.0E-02	2.7E-01	3.1E+00	2.0E+01	9.3E+01	3.3E+02	9.5E+02	2.4E+03	5.3E+03	1.1E+04	2.0E+04	3.6E+04	5.9E+04	9.4E+04
85	→	1.4E-07	2.2E-04	2.1E-02	4.7E-01	4.7E+00	2.8E+01	1.2E+02	3.7E+02	1.0E+03	2.3E+03	4.9E+03	9.3E+03	1.6E+04	2.8E+04	4.4E+04	6.6E+04
85	←	6.2E-11	4.9E-07	1.3E-04	5.9E-03	1.0E-01	9.0E-01	5.3E+00	2.2E+01	7.6E+01	2.2E+02	5.4E+02	1.2E+03	2.4E+03	4.6E+03	8.1E+03	1.4E+04
86	→	5.8E-06	3.7E-03	2.1E-01	3.3E+00	2.6E+01	1.3E+02	4.5E+02	1.3E+03	3.2E+03	6.8E+03	1.3E+04	2.4E+04	4.0E+04	6.3E+04	9.6E+04	1.4E+05
86	←	6.2E-11	3.8E-07	8.4E-05	3.5E-03	5.5E-02	4.6E-01	2.6E+00	1.0E+01	3.4E+01	9.3E+01	2.2E+02	4.8E+02	9.4E+02	1.7E+03	3.0E+03	4.9E+03
87	→	6.0E-07	3.4E-04	1.8E-02	2.7E-01	2.0E+00	9.7E+00	3.4E+01	9.8E+01	2.4E+02	5.1E+02	9.8E+02	1.8E+03	3.0E+03	4.8E+03	7.3E+03	1.1E+04
87	←	1.8E-11	1.7E-07	5.1E-05	2.6E-03	4.6E-02	4.3E-01	2.6E+00	1.2E+01	4.1E+01	1.2E+02	3.0E+02	6.8E+02	1.4E+03	2.7E+03	4.9E+03	8.3E+03

B.4.3. Arrhenius parameters regressed at 1000 K

Table B-16: Standard reaction enthalpy [kJ mol^{-1}], pre-exponential factor [m^3 mol^{-1} s^{-1}], activation energy [kJ mol^{-1}] and rate coefficient [m^3 mol^{-1} s^{-1}] at 1000 K for all C-H-N hydrogen abstraction reactions in the training (T) and validation dataset (V). The Arrhenius parameters exclude tunneling.

No.		Reaction	ΔH_r°	Forward			Reverse		
				$logA$	E_a	k_{for}	$logA$	E_a	k_{rev}
1	T	$CH_3^\bullet + NH_2^\bullet \leftrightarrow CH_4 + NH^\bullet$	11.8	7.231	80.5	5.2E+03	7.807	73.4	4.0E+04
2	T	$CH_3^\bullet + NH_3 \leftrightarrow CH_4 + NH_2^\bullet$	-21.9	7.032	65.8	1.4E+04	7.654	92.1	4.3E+03
3	T	$CH_3^\bullet + NH \leftrightarrow CH_4 + N^\bullet$	-73.1	6.915	44.7	9.1E+04	7.735	120.5	3.0E+02
4	T	$CH_3^\bullet + NH_2 \leftrightarrow CH_4 + NH^\bullet$	-70.4	6.766	63.1	1.0E+04	8.077	139.8	9.6E+01
5	T	$CH_3^\bullet + NH_2 \leftrightarrow CH_4 + NH^\bullet$	-77.8	7.106	54.5	5.3E+04	7.811	136.1	7.6E+01
6	T	$CH_3^\bullet + HN \leftrightarrow CH_4 + N^\bullet$	-46.7	6.908	52.5	4.1E+04	7.666	107.5	9.5E+02
7	T	$CH_3^\bullet + HN \leftrightarrow CH_4 + N^\bullet$	-81.8	6.770	56.1	2.1E+04	8.342	148.2	7.6E+01
8	T	$CH_3^\bullet + HN \leftrightarrow CH_4 + N^\bullet$	-106.5	6.134	56.0	4.9E+03	8.188	162.9	1.2E+01
9	T	$CH_3^\bullet + HN \leftrightarrow CH_4 + N^\bullet$	-91.7	6.768	46.1	5.6E+04	7.714	143.0	3.0E+01
10	T	$+ NH_3 \leftrightarrow + NH_2^\bullet$	85.4	8.392	135.7	3.0E+02	7.414	52.3	1.3E+05
11	T	$NH_2^\bullet + NH_2 \leftrightarrow NH_2 + NH^\bullet$	27.9	7.105	89.4	1.6E+03	7.471	65.8	3.9E+04
12	T	$+ NH_2 \leftrightarrow + NH^\bullet$	-43.8	6.966	44.0	1.1E+05	7.732	90.3	6.2E+03
13	T	$+ NH_2 \leftrightarrow + NH^\bullet$	-6.5	6.726	73.7	3.2E+03	7.604	81.3	1.1E+04
14	T	$+ NH_2 \leftrightarrow + NH^\bullet$	7.1	7.019	76.5	4.8E+03	7.530	67.3	3.9E+04
15	T	$+ NH_2 \leftrightarrow + NH^\bullet$	-30.8	6.799	48.0	5.0E+04	7.035	79.7	3.6E+03
16	T	$+ NH_2 \leftrightarrow + NH^\bullet$	51.6	7.931	113.6	9.5E+02	7.001	63.7	1.7E+04
17	T	$+ NH_2 \leftrightarrow + NH^\bullet$	-4.2	8.260	89.9	2.2E+04	7.411	95.2	1.8E+03
18	T	$+ HN \leftrightarrow + N^\bullet$	-8.2	7.864	89.8	8.8E+03	7.882	105.7	1.9E+03
19	T	$NH_2 + NH_2 \leftrightarrow NH_2 + NH^\bullet$	33.7	7.052	87.4	1.7E+03	7.290	56.4	6.7E+04
20	T	$NH_2 + NH_2 \leftrightarrow NH_2 + NH^\bullet$	-14.8	6.611	68.7	4.1E+03	7.536	87.9	5.0E+03
21	T	$NH_2 + NH_2 \leftrightarrow NH_2 + NH^\bullet$	-22.2	6.606	50.1	2.6E+04	6.925	74.2	4.8E+03
22	T	$NH^\bullet + NH_2 \leftrightarrow NH_2 + NH^\bullet$	38.6	7.107	98.7	6.3E+02	7.024	67.2	1.2E+04
23	T	$NH^\bullet + NH_2 \leftrightarrow NH_2 + NH^\bullet$	-9.9	6.698	91.7	5.0E+02	7.302	110.5	3.0E+02
24	T	$NH^\bullet + NH_2 \leftrightarrow NH_2 + NH^\bullet$	-17.3	7.451	81.6	7.7E+03	7.450	105.4	7.1E+02
25	T	$N + NH_2 \leftrightarrow N + NH^\bullet$	48.1	7.849	110.6	1.1E+03	6.836	67.0	8.1E+03
26	T	$N + NH_2 \leftrightarrow N + NH^\bullet$	-7.8	8.298	92.3	1.9E+04	7.367	103.9	6.9E+02
27	T	$NH + NH_2 \leftrightarrow NH + NH^\bullet$	19.2	6.949	76.5	4.1E+03	7.044	58.1	3.2E+04
28	T	$N + NH_2 \leftrightarrow N + NH^\bullet$	-0.4	7.190	102.4	5.3E+02	7.064	108.2	2.2E+02
29	T	$NH^\bullet + NH_2 \leftrightarrow NH + NH^\bullet$	16.6	7.177	78.7	5.5E+03	7.230	64.5	2.6E+04
30	V	$NH_2^\bullet + NH_3 \leftrightarrow NH_2 + NH_2^\bullet$	61.6	7.133	107.9	2.7E+02	7.452	51.0	1.7E+05
31	V	$+ NH_3 \leftrightarrow + NH_2^\bullet$	28.6	7.126	87.6	2.0E+03	7.938	60.9	1.9E+05
32	V	$+ NH_3 \leftrightarrow + NH_2^\bullet$	40.9	7.224	92.5	1.5E+03	7.687	49.9	3.2E+05
33	V	$+ NH_3 \leftrightarrow + NH_2^\bullet$	-10.0	7.218	60.6	3.7E+04	7.936	73.5	5.3E+04
34	V	$+ NH_3 \leftrightarrow + NH_2^\bullet$	2.9	7.114	64.4	2.0E+04	7.303	62.8	3.6E+04
35	V	$NH^\bullet + NH_2 \leftrightarrow NH + NH_2$	-31.9	6.667	62.1	9.0E+03	7.408	98.3	1.3E+03
36	V	$NH^\bullet + NH \leftrightarrow NH + N^\bullet$	-34.6	7.032	51.7	5.9E+04	7.282	87.0	3.1E+03

37	V		-8.2	6.985	63.2	1.7E+04	7.174	77.8	6.0E+03
38	V	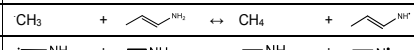	-80.9	6.940	57.3	2.7E+04	8.291	145.1	9.2E+01
39	V	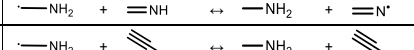	-23.3	6.705	58.3	1.4E+04	7.267	84.2	3.9E+03
40	V	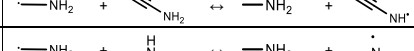	-28.0	6.151	50.5	8.8E+03	6.599	82.1	1.0E+03
41	V	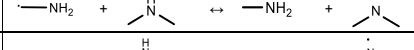	3.1	6.706	71.8	3.7E+03	7.208	77.0	7.0E+03
42	V	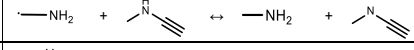	-41.9	6.196	42.8	2.1E+04	6.885	89.8	9.2E+02
43	V		-21.3	6.117	55.2	5.1E+03	6.960	77.2	3.9E+03
44	V	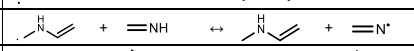	-18.2	6.587	58.9	1.0E+04	7.089	76.3	5.7E+03
45	V		-22.9	6.465	53.6	1.3E+04	6.854	76.9	3.1E+03
46	V		8.3	6.635	74.9	2.3E+03	7.076	71.7	8.8E+03
47	V	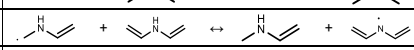	-51.5	5.826	50.2	4.3E+03	7.563	98.9	1.8E+03
48	V	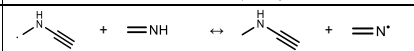	-26.9	6.962	57.4	2.9E+04	7.332	87.9	3.1E+03
49	V	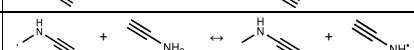	-31.6	6.651	55.7	1.7E+04	7.099	92.5	1.2E+03
50	V	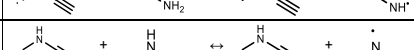	-0.4	6.824	73.1	4.3E+03	7.132	82.9	3.3E+03
51	V	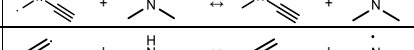	-68.5	6.814	32.6	2.4E+05	7.714	107.6	1.0E+03
52	V	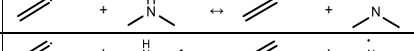	-103.6	6.550	34.2	1.1E+05	8.264	146.3	7.7E+01
53	V	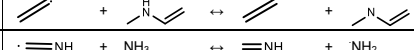	50.3	7.421	97.2	1.5E+03	7.427	49.7	1.8E+05
54	V	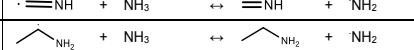	67.5	7.284	107.0	4.1E+02	7.474	42.5	4.1E+05
55	V	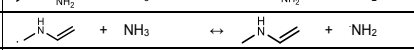	66.8	7.325	111.3	3.0E+02	7.584	46.0	3.7E+05
56	V	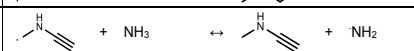	58.1	7.285	106.6	4.3E+02	7.603	54.8	1.6E+05
57	V	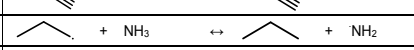	27.3	7.081	85.8	2.2E+03	7.911	60.0	2.0E+05
58	V		-44.1	6.783	52.2	3.2E+04	7.490	92.5	2.9E+03
59	V	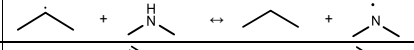	-17.6	6.494	61.1	6.7E+03	7.140	80.6	4.2E+03
60	V	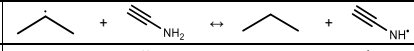	-48.8	6.781	54.6	2.5E+04	7.374	100.6	9.7E+02
61	V	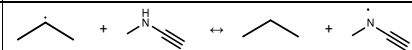	-62.6	6.447	45.9	2.8E+04	7.280	107.3	4.0E+02
62	V		-82.0	6.837	28.3	4.0E+05	7.269	109.4	3.1E+02
63	V	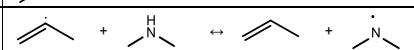	-55.6	6.694	34.1	1.6E+05	7.065	94.6	8.7E+02
64	V		-100.6	6.628	25.9	3.1E+05	7.186	128.3	3.9E+01
65	V	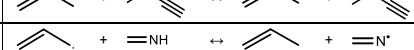	0.5	7.692	83.7	1.1E+04	6.958	83.2	2.1E+03
66	V	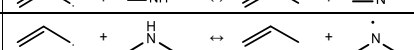	26.9	7.492	93.7	2.5E+03	6.696	72.5	3.4E+03
67	V		68.5	7.339	104.1	6.2E+02	7.558	36.9	8.8E+05
68	V	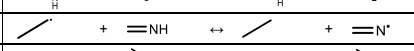	-56.4	6.715	49.3	3.6E+04	7.770	105.5	1.5E+03
69	V	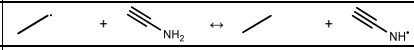	-61.1	6.905	54.2	3.5E+04	7.846	116.1	6.1E+02
70	V	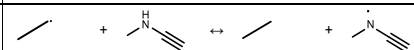	-74.9	6.516	46.2	3.1E+04	7.697	123.5	2.1E+02
71	V	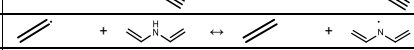	-128.3	6.325	35.9	5.7E+04	8.521	162.8	2.7E+01
72	V	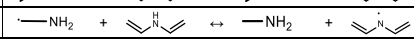	-56.7	5.718	59.3	1.3E+03	7.515	116.3	2.8E+02

73	V		-18.1	7.787	79.2	2.1E+04	7.179	99.9	6.6E+02
74	V	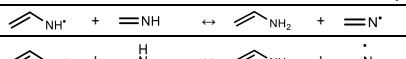	-12.6	7.112	70.2	1.1E+04	7.225	88.1	2.4E+03
75	V	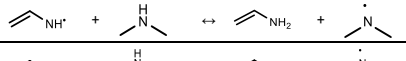	13.8	6.621	77.1	1.8E+03	6.673	74.3	2.7E+03
76	V	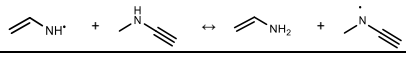	-31.2	6.971	68.6	9.5E+03	7.209	107.6	3.3E+02
77	V		72.4	7.515	119.9	1.9E+02	7.384	55.0	9.5E+04
78	V	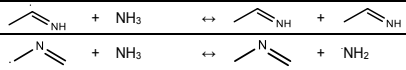	52.9	7.315	99.0	9.9E+02	7.362	47.1	2.0E+05
79	V	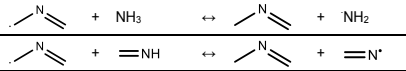	81.8	8.195	129.8	3.5E+02	7.134	52.7	6.8E+04
80	V	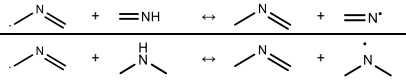	-3.1	7.750	84.2	1.2E+04	6.934	90.0	1.0E+03
81	V		23.3	7.394	91.2	2.6E+03	6.516	76.3	1.5E+03
82	V	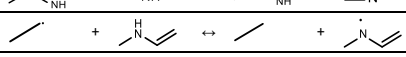	-32.0	6.921	49.1	5.9E+04	7.212	80.1	5.2E+03
83	V	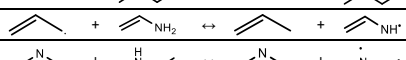	-65.1	6.472	57.2	9.4E+03	8.110	125.9	4.2E+02
84	V	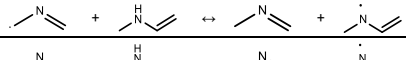	3.1	8.053	101.2	4.4E+03	7.810	101.6	2.4E+03
85	V	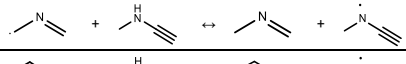	-11.8	7.451	93.6	2.3E+03	7.387	115.7	2.2E+02
86	V	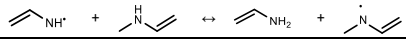	-21.7	7.511	84.3	6.8E+03	6.821	111.3	9.3E+01
87	V		-21.3	6.378	84.2	5.1E+02	7.244	118.5	1.2E+02

B.4.4. Reaction path degeneracy

Table B-17: External and internal symmetry numbers, number of optical isomers and number of single events n_e for all H-H-N hydrogen abstractions of Table B-16.

No.		Reactant 1 R˙			Reactant 2 RH			Transition state			Reaction path degeneracy
		σ_{ext}	σ_{int}	n_{opt}	σ_{ext}	σ_{int}	n_{opt}	σ_{ext}	σ_{int}	n_{opt}	n_e
1	→	2	3	1	3	1	1	1	3	1	6
1	→	1	12	1	2	1	1	1	3	1	8
2	←	2	3	1	1	3	1	1	9	2	4
2	→	1	12	1	3	1	1	1	9	2	8
3	←	2	3	1	1	1	1	1	3	1	2
3	→	1	12	1	1	2	1	1	3	1	8
4	←	2	3	1	1	1	1	1	3	2	4
4	→	1	12	1	1	1	1	1	3	2	8
5	←	2	3	1	1	1	1	1	3	2	4
5	→	1	12	1	1	1	1	1	3	2	8
6	←	2	3	1	1	9	1	1	27	1	2
6	→	1	12	1	2	9	1	1	27	1	8
7	←	2	3	1	1	3	2	1	9	2	2
7	→	1	12	1	1	3	1	1	9	2	8
8	←	2	3	1	1	1	1	1	3	1	2
8	→	1	12	1	1	2	1	1	3	1	8
9	←	2	3	1	1	3	2	1	9	2	2
9	→	1	12	1	1	3	1	1	9	2	8
10	←	1	8	1	3	1	1	1	1	1	24
10	→	1	3	1	2	1	1	1	1	1	6
11	←	1	2	1	1	3	1	1	3	2	4
11	→	1	3	1	3	1	1	1	3	2	6
12	←	1	1	1	1	3	1	1	3	2	2
12	→	1	4	1	3	1	1	1	3	2	8
13	←	1	6	1	1	3	1	1	9	2	4
13	→	2	9	1	3	1	1	1	9	2	12
14	←	2	9	1	1	3	1	1	27	2	4
14	→	2	9	1	3	1	1	1	27	2	4
15	←	1	3	1	1	3	1	1	9	2	2
15	→	1	3	1	3	1	1	1	9	2	2
16	←	1	8	1	1	3	1	1	3	2	16
16	→	1	3	1	3	1	1	1	3	2	6
17	←	1	8	1	1	1	1	1	1	2	16
17	→	1	3	1	1	1	1	1	1	2	6
18	←	1	8	1	1	3	2	1	3	2	8
18	→	1	3	1	1	3	1	1	3	2	6
19	←	1	3	1	1	3	1	1	9	4	4
19	→	1	3	1	3	1	1	1	9	4	4
20	←	1	3	1	1	1	1	1	3	4	4
20	→	1	3	1	1	1	1	1	3	4	4
21	←	1	3	1	1	1	1	1	3	4	4
21	→	1	3	1	1	1	1	1	3	4	4
22	←	1	1	1	1	3	1	1	3	2	2
22	→	1	3	1	3	1	1	1	3	2	6
23	←	1	1	1	1	1	1	1	1	2	2
23	→	1	3	1	1	1	1	1	1	2	6
24	→	1	1	1	1	1	1	1	1	2	2
24	←	1	3	1	1	1	1	1	1	2	6
25	→	1	8	1	1	3	1	1	3	2	16
25	←	1	3	1	3	1	1	1	3	2	6
26	→	1	8	1	1	1	1	1	1	2	16

26	←	1	3	1	1	1	1	1	1	2	6
27	→	1	3	1	1	3	1	1	9	2	2
27	←	1	3	1	3	1	1	1	9	2	2
28	→	1	8	1	1	1	1	1	1	2	16
28	←	1	3	1	1	1	1	1	1	2	6
29	→	1	1	1	1	3	1	1	3	2	2
29	←	1	1	1	3	1	1	1	3	2	2
30	→	1	2	1	3	1	1	1	1	1	6
30	←	1	3	1	2	1	1	1	1	1	6
31	→	1	6	1	3	1	1	1	3	1	6
31	←	2	9	1	2	1	1	1	3	1	12
32	→	2	9	1	3	1	1	1	9	1	6
32	←	2	9	1	2	1	1	1	9	1	4
33	→	1	1	1	3	1	1	1	1	1	3
33	←	1	4	1	2	1	1	1	1	1	8
34	→	1	3	1	3	1	1	1	3	1	3
34	←	1	3	1	2	1	1	1	3	1	2
35	→	1	1	1	1	1	1	1	1	2	2
35	←	1	1	1	1	1	1	1	1	2	2
36	→	1	1	1	1	1	1	1	1	1	1
36	←	1	1	1	1	2	1	1	1	1	2
37	→	1	1	1	1	9	1	1	9	1	1
37	←	1	1	1	2	9	1	1	9	1	2
38	→	2	3	1	1	3	1	1	9	2	4
38	←	1	12	1	1	3	1	1	9	2	8
39	→	1	2	1	1	1	1	1	1	1	2
39	←	1	3	1	1	2	1	1	1	1	6
40	→	1	2	1	1	1	1	1	1	1	2
40	←	1	3	1	1	1	1	1	1	1	3
41	→	1	2	1	1	9	1	1	9	1	2
41	←	1	3	1	2	9	1	1	9	1	6
42	→	1	2	1	1	3	2	1	3	2	2
42	←	1	3	1	1	3	1	1	3	2	6
43	→	1	6	2	1	1	1	1	3	1	1
43	←	1	9	1	1	2	1	1	3	1	6
44	→	1	2	2	1	1	1	1	1	2	2
44	←	1	3	2	1	2	1	1	1	2	6
45	→	1	2	2	1	1	1	1	1	4	4
45	←	1	3	2	1	1	1	1	1	4	6
46	←	1	2	2	1	9	1	1	9	2	2
46	→	1	3	2	2	9	1	1	9	2	6
47	←	1	2	2	1	1	1	1	1	2	2
47	→	1	3	2	1	2	1	1	1	2	6
48	←	1	2	2	1	1	1	1	1	2	2
48	→	1	3	2	1	2	1	1	1	2	6
49	←	1	2	2	1	1	1	1	1	4	4
49	→	1	3	2	1	1	1	1	1	4	6
50	←	1	2	2	1	9	1	1	9	2	2
50	→	1	3	2	2	9	1	1	9	2	6
51	←	1	1	1	1	9	1	1	9	1	1
51	→	1	4	1	2	9	1	1	9	1	8
52	←	1	1	1	1	3	2	1	3	2	1
52	→	1	4	1	1	3	1	1	3	2	8
53	←	1	1	1	3	1	1	1	1	1	3
53	→	1	1	1	2	1	1	1	1	1	2
54	←	1	3	1	3	1	1	1	3	2	6
54	→	1	3	1	2	1	1	1	3	2	4
55	←	1	2	2	3	1	1	1	1	2	6
55	→	1	3	2	2	1	1	1	1	2	6
56	←	1	2	2	3	1	1	1	1	2	6
56	→	1	3	2	2	1	1	1	1	2	6

57	←	1	6	1	3	1	1	1	3	1	6
57	→	2	9	1	2	1	1	1	3	1	12
58	→	2	9	1	1	1	1	1	9	1	2
58	←	2	9	1	1	2	1	1	9	1	4
59	→	2	9	1	1	9	1	1	81	1	2
59	←	2	9	1	2	9	1	1	81	1	4
60	→	2	9	1	1	1	1	1	9	2	4
60	←	2	9	1	1	1	1	1	9	2	4
61	→	2	9	1	1	3	2	1	27	2	2
61	←	2	9	1	1	3	1	1	27	2	4
62	→	1	3	1	1	1	1	1	3	1	1
62	←	1	3	1	1	2	1	1	3	1	2
63	→	1	3	1	1	9	1	1	27	1	1
63	←	1	3	1	2	9	1	1	27	1	2
64	→	1	3	1	1	3	2	1	9	2	1
64	←	1	3	1	1	3	1	1	9	2	2
65	→	1	8	1	1	1	1	1	1	1	8
65	←	1	3	1	1	2	1	1	1	1	6
66	→	1	8	1	1	9	1	1	9	1	8
66	←	1	3	1	2	9	1	1	9	1	6
67	→	1	9	2	3	1	1	1	9	4	6
67	←	1	9	2	2	1	1	1	9	4	4
68	→	1	6	1	1	1	1	1	3	1	2
68	←	2	9	1	1	2	1	1	3	1	12
69	→	1	6	1	1	1	1	1	3	2	4
69	←	2	9	1	1	1	1	1	3	2	12
70	→	1	6	1	1	3	2	1	9	2	2
70	←	2	9	1	1	3	1	1	9	2	12
71	→	1	1	1	1	1	1	1	1	1	1
71	←	1	4	1	1	2	1	1	1	1	8
72	→	1	2	1	1	1	1	1	1	1	2
72	←	1	3	1	1	2	1	1	1	1	6
73	→	1	8	1	1	3	2	1	3	2	8
73	←	1	3	1	1	3	1	1	3	2	6
74	→	1	1	1	1	1	1	1	1	1	1
74	←	1	3	1	1	2	1	1	1	1	6
75	→	1	1	1	1	9	1	1	9	1	1
75	←	1	3	1	2	9	1	1	9	1	6
76	→	1	1	1	1	3	2	1	3	2	1
76	←	1	3	1	1	3	1	1	3	2	6
77	→	1	1	1	3	1	1	1	1	1	3
77	←	1	3	1	2	1	1	1	1	1	6
78	→	1	3	1	3	1	1	1	3	1	3
78	←	1	3	1	2	1	1	1	3	1	2
79	→	1	8	1	3	1	1	1	1	1	24
79	←	1	3	1	2	1	1	1	1	1	6
80	→	1	8	1	1	1	1	1	1	1	8
80	←	1	3	1	1	2	1	1	1	1	6
81	→	1	8	1	1	9	1	1	9	1	8
81	←	1	3	1	2	9	1	1	9	1	6
82	→	1	3	1	1	1	1	1	3	1	1
82	←	1	3	1	1	2	1	1	3	1	2
83	→	1	6	1	1	3	2	1	9	2	2
83	←	2	9	1	1	3	1	1	9	2	12
84	→	1	8	1	1	1	1	1	1	2	16
84	←	1	3	1	1	1	1	1	1	2	6
85	→	1	8	1	1	3	2	1	3	2	8
85	←	1	3	1	1	3	1	1	3	2	6
86	→	1	8	1	1	3	2	1	3	2	8
86	←	1	3	1	1	3	1	1	3	2	6
87	→	1	1	1	1	3	2	1	3	2	1

87	←	1	3	1	1	3	1	1	3	2	6

B.4.5. Group additive values between 300 and 1800 K

Table B-18: Primary group additive values ΔGAV°s between 300 and 1800 K for abstraction of a hydrogen atom from N-H by a carbon-centered radical, deduced from the combined training and test set. For the reference reaction, the single-event pre-exponential factor is expressed in m^3 mol^{-1} s^{-1} and E_a is expressed in kJ mol^{-1}.

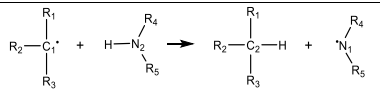

		300 K				400 K				500 K				600 K			
		ΔGAV°(N_1)		ΔGAV°(N_2)		ΔGAV°(N_1)		ΔGAV°(N_2)		ΔGAV°(N_1)		ΔGAV°(N_2)		ΔGAV°(N_1)		ΔGAV°(N_2)	
No.	Group	$log\tilde{A}$	E_a	$log\tilde{A}$	E_a	$log\tilde{A}$	E_a	$log\tilde{A}$	E_a	$log\tilde{A}$	E_a	$log\tilde{A}$	E_a	$log\tilde{A}$	E_a	$log\tilde{A}$	E_a
	Reference:	5.149	48.1	5.471	70.7	5.315	49.3	5.671	72.6	5.395	49.8	5.767	73.4	5.575	51.7	5.984	76.0
1	**N_i-(H)$_2$**	0.461	-12.0	0.194	19.6	0.378	-12.5	0.149	19.2	0.361	-12.7	0.143	19.2	0.325	-13.0	0.133	19.1
2	**$N_{i,I}$**	0.122	24.7	0.077	-26.6	0.102	24.5	0.109	-26.4	0.095	24.5	0.118	-26.3	0.081	24.3	0.140	-26.1
3	**N_i-(C_d)(H)**	0.062	42.2	-0.532	-8.7	0.176	43.0	-0.467	-8.3	0.211	43.3	-0.443	-8.1	0.287	44.0	-0.390	-7.6
4	**N_i-(C_t)(H)**	0.259	41.6	0.127	-14.7	0.223	41.3	0.107	-14.8	0.214	41.3	0.102	-14.8	0.197	41.1	0.093	-14.9
5	**N_i-(C)$_2$**	-0.443	11.0	0.071	-14.1	-0.345	11.7	0.092	-13.9	-0.317	11.9	0.091	-13.9	-0.258	12.5	0.090	-13.9
6	**N_i-(C)(C_d)**	0.147	48.5	-0.265	-14.7	0.259	49.2	-0.220	-14.4	0.296	49.5	-0.201	-14.3	0.375	50.3	-0.158	-13.8
7	**N_i-(C_d)$_2$**	0.886	75.2	-0.426	-8.4	0.972	75.8	-0.471	-8.7	0.970	75.8	-0.479	-8.8	0.958	75.7	-0.492	-8.9
8	**N_i-(C)(C_t)**	-0.147	45.4	-0.074	-24.7	-0.098	45.7	-0.059	-24.6	-0.086	45.8	-0.056	-24.6	-0.061	46.1	-0.049	-24.5
		ΔGAV°(C_1)		ΔGAV°(C_2)		ΔGAV°(C_1)		ΔGAV°(C_2)		ΔGAV°(C_1)		ΔGAV°(C_2)		ΔGAV°(C_1)		ΔGAV°(C_2)	
	Reference:	5.471	70.7	5.149	48.1	5.671	72.6	5.315	49.3	5.767	73.4	5.395	49.8	5.984	76.0	5.575	51.7
1	**C_i-(C)(H)$_2$**	-0.482	2.0	-0.133	-14.7	-0.381	2.7	-0.113	-14.5	-0.358	2.9	-0.117	-14.5	-0.308	3.4	-0.126	-14.6
2	**C_i-(C)$_2$(H)**	-0.700	2.8	0.059	-26.6	-0.509	4.1	0.098	-26.3	-0.461	4.5	0.093	-26.4	-0.360	5.5	0.082	-26.5
3	**$C_{i,d}$-(H)**	0.041	-23.1	0.040	-1.3	0.138	-22.4	0.093	-0.9	0.159	-22.3	0.099	-0.9	0.204	-21.8	0.113	-0.7
4	**$C_{i,d}$-(C)**	-0.170	-20.0	0.054	-11.4	-0.041	-19.1	0.106	-11.0	-0.010	-18.8	0.107	-11.0	0.056	-18.2	0.111	-10.9
5	**C_i-(C_d)(H)$_2$**	-0.160	41.0	-0.920	-35.6	-0.012	42.1	-0.840	-35.0	0.021	42.3	-0.818	-34.8	0.093	43.1	-0.770	-34.4
6	**C_i-(N)(H)$_2$**	-0.514	16.8	-0.611	-34.2	-0.390	17.6	-0.521	-33.6	-0.358	17.9	-0.497	-33.4	-0.286	18.6	-0.444	-32.8
7	**C_i-(C)(N)(H)**	-0.549	14.6	-0.428	-41.8	-0.418	15.5	-0.359	-41.3	-0.377	15.8	-0.340	-41.1	-0.286	16.8	-0.296	-40.7
8	**$C_{i,I}$-(H)**	0.008	5.6	-0.072	-33.4	0.144	6.5	0.008	-32.8	0.177	6.7	0.022	-32.7	0.246	7.5	0.054	-32.4
9	**$C_{i,I}$-(C)**	-0.093	7.5	0.008	-33.8	0.047	8.5	0.056	-33.4	0.079	8.7	0.059	-33.4	0.148	9.4	0.065	-33.4
10	**C_i-(C_t)(H)$_2$**	-0.018	27.2	-0.831	-31.0	0.151	28.4	-0.736	-30.3	0.188	28.7	-0.711	-30.1	0.268	29.5	-0.656	-29.6

11	**C_i-(C_t)(H)$_2$**	-0.127	41.0	-0.956	-29.6	0.020	42.0	-0.873	-29.0	0.050	42.3	-0.854	-28.9	0.114	42.9	-0.812	-28.4

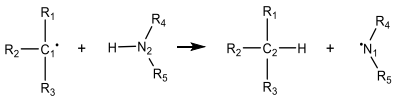

		700 K				**800 K**				**900 K**				**1000 K**			
		ΔGAV°(N_1)		ΔGAV°(N_2)		ΔGAV°(N_1)		ΔGAV°(N_2)		ΔGAV°(N_1)		ΔGAV°(N_2)		ΔGAV°(N_1)		ΔGAV°(N_2)	
No.	Group	$log\tilde{A}$	E_a	$log\tilde{A}$	E_a	$log\tilde{A}$	E_a	$log\tilde{A}$	E_a	$log\tilde{A}$	E_a	$log\tilde{A}$	E_a	$log\tilde{A}$	E_a	$log\tilde{A}$	E_a
	Reference:	5.747	53.7	6.183	78.8	5.908	56.0	6.361	81.5	6.056	58.4	6.520	84.2	6.192	60.8	6.662	86.9
1	**N_i-(H)$_2$**	0.307	-13.3	0.132	19.1	0.296	-13.4	0.135	19.1	0.290	-13.5	0.138	19.2	0.286	-13.6	0.141	19.2
2	**$N_{i,I}$**	0.073	24.2	0.154	-26.0	0.068	24.2	0.163	-25.8	0.066	24.1	0.169	-25.7	0.065	24.1	0.175	-25.6
3	**N_i-(C_d)(H)**	0.341	44.7	-0.351	-7.1	0.379	45.2	-0.323	-6.7	0.407	45.7	-0.303	-6.4	0.428	46.1	-0.287	-6.1
4	**N_i-(C_t)(H)**	0.188	41.0	0.089	-15.0	0.182	40.9	0.087	-15.0	0.179	40.8	0.086	-15.0	0.176	40.8	0.086	-15.0
5	**N_i-(C)$_2$**	-0.217	13.0	0.083	-14.0	-0.189	13.4	0.075	-14.1	-0.167	13.8	0.069	-14.2	-0.151	14.0	0.063	-14.3
6	**N_i-(C)(C_d)**	0.434	51.0	-0.123	-13.4	0.477	51.7	-0.098	-13.0	0.510	52.2	-0.080	-12.8	0.533	52.6	-0.068	-12.5
7	**N_i-(C_d)$_2$**	0.910	75.1	-0.496	-9.0	0.844	74.2	-0.500	-9.0	0.776	73.1	-0.506	-9.1	0.710	72.0	-0.513	-9.2
8	**N_i-(C)(C_t)**	-0.044	46.3	-0.045	-24.5	-0.033	46.4	-0.042	-24.4	-0.025	46.5	-0.040	-24.4	-0.020	46.6	-0.038	-24.4
		ΔGAV°(C_1)		ΔGAV°(C_2)		ΔGAV°(C_1)		ΔGAV°(C_2)		ΔGAV°(C_1)		ΔGAV°(C_2)		ΔGAV°(C_1)		ΔGAV°(C_2)	
	Reference:	6.183	78.8	5.747	53.7	6.361	81.5	5.908	56.0	6.520	84.2	6.056	58.4	6.662	86.9	6.192	60.8
1	**C_i-(C)(H)$_2$**	-0.278	3.8	-0.139	-14.8	-0.259	4.1	-0.151	-14.9	-0.247	4.3	-0.162	-15.1	-0.239	4.4	-0.171	-15.3
2	**C_i-(C)$_2$(H)**	-0.297	6.3	0.064	-26.7	-0.257	6.9	0.046	-26.9	-0.231	7.3	0.030	-27.2	-0.213	7.6	0.018	-27.4
3	**$C_{i,d}$-(H)**	0.230	-21.5	0.117	-0.7	0.246	-21.3	0.117	-0.7	0.255	-21.1	0.117	-0.7	0.260	-21.0	0.116	-0.7
4	**$C_{i,d}$-(C)**	0.096	-17.7	0.105	-11.0	0.122	-17.3	0.098	-11.1	0.138	-17.0	0.092	-11.2	0.148	-16.9	0.086	-11.3
5	**C_i-(C_d)(H)$_2$**	0.136	43.6	-0.731	-33.9	0.165	44.0	-0.699	-33.4	0.185	44.3	-0.671	-33.0	0.200	44.6	-0.647	-32.6
6	**C_i-(N)(H)$_2$**	-0.238	19.2	-0.405	-32.4	-0.204	19.7	-0.376	-32.0	-0.179	20.1	-0.353	-31.6	-0.161	20.4	-0.334	-31.2
7	**C_i-(C)(N)(H)**	-0.216	17.6	-0.257	-40.2	-0.160	18.4	-0.222	-39.7	-0.116	19.1	-0.190	-39.2	-0.080	19.8	-0.162	-38.7
8	**$C_{i,I}$-(H)**	0.288	8.0	0.069	-32.2	0.314	8.3	0.077	-32.1	0.331	8.6	0.081	-32.0	0.343	8.8	0.083	-32.0
9	**$C_{i,I}$-(C)**	0.191	10.0	0.062	-33.4	0.217	10.4	0.056	-33.5	0.236	10.6	0.051	-33.6	0.247	10.9	0.046	-33.6
10	**C_i-(C_t)(H)$_2$**	0.313	30.1	-0.616	-29.1	0.339	30.4	-0.586	-28.7	0.354	30.7	-0.561	-28.3	0.363	30.9	-0.541	-27.9
11	**C_i-(C_t)(H)$_2$**	0.146	43.3	-0.783	-28.1	0.162	43.5	-0.763	-27.8	0.169	43.7	-0.748	-27.5	0.170	43.7	-0.735	-27.3

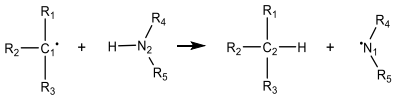

		1100 K				1200 K				1300 K				1400 K			
		ΔGAV°(N_1)		ΔGAV°(N_2)		ΔGAV°(N_1)		ΔGAV°(N_2)		ΔGAV°(N_1)		ΔGAV°(N_2)		ΔGAV°(N_1)		ΔGAV°(N_2)	
No.	Group	$log\tilde{A}$	E_a	$log\tilde{A}$	E_a	$log\tilde{A}$	E_a	$log\tilde{A}$	E_a	$log\tilde{A}$	E_a	$log\tilde{A}$	E_a	$log\tilde{A}$	E_a	$log\tilde{A}$	E_a
	Reference:	6.316	63.3	6.789	89.5	6.430	65.8	6.904	92.1	6.535	68.2	7.008	94.6	6.632	70.7	7.103	97.1
1	**N_i-(H)$_2$**	0.283	-13.7	0.144	19.3	0.281	-13.7	0.146	19.3	0.279	-13.8	0.148	19.4	0.277	-13.8	0.149	19.4
2	**$N_{i,t}$**	0.065	24.1	0.179	-25.5	0.066	24.1	0.182	-25.5	0.067	24.2	0.185	-25.4	0.069	24.2	0.187	-25.4
3	**N_i-(C$_d$)(H)**	0.443	46.4	-0.274	-5.8	0.454	46.6	-0.265	-5.6	0.462	46.8	-0.257	-5.4	0.467	46.9	-0.251	-5.3
4	**N_i-(C$_t$)(H)**	0.174	40.7	0.086	-15.0	0.172	40.7	0.086	-15.0	0.171	40.7	0.086	-15.0	0.170	40.6	0.086	-15.0
5	**N_i-(C)$_2$**	-0.138	14.3	0.058	-14.4	-0.128	14.5	0.054	-14.5	-0.120	14.7	0.050	-14.6	-0.114	14.9	0.047	-14.7
6	**N_i-(C)(C$_d$)**	0.550	52.9	-0.059	-12.4	0.562	53.2	-0.054	-12.2	0.570	53.4	-0.051	-12.2	0.576	53.5	-0.050	-12.2
7	**N_i-(C$_d$)$_2$**	0.651	70.8	-0.522	-9.4	0.599	69.6	-0.533	-9.6	0.553	68.5	-0.544	-9.9	0.514	67.5	-0.556	-10.2
8	**N_i-(C)(C$_t$)**	-0.016	46.7	-0.037	-24.3	-0.012	46.8	-0.036	-24.3	-0.011	46.8	-0.036	-24.3	-0.008	46.9	-0.036	-24.3
		ΔGAV°(C_1)		ΔGAV°(C_2)		ΔGAV°(C_1)		ΔGAV°(C_2)		ΔGAV°(C_1)		ΔGAV°(C_2)		ΔGAV°(C_1)		ΔGAV°(C_2)	
	Reference:	6.789	89.5	6.316	63.3	6.904	92.1	6.430	65.8	7.008	94.6	6.535	68.2	7.103	97.1	6.632	70.7
1	**C_i-(C)(H)$_2$**	-0.233	4.5	-0.177	-15.4	-0.229	4.6	-0.183	-15.5	-0.226	4.7	-0.188	-15.7	-0.224	4.7	-0.192	-15.8
2	**C_i-(C)$_2$(H)**	-0.201	7.9	0.009	-27.6	-0.191	8.1	0.001	-27.8	-0.186	8.2	-0.006	-27.9	-0.181	8.3	-0.011	-28.1
3	**$C_{i,d}$-(H)**	0.264	-20.9	0.116	-0.7	0.266	-20.9	0.117	-0.7	0.268	-20.9	0.117	-0.7	0.268	-20.8	0.118	-0.7
4	**$C_{i,d}$-(C)**	0.155	-16.7	0.082	-11.4	0.160	-16.6	0.078	-11.5	0.162	-16.5	0.076	-11.5	0.164	-16.5	0.074	-11.6
5	**C_i-(C$_d$)(H)$_2$**	0.210	44.8	-0.625	-32.1	0.218	45.0	-0.606	-31.7	0.222	45.1	-0.590	-31.3	0.225	45.1	-0.575	-30.9
6	**C_i-(N)(H)$_2$**	-0.147	20.7	-0.319	-30.9	-0.137	20.9	-0.306	-30.7	-0.129	21.1	-0.295	-30.4	-0.122	21.3	-0.285	-30.1
7	**C_i-(C)(N)(H)**	-0.051	20.3	-0.136	-38.2	-0.027	20.8	-0.114	-37.7	-0.009	21.3	-0.096	-37.3	0.006	21.7	-0.080	-36.9
8	**$C_{i,t}$-(H)**	0.351	9.0	0.085	-32.0	0.357	9.1	0.087	-31.9	0.361	9.2	0.088	-31.9	0.364	9.3	0.090	-31.8
9	**$C_{i,t}$-(C)**	0.257	11.0	0.042	-33.7	0.263	11.2	0.038	-33.8	0.267	11.3	0.035	-33.9	0.269	11.4	0.033	-33.9
10	**C_i-(C$_t$)(H)$_2$**	0.369	31.0	-0.524	-27.6	0.371	31.0	-0.509	-27.2	0.370	31.0	-0.497	-27.0	0.368	31.0	-0.486	-26.7
11	**C_i-(C$_t$)(H)$_2$**	0.167	43.6	-0.726	-27.1	0.163	43.5	-0.718	-27.0	0.157	43.4	-0.712	-26.8	0.150	43.2	-0.707	-26.7

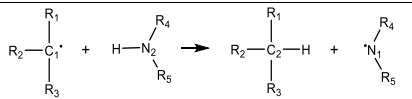

		1500 K				1600 K				1700 K				1800 K			
		ΔGAV°(N_1)		ΔGAV°(N_2)		ΔGAV°(N_1)		ΔGAV°(N_2)		ΔGAV°(N_1)		ΔGAV°(N_2)		ΔGAV°(N_1)		ΔGAV°(N_2)	
No.	**Group**	$logÃ$	E_a	$logÃ$	E_a	$logÃ$	E_a	$logÃ$	E_a	$logÃ$	E_a	$logÃ$	E_a	$logÃ$	E_a	$logÃ$	E_a
	Reference:	6.721	73.2	7.190	99.6	6.803	75.6	7.271	102.0	6.880	78.1	7.346	104.4	6.953	80.5	7.416	106.8
1	**N_i-(H)$_2$**	0.276	-13.8	0.151	19.4	0.275	-13.9	0.152	19.5	0.273	-13.9	0.153	19.5	0.273	-13.9	0.153	19.5
2	**$N_{i,I}$**	0.071	24.3	0.189	-25.3	0.072	24.3	0.191	-25.2	0.074	24.4	0.193	-25.2	0.076	24.4	0.194	-25.1
3	**N_i-(C$_d$)(H)**	0.470	47.0	-0.245	-5.1	0.472	47.1	-0.240	-5.0	0.471	47.1	-0.236	-4.8	0.471	47.1	-0.233	-4.7
4	**N_i-(C$_t$)(H)**	0.169	40.6	0.086	-15.0	0.168	40.6	0.086	-15.0	0.167	40.6	0.086	-15.0	0.167	40.5	0.085	-15.1
5	**N_i-(C)$_2$**	-0.109	15.0	0.044	-14.8	-0.105	15.1	0.042	-14.8	-0.102	15.2	0.040	-14.9	-0.099	15.3	0.037	-15.0
6	**N_i-(C)(C$_d$)**	0.579	53.6	-0.050	-12.1	0.580	53.7	-0.050	-12.2	0.579	53.7	-0.052	-12.2	0.579	53.6	-0.054	-12.3
7	**N_i-(C$_d$)$_2$**	0.480	66.6	-0.566	-10.5	0.451	65.7	-0.576	-10.8	0.424	64.9	-0.586	-11.1	0.403	64.2	-0.595	-11.4
8	**N_i-(C)(C$_t$)**	-0.007	46.9	-0.035	-24.3	-0.006	47.0	-0.035	-24.3	-0.006	47.0	-0.035	-24.3	-0.005	47.0	-0.036	-24.3
		ΔGAV°(C_1)		ΔGAV°(C_2)		ΔGAV°(C_1)		ΔGAV°(C_2)		ΔGAV°(C_1)		ΔGAV°(C_2)		ΔGAV°(C_1)		ΔGAV°(C_2)	
	Reference:	7.190	99.6	6.721	73.2	7.271	102.0	6.803	75.6	7.346	104.4	6.880	78.1	7.416	106.8	6.953	80.5
1	**C_i-(C)(H)$_2$**	-0.222	4.8	-0.196	-15.9	-0.220	4.8	-0.198	-15.9	-0.219	4.9	-0.201	-16.0	-0.218	4.9	-0.203	-16.1
2	**C_i-(C)$_2$(H)**	-0.178	8.4	-0.016	-28.2	-0.175	8.5	-0.020	-28.3	-0.173	8.5	-0.024	-28.4	-0.172	8.6	-0.027	-28.5
3	**$C_{i,d}$-(H)**	0.269	-20.8	0.119	-0.6	0.270	-20.8	0.120	-0.6	0.270	-20.8	0.120	-0.6	0.270	-20.8	0.121	-0.6
4	**$C_{i,d}$-(C)**	0.165	-16.5	0.072	-11.6	0.166	-16.5	0.071	-11.7	0.167	-16.4	0.069	-11.7	0.166	-16.4	0.068	-11.8
5	**C_i-(C$_d$)(H)$_2$**	0.226	45.2	-0.562	-30.6	0.226	45.2	-0.551	-30.3	0.225	45.1	-0.542	-30.0	0.223	45.1	-0.533	-29.7
6	**C_i-(N)(H)$_2$**	-0.117	21.4	-0.277	-29.9	-0.113	21.5	-0.270	-29.7	-0.110	21.6	-0.265	-29.5	-0.108	21.7	-0.259	-29.3
7	**C_i-(C)(N)(H)**	0.019	22.0	-0.067	-36.5	0.030	22.3	-0.055	-36.2	0.038	22.6	-0.046	-35.9	0.044	22.8	-0.037	-35.6
8	**$C_{i,I}$-(H)**	0.367	9.4	0.091	-31.8	0.370	9.5	0.093	-31.8	0.372	9.5	0.094	-31.7	0.373	9.6	0.095	-31.7
9	**$C_{i,I}$-(C)**	0.272	11.4	0.031	-34.0	0.275	11.5	0.029	-34.1	0.276	11.5	0.027	-34.1	0.277	11.6	0.026	-34.2
10	**C_i-(C$_t$)(H)$_2$**	0.365	30.9	-0.477	-26.4	0.362	30.8	-0.469	-26.2	0.358	30.6	-0.463	-26.0	0.353	30.5	-0.456	-25.8
11	**C_i-(C$_t$)(H)$_2$**	0.143	43.0	-0.702	-26.6	0.136	42.8	-0.699	-26.5	0.128	42.6	-0.697	-26.4	0.120	42.3	-0.695	-26.3

B.4.6. Tunneling coefficients

Table B-19: Tunneling coefficients for all reactions from Table B-16 over the temperature range 300-1800 K.

No.	κ(T)															
	300	**400**	**500**	**600**	**700**	**800**	**900**	**1000**	**1100**	**1200**	**1300**	**1400**	**1500**	**1600**	**1700**	**1800**
1	36.9	5.8	2.9	2.1	1.7	1.5	1.4	1.3	1.2	1.2	1.2	1.1	1.1	1.1	1.1	1.1
2	37.8	6.0	3.0	2.1	1.7	1.5	1.4	1.3	1.3	1.2	1.2	1.2	1.1	1.1	1.1	1.1
3	8.0	3.1	2.0	1.6	1.4	1.3	1.3	1.2	1.2	1.1	1.1	1.1	1.1	1.1	1.1	1.1
4	38.5	6.3	3.1	2.2	1.7	1.5	1.4	1.3	1.3	1.2	1.2	1.2	1.1	1.1	1.1	1.1
5	27.8	5.6	2.9	2.1	1.7	1.5	1.4	1.3	1.2	1.2	1.2	1.2	1.1	1.1	1.1	1.1
6	20.8	5.0	2.7	2.0	1.7	1.5	1.4	1.3	1.2	1.2	1.2	1.1	1.1	1.1	1.1	1.1
7	29.8	5.9	3.0	2.1	1.7	1.5	1.4	1.3	1.3	1.2	1.2	1.2	1.1	1.1	1.1	1.1
8	50.0	7.4	3.4	2.3	1.8	1.6	1.4	1.4	1.3	1.2	1.2	1.2	1.1	1.1	1.1	1.1
9	14.4	4.3	2.5	1.9	1.6	1.4	1.3	1.3	1.2	1.2	1.2	1.1	1.1	1.1	1.1	1.1
10	7.2	2.9	1.9	1.6	1.4	1.3	1.2	1.2	1.2	1.1	1.1	1.1	1.1	1.1	1.1	1.1
11	14.3	4.0	2.4	1.8	1.6	1.4	1.3	1.3	1.2	1.2	1.1	1.1	1.1	1.1	1.1	1.1
12	9.1	3.5	2.2	1.8	1.5	1.4	1.3	1.2	1.2	1.2	1.1	1.1	1.1	1.1	1.1	1.1
13	42.7	6.6	3.2	2.2	1.8	1.6	1.4	1.3	1.3	1.2	1.2	1.2	1.1	1.1	1.1	1.1
14	33.3	6.7	3.3	2.3	1.9	1.6	1.5	1.4	1.3	1.3	1.2	1.2	1.2	1.1	1.1	1.1
15	13.9	4.4	2.6	2.0	1.7	1.5	1.4	1.3	1.3	1.2	1.2	1.2	1.1	1.1	1.1	1.1
16	23.2	5.2	2.8	2.0	1.7	1.5	1.4	1.3	1.2	1.2	1.2	1.1	1.1	1.1	1.1	1.1
17	145.3	10.5	4.0	2.5	2.0	1.7	1.5	1.4	1.3	1.3	1.2	1.2	1.2	1.1	1.1	1.1
18	180.3	11.3	4.1	2.6	2.0	1.7	1.5	1.4	1.3	1.3	1.2	1.2	1.2	1.1	1.1	1.1
19	10.4	3.6	2.2	1.8	1.5	1.4	1.3	1.2	1.2	1.2	1.1	1.1	1.1	1.1	1.1	1.1
20	24.8	5.3	2.8	2.1	1.7	1.5	1.4	1.3	1.3	1.2	1.2	1.2	1.1	1.1	1.1	1.1
21	10.3	3.8	2.4	1.9	1.6	1.4	1.3	1.3	1.2	1.2	1.2	1.1	1.1	1.1	1.1	1.1
22	28.1	5.6	2.9	2.1	1.7	1.5	1.4	1.3	1.3	1.2	1.2	1.2	1.1	1.1	1.1	1.1
23	161.9	10.8	4.0	2.5	2.0	1.7	1.5	1.4	1.3	1.3	1.2	1.2	1.2	1.1	1.1	1.1
24	151.0	11.0	4.1	2.6	2.0	1.7	1.5	1.4	1.3	1.3	1.2	1.2	1.2	1.2	1.1	1.1
25	268.2	13.2	4.5	2.7	2.0	1.7	1.5	1.4	1.3	1.3	1.2	1.2	1.2	1.2	1.1	1.1
26	18.8	4.8	2.7	2.0	1.7	1.5	1.4	1.3	1.3	1.2	1.2	1.2	1.1	1.1	1.1	1.1
27	260.6	12.6	4.3	2.7	2.0	1.7	1.5	1.4	1.3	1.3	1.2	1.2	1.2	1.2	1.1	1.1
28	27.0	5.5	2.9	2.1	1.7	1.5	1.4	1.3	1.3	1.2	1.2	1.2	1.1	1.1	1.1	1.1
29	2.8	1.8	1.4	1.3	1.2	1.2	1.1	1.1	1.1	1.1	1.1	1.1	1.0	1.0	1.0	1.0
30	22.5	4.9	2.7	2.0	1.6	1.5	1.4	1.3	1.2	1.2	1.2	1.1	1.1	1.1	1.1	1.1
31	10.9	3.6	2.3	1.8	1.5	1.4	1.3	1.2	1.2	1.2	1.1	1.1	1.1	1.1	1.1	1.1
32	23.1	5.0	2.7	2.0	1.7	1.5	1.4	1.3	1.2	1.2	1.2	1.2	1.1	1.1	1.1	1.1
33	21.0	4.9	2.7	2.0	1.7	1.5	1.4	1.3	1.2	1.2	1.2	1.2	1.1	1.1	1.1	1.1
34	25.0	5.7	3.0	2.1	1.8	1.6	1.4	1.3	1.3	1.2	1.2	1.2	1.1	1.1	1.1	1.1
35	18.5	4.9	2.8	2.0	1.7	1.5	1.4	1.3	1.3	1.2	1.2	1.2	1.1	1.1	1.1	1.1
36	34.4	6.4	3.2	2.2	1.8	1.6	1.4	1.4	1.3	1.2	1.2	1.2	1.2	1.1	1.1	1.1
37	37.4	6.1	3.0	2.1	1.7	1.5	1.4	1.3	1.3	1.2	1.2	1.2	1.1	1.1	1.1	1.1
38	27.8	5.5	2.9	2.1	1.7	1.5	1.4	1.3	1.2	1.2	1.2	1.1	1.1	1.1	1.1	1.1
39	21.1	5.1	2.8	2.0	1.7	1.5	1.4	1.3	1.3	1.2	1.2	1.2	1.1	1.1	1.1	1.1
40	13.8	4.3	2.6	1.9	1.6	1.5	1.4	1.3	1.2	1.2	1.2	1.2	1.1	1.1	1.1	1.1
41	30.1	5.8	3.0	2.1	1.8	1.5	1.4	1.3	1.3	1.2	1.2	1.2	1.1	1.1	1.1	1.1
42	9.4	3.8	2.4	1.9	1.6	1.5	1.4	1.3	1.2	1.2	1.2	1.2	1.1	1.1	1.1	1.1
43	19.7	4.9	2.7	2.0	1.7	1.5	1.4	1.3	1.3	1.2	1.2	1.2	1.1	1.1	1.1	1.1
44	23.1	5.5	2.9	2.1	1.7	1.5	1.4	1.3	1.3	1.2	1.2	1.2	1.1	1.1	1.1	1.1
45	17.3	4.9	2.8	2.1	1.7	1.5	1.4	1.3	1.3	1.2	1.2	1.2	1.1	1.1	1.1	1.1
46	37.0	6.6	3.2	2.3	1.8	1.6	1.5	1.4	1.3	1.2	1.2	1.2	1.2	1.1	1.1	1.1
47	16.3	5.2	3.0	2.2	1.8	1.6	1.4	1.4	1.3	1.2	1.2	1.2	1.2	1.1	1.1	1.1
48	26.5	5.7	3.0	2.1	1.8	1.5	1.4	1.3	1.3	1.2	1.2	1.2	1.1	1.1	1.1	1.1
49	22.7	5.5	2.9	2.1	1.7	1.5	1.4	1.3	1.3	1.2	1.2	1.2	1.1	1.1	1.1	1.1
50	51.7	7.6	3.5	2.4	1.9	1.6	1.5	1.4	1.3	1.3	1.2	1.2	1.2	1.1	1.1	1.1
51	3.3	2.1	1.6	1.4	1.3	1.2	1.2	1.2	1.1	1.1	1.1	1.1	1.1	1.1	1.1	1.1
52	3.1	2.0	1.6	1.4	1.3	1.2	1.2	1.1	1.1	1.1	1.1	1.1	1.1	1.1	1.0	1.0

53	6.6	2.8	1.9	1.6	1.4	1.3	1.2	1.2	1.2	1.1	1.1	1.1	1.1	1.1	1.1	1.1
54	1.9	1.4	1.3	1.2	1.1	1.1	1.1	1.1	1.1	1.0	1.0	1.0	1.0	1.0	1.0	1.0
55	4.7	2.4	1.7	1.5	1.3	1.3	1.2	1.2	1.1	1.1	1.1	1.1	1.1	1.1	1.1	1.1
56	6.7	2.8	1.9	1.6	1.4	1.3	1.2	1.2	1.2	1.1	1.1	1.1	1.1	1.1	1.1	1.1
57	19.6	4.7	2.6	1.9	1.6	1.5	1.4	1.3	1.2	1.2	1.2	1.1	1.1	1.1	1.1	1.1
58	16.3	4.8	2.8	2.0	1.7	1.5	1.4	1.3	1.3	1.2	1.2	1.2	1.1	1.1	1.1	1.1
59	33.3	6.7	3.3	2.3	1.9	1.6	1.5	1.4	1.3	1.3	1.2	1.2	1.2	1.1	1.1	1.1
60	28.3	6.3	3.2	2.3	1.8	1.6	1.5	1.4	1.3	1.2	1.2	1.2	1.2	1.1	1.1	1.1
61	12.4	4.5	2.7	2.1	1.7	1.5	1.4	1.3	1.3	1.2	1.2	1.2	1.2	1.1	1.1	1.1
62	1.7	1.4	1.2	1.2	1.1	1.1	1.1	1.0	1.0	1.0	1.0	1.0	1.0	1.0	1.0	1.0
63	4.0	2.4	1.8	1.6	1.4	1.3	1.2	1.2	1.2	1.1	1.1	1.1	1.1	1.1	1.1	1.1
64	12.4	4.5	2.7	2.1	1.7	1.5	1.4	1.3	1.3	1.2	1.2	1.2	1.2	1.1	1.1	1.1
65	55.9	7.4	3.4	2.3	1.8	1.6	1.4	1.4	1.3	1.2	1.2	1.2	1.2	1.1	1.1	1.1
66	43.6	7.0	3.3	2.3	1.8	1.6	1.5	1.4	1.3	1.2	1.2	1.2	1.2	1.1	1.1	1.1
67	1.7	1.4	1.2	1.2	1.1	1.1	1.1	1.1	1.0	1.0	1.0	1.0	1.0	1.0	1.0	1.0
68	13.8	4.3	2.5	1.9	1.6	1.5	1.3	1.3	1.2	1.2	1.2	1.1	1.1	1.1	1.1	1.1
69	30.6	6.2	3.1	2.2	1.8	1.6	1.4	1.3	1.3	1.2	1.2	1.2	1.1	1.1	1.1	1.1
70	34.7	6.8	3.3	2.3	1.8	1.6	1.5	1.4	1.3	1.2	1.2	1.2	1.2	1.1	1.1	1.1
71	16.3	4.9	2.8	2.1	1.7	1.5	1.4	1.3	1.3	1.2	1.2	1.2	1.1	1.1	1.1	1.1
72	5.6	2.8	2.0	1.6	1.4	1.3	1.3	1.2	1.2	1.1	1.1	1.1	1.1	1.1	1.1	1.1
73	26.7	5.8	3.0	2.1	1.8	1.5	1.4	1.3	1.3	1.2	1.2	1.2	1.1	1.1	1.1	1.1
74	133.2	11.0	4.2	2.6	2.0	1.7	1.5	1.4	1.3	1.3	1.2	1.2	1.2	1.2	1.1	1.1
75	10.2	3.4	2.2	1.7	1.5	1.4	1.3	1.2	1.2	1.2	1.1	1.1	1.1	1.1	1.1	1.1
76	5.4	2.5	1.8	1.5	1.4	1.3	1.2	1.2	1.1	1.1	1.1	1.1	1.1	1.1	1.1	1.1
77	10.2	3.4	2.2	1.7	1.5	1.4	1.3	1.2	1.2	1.2	1.1	1.1	1.1	1.1	1.1	1.1
78	37.5	6.4	3.2	2.2	1.8	1.6	1.4	1.3	1.3	1.2	1.2	1.2	1.2	1.1	1.1	1.1
79	36.1	6.3	3.1	2.2	1.8	1.6	1.4	1.3	1.3	1.2	1.2	1.2	1.2	1.1	1.1	1.1
80	78.4	9.3	3.9	2.5	2.0	1.7	1.5	1.4	1.3	1.3	1.2	1.2	1.2	1.2	1.1	1.1
81	31.5	5.9	3.0	2.1	1.7	1.5	1.4	1.3	1.3	1.2	1.2	1.2	1.1	1.1	1.1	1.1
82	60.2	7.5	3.4	2.3	1.8	1.6	1.4	1.4	1.3	1.2	1.2	1.2	1.2	1.1	1.1	1.1
83	48.1	7.1	3.3	2.3	1.8	1.6	1.4	1.4	1.3	1.2	1.2	1.2	1.2	1.1	1.1	1.1
84	15.2	4.6	2.7	2.0	1.7	1.5	1.4	1.3	1.3	1.2	1.2	1.2	1.1	1.1	1.1	1.1
85	221.4	12.1	4.3	2.6	2.0	1.7	1.5	1.4	1.3	1.3	1.2	1.2	1.2	1.2	1.1	1.1
86	259.7	12.9	4.4	2.7	2.0	1.7	1.5	1.4	1.3	1.3	1.2	1.2	1.2	1.2	1.1	1.1
87	179.3	12.0	4.3	2.7	2.0	1.7	1.5	1.4	1.3	1.3	1.2	1.2	1.2	1.2	1.1	1.1

B.5. References

[1] T. Ko, P. Marshall, A. Fontijn, Rate coefficients for the H+NH3 reaction over a wide temperature range, The Journal of Physical Chemistry 94 (1990) 1401-1404.

[2] C. Willis, A.W. Boyd, O.A. Miller, Primary yields and mechanism in the radiolysis of gaseous ammonia, Canadian Journal of Chemistry 47 (1969) 3007-3016.

[3] K.T. Aganesyan, A.B. Nalbandyan, The determination of the rate constants for the reactions between hydrogen and oxygen atoms and ammonia molecules., Dokl. Phys. Chem. 160 (1965).

[4] W. Hack, P. Rouveirolles, H.G. Wagner, Direct measurements of the reactions NH2+H2→NH3 + H at temperatures from 670 to 1000 K, The Journal of Physical Chemistry 90 (1986) 2505-2511.

[5] J.V. Michael, J.W. Sutherland, R.B. Klemm, Rate constant for the reaction H + NH3 over the temperature range 750-1777 K, The Journal of Physical Chemistry 90 (1986) 497-500.

[6] J.W. Sutherland, R.B. Klemm, Kinetic studies of elementary reactions using the flash photolysis-shock tube technique, Symp. Int. Combus. Proc. 16 (1987).

[7] M. Demissy, R. Lesclaux, Kinetics of hydrogen abstraction by amino radicals from alkanes in the gas phase. A flash photolysis-laser resonance absorption study, J. Am. Chem. Soc. 102 (1980) 2897-2902.

[8] W. Hack, H. Kurzke, P. Rouveirolles, H.G. Wagner, Direct measurements of the reaction NH2+CH4→NH3+CH3 in temperature range 743≤T/K≤1023, Symposium (International) on Combustion 21 (1988) 905-911.

[9] G. Hennig, H.G.G. Wagner, A Kinetic Study About the Reactions of NH2(X2B1) Radicals with Saturated Hydrocarbons in the Gas Phase, Berichte der Bunsengesellschaft für physikalische Chemie 99 (1995) 863-869.

[10] S. Song, D.M. Golden, R.K. Hanson, C.T. Bowman, J.P. Senosiain, C.B. Musgrave, G. Friedrichs, A shock tube study of the reaction NH2 + CH4 → NH3 + CH3 and comparison with transition state theory, Int. J. Chem. Kinet. 35 (2003) 304-309.

[11] W. Hack, H. Kurzke, P. Rouveirolles, H.G. Wagner, Hydrogen Abstraction Reactions by NH2(X̃2B1)-Radicals from Hydrocarbons in the Gas Phase, Berichte der Bunsengesellschaft für physikalische Chemie 90 (1986) 1210-1219.

[12] P. Gray, J.C.J. Thynne, Arrhenius parameters for elementary combustion reactions: H-atom abstraction from N-H bonds, Symp. Int. Combus. Proc. 10 (1965) 435.

[13] P. Gray, A. Jones, J.C.J. Thynne, Kinetics and sites of methyl radical attack on dimethylamine and deuterated dimethylamine, Transactions of the Faraday Society 61 (1965) 474-483.

[14] P. Gray, A. Jones, Methyl radical reactions with ethylamine and deuterated ethylamines, Transactions of the Faraday Society 62 (1966) 112-119.

Appendix C

Supporting information to Chapter 5

C.1. Kinetic model development

The automatically generated model for DEA with Genesys is merged with the mechanism of Glarborg et al. [1]. In the case that the same species or reactions appear in both the automatically generated Genesys mechanism and the Glarborg et al. mechanism, it is opted to retain the kinetic parameters from the Genesys mechanism. A few examples of the difference in rate coefficients when using the kinetic parameters as reported by Glarborg et al. or calculated in this work is given here. Figure C-1 depicts the Arrhenius plots for the hydrogen abstraction from ethanimine ($CH_3CH{=}NH$). The rate coefficients can differ several orders of magnitude depending on the temperature studied. At 600 K, i.e. the temperature at which the conversion of DEA starts at oxidation conditions, the *ab initio* calculated rate coefficient for hydrogen abstraction from the N-H bond is a factor of 100 larger compared to the one reported by Glarborg et al. At 1000 K, this deviation is decreased to a factor of 20. Besides the large differences in rate coefficients, the relative importance of each of the hydrogen abstraction sites differs between models, which can have a large influence on the kinetic model predictions.

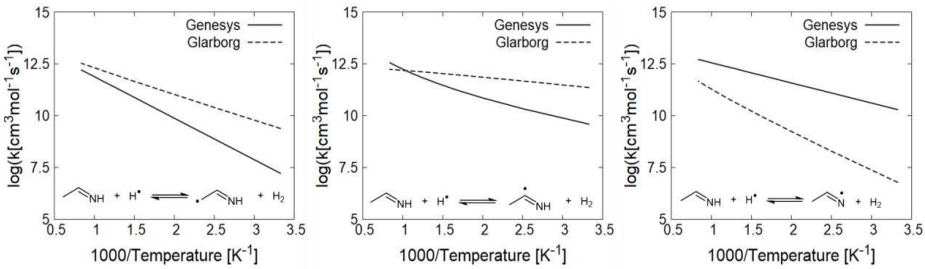

Figure C-1: Arrhenius plot for the hydrogen abstraction from ethanimine ($CH_3CH{=}NH$) by a hydrogen atom, comparing the rate coefficients obtained from *ab initio* calculations (Genesys) and reported in the Glarborg et al. model.

Figure C-2 depicts an Arrhenius plot of the C-H and C-C β-scissions of the radical $CH_3CH_2NH^{\cdot}$ using the *ab initio* calculated kinetic parameters and the kinetic parameters used in the Glarborg et al. model. The kinetic parameters for the C-H β-scission are based on the analogous reaction

of $CH_3NH^{\cdot}$, while for the C-C β-scission they are based on $CH_3CH_2O^{\cdot}$. In both models, the rate coefficient of the C-C β-scission is larger than the C-H β-scission.

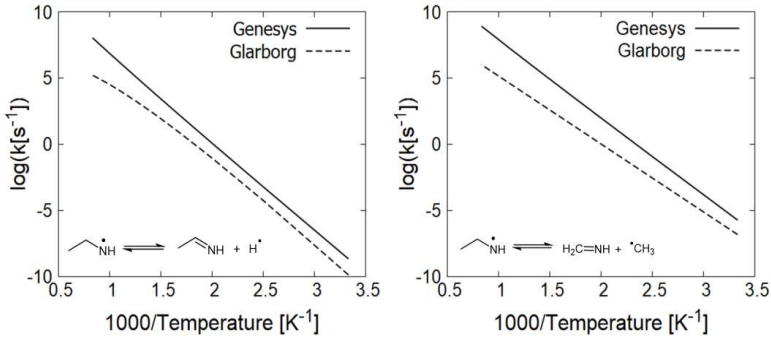

Figure C-2: Arrhenius plot for the C-H and C-C β-scissions of the $CH_3CH_2NH^{\bullet}$ radical comparing the rate coefficients obtained from *ab initio* calculations (Genesys) and reported in the Glarborg et al. model.

Figure C-3 illustrates the influence of the accuracy of these rate coefficients on the simulated mole fractions of HCN for the oxidation of DEA at φ = 1.0.

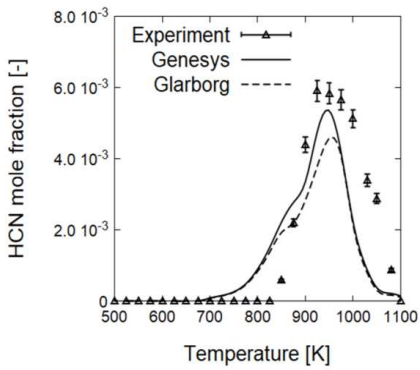

Figure C-3: Simulated mole fraction of HCN during the oxidation of DEA for φ = 1.0 using the respective rate coefficients for the C-C β-scission from the Genesys and Glarborg et al. model.

C.2. Potential energy surfaces

C.2.1. Dimethylamine

The PES for the two radicals formed from DMA is given in Figure C-4. The two radicals that are formed are $CH_3N^{\cdot}CH_3$, labeled as R_1, and $CH_3NHCH_2^{\cdot}$, labeled as R_2. The nitrogen-centered radical R_1 can react via β-scission leading to the formation of $CH_3N{=}CH_2$ with a barrier of 144 kJ mol^{-1}. This important intermediate imine species can also be formed from the carbon-centered radical R_2 via β-scission of the N-H bond. The barrier for this reaction is 157 kJ mol^{-1}. The β-scission of the C-N bond of the carbon-centered radical R_2 leads to the formation of $CH_2{=}NH$ via a barrier of 125 kJ mol^{-1}.

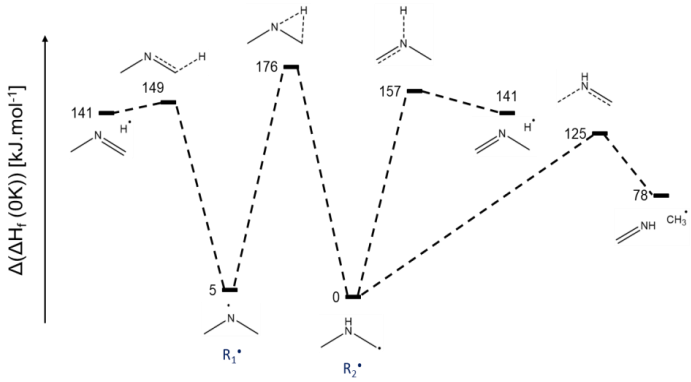

Figure C-4: Relevant part of the potential energy surface for the $CH_3N^{\cdot}CH_3$ ($R_1^{\bullet}$) and CH_3NHCH_2 ($R_2^{\bullet}$) radicals. The values are CBS-QB3 calculated enthalpies of formation at 0 K [kJ mol^{-1}] relative to $CH_3NHCH_2^{\cdot}$ ($R_2^{\bullet}$).

C.2.2. Ethylamine

The PES for the two main radicals formed from EA is given in Figure C-5. The two main radicals that are formed are $CH_3C^{\cdot}HNH_2$, labeled as R_3, and $CH_3CH_2N^{\cdot}H$, labeled as R_4. The carbon-centered radical R_3 can react via β-scission of the N-H bond forming $CH_3CH{=}NH$ with a barrier of 158 kJ mol^{-1}. This important intermediate species can also be formed via β-scission of the radical R_4. Alternatively, the nitrogen-centered radical R_4 undergoes a C-C β-scission leading to the formation of $CH_2{=}NH$ with a barrier of 107 kJ mol^{-1}.

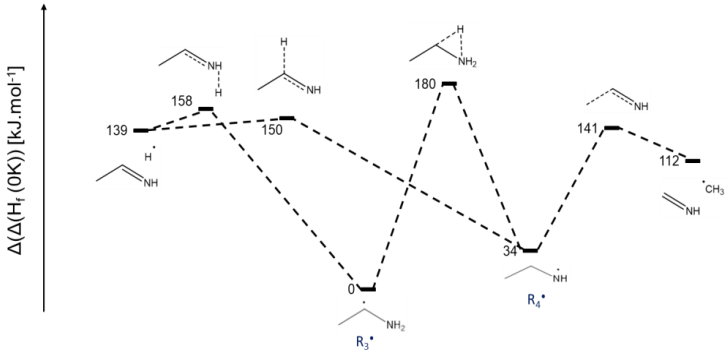

Figure C-5: Relevant part of the potential energy surface for the $CH_3C^{\bullet}HNH_2$ ($R_3^{\bullet}$) and $CH_3CH_2N^{\bullet}H$ ($R_4^{\bullet}$) radicals. The values are CBS-QB3 calculated enthalpies of formation at 0 K [kJ mol^{-1}] relative to $CH_3C^{\bullet}HNH_2$ ($R_3^{\bullet}$).

C.2.3. Diethylamine

The PES for the radicals formed from DEA after hydrogen abstraction is given in Figure C-6.

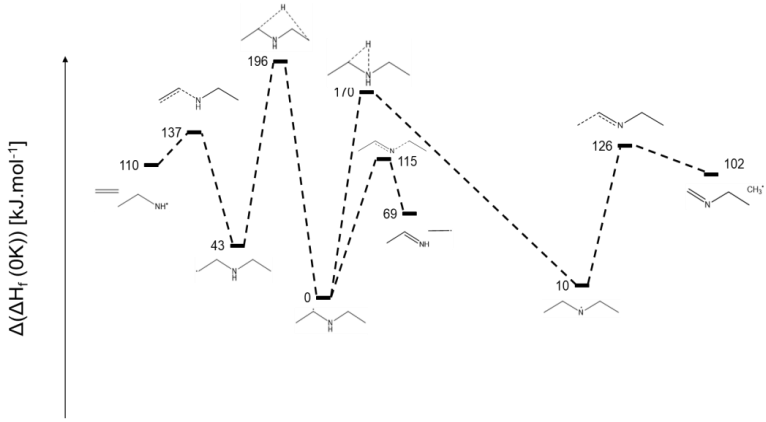

Figure C-6: Relevant part of the potential energy surface for the radicals of DEA. The values are CBS-QB3 calculated enthalpies of formation at 0 K [kJ mol^{-1}] relative to $CH_3C^{\bullet}HNHCH_2CH_3$.

C.3. Pyrolysis and oxidation of DEA

C.3.1. Tubular reactor

C.3.1.1. *Discussion on plug flow reactor assumption*

The tubular reactor (TR) has been modelled as an ideal plug flow reactor. To justify this assumption, the dimensionless Péclet number (Pe) is calculated using Eq. C-1.

$$Pe = \frac{L^2}{D\tau + \frac{QL}{48\pi D}} \qquad \text{(Eq. C-1)}$$

In Eq. C-1, L is the length of the reactor, τ is the residence time, D is the binary diffusion coefficient and Q is the volumetric flow. The calculated values for the Péclet numbers in the TR over the studied temperature range 700 K– 1000 K are given in Table C-1. Based on these numbers ranging from 219 to 114, the use of an ideal plug flow reactor can be justified considering a Péclet number of 100 as threshold value.

Table C-1: Values of the Péclet number during the pyrolysis of diethylamine (0.01 diethylamine inlet mole fraction, τ = 2 s, P = 107 kPa) in the TR.

Temperature [K]	Péclet number [-]
700	219
725	207
750	195
775	184
800	174
825	164
850	155
875	147
900	140
925	133
950	126
975	120
1000	114

C.3.1.2. *Temperatures profiles*

For the simulations of the TR experiments, the temperature profiles measured at unreactive conditions are used as input in the PFR model. In Figure C-7, these temperature profiles are depicted for each value of the set point temperature over the range of 700 to 1000 K in increments of 25 K.

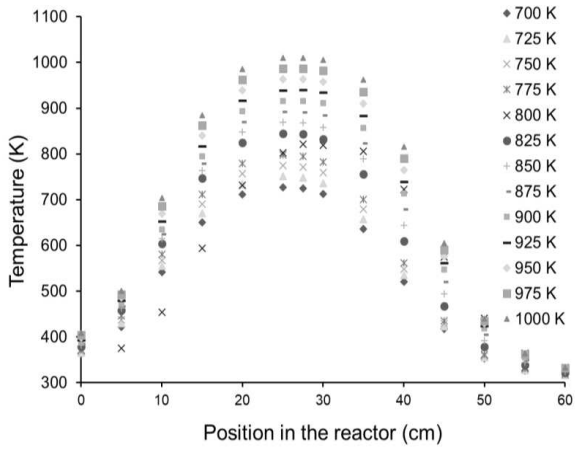

Figure C-7: Temperature profiles [K] in the TR measured at unreactive conditions. The temperatures in the legend correspond to the set point temperatures.

C.3.2. Sensitivity analyses

Sensitivity analyses are performed to better understand the reaction pathways responsible for the consumption of DEA and the formation of the main product species. In the presented sensitivity analyses, a positive sensitivity coefficient for a given reaction indicates that increasing the associated pre-exponential factor increases the mole fraction of the target molecule. Analogously, a negative sensitivity coefficient for a given reaction indicates that increasing the associated pre-exponential factor decreases the mole fraction of the target molecule.

C.3.2.3. *Pyrolysis*

The sensitivity analysis with respect to the mole fraction profile of DEA for pyrolysis conditions at T = 800, 900 and 1000 K is displayed in Figure C-8. The consumption of DEA is very sensitive towards the homolytic scission of the C-N bond. This scission increases the number of radicals in the reactive system and hence has a significant promoting effect on the reactivity. Hydrogen atoms are formed after β-scission of the ethyl and ethylamine ($CH_3CH_2NH^{\bullet}$) radicals.

The homolytic scission of the C-C bond, for which the bond dissociation energy is 5 kJ mol^{-1} higher compared to C-N, results in the formation of the less reactive methyl radicals. Hydrogen abstractions by hydrogen atoms and methyl radicals from DEA have a negative sensitivity coefficient and promote the conversion of DEA. The recombination of two methyl radicals has a negative sensitivity coefficient as it results in a decrease of the number of radicals in the reactive system.

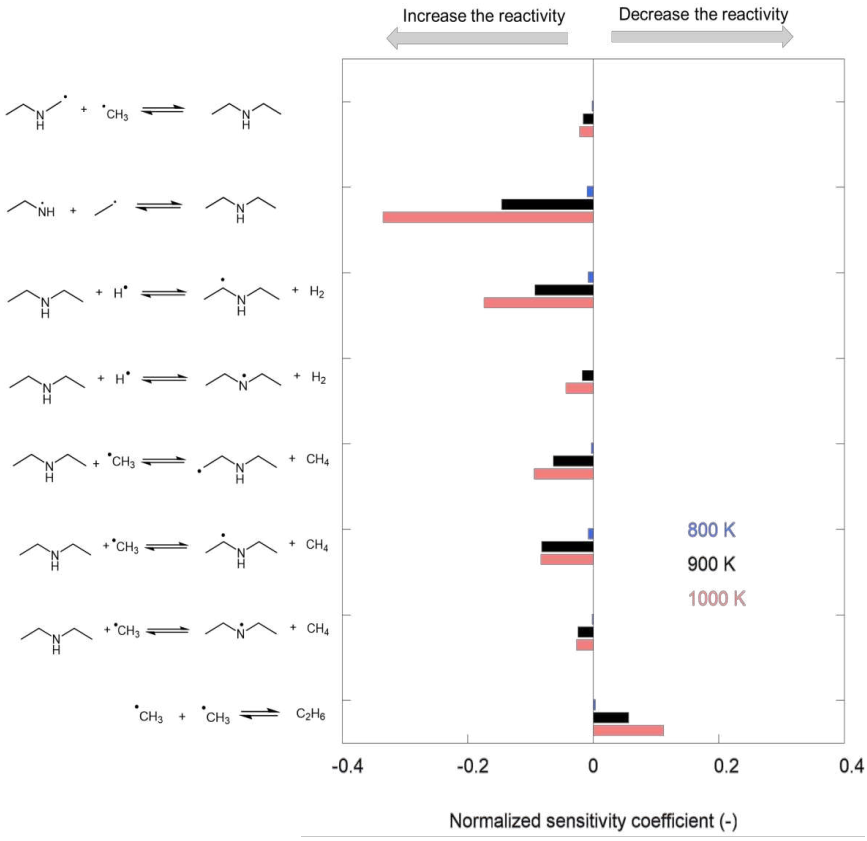

Figure C-8: Normalized sensitivity coefficients for the mole fraction of diethylamine (DEA) in DEA pyrolysis. Experimental conditions correspond to P = 107 kPa, $x_{DEA,0}$ = 0.01, T = 800 K (blue), 900 K (black) and 1000 K (red).

C.3.2.4. *Oxidation*

The sensitivity analysis with respect to the mole fraction of DEA for oxidation at φ = 1 and T = 650, 750 and 850 K is displayed in Figure C-9. The sensitive reactions include hydrogen abstraction reactions by molecular oxygen, hydroxyl radicals and hydroperoxy radicals. Most of these reactions have a negative sensitivity coefficient, as they contribute to the consumption

of DEA. At 650 and 750 K, the main abstracting species is the hydroperoxy radical, which is in agreement with the larger sensitivity coefficient for these reactions. This radical is mainly formed via reactions of methyl and ethyl radicals, which result from the β-scission of fuel radicals. At approximately 750 K, the β-scission of the fuel radicals become more favored compared to O_2 addition, leading to an increased production of these hydroperoxy radicals. Also important for the low-temperature reactivity are reactions of methyl peroxy radicals. Hydrogen abstraction by this radical forms methyl hydrogen peroxide. After homolytic scission, this species can lead to chain branching, forming the reactive hydroxyl radical and enhancing the reactivity. From Figure C-9, it can be seen that the formation of methyl hydrogen peroxide corresponds to a positive sensitivity coefficient for DEA, or equivalently a reduced reactivity of DEA. Self-reaction of hydroperoxy radicals giving hydrogen peroxide and molecular oxygen has a positive sensitivity coefficient as this results in a decrease of radicals in the system. This is also the case for the recombination of a methyl and hydroperoxy radical.

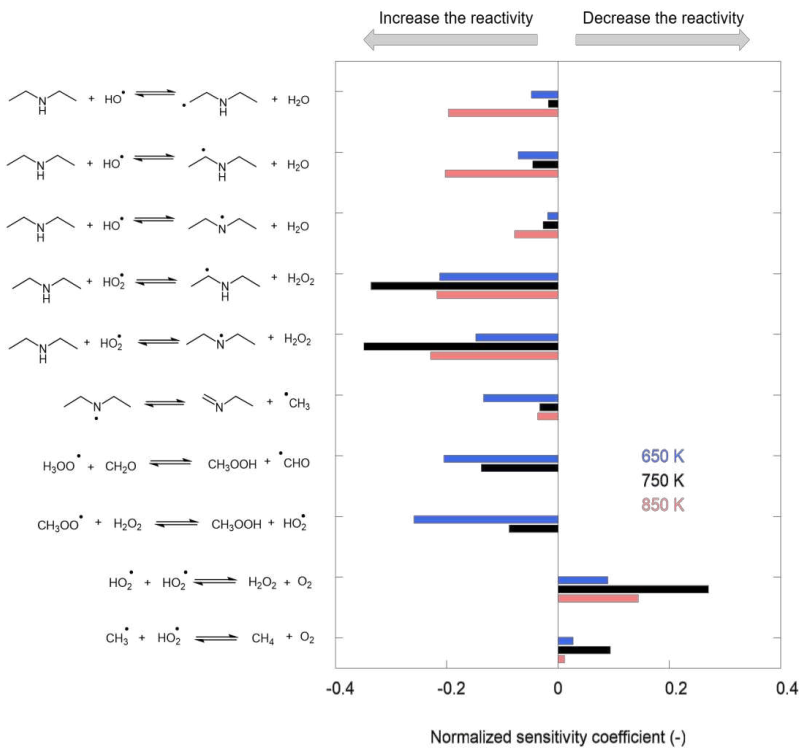

Figure C-9: Normalized sensitivity coefficients for the mole fraction of diethylamine (DEA) in DEA oxidation. Experimental conditions are φ = 1, P = 107 kPa, $x_{DEA,0}$ = 0.01, T = 650 K (blue), 750 K (black) and 850 K (red).

C.4. Laminar premixed flames of DMA/EA

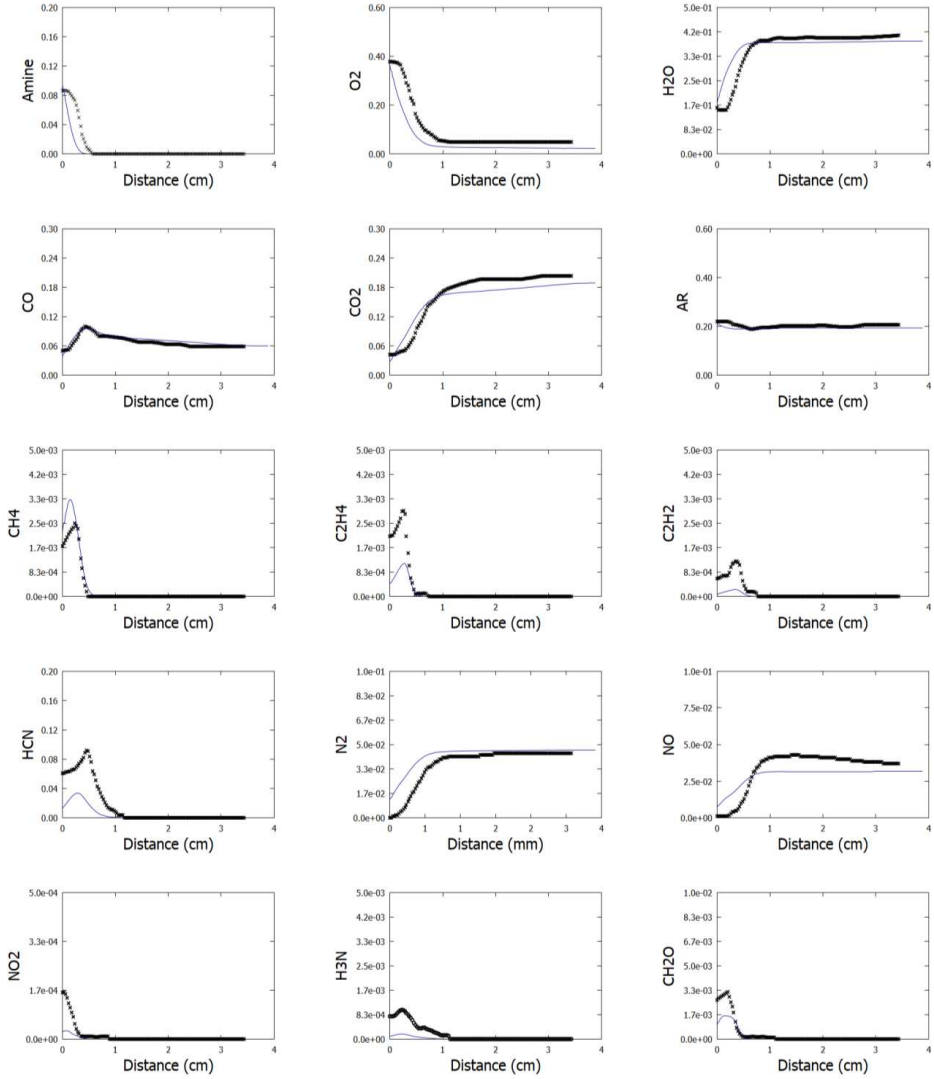

Figure C-10: Species mole fractions as a function of distance [cm] in DMA stoichiometric premixed laminar flames. Experiments (symbols, black) [2] and simulation results (lines, blue) are compared. Experimental conditions are a pressure of 4 kPa and inlet mole fraction of DMA equal to 0.16.

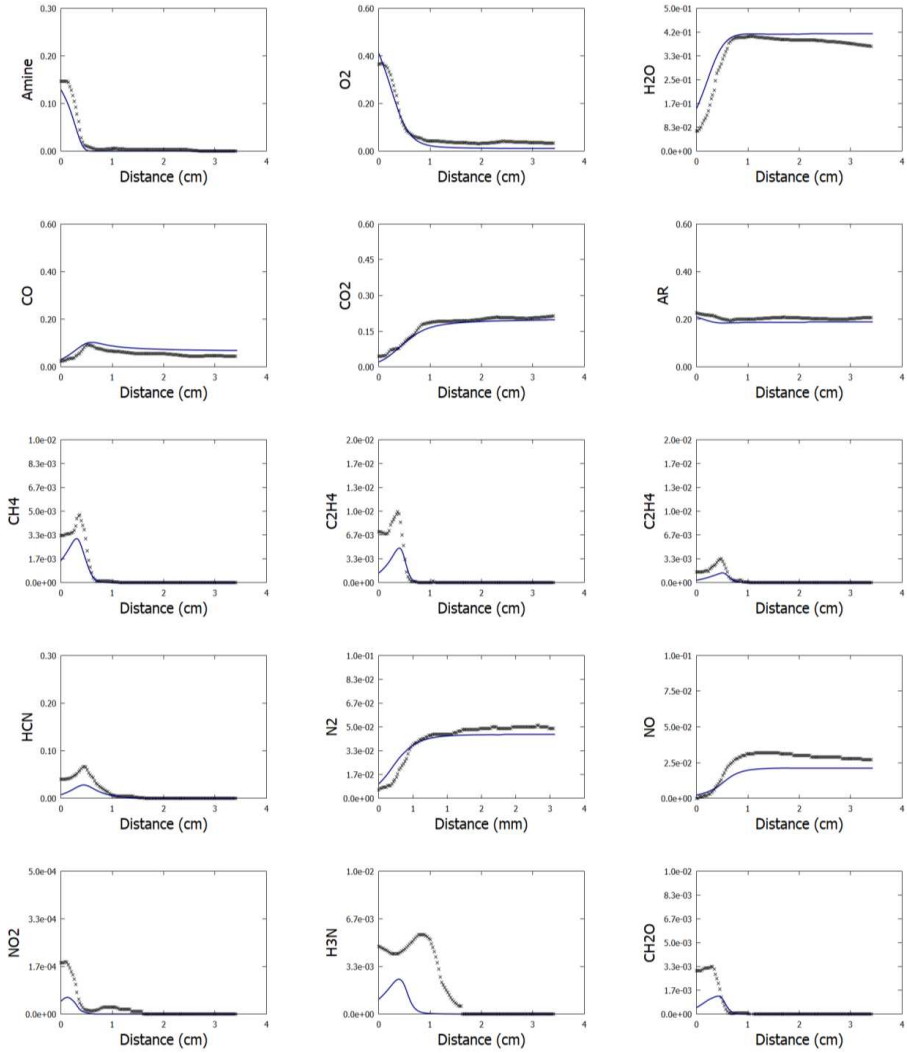

Figure C-11: Species mole fractions as a function of distance [cm] in EA stoichiometric premixed laminar flames. Experiments (symbols, black) [2] and simulation results (lines, blue) are compared. Experimental conditions are a pressure of 4 kPa and inlet mole fraction of EA equal to 0.16.

C.5. References

[1] P. Glarborg, J.A. Miller, B. Ruscic, S.J. Klippenstein, Modeling nitrogen chemistry in combustion, Progress in Energy and Combustion Science 67 (2018) 31-68.

[2] A. Lucassen, K. Zhang, J. Warkentin, K. Moshammer, P. Glarborg, P. Marshall, K. Kohse-Höinghaus, Fuel-nitrogen conversion in the combustion of small amines using dimethylamine and ethylamine as biomass-related model fuels, Combustion and Flame 159 (2012) 2254-2279.

Appendix D

Supporting information to Chapter 6

D.1. Pyrolysis of DMDS in N_2/C_2H_6

D.1.1. Experimental conditions

Table D-1: Overview of the experimental conditions for the pyrolysis of dimethyl disulfide (DMDS) in N_2 and in a C_2H_6 matrix [1].

Experiment	DMDS + N_2					DMDS + C_2H_6				
Set temperature [K]	673	773	873	973	1073	673	773	873	973	1073
Pressure [kPa]	120					120				
N_2 flow [g h^{-1}]	200					-				
C_2H_6 flow [g h^{-1}]	-					200				
H_2O flow [g h^{-1}]	80					80				
DMDS flow [g h^{-1}]	1.16 10^{-2}					1.16 10^{-2}				
Sulfur concentration [ppmwS/total]	286					286				

D.1.2. Temperature profiles

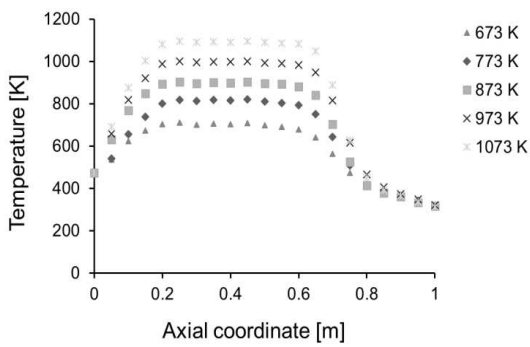

Figure D-1: Temperature profiles along the axial quartz reactor coordinate for the DMDS experiments with N_2. The temperatures in the legend correspond to the set point temperatures.

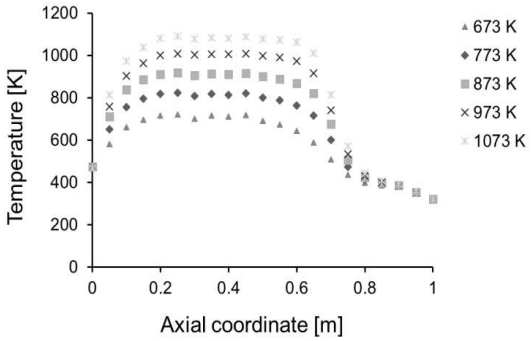

Figure D-2: Temperature profiles along the axial quartz reactor coordinate for the DMDS experiments with C_2H_6. The temperatures in the legend correspond to the set point temperatures.

D.2. Pyrolysis of COS in N_2/C_2H_6

D.2.1. Experimental conditions

Table D-2: Overview of the experimental conditions for the pyrolysis of carbonyl sulfide (COS) in a C_2H_6 matrix.

Experiment	COS + C_2H_6						
Set temperature [K]	973	998	1023	1048	1073	1098	1123
Pressure [kPa]	150						
N_2 flow [g h^{-1}]	120						
C_2H_6 flow [g h^{-1}]	180						
DMDS flow [g h^{-1}]	1.25 10^{-2}						
Sulfur concentration [ppmwS/total]	417						

D.2.2. Temperature profiles

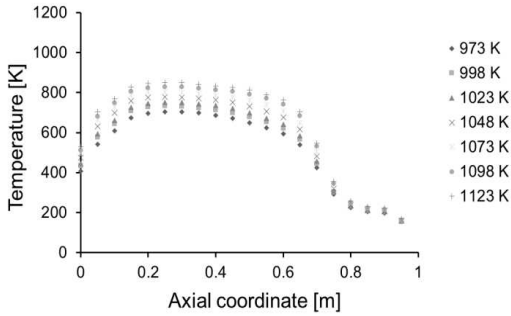

Figure D-3: Temperature profiles along the axial quartz reactor coordinate for the COS experiments with C_2H_6. The temperatures in the legend correspond to the set point temperatures.

D.3. Steam cracking of C_7H_{16} with DMS/DMDS/DMSO/CS_2

Table D-3: Overview of the experimental conditions for the pyrolysis of dimethyl sulfide (DMS), dimethyl disulfide (DMDS), dimethyl sulfoxide (DMSO) and carbon disulfide (CS_2) in a C_2H_6 matrix [2].

Experiment	DMS	DMDS	DMSO	CS_2
CIT [K]	823			
COT [K]	1123			
Pressure [kPa]	170			
Duration [h]	6			
C_7H_{16} flow [g h^{-1}]	4 10^3			
H_2O flow [g h^{-1}]	2 10^3			
Sulfur concentration [ppmwS/HC]	826	841	821	842

D.4. References

[1] N. Olahova, Influence of sulfur compounds on product yields and coke formation during steam cracking of hydrocarbons, 2018.

[2] N. Olahova, M.R. Djokic, R. Van de Vijver, N.D. Ristic, G.B. Marin, M.-F. Reyniers, K.M. Van Geem, Thermal decomposition of sulfur compounds and their role in coke formation during steam cracking of heptane, Chemical Engineering & Technology 39 (2016) 2096-2106.

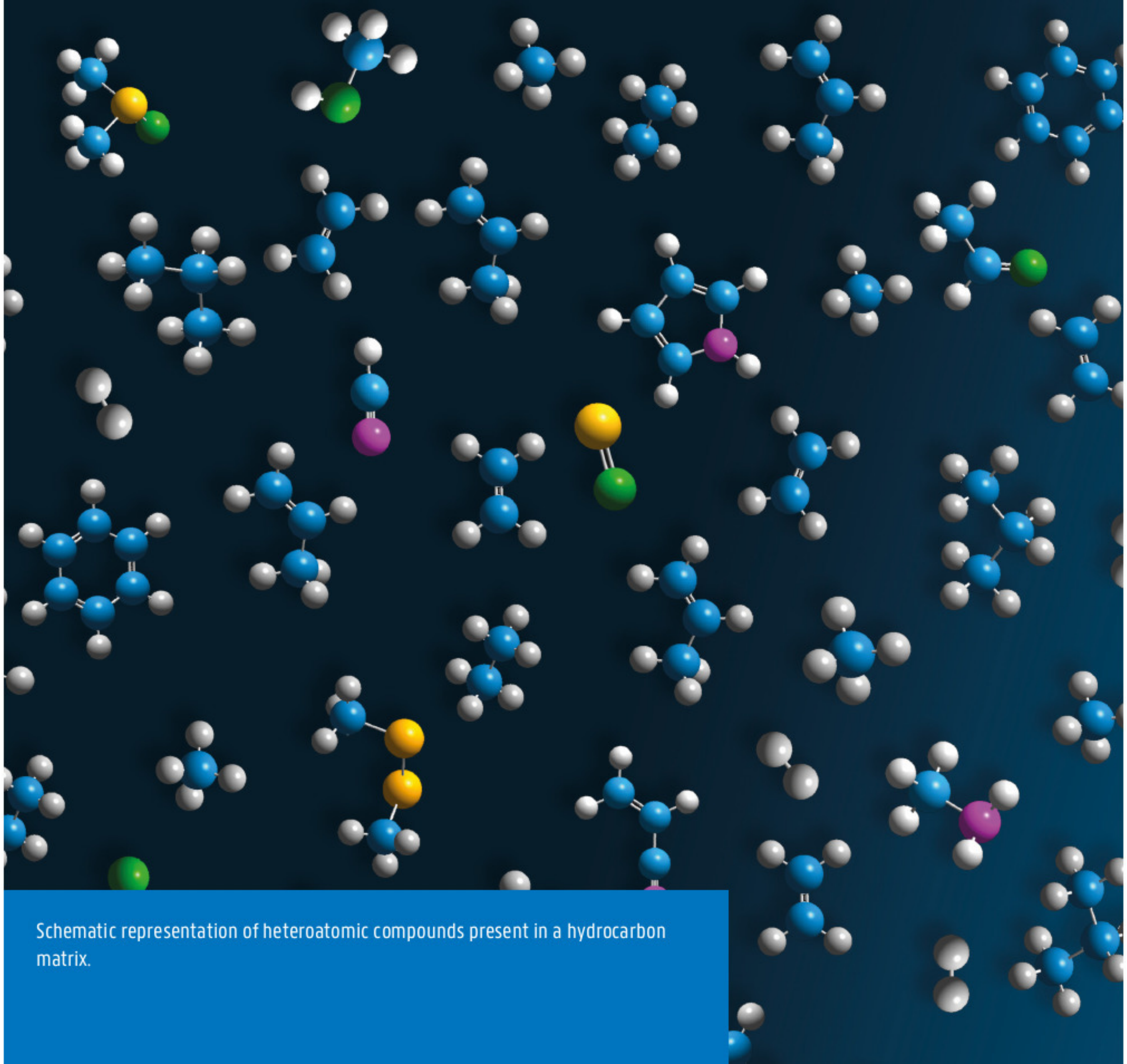

Schematic representation of heteroatomic compounds present in a hydrocarbon matrix.